

UCLA
UCLA Electronic Theses and Dissertations

Title

Tectonic Evolution of the Easternmost Himalayan Collisional System

Permalink

<https://escholarship.org/uc/item/15h7v8tm>

Author

Haproff, Peter Jasura

Publication Date

2018

Peer reviewed|Thesis/dissertation

UNIVERSITY OF CALIFORNIA
Los Angeles

Tectonic Evolution of the
Easternmost Himalayan Collisional System

A dissertation submitted in partial satisfaction of the
requirements for the degree Doctor of Philosophy
in Geology

by

Peter Jasura Haproff

2018

© Copyright by

Peter Jasura Haproff

2018

ABSTRACT OF THE DISSERTATION

Tectonic Evolution of the Easternmost Himalayan Collisional System

by

Peter Jasura Haproff

Doctor of Philosophy in Geology

University of California, Los Angeles, 2018

Professor An Yin, Co-Chair

Professor Timothy Mark Harrison, Co-Chair

The Cenozoic India-Asia collision generated the Tibetan Plateau and the Himalayan collisional system, the latter consisting of the convergence-perpendicular Himalayan orogen and the convergence-parallel Eastern and Western Flanking Belts located along the margins of India. Studying the evolution of each of these tectonic domains is critical to understanding the collision process and differentiating the end-member models of indenter-induced continental deformation. Despite this importance, there is a notable lack of geologic investigations on the development of the flanking belts in comparison to the extensive research of the Tibetan Plateau and east-trending Himalayan orogen. To address this problem, the research of this dissertation is focused on the Mesozoic-Cenozoic tectonic evolution of the northernmost segment of the Eastern Flanking Belt, the northern Indo-Burma Ranges, which are located directly east to southeast of the eastern Himalayan syntaxis. In the following chapters, I integrate the results of geologic field

mapping, balanced cross section construction and restoration, U-Pb zircon geochronology, whole-rock geochemistry, thermobarometry, and (U-Th)/He zircon thermochronology to examine the litho-structural framework of the northern Indo-Burma Ranges and tectonic relationships in time and space with the adjacent eastern Himalayan orogen, the southern Tibetan Plateau, and the Eastern Flanking Belt.

The research of this dissertation shows that the study area exposes a southwest- to west-directed Cenozoic thrust belt cored by a hinterland-dipping duplex system. Thrust faults sole into a northeast- to east-dipping décollement, which extends to >30 km depth. Southwestward forward propagation of the thrust belt in the foreland was coeval with out-of-sequence thrusting in the hinterland. This structural framework combined with the observed southward deflection in the trends of ductile stretching lineations within shear zones (northeast-trending in the north and east-trending in the south) suggest deformation around the eastern Himalayan syntaxis is best approximated by models of clockwise lithospheric flow accommodated by distributed thrusting.

Major lithologic units involved in the northern Indo-Burma thrust belt from south to north include the easternmost continuations of the Tertiary Sub-Himalayan Sequence, Proterozoic-Cambrian Lesser Himalayan Sequence, and Indus-Yarlung suture zone of the Himalayan orogen and the Mesozoic northern Gangdese batholith belt and Mesoproterozoic basement of the Lhasa terrane. However, several Himalayan-Tibetan lithologic units are missing, including the Paleoproterozoic-Ordovician Greater Himalayan Crystalline Complex, Proterozoic-Eocene Tethyan Himalayan Sequence, Mesozoic-Cenozoic Xigaze forearc basin, and Cenozoic igneous rocks of the southern Gangdese batholith. Research suggests that these units were present in the study area at the onset of the Cenozoic India-Asia collision and their present-day absence is related to an eastward increase in post-collisional crustal shortening and continental underthrusting along

the Himalayan collisional system. This interpretation is supported by a Cenozoic shortening strain estimate of ~81% (>156 km) across the northern Indo-Burma Ranges and a dramatic southward decrease in the width of the collisional system from ~200 km across the Himalayan orogen to ~5 km across the study area.

Active deformation across the northern Indo-Burma Ranges and adjacent southeastern Tibetan Plateau is characterized by right-slip transpression partitioned between the range-bounding, oblique-slip Mishmi thrust in the southwest and right-slip Puqu and Parlung faults of Jiali fault zone in the northeast. The leading Mishmi thrust is kinematically-linked with the ~1000-km-long, right-slip Sagaing fault to the south via a previously-unmapped, southwest-trending restraining bend. This structural relationship of the Eastern Flanking Belt provides a key example of the spatial transition from transpressional deformation near the corner of an indenter to discrete right-slip motion along the side of an indenter during continental collision.

The dissertation of Peter Jasura Haproff is approved

Craig Manning

Scott Joseph Brandenberg

Timothy Mark Harrison, Committee Co-Chair

An Yin, Committee Co-Chair

University of California, Los Angeles

2018

TABLE OF CONTENTS

Chapter 1: Introduction	1
1.1. Introduction	2
1.2. Chapter 2: Tectonic evolution of the northern Indo-Burma Ranges: lateral correlation of Himalayan-Tibetan lithologic units across the eastern Himalayan syntaxis	3
1.3. Chapter 3: West-directed thrusting south of the eastern Himalayan syntaxis indicates clockwise crustal flow at the indenter corner during the India-Asia collision	4
1.4. Chapter 4: Tectonic Evolution of the northern Indo-Burma Ranges: Mesozoic-Cenozoic kinematic reconstruction and constraints on the mode of deformation across the easternmost India-Asia collisional zone	6
1.5. Chapter 5: Out of sequence thrusting in the northern Indo-Burma Ranges: evidence from zircon (U-Th)/He thermochronology	7
1.6. Background of the Dissertation	8
1.7. Figures	10
1.8. References	13
 Chapter 2: Tectonic evolution of the northern Indo-Burma Ranges: lateral correlation of Himalayan-Tibetan lithologic units across the eastern Himalayan syntaxis	19
2.1. Abstract	20
2.2. Introduction	21
2.3. Geologic Setting	22
2.3.1. Eastern Himalayan Orogen	23
2.3.2. Indus-Yarlung Suture Zone	25
2.3.3. Lhasa Terrane	25
2.3.4. Cratonal Rocks of Northeast India	27
2.3.5. Northern Indo-Burma Ranges	27
2.4. Sampling and Analytical Methods	28
3.4.1. U-Pb Zircon Geochronology of the Lohit Plutonic Complex	28
3.4.2. U-Pb Detrital Zircon Geochronology	29
3.4.3. Whole-rock Geochemistry	30
2.5. Lithologic Descriptions and Results of U-Pb Zircon Geochronology	31
2.5.1. Lohit Plutonic Complex	31
2.5.1.1. Western Lohit Plutonic Complex Belt	31
2.5.1.2. Eastern Lohit Plutonic Complex Belt	32
2.5.2. Tidding and Mayodia Mélange Complexes	33
2.5.3. Mayodia Gneiss	34
2.5.4. Lalpani Schist	35
2.5.5. Tezu Unit	37
2.5.6. Sewak Unit	37
2.6. Results of Whole-Rock Geochemistry	38
2.6.1. Plutonic Rocks	38
2.6.2. Mafic and Ultramafic Rocks	38

2.6.3. Sr and Nd Isotope Geochemistry	39
2.7. Regional Correlation of Lithologic Units	40
2.7.1. Sub-Himalayan Sequence	40
2.7.2. Lesser Himalayan Sequence and Greater Himalayan Crystalline Complex	41
2.7.3. Indus-Yarlung Suture Zone	42
2.7.4. Mesozoic Magmatic Arc and Mesoproterozoic Basement of the Lhasa Terrane	43
2.8. Discussion	44
2.9. Conclusions	45
2.10. Figures and Tables	47
2.11. References	67
Chapter 3: West-directed thrusting south of the eastern Himalayan syntaxis indicates clockwise crustal flow at the indenter corner during the India-Asia collision	87
3.1. Abstract	88
3.2. Introduction	88
3.3. Structural Geology of the Northern Indo-Burma Ranges	90
3.4. Discussion and Conclusions	94
3.5 Acknowledgements	95
3.6. References	95
Chapter 4: Tectonic Evolution of the northern Indo-Burma Ranges: Mesozoic-Cenozoic kinematic reconstruction and constraints on the mode of deformation across the easternmost India-Asia collisional zone	97
4.1. Abstract	98
4.2. Introduction	99
4.3. Geologic setting	101
4.3.1. Eastern Himalayan Orogen	101
4.3.2. Lhasa Terrane	102
4.3.3. Eastern Flanking Belt	103
4.3.3.1. Northern Indo-Burma Ranges	103
4.3.3.2. Southern Indo-Burma Ranges	105
4.3.3.3. West Burma Microplate	105
4.3.3.4. Central Burma Basin	106
4.3.3.5. Sagaing Fault	107
4.3.4. Lithospheric Structure of the Eastern Flanking Belt	107
4.4. Methods	108
4.4.1. Thermobarometry	108
4.4.2. Construction and Restoration of the Dibang Valley Cross Section	109
4.5. Results of Thermobarometry	110
4.6. Results of the Dibang Valley Cross Section Restoration	112
4.7. Discussion	112
4.7.1. Structural Framework Comparison	113
4.7.2. Crustal Shortening across the Easternmost Himalayan Collisional System	114

4.7.3. Constraints on Models of the India-Asia collision	116
4.7.4. Strain Partitioning surrounding the Eastern Himalayan Syntaxis	117
4.7.5. Transfer of Slip across the Eastern Flanking Belt	118
4.7.6. Mesozoic-Cenozoic Tectonic Evolution	120
4.7.6.1. Stage 1: ~80 Ma	120
4.7.6.2. Stage 2: ~50 Ma	121
4.7.6.3. Stage 3: ~20 Ma	122
4.7.6.4. Stage 4: ~10 Ma	123
4.8. Conclusions	125
4.9. Figures and Tables	127
4.10. References	152
Chapter 5: Out of sequence thrusting in the northern Indo-Burma Ranges: evidence from preliminary zircon (U-Th)/He thermochronology	174
5.1. Abstract	175
5.2. Introduction	175
5.3. Geologic Setting	176
5.3.1. Eastern Himalayan Orogen	176
5.3.2. Southern Lhasa Terrane	179
5.3.3. Northern Indo-Burma Thrust Belt	180
5.4. Sampling and Analytical Methods	181
5.5. Results of Zircon (U-Th)/He Thermochronology	183
5.6. Discussion	184
5.7. Conclusions	186
5.8. Figures and Tables	187
5.9. References	192
Appendices: Supplementary figures and data tables	200
Chapter 2	201
Chapter 4	281
Chapter 5	285

LIST OF FIGURES

1.1. Tectonic map of the India-Asia orogenic system	10
1.2. Simplified tectonostratigraphic column of the Himalayan orogen and the Lhasa terrane	11
1.3. Models of Cenozoic continental deformation around the eastern Himalayan syntaxis	12
2.1. Geologic maps of the India-Asia orogenic system	47
2.2. Tectonostratigraphic column depicting correlation of major lithologic units and faults exposed in the eastern Himalaya, northern Indo-Burma Ranges, and northeast Indian craton	48
2.3. Geologic map of the Dibang Valley traverse	49
2.4. Detailed geologic maps of locations along the Dibang Valley traverse	50
2.5. Geologic map of the Lohit Valley traverse	53
2.6. Outcrop photographs of rocks of the Lohit Plutonic Complex	54
2.7. Outcrop photographs of the Mayodia and Tidding mélange complexes	54
2.8. Outcrop photographs of rocks of the Mayodia gneiss in Dibang Valley	55
2.9. Outcrop photographs of rocks of the Lalpani schist	55
2.10. Outcrop photographs of the Tezu unit and the Sewak unit	56
2.11. Relative probability plots of detrital zircon U-Pb ages for metasedimentary rocks	57
2.12. Geochemical plots for plutonic rocks	59
2.13. Geochemical plots of source and tectonic setting for plutonic rocks	59
2.14. Geochemical plots of mafic and ultramafic rocks	60
2.15. Plot of Σ_{Nd} versus Sr _i for granitoids of the western Lohit Plutonic Complex belt	61
2.16. Plot of the frequency of Σ_{Nd} values for all samples	62
2.17. Schematic geologic cross sections across the northern Indo-Burma Ranges and central Himalaya-southern Tibetan Plateau showing correlation of major lithologic units	63
3.1. Tectonic map of the Indo-Asian collisional zone	89
3.2. End-member models for upper plate continental deformation surrounding the eastern Himalayan syntaxis during the Cenozoic India-Asia collision	89
3.3. Geologic map of the easternmost Himalaya and the northern Indo-Burma Ranges	90
3.4. Geologic map of the Dibang Valley traverse	91
3.5. Geologic map of the Lohit Valley traverse	92
3.6. Cross sections for the Dibang Valley and Lohit Valley traverses	92
3.7. Outcrop photographs of ductile fabrics within and adjacent to the major thrust shear zones	93
3.8. Outcrop photograph of the Mishmi thrust and Google Earth-based map of cut-and-fill terraces along the range-bounding Mishmi thrust	94
3.9. Stereographic plots of stretching lineation orientations across the easternmost Himalayan orogen and northern Indo-Burma thrust belt	95
4.1. Tectonic map of the India-Asia orogenic system	127
4.2 Tectonostratigraphic map of the Eastern Flanking Belt	128
4.3. Tectonostratigraphic map of the Western Flanking Belt	129
4.4. Models of upper plate continental deformation surrounding the eastern Himalayan	

syntaxis during the Cenozoic India-Asia collision	130
4.5. Tectonostratigraphic column of major lithologic units and structures of the Himalayan orogen and Lhasa terrane	131
4.6. Tectonostratigraphic column of major lithologic units and faults of the northern Indo-Burma thrust belt	132
4.7. Geologic map of the Dibang Valley traverse	133
4.8. Geologic map of the Lohit Valley traverse	134
4.9. Balanced cross sections along Dibang Valley and Lohit Valley	135
4.10. Google Earth-based maps of the range-bounding Mishmi thrust	136
4.11. Photomicrographs of schist of the Tidding mélange complex	137
4.12. Photomicrograph of garnet schist of the Tidding mélange complex	138
4.13. Plots of peak pressure-temperature conditions for metamorphic rocks	139
4.14. Reconstruction of the Dibang Valley balanced cross section	140
4.15. Schematic geologic map of the Himalayan orogen showing crustal shortening estimates of existing studies	141
4.16. Schematic cross section of the pre-collisional configuration of major lithologic units comprising the north Indian margin, Neo-Tethys subduction system, and the southern Lhasa terrane during the Cretaceous	142
4.17. Oblique-view block diagram of strain partitioning across the northern Indo-Burma Ranges and southeastern Tibetan Plateau	143
4.18. Google Earth-based maps of the major faults in the study area	144
4.19. Google Earth-based tectonic map of the Namdapha Corridor region	145
4.20. Google Earth-based map of the Namyin fault	147
4.21. Tectonic evolution of the eastern Himalaya, southern Tibet, and southeast Asia since the Late Cretaceous	148
4.22. Schematic lithospheric-scale cross sections of the Mesozoic-Cenozoic evolution of the easternmost Himalayan orogen and southeast Tibet	149
 5.1. Maps of the eastern Himalayan collisional system and southern Lhasa terrane	187
5.2. Geologic map of Dibang Valley, northern Indo-Burma ranges	189
5.3. Geologic cross section along Dibang Valley, northern Indo-Burma ranges	190
 A.2.1. Plots of U-Pb zircon concordia, relative probability, and weighted mean ages for granitoids of the western Lohit Plutonic Complex belt from Chapter 2	201
A.2.2. Plots of U-Pb concordia, relative probability, and weighted mean age plots for granitoids of the eastern Lohit Plutonic Complex belt from Chapter 2	203
A.2.3. Cathodoluminescence images of representative zircons analyzed for U-Pb crystallization ages from Chapter 2	204
A.2.4. Geochemical plots for plutonic rocks from Chapter 2	205
A.2.5. Diagrams of sources for plutonic rocks based on geochemical composition from Chapter 2	206
A.2.6. Rare earth element spider diagrams for granitoids of the western Lohit Plutonic Complex belt from Chapter 2	207
A.2.7. Discriminant diagrams for mafic and ultramafic rocks from Chapter 2	208
A.2.8. Chondrite-normalized rare earth element diagram for mafic and ultramafic rocks from Chapter 2	209

A.4.1. Field photographs of faults exposed along Dibang Valley from Chapter 4	281
A.4.2. Photomicrographs of garnet mica schist from the Tidding mélange complex from Chapter 4	282
A.4.3. Schematic cross section of underthrusted Himalayan-Tibetan lithologic units	283
A.4.4. Block diagram of the paleo-tectonic configuration of the study area at ~55 Ma	284
A.5.1. Plot of (U-Th)/He age versus effective uranium from Chapter 5	285
A.5.2. Plot of (U-Th)/He age versus effective spherical radius from Chapter 5	286

LIST OF TABLES

2.1. Summary of zircon U-Pb geochronology ages for granitoids of the Lohit Plutonic Complex	64
2.2. List of samples used for detrital zircon U-Pb geochronology	65
2.3. Summary of whole-rock Nd and Sr isotopic data	66
4.1. Summary of pressure-temperature determinations	151
5.1. List of samples used for zircon (U-Th)/He thermochronology	191
A.2.1. U-Pb zircon geochronology data for the Western Lohit Plutonic Complex Belt from Chapter 2	210
A.2.2. U-Pb zircon geochronology data for the Eastern Lohit Plutonic Complex Belt from Chapter 2	213
A.2.3. U-Pb detrital zircon geochronologic data of metasedimentary rocks of the Tidding and Mayodia mélange complexes from Chapter 2	216
A.2.4. U-Pb detrital zircon geochronology data of the Mayodia gneiss from Chapter 2	223
A.2.5. U-Pb detrital zircon geochronologic data of the Lalpani schist from Chapter 2	241
A.2.6. U-Pb detrital zircon geochronologic data of the Sewak unit from Chapter 2	272
A.2.7. Whole-rock geochemistry data for plutonic rocks from Chapter 2	276
A.2.8. Whole-rock geochemistry for mafic and ultramafic rocks from Chapter 2	278
A.2.9. Results of the Kolmogorov-Smirnov statistical test from Chapter 2	280
A.5.1. Summary of bedrock zircon (U-Th)/He ages for all aliquots from Chapter 5	286

ACKNOWLEDGEMENTS

During my time at UCLA, I have had the pleasure to interact with many people who have provided invaluable guidance, assistance, and encouragement along the way. I will start by acknowledging the members of my PhD committee for their participation, patience, and advice. I thank Scott Brandenberg for serving as an outstanding committee member and asking thoughtful questions regarding my research. Craig Manning has always been an approachable mentor and a key source of direction with my work. Craig's expertise and constructive advice significantly helped my growth as a geoscientist. I thank Mark Harrison for teaching me the fundamentals of thermochronology, geochronology, and Himalayan-Tibetan tectonics. Without Mark, I never would have come to UCLA or taken the next step in my career. I sincerely appreciate his help and will always remember our great time together in South Africa.

No one has been more influential and supportive at UCLA than An Yin. I thank An for standing by me through the years and imparting his expertise in not only geology, but life as well. An's commitment, advice, and friendship allowed myself to mature as a geoscientist and adult. I thank him for pushing me to achieve my goals, even when I doubted myself. While teaching geologic mapping through CSULA, I found myself taking on An's persona and methods in the field. I am truly proud of being a student of An and will forever cherish our relationship.

I must thank several faculty with whom it has been a pleasure to work with, including Ray Ingersoll, Gilles Peltzer, and Jon Aurnou. Seulgi Moon was incredibly helpful during my later years at UCLA with my writing and presentation skills, and understanding geomorphology. I thank her for leading my third trip to India and am looking forward to collaborating in the future. I also acknowledge Greg Davis for allowing me to take his *Tectonic Evolution of Western North America* course, which remains one of the most informative and enjoyable graduate-level

courses I have taken. Sinan Akciz has been a close friend and critical source of advice with writing, presentations, and interviews.

I acknowledge several UCLA staff, including Lauri Holbrook for her everlasting kindness, approachability, and support, along with Frankie Masi, Mike Rathjen, Kathleen Micham, and Elyse Chou. Many UCLA researchers were integral in aiding with my research, including Rosario Esposito and Frank Kyte with using the electron microprobe, and Axel Schmidt, Matt Wielicki, Rita Economos, Ming-Chang Liu, Beth-Ann Bell, Haolon Tang, and Melanie Barboni with making zircon mounts, using the ion microprobe, and reducing and interpreting my U-Pb data.

My PhD research would not have been possible without the assistance from several colleagues in China, including Wu Chen and Suoya Fan at the Chinese University of Geosciences, Beijing. I thank Ding Lin, Vera Liu, and Chao Wang at the Institute of Tibetan Plateau Research, Chinese Academy of Sciences, for hosting me in Beijing and letting me use their facilities free of charge. Jianlin Chen at the Chinese Academy of Sciences in Guangzhou performed whole-rock geochemical analysis on my samples when time was short. I acknowledge Junpeng Wang and Tim Kusky for hosting me in Wuhan and inviting me to lecture on my research.

Katu Bage is the best Himalayan guide and driver I could have asked for. I thank Katu and Oken Tayeng of Abor Country Travels for committing to working with me for three field seasons and I am excited to continue our relationship.

Without the help and friendship of my fellow graduate students, I would not have succeeded at UCLA. For their support, I must thank Andrew Zuza, Robin Zuza, Paul Burgess, Jessica

Watkins, Erin Leonard, Nate Brown, Kevin Coffey, Ivy Curren, Jeanine Ashe, Chris McGuire, Abijah Simon, Mike Huh, John Mering, Mike Lawson, Margaret Deng, and Ellen Alexander.

Whereas I never overlapped with Mike Taylor, Mike Murphy, or Eric Cowgill during my time at UCLA, I thank them for their influence and advice. Alex Webb has been a key part in my growth as a Himalayan geologist and I am incredibly grateful to him for bringing me to southwest Greenland to study Archean tectonics.

I thank Abby Wesley for her endless support and encouragement, along with the friendship of former UCLA undergraduates including Grace Parker, Sean Ahdi, Hannah Cohen, Margo Odlum, Tomas Capaldi, Bill Pepper, Austin Chadwick, Mike Say, Drew Levy, and Mary Braza.

Lastly, without the unwavering love and care from my parents, Nicholas and Joanne Haproff, and brother Jacob Haproff, none of this would have been possible.

VITA

2011	B. S., Earth Science <i>University of California, Santa Barbara</i>
2011-2012	Staff Geologist <i>San Diego Archaeological Center, Escondido, CA</i>
2012	Geology Intern <i>United States Geological Survey, Menlo Park, CA</i>
2013-2018	Teaching Assistant <i>University of California, Los Angeles (UCLA)</i>
2013-2016	Teaching Assistant for UCLA Summer Field Camp
2016	C. Phil., Geology <i>UCLA</i>
2018	Geology Instructor <i>California State University, Los Angeles (CSULA)</i>
2018	Instructor for CSULA Summer Field Camp
2018	Hired Assistant Professor <i>University of North Carolina-Wilmington</i>

PUBLICATIONS

- Haproff PJ**, Zuza AV, Yin A. 2018. West-directed thrusting south of the eastern Himalayan syntaxis indicates clockwise crustal flow at the indenter corner during the India-Asia collision: *Tectonophysics*, v. 722, p. 277-285.
- Haproff PJ**, Zuza AV, Yin A, Harrison TM, Manning CM, Chen J. 2018 (2nd submission in preparation). Tectonic evolution of the northern Indo-Burma Ranges (Part 1): lateral continuity of tectonostratigraphy across the eastern Himalayan syntaxis: *Geosphere*.
- Haproff PJ**, Zuza AV, Yin A, Harrison TM, Manning CM. 2018 (in preparation). Tectonic Evolution of the northern Indo-Burma Ranges (Part 2): magnitude of continental deformation surrounding the eastern Himalayan syntaxis and constraints on models of the Cenozoic India-Asia collision.
- Haproff PJ**, Odlum ML, Yin A, Zuza AV, Stockli DF. 2018 (in preparation). Out of sequence thrusting in the northern Indo-Burma Ranges: evidence from zircon (U-Th)/He thermochronology.
- Haproff PJ**, Bahamon H, Borda M, Miguel O, Bryce E, Landazabal A, Avila R. 2016. How North America got its shape. *Ted-Ed lesson (YouTube animation)*, Ted Conferences, LLC, <http://ed.ted.com/lessons/how-north-america-got-its-shape-peter-j-haproff>.
- Burton MM, Muniz AA, Abbott PL, Kimbrough DL, **Haproff PJ**, Gehrels GE, Pecha M. 2014. Sourcing sandstone cobble grinding tools in southern California using petrography, U-Pb geochronology, and Hf isotope geochemistry. *Journal of Archaeological Science*, v. 50, p. 273-287.

SELECTED PRESENTATIONS

- Haproff PJ**, Zuza AV, Yin A. 2017. What happens along the flank and corner of a continental indenter? Insights from the easternmost Himalayan orogen and constraints on the models of the India-Asia collision. *AGU Fall Meeting* (oral presentation).
- Haproff PJ**, Zuza AV, Yin A. 2017. Where is the Cenozoic-aged Gangdese batholith in the easternmost Himalayan orogen? *UCLA Fall Geocheminar* (oral presentation).
- Haproff PJ**, Zuza AV, Yin A. 2017. What happens along the flank and corner of a continental indenter? Insights from the easternmost Himalayan orogen and constraints on the models of the India-Asia collision. *UCLA Spring Tectonics and Seismology Seminar* (oral presentation).
- Haproff PJ**, Zuza AV, Yin A. 2017. What happens at the corner of a continental indenter? Insights from the easternmost Himalayan orogen. *University of Southern California Spring Lithospheric Dynamics Seminar* (invited oral presentation).
- Haproff PJ**, Yin A. 2016. Magnitude of crustal shortening and structural framework of the easternmost segment of the Himalayan orogen, the northern Indo-Burman Ranges of northeastern India. *AGU Fall Meeting* (poster).
- Haproff PJ**, Yin A. 2015. Where are Cenozoic-aged granitoids in the easternmost Himalayan orogen? Insights from the N. Gangdese-equivalent Lohit Plutonic Complex, NE India. *GSA Fall Meeting* (oral presentation).
- Haproff PJ**. 2015. U-Pb geochronology, thermobarometry, and geochemistry of L. Cretaceous granitoids in the N. Indo-Burma Ranges, NE India; insights into Gangdese belt rocks in the easternmost Himalayan orogen. *Chinese University of Geosciences, Wuhan* (invited oral presentation).
- Haproff PJ**, Yin A. 2014. Structural controls on the spatial distribution and geochemical composition of volcanism in a continental rift zone; an example from Owens Valley, eastern California. *AGU Fall Meeting* (poster).
- Haproff PJ**, Yin A. 2014. Coupled U-Pb detrital zircon geochronology and field studies of Neoproterozoic-E. Paleozoic White-Inyo strata, eastern California, and implications for a detrital source offshore of southwestern Laurentia. *GSA Fall Meeting* (poster).
- Haproff PJ**, Yin A, Dubey CS. 2013. Tectonic framework of the easternmost Himalayan orogen based on U-Pb zircon geochronology and detailed geologic mapping, NE India. *AGU Fall Meeting* (poster).
- Haproff PJ**, Yin A. 2013. Coupled tectonic, geomorphological, and magmatic processes in a rift zone: an example from the Owens Valley right-slip transtensional system in eastern California. *GSA Fall Meeting* (oral presentation).
- Prentice CS, Zachariasen JA, Kozaci O, Clahan K, Sickler RR, Rosa CM, Hassett W, Feigelson L, **Haproff PJ**, DeLong S, Perkins A, Brooks BA, Delano J, Baldwin JN. 2013. Paleoseismic Studies of the Peninsula San Andreas Fault near Crystal Springs Reservoir, Woodside, California. *AGU Fall Meeting* (poster).
- Schwartz DP, Hecker S, **Haproff PJ**, Beukelman G, Erickson B. 2012. The Bear River Fault Zone, Wyoming and Utah: Complex Ruptures on a Young Normal Fault. *AGU Fall Meeting* (presentation).

-Chapter 1-

Introduction

1.1. Introduction

The Himalayan-Tibetan orogen, generated by the Cenozoic northward indentation of India into Asia, is the largest active collisional system on Earth (Fig. 1) and an ideal testing ground to understand the nature of indenter-induced continental deformation (e.g., Le Fort, 1975; Tapponnier et al., 1982; Dewey et al., 1988; England and Houseman, 1986; Harrison et al., 1992; Yin and Harrison, 2000; Zhang et al., 2004; Yin, 2010). Following the cessation of Neotethys subduction and onset of the India-Asia collision at 55 ± 10 Ma (Rowley, 1998; Yin and Harrison, 2000; Najman et al., 2010; Hu et al., 2015), continental convergence has been accommodated by fault systems across the Himalaya (e.g., Schelling and Arita, 1991; Nelson et al., 1996; DeCelles et al., 2001; Avouac, 2003; Yin, 2006; van Hinsbergen et al., 2011; Webb et al., 2007, 2011), the Tibetan Plateau (e.g., Armijo et al., 1989; Royden et al., 1997; Yin and Harrison, 2000; Tapponnier et al., 2001; Royden et al., 2008; van Hinsbergen et al., 2011; Yin and Taylor, 2011; Zuza et al., 2016), and southeast Asia (e.g., Tapponnier et al., 1990; Lee and Lawver, 1995; Leloup et al., 1995; Harrison et al., 1996; Hall, 2012). These regions have been the focus of most geological investigations into the kinematics, magnitude, and timing of continental deformation during the collision process. However, few studies have centered on the ~1000-km-long, north-trending mountain ranges that bound the eastern and western margins of the Indian subcontinent (Fig. 1). These *Eastern and Western Flanking Belts* are topographic continuations of the Himalayan collisional system (Yin, 2006) (Fig. 1) and establishing their development is key to understanding the holistic evolution of the Himalayan-Tibetan orogen.

The study area of this dissertation is the northernmost segment of the Eastern Flanking Belt, the northern Indo-Burman Ranges, which are located at the intersection of the eastern syntaxis of the Himalayan orogen to the northwest and west and the Tibetan Plateau to the north and

northeast (Fig. 1). Several first-order questions regarding the geologic and structural framework of this area remain unanswered, which have important implications for Himalayan-Tibetan tectonics. These critical questions include:

- (1) Are major lithologic units and structures of the Himalayan-Tibetan orogen laterally continuous across the eastern Himalayan syntaxis to the study area?
- (2) What is the nature of continental deformation along the corner and margin of a rigid indenter and can we differentiate between end-member models (i.e., discrete strike-slip faulting vs. distributed thrust faulting)?
- (3) What are the relationships between the development of the study area and the Mesozoic-Cenozoic evolution of the adjacent eastern Himalayan orogen, southeastern Tibetan Plateau, and Eastern Flanking Belt?
- (4) What is the timing of deformation across the study area?

Each of these questions is examined in Chapters 2-5 of the dissertation, which are outlined below. The topics of the following chapters include (a) the structural and lithologic framework of the study area, (b) kinematic relationships with neighboring tectonic domains of the Himalayan-Tibetan orogen, and (c) temporal constraints to the development of the study area.

1.2. Chapter 2: Tectonic Evolution of the northern Indo-Burma Ranges: lateral correlation of Himalayan-Tibetan lithologic units across the eastern Himalayan syntaxis

In this chapter, we correlate lithologic units of the Himalayan orogen and Lhasa terrane (Fig. 2) with those exposed in the northern Indo-Burma Ranges based on field observations, U-Pb zircon geochronology, and whole-rock geochemistry. Previous lithologic correlations across the eastern Himalayan syntaxis were based solely on comparable lithologies and bounding faults,

without constraints from geochronology and geochemistry (e.g., Thakur and Jain, 1975; Acharyya, 1980; Singh and Chowdhury, 1990; Gururajan and Choudhuri, 2003; Misra, 2009).

Our results show that the northern Indo-Burma Ranges expose the easternmost continuations of the Tertiary Sub-Himalayan Sequence, the Lesser Himalayan Sequence, the Indus-Yarlung suture zone, Mesoproterozoic basement of the Lhasa terrane, and the Mesozoic-Cenozoic northern Gangdese batholith of the Himalayan-Tibetan orogen. However, several Himalayan-Tibetan lithologic units are missing in the study area, including the Mesozoic-Cenozoic southern Gangdese batholith belt and associated Linzizong volcanic sequence, the Xigaze forearc basin, the Greater Himalayan Crystalline Complex, and the Tethyan Himalayan Sequence. The absence of these lithologic units is likely the result of a greater magnitude of crustal shortening and erosion and/or continental underthrusting compared to that across the Himalayan orogen to the west. This interpretation is supported by the southward decrease in the width of the thrust belt measured between the active foreland basin and the Indus-Yarlung suture zone (~33-5 km), compared to ~200 km across the eastern Himalaya.

The work of Chapter 2 is included in a revised manuscript for publication in *Geosphere* with authors Andrew Zuza, An Yin, T. Mark Harrison, Craig E. Manning, Ding Lin, Chen Wu, Jianlin Chen, and Chandra S. Dubey. Peter Zeitler, an anonymous reviewer, and editor Ray Russo provided critical suggestions for the improvement of the second version of the manuscript.

1.3. Chapter 3: West-directed thrusting south of the eastern Himalayan syntaxis indicates clockwise crustal flow at the indenter corner during the India-Asia collision

In Chapter 3, we examine the structural geology of the northern Indo-Burma Ranges and implications regarding the mode of Cenozoic continental deformation surrounding the eastern

Himalayan syntaxis. Existing models to explain this have primarily developed into two end-member forms: (1) lateral extrusion of internally-rigid lithospheric blocks accommodated by discrete strike-slip faults (e.g., Tapponnier et al., 1986; Peltzer and Tapponnier, 1988; England and Molnar; 1990; Mitchell, 1993) (Fig. 3A) and (2) clockwise rotational flow of lithosphere accommodating by distributed thrust faults (e.g., England and Houseman, 1986; Royden et al., 1997; Li et al., 2013) (Fig. 3B). Whereas these models have mostly originated from analogue experiments and numerical simulations for the evolution of the Himalayan-Tibetan orogen, each model makes specific predictions for the style and kinematics of deformation across the northern Indo-Burma Ranges that can be tested with geologic observations.

Based on structural mapping, we show that the northern Indo-Burma Ranges developed primarily as southwest- to west-directed thrust belt. The orientations of ductile stretching lineations within thrust shear zones are northeast-trending in the north (nearest to the syntaxis) and east-trending in the south. This southward deflection in the thrust transport direction suggests deformation is best described by clockwise lithospheric flow around the pole at the eastern Himalayan syntaxis, accommodated by distributed thrust faults. South-trending, sub-horizontal stretching lineations along discrete strike-slip shear zones were not observed in the study area, which precludes the lateral extrusion model for the area.

The research presented in Chapter 3 was originally published in *Tectonophysics* (Haproff et al., 2018) with coauthors Andrew Zuza and An Yin. Editor Zheng-Xiang Li and reviewers A.A.G. Webb and Ding Lin provided excellent feedback for the significant improvement of the manuscript.

1.4. Chapter 4: Tectonic Evolution of the northern Indo-Burma Ranges: Mesozoic-Cenozoic kinematic reconstruction and constraints on the mode of deformation across the easternmost India-Asia collisional zone

In Chapter 4, we expand on descriptions of the structural framework of Haproff et al. (2018) and include new pressure-temperature determinations of metamorphic rocks and an estimate of Cenozoic shortening strain to examine the tectonic evolution of the northern Indo-Burma Ranges. Our work shows that the thrust belt is cored by a hinterland-dipping duplex, which branches from a décollement that exhumed metasedimentary rocks from >30 km depth. Restoration of one balanced cross-section yields a minimum shortening estimate of >156 km, equivalent to ~81% shortening strain. This percent shortening estimate, combined with the absence of several previously-existing Himalayan-Tibetan lithologic units and the dramatic southward decrease in the width of the belt, support the interpretation that an east- to southeastward increase in Cenozoic crustal shortening and/or continental subduction occurred along the eastern Himalayan collisional system.

Google Earth-based mapping of faults active during the Quaternary in the study area reveals that the present-day deformation is expressed by right-slip transpression partitioned between the oblique-slip Mishmi thrust along the range front and right-slip Jiali fault zone in southeastern Tibet. Slip along the leading thrusts of the northern Indo-Burma and Naga Hills thrust belts is likely transferred to the right-slip Sagaing fault to the south via a previously-undiscovered, southwest-trending restraining bend. This spatial transition from transpression near the syntaxis to discrete right-slip faulting along the eastern edge of India provides a key example of the nature of continental deformation along the margins of a collisional indenter.

The last part of the chapter presents a model for the Mesozoic-Cenozoic evolution of the

eastern Himalayan orogen, Eastern Flanking Belt, southeast Tibetan Plateau, and part of southeast Asia in four stages: ~150-80 Ma, ~50 Ma, ~20 Ma, and ~10 Ma. In this model, our findings are integrated with existing research of (1) the paleogeography of the region, (2) the lifespans, kinematics, and displacements of major faults, and (3) the petrogenesis, deformation, and erosion of major lithologic units.

The work of this chapter is included in a manuscript intended for publication in *Geosphere* with authors Andrew V. Zuza, An Yin, T. Mark Harrison, and Craig M. Manning. This manuscript is being prepared as a Part 2 companion study to the research of Chapter 2.

1.5. Chapter 5: Out of sequence thrusting in the northern Indo-Burma Ranges: evidence from preliminary zircon (U-Th)/He thermochronology

In Chapter 5, we use zircon (U-Th)/He thermochronology (ZHe) to quantify the timing of exhumation of major lithologic units across the northern Indo-Burma thrust belt. Our results reveal a southwestward younging trend in ZHe ages, parallel to the thrust transport direction, from ~17 Ma in the Tidding mélange complex to ~5-6 Ma in the Lalpani schist and Sewak unit in the foreland. However, ZHe ages of ~10-6 Ma from the northernmost-exposed Lohit Plutonic Complex in the hinterland suggest renewed exhumation occurred during out-of-sequence thrust motion along the Lohit thrust. The research of this chapter study reveals a more complex exhumation history of the northern Indo-Burma Ranges, such that Late Miocene activity along the Lohit thrust was coeval with exhumation of foreland rocks during southwestward propagation of the thrust belt.

The study presented in Chapter 5 is included in a manuscript intended for publication with authors Margaret L. Odlum, An Yin, Andrew V. Zuza, T. Mark Harrison, and Daniel F. Stockli.

The results presented here are preliminary and further analysis of bedrock ZHe ages is required.

1.6. Background of the Dissertation

The research of this dissertation is based primarily on detailed geologic field mapping in eastern Arunachal Pradesh of northeast India along two deeply-incised river valleys of the northern Indo-Burma Ranges: the northeast-trending, 85-km-long Dibang Valley and east-trending, 45-km-long Lohit Valley. Most of the data presented was derived from fieldwork over two seasons in the winters of 2013 and 2015. During the first three weeks of the 2013 field season, a UCLA group including An Yin and myself collaborated with a Delhi University group led by Dr. Chandra S. Dubey to establish the tectonostratigraphy, map Cenozoic faults, and collect samples for geochronology and thermobarometry. The second three weeks of the 2013 field season were used to conduct neotectonic surveys of right-laterally displaced Quaternary river terraces and deflected channels along the active, range-bounding Mishmi thrust near the villages of Chiddu and Roing. Aside from the inclusion of Quaternary geologic maps of these two sites along the Mishmi thrust, research from this neotectonic study is ongoing. During this same three-week period, I conducted geologic mapping and sample collection along ~2-km-long drainages near the range front between Dibang and Lohit Valleys to test the along-strike continuity of foreland-exposed lithologic units and structures.

In 2015, Andrew V. Zuza and I expanded the work from the 2013 field season by conducting systematic geologic mapping and sample collection over four weeks along the Dibang and Lohit Valleys. One week was spent mapping lithologic units and structures along Siang Valley of the eastern Himalaya, located south of the eastern Himalayan syntaxis. Results of the Siang Valley transect will be presented in separate studies.

During the winter of 2017-2018, I conducted a reconnaissance field season alongside UCLA personnel Professor Seulgi Moon and PhD student Kevin Shao, primarily to study the Quaternary geomorphology of the northern Indo-Burma Ranges. An effort by the Border Roads Organization to clear landslides that occurred during the 2017 summer monsoon resulted in newly-exposed outcrops within the densely-vegetated region. Minor alterations to the geologic maps of Dibang and Lohit Valley made during this field season are included in the dissertation.

1.7. Figures

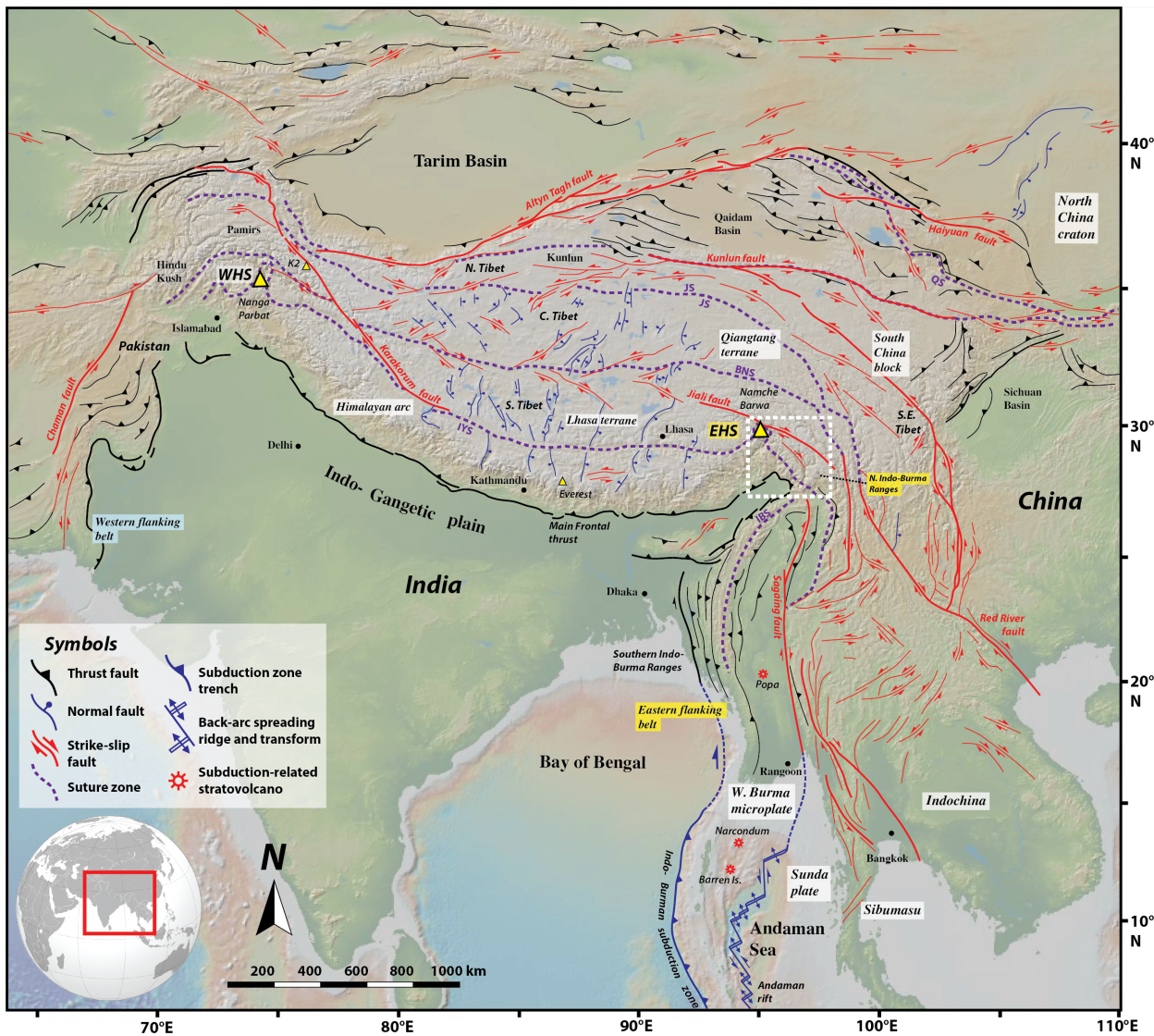


Figure 1.1. Neotectonic map of the India-Asia orogenic system, modified from Haproff et al. (2018). The location of the study area, the northern Indo-Burma Ranges, is shown within the white box. The base digital elevation model was acquired using geomapapp.com (Ryan et al., 2009). The Earth index map was acquired through Generic Mapping Tools (gmt.soest.hawaii.edu). Abbreviations: BNS: Bangong-Nujiang suture, EHS: eastern Himalayan syntaxis, IBS: Indo-Burma suture, IYS: Indus-Yarlung suture, JS: Jinsha suture, WHS: western Himalayan syntaxis.

Himalayan orogen - Lhasa terrane

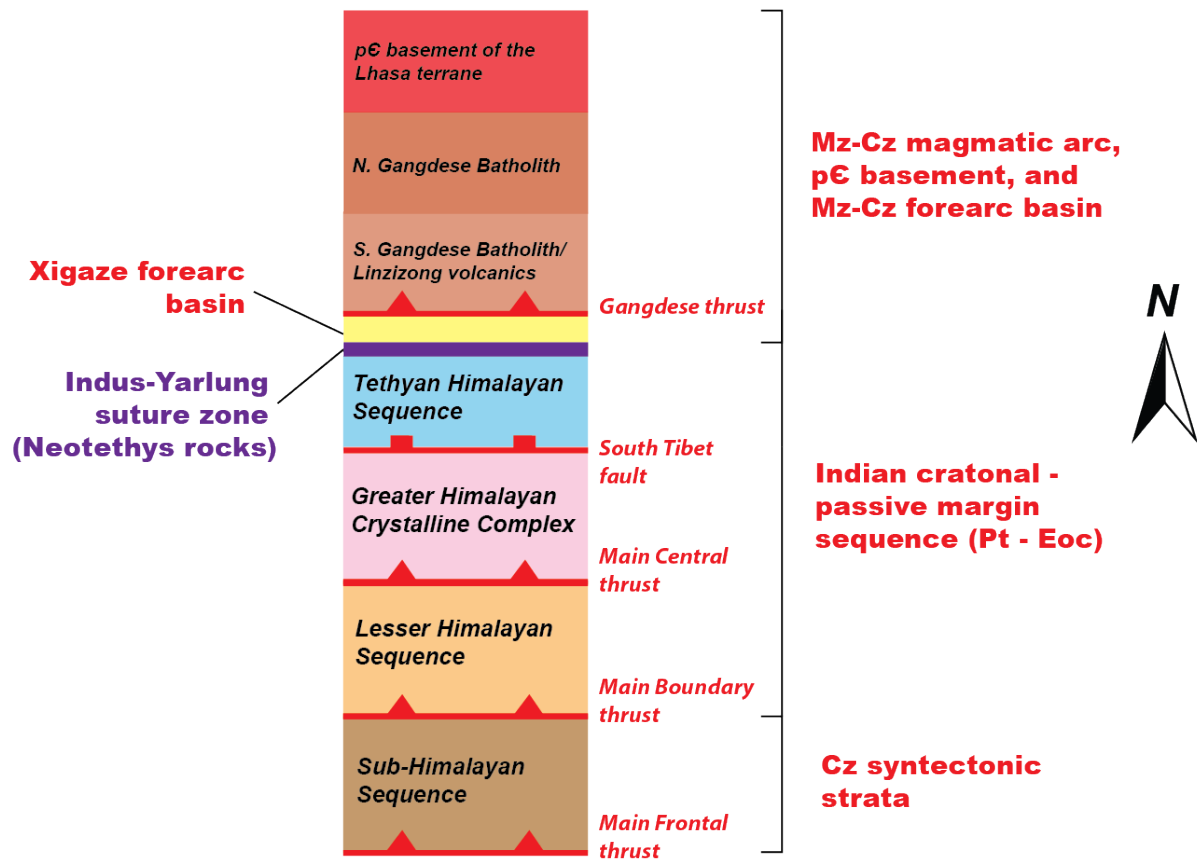


Figure 1.2. Simplified tectonostratigraphic column of major lithologic units and structures of the Himalayan orogen and the Lhasa terrane, modified from Yin (2006). The Gangdese thrust is sparsely-exposed along the northern margin of the Himalayan orogen where the fault is not obscured by the Renbu-Zedong thrust (a.k.a., Great Counter thrust) (Yin et al., 1994; 1999; Harrison et al., 2000).

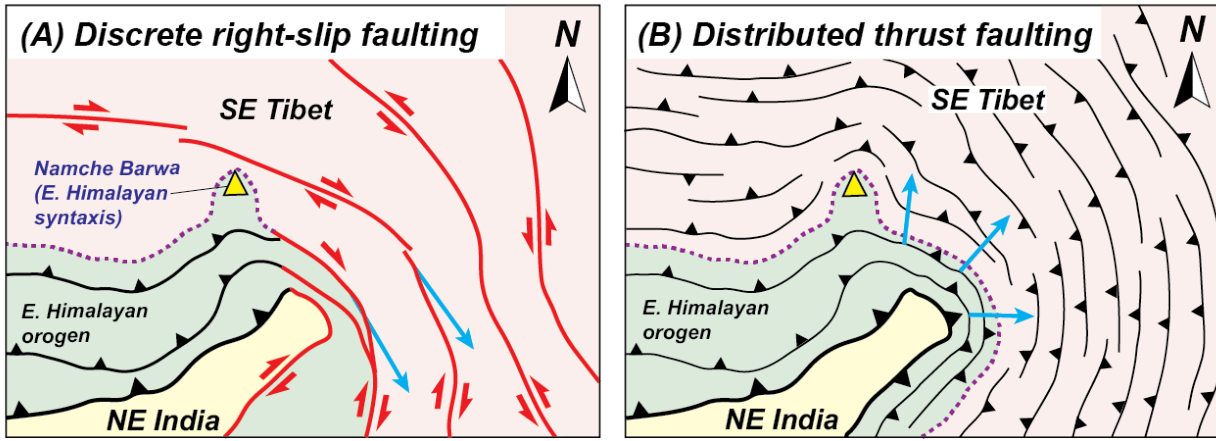


Figure 1.3. End-member models for continental deformation surrounding the eastern Himalayan syntaxis during the Cenozoic India-Asia collision consisting of (A) lateral extrusion of internally-rigid lithospheric blocks along discrete strike-slip faults and (B) distributed thrust faulting during clockwise crustal flow (modified from Haproff et al., 2018). Predictions for the trends of stretching lineations in each model are shown as blue arrows.

1.8. References

- Acharyya, S.K., 1980, Stratigraphy and tectonics of Arunachal Lesser Himalaya: Stratigraphy and Correlations of Lesser Himalayan Formations, p. 231-241.
- Armijo, R., Tapponnier, P., and Han, T., 1989, Late Cenozoic right-lateral strike-slip faulting in southern Tibet: Journal of Geophysical Research: Solid Earth, v. 94, no. B3, p. 2787-2838.
- Avouac, J.P., 2003, Mountain building, erosion, and the seismic cycle in the Nepal Himalaya: Advances in geophysics, v. 46, p. 1-80.
- Avouac, J.P. and Tapponnier, P., 1993, Kinematic model of active deformation in central Asia: Geophysical Research Letters, v. 20, no. 10, p. 895-898.
- DeCelles, P.G., Robinson, D.M., Quade, J., Ojha, T.P., Garzione, C.N., Copeland, P., and Upreti, B.N., 2001, Stratigraphy, structure, and tectonic evolution of the Himalayan fold-thrust belt in western Nepal: Tectonics, v. 20, no. 4, p. 487-509.
- Dewey, J.F., Shackleton, R.M., Chengfa, C., and Yiyin, S., 1988, The tectonic evolution of the Tibetan Plateau: Philosophical Transactions of the Royal Society of London A: Mathematical, Physical and Engineering Sciences, v. 327, no. 1594, p. 379-413.
- England, P. and Houseman, G., 1986, Finite strain calculations of continental deformation 2. Comparison with the India-Asia collision zone, Journal of Geophysical Research, v. 91, p. 3664–3676.
- England, P. and McKenzie, D., 1982, A thin viscous sheet model for continental deformation: Geophysical Journal International, v. 70, no. 2, p. 295-321.
- England, P. and Molnar, P., 1990, Right-lateral shear and rotation as the explanation for strike-slip faulting in eastern Tibet: Nature, v. 344, no. 6262, p. 140-142.
- Gururajan, N.S. and Choudhuri, B.K., 2003, Geology and tectonic history of the Lohit valley,

- Eastern Arunachal Pradesh, India: *Journal of Asian Earth Sciences*, v. 21, no. 7, p. 731-741.
- Hall, R., 2012, Late Jurassic–Cenozoic reconstructions of the Indonesian region and the Indian Ocean: *Tectonophysics*, v. 570, p. 1-41.
- Haproff, P.J., Zuza, A.V., Yin, A., 2018, West-directed thrusting south of the eastern Himalayan syntaxis indicates clockwise crustal flow at the indenter corner during the India-Asia collision: *Tectonophysics*, v. 722, p. 277-285.
- Harrison, T.M., Copeland, P., Kidd, W.S.F., and Yin, A., 1992, Raising Tibet: *Science*, v. 255, no. 5052, p. 1663-1670.
- Harrison, T.M., Leloup, P.H., Ryerson, F.J., Tapponnier, P., Lacassin, R., and Chen, W., 1996, Diachronous initiation of transtension along the Ailao Shan-Red River shear zone, Yunnan and Vietnam: *World and Regional Geology*, p. 208-226.
- Hodges, K.V., 2000, Tectonics of the Himalaya and southern Tibet from two perspectives: *Geological Society of America Bulletin*, v. 112, no. 3, p. 324-350.
- Hu, X., Wang, J., Boudagher-Fadel, M., Garzanti, E., An, W., 2015, New insights into the timing of the India-Asia collision from the Paleogene Quxia and Jialazi Formations of the Xigaze Forearc Basin, South Tibet: *Gondwana Research*, v. 32, p. 76-92.
- Ingalls, M., Rowley, D.B., Currie, B., and Colman, A.S., 2016, Large-scale subduction of continental crust implied by India–Asia mass-balance calculation: *Nature Geoscience*, v. 9, no. 11, p. 848.
- Le Fort, P., 1975, Himalayas: the collided range. Present knowledge of the continental arc: *American Journal of Science*, v. 275, p. 1-44.
- Le Pichon, X., Fournier, M., and Jolivet, L., 1992, Kinematics, topography, shortening, and extrusion in the India-Eurasia collision: *Tectonics*, v. 11, no. 6, p. 1085-1098.

- Lee, T.Y. and Lawver, L.A., 1995. Cenozoic plate reconstruction of Southeast Asia: Tectonophysics, v. 251, no. 1-4, p. 85-138.
- Li, Z.H., Xu, Z., Gerya, T., and Burg, J.P., 2013, Collision of continental corner from 3-D numerical modeling: Earth and Planetary Science Letters, v. 380, p. 98-111.
- Leloup, P. H., et al., 1995, The Ailao Shan-Red River shear zone (Yunnan, China), Tertiary transform boundary of Indochina: Tectonophysics, v. 251, no. 1, p. 3-84.
- Misra, D.K., 2009, Litho-tectonic sequence and their regional correlation along the Lohit and Dibang valleys, eastern Arunachal Pradesh. Journal of the Geological Society of India, v. 73, no. 2, p. 213-219.
- Mitchell, A.H.G., 1993, Cretaceous–Cenozoic tectonic events in the western Myanmar (Burma)–Assam region: Journal of the Geological Society, v. 150, no. 6, p. 1089-1102.
- Najman, Y., et al., 2010, Timing of India-Asia collision: Geological, biostratigraphic, and palaeomagnetic constraints: Journal of Geophysical Research: Solid Earth, v. 115, no. B12.
- Nelson, K.D., Zhao, W., Brown, L.D., and Kuo, J., 1996, Partially molten middle crust beneath southern Tibet: synthesis of project INDEPTH results: Science, v. 274, no. 5293, p. 1684.
- Peltzer, G. and Tapponnier, P., 1988, Formation and evolution of strike-slip faults, rifts, and basins during the India-Asia collision: An experimental approach: Journal of Geophysical Research: Solid Earth, v. 93, no. B12, p. 15085-15117.
- Rowley, D.B., 1998, Minimum age of initiation of collision between India and Asia north of Everest based on the subsidence history of the Zhepure Mountain section: The Journal of Geology, v. 106, no. 2, p. 220-235.
- Royden, L., 1996, Coupling and decoupling of crust and mantle in convergent orogens: Implications for strain partitioning in the crust: Journal of Geophysical Research: Solid

- Earth, v. 101, no. B8, p. 17679-17705.
- Royden, L.H., Burchfiel, B.C., King, R.W., Wang, E., Chen, Z., Shen, F., and Liu, Y., 1997, Surface deformation and lower crustal flow in eastern Tibet: *Science*, v. 276, no. 5313, p. 788-790.
- Royden, L.H., Burchfiel, B.C., and van der Hilst, R.D., 2008, The Geological Evolution of the Tibetan Plateau: *Science*, v. 321, p. 1054-1058.
- Ryan, W.B., et al., 2009, Global multi-resolution topography synthesis: *Geochemistry, Geophysics, Geosystems*, v. 10, no. 3.
- Schelling, D., and Arita, K., 1991, Thrust tectonics, crustal shortening, and the structure of the far-eastern Nepal Himalaya: *Tectonics*, v. 10, no. 5, p. 851-862.
- Singh, S. and Chowdhury, P.K., 1990, An outline of the geological framework of the Arunachal Himalaya: *Journal of Himalayan Geology*, v. 1, no. 2, p. 189-197.
- Tapponnier, P., Peltzer, G., Le Dain, A.Y., Armijo, R., and Cobbold, P. 1982, Propagating extrusion tectonics in Asia: new insights from simple experiments with plasticine: *Geology*, v. 10, p. 611-616.
- Tapponnier, P., Peltzer, G., and Armijo, R., 1986, On the mechanics of the collision between India and Asia: *Geological Society, London, Special Publications*, v. 19, no. 1, p. 113-157.
- Tapponnier, P., et al., 1990, The Ailao Shan/Red River metamorphic belt: tertiary left-lateral shear between Indochina and South China: *Nature*, v. 343, no. 6257, p. 431.
- Tapponnier, P. and Molnar, P., 1976, Slip-line field theory and large-scale continental tectonics: *Nature*, v. 264, no. 5584, p. 319.
- Tapponnier, P., Zhiqin, X., Roger, F., Meyer, B., Arnaud, N., Wittlinger, G., and Jingsui, Y., 2001, Oblique stepwise rise and growth of the Tibet Plateau. *Science*, v. 294, no. 5547, p.

1671-1677.

Thakur, V.C. and Jain, A.K., 1975, Some observations of deformation and metamorphism in the rocks of some parts of Mishmi Hills, Lohit district, (NEFA), Arunachal Pradesh: Himalayan Geology, v. 5, p. 339-364.

van Hinsbergen, D.J., Kapp, P., Dupont-Nivet, G., Lippert, P.C., DeCelles, P.G., and Torsvik, T.H., 2011, Restoration of Cenozoic deformation in Asia and the size of Greater India: Tectonics, v. 30, no. 5.

Webb, A.A.G., Yin, A., Harrison, T.M., Célérier, J., and Burgess, W.P., 2007, The leading edge of the Greater Himalayan Crystalline complex revealed in the NW Indian Himalaya: Implications for the evolution of the Himalayan orogen: Geology, v. 35, no. 10, p. 955-958.

Webb, A.A.G., Yin, A., Harrison, T.M., Célérier, J., Gehrels, G.E., Manning, C.E. and Grove, M., 2011, Cenozoic tectonic history of the Himachal Himalaya (northwestern India) and its constraints on the formation mechanism of the Himalayan orogen: Geosphere, v. 7, no. 4, p. 1013-1061.

Yin, A., 2006, Cenozoic tectonic evolution of the Himalayan orogen as constrained by along-strike variation of structural geometry, exhumation history, and foreland sedimentation: Earth-Science Reviews, v. 76, no. 1, p. 1-131.

Yin, A., 2010, Cenozoic tectonic evolution of Asia: A preliminary synthesis: Tectonophysics, v. 488, no. 1, p. 293-325.

Yin, A., Harrison, T.M., Ryerson, F.J., Wenji, C., Kidd, W.S.F. and Copeland, P., 1994, Tertiary structural evolution of the Gangdese thrust system, southeastern Tibet: Journal of Geophysical Research: Solid Earth, v. 99, no. B9, p. 18175-18201.

Yin, A. and Taylor, M.H., 2011, Mechanics of V-shaped conjugate strike-slip faults and the corresponding continuum mode of continental deformation: Geological Society of America Bulletin, v. 123, no. 9-10, p. 1798-1821.

Zhang, P.Z., et al., 2004, Continuous deformation of the Tibetan Plateau from global positioning system data: Geology, v. 32, no. 9, p. 809-812.

Zuza, A.V., Cheng, X., and Yin, A., 2016, Testing models of Tibetan Plateau formation with Cenozoic shortening estimates across the Qilian Shan–Nan Shan thrust belt: Geosphere, v. 12, no. 2, p. 501-532.

-Chapter 2-

**Tectonic evolution of the northern Indo-Burma Ranges: lateral correlation of
Himalayan-Tibetan lithologic units across the eastern Himalayan syntaxis**

2.1. Abstract

The Cenozoic India-Asia collision generated both the east-trending Himalayan orogen and the north-trending Eastern and Western Flanking Belts located along the margins of the Indian subcontinent. Although the tectonic development of both flanking belts is key to understanding mechanisms of continental deformation during indenter-induced collision, few field-based studies integrated with modern geochronological and geochemical methods have been applied to these tectonic domains. In this study, we investigate the along-strike correlation of lithologic units between the northern Indo-Burma Ranges, the northernmost segment of the Eastern Flanking Belt, and the eastern Himalayan-Tibetan orogen using field observations, U-Pb zircon geochronology, and whole-rock geochemistry. Our findings provide new quantitative constraints to interpretations that the northern Indo-Burma Ranges expose the easternmost continuations of the Tertiary Sub-Himalayan Sequence, the Lesser Himalayan Sequence, the Indus-Yarlung suture zone, and the northern Gangdese batholith belt of the Himalayan-Tibetan orogen. The northernmost-exposed Lohit Plutonic Complex consists of Mesoproterozoic basement rocks (~1286 Ma) and late Jurassic-Cretaceous granitoids (~156-69 Ma) with positive ϵ_{Nd} values and $^{87}\text{Sr}/^{86}\text{Sr}$ (Sr_i) ratios of ~0.705. Mesozoic granitoids of this complex are correlative with the northern Gangdese batholith based on similar zircon crystallization ages and trace element and isotope geochemistry. The Tidding-Mayodia mélange complex, which consists of amalgamated mid-ocean ridge basalts, gabbro, ultramafics, and mafic schist of a dismembered ophiolite sequence, is the easternmost extension of the Indus-Yarlung suture zone. The Mayodia gneiss and Lalpani schist are correlative with the Lesser Himalayan Sequence based on comparable metamorphic lithologies, negative ϵ_{Nd} values, Mesoproterozoic-Cambrian detrital zircon ages, and structural position beneath the suture zone. The structurally lowest Tezu unit contains similar

terrestrial syntectonic strata to the Miocene-Pliocene Siwalik Group of the Himalayan orogen. Despite these correlations, notable Himalayan-Tibetan lithologic units are missing in the northern Indo-Burma Ranges, including the Mesozoic-Cenozoic southern Gangdese batholith belt, Linzizong volcanic sequence, Xigaze forearc basin, Greater Himalayan Crystalline Complex, and Tethyan Himalayan Sequence. We interpret the absence of these lithologic units to be the result of a greater magnitude of crustal shortening and/or continental underthrusting compared to the Himalayan orogen to the west. This interpretation is also supported by a southward decrease in the map-view distance between the active foreland basin and Indus-Yarlung suture zone, from ~200 km in the easternmost Himalaya to ~5 km in the southernmost part of the northern Indo-Burma Ranges.

2.2. Introduction

The Cenozoic India-Asia collision created the Himalayan collisional system that consists of the convergence-perpendicular Himalayan orogen and convergence-parallel flanking belts along the eastern and western margins of the Indian subcontinent (Gansser, 1964; Yin, 2006) (Fig. 1A). Although the geology and tectonic evolution of the Himalayan orogen is well documented (Le Fort, 1996; Hodges, 2000; Yin and Harrison, 2000; DeCelles et al., 2000, 2001; Yin, 2006, 2010; Webb et al., 2013, 2017), few modern geologic studies have focused on the flanking belts (cf., Tapponnier et al., 1981; Ni et al., 1989; Mitchell, 1993; Haq and Davis, 1997; Haproff et al., 2018). Yet, establishing the geologic history of the two flanking belts is crucial for understanding the holistic development of the Himalayan collisional system and differentiating the end-member models of continental deformation during the India-Asia collision (Tapponnier et al., 1982, 2001; England and Houseman, 1986; Cobbold and Davy, 1988; Dewey et al., 1988; England and

Molnar, 1990; Royden et al., 1997).

In this study, we investigate the divisions of major lithologic units exposed in the northern Indo-Burma Ranges, the northernmost segment of the Eastern Flanking Belt (Figs. 1B-C) and correlate these units with the classic lithologic divisions of the Himalayan orogen and the Lhasa terrane (Fig. 2). Correlations are based on the results of new U-Pb zircon geochronology, whole-rock geochemistry, bounding Cenozoic faults, and similar lithologies and metamorphic grades. The key findings of this chapter are that several lithologic units of the Himalayan orogen including the Greater Himalayan Crystalline Complex and Tethyan Himalayan Sequence are absent in the study area. In addition, the Xigaze forearc basin and southern belt of the Gangdese batholith of the Lhasa terrane are missing in the northern Indo-Burma Ranges. If such units were present at during the onset of the Cenozoic India-Asia collision at the longitude of the northern Indo-Burma Ranges, our work implies a greater magnitude of crustal shortening and/or continental underthrusting has occurred compared to the Himalayan orogen to the west.

2.3. Geologic Setting

To provide a regional context for this study, we summarize the existing research of major structures and lithologic units of the eastern Himalayan orogen, the Indus-Yarlung suture zone, the Lhasa terrane, cratonal rocks of northeast India, and the northernmost segment of the Eastern Flanking Belt. The classic lithologic division of the Himalayan orogen include from south to north, the Sub-Himalayan Sequence (SHS), Lesser Himalayan Sequence (LHS), Greater Himalayan Crystalline Complex (GHC), and Tethyan Himalayan Sequence (THS) (Yin, 2006) (Figs. 1B and 2). These Himalayan units are bounded to the north by the Indus-Yarlung suture zone, which has been shortened by two post-collisional thrust systems: the older south-directed Gangdese thrust

system and the younger north-directed Great Counter thrust system (Yin et al., 1994, 1999; Harrison et al., 2000). Located north of the Indus-Yarlung suture zone, the Lhasa terrane exposes three east-west trending tectonic belts from south to north: the Xigaze forearc basin and the southern and northern belts of the Gangdese batholith (Fig. 2).

2.3.1. Eastern Himalayan Orogen

The eastern Himalayan orogen referred in this study extends from the Sikkim-Bhutan border at 89°E to the eastern Himalayan syntaxis at ~95°E (Figs. 1 and 2). The major Himalayan lithologic units are tectonically juxtaposed by the following orogen-scale faults: the Main Frontal thrust (MFT) at the base of the SHS, the Main Boundary thrust (MBT) at the base of the LHS, the Main Central thrust (MCT) at the base of the GHC, and the South Tibetan detachment (STD) at the base of the THS (e.g., Acharyya and Ray, 1977; Acharyya, 1994; Gansser, 1983; Burchfiel et al., 1992; Edwards et al., 1996, 1999; Edwards and Harrison, 1997; Wu et al., 1998; Grujic et al., 2002; McQuarrie et al., 2008; Long et al., 2011a,b,c; Yin et al., 2006, 2010a; Burgess et al., 2012; Webb et al., 2013; DeCelles et al., 2016) (Fig. 2). Each of these faults are not expressed as a single structure, but rather a wide km-scale zone of deformation comprising series of brittle faults and/or ductile shear zones (Hodges, 2000; Yin, 2006).

In the eastern Himalaya, the SHS consists of a 4-6 km thick section of Miocene-Pliocene sandstone and conglomerate (Gansser, 1983; Acharyya, 1994; Dikshitulu et al. 1995; Kumar, 1997; Yin et al., 2006; McQuarrie et al., 2008; Yin et al., 2010a) (Fig. 2). The LHS is composed of Neoproterozoic-Cambrian and Permian strata (Gansser, 1983; McQuarrie et al., 2008; Yin et al., 2010a; Long et al., 2011a) (Fig. 2). Various local names have been assigned for the LHS units in the eastern Himalaya and their correlative relationships are illustrated in Fig. 2. The base of the

Proterozoic strata in the eastern Himalaya is marked by a meter-thick layer of quartz pebble conglomerate that was deposited atop a ~1.7 Ga augen gneiss (Yin et al., 2010a).

The GHC in the eastern Himalaya consists of metasediments, orthogneiss, metavolcanics, and Cenozoic leucogranites (e.g., Gansser, 1983; Yin et al., 2010a; Webb et al., 2013). In Bhutan, the north-dipping Kakhtang thrust, correlative to the Zimithang thrust to the east (Yin et al., 2006), divides the GHC into the upper and lower parts (Gansser, 1983; Swapp and Hollister, 1991; Grujic et al., 1996, 2002; Davidson et al., 1997; Daniel et al., 2003; McQuarrie et al., 2008; Yin et al., 2010a; Long and McQuarrie, 2010; Long et al., 2011a, b) (Fig. 2). The upper GHC consists of upper amphibolite-facies orthogneiss, metasedimentary rocks, and Miocene leucogranites (Gansser 1983; Swapp and Hollister 1991; Davidson et al. 1997; Grujic et al. 1996, 2002; Daniel et al. 2003; Long et al. 2011b, c; Zeiger et al., 2015). In the footwall of the Kakhtang thrust, the lower GHC consists of upper amphibolite facies to upper greenschist-facies metasedimentary rocks and orthogneiss (Davidson et al., 1997; Daniel et al., 2003; Corrie et al., 2012; Zeiger et al., 2015). East of Bhutan, orthogneiss in the GHC yields U-Pb zircon age populations of ~1700 Ma, ~878 Ma, and ~500 Ma (Yin et al., 2010a) (Fig. 2), which are cut by 20-18 Ma leucogranites (Aikman et al. 2012a, b; Harrison and Wielicki, 2016). In the easternmost Himalaya along the Siang River Valley, the MCT splits into two thrusts referred to as the MCT-I and MCT-II by Nandini and Thakur (2011) (Fig. 2).

The THS above the STD consists of pre-Triassic metasedimentary strata (Zeng et al., 2011) and Triassic-Cretaceous isoclinally-folded marine strata (Yin et al., 1994, 1999; Harrison et al., 2000; Aikman et al., 2008) (Fig. 2). Folded THS strata are intruded by ~44 Ma granite (Aikman et al., 2008). Due to the merger of the Great Counter Thrust and the STD northwest of the eastern

Himalayan syntaxis, the THS does not extend to the western margin of the eastern Himalayan syntaxis (Yin, 2006; Webb et al., 2013) (Figs. 1B and 2).

2.3.2. Indus-Yarlung Suture Zone

The Indus-Yarlung suture zone consists of tectonic mélange complexes, dismembered ophiolitic sequences, subduction-related metamorphic rocks, syntectonic conglomerate deposits, and supra-subduction-related igneous rocks (Gansser, 1964; Allegré et al., 1984; Honegger et al., 1982; Malpas et al., 2003; Ziabrev et al., 2003; Dai et al., 2011a, 2011b; Hébert et al., 2011; Cai et al., 2012; An et al., 2014; Laskowski et al., 2016; Leary et al., 2016) (Fig. 2). These features are bounded by two Cenozoic thrust systems: the south-directed Gangdese thrust system of Harrison et al. (1992) and Yin et al. (1994), and the Great Counter thrust of the Heim and Gansser (1939). Late Jurassic-Early Cretaceous ultramafic rocks, volcanics, volcaniclastic strata, granitoids, carbonate, and fossiliferous chert and flysch are intermittently exposed along the northern margin of the Himalayan orogen (McDermid et al., 2002; Maplas et al., 2003; Ziabrev et al., 2003; Dubois-Côté et al., 2005; Dupuis et al., 2005; Zhou et al., 2005; Aitchison et al., 2007; Zhu et al., 2009b).

2.3.3. Lhasa Terrane

The southern edge of the Lhasa terrane is marked by the Gangdese thrust system, which depending on the location, juxtaposes strata of the Xigaze forearc basin strata and the Gangdese batholith (see description below) over the THS (Fig. 2) (Yin et al., 1994). The Xigaze forearc basin sequence consists of Cretaceous to Eocene marine deposits on top of an oceanic basement (Garzanti and Van Haver, 1988; Einsele et al., 1994; Dürr, 1996; Ding et al., 2005; Wang et al., 2012; An et al., 2014; Hu et al., 2015; Orme et al., 2015) (Fig. 2). The forearc strata are only

exposed in south-central Tibet but absent in southwest and southeast Tibet along strike. This map pattern is interpreted to be a result of post-collision underthrusting of the forearc basin below the Gangdese batholith belt (Yin et al., 1994, 1999; Harrison et al., 2000). The Cretaceous strata are cut by a series of north-south trending dikes that yield ages of 18-14 Ma (Yin et al., 1994; Williams et al., 2000).

Located north of the Xigaze forearc basin, the Lhasa terrane is a 200-300-km-wide continental strip that trends east-west in southern Tibet but warps around the eastern Himalayan syntaxis to a north-south trend in northern Myanmar and western Yunnan of China (e.g., Lin et al., 2013; Wang et al., 2014) (Fig. 1B). An east-trending ophiolite belt in the central part of the terrane was interpreted to be a suture zone or a zone of rootless klippe sourced from the Bangong-Nujiang suture zone in the north (Girardeau et al., 1984; Coward et al., 1988; Hsu et al., 1995; Yin and Harrison, 2000; Kapp et al., 2003; Dong et al., 2011, Zhu et al., 2012; Zhang et al., 2014). The Lhasa terrane exposes Mesoproterozoic orthogneiss in the easternmost Bomi-Chayu Complex (~1250-1350 Ma) (at 96°E) (Xu et al., 2013), a composite Neoproterozoic (920–820 Ma) and Cambro-Ordovician (540–460 Ma) gneiss complex along the northern margin of the Lhasa terrane (Guynn et al., 2012), and fragments of Devonian orthogneisses (~366 Ma) in southeast Tibet (Zhu et al., 2011) (Figs. 1-2).

The salient feature of the Lhasa terrane is the >2000-km long Mesozoic to earliest Cenozoic Gangdese batholith belt of Chang and Zheng (1973), which was referred to as the Transhimalayan batholith belt in the early western literature (e.g., Gansser, 1964). The batholith belt can be divided into the northern and southern belts: the northern belt is characterized by late Triassic plutons (Wang et al., 2016), Cretaceous adakite (Zhu et al., 2009a), and S-type granitoids (Wen et al., 2008), whereas the southern belt is dominated by Cretaceous to Eocene granitoids overlain by

Paleocene-Eocene volcanic strata (Schärer et al., 1984; Copeland et al., 1995; Ding et al., 2003; Wen et al., 2008; Zhu et al., 2008; Lee et al., 2009; Ji et al., 2009; Guan et al., 2012). The southern belt is intruded by 18-13 Ma dikes (Coulon et al., 1986; Yin et al., 1994; Williams et al., 2001).

2.3.4. Cratonal Rocks of Northeast India

The 400-km-long, east-trending Shillong Plateau of northeastern India exposes Indian cratonal rocks that are correlative to the Proterozoic metasedimentary strata and Precambrian crystalline rocks of the LHS and GHC (e.g., Gansser, 1983; Yin et al., 2010b) (Fig. 2). Cenozoic deformation is expressed by east-striking thrust faults that bound the margins of the plateau (e.g., Clark and Bilham, 2008; Yin et al., 2010b). Active deformation within the Shillong Plateau is evident by multiple northeast-trending left-slip faults that offset Quaternary geomorphic features and sediments (Yin et al., 2010b).

2.3.5. Northern Indo-Burma Ranges

The research presented in this chapter is focused on the northern Indo-Burma Ranges, the northernmost segment of the Eastern Flanking Belt, located north of latitude 27°N (Fig. 1). Previous geological studies have established the first-order lithologic framework of the northern Indo-Burma Ranges (e.g., Wadia, 1931; Kumar, 1973; Nandy, 1973; Thakur and Jain, 1975; Acharyya, 1980, 1987; Sharma et al., 1991; Singh, 1993; Misra and Singh, 2002; Roy and Singh, 2002; Gururajan and Choudhuri, 2003; Misra, 2009; Sarma et al., 2009; Goswami, 2008, 2011; Sarma et al., 2012; Goswami, 2013a, b; Sharma and Sarma, 2013; Ningthoujam et al., 2015). Most recently, Haproff et al. (2018) divided the rocks exposed in the region into six major units, which from northeast to southwest consist of: (1) igneous rocks of the Lohit Plutonic Complex, (2) the

Tidding and Mayodia mélange complexes, (3) metamorphic rocks of the Mayodia gneiss, (4) metasedimentary rocks of the Lalpani schist, (5) metasedimentary rocks of the Sewak unit, and (6) siliciclastic strata of the Tezu unit (Fig. 2). Each lithologic unit is bounded by south- to west-directed thrust faults including (1) the Walong thrust, (2) the Lohit thrust, (3) the Tidding thrust, (4) the Demwe thrust, (5) the Lalpani thrust, (6) the Tezu thrust, and (7) the Mishmi thrust (Fig. 2). Despite extensive work in the northern Indo-Burma Ranges, disagreement remains regarding whether lithologic units are correlative with those of the Himalayan orogen and the Lhasa terrane (e.g., Thakur and Jain, 1975; Acharyya, 1980; Singh and Chowdhury, 1990; Gururajan and Choudhuri, 2003; Misra, 2009). Although the results of geologic mapping by Haproff et al. (2018) has better constrained the structural framework of the study area, detailed geochronological and geochemical characterization of each lithologic unit is lacking.

2.4. Sampling and Analytical Methods

A total of sixty-five samples were collected along the Lohit and Dibang Valleys for U-Pb zircon geochronology and whole-rock geochemistry (Figs. 3-5). Sampling locations and detailed methodologies are described below. We also present more detailed descriptions of lithologic units building upon on the previous work of Haproff et al. (2018) and additional geologic maps of Dibang Valley (Fig. 4).

2.4.1. U-Pb Zircon Geochronology of the Lohit Plutonic Complex

Zircon grains from ten samples of the Lohit Plutonic Complex were analyzed for U-Pb ages using secondary ion mass spectrometry (SIMS) CAMECA *ims1270* ion microprobe at UCLA (Table 1). Prior to analysis, zircon grains were mounted with standard AS3 (1099 Ma; Paces and

Miller, 1993) on 1-inch diameter epoxy mounts, polished with carbide paper, and coated with ~100 Å of gold. Cathodoluminescence images were taken using the SEM at UCLA to observe any zonation. Zircons were sputtered using a 10–15 nA O[−] primary beam on ~25-μm-diameter spots. U-Pb isotopic ratios (²⁰⁶Pb/²³⁸U and ²⁰⁷Pb/²³⁵U) were calculated based on a calibration curve of UO/U versus Pb/U, and corrected for common lead (Stacey and Kramers, 1975). ²⁰⁶Pb/²⁰⁷Pb ages were reported for zircon grains of >1000 Ma age. Data reduction was accomplished using the program ZIPS 3.0.3. Data tables of all zircon analyses are shown in Tables A.1-A.2. Weighted mean ages and concordia and relative probability plots were generated using Isoplot/Ex (Ludwig, 1991). We interpret that the weighted mean age of the prominent youngest population of concordant analyses yields the best estimate for the crystallization age of the plutonic sample. We excluded age data with low radiogenic lead concentrations, large analytical errors, inherited zircon grains that were significantly older than the dominant zircon-age population, and discordant ages.

2.4.2. U-Pb Detrital Zircon Geochronology

Detrital zircons from fifteen metasedimentary rocks from the Sewak unit, Lalpani schist, Mayodia gneiss, and Tidding and Mayodia mélange complexes were dated via U-Pb geochronology (Table 2). Data tables of all detrital zircon analyses are shown in Tables A.3-A.6. Zircon age distributions were used to determine the detrital provenance, distinguish lithologic units, and test correlations with metasedimentary rocks of the Himalayan orogen to the west of the study area.

Zircon grains were separated from rocks at UCLA using standard procedures (Quidelleur et al., 1997; Schmitt et al., 2003a, 2003b). Zircons were mounted on 1-inch diameter epoxy rounds with 91500 zircon standards (1065 Ma age; Wiedenbeck et al., 1995), and polished with carbide

paper. Zircons from two samples were analyzed U-Pb age by laser ablation inductively coupled plasma mass spectrometry (LA-ICP-MS) at the University of California, Santa Barbara (see Kylander-Clark et al., 2013 for detailed analytical methods). Spots sizes of ~20 µm were each shot twice with an excimer laser at a 5 Hz pulse rate. Zircon grains from another thirteen samples was analyzed using the method of Liu et al. (2018) at the Institute of Tibetan Plateau Research, Chinese Academy of Sciences in Beijing, China.

2.4.3. Whole-Rock Geochemistry

Whole-rock major and trace element geochemical analyses were conducted on six plutonic samples from the Lohit Plutonic Complex and nine mafic and ultramafic samples. Samples selected for whole-rock geochemical analyses were crushed using a steel mortar and pestle and pulverized. Major, minor, and trace element compositions were determined by LA-ICP-MS at Activation Laboratories (Actlabs) in Ontario, Canada. Major and minor element compositions of nine whole-rock samples were determined using at Pomona College by fusion of Li-Tetraborate and X-ray fluorescence (XRF) analysis using a PanAnalytical Axios wavelength-dispersive instrument. XRF instrument calibration and sample preparation methods are based on Johnson et al. (1999). Trace element compositions were determined via ICP-MS at the Institute of Tibetan Plateau Research, Chinese Academy of Sciences in Beijing using the methods of Liu et al. (2018). Results of major and trace element geochemistry are shown on Tables A.7-A.8. Four samples of the western Lohit Plutonic Complex belt were cut into thin sections and viewed in a petrographic microscope to determine the modal abundances of quartz, plagioclase, alkali feldspar for granitoid classification (Fig. A.4B).

Twenty-one plutonic and metasedimentary rock samples from each major lithologic unit were

analyzed for $^{143}\text{Nd}/^{144}\text{Nd}$ and/or initial $^{87}\text{Sr}/^{86}\text{Sr}$ isotopic ratios to understand source and setting of magmagenesis and test correlation with rocks of the Himalayan orogen (Table 3). Prior to analysis, powdered samples were first placed in Teflon bombs, diluted with H_2O , HNO_3 , and HF , and oven heated at 190 °C for 36 hrs. Four ml of H_2O , HClO_4 , and HNO_3 was added to solution, along with 0.1 ml Rh and Re internal standard. Final sample preparation and analyses were performed using the methods of Liu et al. (2018) via both LA-ICP-MS and thermal ionization mass spectrometry (TIMS) at the Institute of Tibetan Plateau Research in Beijing and Guangzhou, China.

2.5. Lithologic Descriptions and Results of U-Pb Zircon Geochronology

2.5.1. Lohit Plutonic Complex

The northernmost mapped unit is the Lohit Plutonic Complex of Nandy (1973), which is divided into western and eastern belts by the north-dipping Walong thrust (Gururajan and Choudhuri, 2003) (Figs. 3, 4A, and 5). Eleven samples were collected from the eastern and western belts to constrain the spatial distribution of U-Pb zircon ages.

2.5.1.1. Western Lohit Plutonic Complex Belt

The western belt of the Lohit Plutonic Complex consists of diorite, granodiorite, monzodiorite, tonalite, quartz monzonite (Fig. 6A), and younger leucogranite and mafic dikes thrust over the Tidding mélange complex (Fig. 4A). The locations of six samples collected for U-Pb zircon geochronology are shown on Figs. 3, 4A, and 5. Samples contain quartz, plagioclase, potassium feldspar, biotite, and variably hornblende and garnet. Cathodoluminescence (CL) images of representative zircons are shown on Fig. A.3A-C. Zircon grains are euhedral and prismatic in shape and transparent to pale brown in color. Long axes of the zircon grains are ~50-150 µm. Most zircon

grains display oscillatory zoning. The outermost rims of the dated zircon grains were targeted with $\sim 25 \mu\text{m}$ ion beam spots to date the youngest crystallization event. Complete U-Pb isotope data can be found in Table A1.

U-Pb zircon ages of the western belt are clustered at 93-115 Ma and 156 Ma (Fig. A.1, Table 1). Weighted mean U-Pb ages (2σ error) of five granitoids from Dibang Valley are 96 ± 3 Ma (*PH-1-8-13-1B*), 105 ± 3 Ma (*PH-1-8-13-3*), 94 ± 20 Ma (*PH-1-8-13-4B*), 94 ± 3 Ma (*PH-1-8-13-7*), and 115 ± 13 Ma (*PH-1-8-13-8*). Lohit Valley sample *PH-1-5-13-9* yields a U-Pb zircon age of 156 ± 7 Ma (Table 1).

2.5.1.2. Eastern Lohit Plutonic Complex Belt

The eastern belt of the Lohit Plutonic Complex consists of foliated diorite, garnet-bearing orthogneiss, and migmatite intermingled with marble bands, intruded by younger aplite, pegmatite, and leucogranite (Fig. 6B). Three foliated granitoid samples were collected from Dibang Valley and one from Lohit Valley (Figs. 3 and 5). Granitoids contain quartz, plagioclase, potassium feldspar, biotite, with variable calcic amphibole, garnet, rutile, epidote, and clinozoisite. Cathodoluminescence (CL) images of dated zircon grains are shown on Fig. A.4D. Analyzed zircon grains are typically ~ 50 - $100 \mu\text{m}$ in the longest dimension, transparent in color, and prismatic in shape. Oscillatory zoning is common. Zircon rims were targeted for dating the youngest crystallization age. Complete isotopic age data can be found in Table A.2.

The eastern belt samples yield a wider range of U-Pb zircon ages compared to those of the western belt (Fig. A.2, Table 1). Sample *PH-11-10-15-15* is a garnet-bearing orthogneiss from the middle part of the eastern belt in Dibang Valley (Fig. 3), which yields U-Pb zircon ages of 57-95 Ma with a bimodal distribution centered at ~ 70 Ma and ~ 92 Ma, respectively. The weighted mean

age of the entire U-Pb age distribution is 76 ± 9 Ma (Fig. A.2A, Table 1).

Orthogneiss sample *PH-11-11-15-1* from the northernmost part of the eastern belt (Fig. 3) has a bimodal age distribution of 68 Ma and 157 Ma, respectively (Fig. A.2B). The weighted mean age of the older age group is 135 ± 6 Ma, whereas the weighted mean age of the younger group is 69 ± 9 Ma (Fig. A.2B).

Sample *PH-11-10-15-13* was collected from a migmatitic garnet-bearing orthogneiss unit in the southernmost part of the eastern belt (Fig. 3). Twelve zircon grains from the sample yield $^{207}\text{Pb}/^{206}\text{Pb}$ ages of 1168-1558 Ma (Tables 1 and A.2), whereas the other nine grains produce an age cluster at 1258-1343 Ma with a weighted mean of 1286 ± 14 Ma (Fig. A.2C).

Sample *PH-1-5-13-5* was collected from a foliated diorite ~ 1 km east of the Walong thrust in Lohit Valley. Zircon grains from the sample yield a U-Pb zircon age of 101 ± 5 Ma (Fig. A.2D, Table 1).

2.5.2. Tidding and Mayodia Mélange Complexes

The ~8-10-km-thick Tidding and Mayodia mélange complexes are exposed in the hanging wall of the Tidding thrust (Figs. 3, 4B, and 5). Both units were originally mapped as the Tidding suture zone (Nandy, 1973; Thakur and Jain, 1975; Gururajan and Choudhuri, 2003) and the Tidding Formation by Misra (2009). In Dibang Valley, the Mayodia mélange complex is exposed as an incoherent mix of dismembered garnet mica schist, metabasite, chert, amphibolite, gabbro, and serpentinized ultramafics within the Mayodia klippe towards the foreland of the thrust belt (Figs. 4A and 7A). To the north, the Tidding mélange complex consists of amphibolite and chlorite muscovite schist (Figs. 3 and 7B). In Lohit Valley, the Tidding mélange complex consists of single exposure of incoherently-mixed amphibolite and chlorite-muscovite schist in the hanging wall of

the Tidding thrust (Fig. 5). In this study, we mapped the Tidding and Mayodia mélange complexes as separate units based on their map-view separation. However, we interpret the units to originate from the same complex, which was telescoped across the orogen in the hanging wall of the Tidding thrust and subsequently folded to form an isolated klippe in the foreland (Figs. 3 and 4B).

One chlorite muscovite schist sample (*PH-1-9-13-10*) from the Mayodia mélange complex (Fig. 4B) yields three youngest zircon ages ($\pm 2\sigma$ error) of 940 ± 9 Ma, 1326 ± 14 Ma, and 1654 ± 15 Ma (Tables 2 and A.3). A wide and significant population occurs at ~ 1200 - 1600 Ma (Fig. 11A).

Garnet-mica schist sample *PH-1-8-13-26* collected from the Tidding mélange complex in Dibang Valley (Fig. 3) contains age populations of ~ 500 - 600 Ma, ~ 800 Ma, and ~ 1000 Ma (Fig. 11A), and a youngest zircon age of 40 ± 1 Ma (3 grains ≤ 51 Ma) (Tables 2 and A.3).

2.5.3. Mayodia Gneiss

The ~ 1.5 - 4 -km-thick Mayodia gneiss was originally mapped as the Mishmi Crystallines by Gururajan and Choudhuri (2003) and later the Mayodia Group by Misra (2009) (Figs. 3, 4C, and 5). Haproff et al. (2018) renamed this unit the “Mayodia gneiss” based on the most prominent lithology exposed in the footwall of the Tidding thrust. Lithologies include paragneiss, augen gneiss, and quartzo-feldspathic schist (Fig. 8A). Meter-wide syntectonic leucogranite dikes intrude the unit near its northernmost exposure (Figs. 3 and 8B). The Mayodia gneiss is in the hanging wall of the north-dipping Demwe thrust, juxtaposed against the Lalpani schist below (Figs. 3, 4C, and 5). In Dibang Valley, the unit is exposed bounding the Mayodia klippe, which originated from the root zone of the Demwe thrust (Figs. 3 and 4B).

Five metasedimentary rocks of the Mayodia gneiss were collected from the basal to uppermost structural sections of the southernmost exposure of the unit in Dibang Valley (Fig. 4C). Mylonitic

paragneiss samples *PH-1-9-13-19A* and *PH-1-9-13-19B* (located ~50 m up-section) from the basal section of the Mayodia gneiss both contain significant age populations at ~1100-1200 Ma and ~1300 Ma and ~1400 Ma (Fig. 11B), and Mesoproterozoic youngest ages of 1073 ± 19 Ma (3 grains ≤ 1181 Ma) and 1022 ± 16 Ma (3 grains ≤ 1035 Ma), respectively (Tables 2 and A.4).

Augen gneiss sample *PH-1-3-13-9*, collected from the structural middle section of the unit (Fig. 4C), contains a large ~1100 Ma peak and smaller populations at ~800 Ma and ~1200-1300 Ma (Fig. 11B), and a youngest zircon age of 499 ± 3 Ma (3 grains ≤ 791 Ma) (Tables 2 and A.4).

Garnet gneiss sample *PH-1-3-13-8*, collected from the structurally uppermost section of the Mayodia gneiss (Fig. 4C), contains a strong peak at ~1200 Ma, and minor populations at ~1100 Ma, ~1300-1400 Ma (Fig. 11B), and a youngest zircon age of 1069 ± 13 Ma (3 grains ≤ 1079 Ma) (Tables 2 and A.4). Schist sample *PH-1-3-13-10A*, collected up-section from *PH-1-3-13-8* (Fig. 4C), contains age populations at ~800 Ma, ~1100-1200 Ma, ~1300-1400 Ma, and ~1700 Ma (Fig. 11A) and a Neoproterozoic youngest zircon age of 646 ± 13 Ma (3 grains ≤ 841 Ma) (Tables 2 and A.4).

2.5.4. Lalpani Schist

The Lalpani schist is exposed in both Lohit and Dibang Valleys (Figs. 3, 4C, and 5) and consists of quartzo-feldspathic schist, paragneiss, quartzite, and carbonate, intruded in some locations by meter-wide mafic dikes (Fig. 9). The unit was originally mapped as the lower section of the Mishmi Crystallines by Gururajan and Choudhuri (2003) and later the Lalpani Group by Misra (2009).

Seven samples of the Lalpani schist were collected for U-Pb zircon geochronology (Fig. 3 and 4C). The youngest U-Pb zircon ages from the samples range from Mesoproterozoic for the

basal unit to Cretaceous in the uppermost section, signaling changes in the source areas (Fig. 11A). Two quartzo-feldspathic paragneiss samples *PH-1-12-13-5* and *PH-1-9-13-27* from the basal section of the Lalpani schist, ~9 km apart from one another along strike (Fig. 4C), yield nearly identical U-Pb age spectra with a significant peak at ~2500 Ma (Fig. 11B) and a youngest individual zircon age of 913 ± 5 Ma (3 grains ≤ 1572 Ma) and 974 ± 6 Ma (3 grains ≤ 1195 Ma), respectively (Tables 2 and A.5).

Schist sample *PH-1-9-13-23* is structurally higher than the previous two samples (Fig. 4C), and yields zircon populations of ~1100-1200 Ma, ~1400 Ma, and ~1600 Ma (Fig. 11B). The youngest individual zircon age was 1054 ± 19 (3 grains ≤ 1166 Ma) (Tables 2 and A.5).

Paragneiss sample *PH-1-3-13-11B*, collected from the upper-middle structural section of the Lalpani schist (Fig. 4C), contains zircon grains with Mesoproterozoic to Cambrian ages clustered at ~1300 Ma, ~800-900 Ma, and ~700 Ma (Fig. 11B), and a youngest age of 525 ± 3 Ma (3 grains ≤ 668 Ma) (Tables 2 and A.5).

Samples *PH-1-12-13-7* and *PH-1-9-13-25* are mylonitic quartzo-feldspathic paragneiss collected from the lowermost structural section of the Lalpani schist (Fig. 4C). Both samples yield identical U-Pb age spectra, with a strong peak at ~500 Ma (Fig. 11A) and youngest zircon ages of 158 ± 1 Ma and 177 ± 1 Ma, respectively (Tables 2 and A.5).

Schist sample *PH-1-9-13-2*, collected from the Hunli half-window (Fig. 3), yields a youngest zircon age of 150 ± 4 Ma (3 grains ≤ 200 Ma), like samples *PH-1-12-13-7* and *PH-1-9-13-25* (Tables 2 and A.5). However, sample *PH-1-9-13-2* has a larger distribution of U-Pb ages with populations at ~150-350 Ma, ~400 Ma, ~500-700 Ma, and ~800-1000 Ma (Fig. 11A).

2.5.5. Tezu Unit

The Tezu unit is a ~2 km thick sequence of non-marine syntectonic strata including interbedded conglomerate, coarse-grained sandstone, and mudstone (Fig. 10A). The unit was observed in only one location along the range front, directly northwest of Lohit Valley (Fig. 5). Conglomeratic layers are defined by cobble-sized clasts exposed in meter-wide channels within a sandy matrix. The north-dipping Tezu unit section is oriented right-way-up to the northeast, evidenced by normal grading and conglomeratic channels. The Tezu unit is in the footwall of the Lalpani thrust, juxtaposed against the Lalpani schist (Fig. 5). U-Pb detrital zircon geochronology was not performed on samples from this unit.

2.5.6. Sewak Unit

The Sewak unit, which was originally mapped by Misra (2009) as the Sewak Group, consists of a ~1.5 km thick section of low-grade metasedimentary rocks including interbedded quartzite, marble, chert, slate, phyllite, and quartzo-feldspathic schist (Fig. 10B). The unit is exposed along the range front in the hanging walls of the Tezu thrust in Lohit Valley and Mishmi thrust in Dibang Valley (Figs. 3, 4C, and 5). In Dibang Valley, the Sewak unit is the southernmost lithologic unit thrust atop Quaternary alluvium by the active Mishmi thrust (Figs. 3 and 4C).

Phyllite sample *PH-1-14-13-4* from the middle structural level of the Sewak unit (Fig. 4C) yields a single youngest zircon age was 27 ± 1 Ma, with three spot analyses of ≤ 30 Ma (Tables 2 and A.6). The sample displays prominent zircon-age populations of ~90 Ma, ~130 Ma, ~500-600 Ma, ~800 Ma, and ~1100-1200 Ma (Fig. 11B).

2.6. Results of Whole-Rock Geochemistry

2.6.1. Plutonic Rocks

The Lohit Plutonic Complex consists of predominantly calc-alkaline diorite suite rocks featuring both I- and S-type major/trace element signatures (Figs. 12A, 13A, and A.5, Table A.7). All granitoid samples are peraluminous diorites with very high Al_2O_3 (> 19 wt. %), A/CNK values (> 1.58), A/NK (> 2.75), and Rb (> 100 ppm) (Fig. 12B, Table A.7). One sample from the eastern Lohit Plutonic Complex belt (*PH-11-10-15-13*) is a garnet-bearing, low-K granodiorite (Fig. 12A, Table A.7).

Trace element signatures of five samples of the Lohit Plutonic Complex are consistent with volcanic arc origins (VAG), along with generation in an orogenic setting (Pearce et al., 1984) (Fig. 13B). Rare earth element concentrations of four granitoids reflect moderate to high fractionation between HREE and LREE (La/Yb : ~7-15) (Figs. A.5-A.6, Table A.7). One granitoid intrusion of the Tidding mélange complex (*PH-1-8-13-22*) is a metaluminous diorite based on moderate to high Na_2O (> 3.75 wt. %), high CaO (> 5.8 wt. %), low Rb (< 35 ppm), and coexisting hornblende and sphene (Table A.7).

2.6.2. Mafic and Ultramafic Rocks

Five mafic samples collected from the Mayodia mélange complex and mafic dikes in the Mayodia gneiss and Lohit Plutonic Complex yield compositions ranging from basalt and basaltic andesite on a SiO_2 vs. total alkalis diagram (Le Bas et al., 1984) (Fig. 14A). One sample (*PH-1-9-13-7B*) from the Mayodia mélange complex contains stichtite and $\text{SiO}_2 < 45\%$, implying the presence of ultramafic blocks within the mélange (Fig. 14A, Table A.8). Seven mafic samples predominantly fall in the MORB (Figs. 14B and A.7) and oceanic-arc fields on trace element

discriminant diagrams (Nb/La vs. La/Yb; V vs. Ti; Ti vs. Zr; Cr vs. Y; Zr/Y vs. Zr) (Pearce, 1982; Shervais, 1982; Condie, 1989) (Fig. A.7, Table A.8). Mafic rock samples display relatively flat trace element slopes (La/Yb: ~1.5-4) on a spider diagram, in contrast to the sample interpreted to have an ultramafic protolith (*PH-1-9-13-7B*) (La/Yb: ~9) (Fig. A.8, Table A.8).

2.6.3 Sr and Nd Isotope Geochemistry

Neodymium and strontium isotopic compositions aid in differentiating protoliths of the LHS from the GHC (e.g., Parrish and Hodges, 1996; Huyghe et al., 2001; Robinson et al., 2001; Aikman et al., 2012a) and identifying the source and evolution of igneous rocks (e.g., Kistler and Ross, 1990; Chung et al., 1998). We determined the isotopic ratios of $^{143}\text{Nd}/^{144}\text{Nd}$ (normalized to CHUR in epsilon notation) and initial $^{87}\text{Sr}/^{86}\text{Sr}$ (Sr_i) for igneous rocks of the western Lohit Plutonic Complex belt (Figs. 15-16) and Tidding and Mayodia mélange complexes to understand source and setting of magmagenesis (Figs. 16). $^{143}\text{Nd}/^{144}\text{Nd}$ and Sr_i ratios were determined for the Mayodia gneiss, Lalpani schist, and Sewak unit to test correlation with the GHC and LHS of the Himalaya orogen (Fig. 16). Results of Sr and Nd isotopic analyses are summarized in Table 3.

Five samples from the western Lohit Plutonic Complex belt yield positive ε_{Nd} values of 2.2 to 5.6 and Sr_i values of 0.704 to 0.705 (Figs. 15-16), comparable to those of I-type Gangdese granitoids of the southern Lhasa terrane (Fig. 15). Three samples from the Mayodia mélange complex samples located near the Tidding thrust yielded positive ε_{Nd} values of 4.97 to 7.69 and Sr_i of 0.703 to 0.706, whereas two samples of the Tidding mélange complex near the Lohit thrust contain ε_{Nd} values of -7.22 and 0.83, and Sr_i values of 0.705 to 0.712 (Fig. 16). Four samples from the Mayodia gneiss yield ε_{Nd} values between -17 and -10, and Sr_i values of 0.715 to 0.721 (Fig. 16). Four Lalpani schist samples yield negative ε_{Nd} values of -27 to -15 (Fig. 16), indicative of a

Lesser Himalayan affinity. The same Lalpani schist samples have Sr_i values between 0.744 and 0.789 (Fig. 16). One phyllite sample of the Sewak unit has a ε_{Nd} value of -10 and Sr_i of 0.712 (Fig. 16).

2.7. Regional Correlation of Lithologic Units

Our results allow us to correlate the major rock units of the northern Indo-Burma Ranges with those of the Himalaya orogen and the Lhasa terrane (Fig. 2). As detailed below, we observe that several Himalayan-Tibetan lithologic units are missing in the study area (Fig. 17), which implies either a unique tectonic process controlled the development of the Eastern Flanking Belt or a greater magnitude of crustal shortening possibly and/or continental subduction occurred across the study area compared to the Himalayan orogen to the west.

2.7.1. Sub-Himalayan Sequence

The Sewak unit and Tezu units are the structurally lowest rocks exposed the study area (Fig. 2). Although the Sewak unit is comparable to the SHS based on structural position alone, the lithology of the Sewak unit including low-grade metamorphic rocks is different. However, the presence of young zircon ages of < 30 Ma (Fig. 11B) makes this unit correlative in age with SHS strata (Yin, 2006) (Fig. 2).

The Tezu unit has a similar lithology to that of the Miocene-Pliocene Siwalik Group in the SHS (e.g., DeCelles et al., 1998). The structural position of the Tezu unit is also like that of the SHS (Yin, 2006), as the unit is juxtaposed atop the Indian foreland basin by an active, range-bounding fault (i.e., Mishmi thrust) (Fig. 2).

2.7.2. Lesser Himalayan Sequence and Greater Himalayan Crystalline Complex

Because both the LHS and GHC consist of medium- to high-grade metamorphic rocks, differentiating the units without a clear structural context can be challenging. Unfortunately, the northeast-striking strike-slip faults bounding the eastern Himalayan syntaxis (Fig. 1C) prevent the testing of the along-strike continuity of major thrusts between the northern Indo-Burma Ranges and Himalayan orogen. However, this problem can be mitigated by comparing U-Pb detrital zircon ages between lithologic units (Gehrels et al., 2011). To do this, we applied the nonparametric K-S statistical test to compare the U-Pb detrital zircon ages between the Mayodia gneiss, Lalpani schist, LHS, and GHC. The tests were conducted using the Excel macro generated by George Gehrels at the University of Arizona LaserChron Center (<https://sites.google.com/a/laserchron.org/laserchron/>). In the test, the observed vertical difference (D_{obs}) between the cumulative probability distributions is compared to a critical value (D_{crit}), determined from the number of zircon analyses per sample. In this study, a maximum D_{obs} value of 0.05 is established. If the D_{obs} is greater than D_{crit} , the null hypothesis that the samples are derived from the same source can be rejected. The P value is the maximum value of the significance level at which the null hypothesis can be accepted. If the P value is greater than 0.05, then the zircon age distributions are derived from the same source at the 95% confidence level. Results of the K-S statistical test are summarized in Table A.9.

The test shows that schist sample *PH-1-3-13-10A* of the Mayodia gneiss may be similar with rocks of the Arunachal Himalaya and Shillong Plateau, specifically sample *AY 02-13-06-7* of the GHC (Webb et al., 2013) and sample *AY9160314A* of the LHS (Yin et al., 2006) (Table A.9). However, sample *AY 02-13-06* from the Arunachal Himalaya is located within the MCT shear

zone, which in some locations extends into the upper LHS (Yin, 2006). We interpret the Mayodia gneiss to correlate with the LHS based on the similarity of detrital zircon ages with sample *AY9160314A*, comparable metamorphic lithologies, and similar negative ϵ_{Nd} values (-17 to -10) (Fig. 16, Table 3). Furthermore, the Mayodia gneiss lacks (1) ~870 Ma and ~500 Ma orthogneiss, (2) large leucogranite sheets or laccolith bodies (e.g., Arunachal and Tsuna leucogranites), and (3) significant U-Pb detrital zircon age populations at ~540-750 Ma and ~800-1200 Ma (Fig. 11B), all of which are common in the GHC (Yin et al., 2010a; Gehrels et al., 2011; Aikman et al. 2012a, b; Webb et al., 2013; Harrison and Wielicki, 2016). Similarly, the Lalpani schist is correlated to the LHS based on (1) similar lithologies and metamorphic grades, (2) negative ϵ_{Nd} values in the range of -27 to -15 (Fig. 16, Table 3), and (3) the presence of the Mesoproterozoic-Cambrian detrital zircon ages (Fig. 11B).

2.7.3. Indus-Yarlung Suture Zone

The Tidding and Mayodia mélange complexes are interpreted to originate from the same complex, which correlates with the Indus-Yarlung suture zone. This is based on (1) amalgamated basalts, gabbro, ultramafics, and mafic schist of a dismembered ophiolite sequence within the Tidding-Mayodia mélange complex, (2) generation of igneous rocks in a mid-ocean ridge setting (Fig. 14B), and (3) the position of the mélange complex between rocks of Indian and Lhasa terrane affinities (Figs. 3 and 5). Metasedimentary rocks containing Eocene zircons (~40 Ma) (Fig. 11A) could have been part of a syntectonic basin within the suture zone.

2.7.4. Mesozoic Magmatic Arc and Mesoproterozoic Basement of the Lhasa Terrane

Following the early suggestion of Lin et al. (2013), we interpret the Lohit Plutonic Complex is the southeastward continuation of the Mesozoic Cenozoic northern Gangdese batholith belt based on (1) similar Jurassic-Cretaceous crystallization ages between ~70-156 Ma (Table 1), (2) low Th/Y (0.07-0.08) and La/Yb ratios in I-type granitoids (Fig. 13A), (3) trace element signatures indicating volcanic arc origins (Fig. 13B), (4) $^{87}\text{Sr}/^{86}\text{Sr}$ values of ≤ 0.704 (Fig. 15, Table 3), (5) positive ϵ_{Hf} values (10-14) (Lin et al., 2013), and (6) positive ϵ_{Nd} values (Figs. 15-16, Table 3). Furthermore, similar Cretaceous zircon ages along with ϵ_{Nd} and initial $^{87}\text{Sr}/^{86}\text{Sr}$ values are found in the Wuntho-Popa and Mogok Metamorphic belts to the south (Mitchell, 1993; Mitchell et al., 2012; Wang et al., 2014). The existence of a continuous magmatic arc stretching from the southern Lhasa terrane to the West Burma block and Sibumasu plate supports the model of continuous Neotethys subduction and Andean-type magmatism along an elongated boundary (Lin et al., 2013).

The eastern Lohit Plutonic Complex belt is distinct in having both Cretaceous (~70-135 Ma) and Mesoproterozoic (~1286 Ma) zircons (Table 1). The ~1286 Ma Mesoproterozoic-aged orthogneiss correlates with the Bomi-Chayu Complex (1276-1342 Ma), which is exposed surrounding the eastern Himalayan syntaxis (Xu et al., 2013) (Fig. 1C). The Bomi-Chayu Complex is notable for being the oldest rocks exposed in the Lhasa terrane (Xu et al., 2013), and our observations suggest that these rocks extend southeast to the northern Indo-Burma Ranges in the hanging-wall of the Walong thrust (Fig. 1C).

Absence of Cenozoic plutonic and volcanic rocks (e.g., analogous to the Linzizong volcanics) of the southern Gangdese batholith belt in the study area raises the question of whether Cenozoic magmatism was occurring along the entire southern Lhasa margin during the Cenozoic. Existing

research has shown that ~50-55 Ma mafic rocks of Gangdese affinity are exposed in the Mogok Metamorphic Belt of northwest Yunnan to the south of the study area (e.g., Wang et al., 2014). Furthermore, Eocene to Oligocene granitoids and Miocene to Quaternary volcanic flows related to Neotethys subduction are exposed throughout the Wuntho-Popa belt in present-day Myanmar (Mitchell, 1993; Mitchell et al., 2012; Lee et al., 2016). The existence of Cenozoic subduction-generated rocks both to the northwest and south of the study area suggests Cenozoic magmatism did occur in the northern Indo-Burma Ranges, but these igneous rocks may have been shortened and eroded and/or underthrusted during development of the orogen (see section 3.7.6).

2.8. Discussion

Correlation of the Lalpani schist and Mayodia gneiss with the LHS (Fig. 2) suggests that prior to the Cenozoic India-Asia collision, rocks comprising the northeast Indian cratonal sequence extended to the east and southeast of the present-day location of the eastern Himalayan syntaxis. Rocks of the Indian passive continental margin (i.e., THS) and Indian cratonal sequence (i.e., GHC and LHS) would have existed along the northeast margin of the Greater Indian continent. The existence of late Jurassic-Cretaceous granitoids within the study area that are equivalent to the northern Gangdese batholith belt implies that subduction of Neotethys oceanic lithosphere and arc magmatism occurred along a continuous belt encompassing both the southern Lhasa terrane and Eastern Flanking Belt (e.g., Lin et al., 2013). Following initial India-Asia collision, Cenozoic magmatism (i.e., southern Gangdese batholith belt) also occurred along an elongated belt from the southern Lhasa terrane to the Eastern Flanking Belt. An accompanying Mesozoic-Cenozoic forearc basin sequence was likely present along the entire Neotethys subduction margin.

We interpret the absence of these major Himalayan-Tibetan units in the northern Indo-Burma Ranges to result from a greater magnitude of (1) Cenozoic shortening and erosion compared to the Himalayan orogen to the west and/or (2) continental underthrusting. Haproff et al. (2018) showed that the southeast- to east-directed northern Indo-Burma thrust belt accommodated clockwise rotation of Himalayan-Tibetan rocks around the eastern Himalayan syntaxis. Progressive clockwise rotation of the thrust belt from an originally east-trending configuration implies a spatial gradient in shortening strain, such that the magnitude of crustal shortening increases with distance from the pole of rotation at the eastern Himalayan syntaxis. This interpretation is supported by the dramatic southward decrease in the map-view distance between the active foreland basin and Tidding mélange complex (=IYSZ), which is ~33 km along Dibang Valley and ~5 km along Lohit Valley further to the southeast. For contrast, the map-view distance between the Main Frontal thrust and IYSZ across the western Arunachal Himalaya, perpendicular to the strike of the orogen, is ~200 km (Yin et al., 2010a). In the northern Indo-Burma Ranges, this width of the thrust belt decreases to ~5 km over a map-view distance of ~250 km from the eastern Himalayan syntaxis. Upper plate shortening at the latitude of the northern Indo-Burma Ranges may also have been coeval with the underthrusting of complete sections of Greater India and southern Lhasa terrane. In this case, the Tethyan Himalayan thrust belt, GHC, Xigaze forearc basin, and southern Gangdese batholith were underthrust during subduction of the Indian slab, removing these lithologic units from the surface.

2.9. Conclusions

Our study presents the results of U-Pb zircon geochronology and whole-rock geochemistry of lithologic units exposed in the northern Indo-Burma Ranges, located east to southeast of the

eastern Himalayan syntaxis. Geochronological and geochemical data were coupled with lithologic and structural observations to test the along-strike continuity of rocks of the easternmost Himalayan collisional system. We infer that lithologic units exposed in the study area are the easternmost continuations of the Cenozoic Sub-Himalayan sequence, Lesser Himalayan Sequence, and Indus-Yarlung suture zone. The eastern Lohit Plutonic Complex contains Mesoproterozoic basement rocks of the Lhasa terrane (i.e., Bomi-Chayu Complex), whereas the western Lohit Plutonic Complex belt correlates with the Mesozoic northern Gangdese batholith belt. Based on comparable U-Pb zircon ages and geochemical composition between the Gangdese batholith and Lohit Plutonic Complex, subduction of Neotethys oceanic lithosphere, Mesozoic arc magmatism, and forearc-basin sedimentation occurred along a continuous belt encompassing the southern Lhasa terrane and Eastern Flanking Belt along the southern margin of Asia. Prior the early Cenozoic India-Asia collision, the northeast continental margin of Greater India was likely a continuous sequence involving rocks of the Lesser Himalayan sequence, Greater Himalayan Crystalline Complex, and the Tethyan Himalayan Sequence. Once collision initiated, rocks of the Himalayan orogen and southern Lhasa terrane experienced coeval clockwise rotation and shortening around northeast India that was accommodated by a southwest- to east-directed thrusting. During progressive development of the northern Indo-Burma thrust belt, a greater magnitude of crustal shortening and/or continental subduction occurred than compared to the Himalayan orogen to the east, resulting in local complete erosion and/or underthrusting of several Himalayan-Tibetan lithologic units.

2.10. Figures and Tables

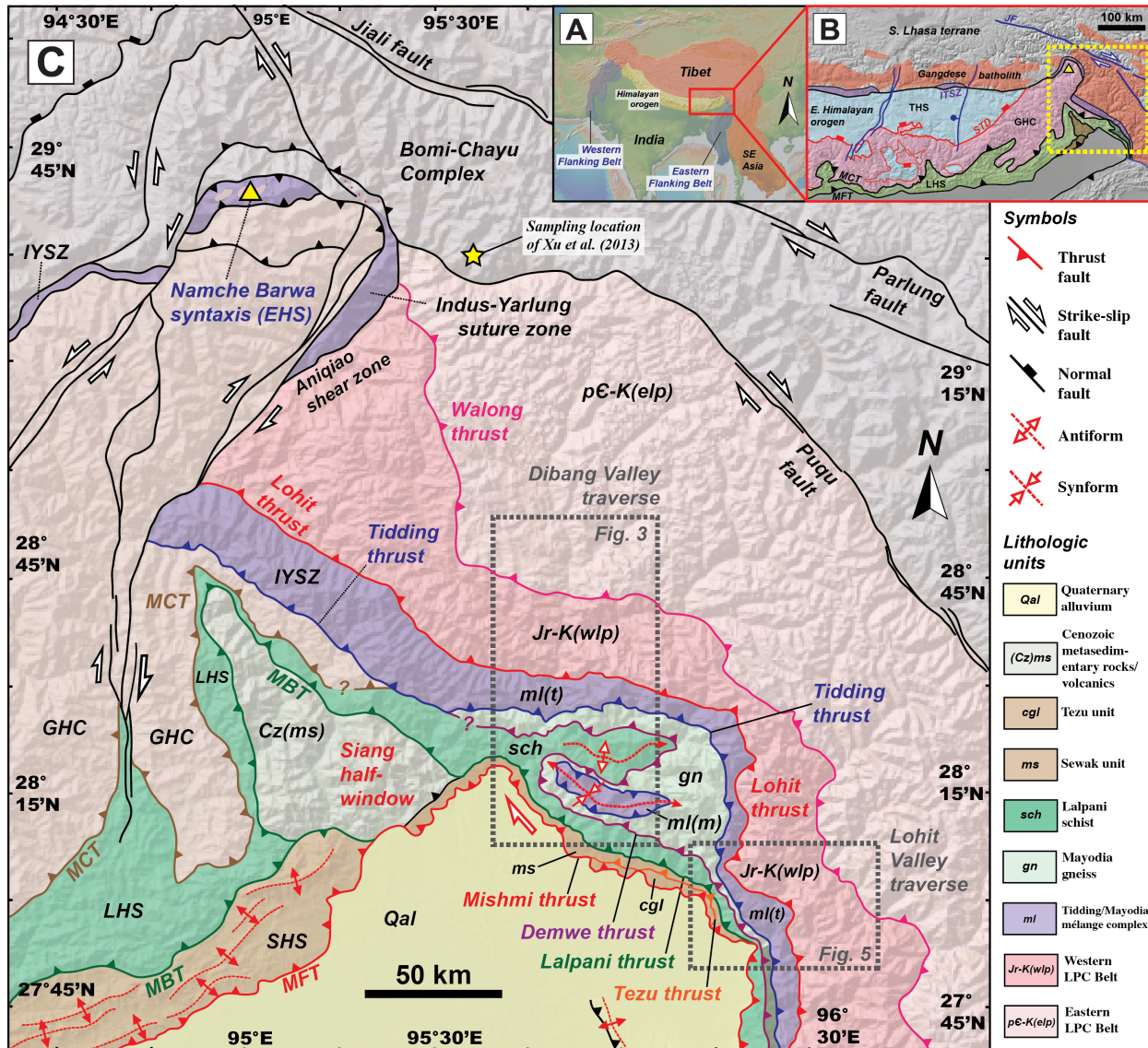


Figure 2.1. Geologic maps of (A) the India-Asia orogenic system including the Eastern and Western Flanking Belts, (B) the easternmost Himalayan orogen and southeastern Tibetan Plateau (modified from Webb et al., 2017), and (C) the northern Indo-Burma Ranges, compiled from Ding et al. (2001) and Hapgood et al. (2018). Abbreviations: GHC: Greater Himalayan Crystalline Complex, IYSZ: Indus-Yarlung suture zone, JS: Jiali fault, LHS: Lesser Himalayan Sequence, MFT: Main Frontal thrust, STD: South Tibetan detachment, and THS: Tethyan Himalayan Sequence.

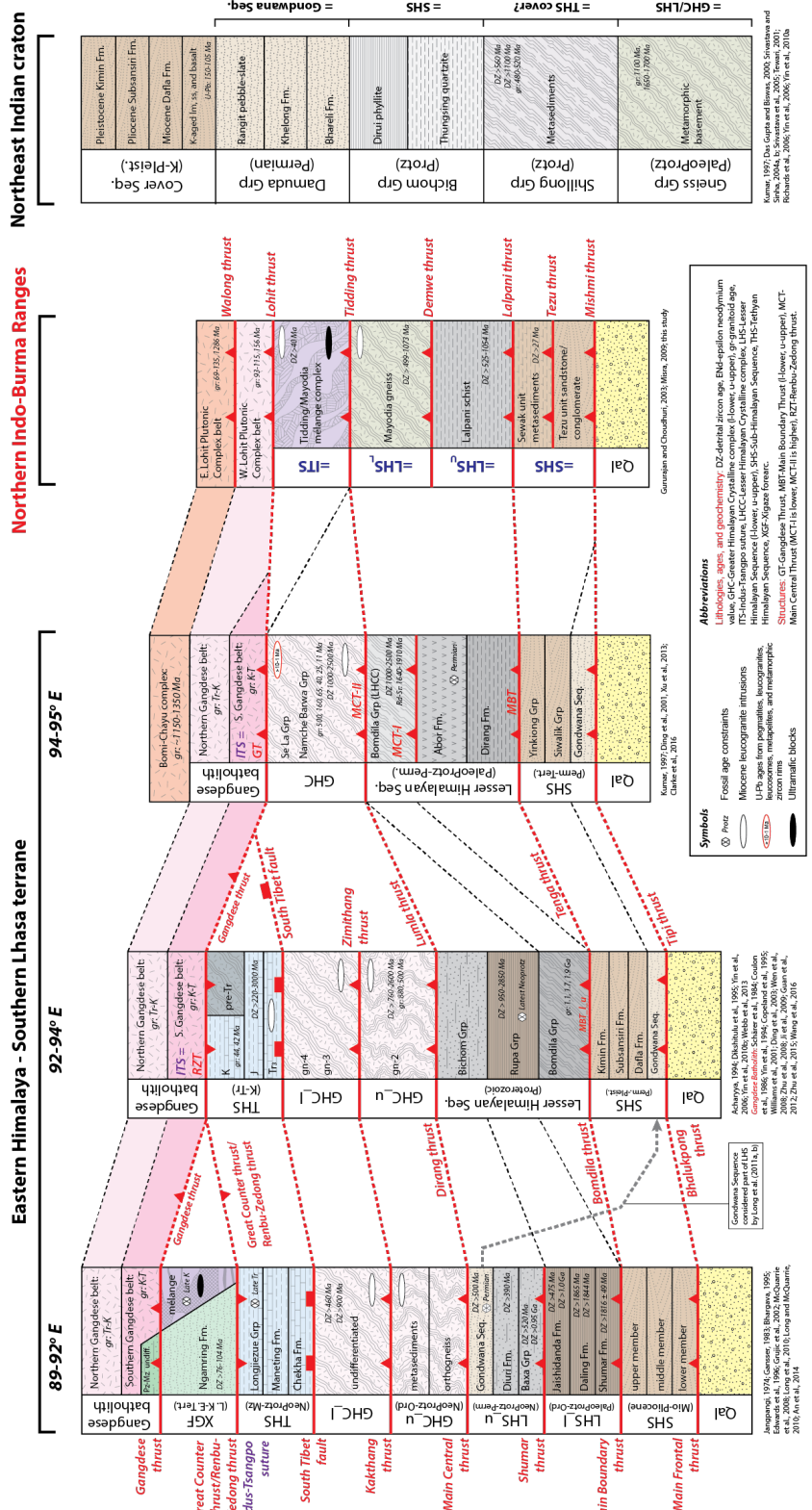


Figure 2.2. Tectonostratigraphic column depicting correlation of major lithologic units and faults exposed in the eastern Himalaya, northern Indo-Burma Ranges, and northeast Indian craton. Thickness of nearly all lithologic units exposed in the study area are likely structural due to the observed internal deformation.

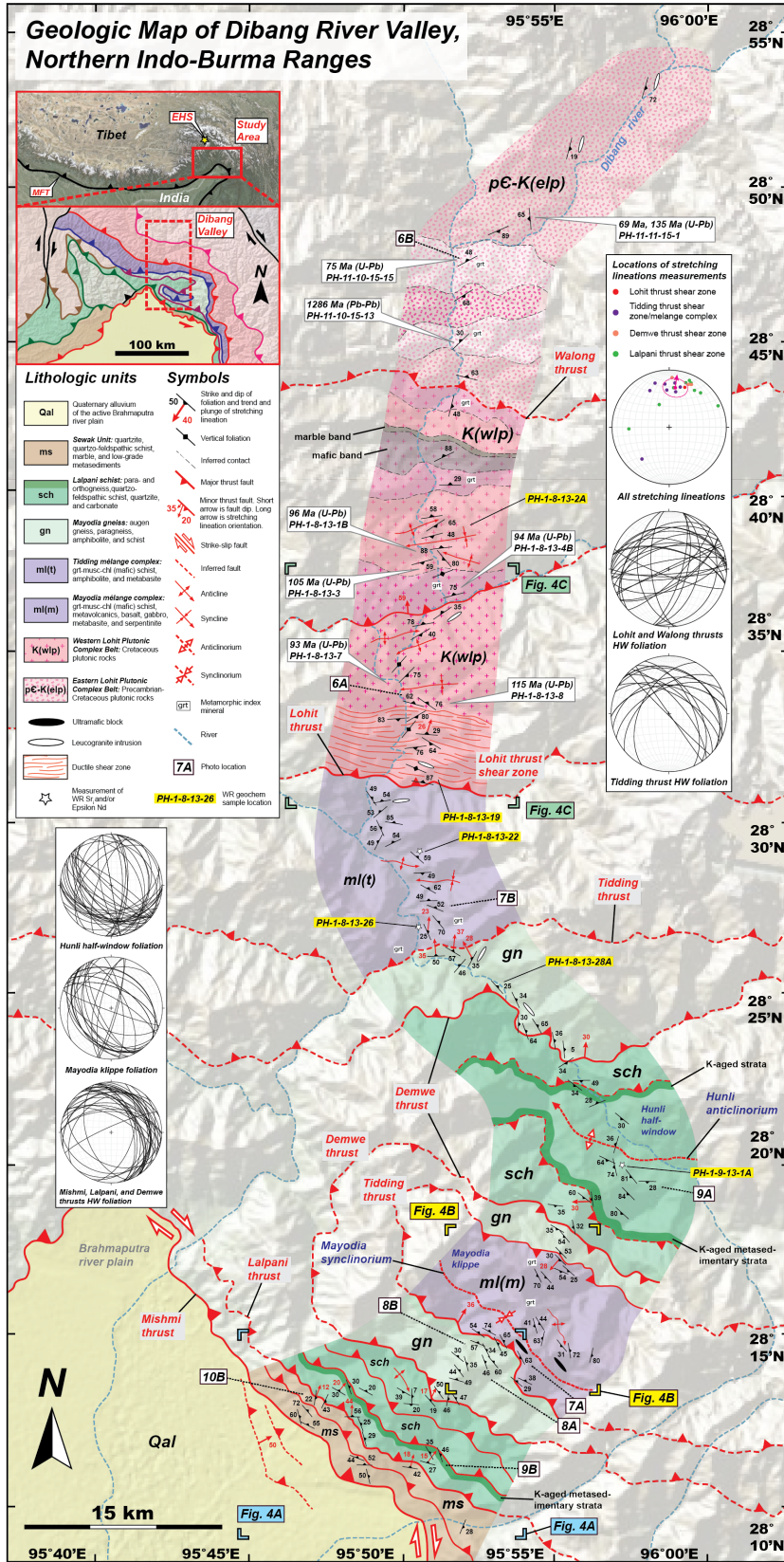
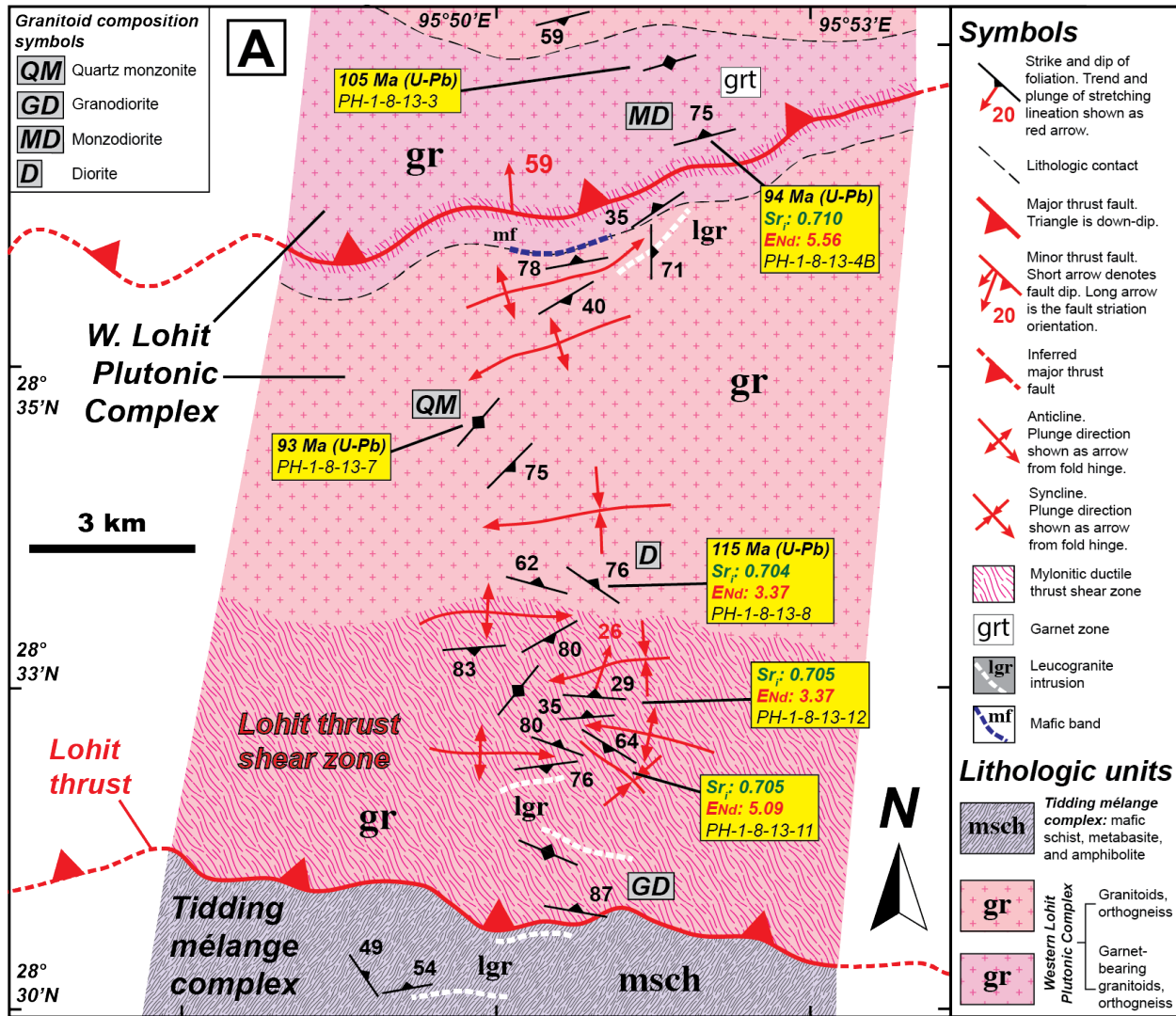
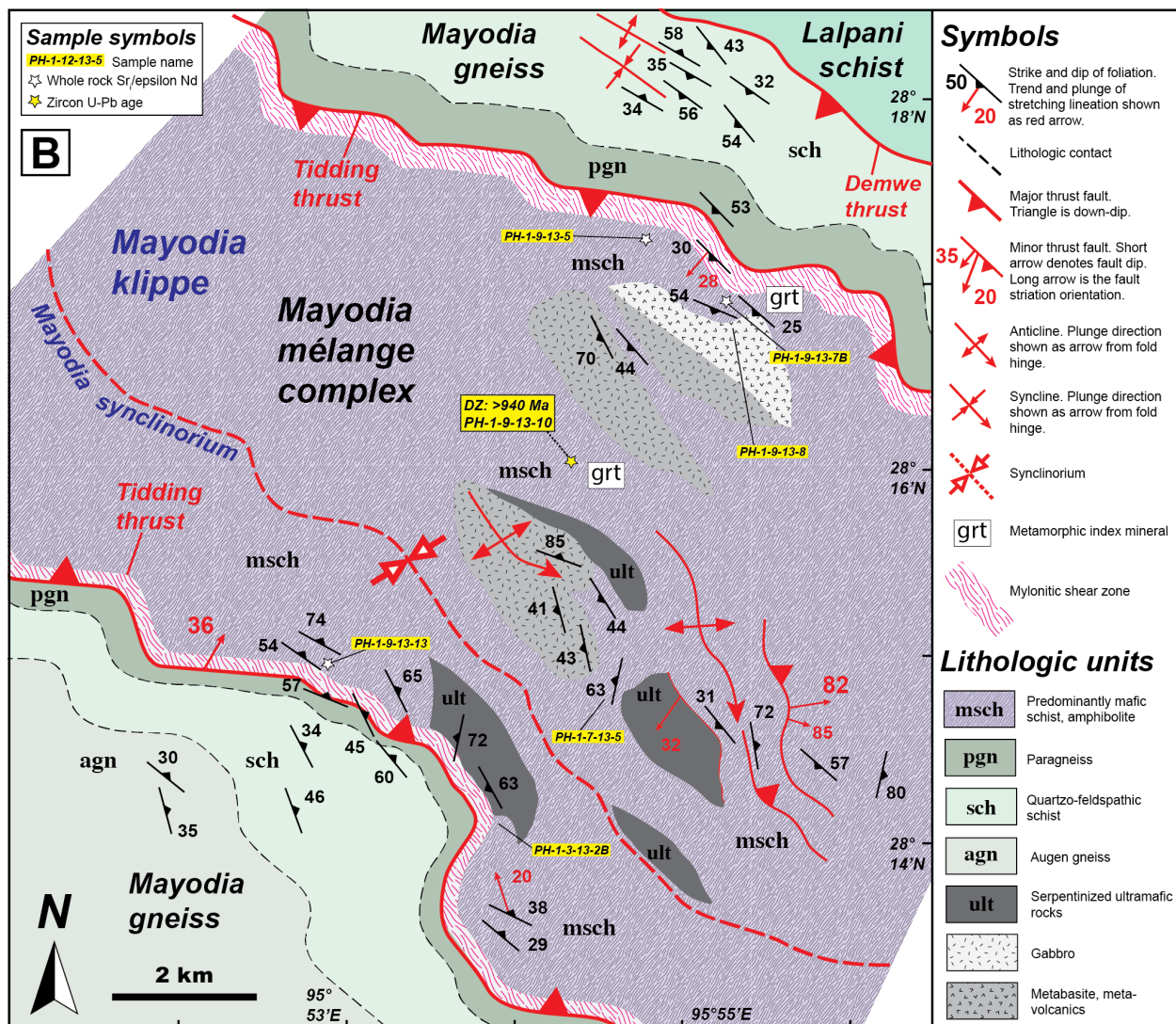


Figure 2.3. Geologic map of the Dibang Valley traverse, modified from Haproff et al. (2018).

Abbreviations: EHS: eastern Himalayan syntaxis, HW: hanging wall, MFT: Main Frontal thrust.





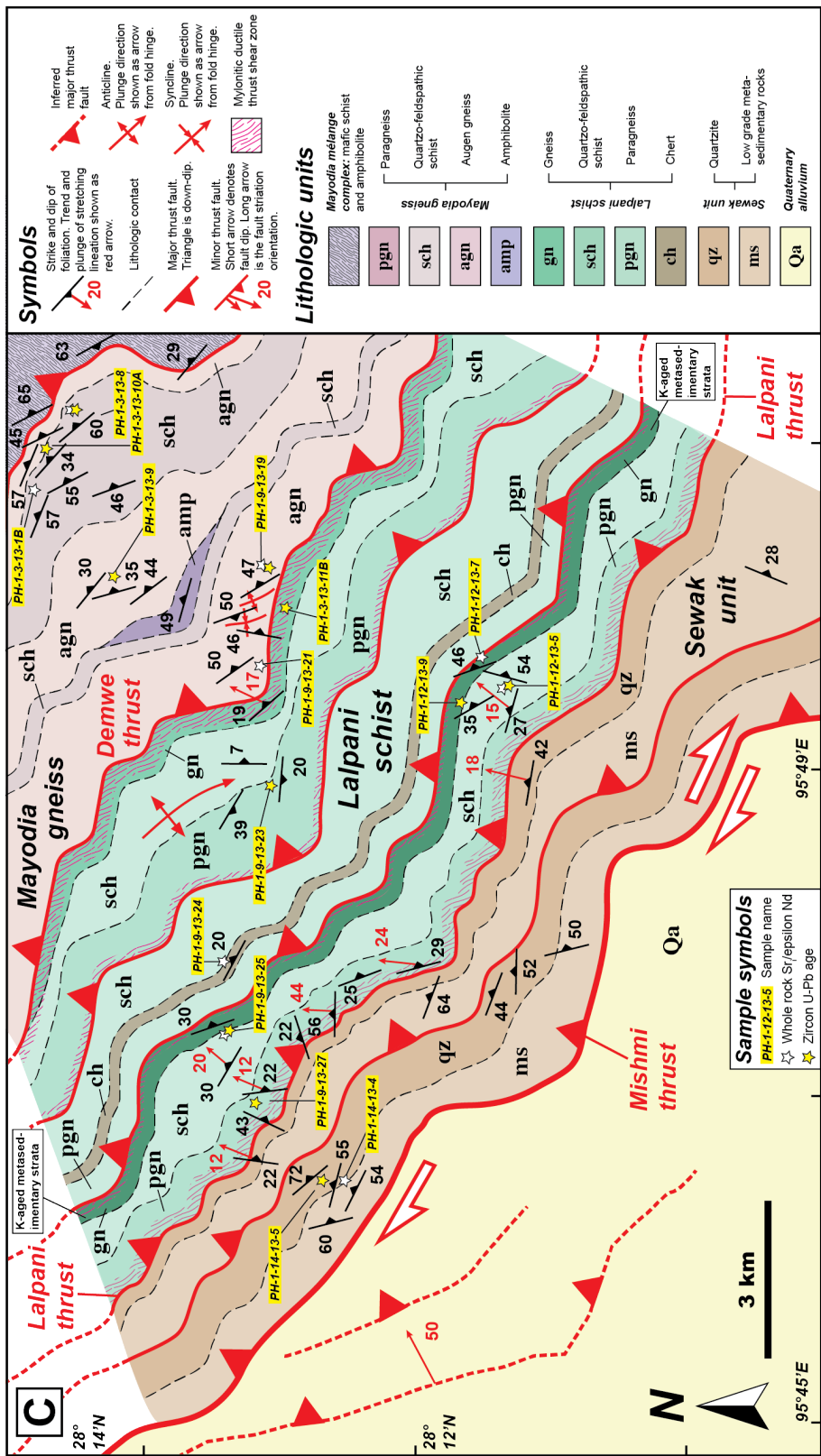


Figure 2.4 (previous two and current page). Detailed geologic maps of locations along the Dibang Valley traverse including

(A) the foreland region, (B) Mayodia klippe, and (C) Lohit thrust shear zone. See Figure 3 for map locations.

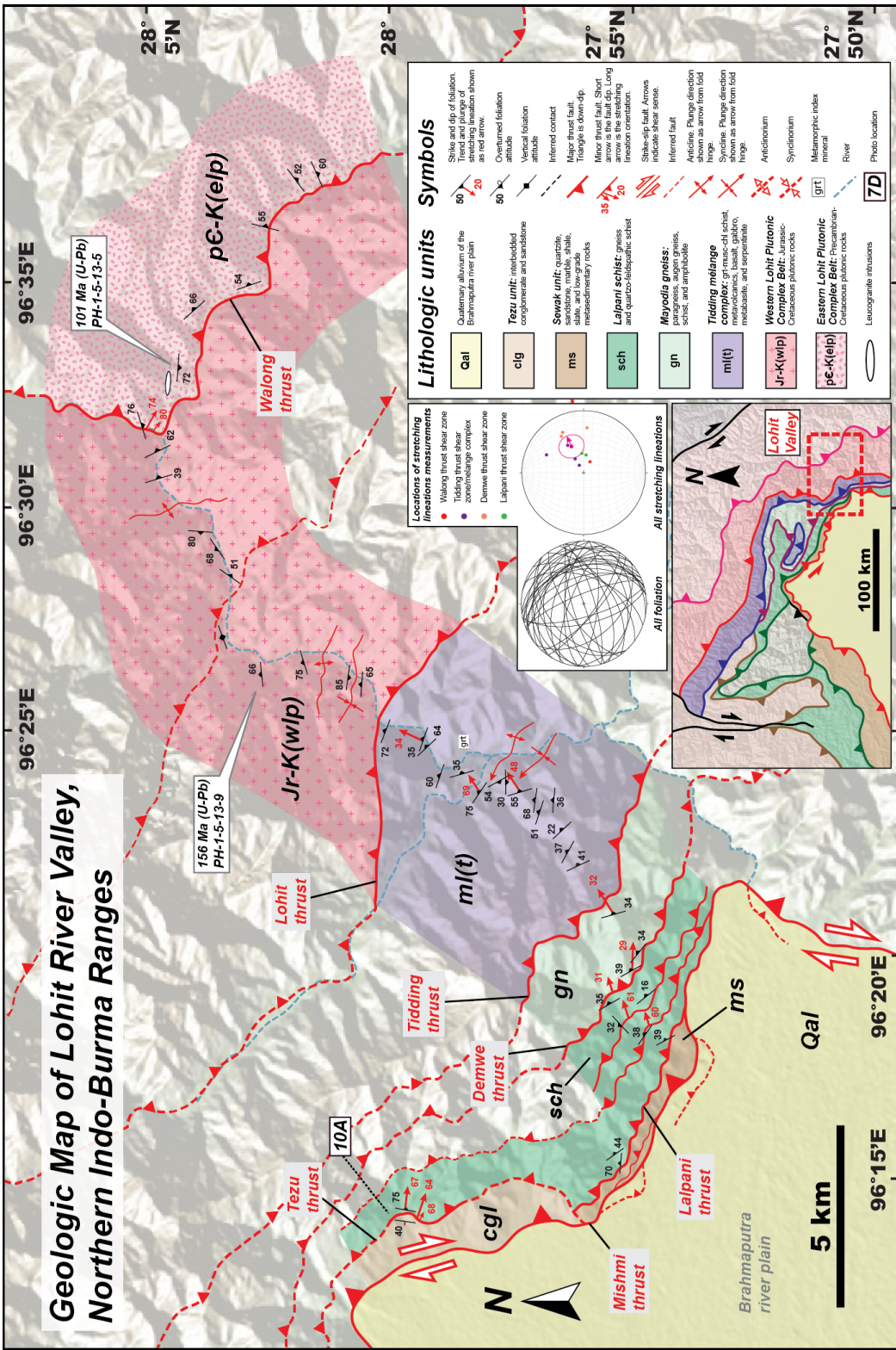


Figure 2.5. Geologic map of the Lohit Valley traverse, modified from Haproff et al. (2018).

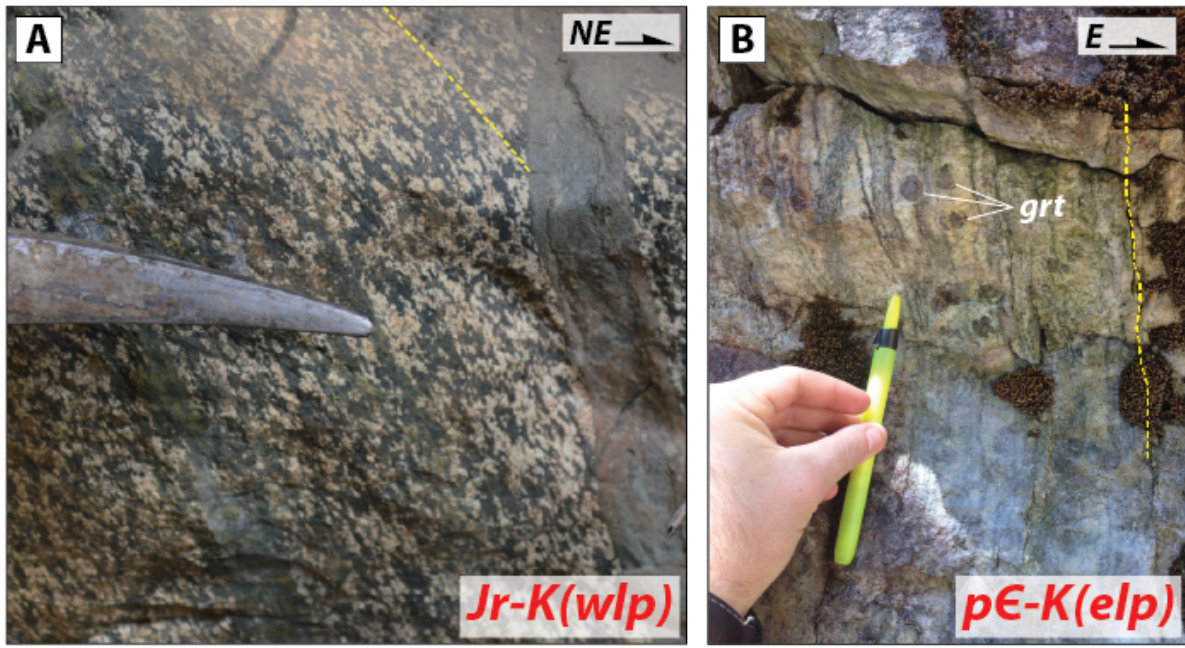


Figure 2.6. Outcrop photographs of rocks of the Lohit Plutonic Complex (LPC); (A) foliated diorites of the western LPC belt (PH-1-8-13-8) and (B) garnet-bearing orthogneiss of the eastern LPC belt (PH-11-10-15-15). Yellow dashed lines depict the orientation of foliation.

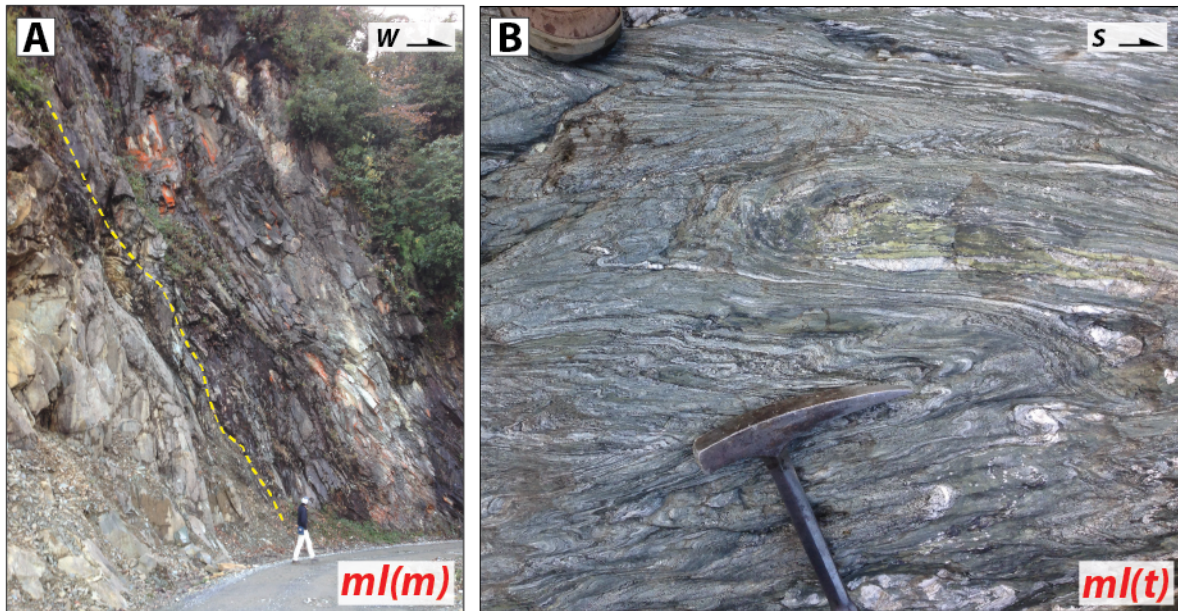


Figure 2.7. Outcrop photographs of (A) sheared serpentinite of the Mayodia mélange complex and (B) isoclinally-folded chlorite schist of the Tidding mélange complex (PH-1-8-13-24). The yellow dashed line depicts the orientation of foliation.

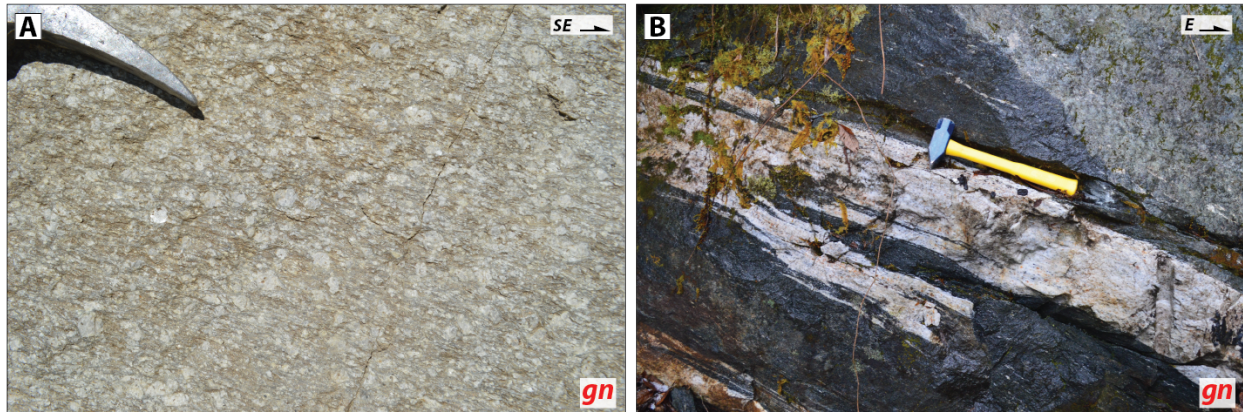


Figure 2.8. Outcrop photographs of rocks of the Mayodia gneiss in Dibang Valley; (A) augen gneiss (PH-1-3-13-9) and (B) gneiss intruded by a m-scale leucogranite dike (PH-1-3-13-1B).

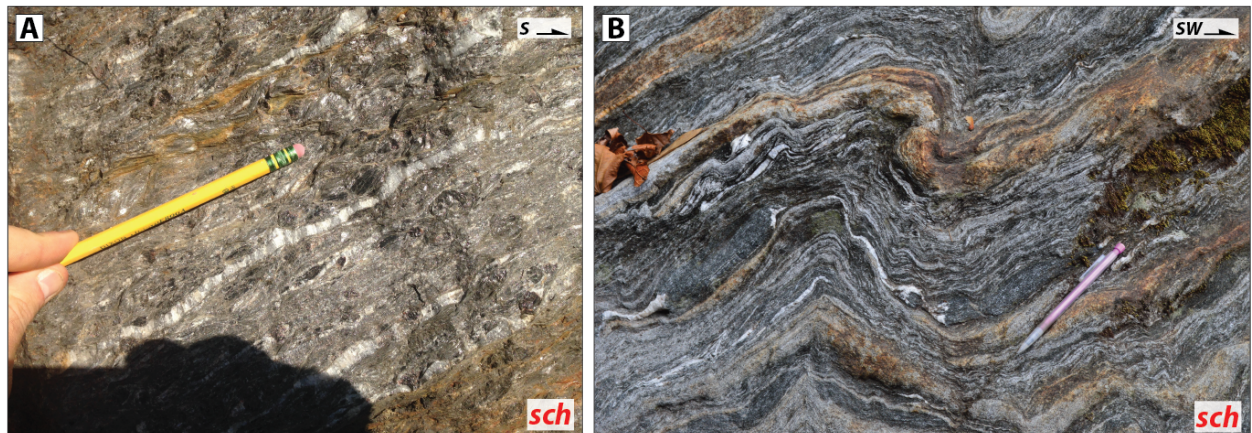


Figure 2.9. Outcrop photographs of rocks of the Lalpani schist (PH-11-9-15-2); (A) foliation within mica schist and (B) southwest-verging isoclinal folds within paragneiss (PH-1-12-13-7) (Haproff et al., 2018).

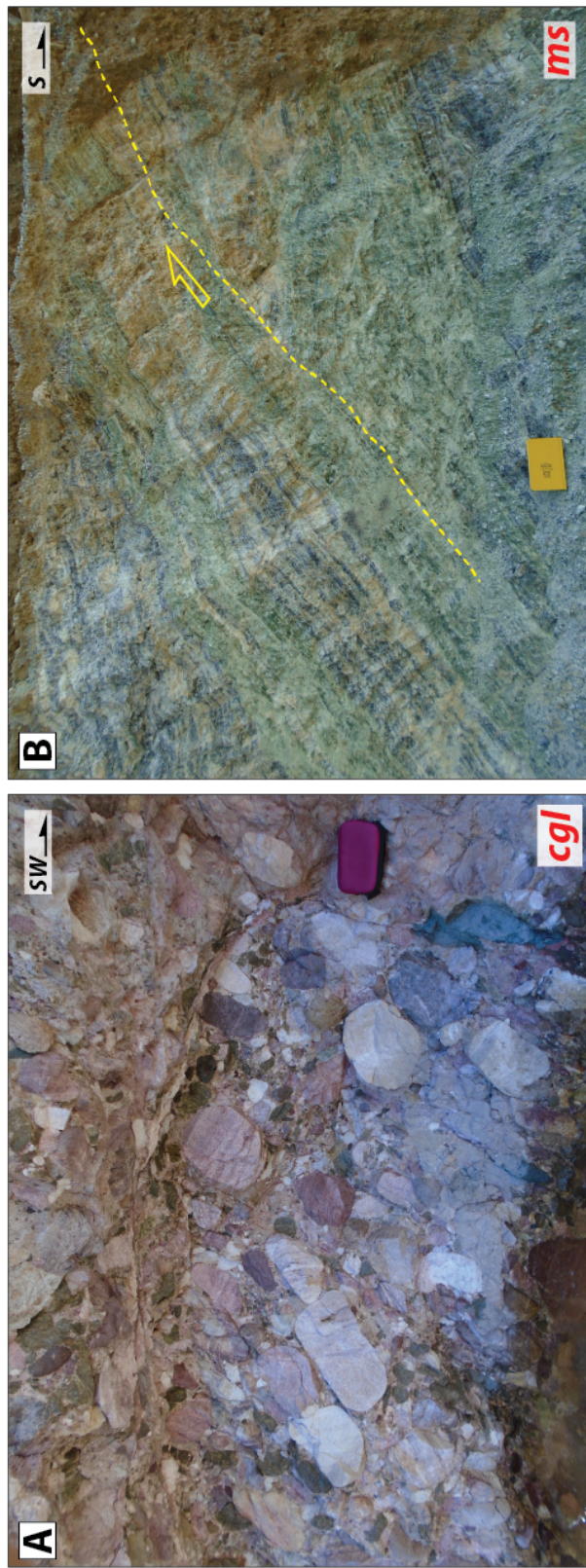
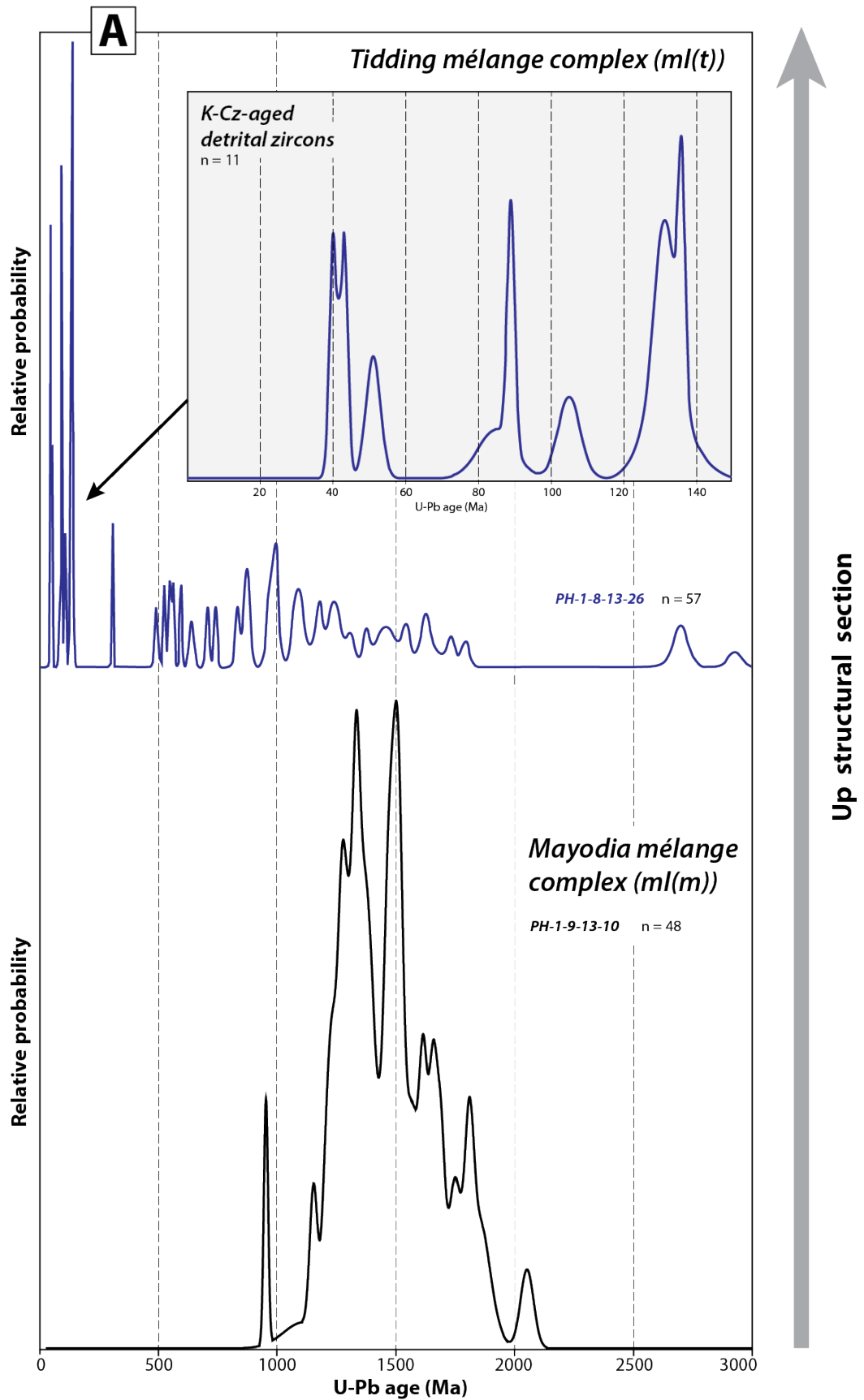


Figure 2.10. Outcrop photographs of (A) conglomerate of the Tezu unit in the footwall of the Tezu thrust (PH-11-13-15-1) and (B) a meter-scale, southeast-directed thrust within quartzite of the Sewak unit (PH-1-14-13-4).



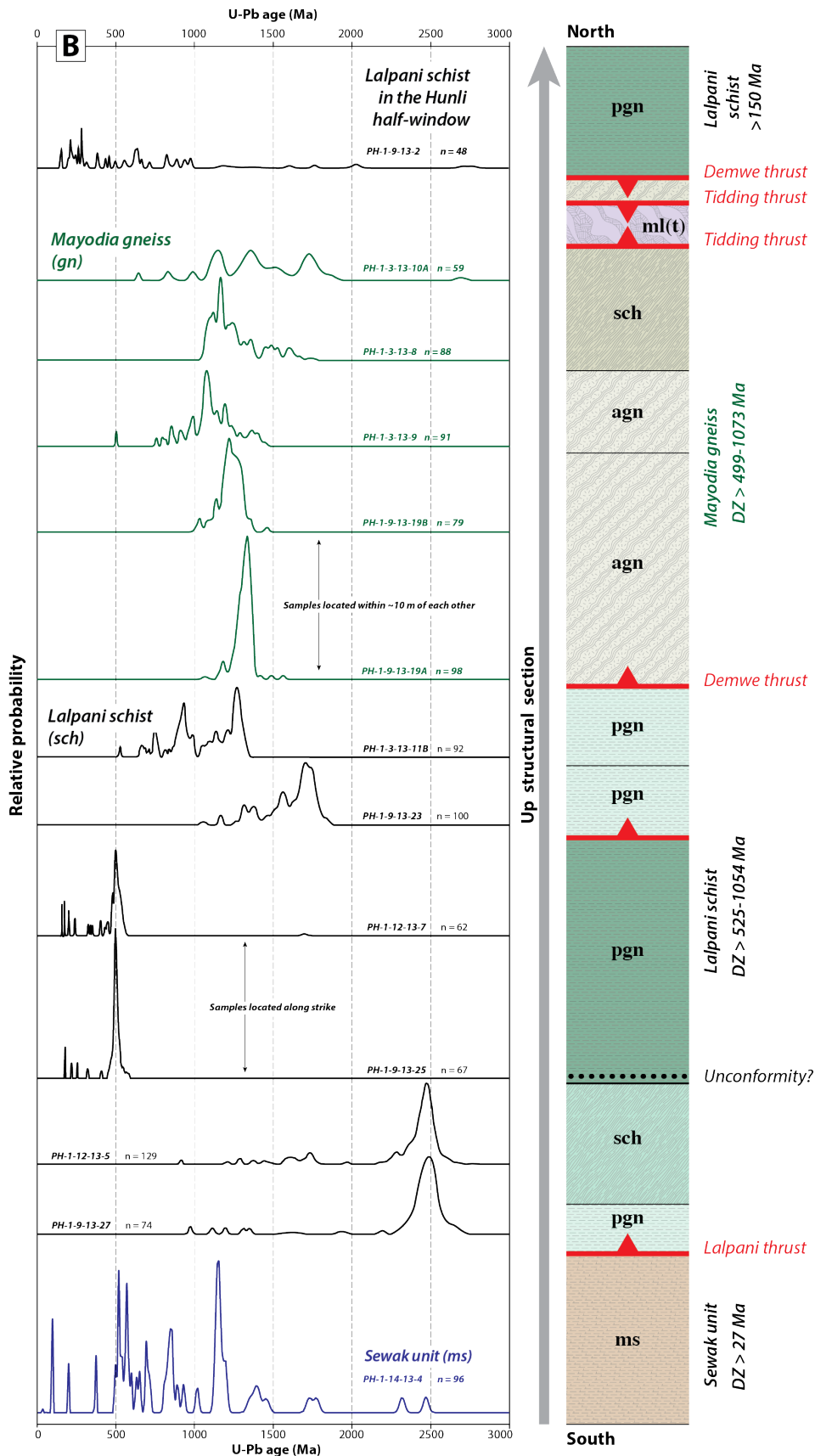


Figure 2.11 (previous and current page). Relative probability plots of detrital zircon U-Pb ages for metasedimentary rocks of the (A) Sewak unit, Lalpani schist, and Mayodia gneiss and (B) the Tidding and Mayodia mélange complexes.

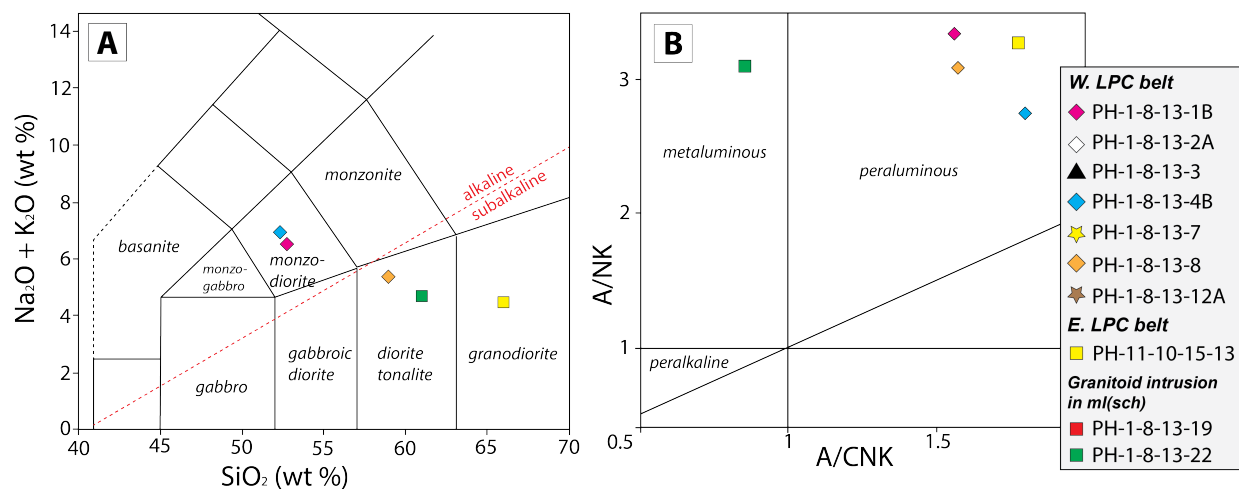


Figure 2.12. Geochemical plots for plutonic rocks including (A) alkalis vs. silica classification (Le Bas et al., 1984) and (B) $\text{Al}_2\text{O}_3/\text{N}_2\text{O} + \text{K}_2\text{O}$ vs. $\text{Al}_2\text{O}_3/\text{CaO} + \text{N}_2\text{O} + \text{K}_2\text{O}$ (Shand, 1943).

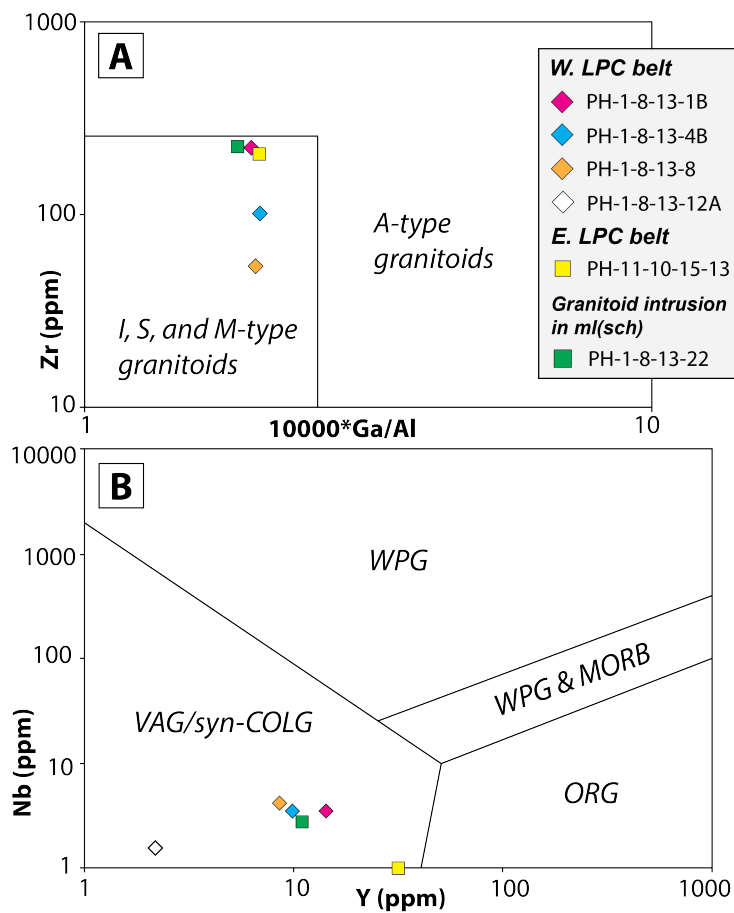


Figure 2.13 (left). Diagrams of (A) source for plutonic rocks including anorogenic (*A*), igneous (*I*), sedimentary (*S*), and mantle (*M*) -types based on Zr vs. $10000*\text{Ga}/\text{Al}$ and (B) tectonic settings diagrams for plutonic rocks including syncollisional (*syn-COLG*), within-plate granite (*WPG*), volcanic arc granite (*VAG*), orogenic (*ORG*) based on Nb vs. Y (Pearce et al., 1984).

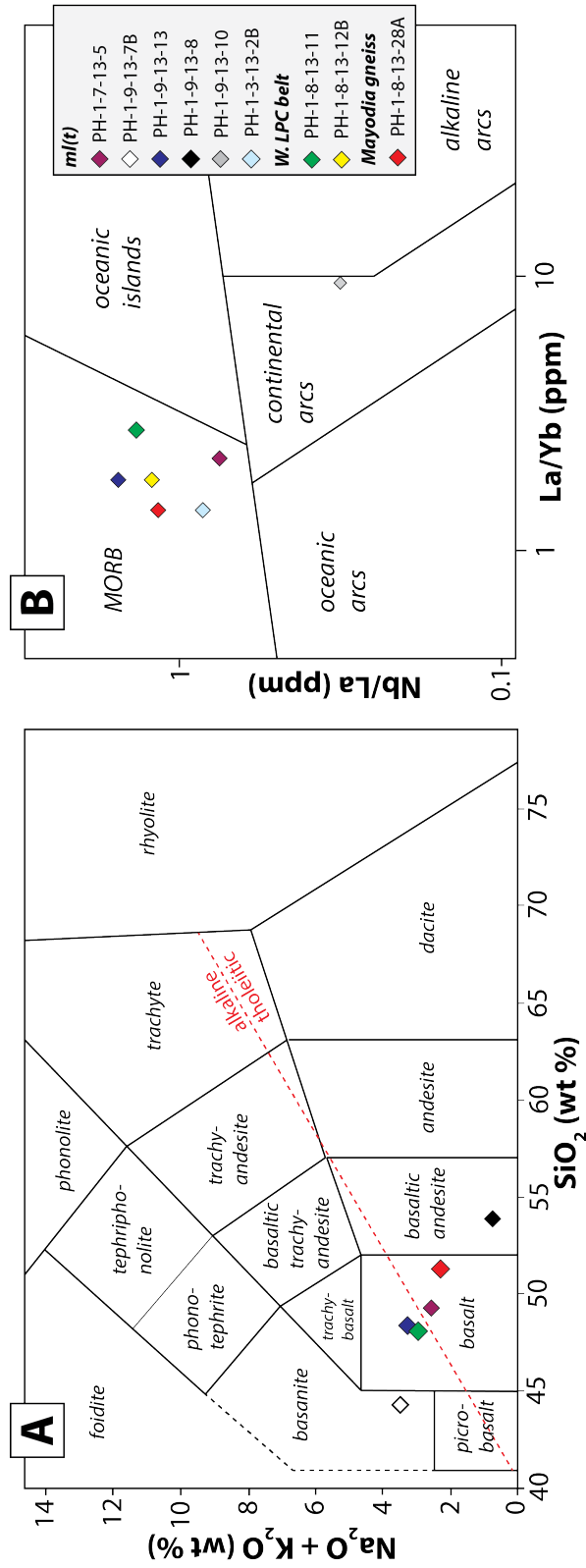


Figure 2.14. Diagrams of (A) alkalis versus silica concentrations in mafic and ultramafic rocks (Le Bas et al., 1984) and (B) tectonic setting including mid-ocean ridge basalts (*MORB*), oceanic island basalts (*OIB*), back-arc basins basalts (*BABB*), island arc tholeiites (*IAT*), oceanic arcs, continental arc or flood basalts (*CFB*), and alkaline arcs based on Nb/La vs. La/Yb (Pearce, 1982; Shervais, 1982; Condie, 1989).

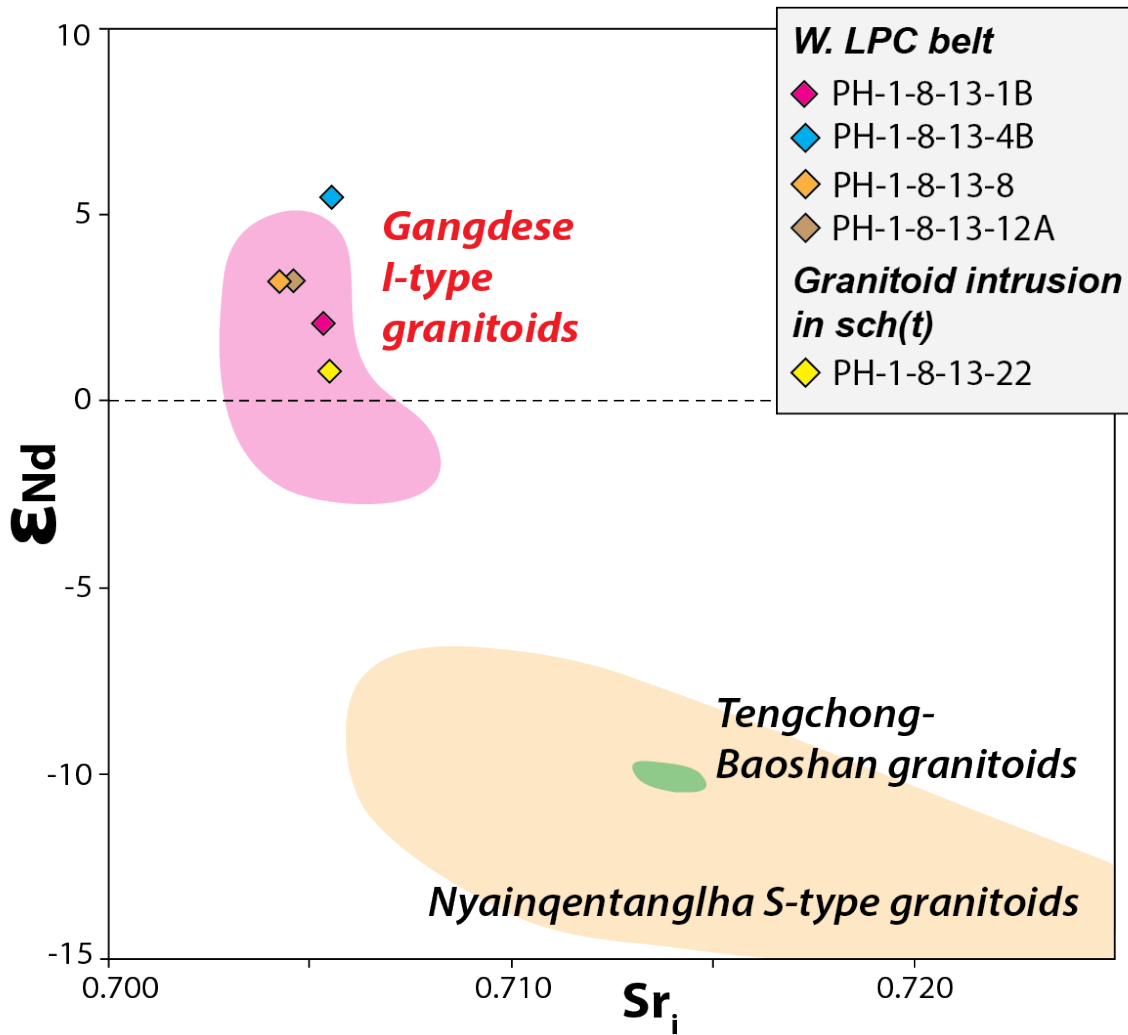


Figure 2.15. Plot of ϵ_{Nd} versus Sr_i , showing granitoids of the western Lohit Plutonic Complex belt within the Gangdese I-type granitoid field, adapted from Mitchell et al. (2012).

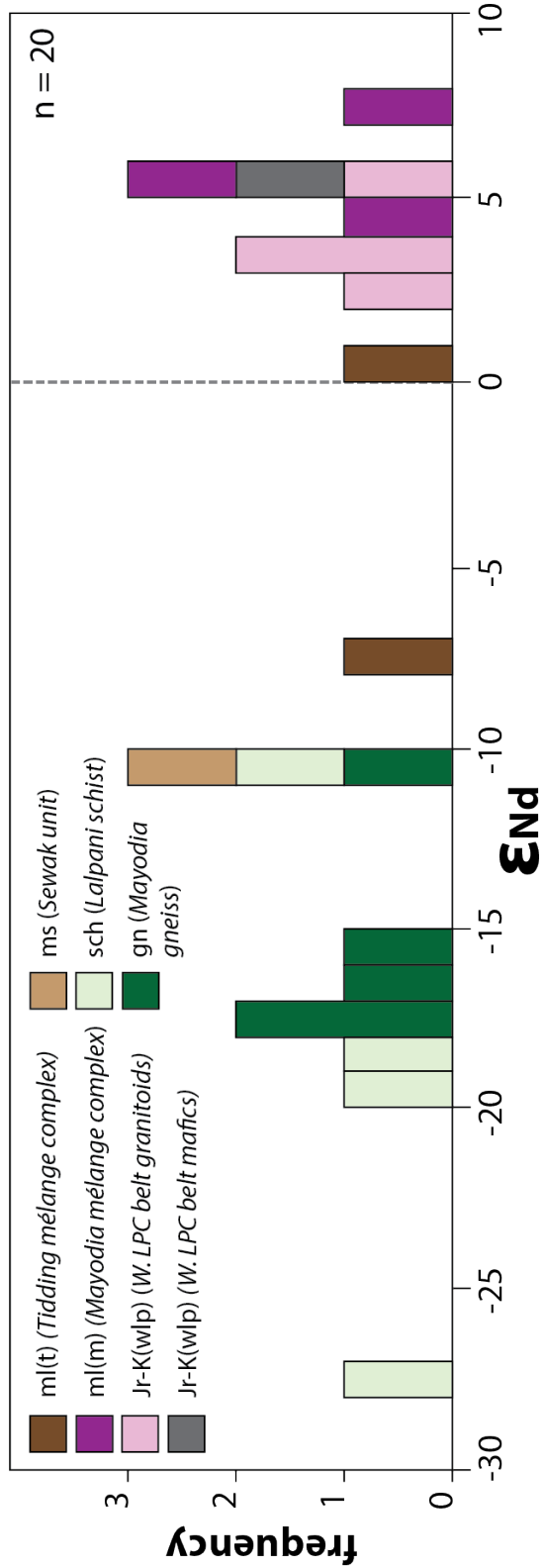
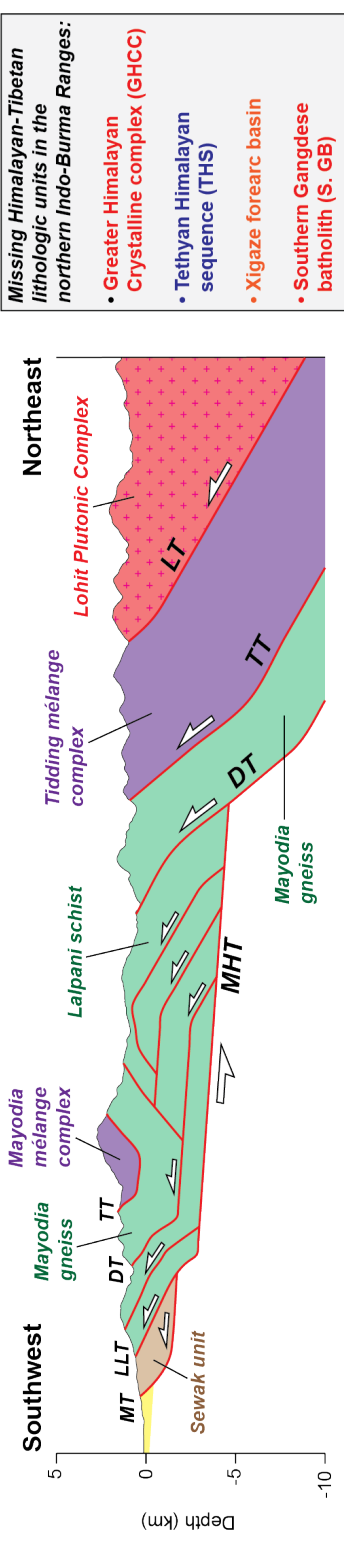


Figure 2.16. Plot of the frequency of ϵ_{Nd} values for all samples ($n = 20$).

A

Northern Indo-Burma Ranges (Dibang Valley)

**B**

Central Himalaya and southern Tibetan Plateau

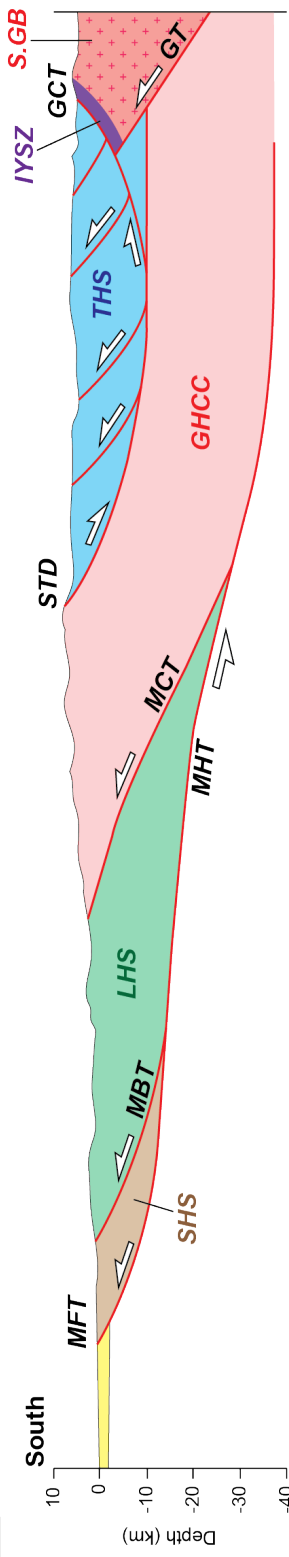


Figure 2.17. Schematic geologic cross sections across (A) the northern Indo-Burma Ranges and (B) central Himalaya-southern Tibetan Plateau showing correlation of major lithologic units. Abbreviations: DT: Denwe thrust, IYSZ: Indus-Yarlung suture zone, GB: Gangdese batholith, GCT: Great Counter thrust, GHCC: Greater Himalayan Crystalline Complex, GT: Gangdese thrust, LLT: Lohit thrust, LHS: Lesser Himalayan sequence, LT: Lohit thrust, MFT: Main Frontal thrust, MCT: Main Central thrust, MBT: Main Boundary thrust, MHT: Main Himalaya thrust, MT: Mishmi thrust, SHS: Sub-Himalayan sequence, STD: South Tibetan detachment, THS: Tethyan Himalayan sequence, TT: Tidding thrust.

Table 2.1. Summary of granitoid zircon U-Pb geochronology results

Sample	Rock type	Latitude	Longitude	Elevation (m)	Age (Ma $\pm 2\sigma$)	MSWD	n
<i>Western Lohit Plutonic complex belt</i>							
PH-1-8-13-1B	Monzodiorite	N28° 37.975	E95° 51.138	798	96.3±3	1.5	13 out of 18
PH-1-8-13-3	Tonalite	N28° 37.309	E95° 51.362	734	105.4±3	1.2	11 out of 11
PH-1-8-13-4B	Monzodiorite	N28° 36.754	E95° 51.718	717	94±20	3.3	3 out of 3
PH-1-8-13-7	Quartz monzonite	N28° 34.809	E95° 50.009	688	93.7±3	0.2	10 out of 10
PH-1-8-13-8	Diorite	N28° 33.579	E95° 50.865	736	115±13	3.5	8 out of 10
PH-1-5-13-9	Diorite	N28° 33.170	E95° 50.510	783	156.7±7	1.5	8 out of 8
<i>Eastern Lohit Plutonic complex belt</i>							
PH-11-10-15-15	Orthogneiss	N28° 45.925	E95° 52.060	1280	75.6±9	7.7	15 out of 15
PH-11-11-15-1 (A) ¹	Orthogneiss	N28° 47.281	E95° 54.543	1357	135.4±6	0.8	21 out of 24
PH-11-11-15-1 (B)	Orthogneiss	N28° 47.281	E95° 54.543	1357	69.3±9	0.1	3 out of 24
PH-11-10-15-13 ²	Orthogneiss	N28° 43.646	E95° 51.839	1080	1286±14	5.7	9 out of 14
PH-1-5-13-5	Diorite	N28° 4.258	E96° 33.112	623	101.2±5	0.3	10 out of 10

¹Sample PH-11-11-15-1 yielded a bimodal age distribution of mid-Cretaceous (A) and Late Cretaceous (B) zircons

²The weighted mean age for sample PH-11-10-15-13 is determined from the single main population of Mesoproterozoic $^{207}\text{Pb}/^{206}\text{Pb}$ ages

Table 2.2. List of samples used for detrital zircon U-Pb geochronology

Sample	Rock type	Latitude	Longitude	Elevation (m)	Youngest Age (Ma $\pm 2\sigma$)
<i>Sewak unit</i>					
PH-1-14-13-4	phyllite	N28° 12.686	E95° 46.841	417	27±1
<i>Lalpani schist</i>					
PH-1-9-13-2	schist	N28° 18.625	E95° 57.287	1196	150±4
PH-1-12-13-7	paragneiss	N28° 11.524	E95° 51.062	571	158±1
PH-1-9-13-25	paragneiss	N28° 13.478	E95° 48.126	1170	177±1
PH-1-3-13-11B	paragneiss	N28° 13.167	E95° 51.687	1810	525±3
PH-1-9-13-23	schist	N28° 13.098	E95° 50.312	1483	1054±19
PH-1-12-13-5	paragneiss	N28° 11.415	E95° 50.882	542	913±5
PH-1-9-13-27	paragneiss	N28° 13.131	E95° 47.572	1064	974±6
<i>Mayodia gneiss</i>					
PH-1-3-13-9	paragneiss	28° 14.484	E95° 53.241	2062	499±3
PH-1-3-13-10A	schist	N28° 14.304	E95° 51.994	1811	646±13
PH-1-3-13-8	paragneiss	N28° 14.745	E95° 53.110'E	2061	1069±13
PH-1-9-13-19A	paragneiss	N28° 13.263	E95° 51.781	1639	1022±16
PH-1-9-13-19B	paragneiss	N28° 13.307	E95° 51.783	1645	1073±19
<i>Tidding/Mayodia mélange complexes</i>					
PH-1-8-13-26	schist	N28° 26.897	E95° 50.957	729	40±1
PH-1-9-13-10	schist	N28° 16.145	E95° 54.358	2363	940±9

Table 2.3. Summary of whole-rock Nd and Sr isotopic data

Sample	Rock type	Rb (ppm)	Sr (ppm)	Sm (ppm)	Nd (ppm)	$^{87}\text{Sr}/^{86}\text{Sr}$	2 S.E.	$^{143}\text{Nd}/^{144}\text{Nd}$	2 S.E.	ϵ_{Nd}^1
<i>Eastern Lohit Plutonic complex belt</i>										
PH-11-10-15-13	orthogneiss	3	197	5.7	18.1	0.705	2.0E-5	-	-	-
<i>Western Lohit Plutonic complex</i>										
PH-1-8-13-1B	monzodiorite	101	814	3.6	15.3	0.705	1.8E-05	0.5127	9.0E-06	2.2
PH-1-8-13-4B	monzodiorite	113	368	4.1	18.3	0.710	1.8E-05	0.5129	6.0E-06	5.6
PH-1-8-13-8	diorite	34	738	2.2	11.1	0.704	2.0E-05	0.5128	9.0E-06	3.4
PH-1-8-13-11	mafic dike	7	188	2.7	9.4	0.705	2.0E-05	0.5129	1.0E-05	5.1
PH-1-8-13-12A	granodiorite	3.1	205	1	4.7	0.705	2.8E-05	0.5128	1.4E-05	3.4
<i>Tidding/Mayodia mélange complexes</i>										
PH-1-9-13-7B	ultramafic rock	22	310	4.8	18.7	0.705	2.3E-05	0.5130	7.0E-06	7.7
PH-1-8-13-22	grt-mica schist	35.3	483.7	2.7	20.9	0.705	1.8E-05	0.5127	8.0E-06	0.8
PH-1-8-13-26	grt-mica schist	70.7	311.3	8.4	42.2	0.712	1.8E-05	0.5123	5.0E-06	-7.2
PH-1-9-13-13	metabasalt	3	180	3.5	10.2	0.706	2.7E-05	0.5129	1.7E-05	5.4
PH-1-9-13-5	mica schist	60	627	8.9	45	0.704	2.8E-05	0.5129	2.1E-05	5.0
<i>Mayodia gneiss</i>										
PH-1-9-13-19B	paragneiss	267	75	9.4	47.2	-	2.1E-05	0.5117	8.0E-06	-17.2
PH-1-9-13-19A	paragneiss	303	58	8	35.7	-	2.6E-05	0.5118	6.0E-06	-15.5
PH-1-3-13-1B	biotite schist	39.3	251.6	1.6	29.2	0.721	2.1E-05	0.5118	8.0E-06	-16.4
PH-1-3-13-9	augen gneiss	73	248.5	2	41.6	0.715	1.6E-05	0.5121	8.0E-06	-10.3
<i>Lalpani schist</i>										
PH-1-9-13-1A	mica schist	124.8	216.8	4	19.7	0.708	1.8E-05	0.5124	9.0E-06	-5.5
PH-1-12-13-9	paragneiss	194	64	11.6	70.6	0.757	2.4E-05	0.5117	7.0E-06	-18.8
PH-1-9-13-25	paragneiss	298.5	11.2	0.4	46	0.894	3.2E-05	0.5117	6.0E-06	-18.1
PH-1-12-13-5	paragneiss	176	136	8.9	51.3	0.744	2.1E-05	0.5112	6.0E-06	-27.8
PH-1-9-13-24	quartzite	32	8	9.7	29.9	0.781	2.2E-05	0.5118	9.0E-06	-16.0
<i>Sewak unit</i>										
PH-1-14-13-4	phyllite	55	150	4.6	22.9	0.711	1.7E-05	0.5121	6.0E-06	-10.2

¹Epsilon notation determined by normalizing $^{143}\text{Nd}/^{144}\text{Nd}$ to chondrite uniform reservoir (CHUR) values

2.11. References

- Acharyya, S.K., 1980, Stratigraphy and tectonics of Arunachal Lesser Himalaya: Stratigraphy and Correlations of Lesser Himalayan Formations, p. 231-241.
- Acharyya, S.K., 1987, Cenozoic plate motions creating the Eastern Himalayan and Indo Burmese range around the northeast corner of India: Ophiolites and Indian plate margins, p. 143-160.
- Acharyya, S.K., 1994, The Cenozoic foreland basin and tectonics of the eastern sub-Himalaya: problems and prospects: Himalayan Geology, v. 15, p. 3-21.
- Acharyya, S.K. and Ray, K.K., 1977, Geology of the Darjeeling-Sikkim Himalaya: Guide to excursion, v. 4.
- Aikman, A.B., Harrison, T.M., and Hermann, J., 2012a. Age and thermal history of Eo-and Neohimalayan granitoids, eastern Himalaya: Journal of Asian Earth Sciences, v. 51, p. 85-97.
- Aikman, A.B., Harrison, T.M., and Hermann, J., 2012b, The origin of Eo-and Neo-himalayan granitoids, Eastern Tibet: Journal of Asian Earth Sciences, v. 58, p. 143-157.
- Aikman, A.B., Harrison, T.M., and Lin, D., 2008, Evidence for early (> 44 Ma) Himalayan crustal thickening, Tethyan Himalaya, southeastern Tibet: Earth and Planetary Science Letters, v. 274, no. 1, p. 14-23.
- Aitchison, J.C., Ali, J.R., and Davis, A.M., 2007, When and where did India and Asia collide?: Journal of Geophysical Research: Solid Earth, v. 112, no. B5.
- Allegré, C.O., Courtillot, V., Tapponnier, P., Hirn, A., Mattauer, M., Coulon, C., Jaeger, J.J., Achache, J., Schärer, U., Marcoux, J. and Burg, J.P., 1984, Structure and evolution of the Himalaya-Tibet orogenic belt: Nature, v. 307, no. 5946, p.17-22.

- An, W., Hu, X., Garzanti, E., BouDagher-Fadel, M.K., Wang, J., and Sun, G., 2014, Xigaze forearc basin revisited (South Tibet): Provenance changes and origin of the Xigaze Ophiolite: Geological Society of America Bulletin, v. 126, no. 11-12, p. 1595-1613.
- Bhargava, O.N., 1995, The Bhutan Himalaya, a geological account: Geological Survey of India Bulletin, no. 39.
- Burchfiel, B.C., Zhiliang, C., Hodges, K.V., Yuping, L., Royden, L.H., Changrong, D., and Jiene, X., 1992, The South Tibetan detachment system, Himalayan orogen: Extension contemporaneous with and parallel to shortening in a collisional mountain belt: Geological Society of America Special Papers, v. 269, p. 1-41.
- Burgess, W.P., Yin, A., Dubey, C.S., Shen, Z.K. and Kelty, T.K., 2012. Holocene shortening across the Main Frontal Thrust zone in the eastern Himalaya: Earth and Planetary Science Letters, v. 357, p. 152-167.
- Cai, F., Ding, L., Leary, R.J., Wang, H., Xu, Q., Zhang, L., and Yue, Y., 2012, Tectonostratigraphy and provenance of an accretionary complex within the Yarlung–Zangpo suture zone, southern Tibet: Insights into subduction–accretion processes in the Neo-Tethys: Tectonophysics, v. 574, p. 181-192.
- Chang, C.F., and Zheng, X.L., 1973, Tectonic features of the mount Jolmo Lungma region in southern Tibet, China. Chinese Journal of Geology, 1, 1-12.
- Chung, S.L., Lo, C.H., Lee, T.Y., Zhang, Y., Xie, Y., Li, X., Wang, K.L. and Wang, P.L., 1998, Diachronous uplift of the Tibetan plateau starting 40 Myr ago: Nature, v. 394, no. 6695, p. 769-773.
- Clark, M.K. and Bilham, R., 2008, Miocene rise of the Shillong Plateau and the beginning of the end for the Eastern Himalaya: Earth and Planetary Science Letters, v. 269, no. 3, p. 337-351.

- Cobbbold, P.R. and Davy, P.H., 1988, Indentation tectonics in nature and experiment. 2. Central Asia: Bull. Geol. Inst. Univ. Uppsala, v. 14, p. 143-162.
- Condie, K.C., 1989. Geochemical changes in basalts and andesites across the Archean-Proterozoic boundary: Identification and significance: *Lithos*, v. 23, no. 1-2, p. 1-18.
- Copeland, P., Harrison, T.M., Yun, P., Kidd, W. S.F., Roden, M., and Zhang, Y., 1995, Thermal evolution of the Gangdese batholith, southern Tibet: A history of episodic unroofing: *Tectonics*, v. 14, no. 2, p. 223-236.
- Corrie, S.L., Kohn, M.J., McQuarrie, N., and Long, S.P., 2012, Flattening the Bhutan Himalaya: *Earth and Planetary Science Letters*, v. 349, p. 67-74.
- Coulon, C., Maluski, H., Bollinger, C., and Wang, S., 1986, Mesozoic and Cenozoic volcanic rocks from central and southern Tibet: ^{39}Ar - ^{40}Ar dating, petrological characteristics and geodynamical significance: *Earth and Planetary Science Letters*, v. 79, no. 3, p. 281-302.
- Coward, M.P., Kidd, W.S.F., Yun, P., Shackleton, R.M., and Hu, Z., 1988, The structure of the 1985 Tibet geotraverse, Lhasa to Golmud: *Philosophical Transactions of the Royal Society of London A: Mathematical, Physical and Engineering Sciences*, v. 327, no. 1594, p. 307-333.
- Dai, J., et al., 2011, Late Devonian OIB alkaline gabbro in the Yarlung Zangbo suture zone: remnants of the Paleo-Tethys?: *Gondwana Research*, v. 19, no. 1, p. 232-243.
- Dai, J.G., Wang, C.S., Hébert, R., Santosh, M., Li, Y.L., and Xu, J.Y., 2011, Petrology and geochemistry of peridotites in the Zhongba ophiolite, Yarlung Zangbo Suture Zone: implications for the Early Cretaceous intra-oceanic subduction zone within the Neo-Tethys: *Chemical Geology*, v. 288, no. 3, p. 133-148.

Daniel, C.G., Hollister, L.S., Parrish, R.T., and Grujic, D., 2003, Exhumation of the Main Central Thrust from lower crustal depths, eastern Bhutan Himalaya: Journal of Metamorphic Geology, v. 21, no. 4, p. 317-334.

Davidson, C., Crujic, D.E., Hollister, L.S., and Schmid, S.M., 1997, Metamorphic reactions related to decompression and synkinematic intrusion of leucogranite, High Himalayan Crystallines, Bhutan: Journal of Metamorphic Geology, v. 15, no. 5, p. 593-612.

DeCelles, P.G., Carrapa, B., Gehrels, G.E., Chakraborty, T., and Ghosh, P., 2016, Along-strike continuity of structure, stratigraphy, and kinematic history in the Himalayan thrust belt: The view from Northeastern India: Tectonics, v. 35, no. 12, p. 2995-3027.

DeCelles, P.G., Gehrels, G.E., Quade, J., LaReau, B., and Spurlin, M., 2000, Tectonic implications of U-Pb zircon ages of the Himalayan orogenic belt in Nepal: Science, v. 288, no. 5465, p. 497-499.

DeCelles, P.G., Gehrels, G.E., Quade, J., and Ojha, T.P., 1998, Eocene-early Miocene foreland basin development and the history of Himalayan thrusting, western and central Nepal: Tectonics, v. 17, no. 5, p. 741-765.

DeCelles, P.G., Robinson, D.M., Quade, J., Ojha, T.P., Garzione, C.N., Copeland, P., and Upreti, B.N., 2001, Stratigraphy, structure, and tectonic evolution of the Himalayan fold-thrust belt in western Nepal: Tectonics, v. 20, no. 4, p. 487-509.

Dewey, J.F., Shackleton, R.M., Chengfa, C., and Yiyin, S., 1988, The tectonic evolution of the Tibetan Plateau: Philosophical Transactions of the Royal Society of London A: Mathematical, Physical and Engineering Sciences, v. 327, no. 1594, p. 379-413.

Dikshitulu, G.R., Pandey, B.K., Krishna, V., and Raju, R.D., 1995, Rb-Sr systematics of granitoids of the central gneissic complex, Arunachal Himalaya: implications on tectonism, stratigraphy and source: Geological Society of India Publications, v. 45, no. 1, p. 51-56.

Ding, L., Kapp, P., Zhong, D., and Deng, W., 2003, Cenozoic volcanism in Tibet: evidence for a transition from oceanic to continental subduction. *Journal of Petrology*, v. 44, no. 10, p. 1833-1865.

Ding, L., Zhong, D., Yin, A., Kapp, P., and Harrison, T.M., 2001. Cenozoic structural and metamorphic evolution of the eastern Himalayan syntaxis (Namche Barwa): Earth and Planetary Science Letters, v. 192, no. 3, p. 423-438.

Dong, X., Zhang, Z., Liu, F., Wang, W., Yu, F., and Shen, K., 2011, Zircon U-Pb geochronology of the Nyainqêntanglha Group from the Lhasa terrane: new constraints on the Triassic orogeny of the south Tibet. *Journal of Asian Earth Sciences*, v. 42, no. 4, p. 732-739.

Dubois-Côté, V., Hébert, R., Dupuis, C., Wang, C.S., Li, Y.L., and Dostal, J., 2005, Petrological and geochemical evidence for the origin of the Yarlung Zangbo ophiolites, southern Tibet: *Chemical Geology*, v. 214, no. 3, p. 265-286.

Dupuis, C., Hébert, R., Dubois-Côté, V., Wang, C.S., Li, Y.L., and Li, Z.J., 2005, Petrology and geochemistry of mafic rocks from melange and flysch units adjacent to the Yarlung Zangbo Suture Zone, southern Tibet: *Chemical Geology*, v. 214, no. 3, p. 287-308.

Dürr, S.B., 1996, Provenance of Xigaze fore-arc basin clastic rocks (Cretaceous, south Tibet): *Geological Society of America Bulletin*, v. 108, no. 6, p. 669-684.

Edwards, M.A. and Harrison, T.M., 1997, When did the roof collapse? Late Miocene north-south extension in the high Himalaya revealed by Th-Pb monazite dating of the Khula Kangri granite: *Geology*, v. 25, no. 6, p. 543-546.

- Edwards, M.A., Kidd, W.S., Li, J., Yue, Y., and Clark, M., 1996, Multi-stage development of the southern Tibet detachment system near Khula Kangri. New data from Gonto La: *Tectonophysics*, v. 260, no. 1-3, p. 1-19.
- Edwards, M.A., Pêcher, A., Kidd, W.S.F., Burchfiel, B. C., and Royden, L.H., 1999, Southern Tibet Detachment System at Khula Kangri, Eastern Himalaya: A Large-Area, Shallow Detachment Stretching into Bhutan?: *The Journal of geology*, v. 107, no. 5, p. 623-631.
- Einsele, G., et al., 1994, The Xigaze forearc basin: evolution and facies architecture (Cretaceous, Tibet): *Sedimentary Geology*, v. 90, no. 1, p. 1-32.
- England, P. and Houseman, G., 1986, Finite strain calculations of continental deformation 2. Comparison with the India-Asia collision zone, *Journal of Geophysical Research*, v. 91, p. 3664–3676.
- England, P. and Molnar, P., 1990, Right-lateral shear and rotation as the explanation for strike-slip faulting in eastern Tibet: *Nature*, v. 344, no. 6262, p. 140-142.
- Gansser, A., 1964, *Geology of the Himalayas*. New York: Wiley Interscience, p. 289.
- Gansser, A., 1983, *Geology of the Bhutan Himalaya*: Birkhauser, Basel, p. 181.
- Garzanti, E. and Van Haver, T., 1988, The Indus clastics: forearc basin sedimentation in the Ladakh Himalaya (India): *Sedimentary Geology*, v. 59, no. 3-4, p. 237-249.
- Gehrels, G., et al., 2011, Detrital zircon geochronology of pre-Tertiary strata in the Tibetan-Himalayan orogen: *Tectonics*, v. 30, no. 5.
- Girardeau, J., et al., 1984, Tectonic environment and geodynamic significance of the Neo-Cimmerian Dongqiao ophiolite, Bangong-Nujiang suture zone, Tibet: *Nature*, v. 307, p. 27-31.
- Goswami, T.K., 2008, Implications of geochemical signatures in the Trans-Himalayan Lohit batholith, Arunachal Pradesh, India: *Himalayan Journal of Sciences*, v. 5, no. 7, p. 53.

- Goswami, T.K., 2011, Collision induces deformation of the Trans Himalayan Lohit Batholith, Arunachal Pradesh, India: Memoir Geological Society of India, v. 77, v. 19-31.
- Goswami, T.K., 2013, Geodynamic significance of leucogranite intrusions in the Lohit batholith near Walong, eastern Arunachal Pradesh, India: Current Science, v. 104, no. 2, p. 229.
- Goswami, T.K., 2013, Subduction Related Magmatism: Constrains from the REE Pattern in the Lohit Batholith, Arunachal Pradesh, India. Geosciences, v. 3, no. 4, p. 128-141.
- Grujic, D., Casey, M., Davidson, C., Hollister, L. S., Kündig, R., Pavlis, T., and Schmid, S., 1996, Ductile extrusion of the Higher Himalayan Crystalline in Bhutan: evidence from quartz microfabrics. Tectonophysics, v. 260, no. 1, p. 21-43.
- Grujic, D., Hollister, L. S., and Parrish, R.R., 2002, Himalayan metamorphic sequence as an orogenic channel: insight from Bhutan: Earth and Planetary Science Letters, v. 198, no. 1, p. 177-191.
- Guan, Q., et al., 2012, Crustal thickening prior to 38 Ma in southern Tibet: evidence from lower crust-derived adakitic magmatism in the Gangdese Batholith. Gondwana Research, v. 21, no. 1, p. 88-99.
- Gupta, A.D. and Biswas, A.K., 2000, Geology of Assam: Geological Society of India Publications, v. 2, no. 1, p. 169.
- Gururajan, N.S. and Choudhuri, B.K., 2003, Geology and tectonic history of the Lohit valley, Eastern Arunachal Pradesh, India: Journal of Asian Earth Sciences, v. 21, no. 7, p. 731-741.
- Guynn, J., Kapp, P., Gehrels, G.E., Ding, L., 2012, U-Pb geochronology of basement rocks in central Tibet and paleogeographic implications: Journal of Asian Earth Sciences, v. 43, no. 1, p. 23-50.
- Haproff, P.J., Zuza, A.V., Yin, and A., 2018, West-directed thrusting south of the eastern

- Himalayan syntaxis indicates clockwise crustal flow at the indenter corner during the India-Asia collision: *Tectonophysics*, v. 722, p. 277-285.
- Haq, S.S.B. and Davis, D., 1997, Oblique convergence and the lobate mountain belts of western Pakistan: *Geology*, v. 25, no. 1, p. 23-26.
- Harrison, T.M. and Wielicki, M.M., 2016, From the Hadean to the Himalaya: 4.4 Ga of felsic terrestrial magmatism: *American Mineralogist*, v. 101, no. 6, p. 1348-1359.
- Harrison, T.M., Yin, A., Grove, M., Lovera, O. M., Ryerson, F. J., and Zhou, X., 2000, The Zedong Window: A record of superposed Tertiary convergence in southeastern Tibet: *Journal of Geophysical Research: Solid Earth*, v. 105, no. B8, p. 19211-19230.
- Hébert, R., Bezard, R., Guilmette, C., Dostal, J., Wang, C.S., and Liu, Z.F., 2012, The Indus-Yarlung Zangbo ophiolites from Nanga Parbat to Namche Barwa syntaxes, southern Tibet: First synthesis of petrology, geochemistry, and geochronology with incidences on geodynamic reconstructions of Neo-Tethys: *Gondwana Research*, v. 22, no. 2, p. 377-397.
- Heim, A. and Gansser, A., 1939, Central Himalaya. Hindustan Publishing; Delhi.
- Hodges, K.V., 2000, Tectonics of the Himalaya and southern Tibet from two perspectives: *Geological Society of America Bulletin*, v. 112, no. 3, p. 324-350.
- Honegger, K., Dietrich, V., Frank, W., Gansser, A., Thöni, M., and Trommsdorff, V., 1982, Magmatism and metamorphism in the Ladakh Himalayas (the Indus-Tsangpo suture zone): *Earth and Planetary Science Letters*, v. 60, no. 2, p. 253-292.
- Hsu, K. et al., 1995, Tectonic evolution of the Tibetan Plateau: a working hypothesis based on the archipelago model of orogenesis: *International Geology Review*, v. 37, p. 473–508.

Hu, X., Wang, J., Boudagher-Fadel, M., Garzanti, E., An, W., 2015, New insights into the timing of the India-Asia collision from the Paleogene Quxia and Jialazi Formations of the Xigaze Forearc Basin, South Tibet: *Gondwana Research*, v. 32, p. 76-92.

Huyghe, P., Galy, A., Mugnier, J.L., and France-Lanord, C., 2001, Propagation of the thrust system and erosion in the Lesser Himalaya: Geochemical and sedimentological evidence: *Geology*, v. 29, no. 11, p. 1007-1010.

Jangpangi, B.S., 1974, Stratigraphy and tectonics of parts of eastern Bhutan: *Himalayan Geology*, v. 4, p. 117-136.

Ji, W.Q., Wu, F.Y., Chung, S.L., Li, J.X., and Liu, C.Z., 2009, Zircon U-Pb geochronology and Hf isotopic constraints on petrogenesis of the Gangdese batholith, southern Tibet: *Chemical Geology*, v. 262, no. 3, p. 229-245.

Johnson, D.M., Hooper, P.R., Conrey, R.M., 1999. GeoAnalytical lab, Washington State University: *Advances in X-Ray Analysis*, v. 41, p. 843-867

Kapp, P., Murphy, M.A., Yin, A., Harrison, T.M., Ding, L., and Guo, J., 2003, Mesozoic and Cenozoic tectonic evolution of the Shiquanhe area of western Tibet: *Tectonics*, v. 22, no. 4.

Kistler, R.W. and Ross, D.C., 1990, A strontium isotopic study of plutons and associated rocks of the southern Sierra Nevada vicinity, California: (No. 1920): USGPO; Books and Open-File Reports Section, US Geological Survey.

Kumar, G., 1997, Geology of Arunachal Pradesh: Bangalore, Geological Society of India, p. 217.

Kumar, G., 1973, Geology of Arunachal Pradesh: Geological Society of India Publications.

Kylander-Clark, A.R., Hacker, B.R., Cottle, J.M., 2013. Laser-ablation split-stream ICP petrochronology: *Chemical Geology*, v. 345, p. 99-112.

- Laskowski, A.K., Kapp, P., Vervoort, J.D., and Ding, L., 2016, High-pressure Tethyan Himalaya rocks along the India-Asia suture zone in southern Tibet: *Lithosphere*, v. 8, no. 5, p. 574-582.
- Lavé, J. and Avouac, J.P., 2000, Active folding of fluvial terraces across the Siwaliks Hills, Himalayas of central Nepal: *Journal of Geophysical Research: Solid Earth*, v. 105, no. B3, p. 5735-5770.
- Le Bas, M.J., Le Maitre, R.W., Streckeisen, A. and Zanettin, B., 1986, A chemical classification of volcanic rocks based on the total alkali-silica diagram: *Journal of Petrology*, v. 27, no. 3, p. 745-750.
- Le Fort, P., 1975, Himalayas: the collided range. Present knowledge of the continental arc: *American Journal of Science*, v. 275, p. 1-44.
- Le Fort, P., 1996, Evolution of the Himalaya: *World and Regional Geology*, v. 1, no. 8, p. 95-109.
- Leary, R.J., DeCelles, P.G., Quade, J., Gehrels, G.E., and Waanders, G., 2016, The Liuqu Conglomerate, southern Tibet: Early Miocene basin development related to deformation within the Great Counter Thrust system: *Lithosphere*, v. 8, no. 5, p. 427-450.
- Lee, H.Y., Chung, S.L., Lo, C.H., Ji, J., Lee, T.Y., Qian, Q., and Zhang, Q., 2009, Eocene Neotethyan slab breakoff in southern Tibet inferred from the Linzizong volcanic record: *Tectonophysics*, v. 477, no. 1, p. 20-35.
- Lee, H.Y., Chung, S.L., and Yang, H.M., 2016, Late Cenozoic volcanism in central Myanmar: Geochemical characteristics and geodynamic significance: *Lithos*, v. 245, p. 174-190.
- Lin, T.H., Chung, S.L., Kumar, A., Wu, F.Y., Chiu, H.Y. and Lin, I., 2013, Linking a prolonged Neo-Tethyan magmatic arc in South Asia: Zircon U-Pb and Hf isotopic constraints from the Lohit Batholith, NE India: *Terra Nova*, v. 25, no. 6, p. 453-458.

Liu, D.L., Shi, R.D., Ding, L., Zou, H. B., 2018. Late Cretaceous transition from subduction to collision along the Bangong-Nujiang Tethys: New volcanic constraints from central Tibet: *Lithos*, v. 296, p. 452-470.

Long, S. and McQuarrie, N., 2010, Placing limits on channel flow: Insights from the Bhutan Himalaya: *Earth and Planetary Science Letters*, v. 290, no. 3, p. 375-390.

Long, S., McQuarrie, N., Tobgay, T., and Grujic, D., 2011, Geometry and crustal shortening of the Himalayan fold-thrust belt, eastern and central Bhutan: *Geological Society of America Bulletin*, p. B30203-1.

Long, S., McQuarrie, N., Tobgay, T., and Hawthorne, J., 2011, Quantifying internal strain and deformation temperature in the eastern Himalaya, Bhutan: Implications for the evolution of strain in thrust sheets: *Journal of Structural Geology*, v. 33, no. 4, p. 579-608.

Long, S., McQuarrie, N., Tobgay, T., Rose, C., Gehrels, G., and Grujic, D., 2011, Tectonostratigraphy of the Lesser Himalaya of Bhutan: Implications for the along-strike stratigraphic continuity of the northern Indian margin: *Geological Society of America Bulletin*: v. 123, no. 7-8, p. 1406-1426.

Malpas, J., Zhou, M.F., Robinson, P.T., and Reynolds, P.H., 2003, Geochemical and geochronological constraints on the origin and emplacement of the Yarlung Zangbo ophiolites, Southern Tibet: *Geological Society, London, Special Publications*, v. 218, no. 1, p. 191-206.

McDermid, I.R., Aitchison, J.C., Davis, A.M., Harrison, T.M., and Grove, M., 2002, The Zedong terrane: a Late Jurassic intra-oceanic magmatic arc within the Yarlung–Tsangpo suture zone, southeastern Tibet: *Chemical Geology*, v. 187, no. 3, p. 267-277.

McQuarrie, N., Robinson, D., Long, S., Tobgay, T., Grujic, D., Gehrels, G., and Ducea, M., 2008, Preliminary stratigraphic and structural architecture of Bhutan: Implications for the along strike architecture of the Himalayan system: *Earth and Planetary Science Letters*, v. 272, no. 1, p. 105-117.

Misra, D.K., 2009, Litho-tectonic sequence and their regional correlation along the Lohit and Dibang valleys, eastern Arunachal Pradesh. *Journal of the Geological Society of India*, v. 73, no. 2, p. 213-219.

Misra, D.K. and Singh, T., 2002, Tectonic setting and neotectonic features along the Eastern Syntaxis Bend (Lohit and Dibang), Arunachal Himalaya: Aspects of Geology and Environment of the Himalaya, p. 19-40.

Mitchell, A.H.G., 1993, Cretaceous–Cenozoic tectonic events in the western Myanmar (Burma)–Assam region: *Journal of the Geological Society*, v. 150, no. 6, p. 1089-1102.

Mitchell, A.H.G., Chung, S.L., Oo, T., Lin, T.H. and Hung, C.H., 2012, Zircon U–Pb ages in Myanmar: Magmatic–metamorphic events and the closure of a neo-Tethys ocean?: *Journal of Asian Earth Sciences*, v. 56, p. 1-23.

Nandini, P. and Thakur, S.S., 2011, Metamorphic evolution of the Lesser Himalayan Crystalline Sequence, Siyom Valley, NE Himalaya, India: *Journal of Asian Earth Sciences*, v. 40, no. 5, p. 1089-1100.

Nandy, D.R., 1973, Geology and structural lineaments of the Lohit Himalaya (Arunachal Pradesh) and adjoining area: Seminar on Geodynamics of the Himalayan Region, NGRI, Hyderabad, p. 167-172.

Ni, J.F., Guzman-Speziale, M., Bevis, M., Holt, W.E., Wallace, T.C., Seager, W.R., 1989: *Geology*, v. 17, no. 1, p. 68-71.

- Ningthoujam, P.S., Dubey, C.S., Lolee, L.K., Shukla, D.P., Naorem, S.S. and Singh, S.K., 2015, Tectonic studies and crustal shortening across Easternmost Arunachal Himalaya: Journal of Asian Earth Sciences, v. 111, p. 339-349.
- Orme, D.A., Carrapa, B., and Kapp, P., 2015, Sedimentology, provenance and geochronology of the Upper Cretaceous–Lower Eocene western Xigaze forearc basin, southern Tibet: Basin Research, v. 27, no. 4, p. 387-411.
- Parrish, R.R. and Hodges, V., 1996, Isotopic constraints on the age and provenance of the Lesser and Greater Himalayan sequences, Nepalese Himalaya: Geological Society of America Bulletin, v. 108, no. 7, p. 904-911.
- Pearce, J.A., 1982, Trace element characteristics of lavas from destructive plate boundaries: Andesites, v. 8, p. 525-548.
- Pearce, J.A., Harris, N.B., and Tindle, A.G., 1984, Trace element discrimination diagrams for the tectonic interpretation of granitic rocks: Journal of Petrology, v. 25, no. 4, p. 956-983.
- Quidelleur, X., Grove, M., Lovera, O.M., Harrison, T.M., and Yin, A., 1997, Thermal evolution and slip history of the Renbu-Zedong Thrust, southeastern Tibet: Journal of Geophysical Research, v. 102, p. 2659-2679.
- Richards, A., Parrish, R., Harris, N., Argles, T. and Zhang, L., 2006, Correlation of lithotectonic units across the eastern Himalaya, Bhutan: Geology, v. 34, no. 5, p. 341-344.
- Robinson, D.M., DeCelles, P.G., Patchett, P.J. and Garzione, C.N., 2001, The kinematic evolution of the Nepalese Himalaya interpreted from Nd isotopes: Earth and Planetary Science Letters, v. 192, no. 4, p. 507-521.
- Royden, L.H., et al., 1997, Surface deformation and lower crustal flow in eastern Tibet: Science, v. 276, p. 788-90.

- Sarma, K.P., Nandy, S., Devi, N.R., and Konwar, P., 2009, Is Mishmi Block a Tectonic Roof?
- Sarma, K.P., Nandy, S., and Mazumdar, N., 2012, Structural studies of the Mishmi block in parts of Dibang Valley of Arunachal Himalaya, Northeast India: International Journal of Geology, Earth and Environmental Sciences, v. 2, no. 3, p. 43-56.
- Schärer, U., Xu, R.H., and Allègre, C.J., 1984, U-Pb geochronology of Gangdese (Transhimalaya) plutonism in the Lhasa-Xigaze region, Tibet: Earth and Planetary Science Letters, v. 69, no. 2, p. 311-320.
- Schmitt, A.K., Grove, M., Harrison, T.M., Lovera, O., Hulen, J., Walters, M., 2003. The Geysers-Cobb Mountain Magma System, California (Part 1): U-Pb zircon ages of volcanic rocks, conditions of zircon crystallization and magma residence times: *Geochimica et Cosmochimica Acta*, v. 67, no. 18, p. 3423-3442.
- Schmitt, A. K., Grove, M., Harrison, T. M., Lovera, O., Hulen, J., Walters, M., 2003. The Geysers-Cobb Mountain Magma System, California (Part 2): timescales of pluton emplacement and implications for its thermal history: *Geochimica et Cosmochimica Acta*, v. 67, no. 18, p. 3443-3458.
- Sharma, K.K., Choubey, V.M. and Chatti, H.R., 1991, Geological setting of the ophiolites and magmatic arc of the Lohit Himalaya (Arunachal Pradesh), India with special reference to their petrochemistry: *Physics and Chemistry of the Earth*, v. 18, p. 277-292.
- Sharma, R., and Sarma, K.P., 2013, Microstructural study and strain history of Mesoproterozoic augen gneiss of Lohit District, Arunachal Himalaya, India: International Journal of Geology, Earth and Environment Sciences, v. 3, no. 2, p. 68-76.
- Singh, B., 1993, Geological set up of a part of the Ladakh Granitoid Complex, Ladakh Himalaya: *Journal of Himalayan Geology*, v. 4, no. 1, p. 57-62.

- Singh, S. and Chowdhury, P.K., 1990, An outline of the geological framework of the Arunachal Himalaya: *Journal of Himalayan Geology*, v. 1, no. 2, p. 189-197.
- Shervais, J.W., 1982, Ti-V plots and the petrogenesis of modern and ophiolitic lavas: *Earth and Planetary Science Letters*, v. 59, no. 1, p. 101-118.
- Srivastava, P., Mitra, G., 1994. Thrust geometries and deep structure of the outer and lesser Himalaya, Kumaon and Garhwal (India): Implications for evolution of the Himalayan fold-and-thrust belt: *Tectonics*, v. 13, no. 1, p. 89-109.
- Srivastava, R.K. and Sinha, A.K., 2004, Geochemistry of Early Cretaceous alkaline ultramafic-mafic complex from Jasra, Karbi Anglong, Shillong plateau, northeastern India: *Gondwana Research*, v. 7, no. 2, p. 549-561.
- Srivastava, R.K. and Sinha, A.K., 2004, Early Cretaceous Sung Valley ultramafic-alkaline-carbonatite complex, Shillong Plateau, Northeastern India: petrological and genetic significance: *Mineralogy and Petrology*, v. 80, no. 3, p. 241-263.
- Srivastava, R.K., Heaman, L.M., Sinha, A.K. and Shihua, S., 2005, Emplacement age and isotope geochemistry of Sung Valley alkaline–carbonatite complex, Shillong Plateau, northeastern India: implications for primary carbonate melt and genesis of the associated silicate rocks: *Lithos*, v. 81, no. 1, p. 33-54.
- Swapp, S.M. and Hollister, L.S., 1991, Inverted metamorphism within the Tibetan slab of Bhutan: Evidence for a tectonically transported heat-source: *Canadian Mineralogist*, v. 29, no. 4, p. 1019-1041.
- Tapponnier, P., Peltzer, G., Le Dain, A.Y., Armijo, R., and Cobbold, P. 1982, Propagating extrusion tectonics in Asia: new insights from simple experiments with plasticine: *Geology*, v. 10, p. 611–616.

Tapponnier, P., Mattauer, M., Proust, F., and Cassaigneau, C., 1981, Mesozoic ophiolites, sutures, and large-scale tectonic movements in Afghanistan: Earth and Planetary Science Letters, v. 52, no. 2, p. 355-371.

Tapponnier, P., Zhiqin, X., Roger, F., Meyer, B., Arnaud, N., Wittlinger, G., and Jingsui, Y., 2001, Oblique stepwise rise and growth of the Tibet Plateau. Science, v. 294, no. 5547, p. 1671-1677.

Tewari, V.C., Lokho, K., Kumar, K. and Siddaiah, N.S., 2010, Late Cretaceous-Paleogene basin architecture and evolution of the Shillong shelf sedimentation, Meghalaya, Northeast India: Journal of the Indian Geological Congress v. 2, no. 2, p. 61-73.

Thakur, V.C. and Jain, A.K., 1975, Some observations of deformation and metamorphism in the rocks of some parts of Mishmi Hills, Lohit district, (NEFA), Arunachal Pradesh: Himalayan Geology, v. 5, p. 339-364.

Tobgay, T., McQuarrie, N., Long, S., Kohn, M.J., and Corrie, S.L., 2012, The age and rate of displacement along the Main Central Thrust in the western Bhutan Himalaya: Earth and Planetary Science Letters, v. 319, p. 146-158.

Wadia, D.N., 1931, The syntaxis of the northwest Himalaya: its rocks, tectonics and orogeny: Rec. Geological Survey of India, v. 65, no. 2, p. 189-220.

Wang, C., Ding, L., Zhang, L. Y., Kapp, P., Pullen, A., and Yue, Y.H., 2016, Petrogenesis of Middle-Late Triassic volcanic rocks from the Gangdese belt, southern Lhasa terrane: Implications for early subduction of Neo-Tethyan oceanic lithosphere: Lithos, v. 262, p. 320-333.

- Wang, C., Li, X., Liu, Z., Li, Y., Jansa, L., Dai, J., and Wei, Y., 2012, Revision of the Cretaceous–Paleogene stratigraphic framework, facies architecture and provenance of the Xigaze forearc basin along the Yarlung Zangbo suture zone: *Gondwana Research*, v. 22, no. 2, p. 415-433.
- Wang, Y., Zhang, L., Cawood, P.A., Ma, L., Fan, W., Zhang, A., Zhang, Y. and Bi, X., 2014, Eocene supra-subduction zone mafic magmatism in the Sibumasu Block of SW Yunnan: Implications for Neotethyan subduction and India–Asia collision: *Lithos*, v. 206, p. 384-399.
- Webb, A.A.G., 2013. Preliminary balanced palinspastic reconstruction of Cenozoic deformation across the Himachal Himalaya (northwestern India): *Geosphere*, v. 9, no. 3, p. 572-587.
- Webb, A.A.G., Yin, A. and Dubey, C.S., 2013, U-Pb zircon geochronology of major lithologic units in the eastern Himalaya: Implications for the origin and assembly of Himalayan rocks: *Geological Society of America Bulletin*, v. 125, no. 3-4, p. 499-522.
- Webb, A. A. G., et al., 2017, The Himalaya in 3D: Slab dynamics controlled mountain building and monsoon intensification: *Lithosphere*, v. L636-1.
- Wen, D.R., et al., 2008, Zircon SHRIMP U–Pb ages of the Gangdese Batholith and implications for Neotethyan subduction in southern Tibet: *Chemical Geology*, v. 252, no. 3, p. 191-201.
- Whalen, J.B., Currie, K.L. and Chappell, B.W., 1987, A-type granites: geochemical characteristics, discrimination and petrogenesis: *Contributions to Mineralogy and Petrology*, v. 95, no. 4, p. 407-419.
- Williams, H., Turner, S., Kelley, S., Harris, N., 2001, Age and composition of dikes in Southern Tibet: New constraints on the timing of east-west extension and its relationship to postcollisional volcanism: *Geology*, v. 29, no. 4, p. 339-342.
- Wu, C., et al., 1998, Yadong cross structure and South Tibetan Detachment in the east central Himalaya (89-90): *Tectonics*, v. 17, no. 1, p. 28-45.

Xu, W.C., Zhang, H.F., Harris, N., Guo, L., Pan, F.B., and Wang, S., 2013, Geochronology and geochemistry of Mesoproterozoic granitoids in the Lhasa terrane, south Tibet: implications for the early evolution of Lhasa terrane: *Precambrian Research*, v. 236, p. 46-58.

Yin, A., 2006, Cenozoic tectonic evolution of the Himalayan orogen as constrained by along-strike variation of structural geometry, exhumation history, and foreland sedimentation: *Earth-Science Reviews*, v. 76, no. 1, p. 1-131.

Yin, A., 2010, Cenozoic tectonic evolution of Asia: A preliminary synthesis: *Tectonophysics*, v. 488, no. 1, p. 293-325.

Yin, A., et al., 1999, Tertiary deformation history of southeastern and southwestern Tibet during the Indo-Asian collision: *Geological Society of America Bulletin*, v. 111, no. 11, p. 1644-1664.

Yin, A., Dubey, C.S., Webb, A.A.G., Kelty, T.K., Grove, M., Gehrels, G.E. and Burgess, W.P., 2010, Geologic correlation of the Himalayan orogen and Indian craton: Part 1. Structural geology, U-Pb zircon geochronology, and tectonic evolution of the Shillong Plateau and its neighboring regions in NE India: *Geological Society of America Bulletin*, v. 122, no. 3-4, p. 336-359.

Yin, A., Dubey, C.S., Kelty, T.K., Gehrels, G.E., Chou, C.Y., Grove, M., and Lovera, O., 2006, Structural evolution of the Arunachal Himalaya and implications for asymmetric development of the Himalayan orogen: *Current Science*, v. 90, no. 2, p. 195-200.

Yin, A., Dubey, C.S., Kelty, T.K., Webb, A.A.G., Harrison, T.M., Chou, C.Y. and Célérier, J., 2010, Geologic correlation of the Himalayan orogen and Indian craton: Part 2. Structural geology, geochronology, and tectonic evolution of the Eastern Himalaya: *Geological Society of America Bulletin*, p. B26461-1.

- Yin, A. and Harrison, T.M., 2000, Geologic Evolution of the Himalayan-Tibetan Orogen: Annual Review of Earth and Planetary Sciences, v. 28, p. 211-280.
- Yin, A., Harrison, T.M., Ryerson, F.J., Wenji, C., Kidd, W.S.F. and Copeland, P., 1994, Tertiary structural evolution of the Gangdese thrust system, southeastern Tibet: Journal of Geophysical Research: Solid Earth, v. 99, no. B9, p. 18175-18201.
- Zeiger, K., Gordon, S.M., Long, S.P., Kylander-Clark, A.R.C., Agustsson, K., and Penfold, M., 2015, Timing and conditions of metamorphism and melt crystallization in Greater Himalayan rocks, eastern and central Bhutan: insight from U–Pb zircon and monazite geochronology and trace-element analyses: Contributions to Mineralogy and Petrology, v. 169, no. 5, p. 1-19.
- Zeng, L., Gao, L.E., Xie, K., Liu-Zeng, J., 2011, Mid-Eocene high Sr/Y granites in the Northern Himalayan Gneiss Domes: melting thickened lower continental crust: Earth and Planetary Science Letters, v. 303, no. 3, p. 251-266.
- Zhang, X., et al., 2014, Early Jurassic high-pressure metamorphism of the Amdo terrane, Tibet: Constraints from zircon U–Pb geochronology of mafic granulites: Gondwana Research, v. 26, no. 3, p. 975-985.
- Zhou, M.F., Robinson, P.T., Malpas, J., Edwards, S.J., and Qi, L., 2005, REE and PGE geochemical constraints on the formation of dunites in the Luobusa ophiolite, Southern Tibet: Journal of Petrology, v. 46, no. 3, p. 615-639.
- Zhu, D.C., et al., 2009, Early cretaceous subduction-related adakite-like rocks of the Gangdese Belt, southern Tibet: Products of slab melting and subsequent melt–peridotite interaction?: Journal of Asian Earth Sciences, v. 34, no. 3, p. 298-309.

Zhu, D.C., et al., 2012, Cambrian bimodal volcanism in the Lhasa Terrane, southern Tibet: record of an early Paleozoic Andean-type magmatic arc in the Australian proto-Tethyan margin: *Chemical Geology*, v. 328, p. 290-308.

Zhu, D.C., Chung, S.L., Mo, X.X., Zhao, Z.D., Niu, Y., Song, B., and Yang, Y.H., 2009, The 132 Ma Comei-Bunbury large igneous province: Remnants identified in present-day southeastern Tibet and southwestern Australia: *Geology*, v. 37, no. 7, p. 583-586.

Zhu, D.C., Pan, G.T., Chung, S.L., Liao, Z.L., Wang, L.Q., and Li, G.M., 2008, SHRIMP zircon age and geochemical constraints on the origin of Lower Jurassic volcanic rocks from the Yeba Formation, southern Gangdese, South Tibet: *International Geology Review*, v. 50, no. 5, p. 442-471.

Zhu, D.C., Zhao, Z.D., Niu, Y., Dilek, Y., and Mo, X.X., 2011, Lhasa terrane in southern Tibet came from Australia: *Geology*, v. 39, no. 8, p. 727-730.

Ziabrev, S., Aitchison, J., Abrajevitch, A., Davis, A., and Luo, H., 2003, Precise radiolarian age constraints on the timing of ophiolite generation and sedimentation in the Dazhuqu terrane, Yarlung–Tsangpo suture zone, Tibet: *Journal of the Geological Society*, v. 160, no. 4, p. 591-599.

-Chapter 3-

West-directed thrusting south of the eastern Himalayan syntaxis indicates clockwise crustal flow at the indenter corner during the India-Asia collision



West-directed thrusting south of the eastern Himalayan syntaxis indicates clockwise crustal flow at the indenter corner during the India-Asia collision



Peter J. Hapgood^{a,*}, Andrew V. Zupa^{a,b}, An Yin^a

^a Department of Earth, Planetary, and Space Sciences, University of California, Los Angeles, CA 90095-156702, USA

^b Nevada Bureau of Mines and Geology, University of Nevada, Reno, NV 89557, USA

ARTICLE INFO

Keywords:
Himalaya
Tibet
Eastern Himalayan syntaxis
Extrusion tectonics
Crustal flow
Thrust tectonics

ABSTRACT

Whether continental deformation is accommodated by microplate motion or continuum flow is a central issue regarding the nature of Cenozoic deformation surrounding the eastern Himalayan syntaxis. The microplate model predicts southeastward extrusion of rigid blocks along widely-spaced strike-slip faults, whereas the crustal-flow model requires clockwise crustal rotation along closely-spaced, semi-circular right-slip faults around the eastern Himalayan syntaxis. Although global positioning system (GPS) data support the crustal-flow model, the surface velocity field provides no information on the evolution of the India-Asia orogenic system at million-year scales. In this work, we present the results of systematic geologic mapping across the northernmost segment of the Indo-Burma Ranges, located directly southeast of the eastern Himalayan syntaxis. Early research inferred the area to have experienced either right-slip faulting accommodating northward indentation of India or thrusting due to the eastward continuation of the Himalayan orogen in the Cenozoic. Our mapping supports the presence of dip-slip thrust faults, rather than strike-slip faults. Specifically, the northern Indo-Burma Ranges exposes south- to west-directed ductile thrust shear zones in the hinterland and brittle fault zones in the foreland. The trends of ductile stretching lineations within thrust shear zones and thrust sheets rotate clockwise from the northeast direction in the northern part of the study area to the east direction in the southern part of the study area. This clockwise deflection pattern of lineations around the eastern Himalayan syntaxis mirrors the clockwise crustal-rotation pattern as suggested by the crustal-flow model and contemporary GPS velocity field. However, our finding is inconsistent with discrete strike-slip deformation in the area and the microplate model.

1. Introduction

Fundamental questions in studies of continental tectonics are whether continental deformation is accommodated by the interaction of microplate motion (McKenzie, 1972; Avouac and Tapponnier, 1993) or continuum flow (England and McKenzie, 1982; England and Houseman, 1986) and how this interaction might have impacted regional topographic evolution and climate changes (e.g., Ding et al., 2014, 2017). The question of how the continental lithosphere deforms is manifested in the ongoing debate about the nature of Cenozoic tectonic deformation across Southeast Asia surrounding the eastern Himalayan syntaxis (Fig. 1). The microplate model predicts south-eastward translation of rigid blocks such as Indochina along relatively linear conjugate strike-slip faults (Tapponnier et al., 1986; Leloup et al., 2001; Akciz et al., 2008), whereas the crustal-flow model requires the development of closely spaced, semi-circular, thrust and right-slip faults surrounding the eastern Himalayan syntaxis to accommodate clockwise crustal rotation (Cobbold and Davy, 1988; Royden et al., 1997; Wang

et al., 1998). Although the results of several global positioning system (GPS) velocity-field studies (Zhang et al., 2004; Gan et al., 2007; Maurin et al., 2010) and modeling efforts (e.g., Chang et al., 2015) support the crustal flow model, the surface velocity field provides no information on the long-term tectonic development of the India-Asia collision zone. For example, it is possible that microplate motion as expressed by extrusion tectonics occurred first followed by crustal flow around the eastern Himalayan syntaxis (e.g., Kornfeld et al., 2014). Such a two-phase scenario would require early formation of widely spaced, linear strike-slip faulting that was followed by younger closely-spaced and curved strike-slip faults (e.g., Wang and Burchfiel, 1997; Royden et al., 1997).

A key test of these two competing models is whether upper plate continental deformation directly south of the eastern Himalayan syntaxis across the northernmost Indo-Burma Ranges is accommodated by right-slip faulting (Fig. 2A) (Mitchell, 1993) or west-directed thrusting (Fig. 2B) (Gururajan and Choudhuri, 2003; Misra, 2009). In this study, we present the results of systematic geologic mapping in this key area

* Corresponding author.

E-mail addresses: peterhapgood@ucla.edu, peterhapgood@gmail.com (P.J. Hapgood).

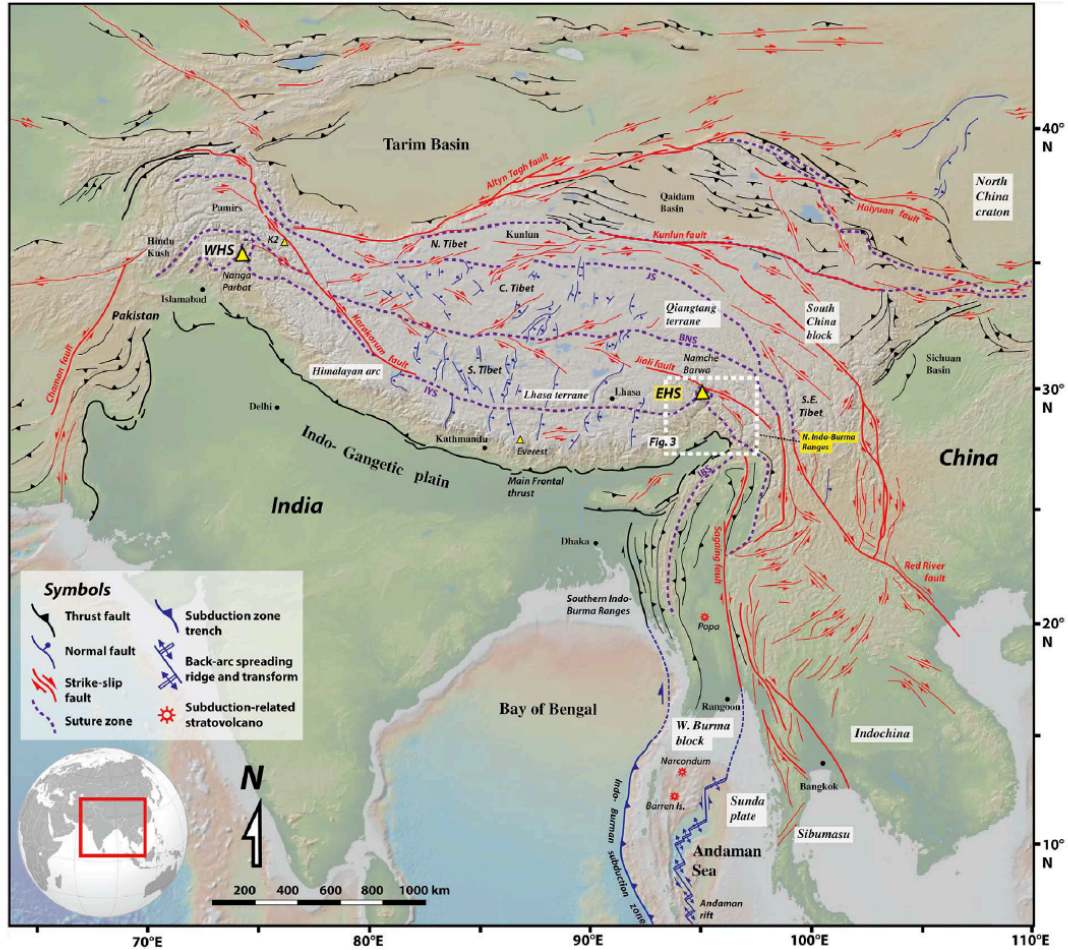
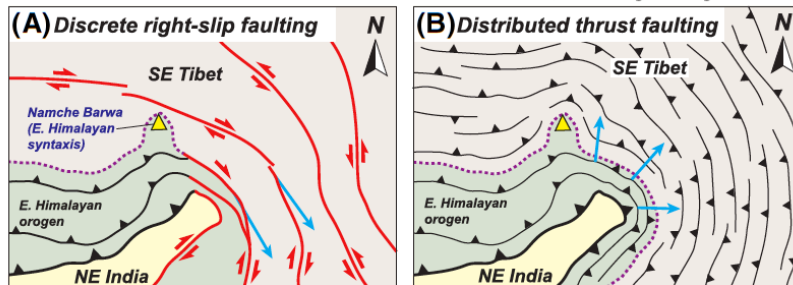


Fig. 1. Tectonic map of the Indo-Asian collision zone modified from Taylor and Yin (2009). The northern Indo-Burma Ranges are shown within the white box (Fig. 3). The digital elevation map was acquired using geomapapp.com (Ryan et al., 2009). The Earth index map was acquired through Generic Mapping Tools (gmt.soest.hawaii.edu). Abbreviations: BNS: Bangong-Nujiang suture, EHS: eastern Himalayan syntaxis, IYS: Indus-Yarlung suture, JS: Jinsha suture, WHS: western Himalayan syntaxis.

Models of deformation around the eastern Himalayan syntaxis



(Figs. 1 and 3). Our work shows that the dominant structures across a ~100-km wide deformation zone are southwest-directed thrusts that have accommodated > 10's km of crustal shortening during the Cenozoic. This finding is consistent with the continuum flow models of England and Houseman (1986), Cobbold and Davy (1988), and Royden et al. (1997) that predict that the overriding Asian plate during the India-Asia collision is highly mobile and capable of flowing along the

maximum gradient of the gravitational potential energy stored in the thickened Tibetan lithosphere. To focus on the results of our geologic mapping, we provide only a general overview of the lithologic descriptions and timing constraints for the rock units and deformation events, as these materials will be presented in separate papers.

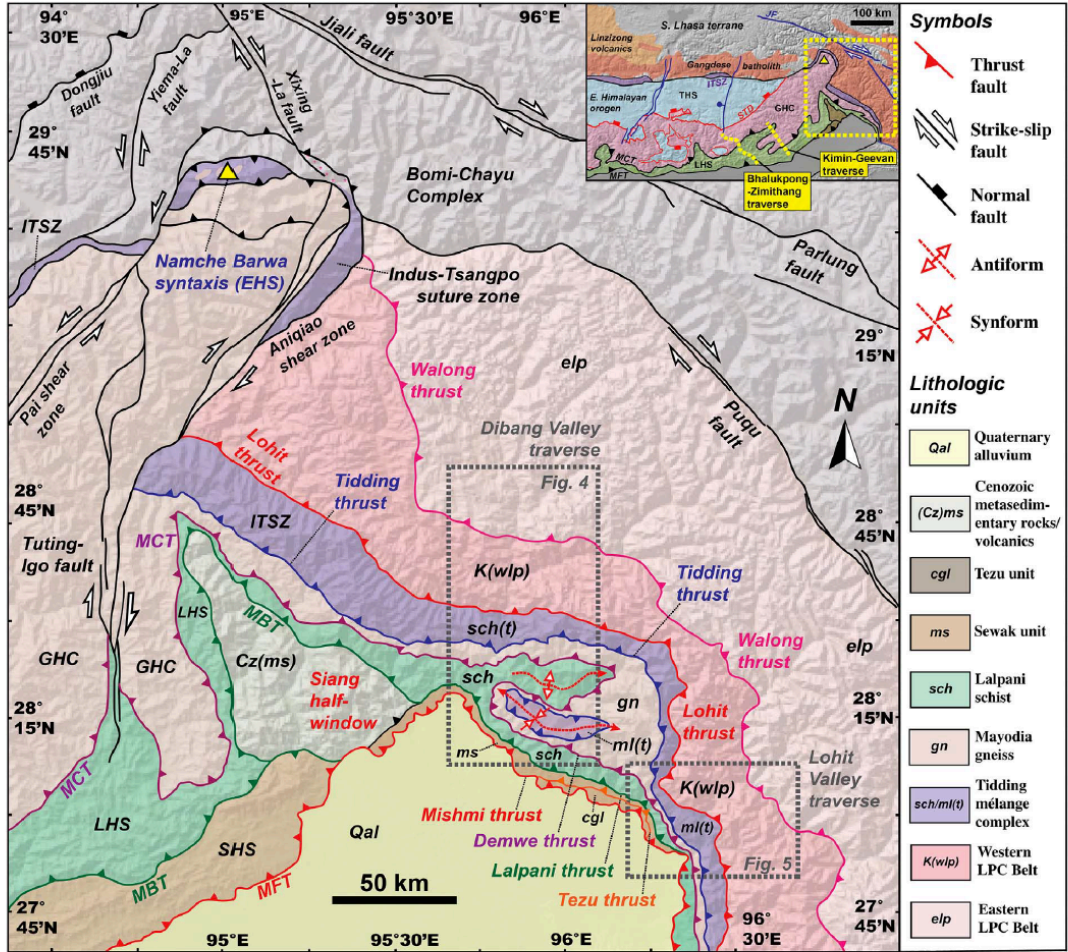


Fig. 3. Geologic map of the easternmost Himalaya and the northern Indo-Burma Ranges compiled from our mapping and that of Ding et al. (2001). Locations of the Dibang Valley (Fig. 4) and Lohit Valley (Fig. 5) traverses are shown in gray boxes. Locations of the Bhalukpong-Zimithang and Kimin-Geevan traverses of Yin et al. (2010a) across the easternmost Himalaya are shown as yellow dashed lines. Index geologic map of the eastern Himalayan orogen is adapted from Webb et al. (2017). Abbreviations: GHC: Greater Himalayan Crystalline complex, ITSZ: Indus-Tsangpo suture zone, JS: Jiali fault, LHS: Lesser Himalayan sequence, MFT: Main Frontal thrust, STD: South Tibetan detachment, and THS: Tethyan Himalayan sequence.

2. Structural geology of the Northern Indo-Burma ranges

The north-trending Indo-Burma Ranges and Central Burma Basin, extending southward from the eastern Himalayan syntaxis to the Andaman Sea, has a linear eastern edge along the right-slip Sagaing fault and a westward convex margin that truncates the west-trending Shillong plateau (Fig. 1) (Mitchell, 1993; Tapponnier et al., 2001; Acharyya, 2010; Yin, 2010). Our study area is located at the northernmost segment of the Indo-Burma Ranges where structures trend northwest, perpendicular to the northeast trend of the eastern Himalayan arc (Figs. 1 and 3). The area exposes drastically different lithologic units, including metasedimentary rocks, mélange complexes, and plutonic rocks, that are bounded by northwest-striking faults (Mitchell, 1993; Gururajan and Choudhuri, 2003; Misra, 2009; Acharyya, 2010). Due to the lack of detailed kinematic studies, the faults in the area have been interpreted as either strike-slip faults accommodating 100's km of northward indentation of India (e.g., Mitchell, 1993), or northeast-dipping thrusts that are laterally correlative to those of the Himalayan orogen (e.g., the Main Central Thrust) (Gururajan and Choudhuri, 2003; Misra, 2009). To resolve this key issue, we conducted detailed geologic mapping along two deeply-incised river valleys: the north

trending Dibang and east trending Lohit Valleys, respectively (Fig. 3). Our work refines the early established tectonostratigraphic framework of previous researchers and provides new constraints on the geometry and kinematics of the major faults in the area.

A total of seven major north- to northeast-dipping thrusts are mapped in the study area (Figs. 3–5). As described below, the strike and slip directions of faults change systematically across the study area: east-striking faults with down-dip stretching lineations occur in the southern region of the study area, whereas northwest-striking faults with down-dip stretching lineations are observed in the northern region of the study area. Structures are shown in cross sections in Fig. 6. The northernmost structure in the map area is the north-dipping Walong thrust of Gururajan and Choudhuri (2003), which places the eastern belt of the Lohit Plutonic Complex (foliated diorite, garnet orthogneiss, migmatite, and marble bands) over the western belt (dominantly foliated Cretaceous diorite suite rocks) (Figs. 4 and 5). The Lohit Plutonic Complex is the eastern extension of the Gangdese batholith in southern Tibet directly north of the Himalaya (Yin and Harrison, 2000; Lin et al., 2013). Along the Dibang Valley traverse (Fig. 4), the Walong thrust is east-striking and north-dipping, placing migmatitic orthogneiss over a foliated diorite intrusive complex that yielded a crystallization age of

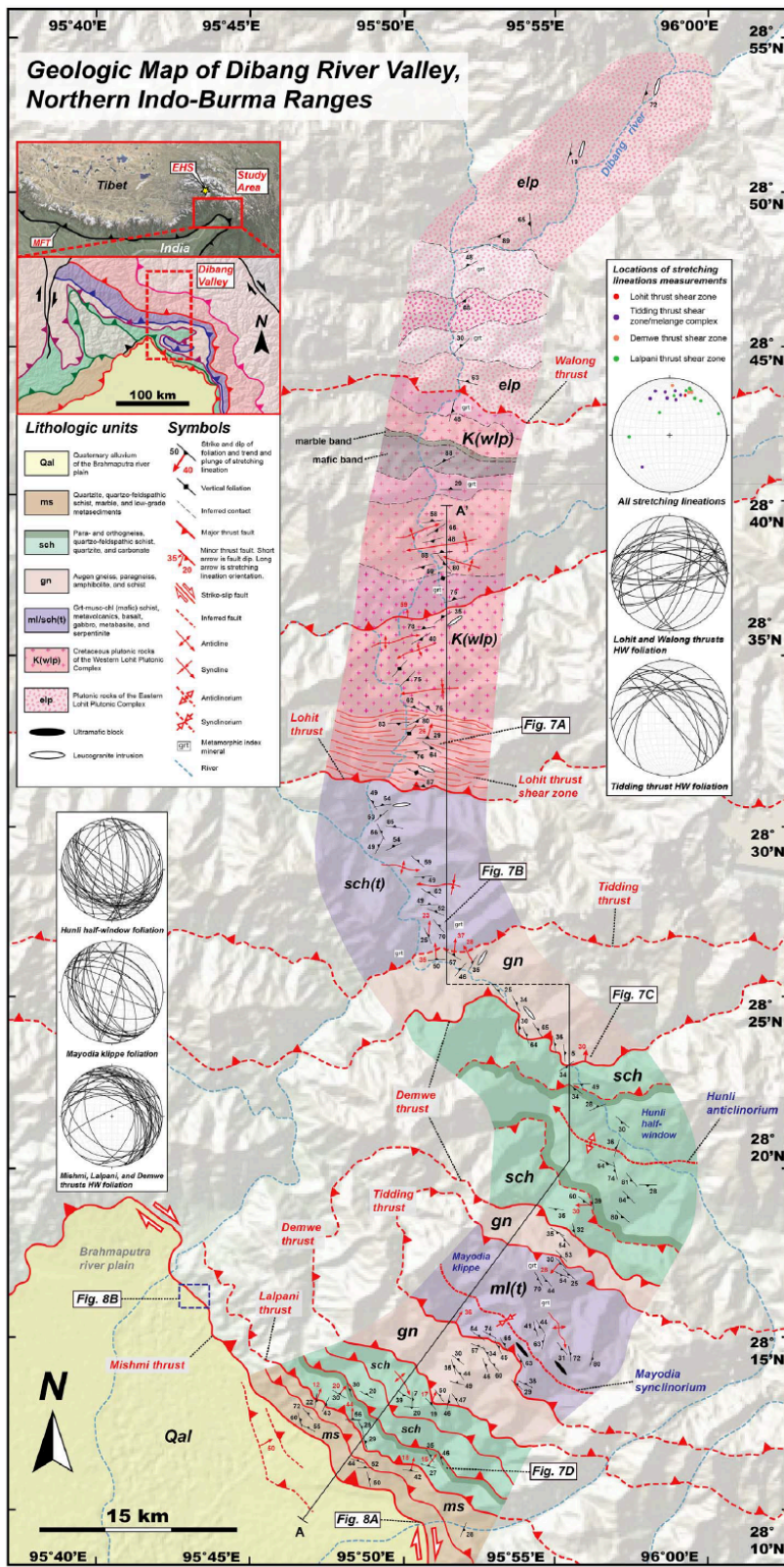


Fig. 4. Geologic map of the Dibang Valley traverse. Abbreviations: EHS: eastern Himalayan syntaxis, HW: hanging wall, MFT: Main Frontal thrust.

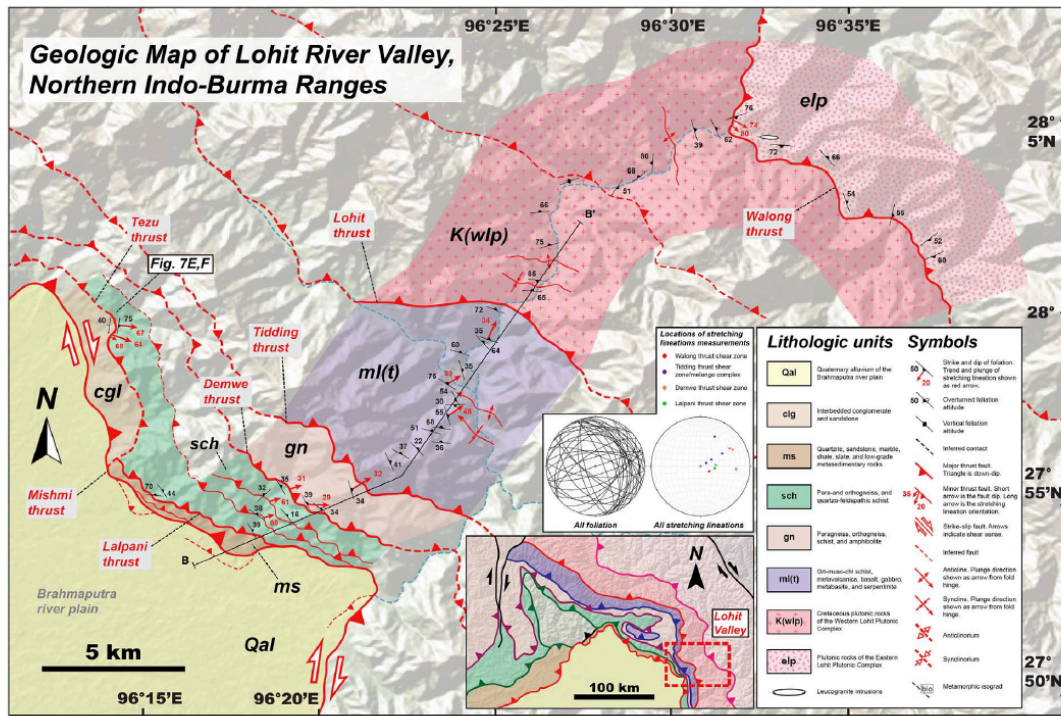


Fig. 5. Geologic map of the Lohit Valley traverse.

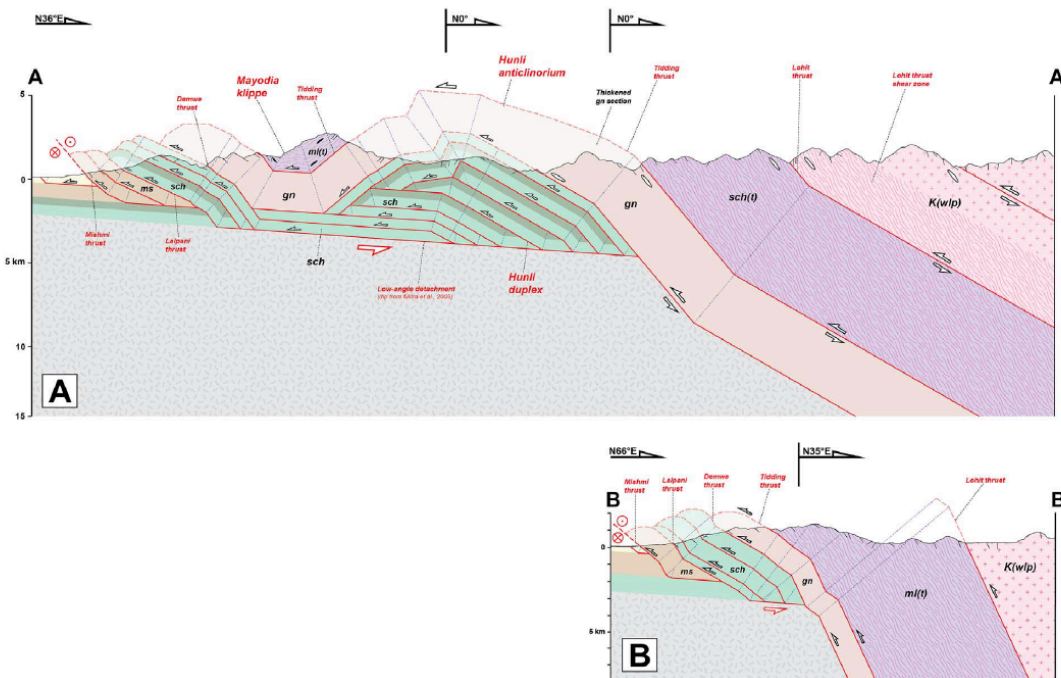


Fig. 6. Cross sections for the (A) Dibang Valley traverse, oriented SW-NE (A-A'), and (B) Lohit Valley traverse, oriented SW-NE (B-B'). See Figs. 4 and 5 for unit descriptions.

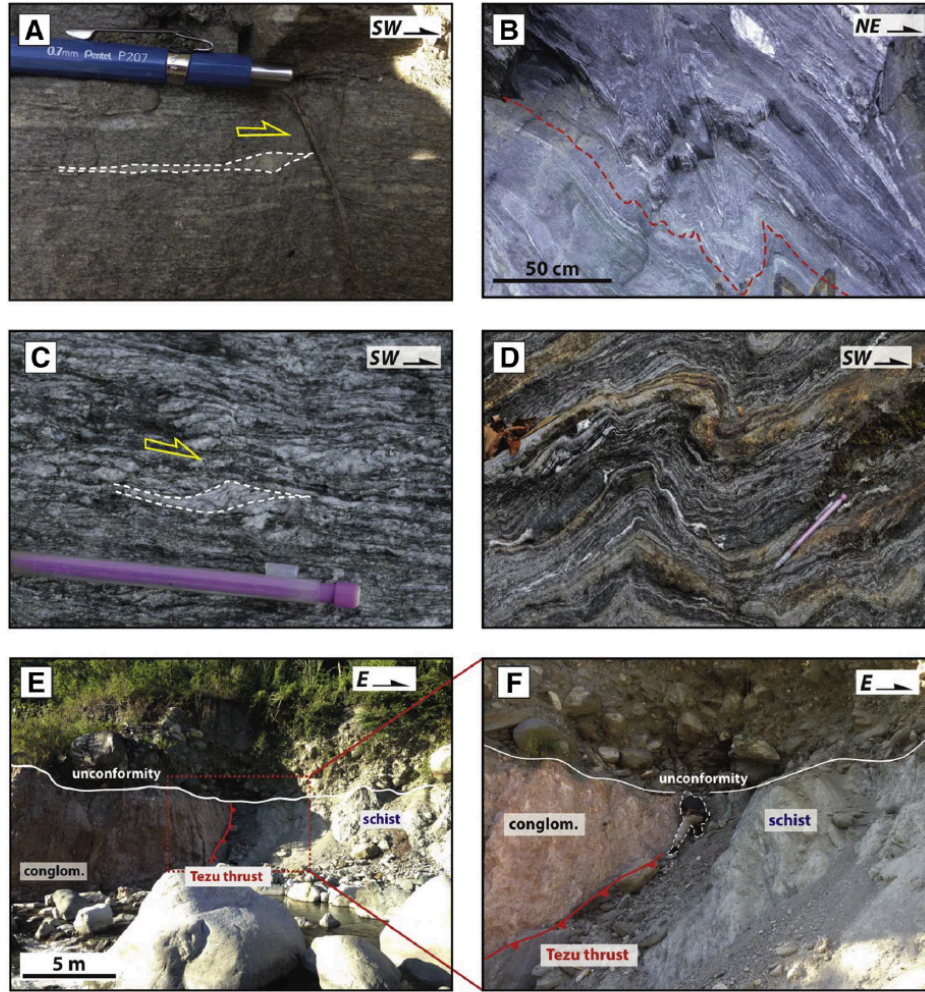


Fig. 7. Outcrop photographs of ductile fabrics within and adjacent to the major thrust shear zones. (A) Foliated diorite displaying asymmetric porphyroclasts indicating top-south shear in the Lohit thrust zone. (B) Chlorite schist containing south-verging tight asymmetric folds within the Tidding thrust shear zone. (C) Augen gneiss displaying asymmetric porphyroclasts and S-C fabric indicating top-southwest shear within the Demwe thrust shear zone. (D) Southwest-verging asymmetric folds in the Lalpani thrust shear zone. (E) and (F) Field relationship of the Tezu thrust placing schist atop conglomerate (conglom.) beds.

~100 Ma (Lin et al., 2013). Along the Lohit traverse, the fault is expressed as a 1-km thick mylonitic shear zone featuring steeply-plunging ($> 70^\circ$), east-trending stretching lineations (Figs. 4 and 5). S-C fabrics and asymmetric porphyroclasts are well developed in the Walong thrust zone and indicate a top-south sense of shear.

The generally east-striking and north-dipping Lohit thrust of Gururajan and Choudhuri (2003) lies structurally below the Walong thrust (Figs. 4 and 5). This structure places the Lohit Plutonic Complex atop the Tidding mélange complex, which represents the southward continuation of the Indus-Yarlung suture zone in the Indo-Burma Ranges separating Asia in the northeast from India in the southwest (Mitchell, 1993; Yin and Harrison, 2000; Ding et al., 2001; Acharyya, 2010). The Lohit thrust is expressed as a mylonitic shear zone within which foliation is tightly folded with steep dips of 60–80°. Stretching lineations trend to the northeast along both Dibang and Lohit Valleys (Figs. 4 and 5). Asymmetric σ and S-C porphyroclasts and S-C fabric indicate top-southwest shear sense (Fig. 7A). Meter-scale leucogranites are also ductily deformed within the Lohit thrust shear zone. The terminations of both the Lohit and Walong thrusts at the left-slip Aniqiao shear zone to the northwest of the study area was mapped from satellite

imagery and digital elevation models.

The Tidding mélange complex in the footwall of the Lohit thrust consists of garnet-chlorite schist, metabasite, chert, amphibolite, gabbro, and serpentinized ultramafic rocks. The mélange complex is bounded below by the Tidding thrust with its root zone mapped by Gururajan and Choudhuri (2003) (Figs. 4 and 5). The frontal portion of the Tidding thrust sheet is recognized in our mapping, which is expressed as a flat-lying, mélange-bearing klippe due to folding of the Tidding thrust (Figs. 3 and 4). The ultramafic rocks in the klippe were originally interpreted as the location of the Indus-Tsangpo suture zone (Mitchell, 1993; Acharyya, 2010), but the rootless nature of this lithologic unit and its correlation with the Tidding mélange complex exposed in the root zone of the Tidding thrust reject this early hypothesis. The Tidding thrust in the root zone is characterized by a ~1-km-thick mylonitic shear zone with kinematic indicators such as S-C fabrics, asymmetric folds, and rotated porphyroclasts all indicate a top-south sense of shear (Fig. 7B). Stretching lineations within the Tidding thrust shear zone and throughout the Tidding mélange complex trend to the north along Dibang Valley and northeast along Lohit Valley (Figs. 4 and 5). Similar to the structurally higher Lohit thrust zone, meter-scale

leucogranites are involved in the ductile deformation along the Tidding thrust zone.

The north-dipping Demwe thrust is a km-scale ductile shear zone juxtaposing the hanging wall unit of paragneiss, augen gneiss, and quartzo-feldspathic schist against the footwall unit of mostly of lower grade schist. Kinematic indicators show a top-south sense of shear (Fig. 7C). Like the overlying Tidding thrust, the Demwe thrust is also folded, which is expressed by an antiform in the north and synform in the south (Fig. 4). The width of the folded thrust sheet is ~20 km in the thrust-transport direction, which constrains its minimum magnitude of slip. Note that the fault trace strikes nearly east-west along the northernmost exposure but the strike changes to a northwest direction along the southernmost exposure (Fig. 4). Stretching lineations trend to the northeast along Dibang Valley and east along Lohit Valley (Figs. 4 and 5).

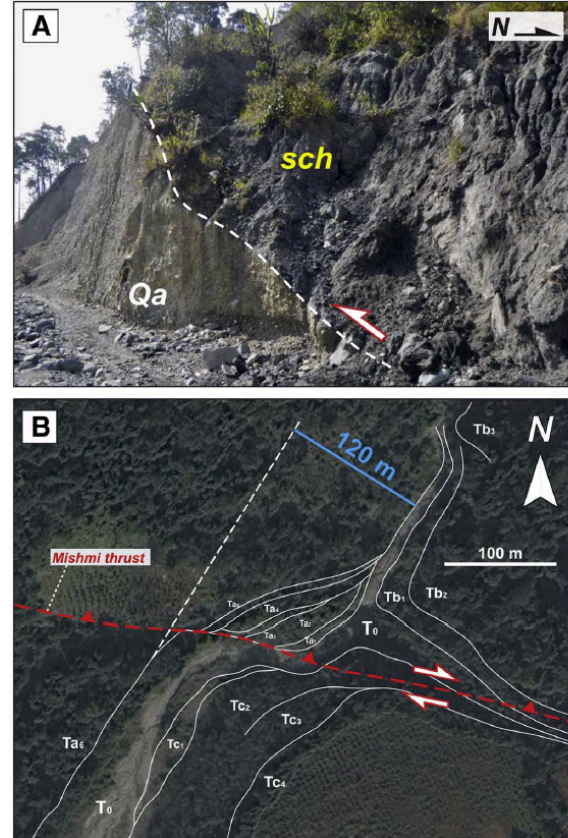
The northeast-dipping Lalpani thrust of Misra (2009) is expressed as a km-thick shear zone juxtaposing schist in the hanging wall over dominantly phyllite, quartzite, and schist in the footwall. Well-developed mylonitic foliation and north- to northeast-trending stretching lineations are present directly above and below the thrust contact. Stretching lineations within the Lalpani thrust shear zone trend to the north along Dibang Valley and to the east along Lohit Valley (Figs. 4 and 5). Kinematic indicators associated with the mylonitic fabrics, including asymmetric porphyroclasts, asymmetric folds, and S-C fabric indicate top-south to southwest shear (Fig. 7D). The Lalpani thrust and the shear zones at the higher structural levels is that it dips at a much shallower angle of 10–20° rather than mostly >60° to the north and northeast. In cross section, the Lalpani thrust merges with an inferred décollement at ~3 km depth along both the Dibang (Fig. 6A) and Lohit Valley traverses (Fig. 6B) (Mitra et al., 2005).

The east-dipping Tezu thrust, which is only recognized along the Lohit traverse, strikes north and displays down-dip striae (Fig. 5). The fault is expressed by a meter-thick cataclastic shear zone that juxtaposes metasediments in the hanging wall over a sequence of Tertiary (?) conglomerate and sandstone. The footwall unit is referred here to as the Tezu unit that may be correlative to the Neogene Siwalik Group in the Himalayan foreland basin (Yin, 2006), as the clasts in the conglomerate beds are clearly derived from the nearby thrust sheets mapped in this study. Foliated fault gouge materials in the shear zone display cleavage-defined S-C fabric, which indicate top-west shear (Fig. 7E and F).

The northeast-dipping, range-bounding Mishmi thrust places the Tezu unit over Quaternary deposits (Figs. 3–5, 8A). In addition to the range-bounding thrust, active faults cutting Quaternary sediments are expressed by prominent southwest-facing escarpments within the foreland basin (Figs. 4 and 5). Escarpments are 10's m in height and 5–10 km in length along strike. The trace of the Mishmi thrust is locally associated with right-lateral stream deflection near Chiddu, which may have resulted from some component of right-slip faulting (Fig. 8B). Based on the sinuous trace of the fault along the range front, the Mishmi thrust appears to be the surface expression of the active, low-angle thrust décollement that serves as the main interface between the Indian plate and upper plate orogenic wedge (Fig. 6), similar to the Main Frontal thrust to the west (Fig. 1). Slip along the décollement triggered the M_W 8.6 1950 Assam earthquake, which has been interpreted to have either strike-slip (Ben-Menahem et al., 1974) or low-angle thrust kinematics (Chen and Molnar, 1977; Coudurier-Curveur et al., 2016).

3. Discussion and conclusions

The most important finding of this work is that the northern Indo-Burma Ranges, directly south of the eastern Himalayan syntaxis, is dominated by dip-slip thrust faults. The only structure that accommodates right-slip deformation is the range-bounding oblique thrust that right laterally displaces active stream channels along its trace (Fig. 8B). Despite local variabilities, our field mapping and systematic



Orientations of stretching lineations across the easternmost Himalayan orogen and northern Indo-Burma thrust belt

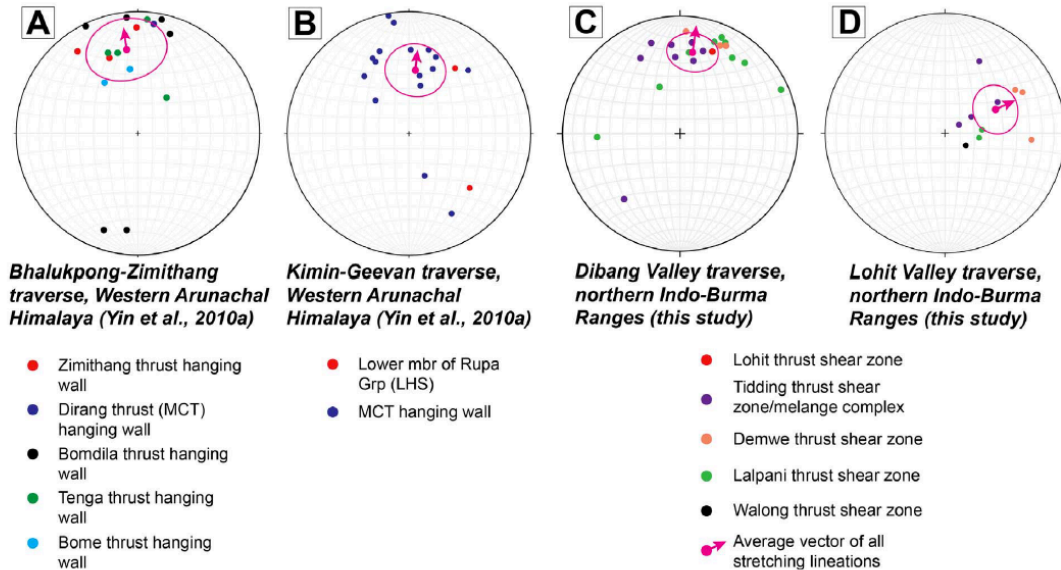


Fig. 9. Stereographic plots of stretching lineation orientations across the easternmost Himalayan orogen and northern Indo-Burma thrust belt (this study), including the (A) Bhalukpong-Zimithang and (B) Kimin-Geevan traverses of Yin et al. (2010a), and (C) Dibang Valley and (D) Lohit Valley traverses of this study.

and Davy (1988) and Royden et al. (1997). The dominance of thrusting across the northernmost Indo-Burma Ranges and varying slip vectors are inconsistent with the right-slip fault-zone model of Mitchell (1993).

The transport direction of thrusts across the northern Indo-Burma Ranges is nearly westward along Lohit Valley (Fig. 9C and D), which is nearly orthogonal to the top-south to top-southeast transport direction of major thrusts across the easternmost Himalayan (Fig. 9A–B) (Yin et al., 2006, 2010a; Burgess et al., 2012; Webb et al., 2013; DeCelles et al., 2016). As the northeast Indian craton is little deformed except along the Oldham and Dauki thrusts bounding the northern and southern margins of the Shillong plateau (Clark and Bilham, 2008; Yin et al., 2010b), the discrepancy in thrust transport directions directly west and south of the eastern Himalayan syntaxis can be attributed to the non-rigid behavior of the overriding Asian plate. Specifically, deformation of overriding-plate lithosphere is best described by distributed shortening approximated by continuum flow. The flow pattern may have been controlled by the combined effects of releasing the gravitational energy potential stored in the thickened Tibetan lithosphere and basal shear caused by westward slab rollback of the Indian oceanic slab below the Indo-Burma Ranges (Ni et al., 1989; Russo, 2012; Rangin et al., 2013).

At this stage of our research, the timing of deformation across the study area is not well constrained. However, the northern Indo-Burma thrust belt features a foreland-ward decrease in deformational fabric temperatures combined with active shortening along the range front, comparable to the style of deformation related to the Cenozoic India-Asia collision across the adjacent easternmost Himalaya. Therefore, the simplest interpretation is that westward younging deformation is consistent with the development of an accretionary fold-thrust belt across the northern Indo-Burma Ranges, as observed along the Himalayan arc (e.g., Ding et al., 2001; Yin et al., 2010a, 2010b; Webb et al., 2013). Although our assertion that the varying trend of stretching lineations supports the crustal flow model may be non-unique, it is the simplest explanation regarding the two competing models in this area: (a) right-slip faulting model of Mitchell (1993) versus (b) the westward thrusting model predicted by the crustal-flow model of Royden et al. (1997).

An important question regarding the spatial deflection of stretching lineation orientations across our study area is whether the trend developed during or after thrusting. In the first case, all thrusts were active simultaneously, but had different transport directions: southward in the north and westward in the south. In the second case, thrust transport in the study area was entirely southward and later distributed right-slip shear resulted in clockwise rotation of the southern part of the thrust belt. Distributed right-slip shear also supports a crustal-flow model, but with different kinematics than predicted by the model of Royden et al. (1997). Note that distributed right-slip shear across the study area is inconsistent with the discrete right-slip faulting model of Mitchell (1993).

The spatial deflection of stretching lineation orientations could also be related to a forward-propagating thrust system in which new thrusts initiate at slight angles to deactivated thrusts towards the front of a radially expanding accretionary complex or around a syntaxis of an orogenic belt (Capitanio and Replumaz, 2013; Moresi et al., 2014). Our field observations favor the simplest interpretation that the trend of stretching lineation is original. If distributed right-slip-shear occurred after the cessation of thrusting, one would expect the development of north-striking strike-slip faults that cut through the ductile thrusts. However, such a cross-cutting relationship was not observed in the study area.

Acknowledgements

This work is supported by grant award #1145038 from the Tectonics Program of the US National Science Foundation. We thank two anonymous reviewers for their detailed comments that improved this manuscript.

References

- Acharyya, S.K., 2010. Tectonic evolution of Indo-Burma range with special reference to Naga-Manipur Hills. Geol. Soc. India Mem. 75, 25–43.
- Akciz, S., Burchfiel, B.C., Crowley, J.L., Jiayun, Y., Liangzhong, C., 2008. Geometry, kinematics, and regional significance of the Chong Shan shear zone, Eastern Himalayan

- Syntaxis, Yunnan, China. *Geosphere* 4 (1), 292–314.
- Avouac, J.P., Tapponier, P., 1993. Kinematic model of active deformation in central Asia. *Geophys. Res. Lett.* 20 (10), 895–898.
- Ben-Menahem, A., Aboodi, E., Schild, R., 1974. The source of the great Assam earthquake—an interplate wedge motion. *Phys. Earth Planet. Inter.* 9 (4), 265–289.
- Burchfiel, B.C., Royden, L.H., van der Hilst, R.D., Hager, B.H., Chen, Z., King, R.D., Li, C., Lu, J., Yao, H., Kirby, E., 2008. A Geological and Geophysical Context for the Wenchuan Earthquake of 12 May 2008, Sichuan, People's Republic of China, GSA Today. 18, pp. 4–11. <http://dx.doi.org/10.1130/GSATG18A.1>.
- Burgess, W.P., Yin, A., Dubey, C.S., Shen, Z.K., Kelty, T.K., 2012. Holocene shortening across the main frontal thrust zone in the eastern Himalaya. *Earth Planet. Sci. Lett.* 357, 152–167.
- Capitanio, F.A., Replumaz, A., 2013. Subduction and slab breakoff controls on Asian indentation tectonics and Himalayan western syntaxis formation. *Geochem. Geophys. Geosyst.* 14 (9), 3515–3531.
- Chang, L., Flesch, L.M., Wang, C.Y., Ding, Z., 2015. Vertical coherence of deformation in lithosphere in the eastern Himalayan syntaxis using GPS, quaternary fault slip rates, and shear wave splitting data. *Geophys. Res. Lett.* 42 (14), 5813–5819.
- Chen, W.P., Molnar, P., 1977. Seismic moments of major earthquakes and the average rate of slip in central Asia. *J. Geophys. Res. Solid Earth* 82 (20), 2945–2969.
- Clark, M.K., Bilham, R., 2008. Miocene rise of the Shillong Plateau and the beginning of the end for the Eastern Himalaya. *Earth Planet. Sci. Lett.* 269 (3), 337–351.
- Cobbold, P.R., Davy, P.H., 1988. Indentation tectonics in nature and experiment. 2. Central Asia. *Bull. Geol. Inst. Univ.* 14, 143–162 (Uppsala).
- Coudurier-Curvent, A., Kali, E., Tapponier, P., Karakas, Ç., Ildefonso, S., van der Woerd, J., ... Banerjee, P., 2016. Surface rupture of the 1950 Assam earthquake: active faults and recurrence interval along the Eastern Himalayan syntaxis. In: EGU General Assembly Conference Abstracts. vol. 18, pp. 15794.
- DeCelles, P.G., Carrapa, B., Gehrels, G.E., Chakraborty, T., Ghosh, P., 2016. Along-strike continuity of structure, stratigraphy, and kinematic history in the Himalayan thrust belt: the view from Northeastern India. *Tectonics* 35 (12), 2995–3027.
- Ding, L., Zhong, D., Yin, A., Kapp, P., Harrison, T.M., 2001. Cenozoic structural and metamorphic evolution of the eastern Himalayan syntaxis (Namche Barwa). *Earth Planet. Sci. Lett.* 192 (3), 423–438.
- Ding, L., Xu, Q., Yue, Y., Wang, H., Cai, F., Li, S., 2014. The Andean-type Gangdese Mountains: paleoelevation record from the Paleocene-Eocene Linzhou Basin. *Earth Planet. Sci. Lett.* 392, 250–264. <http://dx.doi.org/10.1016/j.epsl.2014.01.045>.
- Ding, L., Spicer, R.A., Yang, J., Xu, Q., Cai, F., Li, S., Lai, Q., Wang, H., Spicer, T.E.V., Yue, Y., Shukla, A., Srivastava, G., Ali Khan, M., Bera, S., Mehrotra, R., 2017. Quantifying the rise of the Himalaya orogen and implications for the South Asian monsoon. *Geology* 45 (3), 215–218.
- England, P., Houseman, G., 1986. Finite strain calculations of continental deformation: 2. Comparison with the India-Asia collision zone. *J. Geophys. Res. Solid Earth* 91 (B3), 3664–3676.
- England, P., McKenzie, D., 1982. A thin viscous sheet model for continental deformation. *Geophys. J. Int.* 70 (2), 295–321.
- Gan, W., Zhang, P., Shen, Z.K., Niu, Z., Wang, M., Wan, Y., Cheng, J., 2007. Present-day crustal motion within the Tibetan Plateau inferred from GPS measurements. *J. Geophys. Res. Solid Earth* 112 (B8).
- Garunjan, N.S., Choudhuri, B.K., 2003. Geology and tectonic history of the Lohit valley, Eastern Arunachal Pradesh, India. *J. Asian Earth Sci.* 21 (7), 731–741.
- Kornfeld, D., Eckert, S., Appel, E., Ratschbacher, L., Sonntag, B.L., Pfänder, J.A., Ding, L., Liu, D., 2014. Cenozoic clockwise rotation of the Tengchong block, southeastern Tibetan Plateau: a paleomagnetic and geochronologic study. *Tectonophysics* 628, 105–122.
- Leloup, P.H., Arnaud, N., Lacassin, R., Kienast, J.R., Harrison, T.M., Trong, T.T., Replumaz, A., Tapponier, P., 2001. New constraints on the structure, thermochronology, and timing of the Ailaoshan-Shan-Red River shear zone, SE Asia. *J. Geophys. Res. Solid Earth* 106 (B4), 6683–6732.
- Lin, T.H., Chung, S.I., Kumar, A., Wu, F.Y., Chiu, H.Y., Lin, I., 2013. Linking a prolonged Neo-Tethyan magmatic arc in South Asia: Zircon U-Pb and Hf isotopic constraints from the Lohit Batholith, NE India. *Terra Nova* 25 (6), 453–458.
- Maurin, T., Masson, F., Rangin, C., Min, U.T., Collard, P., 2010. First global positioning system results in northern Myanmar: constant and localized slip rate along the Sagaing fault. *Geology* 38 (7), 591–594.
- McKenzie, D., 1972. Active tectonics of the Mediterranean region. *Geophys. J. Int.* 30 (2), 109–185.
- Misra, D.K., 2009. Litho-tectonic sequence and their regional correlation along the Lohit and Dibang valleys, eastern Arunachal Pradesh. *J. Geol. Soc. India* 73 (2), 213–219.
- Mitchell, A.H.G., 1993. Cretaceous–Cenozoic tectonic events in the western Myanmar (Burma)–Assam region. *J. Geol. Soc. India* 150 (6), 1089–1102.
- Mitra, S., Priestley, K., Bhattacharyya, A.K., Gaur, V.K., 2005. Crustal structure and earthquake focal depths beneath northeastern India and southern Tibet. *Geophys. J. Int.* 160 (1), 227–248.
- Moresi, L., Betts, P.G., Miller, M.S., Cayley, R.A., 2014. Dynamics of continental accretion. *Nature* 508 (7495), 245–248.
- Ni, J.F., Guzman-Speziale, M., Bevis, M., Holt, W.E., Wallace, T.C., Seager, W.R., 1989. Accretionary tectonics of Burma and the three-dimensional geometry of the Burma subduction zone. *Geology* 17 (1), 68–71.
- Rangin, C., Maurin, T., Masson, F., 2013. Combined effects of Eurasia/Sunda oblique convergence and East-Tibetan crustal flow on the active tectonics of Burma. *J. Asian Earth Sci.* 76, 185–194.
- Royden, L.H., Burchfiel, B.C., King, R.W., Wang, E., Chen, Z., Shen, F., Liu, Y., 1997. Surface deformation and lower crustal flow in eastern Tibet. *Science* 276 (5313), 788–790.
- Russo, R.M., 2012. Source-side shear-wave splitting and upper-mantle flow beneath the Arakan slab, India-Asia-Sundaland triple junction. *Geosphere* 8 (1), 158–178.
- Ryan, W.B., Carbotte, S.M., Coplan, J.O., O'Hara, S., Melkonian, A., Arko, R., Bonczkowski, J., 2009. Global multi-resolution topography synthesis. *Geochem. Geophys. Geosyst.* 10 (3).
- Tapponier, P., Peltzer, G., Armijo, R., 1986. On the mechanics of the collision between India and Asia. *Geol. Soc. Lond. Spec. Publ.* 19 (1), 113–157.
- Tapponier, P., Zhiqin, X., Roger, F., Meyer, B., Arnaud, N., Wittlinger, G., Jingsui, Y., 2001. Oblique stepwise rise and growth of the Tibet Plateau. *Science* 294 (5547), 1671–1677.
- Taylor, M., Yin, A., 2009. Active structures of the Himalayan-Tibetan orogen and their relationships to earthquake distribution, contemporary strain field, and Cenozoic volcanism. *Geosphere* 5 (3), 199–214.
- Wang, E., Burchfiel, B.C., 1997. Interpretation of Cenozoic tectonics in the right-lateral accommodation zone between the Ailaoshan shear zone and the eastern Himalayan syntaxis. *Int. Geol. Rev.* 39 (3), 191–219.
- Wang, E., Burchfiel, B.C., Royden, L.H., Chen, Z., Chen, J., 1998. Late Cenozoic Xiangshuihe-Xiaojiang, Red River, and Dali fault systems of southwestern Sichuan and central Yunnan, China. *Geol. Soc. Am. Spec. Pap.* 327, 1–108.
- Webb, A.A.G., Yin, A., Dubey, C.S., 2013. U-Pb zircon geochronology of major lithologic units in the eastern Himalaya: implications for the origin and assembly of Himalayan rocks. *Geol. Soc. Am. Bull.* 125 (3–4), 499–522.
- Webb, A.A.G., Guo, H., Clift, P.D., Husson, L., Müller, T., Costantino, D., ... Wang, Q., 2017. The Himalaya in 3D: slab dynamics controlled mountain building and monsoon intensification. *Lithosphere* 9, L636–L636.
- Yin, A., 2006. Cenozoic tectonic evolution of the Himalayan orogen as constrained by along-strike variation of structural geometry, exhumation history, and foreland sedimentation. *Earth Sci. Rev.* 76 (1), 1–131.
- Yin, A., 2010. Cenozoic tectonic evolution of Asia: a preliminary synthesis. *Tectonophysics* 488 (1), 293–325.
- Yin, A., Harrison, T.M., 2000. Geologic evolution of the Himalayan-Tibetan orogen. *Annu. Rev. Earth Planet. Sci.* 28 (1), 211–280.
- Yin, A., Dubey, C.S., Kelty, T.K., Gehrels, G.E., Chou, C.Y., Grove, M., Lovera, O., 2006. Structural evolution of the Arunachal Himalaya and implications for asymmetric development of the Himalayan orogen. *Curr. Sci.* 195–206.
- Yin, A., Dubey, C.S., Kelty, T.K., Webb, A.A.G., Harrison, T.M., Chou, C.Y., Célérrier, J., 2010a. Geologic correlation of the Himalayan orogen and Indian craton: part 2. Structural geology, geochronology, and tectonic evolution of the Eastern Himalaya. *Geol. Soc. Am. Bull.* B26461–1.
- Yin, A., Dubey, C.S., Webb, A.A.G., Kelty, T.K., Grove, M., Gehrels, G.E., Burgess, W.P., 2010b. Geologic correlation of the Himalayan orogen and Indian craton: part 1. Structural geology, U-Pb zircon geochronology, and tectonic evolution of the Shillong Plateau and its neighboring regions in NE India. *Geol. Soc. Am. Bull.* 122 (3–4), 336–359.
- Zhang, P.Z., Shen, Z., Wang, M., Gan, W., Bürgmann, R., Molnar, P., Wang, Q., Niu, Z., Sun, J., Wu, J., Hanrong, S., 2004. Continuous deformation of the Tibetan Plateau from global positioning system data. *Geology* 32 (9), 809–812.

-Chapter 4-

Tectonic evolution of the northern Indo-Burma Ranges: Mesozoic-Cenozoic kinematic reconstruction and constraints on the mode of deformation across the easternmost India-Asia collisional zone

4.1. Abstract

The ~1000-km-long, north-trending Eastern Flanking Belt is a key segment of the Cenozoic India-Asia orogenic system and studying its evolution is critical to understanding the collision process. Yet, the development of the belt is poorly understood in comparison to the Cenozoic east-trending Himalayan orogen and the Tibetan Plateau. In this study, we examine the structural framework, *P-T* conditions of metamorphic rocks, magnitude of Cenozoic shortening strain, and tectonic evolution of the northernmost segment of the Eastern Flanking Belt, the northern Indo-Burma Ranges, located directly east to southeast of the eastern Himalayan syntaxis. Based on geologic field mapping, the study area exposes a southwest- to west-directed, arcuate thrust belt cored by a hinterland-dipping duplex, which is consistent with deformation models of clockwise continuum flow around the syntaxis. The décollement of the thrust belt is deeply rooted, having exhumed metasedimentary rocks from >30 km depth. Restoration of one balanced cross-section across the thrust belt yields a minimum shortening estimate of >156 km, equivalent to ~81% shortening strain. Whereas the magnitude of crustal shortening across the northern Indo-Burma thrust belt is significantly less compared to the Himalayan orogen to the west, percent shortening is comparable or greater. Our shortening estimate combined with (1) an absence of several previously-existing Himalayan-Tibetan lithologic units (i.e., Tethyan Himalayan Sequence, Greater Himalayan Crystalline Complex, Xigaze forearc sequence, and southern Gangdese batholith belt) and (2) the southward decrease in the width of the belt (33-5 km) suggest an east-to southeastward increase in Cenozoic crustal shortening and/or continental subduction occurred along the eastern segment of the Himalayan collisional system. At the present day, continental deformation around the eastern syntaxis is expressed by right-slip transpression partitioned between the oblique-slip Mishmi thrust along the range front to the southwest and right-slip Jiali

fault zone in southeast Tibet to the northeast. Slip along the Mishmi thrust and Naga thrust is transferred to the right-slip Sagaing fault via southwest-trending restraining bend. This structural relationship provides a key example of the spatial transition of continental deformation from clockwise continuum flow and transpression around the corner of an indenter to discrete right-slip faulting along the side of an indenter during collision. By integrating the findings of this study with existing knowledge of the regional lithologic and structural framework, we present a comprehensive model for the Mesozoic-Cenozoic tectono-magmatic evolution of the eastern Himalaya, southeastern Tibetan Plateau, and Eastern Flanking Belt.

4.2. Introduction

The Himalayan-Tibetan orogen has served as a testing ground for competing models of mountain building and continental deformation since the advent of the plate tectonics theory (e.g., Dewey and Burke, 1973; Molnar and Tapponnier, 1975; Le Fort, 1975; Allégre et al., 1984; England and Houseman, 1986; Dewey et al., 1988; Hodges, 2000; Yin and Harrison, 2000; Tapponnier et al., 2001; Royden et al., 2008; Yin, 2010; Zuza et al., 2016). In addition to generating the Himalayan orogen and the Tibetan plateau, the Cenozoic indentation of India into Asia has also resulted in the development of >1000-km-long, north-trending Eastern and Western Flanking Belts that bound the margins of the Indian subcontinent (Gansser, 1964; Tapponnier et al., 2001; Yin, 2006, 2010; Haproff et al., in preparation) (Fig. 1). Despite the large aerial extent of the Western and Eastern Flanking Belts (Figs. 2-3), existing research efforts have been centered almost exclusively on the Himalayan orogen between the eastern and western syntaxes (e.g., Schelling and Arita, 1991; Nelson et al., 1996; Murphy et al., 1997; DeCelles et al., 2001; Avouac, 2003; Yin, 2006; Yin et al., 2010a; Webb et al., 2007, 2011, 2013) and the Tibetan plateau (e.g.,

Armijo et al., 1986, 1989; Wang et al., 2001; Murphy et al., 2003; Yin et al., 2007, 2008a,b; Taylor and Yin, 2009; Yin and Taylor, 2011; Zuza et al., 2016).

The structural framework and kinematics of the flanking belts have been predicted in models based on analogue experiments and numerical simulations of the India-Asia collision (e.g., Tapponnier et al., 1982; England and Houseman, 1986; Davy and Cobbold, 1988; Cobbold and Davy, 1988; Royden et al., 1997). The lateral extrusion model of Tapponnier et al. (1986) and Peltzer and Tapponnier (1988) (Fig. 4B) and the bookshelf faulting model of England and Molnar (1990) (i.e., right-slip mega-shear zone) (Fig. 4C) require the Eastern Flanking belt to be dominated by discrete right-slip faults that accommodate the northward indentation of India into Asia.

In contrast to the discrete strike-slip faulting models, the continuum-flow models of England and Houseman (1986), Royden et al. (1997), and Li et al. (2013), and the analogue experiment model of Cobbold and Davy (1988) all predict clockwise viscous flow of Asian lithosphere around the eastern Himalayan syntaxis (Fig. 4A), which requires the Eastern Flanking Belt to have formed as an east-striking thrust system that subsequently rotated clockwise to the current north-striking orientation (Haproff et al., 2018). Clockwise rotation of the thrust belt implies the existence of a spatial strain gradient such that Cenozoic crustal shortening increases with distance southward from the pole of rotation at the eastern Himalayan syntaxis (Haproff et al., in preparation). However, total crustal shortening estimates across the Eastern Flanking Belt via the construction and restoration of balanced cross sections have yet to be determined.

In this chapter, we present the results of a geologic investigation across the northern Indo-Burma Ranges, the northernmost segment of the Eastern Flanking Belt, located directly east to southeast of the eastern Himalayan syntaxis (Figs. 1-2). Our work includes new metamorphic

pressure-temperature (P - T) constraints of metasedimentary rocks associated with Cenozoic deformation and an estimate of minimum Cenozoic horizontal shortening based on the restoration of one balanced cross section across the study area. We also present Google Earth-based maps of active faults to show the mode of strain partitioning and fault linkage within the Eastern Flanking Belt. These findings are integrated with previously presented descriptions of lithologic units and structures, U-Pb zircon geochronology, and geochemistry in the study area (Haproff et al., 2018, in preparation), and knowledge of the paleogeography of southern Asia to produce a model for the tectono-magmatic evolution of the easternmost Himalayan collisional system since the latest Jurassic.

4.3. Geologic Setting

To provide a geologic context of the region, we summarize the major lithostratigraphic units and structures of the (1) eastern Himalayan orogen, (2) the southern Lhasa terrane, (3) the Eastern Flanking Belt. Lastly, we discuss the lithospheric structure of the Eastern Flanking Belt derived from existing geophysical studies.

4.3.1. Eastern Himalayan Orogen

The eastern Himalayan orogen extends from longitude 89°E in the west to the eastern Himalayan syntaxis at longitude 95°E, and is bounded by the Indus-Yarlung suture zone and the southern Lhasa terrane to the north and the Main Frontal thrust (MFT) and active Himalayan foreland basin to the south (Yin, 2006) (Fig. 1). The eastern segment of the orogen exposes from north to south the Proterozoic-Eocene siliclastic and carbonate sedimentary rocks interbedded with Paleozoic and Mesozoic volcanics of the Tethyan Himalayan Sequence (THS), Paleoproterozoic-

Ordovician high-grade metamorphic rocks and ~500 Ma granitoids of the Greater Himalayan Crystalline Complex (GHC), Proterozoic-Cambrian medium- to low-grade metamorphic rocks of the Lesser Himalayan Sequence (LHS), and Tertiary siliciclastic strata of the Sub-Himalayan Sequence (SHS), each bounded by the South Tibetan detachment (STD), the Main Central thrust (MCT), the Main Boundary thrust (MBT), and the Main Frontal thrust (MFT), respectively (e.g., Gansser, 1964; Le Fort, 1975, 1996; Acharyya and Ray, 1977; Acharyya, 1994; Gansser, 1983; Burchfiel et al., 1992; Edwards et al., 1996, 1999; Edwards and Harrison, 1997; Wu et al., 1998; Grujic et al., 2002; McQuarrie et al., 2008; Long et al., 2011a, b, c; Yin et al., 2010a, b; Burgess et al., 2012; Webb et al., 2013; DeCelles et al., 2016) (Fig. 5).

4.3.2. Southern Lhasa Terrane

The southern Lhasa terrane is located between the east-trending Indus-Yarlung suture zone (IYSZ) in the south and a cryptic zone of metamorphic rocks and ultramafic fragments interpreted as rocks in a Permian suture zone (e.g., Hsü et al., 1995; Dong et al., 2011, Zhu et al., 2012; Zhang et al., 2014) or telescoped fragments of the Late Jurassic Bangong-Nujiang suture zone to the north (Girardeau et al., 1984; Coward et al., 1988; Yin and Harrison, 2000; Kapp et al., 2003) (Fig. 1). The >2000-km long Gangdese Batholith is the most prominent feature of the southern Lhasa terrane, which is divided into a northern belt of late Triassic plutonic rocks (Wang et al., 2016), Cretaceous adakite (Zhu et al., 2009a) and S-type granitoids (Wen et al., 2008), and a southern belt of Cretaceous to Eocene granitoids, the Paleocene-Eocene Linzizong volcanic sequence (Schärer et al., 1984; Copeland et al., 1995; Ding et al., 2003; Wen et al., 2008; Zhu et al., 2008, 2009b,c; Lee et al., 2009; Ji et al., 2009; Guan et al., 2012; Guo et al., 2013; Zhu et al., 2013), and Neogene volcanics and dikes (Coulon et al., 1986; Yin et al., 1994; Guo et al., 2012) (Fig. 5).

4.3.3. Eastern Flanking Belt

The ~1000-km-long, north-trending Eastern Flanking Belt extends southward from the eastern Himalayan syntaxis in the north to the Andaman subduction zone in the south and is bounded by the Indian subcontinent and Bengal basin to the west and north-striking Sagaing fault and Sibumasu plate to the east (longitude 90-97°E) (Figs. 1-2). From north to south, the Eastern Flanking belt consists of three zones: (1) the northern Indo-Burma Ranges (N28°-N27°), (2) a central zone that includes the southern Indo-Burma Ranges to the west and West Burma microplate and Central Burma basin to the east (N27°-N17°) (Fig. 2), and (3) the Andaman subduction zone and back-arc rift system (N17°-N6°) (Fig. 2). In following sections, I discuss the lithologic and structural framework of each of these tectonic domains.

4.3.3.1. Northern Indo-Burma Ranges

Our study is focused on the northern Indo-Burma Ranges, the northernmost segment of the Eastern Flanking Belt (Figs. 1-2). Rocks exposed along the Dibang Valley and Lohit Valley across the study area are divided into six major lithologic units, each bounded by ~1-10-km-wide, south-to west-directed thrust shear zones (Fig. 6). The northernmost exposed unit is the Lohit Plutonic Complex, which consists of a western belt of Mesozoic-aged, southern Gangdese-equivalent granitoids and an eastern belt of Mesoproterozoic plutonic rocks, separated by the Walong thrust (Fig. 7 and 9). The eastern Lohit Plutonic Complex belt is bounded to the northeast by two northwest-striking strands of the right-slip Jiali fault zone: the northern Parlung fault and southern Puqu fault (Fig. 2), which have been active since at least ~18-12 Ma (Lee et al., 2003).

The Lohit thrust places the western belt of the Lohit Plutonic Complex atop the Tidding mélange complex (Figs. 6-9), which is a tectonic mélange of dismembered garnet mica schist, metabasite, and amphibolite. The Tidding mélange complex is considered the easternmost continuation of the IYSZ (Haproff et al., 2018). To the southwest, the Mayodia mélange complex is exposed in a thrust-bound klippe exposing serpentinized ultramafics, amphibolite, garnet mica schist, gabbro, and metabasite.

The Tidding thrust places the Tidding mélange complex atop rocks correlative with the LHS (Haproff et al., in preparation), which are divided into the Mayodia gneiss and structurally-lower Lalpani schist (Figs. 6-9). The Mayodia gneiss contains paragneiss, augen gneiss, migmatite, and quartzo-feldspathic schist with youngest Mesoproterozoic-Cambrian-aged detrital zircons and negative ε_{Nd} values of -17 to -10 (Fig. 6). Across the Demwe thrust, the Lalpani schist contains quartzo-feldspathic schist, paragneiss, quartzite, and carbonate with youngest Mesoproterozoic-Cretaceous-aged detrital zircons and more negative ε_{Nd} values -27 to -15 (Fig. 6).

The Lalpani thrust places the Lalpani schist atop the southernmost-exposed Sewak unit (Figs. 6-9), which contains quartzite, marble, chert, slate, phyllite, and quartzo-feldspathic schist with youngest Tertiary-aged detrital zircons. The Tezu unit is exposed in one location along the range front of Lohit Valley (Fig. 8) and contains syntectonic siliciclastic strata including sandstone and conglomerate. The Sewak and Tezu units are in the hanging wall of the Mishmi thrust, the southernmost fault in the northern Indo-Burma Ranges (Fig. 7-9). Unlike other faults mapped in the study area, the brittle Mishmi thrust has a component of right-slip shear, based on right-lateral displacement of Quaternary river terraces and stream deflection along the range front (Fig. 10) (Haproff et al., 2018).

4.3.3.2. Southern Indo-Burma Ranges

The southern Indo-Burma Ranges expose a westward-tapering, thin-skinned fold and thrust belt that is divided into two salients: (1) an outer belt to the west involving Lower Miocene submarine deposits, upper Miocene continental shelf deposits, and Pliocene-Pleistocene fluvial deposits (Maurin and Rangin, 2009a), and (2) an onshore inner belt to the east involving Eocene flysch deposits (Maurin and Rangin, 2009a; Rangin et al., 2013) (Fig. 2). The inner belt is considered part of the Early Cenozoic accretionary prism of the India-Burma subduction zone and includes the Naga Hills thrust belt (a.k.a., Assam-Arakan thrust belt) (Maurin and Rangin, 2009a; Rangin et al., 2013) (Fig. 2). The outer belt includes the Chin-Chittagong Hills thrust belt, which is bounded by the leading Chittagong Coastal fault (Fig. 2). Thrust faults of both belts exhibit subhorizontal fault striations and right-lateral thrust sense of shear (Maurin and Rangin, 2009a). The outer and inner belts of the southern Indo-Burma Ranges are divided by the oblique-slip Kaladan fault, which terminates to the north near the merger of the Naga and Dauki thrusts (Fig. 2).

4.3.3.3. West Burma Microplate

East of the southern Indo-Burma Ranges, the West Burma microplate (a.k.a., West Burma block) is divided into the Mt. Victoria block to the west and Central Burma Basin to the east, separated by the oblique-slip Kabaw fault (Fig. 2). The core of the Mt. Victoria block consists of Jurassic-Cretaceous ophiolitic fragments of the Western Belt Ophiolites (Maurin and Rangin, 2009a, b; Rangin et al., 2013; Ao and Bhowmik, 2014; Morley and Searle, 2017) (Fig. 2), which are considered the southern continuation of the IYSZ (e.g., Maurin and Rangin, 2009a, b; Rangin et al., 2013). The Western Belt Ophiolites are thrust atop Late Triassic to Late Cretaceous carbonate and shale and the Paleozoic (?) Kanpetlet schist (Socquet et al., 2002). In the Chin Hills

of Myanmar, the Western Belt Ophiolites are overlain by fossiliferous flysch and conglomerate of the Late Cretaceous-Early Paleogene Kabaw Formation (Socquet et al., 2002). In the Naga Hills of northeast India, mylonitic limestone and metasedimentary rocks of the Mesozoic (?) Nimi Formation are thrust atop the Late Eocene-Oligocene Jopi-Phokphur Formation and eclogite-bearing Naga ophiolitic mélange, which are placed atop Upper Cretaceous-Eocene Disang Flysch (Chatterjee and Ghose, 2010).

4.3.3.4. Central Burma Basin

East of the Mt. Victoria block, the north-trending Central Burma basin is filled with Cenozoic terrestrial and marine strata (Rangin et al., 1999, 2013) (Fig. 2). The Central Burma basin is considered either a series of forearc and backarc basins related to subduction of the oceanic lithosphere beneath the West Burma microplate (e.g., Mitchell, 1993) or Cenozoic right-slip pull-apart basins related to slip along the Sagaing fault (Rangin et al., 1999; Bertrand and Rangin, 2003). The Central Burma basin is bisected by intermittent exposures of the Wuntho-Popa magmatic belt (Fig. 2), which consists of Cretaceous (~91-106 Ma) and Eocene to Oligocene I-type granitoids (~52-37 Ma) (Mitchell, 1993; Barley et al., 2003; Barley and Zaw, 2009; Mitchell et al., 2012), igneous rocks of the Maygyi Formation, metasedimentary roof pendants, Permian limestone, and dismembered ophiolites (Mitchell, 1993). Detrital zircon U-Pb ages from the adjacent basin are derived from the Wuntho-Popa belt and further constrain magmatism to ~110-80 Ma and ~70-40 Ma (Wang et al., 2014). The youngest exposed igneous rocks are Eocene to Oligocene granitoids and Miocene (16-13 Ma) to Quaternary volcanic flows (Lee et al., 2016). Morley and Searle (2017) interpret the Wuntho-Popa and Mogok Metamorphic belts of the Sibumasu plate as a coupled magmatic arc generated during subduction of Neotethys and Indian

oceanic lithosphere beneath the West Burma microplate and correlates with the Gangdese batholith.

4.3.3.5. Sagaing Fault

Bounding the Central Burma basin to the east, the ~1000-km right-slip Sagaing fault extends from the southeast-striking restraining bend in northern Myanmar to the Andaman Sea where the fault transitions into series of right-stepping transform faults and spreading centers of the Andaman back-arc rift system (Fig. 2). The GPS-derived, instantaneous slip rates along the northern and central segments of the Sagaing fault are ~18-20 mm/yr, slightly greater than half of the relative India-Sibumasu plate velocity (~35 mm/yr) (Vigny et al., 2003; Maurin et al., 2010). One paleoseismic study by Wang et al. (2011) determined a Holocene slip rate of 14 mm/yr along the southernmost segment of the Sagaing fault. The initiation age of the Sagaing fault has been bracketed to Middle Miocene to Early Pliocene based on the onset of seafloor spreading in the Andaman rift (Raju et al., 2004). Estimates of the net right-slip displacement since the Miocene are between 400-460 km (Curay et al., 1979; Maung, 1987) to as much as ~600 km, exemplified by Morley and Searle (2017).

4.3.4. Lithospheric Structure of the Eastern Flanking Belt

Across the Eastern Flanking Belt, more than half of the India-Sibumasu block motion (~35 mm/yr) is accommodated by the right-slip Sagaing fault (~18 mm/yr), whereas the remaining motion is accommodated by either oblique subduction (Curay et al., 1979; Le Dain et al., 1984; Acharyya et al., 1990) or distributed transpression across thrust belts of the southern Indo-Burma Ranges (Maurin and Rangin, 2009a; Rangin et al., 2013) (Fig. 2). Maurin and Rangin (2009a)

postulate no subduction of oceanic lithosphere is occurring now, as geophysical data suggest the east-dipping Bengal slab has detached, leaving broken segments in the upper mantle (Russo, 2012). Mantle tomography studies beneath the Eastern Flanking Belt by Li et al. (2008) delineated a steep, east-dipping high-velocity zone reaching depths up to 500 km, interpreted to be the relict Neotethys slab.

4.4. Methods

The findings of this chapter are based on field mapping of lithologic units and faults and the collection of rock samples along the 45-km-long, east-trending Lohit Valley and 85-km-long, northeast-trending Dibang Valley across the northern Indo-Burma Ranges (Figs. 7-9). Details of geologic mapping, descriptions of lithologic units and faults, and summaries of geochronology and geochemistry data are presented in Chapters 2 and 3. In this study, active faults located between the study area and the central section of the Eastern Flanking Belt were mapped on Google Earth imagery from their geomorphic expression. Below, we describe the methods involved in (1) thermobarometry of metasedimentary rocks of the Tidding and Mayodia mélange complexes and (2) the construction and restoration of the balanced cross section across Dibang Valley.

4.4.1. Thermobarometry

Thermobarometry was conducted on five garnet mica schist samples of the Tidding and Mayodia mélange complexes to constrain the temperature and pressure conditions of metamorphism associated with Cenozoic deformation. All samples selected for thermobarometry are mylonitized L-S tectonites with recrystallized quartz and plagioclase forming primary foliation and lineations. Ductile deformation is assumed to be related to the Cenozoic development of the

orogen. Samples *PH-11-12-15-17* and *PH-1-9-13-8* were selected ~50 m from each other from the northern section of the Mayodia klippe in Dibang Valley (Fig. 7). Samples *PH-1-8-13-26* and structurally-higher *PH-11-9-15-40* were selected ~100 m from each other within the Tidding mélange complex in Dibang Valley (Fig. 7). Sample *PH-11-14-15-24* was selected from the middle section of the Tidding mélange complex in Lohit Valley (Fig. 8).

Whole rock samples were cut into half-cover 30 mm thin sections, polished with carbide paper, and coated in carbon. Photomicrographs and back-scattered electron compositional images of selected mineral phases were taken with a scanning electron microscope (SEM) at the University of California, Los Angeles (UCLA). Selected mineral phases located adjacent to each other were shot with a 15 nA electron current on spots of 10 μm using a JEOL 8200 electron microprobe. Oxide weight percentages and activity coefficients were calculated using the program AX and inputted into the *average P-T mode* of the THERMOCALC 3.37 program (Holland and Powell, 1998). Intersections of equilibria reactions in *P-T* space were determined the internally-consistent dataset of Holland and Powell (1998). Titanium concentrations in biotite (Ti-in bio) were measured to verify peak temperature conditions (Henry et al., 2005). Results of metamorphic *P-T* determinations are summarized in Table 1. Element maps of selected garnet grains were generated using energy-dispersive X-ray spectroscopy (EDS) to show chemical zonation.

4.4.2. Construction and Restoration of the Dibang Valley Cross Section

Two northeast-oriented balanced cross sections were constructed for the Dibang and Lohit Valley traverses (Fig. 9). Lines of cross section are oriented perpendicular to the trend of the orogen and parallel to the principle shortening direction defined by the trend of stretching lineations (Figs. 7-8). We utilized the kink-bend method of Suppe (1983) and adhered to typical

thrust geometries (e.g., Dahlstrom, 1970; Boyer and Elliott, 1982; Butler, 1987). Field measurements were projected along strike to the line of cross section, assuming all structures are laterally continuous and folds have cylindrical geometries. Dip measurements converted to apparent values and grouped into average dip domains. Fold axial planes were calculated by bisecting the interlimb angle between dip domains. The orientation of fault planes at depth are assumed to parallel hanging wall foliation.

Restoration of the Dibang Valley cross section was completed using the line balancing method of Dahlstrom (1969). To maintain a minimum estimate of horizontal shortening, exposed thrust faults are assumed to sole into a single décollement at depth (e.g., Yin et al., 2007; 2008b). Furthermore, internal shortening of units (e.g., isoclinal folding and transposed bedding) are excluded and lateral projections of hanging wall cutoffs are minimized. Propagation of thrust ramps and bedding-parallel flats are not viable within plutonic rocks, preventing estimation of slip along the Lohit and Walong thrusts within the Lohit Plutonic Complex (Figs. 7-8). Lastly, right slip shear along the range-bounding Mishmi thrust was assumed to be negligible to maintain the plane requirement.

4.5. Results of Thermobarometry

Garnet mica schist *PH-1-8-13-26* from Dibang Valley (Fig. 7) contains plagioclase (An_{31}), biotite ($X_{Mg}=0.54$), muscovite ($X_{Mg}=0.60$), and quartz+sphene+hornblende+ilmenite+rutile+Fe-rich garnet ($X_{Mg}=0.15$, 69% alm, 16% grs, 3% sps, 12% pyp) (Fig. 11) with relatively homogenous, unzoned composition. Garnets display “snowball” texture indicative of rotation during shear (Fig. 12). Fluid and quartz inclusions are observed within garnet grains, while mica has predominantly grown along garnet rims. Use of THERMOCALC 3.37 yields upper amphibolite conditions of

10.4 ± 1.1 kbar and 627 ± 28 °C (Table 1; Fig. 13A). Given a constant lithostatic gradient and crustal density of 2.7 g/cm^3 , ~ 10 kbar equates to ~ 35 km depth in the crust. Application of the Ti-in biotite thermometer to *PH-1-8-13-26* yields slightly lower temperatures of $\sim 620 \pm 24$ °C (Table 1; Fig. 13A). Garnet mica schist sample *PH-11-9-15-40* from Dibang Valley (Fig. 7) contains the same mineral assemblage as *PH-1-8-13-26* with garnets displaying Mn-rich and Mg-depleted cores (Fig. 13B). Use of THERMOCALC 3.37 yields upper amphibolite conditions of 616 ± 11 °C and 9 ± 0.5 kbar ($= \sim 30$ km depth) (Table 1; Fig. 13A).

Garnet mica schist sample *PH-11-14-15-24* collected from Lohit Valley (Fig. 8) contains a mineral assemblage of plagioclase (Ab_{75}), biotite ($X_{\text{Mg}}=0.68$), muscovite ($X_{\text{Mg}}=0.74$), and quartz+ilmenite+titanite+kyanite+rutile+garnet ($X_{\text{Mg}}=0.29$, 58% alm, 12% grs, 6% sps, 24% pyp) (Figs. 13C and G). Use of THERMOCALC 3.37 yields temperatures and pressure of 679 ± 18 °C and 13.1 ± 0.8 kbar ($= \sim 45$ km depth) (Table 1; Fig. 13A). Application of the Ti-in biotite and garnet-biotite Mg-Fe exchange thermometers yield lower temperatures of 600 ± 24 °C and 644 ± 50 °C, respectively (Table 1; Fig. 13A).

Sample *PH-11-12-15-17* from the Mayodia klippe in Dibang Valley (Fig. 7) is a garnet chlorite schist containing plagioclase (An_{27}), muscovite ($X_{\text{Mg}}=0.66$), chlorite ($X_{\text{Mg}}=0.55$), clinozoisite ($\text{Al}=2.5$ pfu), and quartz+titanite+rutile+garnet ($X_{\text{Mg}}=0.09$, 65% alm, 23% grs, 0.4% sps, and 10% pyp). Garnet cores are rich in Mn and depleted in Mg, indicative of temperatures of metamorphism below 650 °C (Fig. 13D). Use of THERMOCALC 3.37 yields upper greenschist conditions of 4.7 ± 2.3 kbar and 440 ± 76 °C (Table 1; Fig. 13A). Garnet chlorite schist *PH-1-9-13-8* also from the Mayodia klippe (Fig. 7) contains the same mineral assemblage of chlorite+clinozoisite+quartz+titanite+rutile+Fe-rich garnet ($X_{\text{Mg}}=0.14$, 60% alm, 28% grs, 0.4% sps, 11% pyp). Garnets show similar prograde growth zonation indicative of metamorphic

temperatures below 650 °C (Figs. 13E-F).

Metamorphic conditions experienced by garnet mica schist of the Tidding and Mayodia mélange complexes suggests a *P-T* path involving metamorphism through upper amphibolite-facies at deep crustal levels of >30 km and subsequent exhumation through greenschist facies conditions. Temporal constraints to metamorphism remain unconstrained.

4.6. Results of the Dibang Valley Cross Section Restoration

Restoration of the Dibang Valley balanced cross section yields a minimum shortening estimate of >156 km, equivalent to ~81% shortening strain (Fig. 14). The deformed width of the section measured from the southernmost Mishmi thrust to the Tidding thrust and Tidding mélange complex is ~33 km. The restored length of the section is ~192 km, over 70% of which is accommodated by thrust systems within the Lalpani schist, including the Hunli duplex (~137 km). The Hunli duplex is interpreted to consist of 8 horses, two of which are exposed at the surface (Fig. 9). The Demwe thrust alone accommodated >34 km or 22% of the total minimum shortening estimate (Fig. 14). Variations in the structural thickness of thrust sheets involving the Lalpani schist are based on the inclusion and exclusion of metasedimentary rocks containing Jurassic-Cretaceous-aged detrital zircons (Haproff et al., in preparation). The Tidding and Mayodia mélange complexes are interpreted to originate from the same complex, which was telescoped across the orogen along a thrust flat and subsequently folded during development of the Hunli duplex (Figs. 9 and 14).

4.7. Discussion

The tectonic evolution of the Eastern Flanking Belt and relationships with the development of

the Tibetan Plateau and east-trending Himalayan orogen are largely unknown, despite the belt being an important segment of the Cenozoic India-Asia collisional system. This chapter presents an investigation of the structural framework, magnitude of Cenozoic shortening strain, and *P-T* conditions associated with Cenozoic deformation across the northern Indo-Burma Ranges. The main findings of this chapter include (1) the study area exposes a south- to east- directed thrust belt involving some but not all major lithologic units of the Himalayan-Tibetan orogen, (2) metamorphic rocks of the Tidding and Mayodia mélange complexes were exhumed along a thrust ramp from >30 km depth, and (3) Cenozoic shortening strain exceeds ~156 km (~81%) across the thrust belt.

In the following sections, we discuss implications of this work including a comparison of the structural geometries and shortening estimates between the Himalayan orogen and northern Indo-Burma thrust belt to determine the nature of crustal deformation along the easternmost Himalayan collisional system. In addition, we differentiate between end-member models of continental deformation surrounding the eastern Himalayan syntaxis and discuss of active partitioning and transfer of slip between faults of the study area to the central segment of the Eastern Flanking Belt to the south. Lastly, we present a model for the Mesozoic-Cenozoic tectono-magmatic evolution of the eastern Himalayan orogen, southeast Tibetan Plateau, and Eastern Flanking Belt.

4.7.1. Structural Framework Comparison

Like the Himalayan orogen, the northern Indo-Burma Ranges expose a Cenozoic south-to east-directed, imbricate thrust belt featuring a hinterland-dipping duplex system that involves mostly rocks of the Lalpani schist (=LHS) (Figs. 7-9). North-dipping thrusts branch from a single low-angle, northeast- to east-dipping décollement (i.e., Main Himalayan detachment), which is exposed

on the surface as the southernmost Mishmi thrust (=MFT). Individual thrusts have accommodated a significant percentage of crustal shortening across the orogen (e.g., Demwe thrust: 22% or >34 km of total minimum shortening of >156 km) (Fig. 14).

However, the northern Indo-Burma thrust belt is distinct from the Himalayan orogen based on right-slip kinematics along the southeast- to south-striking Mishmi thrust and the absence of faults with top-to-Lhasa terrane kinematics such as the STD or Great Counter thrust. Furthermore, the width of the thrust belt measured from the Mishmi thrust to the Neotethys suture zone decreases dramatically from north to south (33-5 km) (Fig. 8), in contrast to ~200 km across the Himalayan orogen (Fig. 1). The northern Indo-Burma Ranges also expose a kilometer-scale ophiolitic mélange zone and subduction complex that was exhumed from >30 km depth. These rocks were thrust across the orogen and subsequently folded and partially eroded to form an isolated klippe (Fig. 9). Such a feature is seldom seen in the Himalayan orogen, except for the southern Ladakh ophiolites exposed as klippen atop the THS in the western Himalaya (e.g., Hodges, 2000; Searle et al., 1988; Corfield et al., 2001). Thus, the northern Indo-Burma thrust belt developed as a similar contractional orogen compared to the Himalaya, but details of the structural geometry are distinct, implying a somewhat unique geological evolution.

4.7.2. Crustal Shortening across the Easternmost Himalayan Collisional System

Reconstruction of the Dibang Valley cross section produces a minimum horizontal shortening estimate of ~156 km (~81%) (Fig. 14). This shortening magnitude is significantly less compared to the Himalayan orogen to the west (Fig. 15) (e.g., 515-775 km in Western Arunachal, Yin et al., 2010b). Percent shortening across the northern Indo-Burma Ranges, however, exceeds that of the western Arunachal Himalaya (~70-76%) (Yin et al., 2010b) and compares only in Sikkim and

southern Tibet (~80%) near the center of the Himalayan orogen (Ratschbacher et al., 1994; Mitra et al., 2010; Long et al., 2011b) (Fig. 15).

Major lithologic units of the Himalayan-Tibetan orogen including the Tethyan Himalayan Sequence, Greater Himalayan Crystalline Complex, Mesozoic-Cenozoic igneous rocks of the southern Gangdese batholith and Linzizong volcanic sequence, and Xigaze forearc sequence are not exposed in the study area (Haproff et al., in preparation). However, Gangdese-equivalent Mesozoic-Cenozoic igneous rocks and adjacent forearc basin sediments are exposed in the central zone of the Eastern Flanking Belt (Mitchell, 1993; Mitchell et al., 2012; Wang et al., 2014). The existence of these rocks to the northeast and south of the study area suggests Mesozoic-Cenozoic arc magmatism and forearc sedimentation occurred along a laterally-continuous belt parallel to the southern margin of the southern Lhasa terrane and West Burma microplate (Lin et al., 2013; Haproff et al., in preparation).

We interpret that the local absence of these lithologic units in the northern Indo-Burma Ranges, along with the discrepancies in shortening strain across syntaxis, to be the result of a greater magnitude of Cenozoic shortening and erosion, and/or continental underthrusting at the longitude of the study area (Figs. 16 and A.3). The pre-collisional configuration of northeast Greater India likely comprised a laterally-continuous cratonal sequence and passive margin sequence including the LHS, GHC, and THS (Figs. 16 and A.4). Following the Cenozoic India-Asia collision, thrusting of these lithologic units accommodated a significant portion of crustal shortening across the study area. For example, in northwest Nepal and southwest Tibet, the Tethyan Himalayan fold and thrust belt accommodated 112 km of shortening, approximately 20% of the total 597 km across that segment of the Himalayan orogen (Murphy and Yin, 2003). Complete sections of these rocks could also have been subducted with the down-going Indian plate. This interpretation that a greater

magnitude of crustal shortening and/or continental underthrusting occurred across the study area is supported by the southward decrease in the width of the thrust belt of 33 km and 5 km along the Dibang and Lohit Valleys, respectively (Figs. 7-8).

4.7.3. Constraints on Models of the India-Asia Collision

Models of deformation surrounding the eastern Himalayan syntaxis during the India-Asia collision have developed into two end-member forms: (1) clockwise crustal flow of lithosphere accommodated by distributed thrusting (e.g., England and Houseman, 1986; England and Molnar, 1990; Royden et al., 1996, 1997; Li et al., 2013), and (2) southeastward lateral extrusion along north-striking discrete strike-slip faults (e.g., Tapponnier et al., 1986; Peltzer and Tapponnier, 1988) (Fig. 4).

Geologic mapping across the northern Indo-Burma Ranges has shown that the mode of deformation is dominated by southwest-directed thrusting along Dibang Valley in the north and west-directed thrusting along Lohit Valley in the south, defined by the orientations of thrust faults and perpendicular trends of stretching lineations within shear zones (Figs. 7-8). This southward deflection in the thrust transport direction across the study area is evidence of clockwise crustal flow around the eastern Himalayan syntaxis accommodated by thrusts (Haproff et al., 2018). South-trending, sub-horizontal stretching lineations along discrete strike-slip shear zones were not observed, which precludes the lateral extrusion model for the study area. Our interpretation that crustal shortening increases to the east from the Himalayan orogen to the northern Indo-Burma thrust belt supports the clockwise flow model, as progressive rotation of the Eastern Flanking Belt requires an increase in strain with distance from the pole at the eastern Himalayan syntaxis.

4.7.4. Strain Partitioning surrounding the Eastern Himalayan Syntaxis

Based on the structural framework of the northern Indo-Burma Ranges and southeastern Tibetan Plateau, we present a model for the active mode of strain partitioning adjacent the eastern Himalayan syntaxis (Fig. 17). Present-day deformation in the study area is expressed by two fault systems: the oblique-slip Mishmi thrust along the range front in the southwest and right-slip Puqu and Parlung faults of Jiali fault zone of southeast Tibet in the northeast (Fig. 17). The surface trace of the Mishmi thrust along the range front is irregular, suggesting a low-angle geometry at depth like the MFT to the west (Figs. 7-9). However, the fault has some component of right-slip shear, based on the displacement of Quaternary river terraces and stream deflection (Haproff et al., 2018) (Fig. 10). Slip along the low-angle fault triggered the M_w 8.6 1950 Assam earthquake at ~15 km depth, which has been interpreted to have either strike-slip (Ben-Menahem et al., 1974) or low-angle thrust kinematics (Chen and Molnar, 1977). In southeast Tibet, the right-slip Puqu and Parlung faults are the southeastern extensions of the Jiali fault zone, located directly north of the eastern Himalayan syntaxis (Fig. 18). Both the Puqu and Parlung faults are easily identified by their geomorphic expression along linear, southeast-trending river valleys (Fig. 18). The surface traces of both right-slip faults are expressed ~10-km-long scarps and several beheaded channels and right-laterally-deflected channels (Fig. 18). Based on their surface traces, both the Puqu and Parlung faults are interpreted to have pure right-slip kinematics and sub-vertical geometries (Fig. 17-18).

In our strain partitioning model, components of thrust and right-slip motion occur along the Main Himalayan detachment, which is exposed on the surface as the Mishmi thrust (Fig. 17). In the hinterland of the thrust belt, the detachment merges at depth with the Puqu fault (Fig. 17). Deformation across the region is expressed by right-slip transpression partitioned between the

Mishmi thrust and Puqu-Parlung fault system, along which coeval slip accommodates oblique convergence between India and Asia and clockwise rotation of lithosphere around the eastern Himalayan syntaxis. A similar tectonic regime can be inferred for the Suliman-Kirthar mountains in Pakistan and Afghanistan, southwest of the western Himalayan syntaxis (i.e., Nanga Parbat). There, a southeast-directed décollement of the foreland fold and thrust belt likely merges with the northeast-striking, left-slip Gardaiz-Chaman-Ghazaband fault system in the hinterland (e.g., Ul-Hadi et al., 2013) (Fig. 3).

4.7.5. Transfer of Slip across the Eastern Flanking Belt

The southwest- to west-directed Mishmi thrust and southeast-directed Naga thrust are both range-bounding faults that accommodate some percent of India-Asia convergence along the easternmost Himalayan collisional system (Wang et al., 2014). The active slip rate along the Mishmi thrust is unknown, but may be comparable to the ~23 mm/yr Holocene slip rate of the MFT in the western Arunachal Himalaya (Burgess et al., 2012). South of the MFT, the Naga thrust is the leading fault of the northeast-trending Naga Hills thrust belt (a.k.a., Assam-Araken thrust belt) and places Cenozoic continental shelf sediments atop Quaternary alluvium along the southern margin of the Brahmaputra river basin (Kent et al., 2002; Kent and Dasgupta, 2003; Aier et al., 2011) (Fig. 2). The active slip rate along the Naga thrust has yet to be determined. Whereas the Mishmi thrust has some right-slip component, the Naga thrust has pure-dip slip kinematics (Kent et al., 2002). Southeast of the Naga Hills thrust belt, the ~1000-km-long, right-slip Sagaing fault bounds the eastern margin of the West Burma microplate and slips ~14-20 mm/yr, accommodating a large percentage of the India-Sibumasu relative plate velocity of ~35 mm/yr (Vigny et al., 2003; Wang et al., 2011). The north-striking Namyin fault is the northernmost segment of the Sagaing

fault in northern Myanmar (Fig. 2). The Namyin fault has yet to be studied in detail, however, its geomorphic expression clearly delineates active right-slip kinematics from ~100-km-long scarps and beheaded and deflected stream channels (Fig. 19-20). Despite being key faults in accommodating India-Asia convergence across the region, much remains unknown regarding the geometry and kinematics of linkage between the Mishmi thrust and Naga thrust, along with the nature of slip transfer to the Namyin-Sagaing fault to the southeast.

To reconcile these problems, we mapped active faults of the central zone of the Eastern Flanking Belt, including the southern and northeastern terminations of the Mishmi thrust and Naga thrust, respectively, and northern termination of the Sagaing fault from their geomorphic expression on Google Earth imagery (Fig. 20). Our work revealed that the Mishmi thrust and Naga thrust merge at the western opening of an ~100-km-long and ~25-km-wide, southeast-trending valley near the southeastern termination of the Manabum anticline (Fig. 20). At least 10 southeast-striking faults were identified paralleling the valley, which link the Mishmi thrust and Naga thrust with the north-striking, right-slip Namyin fault (Fig. 20). We interpret this southeast-trending corridor of faults to be a left-stepping restraining bend that transfers motion from the oblique-slip Mishmi thrust and dip-slip Naga thrust to the right-slip Sagaing fault (Fig. 2). We name the restraining bend the Namdapha Corridor, based on the Namdapha National Park of northeast India located within its northwest segment. The Namdapha Corridor is a key example of a slip transfer structure from diffuse contractional belts in the north to discrete right-slip faults in the south that both accommodate continental deformation attributed to the indentation of India into Asia.

4.7.6. Mesozoic-Cenozoic Tectonic Evolution of the Easternmost Himalayan Collisional System

We present a model for the Mesozoic-Cenozoic evolution of the easternmost Himalayan collisional system including the eastern Himalayan orogen, Eastern Flanking Belt, southeast Tibetan Plateau, and part of southeast Asia, compiled from research of this dissertation and previously published information of the geological framework and paleogeography of the region (Fig. 21). The Mesozoic-Cenozoic evolution is shown in four stages: (A) ~150-80 Ma, (B) ~50 Ma, (C) ~20 Ma, and (D) ~10 Ma (Fig. 21). The paleogeographic configuration of the Eastern Flanking Belt and southeast Asia in map view is based on Hall (2012), Lee and Lawver (1995), and Morley and Searle (2017). Important elements of the reconstruction are the locations and migrations of major lithospheric blocks and terranes, the lifespans, kinematics, and displacements of major faults, and the petrogenesis, deformation, and erosion of major lithologic units. Deformation accommodated north of the Bangong-Nujiang suture is not included in the model. The longitudinal size of northeast Greater India is based on van Hinsbergen et al. (2011). The Mesozoic-Cenozoic evolution of only the northern Indo-Burma Ranges is shown on series of schematic cross sections with the addition of a ~40 Ma stage (Fig. 22).

4.7.6.1. Stage 1: ~150-80 Ma

Continuous northward subduction of Neotethys oceanic lithosphere occurred along a concave-shaped, northwest-trending southern Asian margin comprising the Lhasa terrane, West Burma microplate, and Sibumasu plate (e.g., Replumaz and Tapponnier, 2003; Hall, 2012; Morley and Searle, 2017) (Figs. 21 and 22A). Mesozoic arc magmatism encompassing the northern Gangdese batholith belt, western Lohit Plutonic Complex belt, and Wuntho-Popa arc, along with forearc

sedimentation in the Xigaze basin and Central Burma basin occurred along a continuous belt paralleling the Neotethys trench (Figs. 21 and 22A). Mesozoic arc granitoids intruded preexisting basement rocks including Mesoproterozoic orthogneiss of the eastern Lohit Plutonic Complex belt and Bomi-Chayu Complex of the southern Lhasa terrane (Xu et al., 2013). Tectonic mélange sequences developed as part of a subduction-related accretionary prism to the south of the forearc basin sequence (Figs. 21 and 22 A). By ~80 Ma, the Greater India was located > 4000 km south of the southern Lhasa terrane at latitude 20°S (Torsvik et al., 2012).

4.7.6.2. Stage 2: ~50 Ma

Closure of the Neotethys ocean and initial India-Asia collision resulted in the obduction of ophiolitic rocks atop the margin of Greater India (Figs. 21 and 22B). Ophiolitic belts of the Himalayan orogen and Eastern Flanking Belt emplaced during this time include the IYSZ, Tidding-Mayodia mélange complex, Western Belt Ophiolites, Naga ophiolitic mélange, and Andaman ophiolite (Fig. 21). In the northern Indo-Burma Ranges, the Tidding-Mayodia mélange complex was thrust atop the Indian margin by the Tidding thrust (Figs. 21 and 22B). Initial shortening across the Tethyan thrust belt occurred along the India-Asia collisional margin (e.g., Murphy and Yin, 2003) (Fig. 21 and 22B). The northeastern margin of Greater India collided with the West Burma microplate at a highly-oblique angle, suggesting some component of right-slip shear along the plate boundary (Fig. 21).

Magmatism continued into the Cenozoic along a belt encompassing the southern Lhasa terrane and northern Indo-Burma Ranges (Fig. 21). In the central to southern zones of the Eastern Flanking Belt, northward subduction of relict Neotethys lithosphere attached to the eastern margin of India resulted in Cenozoic magmatism along parallel “dual arcs” including the Wuntho-Popa arc and

Mogok-Mandalay-Mergui belt (Morley and Searle, 2017; Replumaz and Tapponnier, 2003) (Fig. 21).

4.7.6.3. Stage 3: ~20 Ma

By Miocene time, widespread arc magmatism ceased throughout the Lhasa terrane (Fig. 21), whereas the generation of sparse igneous rocks occurred till ~10 Ma (Coulon et al., 1986). Along the Himalayan orogen, an initial phase of shortening along the IYSZ occurred as the Gangdese thrust placed the southern Gangdese batholith atop Xigaze forearc sediments and ophiolitic mélange rocks (Yin et al., 1994; 1999). In the northern Indo-Burma Ranges, slip along the south-directed Walong and Lohit thrusts shortened the Lohit Plutonic Complex (Figs. 21 and 22C-D). Mesozoic granitoids of the western Lohit Plutonic Complex belt were thrust atop Cenozoic granitoids equivalent to the southern Gangdese batholith (Figs. 21 and 22C-D). Continued motion along the structurally-lower Tidding thrust resulted in (1) uplift of Cenozoic granitoids and (2) exhumation and retrograde metamorphism of metasedimentary rocks of the Tidding-Mayodia mélange complex from >30 km depth (Figs. 22C-D). By Miocene(?) time, the northern Indo-Burma thrust belt propagated southwards to include the GHC and LHS (i.e., Mayodia gneiss and Lalpani schist) of the Indian cratonal sequence as the Demwe thrust initiated (Figs. 22C-D). Tethyan Himalayan rocks and Cenozoic granitoids of the Lhasa terrane thrust atop the Indian cratonal sequence were eroded and deposited in a syntectonic foreland basin along the range front (i.e., deposition of the Sewak and Tezu units) (Fig. 21D). In the eastern Himalayan orogen, a second phase of shortening occurred along the IYSZ as the Greater Counter thrust (=Renbu-Zedong thrust) placed the ophiolitic mélange rocks atop the Xigaze forearc basin (Yin et al., 1999).

Clockwise rotation and crustal shortening of the Eastern Flanking Belt increased with distance from the pole at the eastern Himalayan syntaxis, resulting in a northwest-trend of the belt (Fig. 21). By 20 Ma, the right-slip Jiali fault zone initiated in the eastern segment of Lhasa terrane to accommodate further clockwise rotation of overriding plate lithosphere (Lee et al., 2003) (Figs. 21 and 22D).

In the southern Indo-Burma Ranges, southwest- to west-directed thrust belts developed within continental shelf deposits to the west of the Central Burma basin as the Indian continent was underthrusted below (Morley and Searle, 2017) (Figs. 21). Magmatism continued throughout the central and southern zones of the Eastern Flanking Belt due to subduction of relict Neotethys lithosphere (Mitchell et al., 2012) (Fig. 21). Opening of the Andaman rift system in the back-arc region of the Andaman subduction zone was coeval with right-slip transtension along the incipient Sagaing fault between the West Burma microplate and Sibumasu plate (Morley and Searle, 2017) (Fig. 21). Slip along the Sagaing fault resulted in transpressional deformation and basin inversion in eastern sections of the Central Burma basin (Morley, 2004; Morley and Searle, 2017).

In southeast Tibet, motion along the left-slip Red River and Gaoligong faults and right-slip Chong Shan fault occurred during southeastward extrusion and clockwise rotation of Indochina (Leloup et al., 1995; Harrison et al., 1996; Akciz et al., 2008; Eroğlu et al., 2013; Wang et al., 2000) (Fig. 21). Cessation of left-slip along the Red River fault at ~20-17 Ma coincides with initiation of slip along the MCT in the Himalayan orogen (Harrison et al., 1992, 1996).

4.7.6.4. Stage 4: ~10 Ma

By the late Miocene, the right-slip Parlung and Puqu faults of the Jiali fault zone initiated in southeastern Tibet to accommodate continued clockwise rotation of overriding plate lithosphere

around the eastern Himalayan syntaxis (Figs. 21 and 22E). In the northern Indo-Burma Ranges, the Cenozoic southern Gangdese batholith, forearc basin sequence, GHS, and THS had been involved in the thrust belt and were completely eroded or underthrusted (Figs. 21 and 22D). The Lalpani thrust initiated in the foreland of the thrust belt, while the Hunli duplex developed at depth within rocks of the Lalpani schist, which folded the overlying Demwe thrust and hanging wall of the Mayodia gneiss and Tidding-Mayodia mélange complexes. Subsequent erosion resulted in exposure of the Hunli half-window and Mayodia klippe (Fig. 9). Tertiary syntectonic strata including the Sewak and Tezu units were incorporated in the thrust belt as the Tezu and Mishmi thrusts initiated (Fig. 22D). At some point during clockwise rotation of the Eastern Flanking Belt to a trend of north-south, the Mishmi thrust developed a right-slip component to accommodate northward indentation of India (Fig. 22D).

In the central and southern zones of the Eastern Flanking Belt, right-slip faults including the Sagaing fault and Sumatra and West Andaman faults were active (Raju et al., 2004; Morley and Searle, 2017), while the Andaman rift developed series of right-stepping transforms and spreading centers (Raju et al., 2004) (Fig. 21). Thrust belts of the southern Indo-Burma Ranges propagated further westward to include Cenozoic sediments of the Bengal Basin (Fig. 21). By the Late Miocene, the present-day strain regime across the Eastern Flanking Belt developed including distributed right-slip transpression across the Indo-Burma Ranges and West Burma block (Morley and Searle, 2017). Alkaline and calc-alkaline volcanism continued throughout the central zone of the Eastern Flanking Belt, likely due to dehydration of a piece of Neotethys lithosphere still attached to the eastern margin of India (Maury et al., 2004; Mitchell et al., 2012). Continued subduction of this relict slab of Neotethys lithosphere occurred at a highly oblique angle, resulting

in a large component of right-slip shear along the plate boundary at depth (i.e., Southern Myanmar shear zone) (Nielsen et al., 2004; Rangin et al., 2013).

By the mid-Miocene, the Chong Shan and Gaoligong faults became inactive in southeastern Tibet. Left-slip motion along the Red River fault fully transitioned to right-slip at ~5 Ma (Leloup et al., 1995; Replumaz et al., 2001). South of the Himalayan orogen, the Dauki and Oldham thrusts accommodated uplift of the Shillong Plateau (Clark and Bilham, 2008).

4.8. Conclusions

In this chapter, we presented an investigation of the structural framework, metamorphic *P-T* conditions, and tectonic evolution of the northern Indo-Burma Ranges, the easternmost segment of the Himalayan collisional system. Main findings include (1) the study area is dominated by south- to east- directed thrusts, consistent with end-member models of clockwise continuum flow around the eastern Himalayan syntaxis, (2) the décollement of the thrust belt extends to >30 km depth, based on *P-T* constraints of metamorphic rocks, and (3) reconstruction of one balanced cross-section across the study area yields a minimum shortening estimate of >156 km (~81%) shortening strain. Our shortening estimate combined with the absence of several previously-existing Himalayan-Tibetan lithologic units and the southward decrease in the width of the thrust belt suggest Cenozoic crustal shortening and/or continental underthrusting increases to the east across the eastern Himalayan syntaxis. The mode of active deformation in the study area is expressed by right-slip transpression partitioned between the oblique-slip Mishmi thrust and the right-slip Jiali fault zone to accommodate clockwise flow of lithosphere around the eastern Himalayan syntaxis. The Mishmi thrust and Naga thrust are both kinematically linked to the right-slip Sagaing fault by a left-stepping restraining bend (i.e., Namdapha Corridor). This structural

relationship provides a key example of the spatial transition in continental deformation of clockwise flow and transpression around the corner of an indenter to discrete right-slip motion along the side of an indenter during the collision process. Our findings show that the structural development of the northern Indo-Burma Ranges was not exclusive, but had an integral relationship with the Mesozoic-Cenozoic tectono-magmatic evolution of the eastern Himalaya, southeast Tibetan Plateau, and Eastern Flanking Belt.

4.9. Figures and Tables

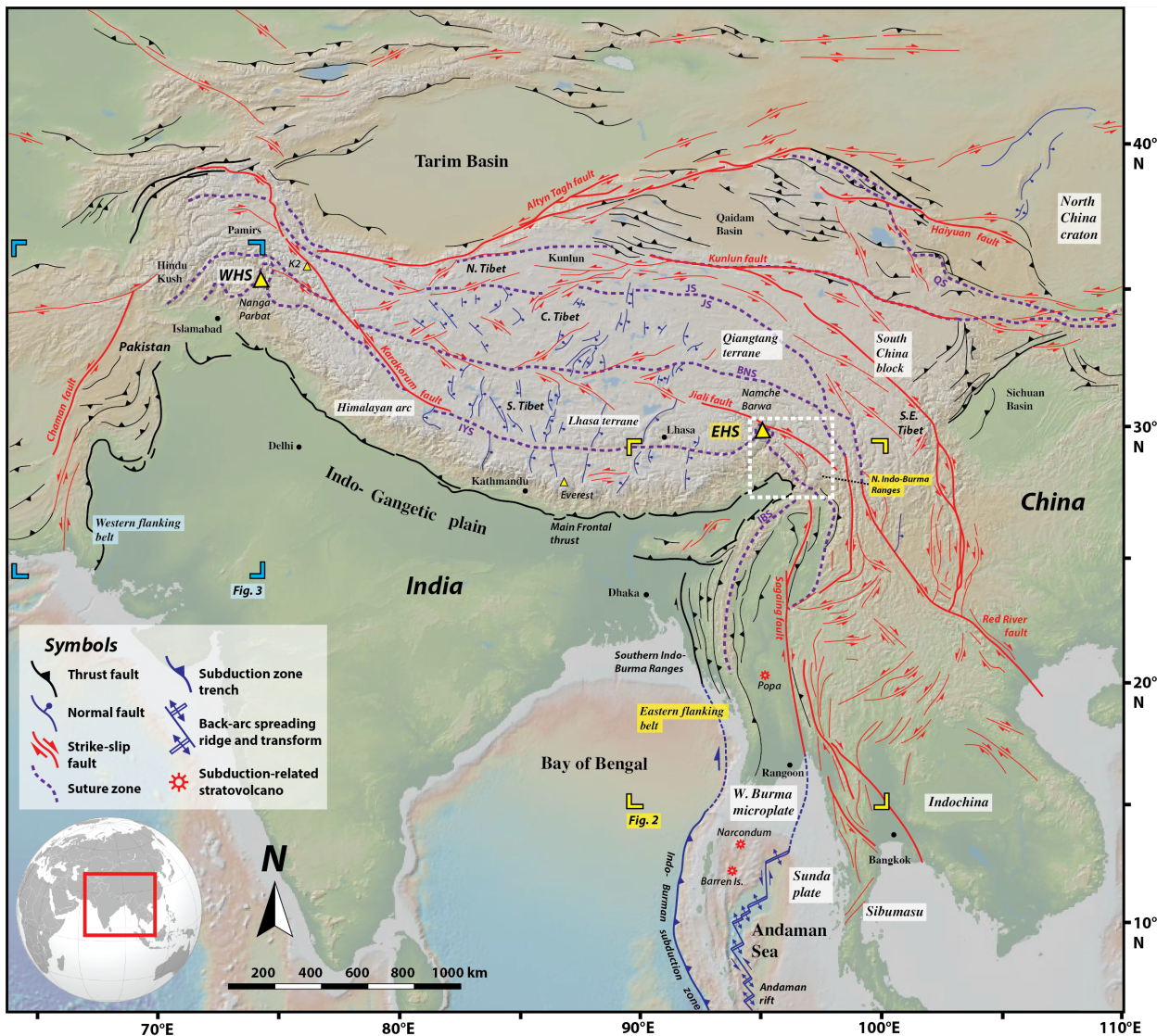


Figure 4.1. Neotectonic map of the India-Asia orogenic system, adapted from Hapgood et al. (2018). The northern Indo-Burma Ranges is shown within the white box. The base digital elevation model was acquired using geomapapp.com (Ryan et al., 2009). The Earth index map was acquired through Generic Mapping Tools (gmt.soest.hawaii.edu). Abbreviations: BNS: Bangong-Nujiang suture, EHS: eastern Himalayan syntaxis, IBS: Indo-Burma suture, IYS: Indus-Yarlung suture, JS: Jinsha suture, QS: Qilian suture, WHS: western Himalayan syntaxis.

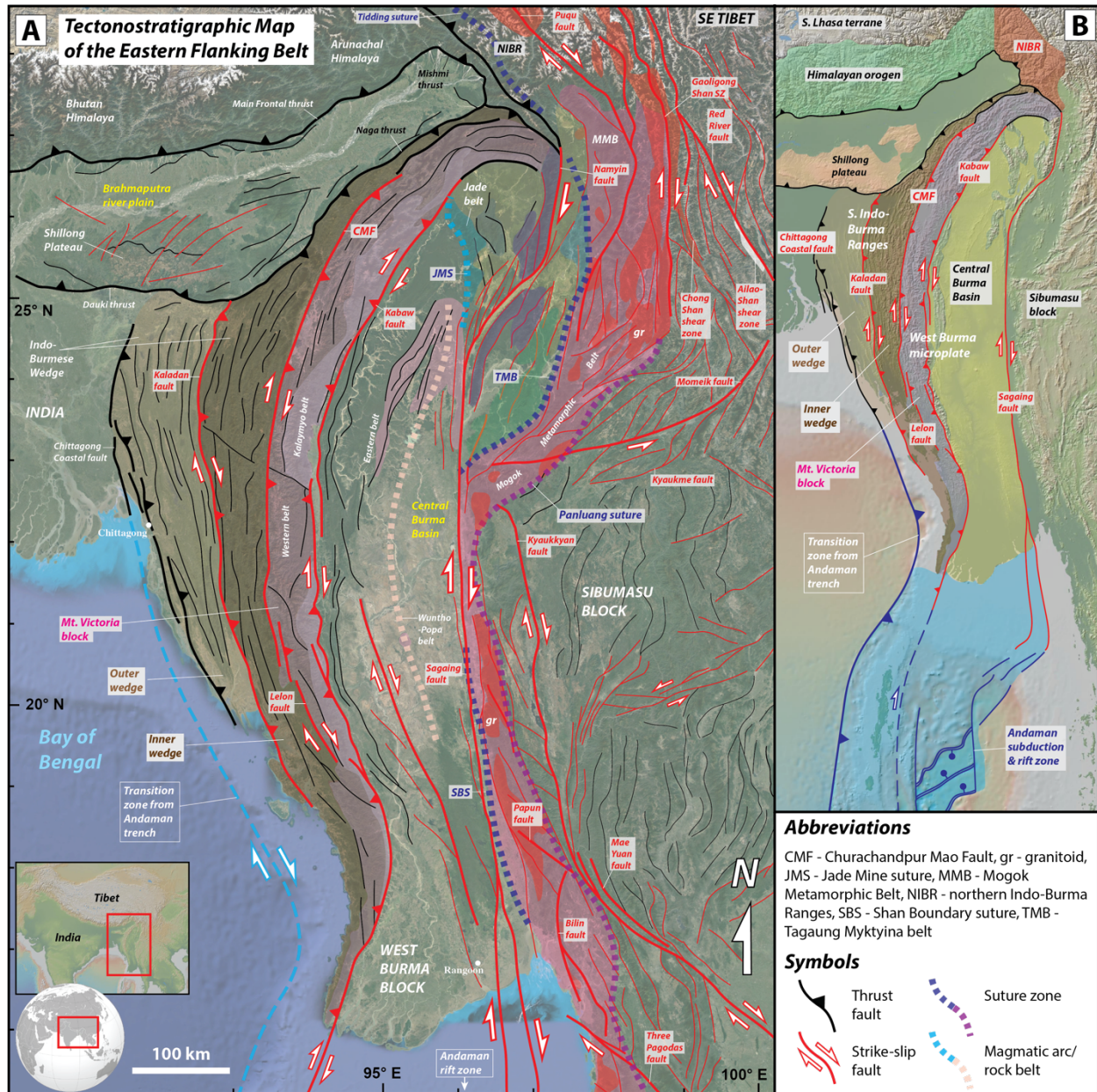


Figure 4.2. Tectonostratigraphic map of the Eastern Flanking Belt. Map location is shown on Fig. 1. Map is compiled from Archaryya, (1987), Morley (2004), Mitchell et al. (2007), Searle et al. (2007), Searle and Morley (2011), Watkinson et al. (2011), Watkinson (2011), Tun et al. (2014), Ridd and Watkinson (2013), and Morley and Searle (2017).

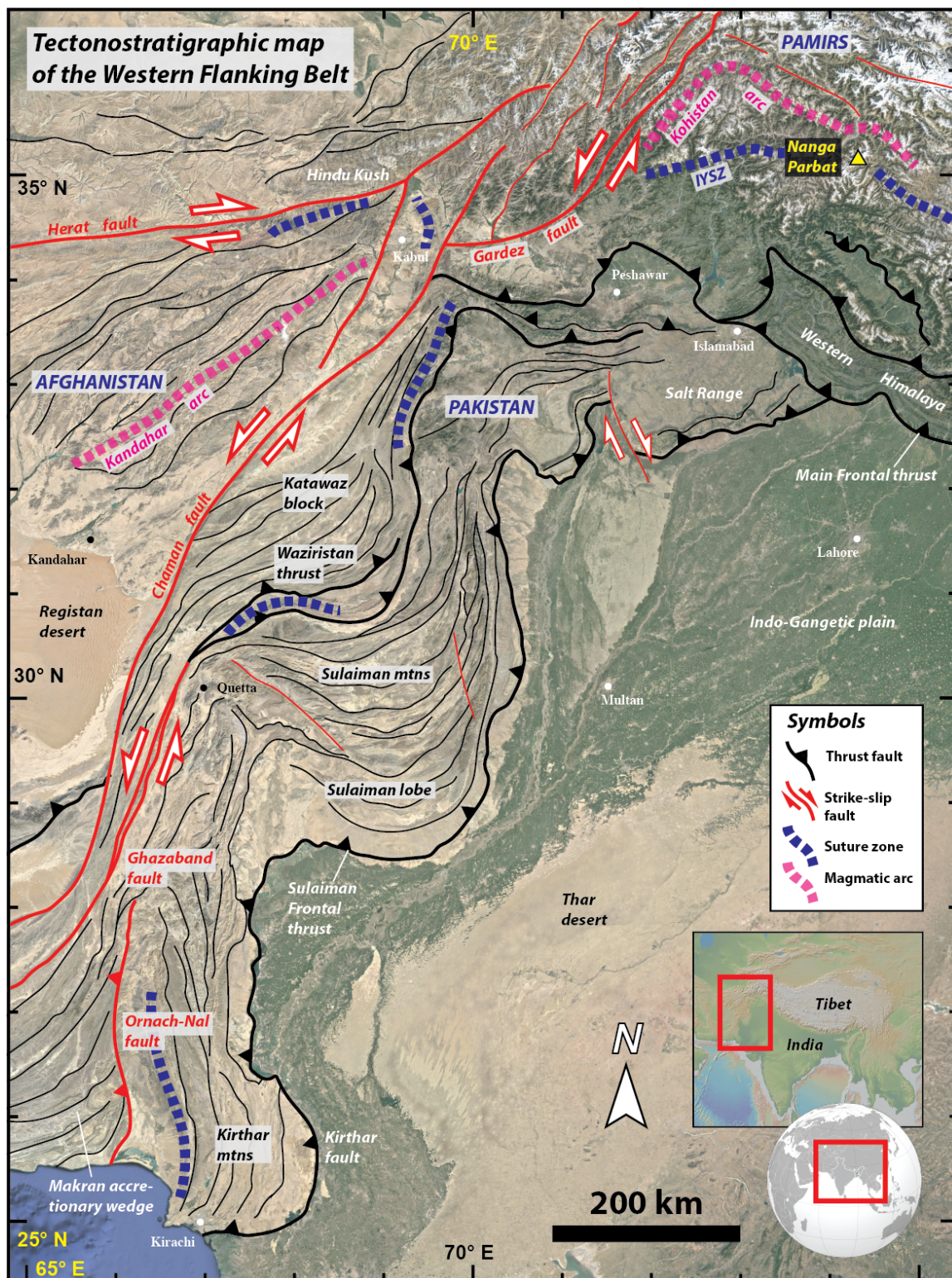


Figure 4.3. Tectonostratigraphic map of the Western Flanking Belt, compiled from Haq and Davis (1997) and Schelling (1999).

Models of deformation around the eastern Himalayan syntaxis

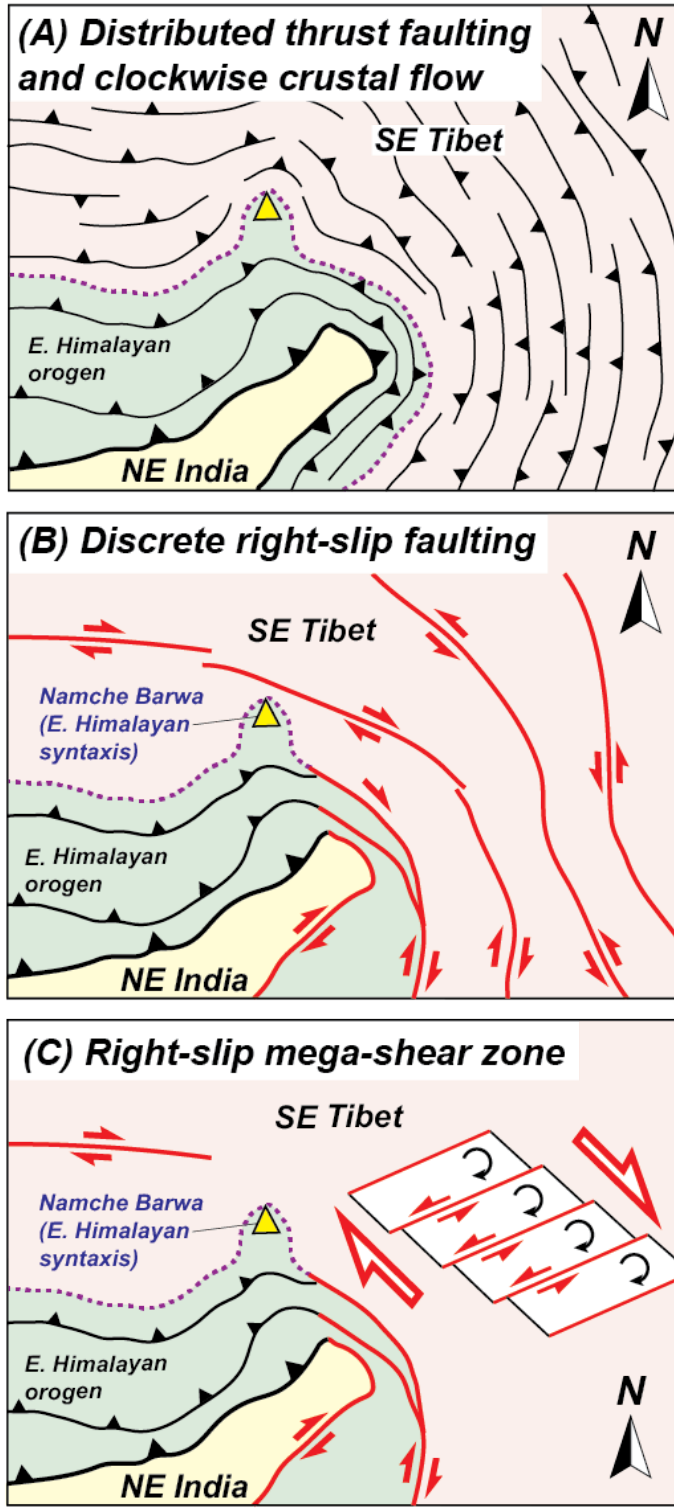


Figure 4.4. Models for upper plate continental deformation surrounding the eastern Himalayan syntaxis during the Cenozoic India-Asia collision consisting of (A) distributed thrust faulting during clockwise crustal flow, (B) discrete strike-slip faulting, and (C) series of northwest-striking, left-slip bookshelf faults accommodating southeast-oriented, right-slip shear (modified from Haproff et al., 2018).

Himalayan orogen - Lhasa terrane

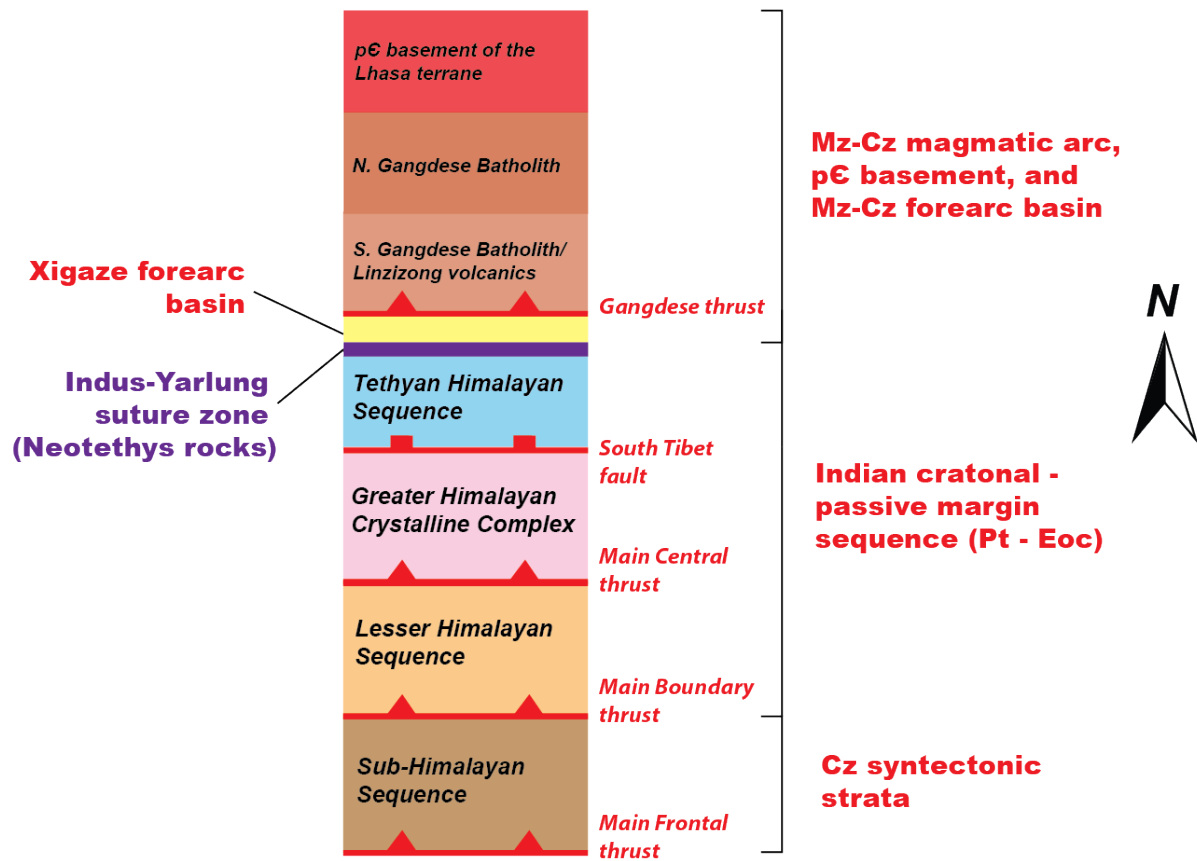


Figure 4.5. Simplified tectonostratigraphic column of major lithologic units and structures of the Himalayan orogen and Lhasa terrane, modified from Yin (2006).

Northern Indo-Burma Ranges

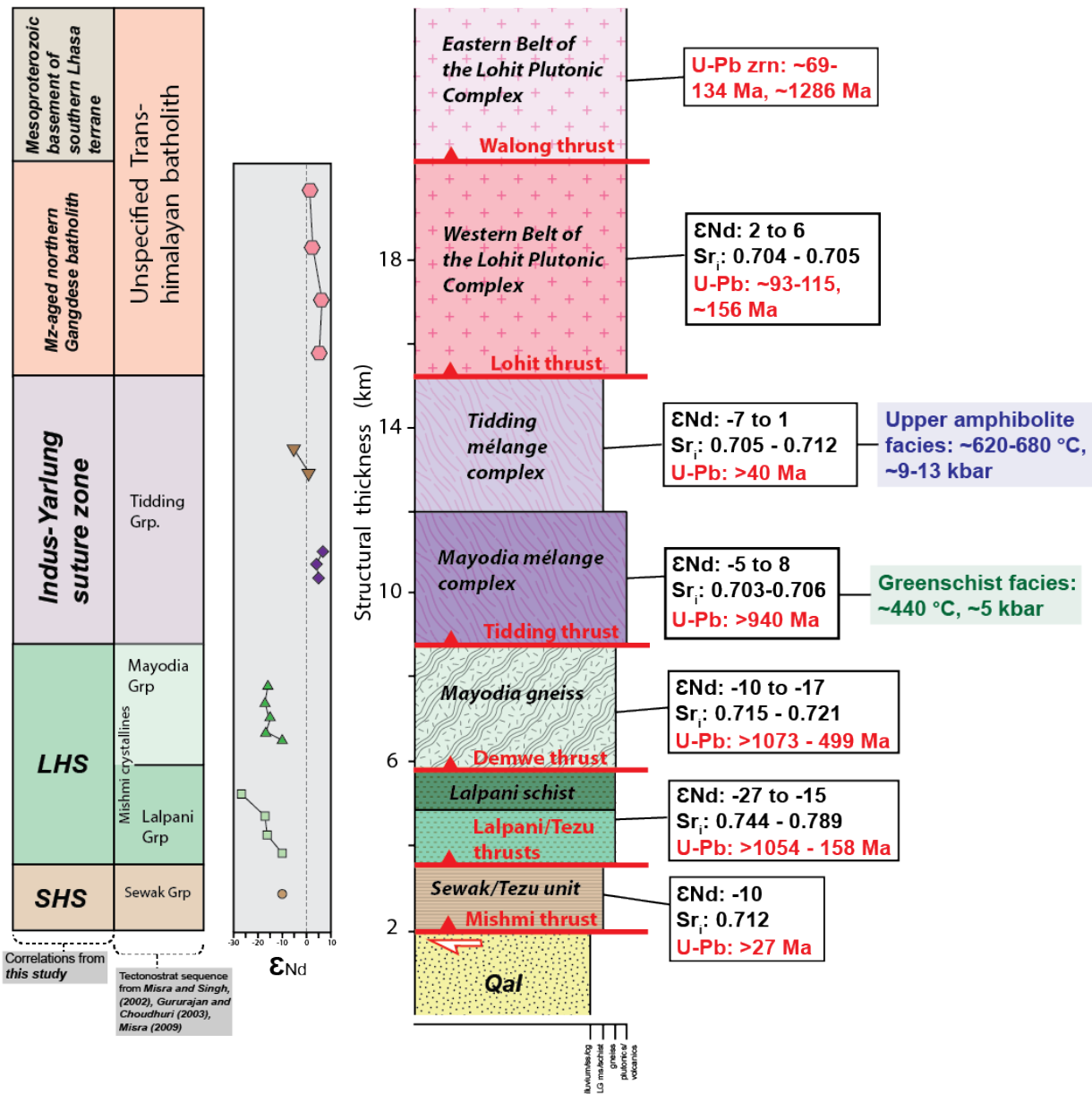


Figure 4.6. Tectonostratigraphic column of major lithologic units and faults of the northern Indo-Burma thrust belt, including P - T determinations, U-Pb ages, and ϵ_{Nd} and Sr_i values (Haproff et al., 2018, in preparation). Interpretations of tectonostratigraphic correlation between the study area and Himalayan orogen are shown for this study and Misra and Singh (2002), Gururajan and Choudhuri (2003), and Misra (2009).

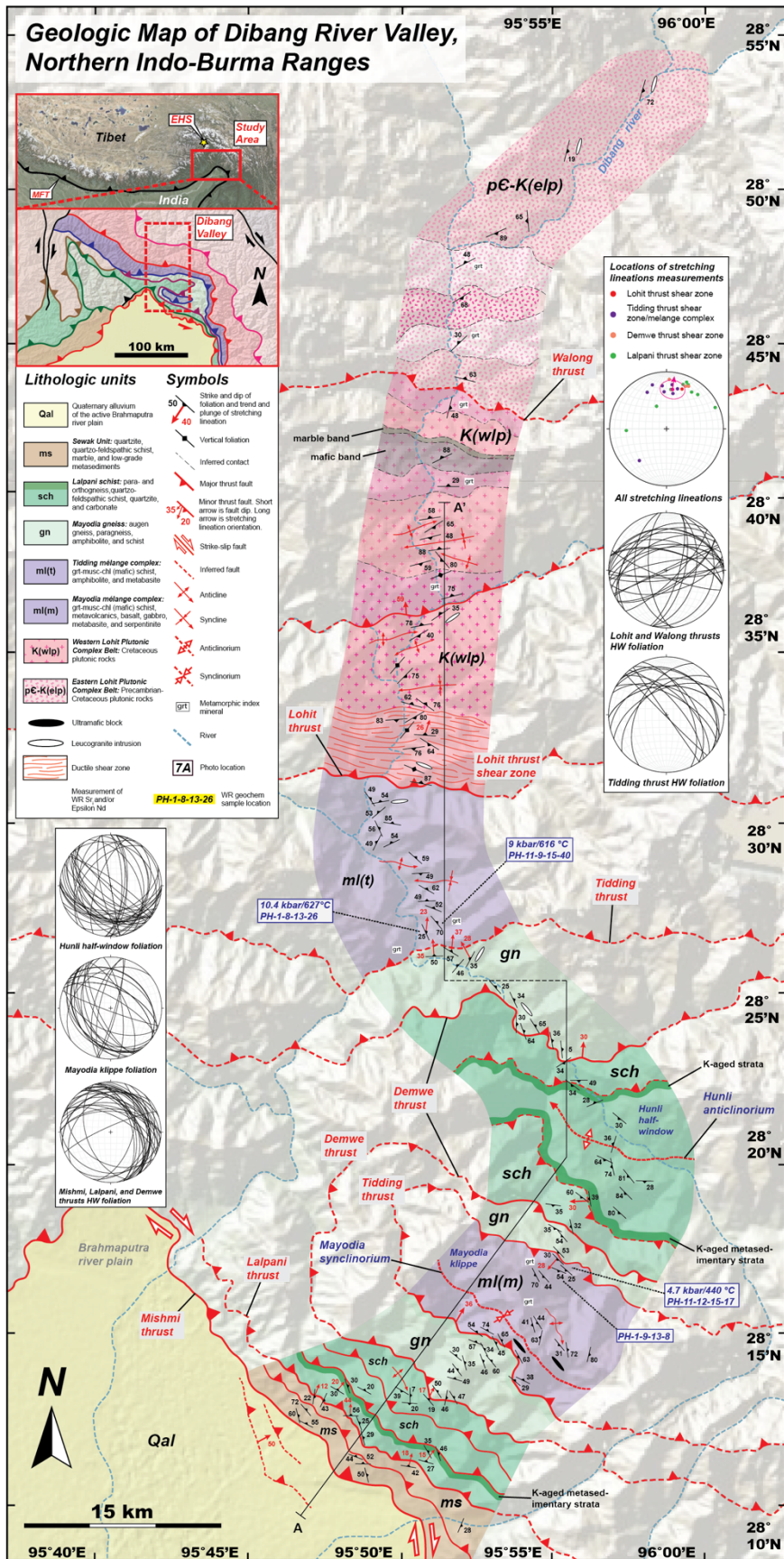


Figure 4.7. Geologic map of the Dibang Valley traverse, modified from Haproff et al. (2018).

Abbreviations: EHS: eastern Himalayan syntaxis, HW: hanging wall, MFT: Main Frontal thrust.

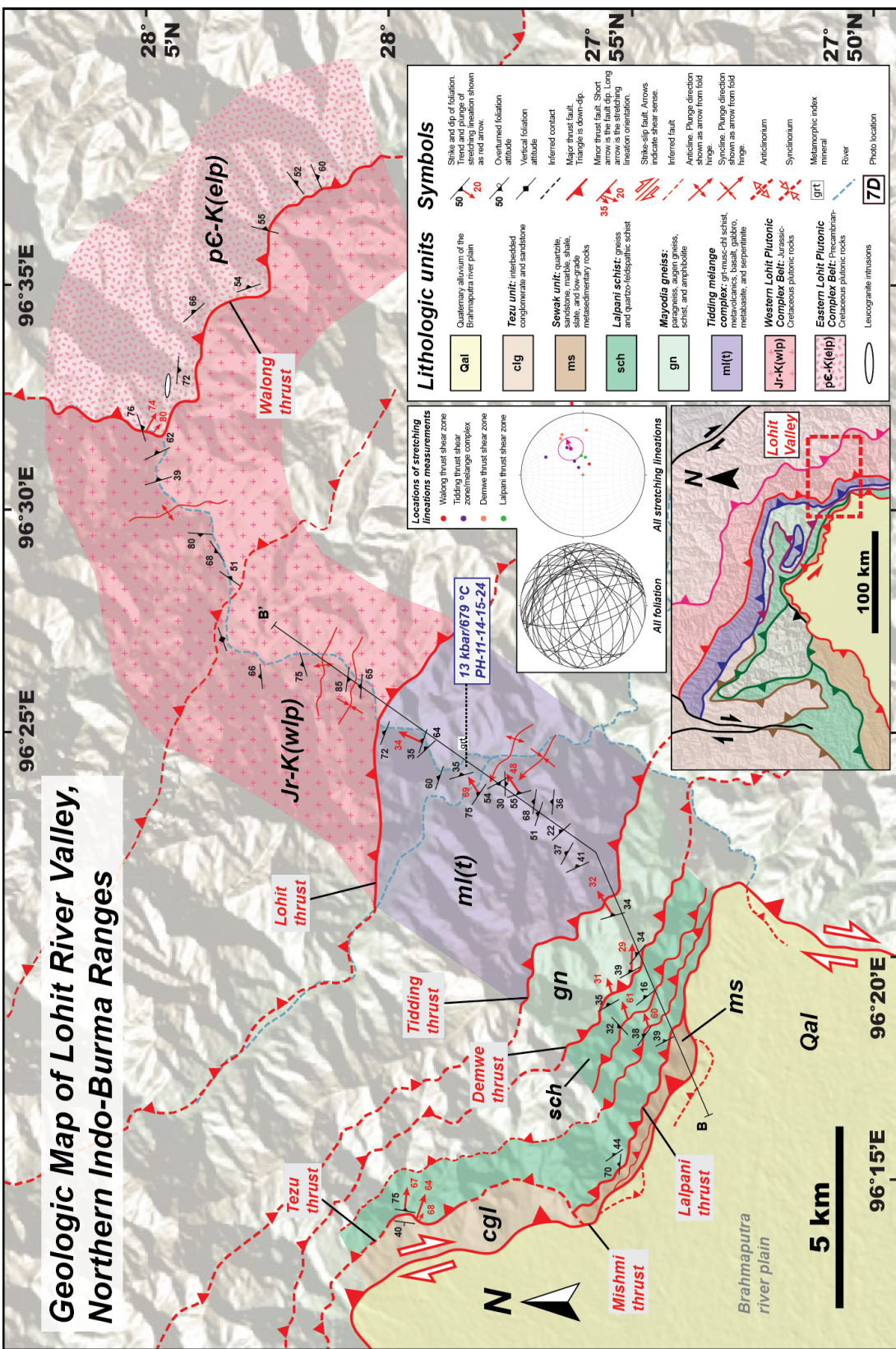


Figure 4.8. Geologic map of the Lohit Valley traverse, modified from Haproff et al. (2018).

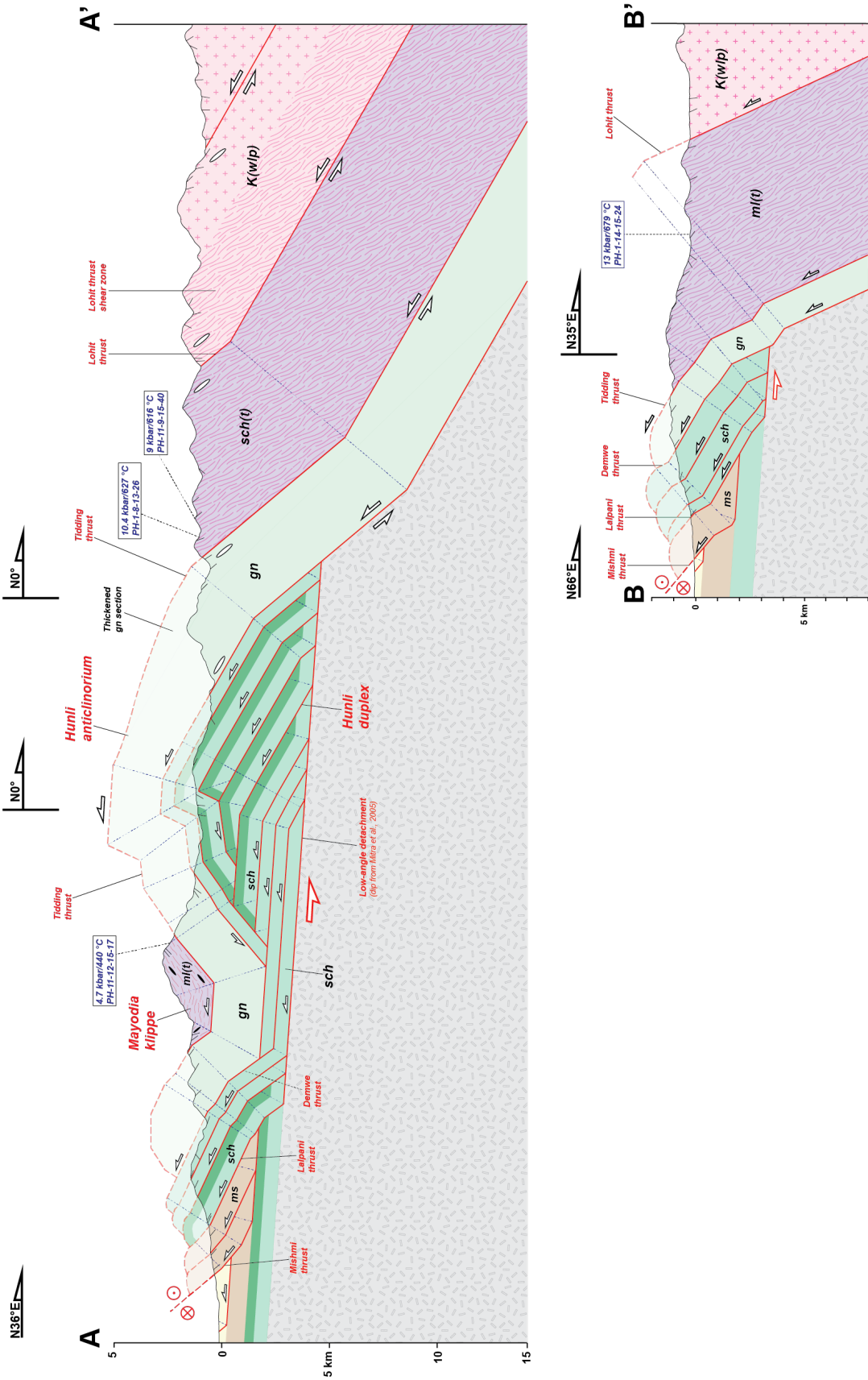


Figure 4.9. Balanced cross sections along the (A) Dibang Valley traverse oriented SW-NE (A-A') and (B) Lohit Valley traverse oriented SW-NE (B-B'), modified from Haproff et al. (2018).

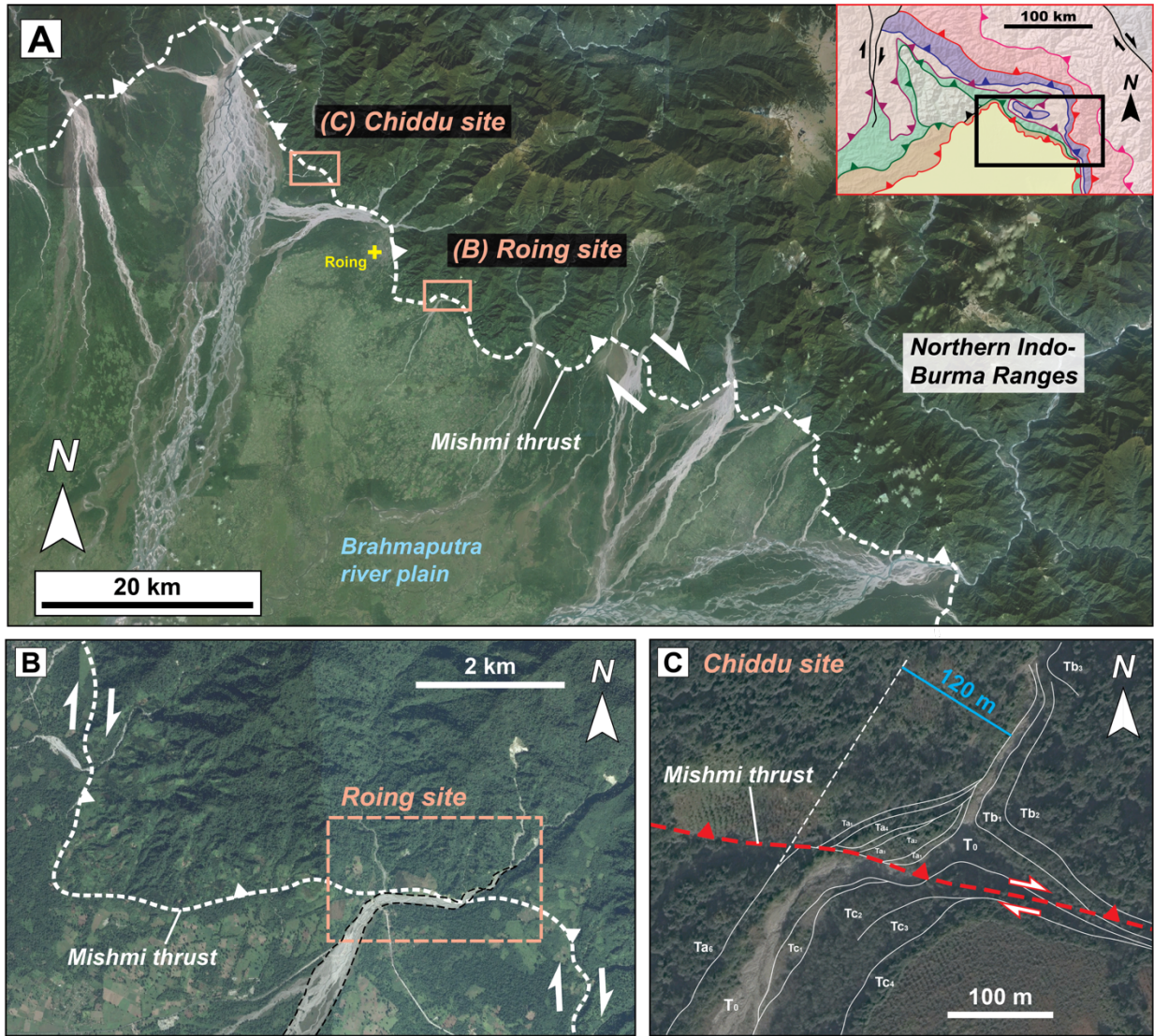


Figure 4.10. Google Earth-based maps of the range-bounding Mishmi thrust, including (A) the surface trace of the fault along the southwest margin of the northern Indo-Burma Ranges, (B) the Roing site along the fault showing a right-lateral deflection of an active stream channel, and (C) the Chiddu site along the fault showing right-lateral displacement of fluvial terraces (Haproff et al., 2018).

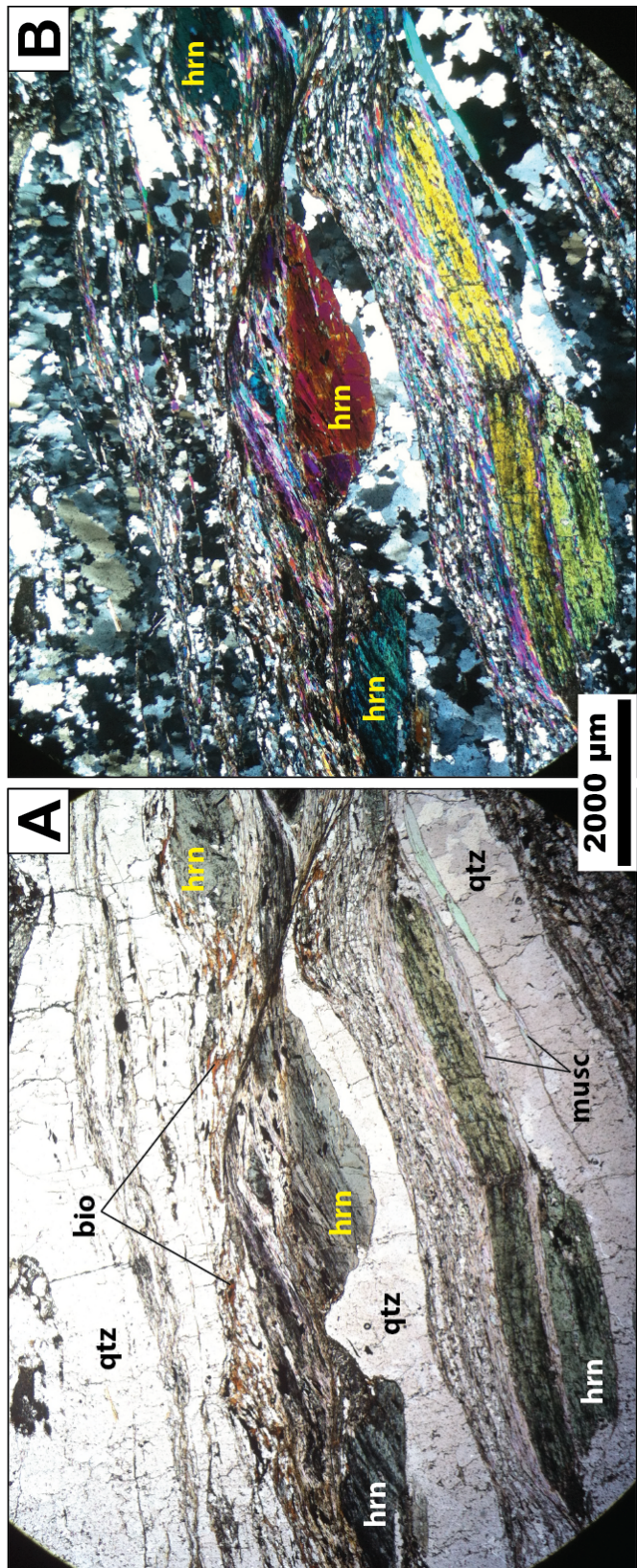


Figure 4.11. Photomicrographs of garnet mica hornblende schist *PH-1-8-13-26* of the Tidding mélange complex in (A) ppl and (B) xpl. (C) Large (~8 mm diameter) garnets display snowball texture indicative of top-southwest rotation during shear.

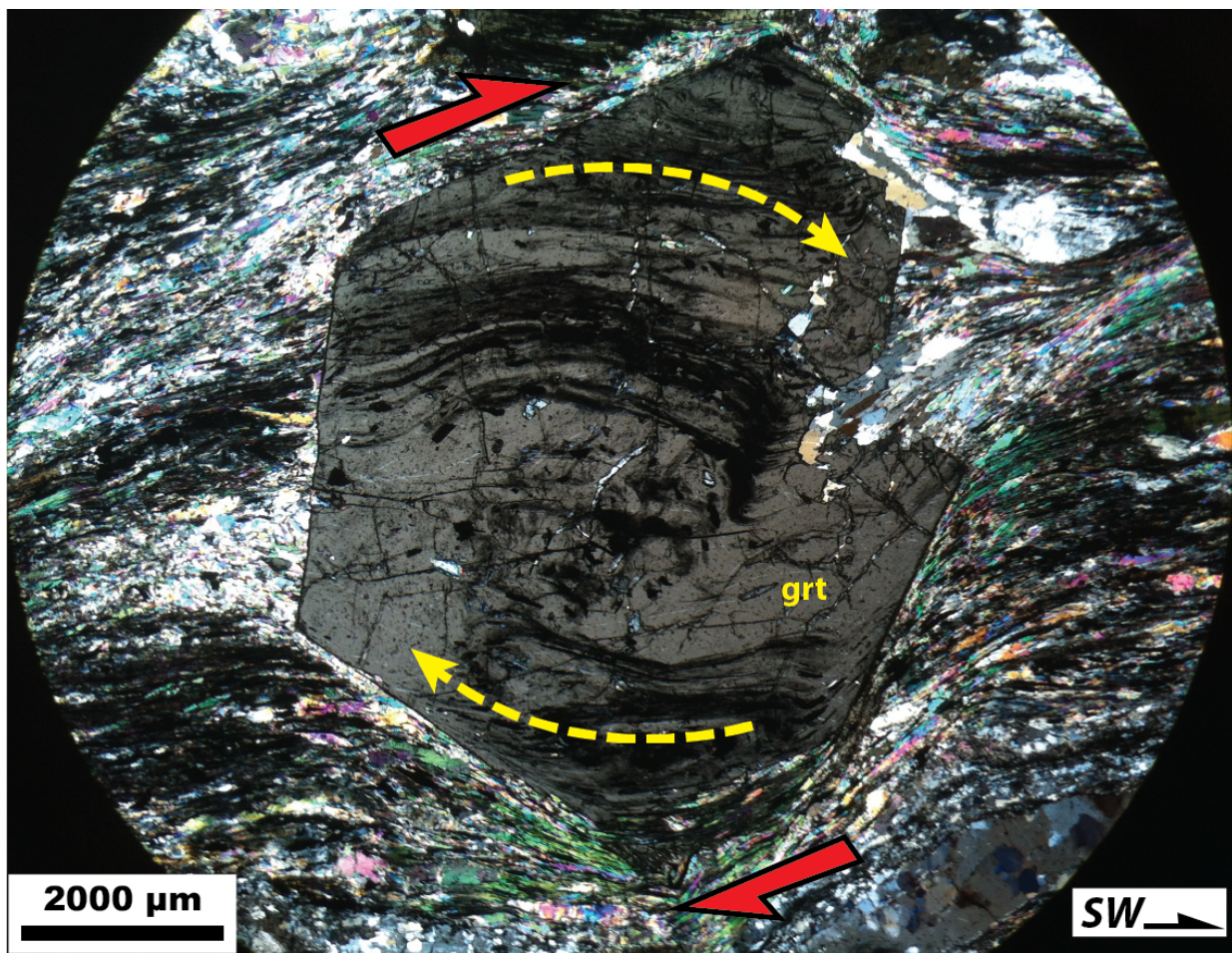


Figure 4.12. Photomicrograph of garnet mica hornblende schist *PH-1-8-13-26* of the Tiddings mélange complex showing snowball garnet texture indicative of rotation during southwest-directed shear.

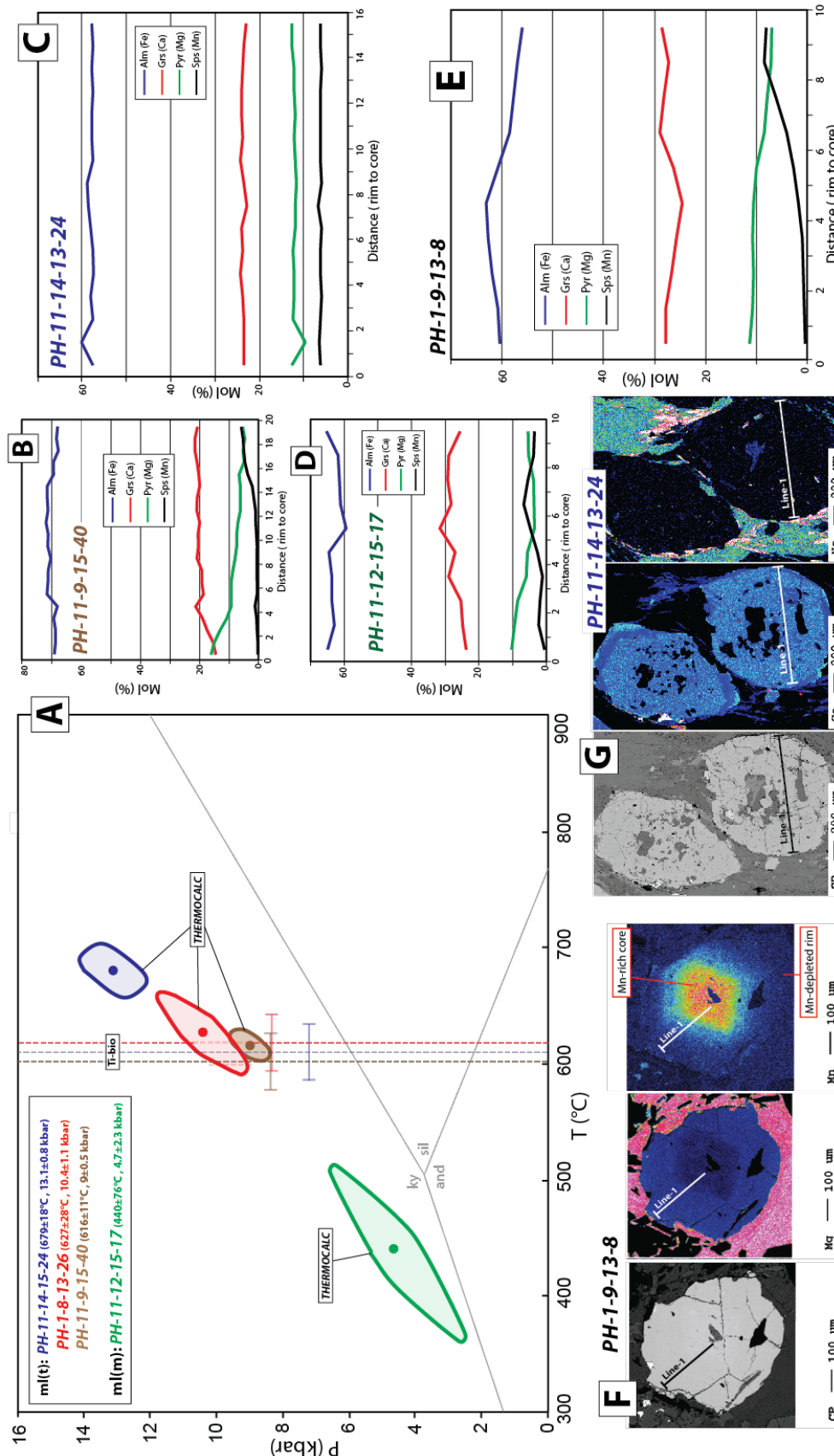


Figure 4.13. (A) Plot of peak pressure and temperature determinations for metamorphic rocks of the Tidding and Mayodia mélange complexes, calculated using THERMOCALC 3.37. (B-E) Garnet traverse plots of almandine, grossular, pyrope, and spessartine contents derived from electron microprobe data for the Tidding and Mayodia mélange complexes. Samples *PH-11-12-15-17*, *PH-11-9-13-8* show prograde growth zoning (Mn-rich, Mg-depleted core), whereas *PH-11-8-13-26* shows a homogenous composition equilibrated at higher temperatures. (F-G) Backscatter electron images and Mn-Mg element maps of measured garnets from *PH-11-9-13-8* and *PH-11-14-15-24*.

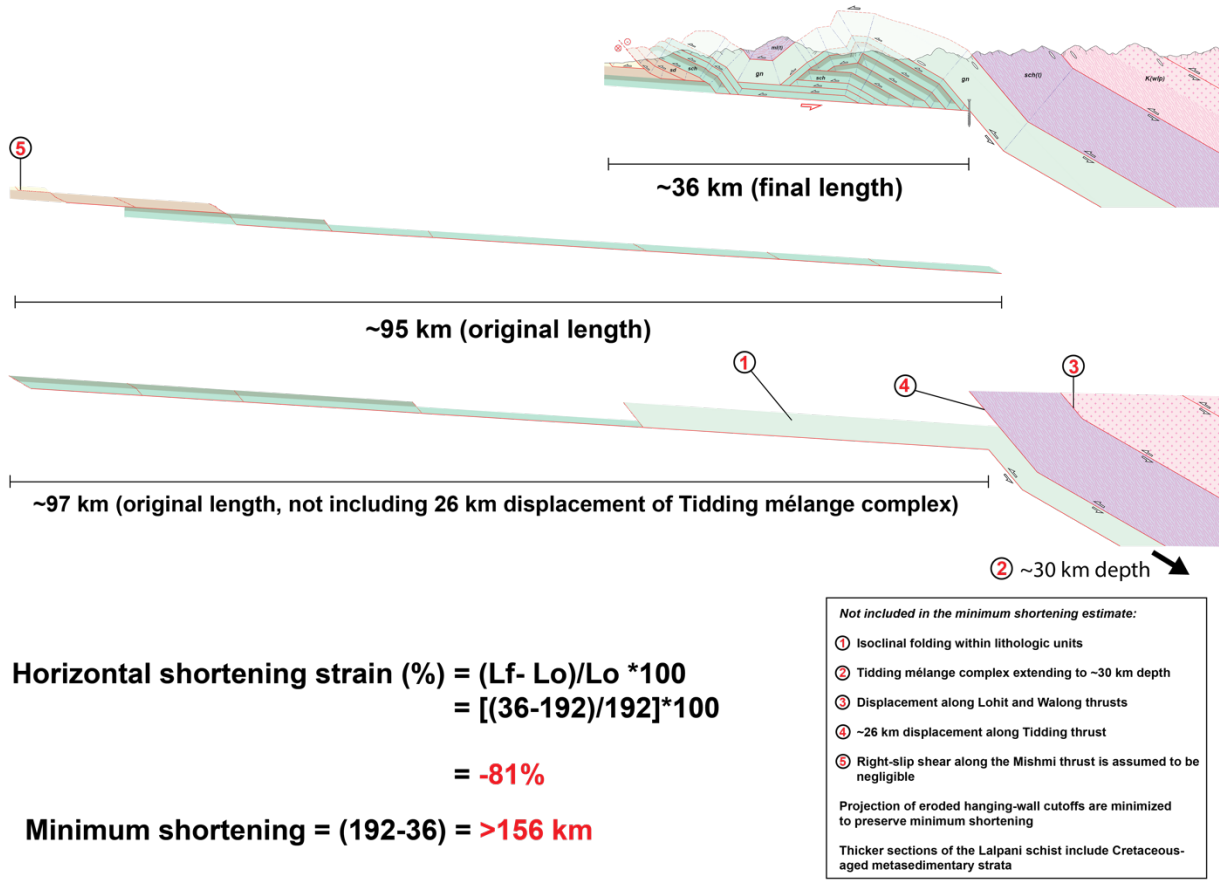


Figure 4.14. Reconstruction of the Dibang Valley balanced cross section. The original ~192-km-long section was shortened to 36 km, yielding >156 km (~81%) strain. Assumptions and factors not included in the minimum shortening estimate are described in the bottom-right box.

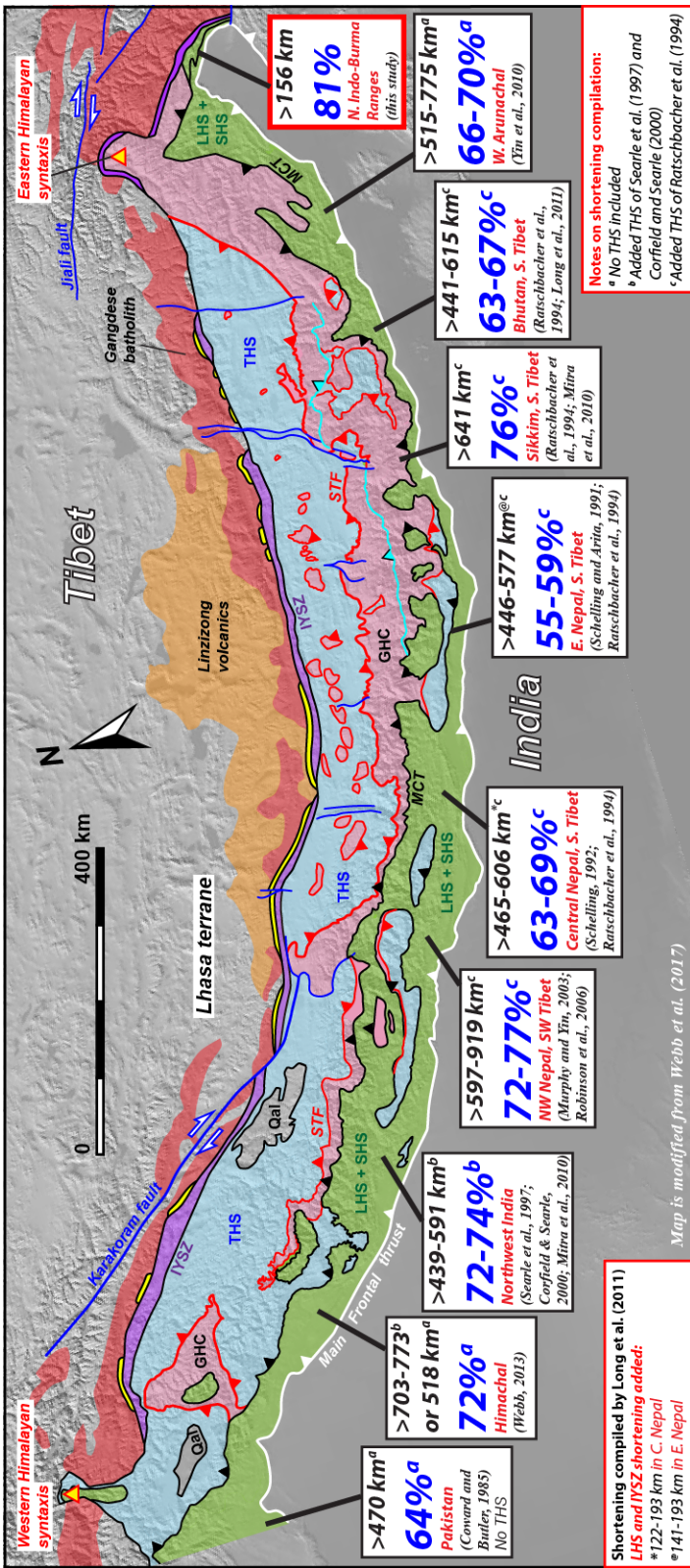


Figure 4.15. Schematic geologic map showing crustal shortening estimates of studies across the Himalayan orogen and northern Indo-Burma thrust belt. Base geologic map is modified from Webb et al. (2017).

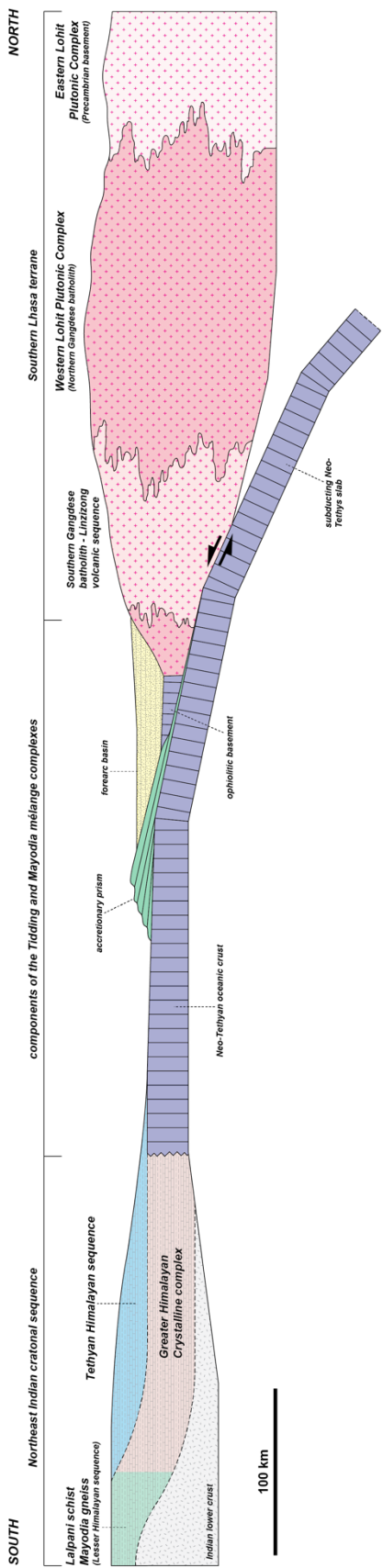


Figure 4.16. Schematic cross section of the pre-collisional configuration of major lithologic units of the northern Indo-Burma Ranges including the northeast Indian cratonal sequence, Neotethys subduction system, and the southern Lhasa terrane during the Cretaceous.

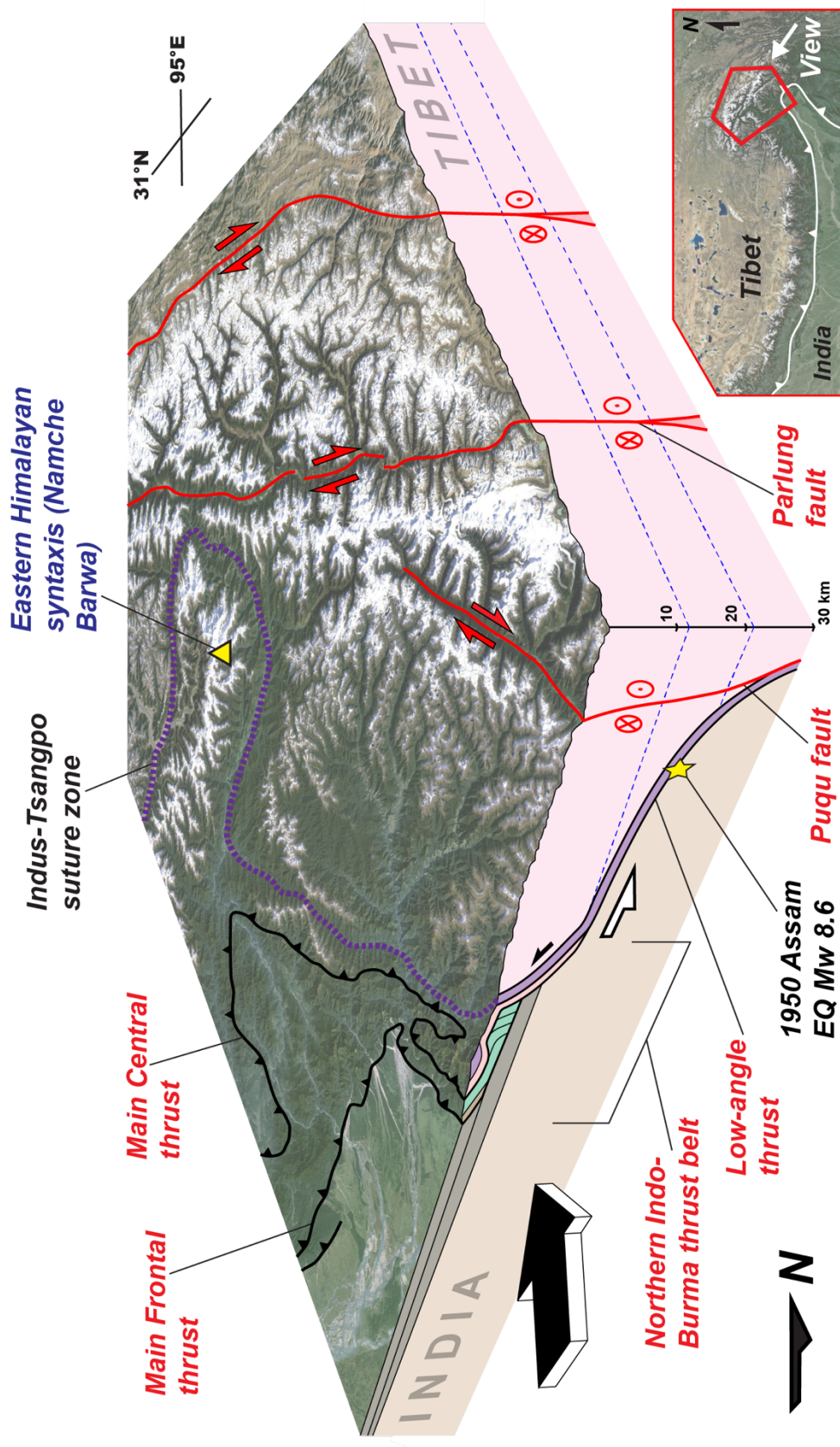


Figure 4.17. Oblique-view block diagram of lithospheric deformation across the northern Indo-Burma Ranges and southeastern Tibetan Plateau.

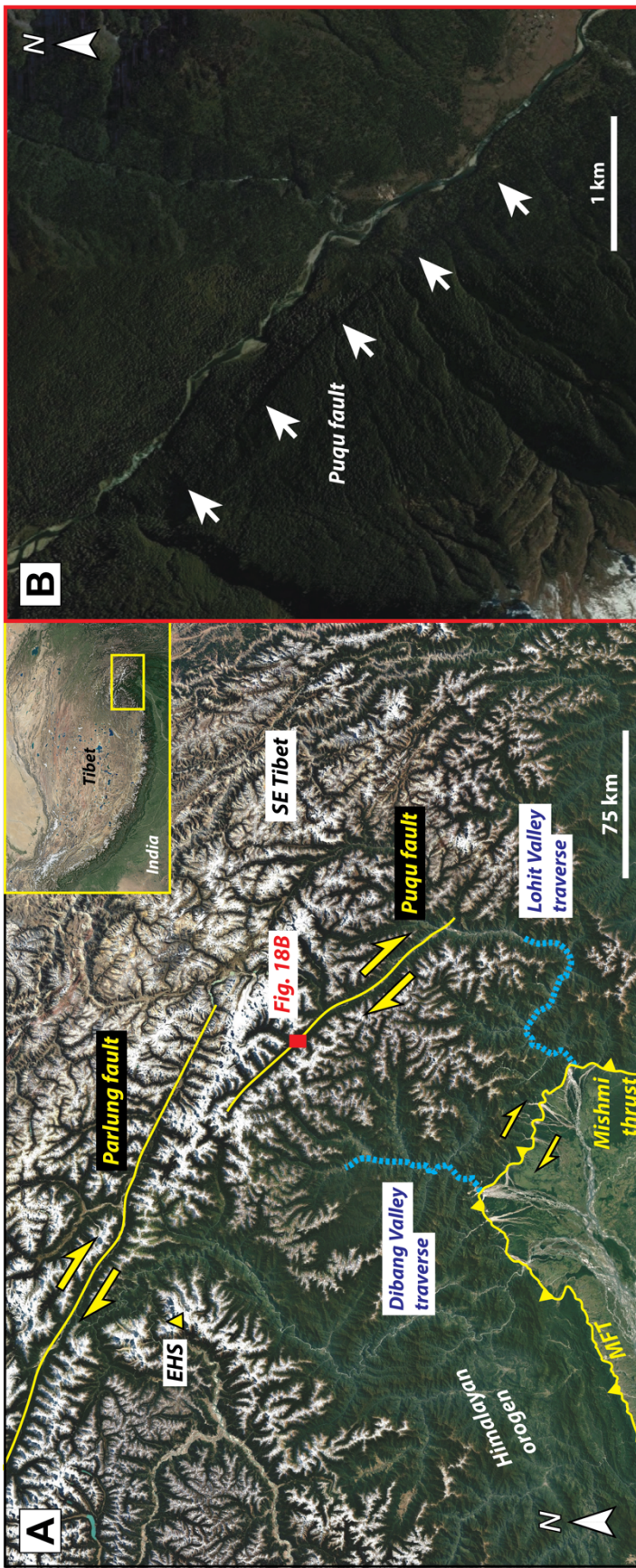


Figure 4.18. Google-Earth-based maps of (A) the northern Indo-Burma Ranges, showing the locations of the major faults including the Mishmi thrust, Puqu fault, and Parlung fault. The locations of the Dibang Valley and Lohit Valley traverses and Eastern Himalayan syntaxis (EHS) are also shown and (B) the geomorphic expression of the active Puqu fault, including linear scarps and beheaded river. Map location is shown in Fig. 18A.

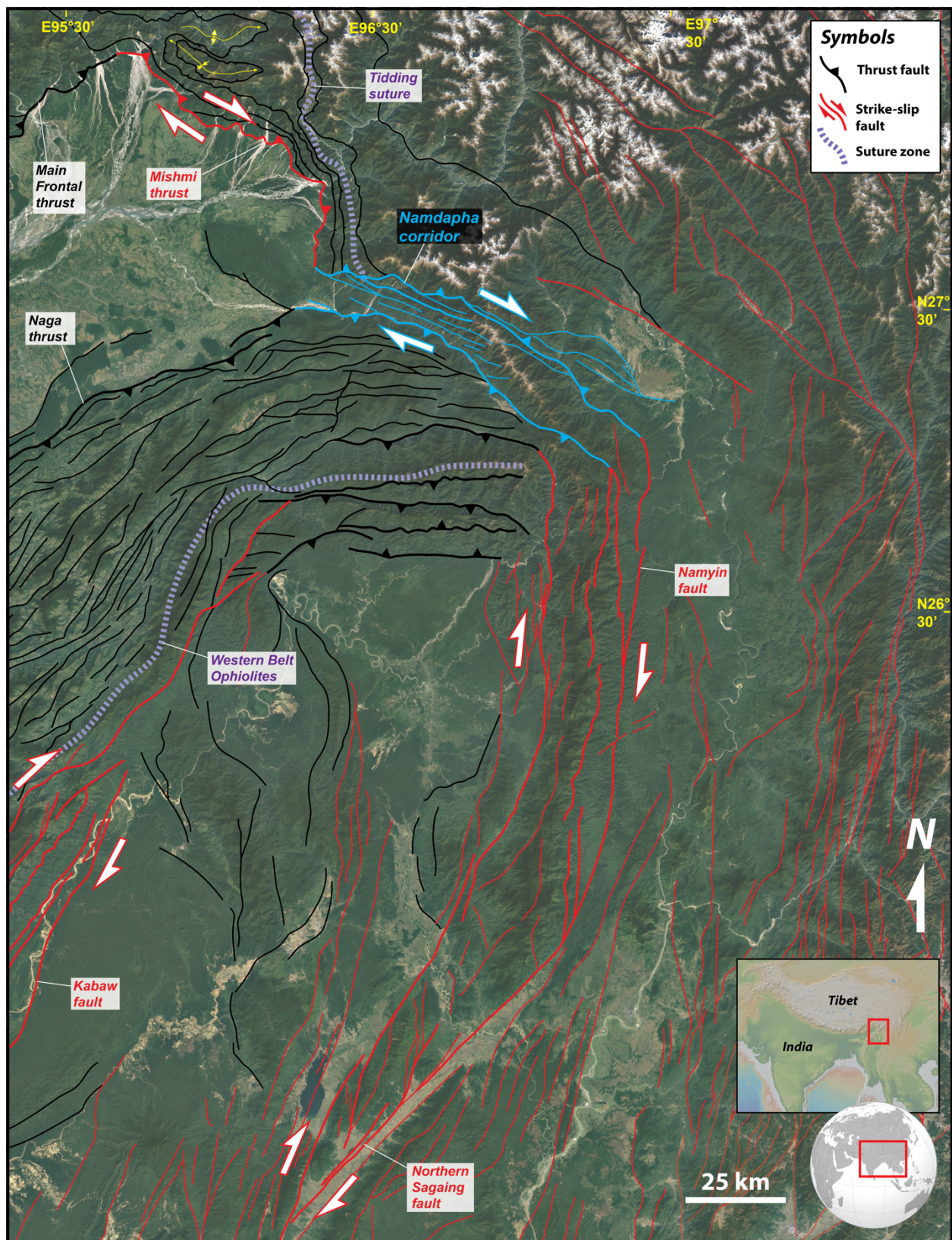


Figure 4.19 (previous page). Google Earth-based fault map of the northern and central zones of the Eastern Flanking Belt, including the location of the Namdapha Corridor (blue faults) linking the Mishmi thrust, Naga thrust, and Namyin fault (northern segment of the right-slip Sagaing fault). The base digital elevation model was acquired using geomapapp.com (Ryan et al., 2009). The Earth index map was acquired through Generic Mapping Tools (gmt.soest.hawaii.edu).

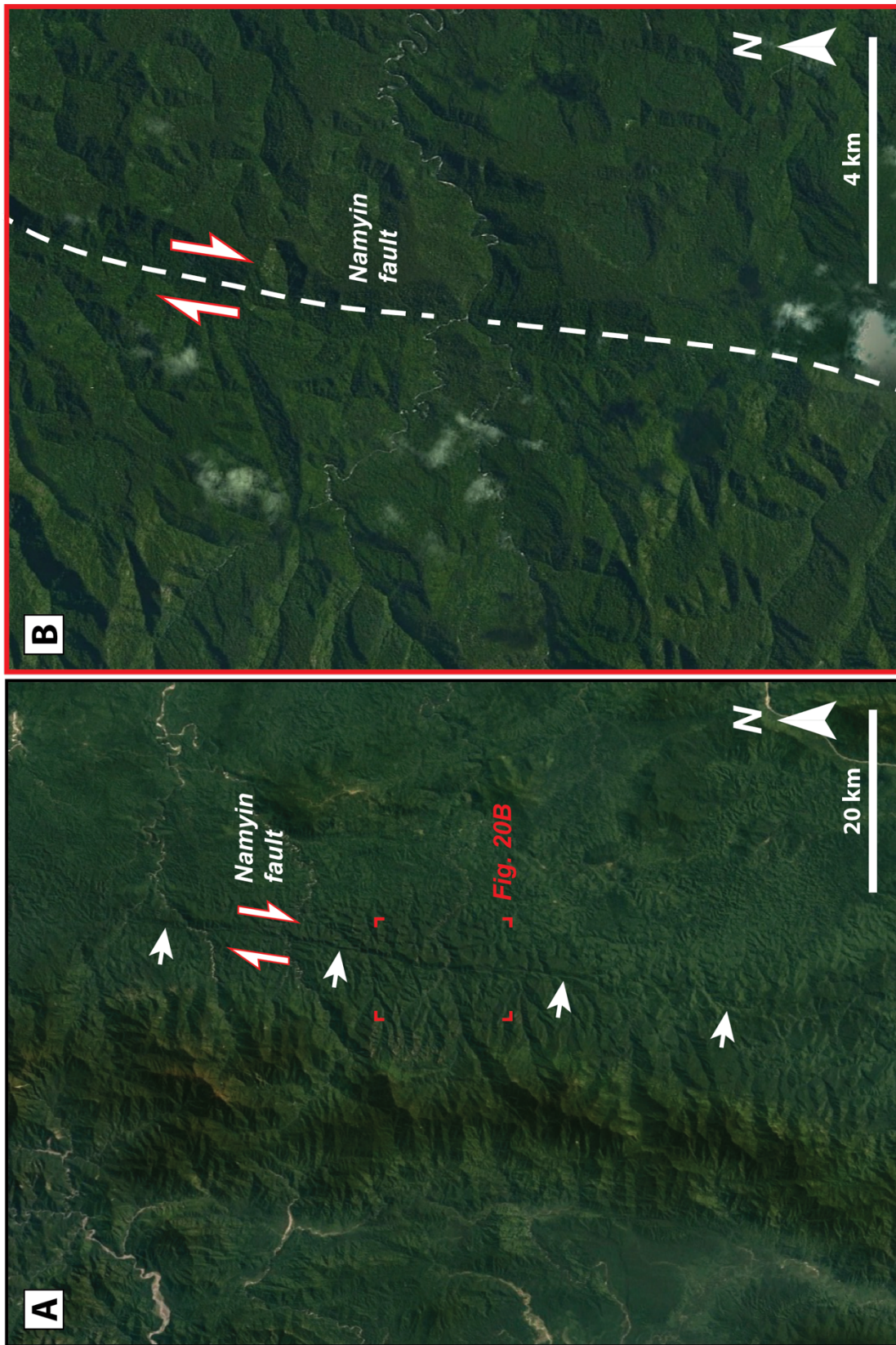


Figure 4.20. Google-Earth-based maps of the surface trace of the right-slip Namyin fault, the northernmost segment of the Sagang fault, showing linear scars and beheaded stream channels. Map location is shown on Fig. 19.

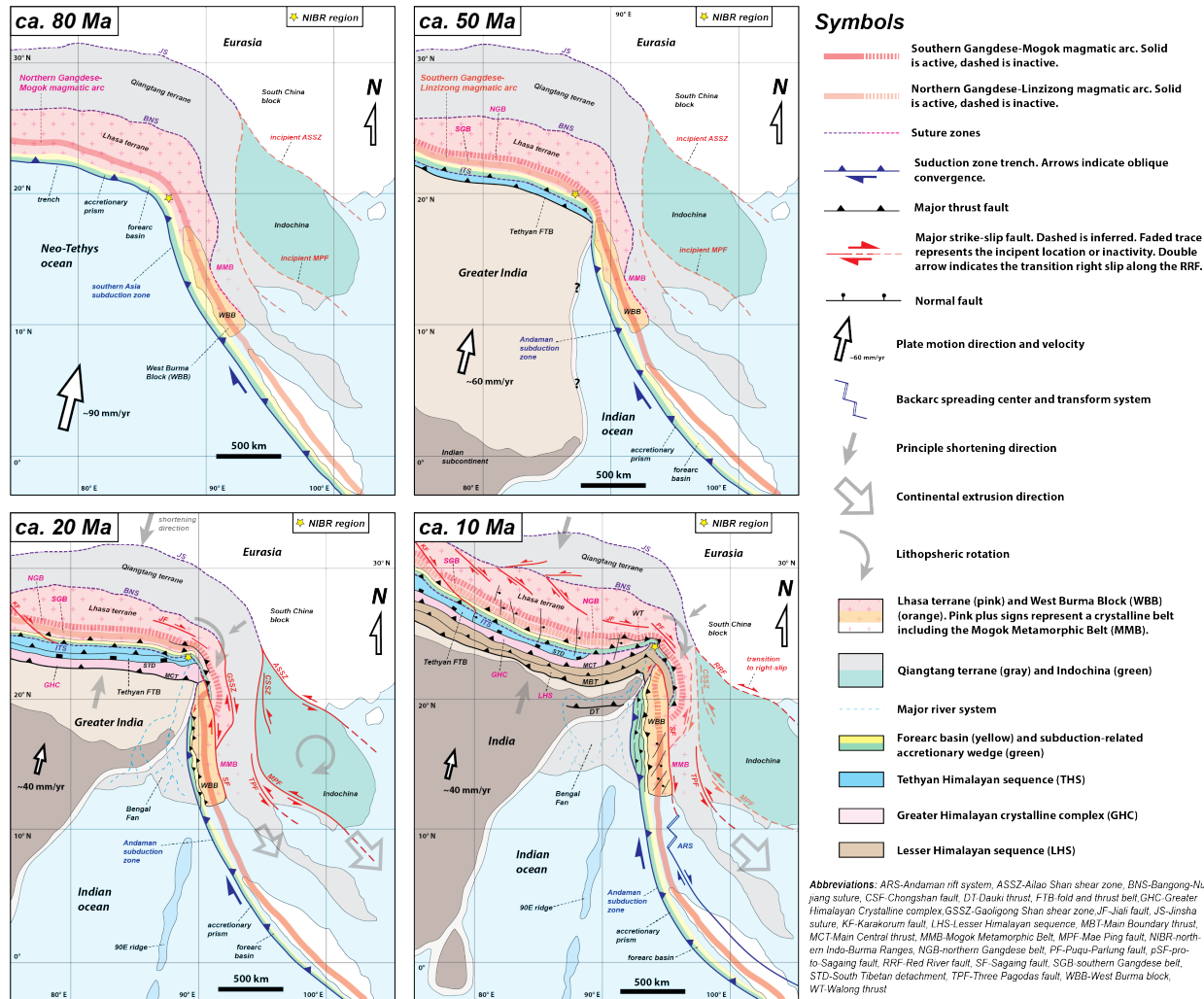
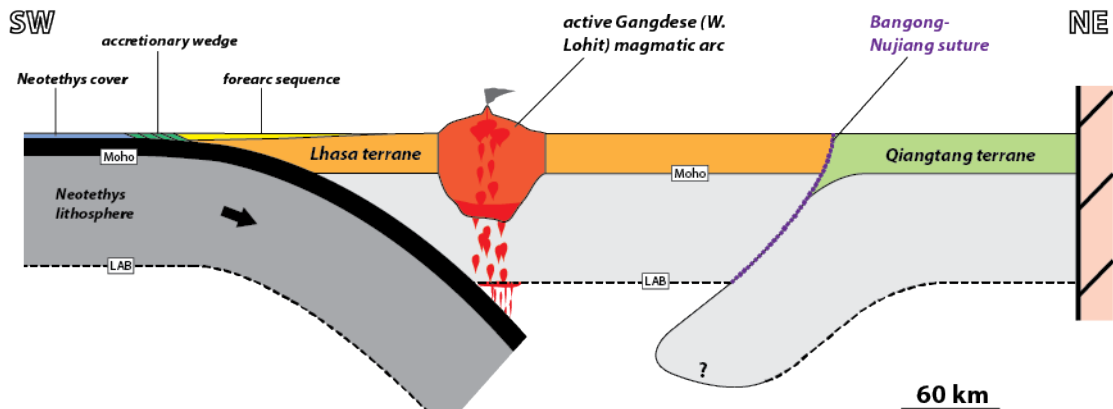


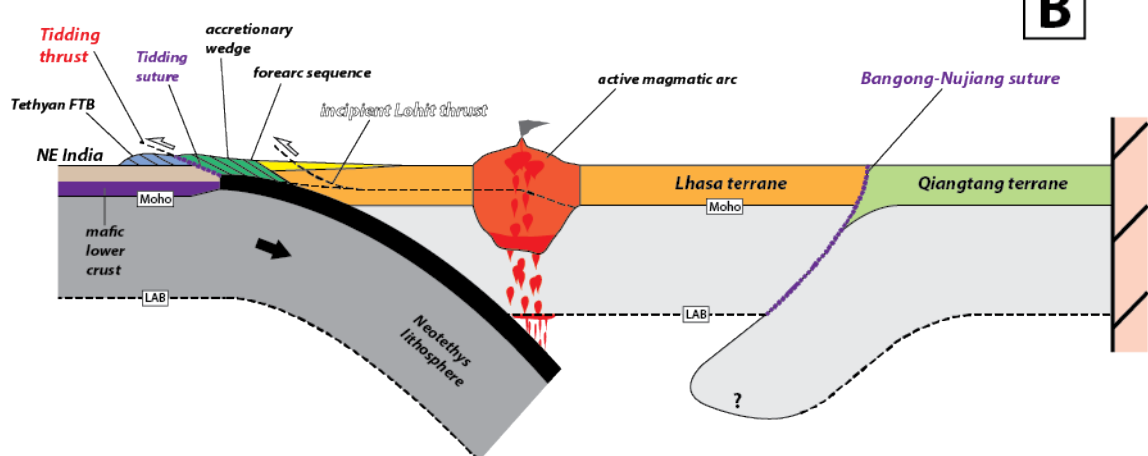
Figure 4.21. Tectonic evolution of the eastern Himalayan collisional system, southeastern Tibetan Plateau, and southeast Asia since the Cretaceous, depicted at ~80 Ma, ~50 Ma, ~20 Ma, and ~10 Ma.

c. 150-80 Ma



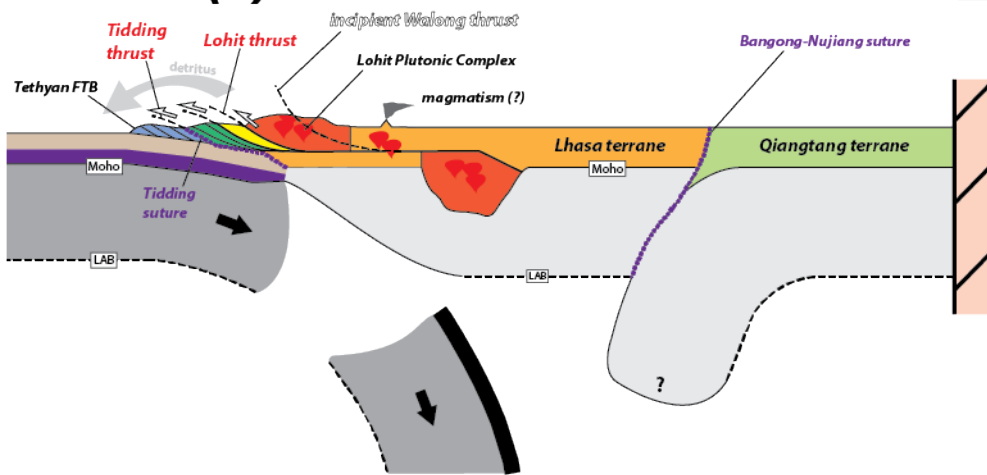
A

c. 50 Ma



B

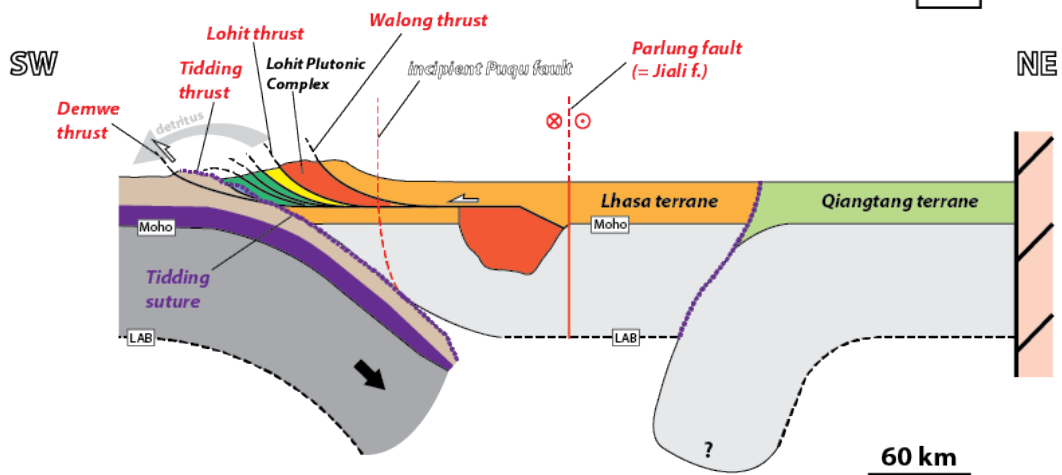
c. 40 Ma(?)



C

c. 20 Ma(?)

D



c. 10 Ma(?)

E

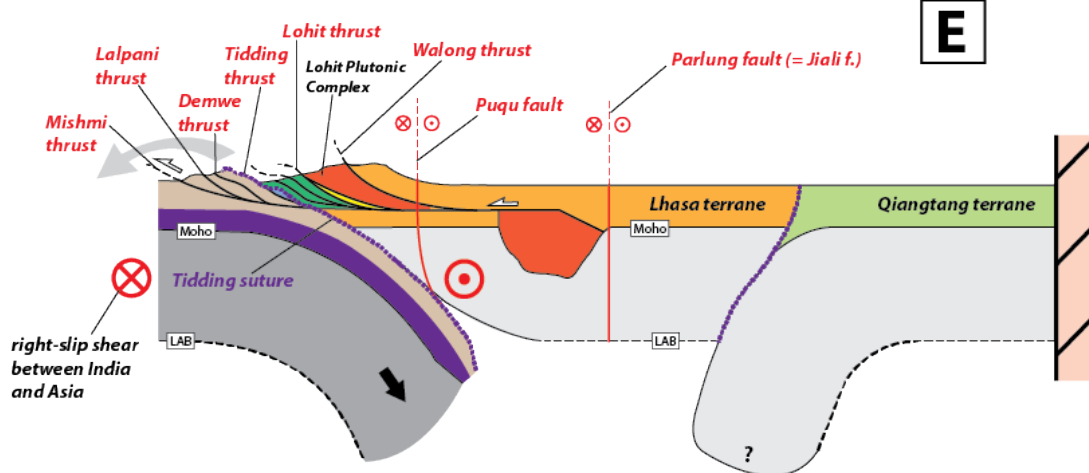


Figure 4.22 (previous and current page). Schematic lithospheric-scale cross sections depicting the latest Jurassic-Cenozoic evolution of the easternmost Himalayan orogen and southeast Tibet at (A) 150-80 Ma, (B) 65-52 Ma, (C) 40 Ma, (D) 20 Ma, and (E) 10 Ma to present. The timing of stages C-E are inferred.

Table 4.1. Summary of *P-T* determinations for selected metamorphic rocks of the Tidding and Mayodia mélange complexes

Sample and lithology	Technique	Minerals analyzed [%]	T (°C)	S.D. (°C)	P (kbar)	S.D. (kbar)	Cor [@]
<i>Tidding mélange complex</i>							
PH-1-8-13-26 (garnet-mica schist)	THERMOCALC*	plg, bio, musc, qtz, sph, hrn, ilm, ru, grt	627	28	10.4	1.1	0.841
	Ti-in-Bio ^{&}	bio	620	24	-	-	-
PH-11-14-15- 24 (garnet-mica schist)	THERMOCALC	plg, bio, musc, qtz, ilm, ti, ky, ru, grt	679	18	13.1	0.8	0.498
	Ti-in-Bio	bio	596	24	-	-	-
PH-11-9-15- 40 (garnet-mica schist)	THERMOCALC	plg, bio, musc, qtz, sph, hrn, ilm, ru, grt	616	11	9	0.5	0.604
	Ti-in-Bio	bio	602	24	-	-	-
<i>Mayodia mélange complex</i>							
PH-1-9-13-8 (garnet-mica schist)	Grt growth zoning	grt	< 650	-	-	-	-
PH-11-12-15- 17 (garnet-mica schist)	THERMOCALC	plg, musc, chl, clz, qtz, ti, ru, grt	450	50	3.6	1.1	0.957
	Grt growth zoning	grt	< 650	-	-	-	-

[%]Mineral abbreviations are plg-plagioclase, bio-biotite, musc-muscovite, qtz-quartz, ilm-ilmenite, ti-titanite

ky-kyanite, ru-rutile, grt-garnet, sph-spheine, amp-amphibole, ep-epidote, chl-chlorite, clz-clinozoesite

*Version 3.37 of THERMOCALC by Holland and Powell (1998)

"@" Correlation coefficient used in THERMOCALC

[&]Ti-in-Bio thermometer of Henry et al. (2005)

"-" Dashes are immeasurable values

4.10. References

- Acharyya, S.K., 1987, Cenozoic plate motions creating the Eastern Himalayan and Indo Burmese range around the northeast corner of India: Ophiolites and Indian plate margins, p. 143-160.
- Acharyya, S.K., 1994, The Cenozoic foreland basin and tectonics of the eastern sub-Himalaya: problems and prospects: *Himalayan Geology*, v. 15, p. 3-21.
- Acharyya, S.K. and Ray, K.K., 1977, Geology of the Darjeeling-Sikkim Himalaya: Guide to excursion, v. 4.
- Acharyya, S.K., Ray, K.K., and Sengupta, S., 1990, Tectonics of the ophiolite belt from Naga Hills and Andaman Islands, India: *Journal of Earth System Science*, v. 99, no. 2, p. 187-199.
- Aier, I., Luirei, K., Bhakuni, S., Thong, G.T., and Kothyari, G.C., 2011, Geomorphic evolution of Medziphema intermontane basin and Quaternary deformation in the schuppen belt, Nagaland, NE India: *Geomorphology*, v. 55, no. 2, p. 247–265
- Akciz, S., Burchfiel, B.C., Crowley, J.L., Jiyun, Y., and Liangzhong, C., 2008, Geometry, kinematics, and regional significance of the Chong Shan shear zone, Eastern Himalayan Syntaxis, Yunnan, China: *Geosphere*, v. 4, no. 1, p. 292-314.
- Allégre, C.J., et al., 1984, Structure and evolution of the Himalaya–Tibet orogenic belt: *Nature*, v. 307, p. 17-22.
- Ao, A. and Bhowmik, S.K., 2014, Cold subduction of the Neotethys: the metamorphic record from finely banded lawsonite and epidote blueschists and associated metabasalts of the Nagaland Ophiolite Complex, India: *Journal of Metamorphic Geology*, v. 32, no. 8, p. 829-860.

- Armijo, R., Tapponnier, P., and Han, T., 1989, Late Cenozoic right-lateral strike-slip faulting in southern Tibet: *Journal of Geophysical Research: Solid Earth*, v. 94, no. B3, p. 2787-2838.
- Armijo, R., Tapponnier, P., Mercier, J.L., and Han, T.L., 1986, Quaternary extension in southern Tibet: Field observations and tectonic implications: *Journal of Geophysical Research: Solid Earth*, v. 91, no. B14, p. 13803-13872.
- Avouac, J.P., 2003, Mountain building, erosion, and the seismic cycle in the Nepal Himalaya: *Advances in geophysics*, v. 46, p. 1-80.
- Barley, M.E., Pickard, A.L., Zaw, K., Rak, P., and Doyle, M.G., 2003, Jurassic to Miocene magmatism and metamorphism in the Mogok metamorphic belt and the India-Eurasia collision in Myanmar: *Tectonics*, v. 22, no. 3, p. 1019.
- Barley, M.E. and Zaw, K., 2009, SHRIMP U-Pb in zircon geochronology of granitoids from Myanmar: temporal constraints on the tectonic evolution of Southeast Asia: EGU General Assembly Conference Abstracts, v. 11, no. 3842.
- Ben-Menahem, A., Aboodi, E., and Schild, R., 1974, The source of the great Assam earthquake—an interplate wedge motion: *Physics of the Earth and Planetary Interiors*, v. 9, no. 4, p. 265-289.
- Bertrand, G. and Rangin, C., 2003, Tectonics of the western margin of the Shan plateau (central Myanmar): implication for the India-Indochina oblique convergence since the Oligocene: *Journal of Asian Earth Sciences*, v. 21, no. 10, p. 1139-1157.
- Bilham, R. and England, P., 2001, Plateau ‘pop-up’ in the great 1897 Assam earthquake: *Nature*, v. 410, no. 6830, p. 806-809
- Boyer, S.E. and Elliott, D., 1982, Thrust systems: *AAPG Bulletin*, v. 66, no. 9, p. 1196-1230.

- Burchfiel, B.C., Zhiliang, C., Hodges, K.V., Yuping, L., Royden, L.H., Changrong, D., and Jiene, X., 1992, The South Tibetan detachment system, Himalayan orogen: Extension contemporaneous with and parallel to shortening in a collisional mountain belt: Geological Society of America Special Papers, v. 269, p. 1-41.
- Burgess, W.P., Yin, A., Dubey, C.S., Shen, Z.K. and Kelty, T.K., 2012. Holocene shortening across the Main Frontal Thrust zone in the eastern Himalaya: Earth and Planetary Science Letters, v. 357, p. 152-167.
- Butler, R.W.H., 1987. Thrust sequences: Journal of the Geological Society, v. 144, no. 4, p. 619-634.
- Chatterjee, N. and Ghose, N.C., 2010, Metamorphic evolution of the Naga Hills eclogite and blueschist, Northeast India: implications for early subduction of the Indian plate under the Burma microplate: Journal of Metamorphic Geology, v. 28, no. 2, p. 209-225.
- Chen, W.P. and Molnar, P., 1977, Seismic moments of major earthquakes and the average rate of slip in central Asia: Journal of Geophysical Research, v. 82. No. 20, p. 2945-2969.
- Clark, M.K. and Bilham, R., 2008, Miocene rise of the Shillong Plateau and the beginning of the end for the Eastern Himalaya: Earth and Planetary Science Letters, v. 269, no. 3, p. 337-351.
- Clark, M.K., and Royden, L.H., 2000, Topographic ooze: Building the eastern margin of Tibet by lower crustal flow: Geology, v. 28, no. 8, p. 703-706.
- Cobbbold, P.R. and Davy, P.H., 1988, Indentation tectonics in nature and experiment. 2. Central Asia: Bull. Geol. Inst. Univ. Uppsala, v. 14, p. 143-162.
- Copeland, P., Harrison, T.M., Yun, P., Kidd, W. S.F., Roden, M., and Zhang, Y., 1995, Thermal evolution of the Gangdese batholith, southern Tibet: A history of episodic unroofing: Tectonics, v. 14, no. 2, p. 223-236.

- Corfield, R.I. and Searle, M.P., 2000, Crustal shortening estimates across the north Indian continental margin, Ladakh, NW India: Geological Society, London, Special Publications, v. 170, no. 1, p. 395-410.
- Corfield, R.I., Searle, M.P. and Pedersen, R.B., 2001, Tectonic setting, origin, and obduction history of the Spontang Ophiolite, Ladakh Himalaya, NW India: The Journal of Geology, v. 109, no. 6, p. 715-736.
- Coulon, C., Maluski, H., Bollinger, C., and Wang, S., 1986, Mesozoic and Cenozoic volcanic rocks from central and southern Tibet: 39 Ar-40 Ar dating, petrological characteristics and geodynamical significance: Earth and Planetary Science Letters, v. 79, no. 3, p. 281-302.
- Coward, M.P. and Butler, R.W.H., 1985, Thrust tectonics and the deep structure of the Pakistan Himalaya: Geology, v. 13, no. 6, p. 417-420.
- Coward, M.P., Kidd, W.S.F., Yun, P., Shackleton, R.M., and Hu, Z., 1988, The structure of the 1985 Tibet geotraverse, Lhasa to Golmud: Philosophical Transactions of the Royal Society of London A: Mathematical, Physical and Engineering Sciences, v. 327, no. 1594, p. 307-333.
- Curry, J.R., Moore, D.G., Lawver, L. A., Emmel, F.J., Raith, R.W., Henry, M., and Kieckhefer, R., 1979, Tectonics of the Andaman Sea and Burma: convergent margins: Geological and Geophysical Investigations of Continental Margins, p. 189-198.
- Dahlstrom, C.D., 1969, Balanced cross sections: Canadian Journal of Earth Sciences, v. 6, no. 4, p. 743-757.
- Dahlstrom, C.D., 1970, Structural geology in the eastern margin of the Canadian Rocky Mountains: Bulletin of Canadian Petroleum Geology, v. 18, no. 3, p. 332-406.

- Davy, P. and Cobbold, P.R., 1988, Indentation tectonics in nature and experiment. 1. Experiments scaled for gravity: Bull. Geol. Inst. Univ. Uppsala, v. 14, p. 129-141.
- DeCelles, P.G., Carrapa, B., Gehrels, G.E., Chakraborty, T., and Ghosh, P., 2016, Along-strike continuity of structure, stratigraphy, and kinematic history in the Himalayan thrust belt: The view from Northeastern India: Tectonics, v. 35, no. 12, p. 2995-3027.
- DeCelles, P.G., Robinson, D.M., Quade, J., Ojha, T.P., Garzione, C.N., Copeland, P., and Upreti, B.N., 2001, Stratigraphy, structure, and tectonic evolution of the Himalayan fold-thrust belt in western Nepal: Tectonics, v. 20, no. 4, p. 487-509.
- DeCelles, P. G., Robinson, D. M., and Zandt, G., 2002, Implications of shortening in the Himalayan fold-thrust belt for uplift of the Tibetan Plateau: Tectonics, v. 21, no. 6, p. 12.1-12.25.
- Dewey, J.F. and Burke, K.C., 1973, Tibetan, Variscan, and Precambrian basement reactivation: products of continental collision: The Journal of Geology, v. 81, no. 6, p. 683-692.
- Dewey, J.F., Shackleton, R.M., Chengfa, C., and Yiyin, S., 1988, The tectonic evolution of the Tibetan Plateau: Philosophical Transactions of the Royal Society of London A: Mathematical, Physical and Engineering Sciences, v. 327, no. 1594, p. 379-413.
- Ding, L., Kapp, P., Zhong, D., and Deng, W., 2003, Cenozoic volcanism in Tibet: evidence for a transition from oceanic to continental subduction. Journal of Petrology, v. 44, no. 10, p. 1833-1865.
- Ding, L., Zhong, D., Yin, A., Kapp, P., and Harrison, T.M., 2001, Cenozoic structural and metamorphic evolution of the eastern Himalayan syntaxis (Namche Barwa): Earth and Planetary Science Letters, v. 192, no. 3, p. 423-438.

- Dong, X., Zhang, Z., Liu, F., Wang, W., Yu, F., and Shen, K., 2011, Zircon U–Pb geochronology of the Nyainqêntanglha Group from the Lhasa terrane: new constraints on the Triassic orogeny of the south Tibet. *Journal of Asian Earth Sciences*, v. 42, no. 4, p. 732-739.
- Edwards, M.A. and Harrison, T.M., 1997, When did the roof collapse? Late Miocene north-south extension in the high Himalaya revealed by Th-Pb monazite dating of the Khula Kangri granite: *Geology*, v. 25, no. 6, p. 543-546.
- Edwards, M.A., Kidd, W.S., Li, J., Yue, Y., and Clark, M., 1996, Multi-stage development of the southern Tibet detachment system near Khula Kangri. New data from Gonto La: *Tectonophysics*, v. 260, no. 1-3, p. 1-19.
- Edwards, M.A., Pêcher, A., Kidd, W.S.F., Burchfiel, B. C., and Royden, L.H., 1999, Southern Tibet Detachment System at Khula Kangri, Eastern Himalaya: A Large-Area, Shallow Detachment Stretching into Bhutan?: *The Journal of geology*, v. 107, no. 5, p. 623-631.
- England, P. and Houseman, G., 1986, Finite strain calculations of continental deformation 2. Comparison with the India-Asia collision zone, *Journal of Geophysical Research*, v. 91, p. 3664–3676.
- England, P. and Molnar, P., 1990, Right-lateral shear and rotation as the explanation for strike-slip faulting in eastern Tibet: *Nature*, v. 344, no. 6262, p. 140-142.
- Eroğlu, S., Siebel, W., Danišík, M., Pfänder, J.A., and Chen, F., 2013, Multi-system geochronological and isotopic constraints on age and evolution of the Gaoligongshan metamorphic belt and shear zone system in western Yunnan, China: *Journal of Asian Earth Sciences*, v. 73, p. 218-239.
- Gansser, A., 1964, *Geology of the Himalayas*. New York: Wiley Interscience, p. 289.
- Gansser, A., 1983, *Geology of the Bhutan Himalaya*: Birkhauser, Basel, p. 181.

- Girardeau, J., et al., 1984, Tectonic environment and geodynamic significance of the Neo-Cimmerian Donqiao ophiolite, Bangong-Nujiang suture zone, Tibet: *Nature*, v. 307, p. 27-31.
- Grujic, D., Hollister, L. S., and Parrish, R.R., 2002, Himalayan metamorphic sequence as an orogenic channel: insight from Bhutan: *Earth and Planetary Science Letters*, v. 198, no. 1, p. 177-191.
- Guan, Q., et al., 2012, Crustal thickening prior to 38 Ma in southern Tibet: evidence from lower crust-derived adakitic magmatism in the Gangdese Batholith. *Gondwana Research*, v. 21, no. 1, p. 88-99.
- Guo, L., Zhang, H.F., Harris, N., Parrish, R., Xu, W.C., and Shi, Z. L., 2012, Paleogene crustal anatexis and metamorphism in Lhasa terrane, eastern Himalayan syntaxis: evidence from U-Pb zircon ages and Hf isotopic compositions of the Nyingchi Complex. *Gondwana Research*, v. 21, no. 1, p. 100-111.
- Guo, L., Zhang, H.F., Harris, N., Pan, F.B., and Xu, W.C., 2013, Late Cretaceous (~ 81Ma) high-temperature metamorphism in the southeastern Lhasa terrane: Implication for the Neo-Tethys ocean ridge subduction: *Tectonophysics*, v. 608, p. 112-126.
- Gururajan, N.S. and Choudhuri, B.K., 2003, Geology and tectonic history of the Lohit valley, Eastern Arunachal Pradesh, India: *Journal of Asian Earth Sciences*, v. 21, no. 7, p. 731-741.
- Hall, R., 2012, Late Jurassic–Cenozoic reconstructions of the Indonesian region and the Indian Ocean: *Tectonophysics*, v. 570, p. 1-41.
- Haproff, P.J., Zuza, A.V., Yin, A., 2018, West-directed thrusting south of the eastern Himalayan syntaxis indicates clockwise crustal flow at the indenter corner during the India-Asia collision: *Tectonophysics*, v. 722, p. 277-285.
- Haproff, P.J., Zuza, A.V., Yin, A., Harrison, T.M., Manning, C.M., Ding, L., Wu, C., Chen, J.,

- Dubey, C.S., Tectonic evolution of the northern Indo-Burma Ranges (Part 1): lateral tectonostratigraphy correlation across the eastern Himalayan syntaxis: in preparation.
- Haq, S.S., and Davis, D.M., 1997, Oblique convergence and the lobate mountain belts of western Pakistan: *Geology*, v. 25, no. 1, p. 23-26.
- Harrison, T.M., Leloup, P.H., Ryerson, F.J., Tapponnier, P., Lacassin, R., and Chen, W., 1996, Diachronous initiation of transtension along the Ailao Shan-Red River shear zone, Yunnan and Vietnam: *World and Regional Geology*, p. 208-226.
- Harrison, T.M., Wenji, C., Leloup, P.H., Ryerson, F.J., and Tapponnier, P., 1992, An early Miocene transition in deformation regime within the Red River fault zone, Yunnan, and its significance for Indo-Asian tectonics: *Journal of Geophysical Research: Solid Earth*, v. 97, no. B5, p. 7159-7182.
- Henry, D.J., Guidotti, C.V., and Thomson, J.A., 2005, The Ti-saturation surface for low-to-medium pressure metapelitic biotites: Implications for geothermometry and Ti-substitution mechanisms. *American Mineralogist*, v. 90, no. 2-3, p. 316-328.
- Hodges, K.V., 2000, Tectonics of the Himalaya and southern Tibet from two perspectives: *Geological Society of America Bulletin*, v. 112, no. 3, p. 324-350.
- Holland, T.J.B. and Powell, R., 1998, An internally consistent thermodynamic data set for phases of petrological interest: *Journal of Metamorphic Geology*, v. 16, no. 3, p. 309-343.
- Hsü, K. et al., 1995, Tectonic evolution of the Tibetan Plateau: a working hypothesis based on the archipelago model of orogenesis: *International Geology Review*, v. 37, p. 473–508.
- Ji, W.Q., Wu, F.Y., Chung, S.L., Li, J.X., and Liu, C.Z., 2009, Zircon U-Pb geochronology and Hf isotopic constraints on petrogenesis of the Gangdese batholith, southern Tibet: *Chemical*

- Geology, v. 262, no. 3, p. 229-245.
- Kapp, P., Murphy, M.A., Yin, A., Harrison, T.M., Ding, L., and Guo, J, 2003, Mesozoic and Cenozoic tectonic evolution of the Shiquanhe area of western Tibet: *Tectonics*, v. 22, no. 4.
- Kent, W.N., Hickman, R.G., and Dasgupta, U., 2002, Application of a ramp/flat-fault model to interpretation of the Naga thrust and possible implications for petroleum exploration along the Naga thrust front: *AAPG bulletin*, v. 86, no. 12, p. 2023-2045.
- Kent, W.N. and Dasgupta, U., (2004, Structural evolution in response to fold and thrust belt tectonics in northern Assam. A key to hydrocarbon exploration in the Jaipur anticline area: *Marine and Petroleum Geology*, v. 21, no. 7, p. 785-803.
- Kundu, B. and Gahalaut, V.K., 2012, Earthquake occurrence processes in the Indo-Burmese wedge and Sagaing fault region: *Tectonophysics*, v. 524, p. 135-146.
- Le Dain, A. Y., Tapponnier, P., and Molnar, P., 1984, Active faulting and tectonics of Burma and surrounding regions. *Journal of Geophysical Research: Solid Earth*, v. 89, no. B1, p. 453-472.
- Le Fort, P., 1975, Himalayas: the collided range. Present knowledge of the continental arc: *American Journal of Science*, v. 275, p. 1-44.
- Le Fort, P., 1996, Evolution of the Himalaya: *World and Regional Geology*, v. 1, no. 8, p. 95-109.
- Lee, H.Y., et al., 2003, Miocene Jiali faulting and its implications for Tibetan tectonic evolution: *Earth and Planetary Science Letters*, v. 205, no. 3, p. 185-194.
- Lee, H.Y., Chung, S.L., Lo, C.H., Ji, J., Lee, T.Y., Qian, Q., and Zhang, Q., 2009, Eocene Neotethyan slab breakoff in southern Tibet inferred from the Linzizong volcanic record: *Tectonophysics*, v. 477, no. 1, p. 20-35.

Lee, H.Y., Chung, S.L., and Yang, H.M., 2016. Late Cenozoic volcanism in central Myanmar: Geochemical characteristics and geodynamic significance: *Lithos*, v. 245, p. 174-190.

Lee, T.Y. and Lawver, L.A., 1995. Cenozoic plate reconstruction of Southeast Asia: *Tectonophysics*, v. 251, no. 1-4, p. 85-138.

Leloup, P. H., et al., 1995, The Ailao Shan-Red River shear zone (Yunnan, China), Tertiary transform boundary of Indochina: *Tectonophysics*, v. 251, no. 1, p. 3-84.

Li, C., Van der Hilst, R.D., Meltzer, A.S., and Engdahl, E.R., 2008, Subduction of the Indian lithosphere beneath the Tibetan Plateau and Burma: *Earth and Planetary Science Letters*, v. 274, no. 1, p. 157-168.

Li, Z.H., Xu, Z., Gerya, T., and Burg, J.P., 2013, Collision of continental corner from 3-D numerical modeling: *Earth and Planetary Science Letters*, v. 380, p. 98-111.

Lin, T.H., Chung, S.L., Kumar, A., Wu, F.Y., Chiu, H.Y. and Lin, I., 2013, Linking a prolonged Neo-Tethyan magmatic arc in South Asia: Zircon U-Pb and Hf isotopic constraints from the Lohit Batholith, NE India: *Terra Nova*, v. 25, no. 6, p. 453-458.

Liu, G. and Einsele, G., 1994, Sedimentary history of the Tethyan basin in the Tibetan Himalayas: *Geologische Rundschau*, v. 83, no. 1, p. 32-61.

Long, S., McQuarrie, N., Tobgay, T., and Grujic, D., 2011b, Geometry and crustal shortening of the Himalayan fold-thrust belt, eastern and central Bhutan: *Geological Society of America Bulletin*, p. B30203-1.

Long, S., McQuarrie, N., Tobgay, T., and Hawthorne, J., 2011c, Quantifying internal strain and deformation temperature in the eastern Himalaya, Bhutan: Implications for the evolution of strain in thrust sheets: *Journal of Structural Geology*, v. 33, no. 4, p. 579-608. C

- Long, S., McQuarrie, N., Tobgay, T., Rose, C., Gehrels, G., and Grujic, D., 2011a, Tectonostratigraphy of the Lesser Himalaya of Bhutan: Implications for the along-strike stratigraphic continuity of the northern Indian margin: Geological Society of America Bulletin: v. 123, no. 7-8, p. 1406-1426.
- Maung, H., 1987, Transcurrent movements in the Burma–Andaman Sea region, Geology, v. 15, no. 10, p. 911-912.
- Maury, R. C., et al., 2004, Quaternary calc-alkaline and alkaline volcanism in a hyper-oblique convergence setting, central Myanmar and western Yunnan: Bulletin de la Société Géologique de France, v. 175, no. 5, p. 461-472.
- Maurin, T., Masson, F., Rangin, C., Min, U.T. and Collard, P., 2010, First global positioning system results in northern Myanmar: Constant and localized slip rate along the Sagaing fault: Geology, v. 38, no. 7, p. 591-594.
- Maurin, T. and Rangin, C., 2009b, Impact of the 90 E ridge at the Indo-Burmese subduction zone imaged from deep seismic reflection data: Marine Geology, v. 266, no. 1, p. 143-155.
- Maurin, T. and Rangin, C., 2009a, Structure and kinematics of the Indo-Burmese Wedge: Recent and fast growth of the outer wedge: Tectonics, v. 28, no. 2.
- McQuarrie, N., Robinson, D., Long, S., Tobgay, T., Grujic, D., Gehrels, G., and Ducea, M., 2008, Preliminary stratigraphic and structural architecture of Bhutan: Implications for the along strike architecture of the Himalayan system: Earth and Planetary Science Letters, v. 272, no. 1, p. 105-117.
- Metcalfe, I., 2013, Gondwana dispersion and Asian accretion: tectonic and palaeogeographic evolution of eastern Tethys: Journal of Asian Earth Sciences, v. 66, p. 1-33.
- Mitra, G., Bhattacharyya, K. and Mukul, M., 2010, The Lesser Himalayan duplex in Sikkim:

- Implications for variations in Himalayan shortening: Journal of the Geological Society of India, v. 75, no. 1, p. 289-301.
- Misra, D.K., 2009, Litho-tectonic sequence and their regional correlation along the Lohit and Dibang valleys, eastern Arunachal Pradesh. Journal of the Geological Society of India, v. 73, no. 2, p. 213-219.
- Misra, D.K. and Singh, T., 2002, Tectonic setting and neotectonic features along the Eastern Syntaxial Bend (Lohit and Dibang), Arunachal Himalaya: Aspects of Geology and Environment of the Himalaya, p. 19-40.
- Mitchell, A.H.G., 1993, Cretaceous–Cenozoic tectonic events in the western Myanmar (Burma)–Assam region: Journal of the Geological Society, v. 150, no. 6, p. 1089-1102.
- Mitchell, A.H.G., Chung, S.L., Oo, T., Lin, T.H. and Hung, C.H., 2012, Zircon U–Pb ages in Myanmar: Magmatic–metamorphic events and the closure of a neo-Tethys ocean?: Journal of Asian Earth Sciences, v. 56, p. 1-23.
- Mitchell, A.H.G., Htay, M.T., Htun, K.M., Win, M.N., Oo, T., and Hlaing, T, 2007, Rock relationships in the Mogok metamorphic belt, Tatkon to Mandalay, central Myanmar: Journal of Asian Earth Sciences, v. 29, no. 5, p. 891-910.
- Mitra, S., Priestley, K., Bhattacharyya, A.K. and Gaur, V.K., 2005, Crustal structure and earthquake focal depths beneath northeastern India and southern Tibet: Geophysical Journal International, v. 160, no. 1, p. 227-248.
- Molnar, P. and Tapponnier, P., 1975, Cenozoic tectonics of Asia: effects of a continental collision: Science, v. 189, no. 4201, p. 419-426.

- Morley, C.K., 2004, Nested strike-slip duplexes, and other evidence for Late Cretaceous–Palaeogene transpressional tectonics before and during India–Eurasia collision, in Thailand, Myanmar and Malaysia: Journal of the Geological Society, v. 16, no. 5, p. 799–812.
- Morley, C.K. and Searle, M., 2017, Regional tectonics, structure and evolution of the Andaman–Nicobar Islands from ophiolite formation and obduction to collision and back-arc spreading: Geological Society, London, Memoirs, v. 47, no. 1, p. 51–74.
- Murphy, M.A., et al., 1997, Did the Indo-Asian collision alone create the Tibetan plateau?: Geology, v. 25, no. 8, p. 719–722.
- Murphy, M. A. and Yin, A., 2003, Structural evolution and sequence of thrusting in the Tethyan fold-thrust belt and Indus-Yalu suture zone, southwest Tibet: Geological Society of America Bulletin, v. 115, no. 1, p. 21–34.
- Nelson, K.D., Zhao, W., Brown, L.D., and Kuo, J., 1996, Partially molten middle crust beneath southern Tibet: synthesis of project INDEPTH results: Science, v. 274, no. 5293, p. 1684.
- Nielsen, C., Chamot-Rooke, N., and Rangin, C., 2004, From partial to full strain partitioning along the Indo-Burmese hyper-oblique subduction: Marine Geology, v. 209, no. 1–4, p. 303–327.
- Peltzer, G. and Tapponnier, P., 1988, Formation and evolution of strike-slip faults, rifts, and basins during the India-Asia collision: An experimental approach: Journal of Geophysical Research: Solid Earth, v. 93, no. B12, p. 15085–15117.
- Raju, K.K., Ramprasad, T., Rao, P.S., Rao, B.R., and Varghese, J., 2004, New insights into the tectonic evolution of the Andaman basin, northeast Indian Ocean: Earth and Planetary Science Letters, v. 221, no. 1, p. 145–162.
- Rangin, C., Jolivet, L., Pubellier, M., and Tethys Pacific Working Group, 1990, A simple model

- for the tectonic evolution of southeast Asia and Indonesia region for the past 43 my: Bull. Soc. Geol. Fr. v. 6, no. 6, p. 889-905.
- Rangin, C., Maurin, T., and Masson, F., 2013, Combined effects of Eurasia/Sunda oblique convergence and East-Tibetan crustal flow on the active tectonics of Burma: Journal of Asian Earth Sciences, v. 76, p. 185-194.
- Rangin, C., Spakman, W., Pubellier, M., and Bijwaard, H., 1999, Tomographic and geological constraints on subduction along the eastern Sundaland continental margin (South-East Asia): Bulletin de la Société géologique de France, v. 170, no. 6, p. 775-788.
- Ratschbacher, L., Frisch, W., Liu, G., and Chen, C., 1994, Distributed deformation in southern and western Tibet during and after the India-Asia collision: Journal of Geophysical Research: Solid Earth, v. 99, no. B10, p. 19917-19945.
- Replumaz, A. and Tapponnier, P., 2003, Reconstruction of the deformed collision zone between India and Asia by backward motion of lithospheric blocks: Journal of Geophysical Research: Solid Earth, v. 108, no. B6.
- Replumaz, A., Lacassin, R., Tapponnier, P., and Leloup, P.H., 2001, Large river offsets and Plio-Quaternary dextral slip rate on the Red River fault (Yunnan, China): Journal of Geophysical Research: Solid Earth, v. 106, no. B1, p. 819-836.
- Ridd, M.F. and Watkinson, I., 2013, The Phuket-Slate Belt terrane: tectonic evolution and strike-slip emplacement of a major terrane on the Sundaland margin of Thailand and Myanmar: Proceedings of the Geologists' Association v. 124, no. 6, p. 994-1010.
- Ryan, W.B., et al., 2009, Global multi-resolution topography synthesis: Geochemistry, Geophysics, Geosystems, v. 10, no. 3.
- Royden, L., 1996. Coupling and decoupling of crust and mantle in convergent orogens:

- Implications for strain partitioning in the crust: Journal of Geophysical Research: Solid Earth, v. 101, no. B8, p. 17679-17705.
- Royden, L.H., et al., 1997, Surface deformation and lower crustal flow in eastern Tibet: Science, v. 276, p. 788–90.
- Royden, L.H., Burchfiel, B.C., and van der Hilst, R.D., 2008, The Geological Evolution of the Tibetan Plateau: Science, v. 321, p. 1054-1058.
- Russo, R.M., 2012, Source-side shear-wave splitting and upper-mantle flow beneath the Arakan slab, India-Asia-Sundaland triple junction: Geosphere, p. GES00534-1.
- Schärer, U., Xu, R.H., and Allègre, C.J., 1984, U-Pb geochronology of Gangdese (Transhimalaya) plutonism in the Lhasa-Xigaze region, Tibet: Earth and Planetary Science Letters, v. 69, no. 2, p. 311-320.
- Schelling, D., and Arita, K., 1991, Thrust tectonics, crustal shortening, and the structure of the far-eastern Nepal Himalaya: Tectonics, v. 10, no. 5, p. 851-862.
- Schelling, D.D., 1999, Frontal structural geometries and detachment tectonics of the northeastern Karachi arc, southern Kirthar range, Pakistan, Geological Society of America Special Papers, p. 287-302.
- Searle, M.P., Cooper, D.J.W., Rex, A.J., and Colchen, M., 1988, Collision tectonics of the Ladakh-Zanskar Himalaya: Phil. Trans. R. Soc. Lond. A, v. 326, no. 1589, p. 117-150.
- Searle, M.P., Corfield, R.I., Stephenson, B.E.N., and McCarron, J.O.E., 1997, Structure of the North Indian continental margin in the Ladakh-Zanskar Himalayas: implications for the timing of obduction of the Spontang ophiolite, India-Asia collision and deformation events in the Himalaya. Geological Magazine, v. 134, no. 3, p. 297-316.

- Searle, M.P., Noble, S.R., Cottle, J.M., Waters, D.J., Mitchell, A.H.G., Hlaing, T., and Horstwood, M.S.A., 2007, Tectonic evolution of the Mogok metamorphic belt, Burma (Myanmar) constrained by U-Th-Pb dating of metamorphic and magmatic rocks: *Tectonics*, v. 26, no. 3).
- Searle, M.P. and Morley, C.K., 2011, Tectonic and thermal evolution of Thailand in the regional context of SE Asia: *The Geology of Thailand*, chapter 20, p. 539-571.
- Socquet, A., Goffe, B., Pubellier, M., and Rangin, C., 2002, Late Cretaceous to Eocene metamorphism of the internal zone of the Indo-Burma range (western Myanmar): geodynamic implications: *Comptes Rendus Geoscience*, v. 334, no. 8, p. 573-580.
- Suppe, J., 1983, Geometry and kinematics of fault-bend folding: *American Journal of science*, v. 283, no. 7, p. 684-721.
- Tapponnier, P., Peltzer, G., Le Dain, A.Y., Armijo, R., and Cobbold, P. 1982, Propagating extrusion tectonics in Asia: new insights from simple experiments with plasticine: *Geology*, v. 10, p. 611–616.
- Tapponnier, P., Mattauer, M., Proust, F., and Cassaigneau, C., 1981, Mesozoic ophiolites, sutures, and large-scale tectonic movements in Afghanistan: *Earth and Planetary Science Letters*, v. 52, no. 2, p. 355-371.
- Tapponnier, P., Peltzer, G., and Armijo, R., 1986, On the mechanics of the collision between India and Asia: *Geological Society, London, Special Publications*, v. 19, no. 1, p. 113-157.
- Tapponnier, P., Zhiqin, X., Roger, F., Meyer, B., Arnaud, N., Wittlinger, G., and Jingsui, Y., 2001, Oblique stepwise rise and growth of the Tibet Plateau. *Science*, v. 294, no. 5547, p. 1671-1677.
- Taylor, M. and Yin, A., 2009, Active structures of the Himalayan-Tibetan orogen and their

- relationships to earthquake distribution, contemporary strain field, and Cenozoic volcanism: *Geosphere*, v. 5, no. 3, p. 199-214.
- Torsvik, T.H., et al., 2012, Phanerozoic polar wander, palaeogeography and dynamics: *Earth-Science Reviews*, v. 114, no. 3, p. 325-368.
- Tun, S.T., Thein, M., Htay, N. and Sein, K., 2014, Geological Map of Myanmar (1:2,250,000): Myanmar Geosciences Society.
- Ul-Hadi, S., Khan, S.D., Owen, L.A. and Khan, A.S., 2013, Geomorphic response to an active transpressive regime: a case study along the Chaman strike-slip fault, western Pakistan: *Earth Surface Processes and Landforms*, v. 38, no. 3, p. 250-264.
- van Hinsbergen, D.J., Kapp, P., Dupont-Nivet, G., Lippert, P.C., DeCelles, P.G., and Torsvik, T.H., 2011, Restoration of Cenozoic deformation in Asia and the size of Greater India: *Tectonics*, v. 30, no. 5.
- Vigny, C., et al., 2003, Present-day crustal deformation around Sagaing fault, Myanmar: *Journal of Geophysical Research: Solid Earth*, v. 108, no. B11.
- Wang, C., Ding, L., Zhang, L. Y., Kapp, P., Pullen, A., and Yue, Y.H., 2016, Petrogenesis of Middle–Late Triassic volcanic rocks from the Gangdese belt, southern Lhasa terrane: Implications for early subduction of Neo-Tethyan oceanic lithosphere: *Lithos*, v. 262, p. 320-333.
- Wang, P.L., Lo, C.H., Chung, S.L., Lee, T.Y., Lan, C.Y., and Van Thang, T., 2000, Onset timing of left-lateral movement along the Ailao Shan–Red River shear zone: $40\text{Ar}/39\text{Ar}$ dating constraint from the Nam Dinh area, northeastern Vietnam: *Journal of Asian Earth Sciences*, v. 18, no. 3, p. 281-292.

- Wang, Y., Sieh, K., Aung, T., Min, S., Khaing, S.N., and Tun, S.T., 2011, Earthquakes and slip rate of the southern Sagaing fault: insights from an offset ancient fort wall, lower Burma (Myanmar): *Geophysical Journal International*, v. 185, no. 1, p. 49-64.
- Wang, J.H., Yin, A., Harrison, T.M., Grove, M., Zhang, Y.Q., and Xie, G.H., 2001, A tectonic model for Cenozoic igneous activities in the eastern Indo–Asian collision zone: *Earth and Planetary Science Letters*, v. 188, no. 1, p. 123-133.
- Wang, Y., Zhang, L., Cawood, P.A., Ma, L., Fan, W., Zhang, A., Zhang, Y. and Bi, X., 2014, Eocene supra-subduction zone mafic magmatism in the Sibumasu Block of SW Yunnan: Implications for Neotethyan subduction and India–Asia collision: *Lithos*, v. 206, p. 384-399.
- Wang, J.G., Wu, F.Y., Tan, X.C., and Liu, C.Z., 2014, Magmatic evolution of the Western Myanmar Arc documented by U–Pb and Hf isotopes in detrital zircon: *Tectonophysics*, v. 612, p. 97-105.
- Watkinson, I., 2011. Structural geology of Thailand during the Cenozoic: *The Geology of Thailand*, p. 273.
- Watkinson, I., Elders, C., Batt, G., Jourdan, F., Hall, R., and McNaughton, N.J., 2011, The timing of strike-slip shear along the Ranong and Khlong Marui faults, Thailand: *Journal of Geophysical Research: Solid Earth* v. 116, no. B9.
- Webb, A.A.G., 2013, Preliminary balanced palinspastic reconstruction of Cenozoic deformation across the Himachal Himalaya (northwestern India): *Geosphere*, v. 9, no. 3, p. 572-587.
- Webb, A. A. G., et al., 2017, The Himalaya in 3D: Slab dynamics controlled mountain building and monsoon intensification: *Lithosphere*, v. L636-1.
- Webb, A.A.G., Yin, A. and Dubey, C.S., 2013, U-Pb zircon geochronology of major lithologic units in the eastern Himalaya: Implications for the origin and assembly of Himalayan rocks:

- Geological Society of America Bulletin, v. 125, no. 3-4, p. 499-522.
- Webb, A.A.G., Yin, A., Harrison, T.M., Célérier, J., and Burgess, W.P., 2007, The leading edge of the Greater Himalayan Crystalline complex revealed in the NW Indian Himalaya: Implications for the evolution of the Himalayan orogen: Geology, v. 35, no. 10, p. 955-958.
- Webb, A.A.G., Yin, A., Harrison, T.M., Célérier, J., Gehrels, G.E., Manning, C.E. and Grove, M., 2011, Cenozoic tectonic history of the Himachal Himalaya (northwestern India) and its constraints on the formation mechanism of the Himalayan orogen: Geosphere, v. 7, no. 4, p. 1013-1061.
- Wen, D.R., et al., 2008, Zircon SHRIMP U-Pb ages of the Gangdese Batholith and implications for Neotethyan subduction in southern Tibet: Chemical Geology, v. 252, no. 3, p. 191-201.
- Wu, C., et al., 1998, Yadong cross structure and South Tibetan Detachment in the east central Himalaya (89°-90°E): Tectonics, v. 17, no. 1, p. 28-45.
- Yin, A., 2006, Cenozoic tectonic evolution of the Himalayan orogen as constrained by along-strike variation of structural geometry, exhumation history, and foreland sedimentation: Earth-Science Reviews, v. 76, no. 1, p. 1-131.
- Yin, A., 2010, Cenozoic tectonic evolution of Asia: A preliminary synthesis: Tectonophysics, v. 488, no. 1, p. 293-325.
- Yin, A., et al., 1999, Tertiary deformation history of southeastern and southwestern Tibet during the Indo-Asian collision: Geological Society of America Bulletin, v. 111, no. 11, p. 1644-1664.
- Yin, A., Dang, Y., Zhang, M., McRivette, M.W., Burgess, W.P., and Chen, X., 2007, Cenozoic tectonic evolution of Qaidam basin and its surrounding regions (part 2): wedge tectonics in

southern Qaidam basin and the Eastern Kunlun Range: Geological Society of America Special Papers, v. 433, p. 369-390.

Yin, A., Dang, Y.Q., Wang, L.C., Jiang, W.M., Zhou, S.P., Chen, X.H., Gehrels, G., and McRivette, M.W., 2008a, Cenozoic tectonic evolution of Qaidam basin and its surrounding regions (Part 1): The southern Qilian Shan-Nan Shan thrust belt and northern Qaidam basin: Geological Society of America Bulletin, v. 120, no. 7-8, p. 813-846.

Yin, A., Dang, Y.Q., Zhang, M., Chen, X.H., and McRivette, M.W., 2008b, Cenozoic tectonic evolution of the Qaidam basin and its surrounding regions (Part 3): Structural geology, sedimentation, and regional tectonic reconstruction: Geological Society of America Bulletin, v. 120, no. 7-8, p. 847-876.

Yin, A., Dubey, C.S., Webb, A.A.G., Kelty, T.K., Grove, M., Gehrels, G.E. and Burgess, W.P., 2010, Geologic correlation of the Himalayan orogen and Indian craton: Part 1. Structural geology, U-Pb zircon geochronology, and tectonic evolution of the Shillong Plateau and its neighboring regions in NE India: Geological Society of America Bulletin, v. 122, no. 3-4, p. 336-359.

Yin, A., Dubey, C.S., Kelty, T.K., Gehrels, G.E., Chou, C.Y., Grove, M., and Lovera, O., 2006, Structural evolution of the Arunachal Himalaya and implications for asymmetric development of the Himalayan orogen: Current Science, v. 90, no. 2, p. 195-200.

Yin, A., Dubey, C.S., Kelty, T.K., Webb, A.A.G., Harrison, T.M., Chou, C.Y. and Célérier, J., 2010, Geologic correlation of the Himalayan orogen and Indian craton: Part 2. Structural geology, geochronology, and tectonic evolution of the Eastern Himalaya: Geological Society of America Bulletin, p. B26461-1.

Yin, A. and Harrison, T.M., 2000, Geologic Evolution of the Himalayan-Tibetan Orogen:

Annual Review of Earth and Planetary Sciences, v. 28, p. 211-280.

Yin, A., Harrison, T.M., Ryerson, F.J., Wenji, C., Kidd, W.S.F. and Copeland, P., 1994, Tertiary structural evolution of the Gangdese thrust system, southeastern Tibet: *Journal of Geophysical Research: Solid Earth*, v. 99, no. B9, p. 18175-18201.

Yin, A. and Taylor, M.H., 2011, Mechanics of V-shaped conjugate strike-slip faults and the corresponding continuum mode of continental deformation: *Geological Society of America Bulletin*, v. 123, no. 9-10, p. 1798-1821.

Zhang, X., et al., 2014, Early Jurassic high-pressure metamorphism of the Amdo terrane, Tibet: Constraints from zircon U-Pb geochronology of mafic granulites: *Gondwana Research*, v. 26, no. 3, p. 975-985.

Zhu, D.C., et al., 2009a, Early cretaceous subduction-related adakite-like rocks of the Gangdese Belt, southern Tibet: Products of slab melting and subsequent melt–peridotite interaction?: *Journal of Asian Earth Sciences*, v. 34, no. 3, p. 298-309.

Zhu, D.C., et al., 2012, Cambrian bimodal volcanism in the Lhasa Terrane, southern Tibet: record of an early Paleozoic Andean-type magmatic arc in the Australian proto-Tethyan margin: *Chemical Geology*, v. 328, p. 290-308.

Zhu, D.C., Chung, S.L., Mo, X.X., Zhao, Z.D., Niu, Y., Song, B., and Yang, Y.H., 2009b, The 132 Ma Comei-Bunbury large igneous province: Remnants identified in present-day southeastern Tibet and southwestern Australia: *Geology*, v. 37, no. 7, p. 583-586.

Zhu, D.C., Mo, X., Niu, Y., Zhao, Z., Wang, L., Liu, Y., and Wu, F., 2009c, Geochemical investigation of Early Cretaceous igneous rocks along an east–west traverse throughout the central Lhasa Terrane, Tibet: *Chemical Geology*, v. 268, no. 3, p. 298-312.

Zhu, D.C., Pan, G.T., Chung, S.L., Liao, Z.L., Wang, L.Q., and Li, G.M., 2008, SHRIMP zircon age and geochemical constraints on the origin of Lower Jurassic volcanic rocks from the

Yeba Formation, southern Gangdese, South Tibet: International Geology Review, v. 50, no. 5, p. 442-471.

Zhu, D.C., Zhao, Z.D., Niu, Y., Dilek, Y., Hou, Z.Q., and Mo, X.X., 2013, The origin and pre-Cenozoic evolution of the Tibetan Plateau: Gondwana Research, v. 23, no. 4, p. 1429-1454.

Zuza, A.V., Cheng, X., and Yin, A., 2016, Testing models of Tibetan Plateau formation with Cenozoic shortening estimates across the Qilian Shan–Nan Shan thrust belt: Geosphere, v. 12, no. 2, p. 501-532.

-Chapter 5-

**Out of sequence thrusting in the northern Indo-Burma Ranges: evidence from
preliminary zircon (U-Th)/He thermochronology**

5.1. Abstract

Zircon (U-Th)/He (ZHe) cooling ages are used to quantify the timing of exhumation across the northern Indo-Burma thrust belt, the easternmost segment of the Cenozoic Himalayan collisional system. Single grain ZHe ages were determined for fourteen bedrock samples of major lithologic units exposed along Dibang Valley, which consist from northeast to southwest: (1) the Mesoproterozoic and latest Jurassic-Cretaceous granitoids of the Lohit Plutonic Complex, (2) Tidding and Mayodia mélange complexes, (3) Mesoproterozoic-Cambrian Mayodia gneiss, (4) Mesoproterozoic-Jurassic Lalpani schist, and (5) Tertiary Sewak unit. Zircons from Cretaceous granitoids of the Lohit Plutonic Complex yield ZHe ages of ~10-6 Ma. Garnet schist from the Tidding mélange complex yields an older ZHe age of ~17 Ma. Samples of the Lalpani schist in the Hunli duplex and Mayodia mélange complex in the Mayodia klippe both yield ZHe ages of ~7 Ma. In the foreland of the thrust belt, ZHe ages of the Mayodia gneiss, Lalpani schist, and Sewak unit have ages of ~9-5 Ma. The spatial distribution of ZHe ages of ~17 Ma in the Tidding mélange complex to ~5-6 Ma in the Lalpani schist and Sewak unit in the foreland suggest a younging trend from northeast to southwest, parallel to the thrust transport direction. However, ZHe ages of ~10-6 Ma from the Lohit Plutonic Complex in the hinterland of the thrust belt suggest renewed exhumation via out of sequence thrust motion along the southwest-directed Lohit thrust. This study reveals a complex exhumation history of the northern Indo-Burma Ranges, such that Late Miocene activity along the Lohit thrust was coeval with exhumation of foreland rocks during southwestward forward propagation of the thrust belt.

5.2. Introduction

The Cenozoic India-Asia collision generated the east-trending Himalayan orogen and the

north-trending Eastern and Western Flanking Belts, which bound the margins of the Indian subcontinent (Fig. 1A) (Gansser, 1964; Yin, 2006). Studying the Cenozoic development of both flanking belts is critical to understanding the India-Asia collision process, however, the kinematic and exhumation histories of each belt remain inadequately understood. In this study, we present preliminary zircon (U-Th)/He (ZHe) thermochronology data to constrain the timing of exhumation through ~150–200 °C (Reiners, 2005) across the northern Indo-Burma thrust belt, the northernmost segment of the Eastern Flanking Belt (Fig. 1B). Our results show an Early Miocene to Pliocene younging trend of ZHe ages from northeast to southwest, which parallels the thrust transport direction across the thrust belt. However, Late Miocene ZHe ages from the hanging-wall of the Lohit thrust in the hinterland of the thrust belt suggest out-of-sequence thrusting was coeval with southeastward foreland propagation.

5.3. Geologic Setting

To provide a geologic context, we summarize the major lithologic units and structures of the (1) eastern Himalayan orogen, (2) southern Lhasa terrane, and (3) northern Indo-Burma thrust belt. We also include results of existing low-temperature thermochronology studies for each tectonic domain.

5.3.1. Eastern Himalayan Orogen

The eastern Himalayan orogen (89°E to 95°E) is a south-directed thrust belt bounded by the Indus-Yarlung suture zone (IYSZ) in the north and active Brahmaputra river plain in the south (Fig. 1B). The thrust belt involves, from north to south, the Paleoproterozoic-Eocene Tethyan Himalayan Sequence (THS), Paleoproterozoic-Ordovician Greater Himalayan Crystalline

Complex (GHC), Proterozoic-Cambrian Lesser Himalayan Sequence (LHS), and Tertiary Sub-Himalayan Sequence (SBS). These lithologic units are bounded by the following faults: the South Tibet detachment (STD), Main Central thrust (MCT), Main Boundary thrust (MBT), and Main Frontal thrust (MFT), respectively (Fig. 1B) (e.g., Gansser, 1964; Le Fort, 1975; Gansser, 1983; Burchfiel et al., 1992; Edwards et al., 1996, 1999; Edwards and Harrison, 1997; Grujic et al., 2002; McQuarrie et al., 2008; Long et al., 2011a, b, c; Yin et al., 2006, 2010a; Webb et al., 2013; DeCelles et al., 2016).

The application of low-temperature thermochronology (e.g., fission track and (U-Th/He) dating) in the eastern Himalayan orogen has proven to be a key tool for constraining the timing of Cenozoic exhumation (e.g., Burg et al., 1997, 1998; Grujic et al., 2006; Seward and Burg, 2008; Stewart et al., 2008; McQuarrie et al., 2014; Enkelmann et al., 2011; Long et al., 2012; Adlakha et al., 2013; DeCelles et al., 2016). In western Bhutan, exhumation of the GHS and LHS in the respective hanging walls of the MCT and MBT occurred prior to ~9-6 Ma (ZHe) (McQuarrie et al., 2014). Spatial variations in ZHe ages of the GHC (~5-8 Ma) and LHS (~2-3 Ma, 6-9 Ma, and 13 Ma) in western Bhutan are related to variations in the location, geometry, and lifespans of thrust systems at depth (McQuarrie et al., 2014). Exhumation of the SHS in the hanging wall of the MFT occurred from ~1.4-2 Ma following cessation of slip along the MBT and MCT (Grujic et al., 2006; McQuarrie et al., 2014).

In eastern Bhutan, exhumation of the LHS occurred from ~15-10 Ma (ZHe and apatite fission track (AFT) dating) during development of the upper Lesser Himalayan duplex at depth (Long et al., 2012), which followed exhumation of the GHC in the hanging wall of the MCT from ~23-16 Ma (Chambers et al., 2011). AFT ages of the LHS and SHS from the respective hanging walls of the MBT and MFT are <10 Ma, signaling southward propagation of Himalayan thrust belt

following development of the Lesser Himalayan duplex system (Grujic et al., 2006; Long et al., 2012).

Apatite and zircon fission track ages from the LHS in the western Arunachal Himalaya are ~6-10 Ma and ~11-14 Ma, respectively (Adlanka et al., 2013; DeCelles et al., 2016). Cooling ages of GHC samples in the hanging wall of the MCT have a younger age of ~2 Ma compared to those of the structurally-lower LHS (Adlanka et al., 2013). This contrast in exhumation ages between the LHS and GHC is supported by out-of-sequence thrust motion at 6-7 Ma along the Bomdila thrust in the footwall of the MCT, which followed the onset of thrust motion at structurally lower levels at ~13 Ma (Yin et al., 2010b).

The eastern Himalayan syntaxis is the eastern termination of the east-trending segment of Himalayan orogen and transition zone to the northern Indo-Burma thrust belt to the east and southeast (Fig. 1B). The syntaxis is expressed by a north-plunging antiform with a core of GH-equivalent, high-grade metamorphic rocks, ~160-65 Ma orthogneiss, and Late Cenozoic leucogranites (Kumar, 1997; Burg et al., 1998; Ding et al., 2001; Yin, 2006) (Fig. 1C).

The core of the antiform is the Namche Barwa-Gyala Peri massif, which has been the focus of many low-temperature thermochronologic studies due to the high relief (>4 km) and deep incision by the surrounding Indus-Yarlung (=Tsangpo) river (e.g., Burg et al., 1998; Seward and Burg, 2008; Stewart et al., 2008; Booth et al., 2009; Enkelmann et al., 2011). Fission track and (U-Th)/He dating of apatite and zircon from bedrock and detrital samples surrounding the massif have delineated a circular map-view pattern of incredibly young exhumation ages of <1-3 Ma (Burg et al., 1998; Malloy, 2004; Seward and Burg, 2008; Enkelmann et al., 2011). These cooling ages are complemented with higher-temperature accessory mineral U-Th-Pb ages of <4 Ma from the massif (Burg et al., 1998; Ding et al., 2001; Booth et al., 2009). Fission track and (U-Th)/He ages are

older with distance from Namche Barwa-Gyala Peri, shown by ages of ~3-5 Ma near the massif to >20 Ma from samples of the surrounding Gangdese and Bomi-Chayu batholiths (Seward and Burg, 2008; Stewart et al., 2008; Enkelmann et al., 2011). Models to explain the Cenozoic structural development and rapid exhumation of Namche Barwa-Gyala Peri include (1) uplift accommodated by thrust duplexing and crustal-scale folding (e.g., Burg et al., 1998; Ding et al., 2001) and (2) local feedbacks between focused tectonics and erosion (e.g., Zeitler et al., 2001; Koons et al., 2013).

5.3.2. Southern Lhasa Terrane

North of the eastern Himalayan orogen, the southern Lhasa terrane consists of predominantly Cretaceous to Eocene granitoids of the southern Gangdese batholith and the Paleocene-Eocene Linzizong volcanic sequence (Fig. 1B) (Schärer et al., 1984; Copeland et al., 1995; Ding et al., 2003; Wen et al., 2008; Zhu et al., 2008; Ji et al., 2009; Guan et al., 2012). These igneous rocks are placed atop the Late Jurassic-Early Cretaceous IYSZ and Cretaceous-Eocene Xigaze forearc sequence by the north-dipping Gangdese thrust (Fig. 1B) (Yin et al., 1994, 1999; Harrison et al., 2000).

Application of low-temperature thermochronology to the eastern part of the southern Gangdese batholith in southern Lhasa terrane has revealed a protracted exhumation history spanning Eocene to Miocene time (e.g., Copeland et al., 1995; Dai et al., 2012; Rohrmann et al., 2012; Tremblay et al., 2015). Eocene fission track and (U-Th)/He ages of Cretaceous-Cenozoic granitoids near Lhasa are between ~55 and 40 Ma (Copeland et al., 1995; Rohrmann et al., 2012; Dai et al., 2013; Tremblay et al., 2015) and may be related to uplift during initial continental subduction of India beneath Asia (Dai et al., 2013). Oligocene-Miocene cooling ages from the same region of ~33-15

Ma (Copeland et al., 1995; Rohrmann et al., 2012; Dai et al., 2013; Tremblay et al., 2015) are interpreted to be related to (1) exhumation accommodated by slip along the south-dipping Renbu-Zedong thrust (Copeland et al., 1995) or (2) Gangdese thrust (Dai et al., 2013), and/or (3) dynamic uplift of Lhasa terrane (Dai et al., 2013; Carrapa et al., 2014). Miocene ages of ~13-8 Ma (Copeland et al., 1995; Dai et al., 2013; Tremblay et al., 2013) are either related to (1) capture of the Yarlung-Zangbo river, (2) east-west-directed normal faulting (Dai et al., 2013), or (3) southward migration of the main river drainage divide to the Himalaya (Tremblay et al., 2015).

5.3.3. Northern Indo-Burma Thrust Belt

The northern Indo-Burma Ranges expose a southeast- to east-directed thrust belt bounded by the Mishmi thrust and Brahmaputra river plain to the southwest and right-slip Jiali fault zone to the northeast (Fig. 1C) (e.g., Gururajan and Choudhuri, 2003; Misra, 2009; Ningthoujam et al., 2015; Haproff et al., 2018). Except for the southernmost, range-bounding Mishmi thrust, faults are expressed as ~1- to 10-km-wide mylonitic thrust shear zones (Fig. 2). Thrust shear zones bound major lithologic units, which along Dibang Valley from northeast to southwest consist of (1) Mesoproterozoic and latest Jurassic-Cretaceous granitoids of the Lohit Plutonic Complex, (2) dismembered ophiolitic fragments of the Tidding and Mayodia mélange complexes (= Indus-Yarlung suture zone), (3) Mesoproterozoic-Cambrian metamorphic rocks of the Mayodia gneiss, (4) Mesoproterozoic-Jurassic metasedimentary rocks of the Lalpani schist, and (5) Tertiary metasedimentary rocks of the Sewak unit (Figs. 2-3). Haproff et al. (2018, in preparation) showed that the Lohit Plutonic Complex is correlative with the Mesoproterozoic Bomi-Chayu complex and latest Jurassic-Cretaceous granitoids of the southern Gangdese batholith belt. Metamorphic rocks of the Mayodia gneiss and Lalpani schist are correlative with the Lesser Himalayan sequence

of the Himalayan orogen.

Despite recent advances in understanding the lithologic framework and structural geometry of the northern Indo-Burma Ranges (e.g., Ningthoujam et al., 2015; Haproff et al., 2018), temporal constraints to the development of the thrust belt are unknown. Whereas the data presented in this chapter is preliminary, further analysis of ZHe ages across the study area will allow for the comparison of exhumation histories along the easternmost Himalayan orogen and provide temporal constraints to the Cenozoic reconstruction of the northernmost Eastern Flanking Belt.

5.4. Sampling and Analytical Methods

Fourteen samples were collected for (U-Th)/He thermochronology from each lithologic unit exposed along the northeast-trending Dibang Valley in the northern Indo-Burma Ranges (Fig. 2). Sampling locations from each lithologic unit are described from southwest to northeast. One quartzite sample (*PH-1-14-13-5*) was collected from the middle section of the southernmost-exposed Sewak unit in the foreland of the thrust belt (Figs. 2-3). Four metasedimentary rock samples from the southernmost exposure of the Lalpani schist were collected from the structural lowermost (*PH-1-12-13-5* and *PH-1-9-13-27*) and uppermost sections (*PH-1-9-13-23* and *PH-1-3-13-11B*) of the unit (Figs. 2-3). Three metamorphic rock samples from the southeasternmost exposure of the Mayodia gneiss were collected from the structural lowermost (*PH-1-9-13-19*) and uppermost sections of the unit (*PH-1-3-13-9* and *PH-1-3-13-8*). Garnet schist sample *PH-1-9-13-10* was collected from the Mayodia mélange complex in the Mayodia klippe. Quartzofeldspathic schist sample *PH-1-9-13-2* was collected from the Lalpani schist in the Hunli half-window in the core of the thrust belt (Figs. 2-3). Garnet schist sample *PH-1-8-13-26* was collected from the Tidding mélange complex located in the hinterland of the thrust belt (Figs. 2-

3). The northeasternmost three granitoid samples (*PH-1-8-13-8*, *PH-1-8-13-7*, and *PH-1-8-13-1B*) were collected from the structural lowermost and middle parts of the western belt of the Lohit Plutonic Complex (Figs. 2-3).

Prior to (U-Th)/He analyses, whole rocks were crushed and separated for zircons at the University of California, Los Angeles (UCLA) using standard procedures (Quidelleur et al., 1997). Picking of zircon grains and (U-Th)/He analyses were performed at the Geo- and Thermochronometry Lab at the University of Texas at Austin. Euhedral and inclusion-free zircon grains of $\geq 70 \mu\text{m}$ width were hand selected using a Nikon SMZ-U/100 stereomicroscope. Approximately three zircon grains per sample were selected for analysis, except for samples yielding significant variation in ZHe ages. Dimensions of each grain were measured to calculate the alpha ejection correction factor (Ft, Farley et al., 1996; Farley, 2002).

Single grains were packed into platinum tubes and heated with a diode laser for 10 minutes at 1250 °C. Single grains were reheated until ${}^4\text{He}$ yield dropped to <1% to ensure complete degassing of the sample. Extracted gas was spiked with a ${}^3\text{He}$ tracer, cryogenically purified, and measured by isotope dilution on a quadrupole noble gas mass spectrometer. Following degassing, zircon grains were dissolved using U-Pb double pressure vessel digestion procedures, including spiking with an enriched ${}^{230}\text{Th}$, ${}^{235}\text{U}$, and ${}^{149}\text{Sm}$ tracer and two-stage dissolution with hydrofluoric acid-nitric acid for 96 hours at 225°C and hydrochloric acid for 12 hours at 180°C. Parent concentrations of U, Th, and Sm were measured via isotope dilution-inductively coupled plasma-mass spectrometry (ID-ICP-MS). ZHe ages were corrected for alpha ejection (F_T) using Helios software with standard errors of 8% (2σ) based on reproducibility of the Fish Canyon Tuff standard (Reiners et al., 2002). Reported ages in this study are the averages and standard deviations of analytical ages for multiple zircon grains per sample. Complete isotopic data for

each analysis is shown on Table A.1. Relationships between ZHe ages and effective uranium ($eU = U + 0.235 \times Th$), which is proportional to radiation damage, is shown on Fig. A.5.1.

Relationships between ZHe age and zircon grain size (effective spherical radius = ESR) for each analysis is shown on Fig. A.5.2.

5.5. Results of Zircon (U-Th)/He Thermochronology

In this section, we describe preliminary ZHe ages from each lithologic unit along Dibang Valley from southeast to northwest (Table 1). The spatial relationship of ZHe ages are shown in Figs. 2-3.

In the foreland of the thrust belt, quartzite sample *PH-1-14-13-5* from the Sewak unit has a ZHe age of 5.8 ± 0.2 Ma. For this sample, we average the youngest two ages ($\pm 2\sigma$) of 5.7 ± 0.5 Ma and 5.9 ± 0.47 Ma and excluded an older age of 12.1 ± 1 Ma. Structurally above the Sewak unit, samples of phyllite (*PH-1-12-13-5*) and quartzo-feldspathic augen gneiss (*PH-1-9-13-27*) of the Lalpani schist towards the foreland have ZHe ages of 4.9 ± 1.9 Ma and 5.6 ± 0.8 Ma, respectively. Samples of quartzo-feldspathic augen gneiss (*PH-1-9-13-23*) and paragneiss (*PH-1-3-13-11B*) from the structural uppermost section of the Lalpani schist in the foreland yields ages of 7.8 ± 1.6 Ma and 8.1 ± 1.4 Ma, respectively. For sample *PH-1-9-13-23*, we average the three youngest ages ($\pm 2\sigma$) of 9.6 ± 0.8 Ma, 6.6 ± 0.5 Ma, and 7.3 ± 0.6 Ma and excluded an older age of 15 ± 1.2 Ma.

Structurally above the Lalpani schist, one paragneiss sample (*PH-1-9-13-19*) from the southwesternmost Mayodia gneiss has a ZHe age of 6.5 ± 1.3 Ma. Two samples of biotite muscovite schist (*PH-1-3-13-9*) and augen gneiss (*PH-1-3-13-8*) from the structural uppermost section of the same exposure of the Mayodia gneiss have ZHe ages of 9.1 ± 1.8 Ma and 8.1 ± 1.2 Ma, respectively.

Garnet schist sample *PH-1-9-13-10* of the Mayodia mélange complex in the center of thrust

belt has a ZHe age of 7.1 ± 0.8 Ma. Quartzo-feldspathic schist sample *PH-1-9-13-2* of the Lalpani schist within the Hunli half-window, located structurally above the Mayodia klippe, has a ZHe age of 7.1 ± 1.4 Ma.

Towards the hinterland of the thrust belt, garnet biotite muscovite schist sample *PH-1-8-13-26* of the Tidding mélange complex, located structurally above the Hunli half-window, yields a range of six ZHe ages ($\pm 2\sigma$) of 16.3 ± 1.3 Ma, 17.4 ± 1.4 Ma, 18.1 ± 1.5 Ma, 26.1 ± 2.1 Ma, 27.6 ± 2.2 Ma, and 32.6 ± 2.6 Ma. The youngest three ZHe ages have an average of 17.3 ± 0.9 Ma. The northernmost three granitoid samples of this study from latest Jurassic-Cretaceous western belt of the Lohit Plutonic Complex have ZHe ages from southwest to northeast of 6 ± 0.8 Ma (*PH-1-8-13-8*), 7.9 ± 0.1 Ma (*PH-1-8-13-7*), and 10.5 ± 0.6 Ma (*PH-1-8-13-1B*).

Samples *PH-1-4-13-5*, *PH-1-3-13-9*, *PH-1-3-13-9*, and the older ZHe age population of ~ 28 Ma in *PH-1-8-13-26* have positive correlations with effective uranium (Fig. A.5.1). This suggests radiation damage such as fission tracks may have trapped ^4He , which delays diffusion and results in older ZHe ages (Danišík et al., 2017). Similarly, the ZHe ages of several samples display a positive correlation with grain size (Fig. A.5.2). These samples include *PH-1-8-13-1B*, *PH-1-3-13-9*, *PH-1-12-13-5*, *PH-1-9-13-27*, *PH-1-9-13-23*, *PH-1-8-13-8*, *PH-1-9-13-19A*, and the older ZHe age population in *PH-1-8-13-26*. Closure temperature for the ZHe system has been shown to be proportional to grain size, which results in older ages for larger grains (Farley, 2002; Reiners, 2005).

5.6. Discussion

Low-temperature thermochronologic ages of major Himalayan lithologic units including the SBS, LHS, and GHC indicate that exhumation primarily occurred from Miocene-Pliocene time

with some variability along strike related to the different slip histories of bounding faults (e.g., Grujic et al., 2006; Stewart et al., 2008; McQuarrie et al., 2014; Enkelmann et al., 2011; Long et al., 2012; Adlakha et al., 2013, 2018). An exception to this include exhumation ages of the GHC in the core of the Namche Barwa-Gyala Peri massif, which are as young as <1 Ma (e.g., Burg et al., 1998; Malloy, 2004; Seward and Burg, 2008; Enkelmann et al., 2011). The application of low-temperature thermochronology across the Himalayan orogen often yields not only a southward younging trend related to forward thrust propagation, but also younger ages at higher structural levels, reflecting temporal variations in slip along thrust systems at depth and/or out-of-sequence thrusting (e.g., Adlanka et al., 2013; McQuarrie et al., 2014).

In the northern Indo-Burma Ranges, the spatial distribution of Miocene ZHe ages from the Tidding mélange complex (~17 Ma) in the northeast to the Lalpani schist and Sewak unit (~5-6 Ma) in the southwest signal a general southwestward younging trend, parallel to the thrust transport direction (Figs. 2-3). Exhumation of the Tidding mélange complex occurred at ~17 Ma was likely related to slip along the Tidding thrust, located at the base of the unit (Fig. 3). To the southwest, exhumation of samples from the Hunli half window and Mayodia mélange complex at ~7 Ma occurred during the development of the Hunli duplex at depth (Fig. 3). Development of the duplex may have been coeval with exhumation of the Mayodia gneiss towards the foreland at ~6.5-9 Ma (Fig. 3). Exhumation of the southeasternmost-exposed Lalpani schist and Sewak unit in the hanging walls of the Lalpani thrust and Mishmi thrust, respectively, occurred from ~5-6 Ma (Fig. 3).

In contrast with the southwestward-younging ZHe ages from the Tidding mélange complex to the foreland (~17-5 Ma), samples of the northernmost-exposed Lohit Plutonic Complex in the hinterland of the thrust belt yield ZHe ages of ~10-6 Ma. These samples are from the hanging wall

of the Lohit thrust, which is the northernmost major fault (Figs. 2-3). These Late Miocene ZHe ages suggest exhumation of the Lohit Plutonic Complex was accommodated via out-of-sequence thrusting, which occurred after cooling of the Tidding mélange complex and was coeval with exhumation in the foreland (Fig. 3). The initial timing of slip along the Lohit thrust has yet to be determined via high-temperature thermochronology or geochronology. However, the Lohit thrust is analogous to the Gangdese thrust in the central segment of the southern Lhasa terrane based on the juxtaposition of granitoids of the Gangdese batholith atop the Indus-Yarlung suture zone (Yin et al., 1994, 1999; Harrison et al., 2000). Although speculative, the Lohit thrust may have initiated at a similar time as the Gangdese thrust (~30-23 Ma) (Yin et al., 1994, 1999; Harrison et al., 2000) during early stages of orogenesis. After a period of inactivity, slip along the Lohit thrust resumed, further exhuming granitoids of the Lohit Plutonic Complex at ~10 Ma.

5.7. Conclusions

Preliminary bedrock zircon (U-Th)/He (ZHe) cooling ages are used to quantify the timing of exhumation across the northern Indo-Burma thrust belt, the easternmost segment of the Himalayan collisional system. The spatial distribution of ZHe ages of ~17-5 Ma from the Tidding mélange complex (=IYSZ) in the northeast to the Sewak unit in the southwest towards the foreland suggests the thrust belt developed as a forward propagating thrust system. However, ZHe ages of ~10-6 Ma from Gangdese-equivalent granitoids in the hinterland of thrust belt suggest renewed exhumation occurred during out-of-sequence thrust motion along the Lohit thrust. This study reveals a more complex exhumation history of the easternmost segment of the Himalayan collisional system, such that Late Miocene slip along the northernmost-exposed Lohit thrust was coeval with the development of the Hunli duplex at depth and imbricate thrust faulting in the foreland.

5.8. Figures and Tables

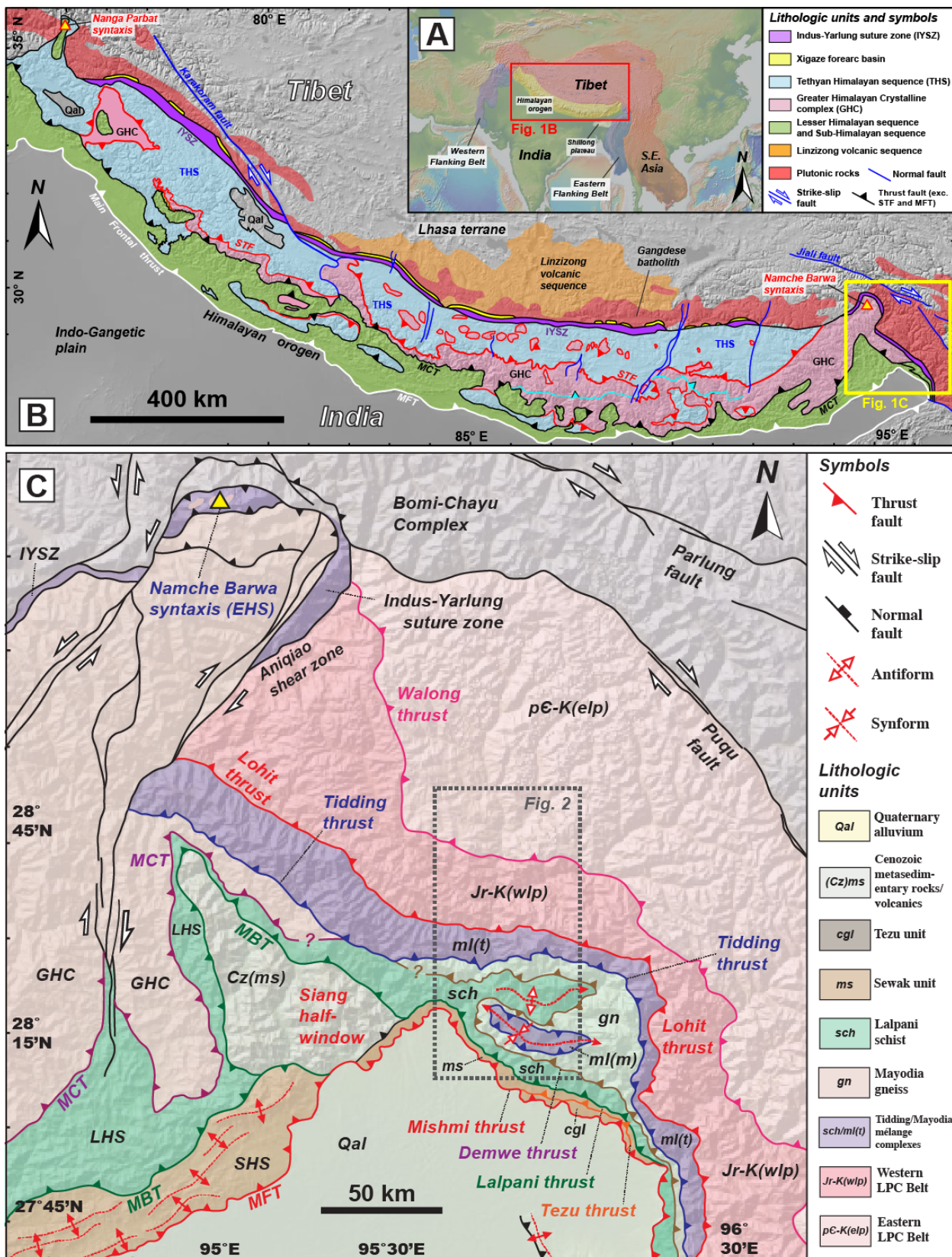


Figure 5.1 (previous page). (A) Map of the southern Asia, showing the locations of the Indian continent, Tibet and southeast Asia (orange), Eastern and Western Flanking belts (blue), Himalayan orogen (yellow), and Shillong plateau (white). The base digital elevation model was acquired using geomapapp.com (Ryan et al., 2009). (B) Simplified geologic map of the Himalayan orogen and southern Lhasa terrane, modified from Webb et al. (2017). The location of the northern Indo-Burma Ranges is shown in the yellow box. (C) Geologic map of the easternmost Himalaya and the northern Indo-Burma Ranges, compiled from Ding et al. (2001) and Haproff et al. (2018). The location of the geologic map of the Dibang Valley traverse is shown in the gray box (Fig. 2). Abbreviations: EHS: eastern Himalayan syntaxis, GHC: Greater Himalayan Crystalline complex, IYSZ: Indus-Yarlung suture zone, JS: Jiali fault, LHS: Lesser Himalayan Sequence, MFT: Main Frontal thrust, STD: South Tibetan detachment, and THS: Tethyan Himalayan Sequence.

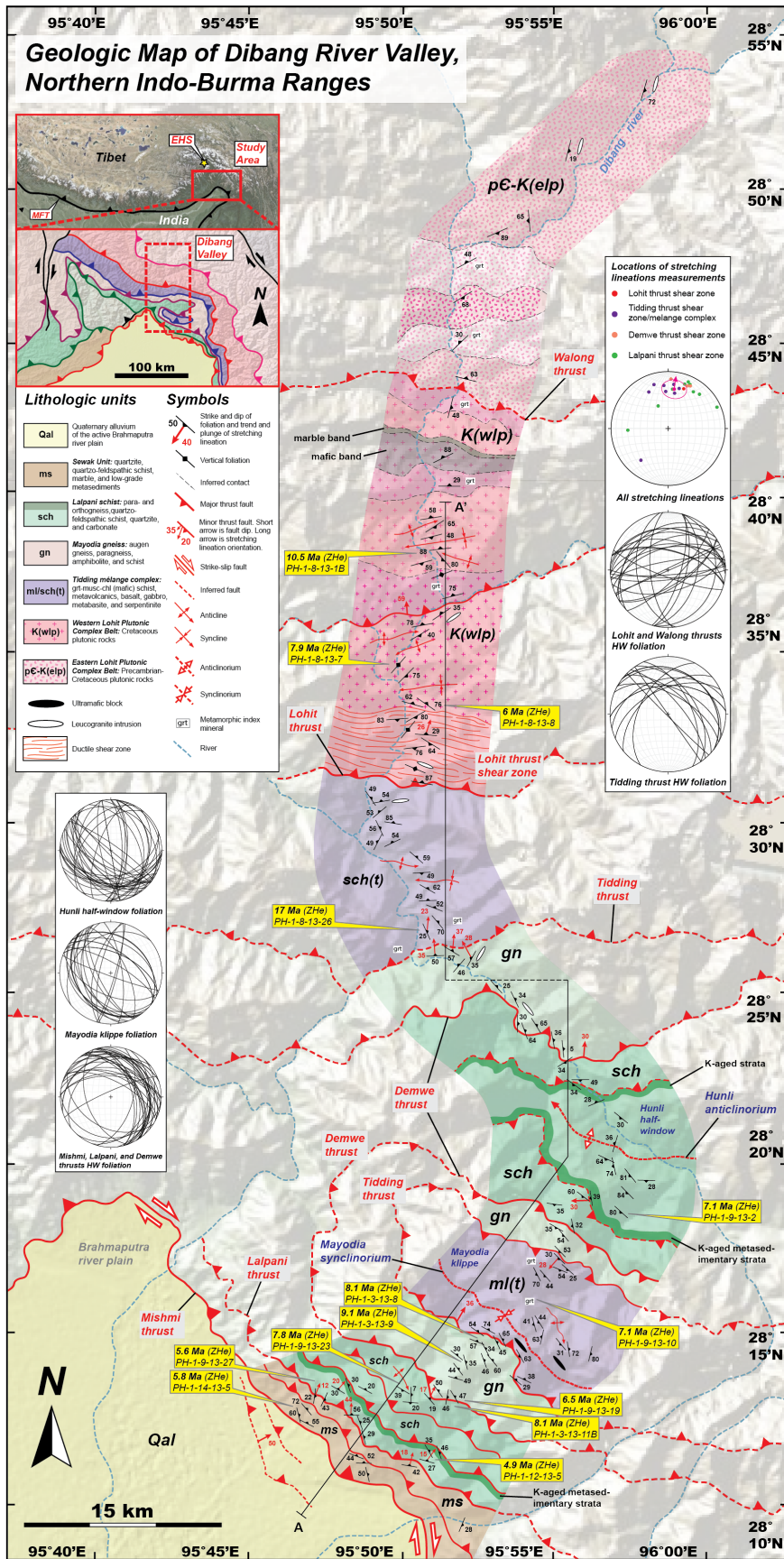


Figure 5.2. Geologic map of Dibang Valley of the northern Indo-Burma Ranges, showing the locations of bedrock ZHe ages (modified from Haproff et al., 2018).

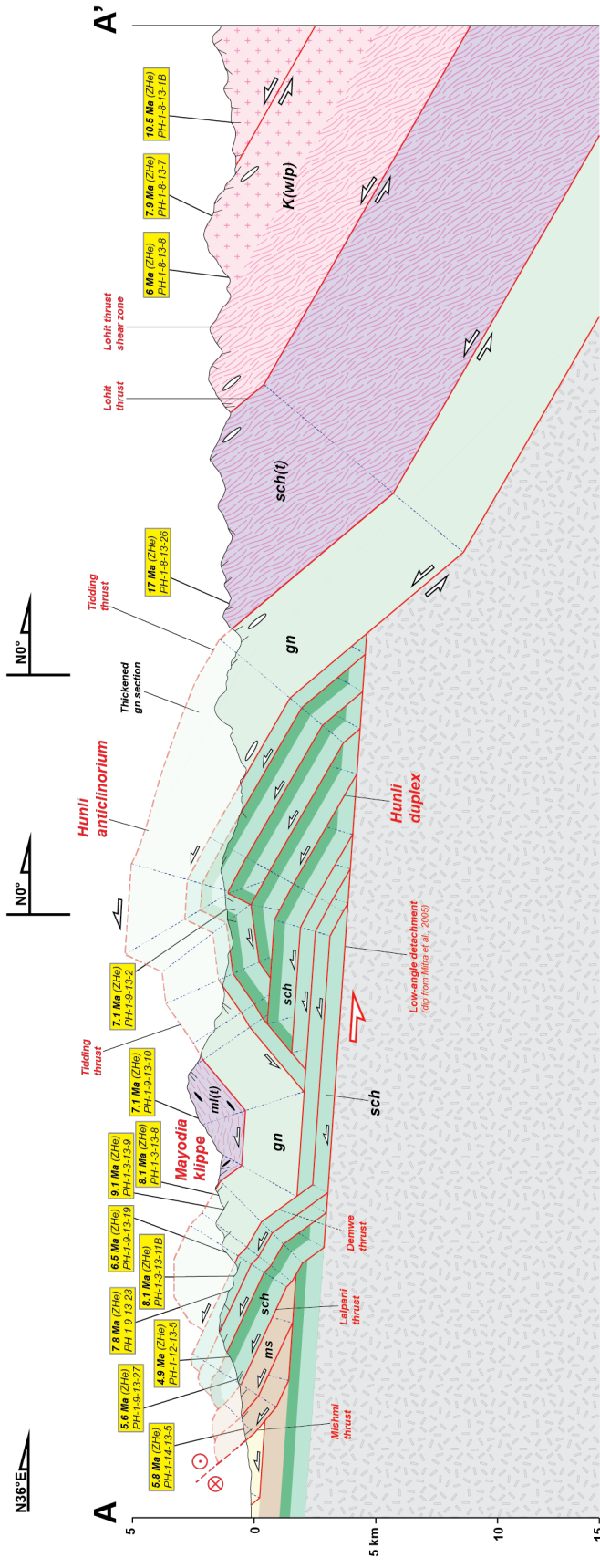


Figure 5.3. Geologic cross section along Dibang Valley of the northern Indo-Burma Ranges, showing the structural locations of ZHe ages (modified from Haproff et al., 2018).

Table 5.1. List of samples used for zircon (U-Th)/He thermochronology

Sample	Rock type	Latitude	Longitude	Elevation (m)	Average ZHe age (Ma)	Std Dev	n
Sewak unit							
PH-1-14-13-4 ¹	phyllite	N28° 12.686	E95° 46.841	417	5.8	0.2	2 out of 3
Lalpani schist							
PH-1-9-13-2	schist	N28° 18.625	E95° 57.287	1196	7.1	1.4	3 out of 3
PH-1-3-13-11B	paragneiss	N28° 13.167	E95° 51.687	1810	8.1	1.4	3 out of 3
PH-1-9-13-23 ²	schist	N28° 13.098	E95° 50.312	1483	7.8	1.6	3 out of 4
PH-1-12-13-5	paragneiss	N28° 11.415	E95° 50.882	542	4.9	1.9	3 out of 3
PH-1-9-13-27	paragneiss	N28° 13.131	E95° 47.572	1064	5.6	0.8	3 out of 3
Mayodia gneiss							
PH-1-3-13-9	paragneiss	28° 14.484	E95° 53.241	2062	9.1	1.8	3 out of 3
PH-1-3-13-8	paragneiss	N28° 14.745	E95° 53.110'E	2061	8.1	1.2	3 out of 3
PH-1-9-13-19A	paragneiss	N28° 13.263	E95° 51.781	1639	6.5	1.3	3 out of 3
Tidding mélange complex							
PH-1-8-13-26 ³	schist	N28° 26.897	E95° 50.957	729	17.3	0.9	3 out of 6
Mayodia mélange complex							
PH-1-9-13-10	schist	N28° 16.145	E95° 54.358	2363	7.1	0.8	3 out of 3
Western Lohit Plutonic Complex belt							
PH-1-8-13-1B	monzodiorite	N28° 37.975	E95° 51.138	798	10.5	0.6	3 out of 3
PH-1-8-13-7	quartz monzonite	N28° 34.809	E95° 50.009	688	7.9	0.1	3 out of 3
PH-1-8-13-8	diorite	N28° 33.579	E95° 50.865	736	6	0.8	3 out of 3

¹Average age for sample PH-1-14-13-4 excludes one ZHe age of 12.1 Ma

²Average age for sample PH-1-9-13-23 excludes one ZHe age of 15 Ma

³Average age for sample PH-1-8-13-26 excludes an older population of four ZHe ages of 32.6 Ma, 27.6 Ma, and 26.1 Ma

5.9. References

- Adlakha, V., Lang, K.A., Patel, R.C., Lal, N., and Huntington, K.W., 2013, Rapid long-term erosion in the rain shadow of the Shillong Plateau, Eastern Himalaya: Tectonophysics, v. 582, p. 76-83.
- Adlakha, V., Patel, R.C., Kumar, A., and Lal, N., 2018, Tectonic control over exhumation in the Arunachal Himalaya: new constraints from Apatite Fission Track Analysis: Geological Society, London, Special Publications, v. 481, no. SP481-1.
- Booth, A.L., Chamberlain, C.P., Kidd, W.S., and Zeitler, P.K., 2009, Constraints on the metamorphic evolution of the eastern Himalayan syntaxis from geochronologic and petrologic studies of Namche Barwa: Geological Society of America Bulletin, v. 121, no. 3-4, p. 385-407.
- Burchfiel, B.C., Zhiliang, C., Hodges, K.V., Yuping, L., Royden, L.H., Changrong, D., and Jiene, X., 1992, The South Tibetan detachment system, Himalayan orogen: Extension contemporaneous with and parallel to shortening in a collisional mountain belt: Geological Society of America Special Papers, v. 269, p. 1-41.
- Burg, J.P., Davy, P., Nievergelt, P., Oberli, F., Seward, D., Diao, Z., and Meier, M., 1997, Exhumation during crustal folding in the Namche-Barwa syntaxis: Terra Nova, v. 9, no. 2, p. 53-56.
- Burg, J.P., et al., 1998, The Namche Barwa syntaxis: evidence for exhumation related to compressional crustal folding: Journal of Asian Earth Sciences, v. 16, no. 2, p. 239-252.
- Carrapa B, et al., 2014, Miocene burial and exhumation of the India-Asia collision zone in southern Tibet: Response to slab dynamics and erosion: Geology, v. 42, no. 5, p. 443–446

- Chambers, J., Parrish, R., Argles, T., Harris, N., and Horstwood, M., 2011, A short-duration pulse of ductile normal shear on the outer South Tibetan detachment in Bhutan: Alternating channel flow and critical taper mechanics of the eastern Himalaya: *Tectonics*, v. 30, no. 2.
- Copeland, P., Harrison, T.M., Yun, P., Kidd, W. S.F., Roden, M., and Zhang, Y., 1995, Thermal evolution of the Gangdese batholith, southern Tibet: A history of episodic unroofing: *Tectonics*, v. 14, no. 2, p. 223-236.
- Dai, J., Wang, C., Hourigan, J., Li, Z., and Zhuang, G., 2013, Exhumation history of the Gangdese batholith, southern Tibetan Plateau: Evidence from apatite and zircon (U-Th)/He thermochronology: *The Journal of Geology*, v. 121, no. 2, p. 155-172.
- Danišík, M., McInnes, B.I., Kirkland, C.L., McDonald, B.J., Evans, N.J., and Becker, T., 2017, Seeing is believing: Visualization of He distribution in zircon and implications for thermal history reconstruction on single crystals: *Science advances*, v. 3, no. 2, e1601121.
- DeCelles, P.G., Carrapa, B., Gehrels, G.E., Chakraborty, T., and Ghosh, P., 2016, Along-strike continuity of structure, stratigraphy, and kinematic history in the Himalayan thrust belt: The view from Northeastern India: *Tectonics*, v. 35, no. 12, p. 2995-3027.
- Ding, L., Kapp, P., Zhong, D., and Deng, W., 2003, Cenozoic volcanism in Tibet: evidence for a transition from oceanic to continental subduction. *Journal of Petrology*, v. 44, no. 10, p. 1833-1865.
- Ding, L., Zhong, D., Yin, A., Kapp, P., and Harrison, T.M., 2001, Cenozoic structural and metamorphic evolution of the eastern Himalayan syntaxis (Namche Barwa): *Earth and Planetary Science Letters*, v. 192, no. 3, p. 423-438.

Edwards, M.A. and Harrison, T.M., 1997, When did the roof collapse? Late Miocene north-south extension in the high Himalaya revealed by Th-Pb monazite dating of the Khula Kangri granite: *Geology*, v. 25, no. 6, p. 543-546.

Edwards, M.A., Kidd, W.S., Li, J., Yue, Y., and Clark, M., 1996, Multi-stage development of the southern Tibet detachment system near Khula Kangri. New data from Gonto La: *Tectonophysics*, v. 260, no. 1-3, p. 1-19.

Edwards, M.A., Pêcher, A., Kidd, W.S.F., Burchfiel, B. C., and Royden, L.H., 1999, Southern Tibet Detachment System at Khula Kangri, Eastern Himalaya: A Large-Area, Shallow Detachment Stretching into Bhutan?: *The Journal of geology*, v. 107, no. 5, p. 623-631.

Enkelmann, E., Ehlers, T.A., Zeitler, P.K., and Hallet, B., 2011, Denudation of the Namche Barwa antiform, eastern Himalaya: *Earth and Planetary Science Letters*, v. 307, no. 3-4, p. 323-333.

Farley, K.A., 2002, (U-Th)/He dating: Techniques, calibrations, and applications: *Reviews in Mineralogy and Geochemistry*, v. 4, no. 1, p. 819-844.

Farley, K.A., Wolf, R.A., and Silver, L.T., 1996, The effects of long alpha-stopping distances on (U-Th)/He ages: *Geochimica et cosmochimica acta*, v. 60, no. 21, p. 4223-4229.

Gansser, A., 1964, *Geology of the Himalayas*. New York: Wiley Interscience, p. 289.

Gansser, A., 1983, *Geology of the Bhutan Himalaya*: Birkhauser, Basel, p. 181.

Grujic, D., Hollister, L. S., and Parrish, R.R., 2002, Himalayan metamorphic sequence as an orogenic channel: insight from Bhutan: *Earth and Planetary Science Letters*, v. 198, no. 1, p. 177-191.

Grujic, D., Coutand, I., Bookhagen, B., Bonnet, S., Blythe, A., and Duncan, C., 2006, Climatic forcing of erosion, landscape, and tectonics in the Bhutan Himalayas: *Geology*, v. 34, no. 10, p. 801-804.

Guan, Q., et al., 2012, Crustal thickening prior to 38 Ma in southern Tibet: evidence from lower crust-derived adakitic magmatism in the Gangdese Batholith: *Gondwana Research*, v. 21, no. 1, p. 88-99.

Gururajan, N.S. and Choudhuri, B.K., 2003, Geology and tectonic history of the Lohit valley, Eastern Arunachal Pradesh, India: *Journal of Asian Earth Sciences*, v. 21, no. 7, p. 731-741.

Haproff, P.J., Zuza, A.V., Yin, A., 2018, West-directed thrusting south of the eastern Himalayan syntaxis indicates clockwise crustal flow at the indenter corner during the India-Asia collision: *Tectonophysics*, v. 722, p. 277-285.

Haproff, P.J., Zuza, A.V., Yin, A., Harrison, T.M., Manning, C.M., Ding, L., Wu, C., Chen, J., Dubey, C.S., 2018, Tectonic evolution of the northern Indo-Burma Ranges (Part 1): lateral tectonostratigraphy correlation across the eastern Himalayan syntaxis: in preparation.

Harrison, T.M., Yin, A., Grove, M., Lovera, O. M., Ryerson, F. J., and Zhou, X., 2000, The Zedong Window: A record of superposed Tertiary convergence in southeastern Tibet: *Journal of Geophysical Research: Solid Earth*, v. 105, no. B8, p. 19211-19230.

Ji, W.Q., Wu, F.Y., Chung, S.L., Li, J.X., and Liu, C.Z., 2009, Zircon U-Pb geochronology and Hf isotopic constraints on petrogenesis of the Gangdese batholith, southern Tibet: *Chemical Geology*, v. 262, no. 3, p. 229-245.

Koons, P.O., Zeitler, P.K., and Hallet, B., 2013, Tectonic aneurysms and mountain building: *Treatise on geomorphology*, v. 5, p. 318-349.

Kumar, G., 1997, Geology of Arunachal Pradesh: Bangalore, Geological Society of India, p. 217.

Le Fort, P., 1975, Himalayas: the collided range. Present knowledge of the continental arc: *American Journal of Science*, v. 275, p. 1-44.

Long, S., McQuarrie, N., Tobgay, T., and Grujic, D., 2011, Geometry and crustal shortening of

the Himalayan fold-thrust belt, eastern and central Bhutan: Geological Society of America Bulletin, p. B30203-1.

Long, S.P., McQuarrie, N., Tobgay, T., and Hawthorne, J., 2011, Quantifying internal strain and deformation temperature in the eastern Himalaya, Bhutan: Implications for the evolution of strain in thrust sheets: *Journal of Structural Geology*, v. 33, no. 4, p. 579-608.

Long, S.P., McQuarrie, N., Tobgay, T., Rose, C., Gehrels, G., and Grujic, D., 2011, Tectonostratigraphy of the Lesser Himalaya of Bhutan: Implications for the along-strike stratigraphic continuity of the northern Indian margin: Geological Society of America Bulletin: v. 123, no. 7-8, p. 1406-1426.

Long, S.P., et al., 2012, Variable shortening rates in the eastern Himalayan thrust belt, Bhutan: Insights from multiple thermochronologic and geochronologic data sets tied to kinematic reconstructions: *Tectonics*, v. 31, no. 5.

Malloy, M., 2004, Rapid erosion at the Tsangpo knickpoint and exhumation of southeastern Tibet: M.S. thesis, Lehigh University.

McQuarrie, N., Robinson, D., Long, S., Tobgay, T., Grujic, D., Gehrels, G., and Ducea, M., 2008, Preliminary stratigraphic and structural architecture of Bhutan: Implications for the along strike architecture of the Himalayan system: *Earth and Planetary Science Letters*, v. 272, no. 1, p. 105-117.

McQuarrie, N., Tobgay, T., Long, S.P., Reiners, P.W., and Cosca, M.A., 2014, Variable exhumation rates and variable displacement rates: Documenting recent slowing of Himalayan shortening in western Bhutan: *Earth and Planetary Science Letters*, v. 386, p. 161-174.

Misra, D.K., 2009, Litho-tectonic sequence and their regional correlation along the Lohit and Dibang valleys, eastern Arunachal Pradesh: *Journal of the Geological Society of India*, v. 73,

no. 2, p. 213-219.

Misra, D.K. and Singh, T., 2002, Tectonic setting and neotectonic features along the Eastern Syntaxial Bend (Lohit and Dibang), Arunachal Himalaya: Aspects of Geology and Environment of the Himalaya, p. 19-40.

Mitra, S., Priestley, K., Bhattacharyya, A.K., and Gaur, V.K., 2005, Crustal structure and earthquake focal depths beneath northeastern India and southern Tibet: Geophysical Journal International, v. 160, no. 1, p. 227-248.

Ningthoujam, P.S., Dubey, C.S., Lolee, L.K., Shukla, D.P., Naorem, S.S., and Singh, S.K., 2015, Tectonic studies and crustal shortening across Easternmost Arunachal Himalaya: Journal of Asian Earth Sciences, v. 111, p. 339-349.

Quidelleur, X., Grove, M., Lovera, O.M., Harrison, T.M., and Yin, A., 1997, Thermal evolution and slip history of the Renbu-Zedong Thrust, southeastern Tibet: Journal of Geophysical Research, v. 102, p. 2659-2679.

Reiners, P.W., Farley, K.A., and Hickes, H.J., 2002, He diffusion and (U-Th)/He thermochronometry of zircon: initial results from Fish Canyon Tuff and Gold Butte: Tectonophysics, v. 349, no. 1-4, p. 297-308.

Reiners, P.W., 2005, Zircon (U-Th)/He Thermochronometry: Reviews in Mineralogy and Geochemistry, v. 58, no. 1, p. 151-179.

Rohrmann, A., Kapp, P., Carrapa, B., Reiners, P.W., Guynn, J., Ding, L., and Heizler, M., 2012, Thermochronologic evidence for plateau formation in central Tibet by 45 Ma: Geology, v. 4, no. 2, p. 187-190.

Ryan, W. B., et al., 2009, Global multi-resolution topography synthesis: Geochemistry, Geophysics, Geosystems, v. 10, no. 3.

Schärer, U., Xu, R.H., and Allègre, C.J., 1984, UPb geochronology of Gangdese (Transhimalaya) plutonism in the Lhasa-Xigaze region, Tibet: Earth and Planetary Science Letters, v. 69, no. 2, p. 311-320.

Seward, D. and Burg, J.P., 2008, Growth of the Namche Barwa Syntaxis and associated evolution of the Tsangpo Gorge: Constraints from structural and thermochronological data: Tectonophysics, v. 451, no. 1-4, p. 282-289.

Stewart, R.J., Hallet, B., Zeitler, P.K., Malloy, M.A., Allen, C.M., and Trippett, D., 2008, Brahmaputra sediment flux dominated by highly localized rapid erosion from the easternmost Himalaya: Geology, v. 36, no. 9, p. 711-714.

Tremblay, M.M., et al., 2015, Erosion in southern Tibet shut down at~ 10 Ma due to enhanced rock uplift within the Himalaya: Proceedings of the National Academy of Sciences, v. 112, no. 39, p. 12030-12035.

Webb, A.A.G., Yin, A. and Dubey, C.S., 2013, U-Pb zircon geochronology of major lithologic units in the eastern Himalaya: Implications for the origin and assembly of Himalayan rocks: Geological Society of America Bulletin, v. 125, no. 3-4, p. 499-522.

Webb, A. A. G., et al., 2017, The Himalaya in 3D: Slab dynamics controlled mountain building and monsoon intensification: Lithosphere, v. L636-1.

Wen, D.R., et al., 2008, Zircon SHRIMP U–Pb ages of the Gangdese Batholith and implications for Neotethyan subduction in southern Tibet: Chemical Geology, v. 252, no. 3, p. 191-201.

Yin, A., 2006, Cenozoic tectonic evolution of the Himalayan orogen as constrained by along-strike variation of structural geometry, exhumation history, and foreland sedimentation: Earth-Science Reviews, v. 76, no. 1, p. 1-131.

Yin, A., et al., 1999, Tertiary deformation history of southeastern and southwestern Tibet during the Indo-Asian collision: Geological Society of America Bulletin, v. 111, no. 11, p. 1644-1664.

Yin, A., Dubey, C.S., Webb, A.A.G., Kelty, T.K., Grove, M., Gehrels, G.E. and Burgess, W.P., 2010, Geologic correlation of the Himalayan orogen and Indian craton: Part 1. Structural geology, U-Pb zircon geochronology, and tectonic evolution of the Shillong Plateau and its neighboring regions in NE India: Geological Society of America Bulletin, v. 122, no. 3-4, p. 336-359.

Yin, A., Dubey, C.S., Kelty, T.K., Gehrels, G.E., Chou, C.Y., Grove, M., and Lovera, O., 2006, Structural evolution of the Arunachal Himalaya and implications for asymmetric development of the Himalayan orogen: Current Science, v. 90, no. 2, p. 195-200.

Yin, A., Dubey, C.S., Kelty, T.K., Webb, A.A.G., Harrison, T.M., Chou, C.Y. and Célérier, J., 2010, Geologic correlation of the Himalayan orogen and Indian craton: Part 2. Structural geology, geochronology, and tectonic evolution of the Eastern Himalaya: Geological Society of America Bulletin, p. B26461-1.

Yin, A., Harrison, T.M., Ryerson, F.J., Wenji, C., Kidd, W.S.F. and Copeland, P., 1994, Tertiary structural evolution of the Gangdese thrust system, southeastern Tibet: Journal of Geophysical Research: Solid Earth, v. 99, no. B9, p. 18175-18201.

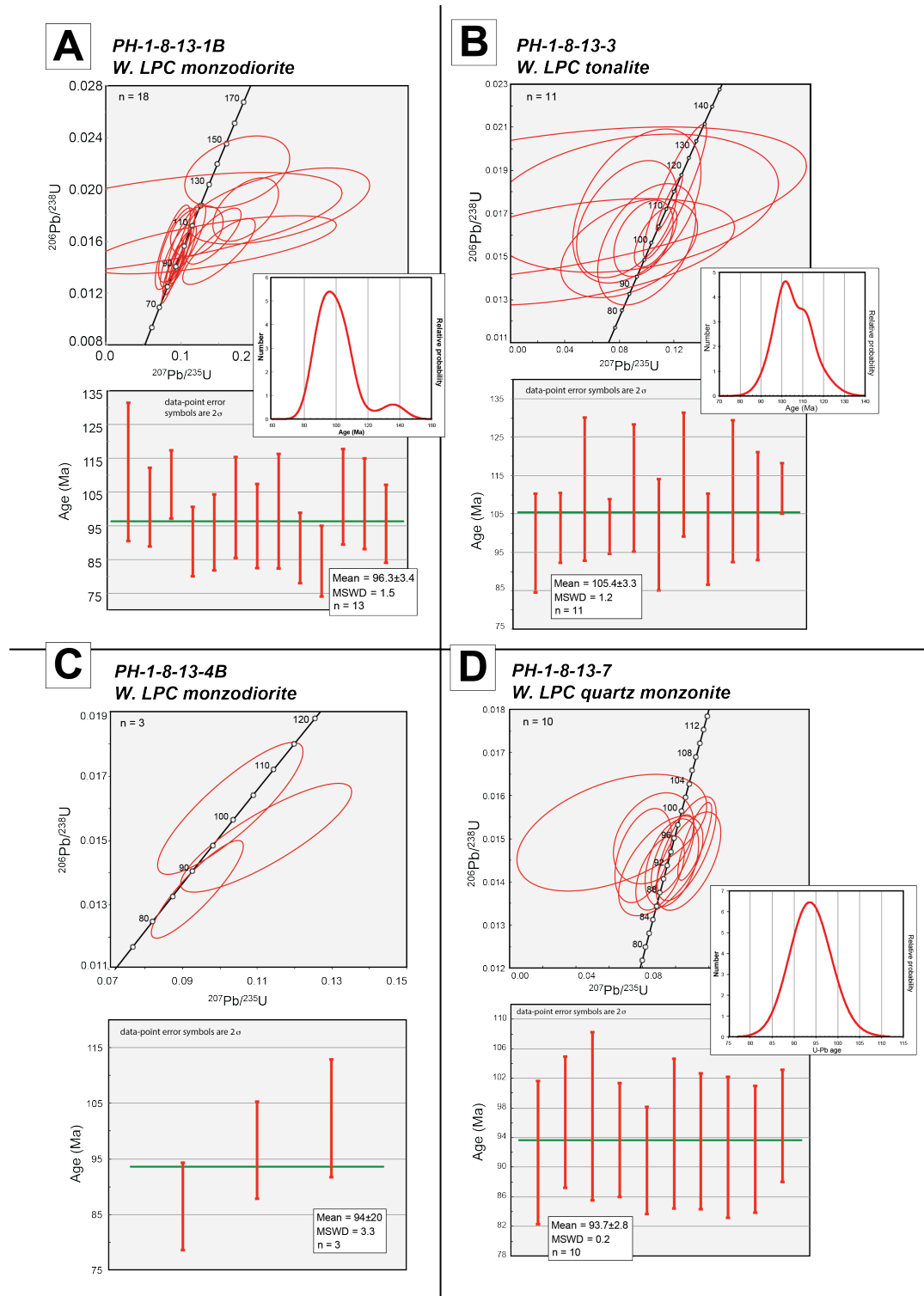
Zeitler, P. K., et al., 2001, Erosion, Himalayan geodynamics, and the geomorphology of metamorphism: GSA Today, v. 11, p. 4-9.

Zhu, D.C., Pan, G.T., Chung, S.L., Liao, Z.L., Wang, L.Q., and Li, G.M., 2008, SHRIMP zircon age and geochemical constraints on the origin of Lower Jurassic volcanic rocks from the Yeba Formation, southern Gangdese, South Tibet: International Geology Review, v. 50, no. 5, p. 442-471.

-Appendices-

Supplementary figures and data tables

Chapter 2: Tectonic evolution of the northern Indo-Burma Ranges: lateral correlation of Himalayan-Tibetan lithologic units across the eastern Himalayan syntaxis



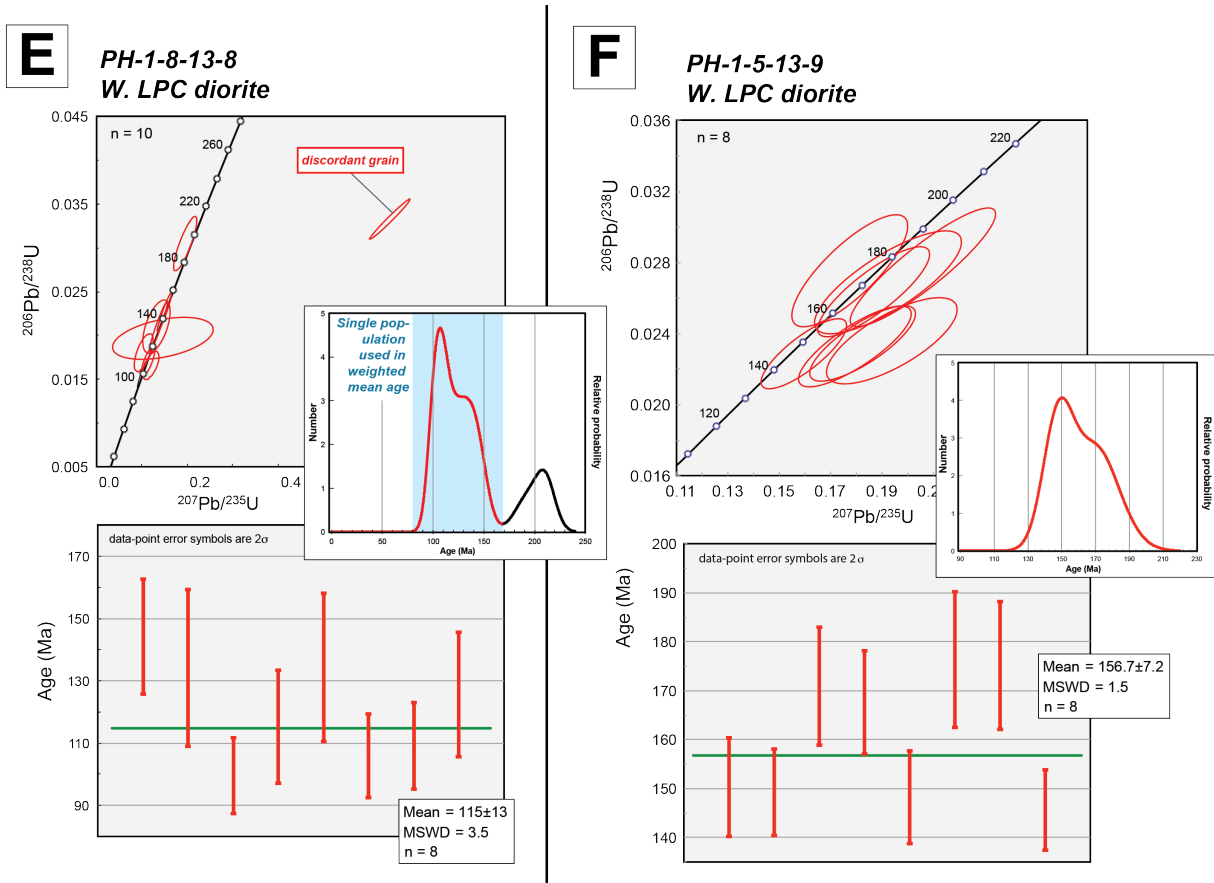


Figure A.2.1 (previous and current page). U-Pb zircon concordia, relative probability, and weighted mean age plots for granitoids of the western Lohit Plutonic Complex belt: (A) *PH-1-8-13-1B*, (B) *PH-1-8-13-3*, (C) *PH-1-8-13-4B*, (D) *PH-1-8-13-7*, (E) *PH-1-8-13-8*, and (F) *PH-1-5-13-9*.

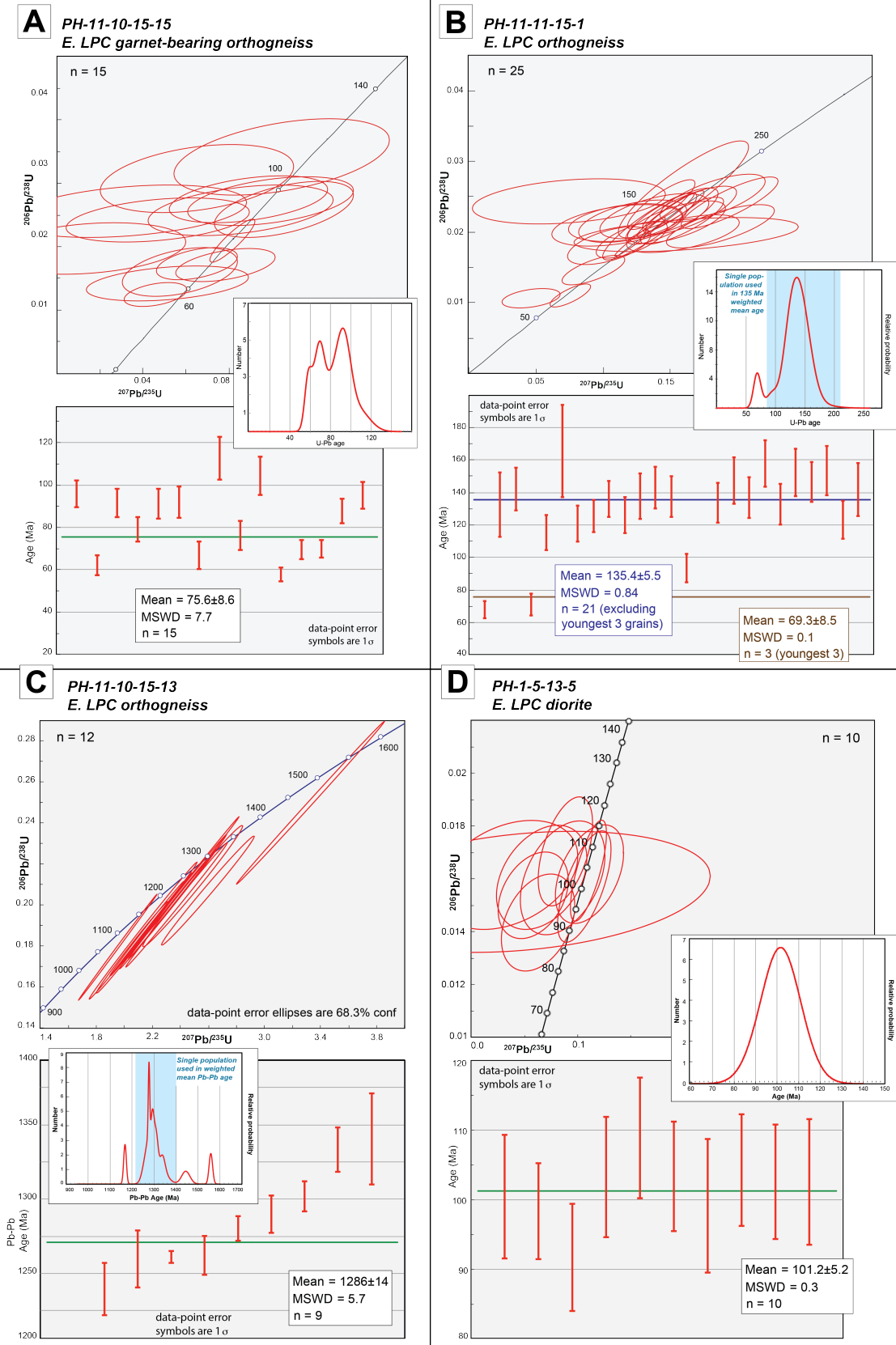


Figure A.2.2 (previous page). U-Pb concordia, relative probability, and weighted mean age plots for granitoids of the eastern Lohit Plutonic Complex belt: (A) PH-11-10-15-15, (B) PH-11-11-15-1, (C) PH-11-10-15-13, and (D) PH-1-5-13-5.

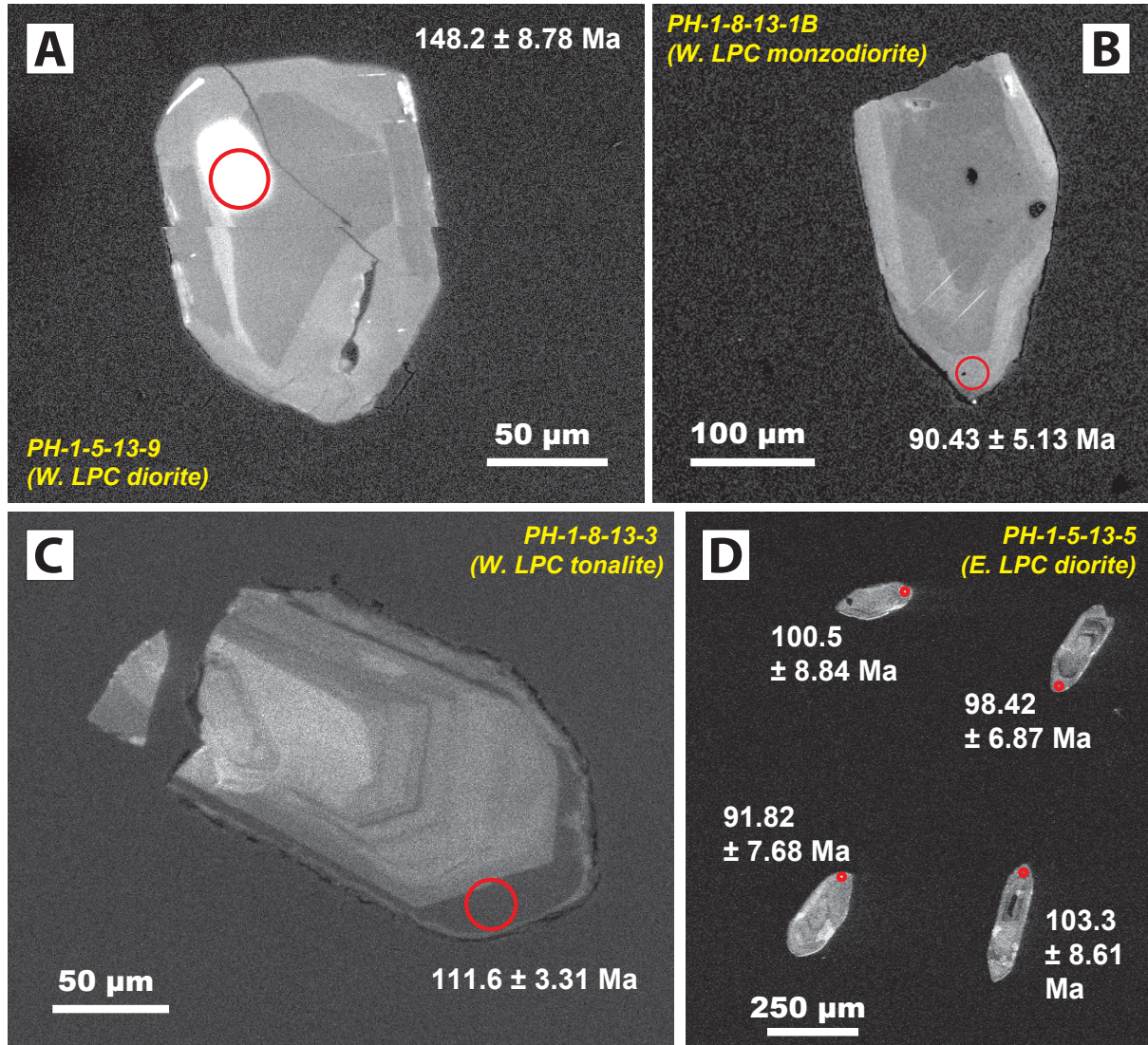


Figure A.2.3. Cathodoluminescence (CL) images of representative zircons analyzed for U-Pb crystallization ages from (A-C) granitoids of the western Lohit Plutonic Complex belt and (D) diorite of the eastern Lohit Plutonic Complex belt.

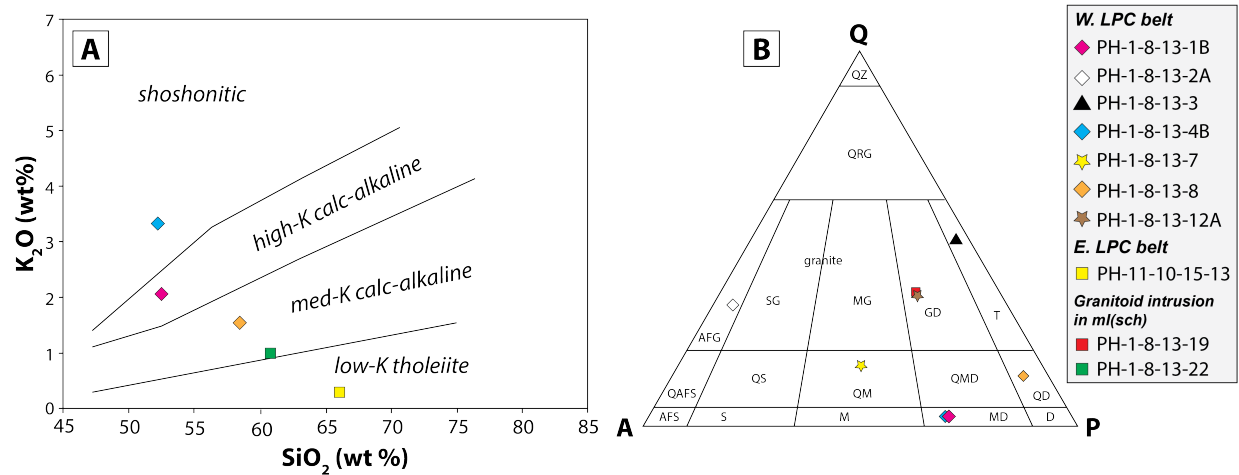


Figure A.2.4. Geochemical plots for plutonic rocks including (A) K₂O vs. SiO₂ (Le Bas et al., 1984) and (B) granitoid-type based on quartz-alkali feldspar-plagioclase feldspar (QAP) abundances based on mineral point counting in thin section.

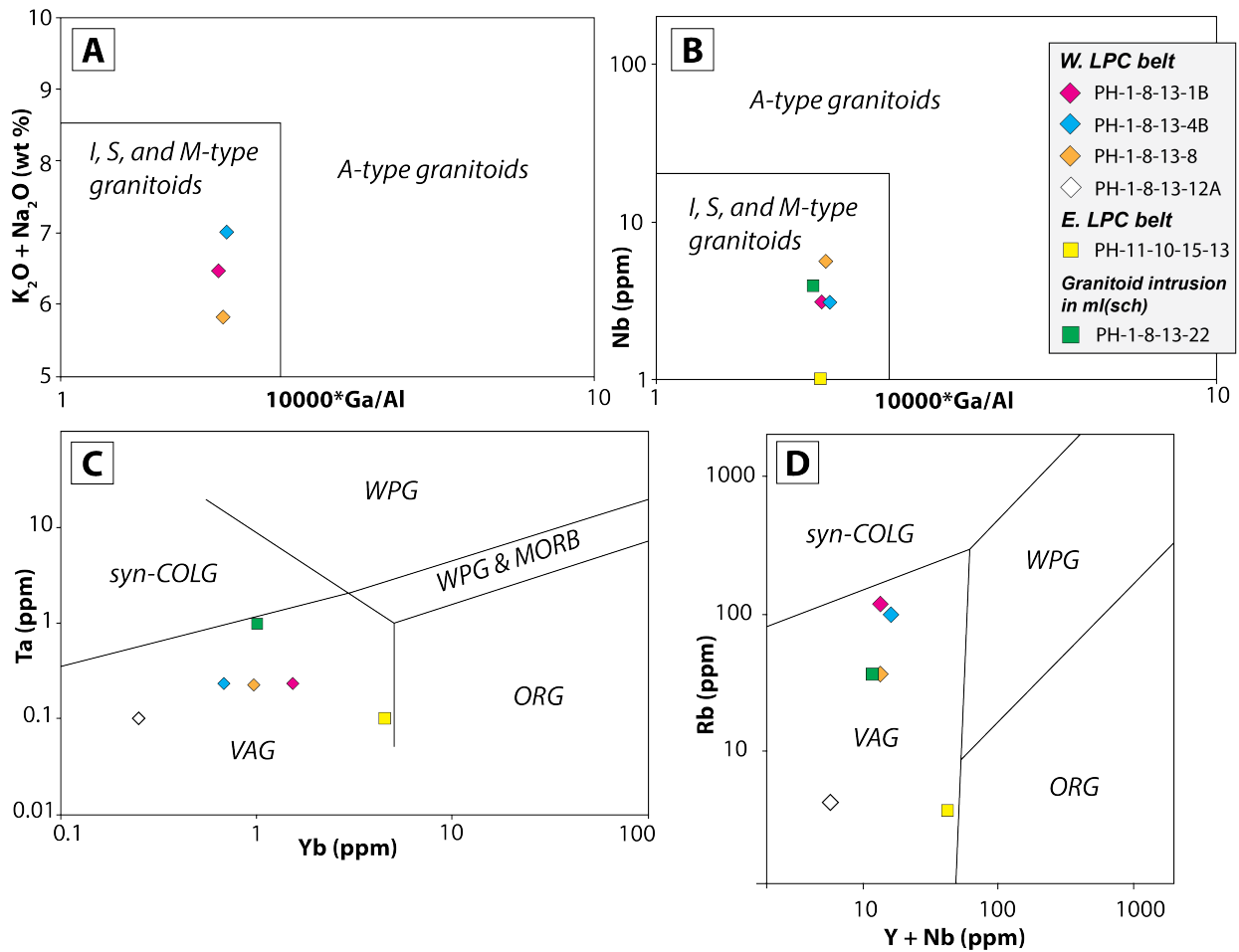


Figure A.2.5. Diagrams of sources for plutonic rocks including anorogenic (A), igneous (I), sedimentary (S), and mantle (M)-types based on (A) $K_2O + Na_2O$ vs. $10000^*Ga/Al$ and (B) Nb vs. $10000^*Ga/Al$. Tectonic settings diagram for plutonic rocks including syncollisional (*syn-COLG*), within-plate granite (*WPG*), volcanic arc granite (*VAG*), orogenic (*ORG*) based on (C) Ta vs. Yb and (D) Rb vs. $Y + Nb$ (Pearce et al., 1984).

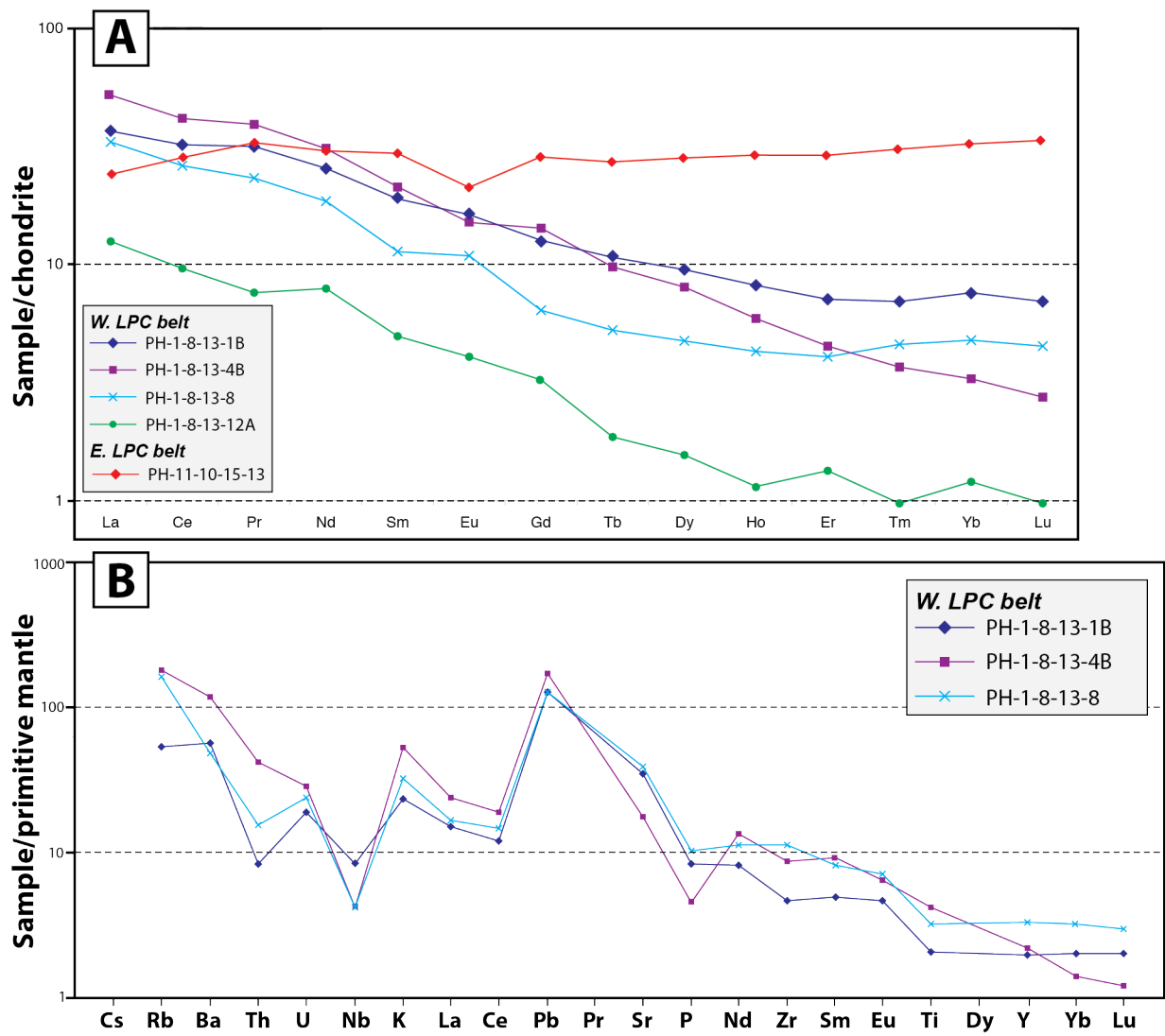


Figure A.2.6. (A) Chondrite-normalized and (B) primitive mantle-normalized rare earth element spider diagram for granitoids of the western Lohit Plutonic Complex belt.

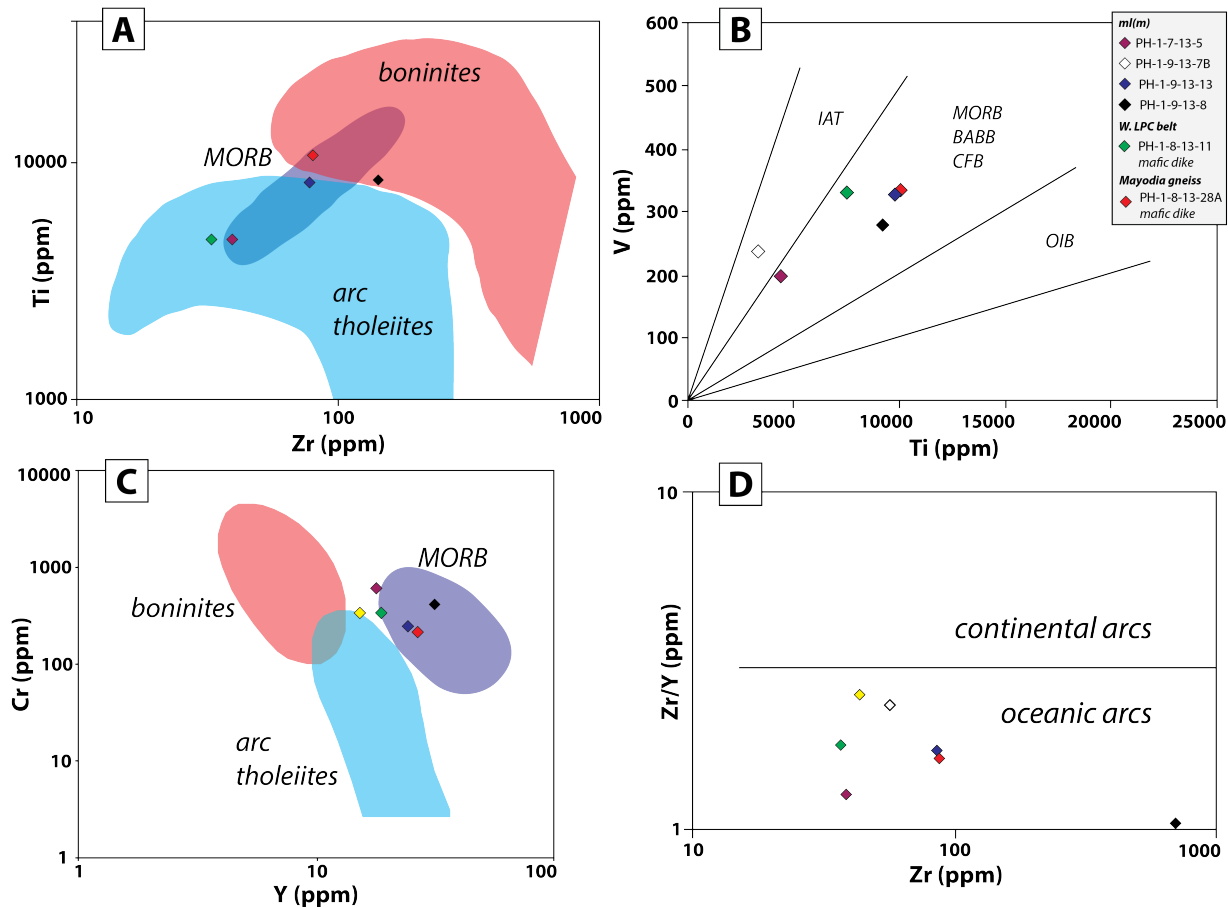


Figure A.2.7. Tectonic setting discriminant diagrams of mafic and ultramafic rocks including mid-ocean ridge basalts (*MORB*), oceanic island basalts (*OIB*), back-arc basins basalts (*BABB*), island arc tholeiites (*IAT*), oceanic arcs, continental arc or flood basalts (*CFB*), and alkaline arcs, based on (A) Ti vs. Zr, (B) V vs. Ti, (C) Cr vs. Y, and (D) Zr/Y vs. Zr.

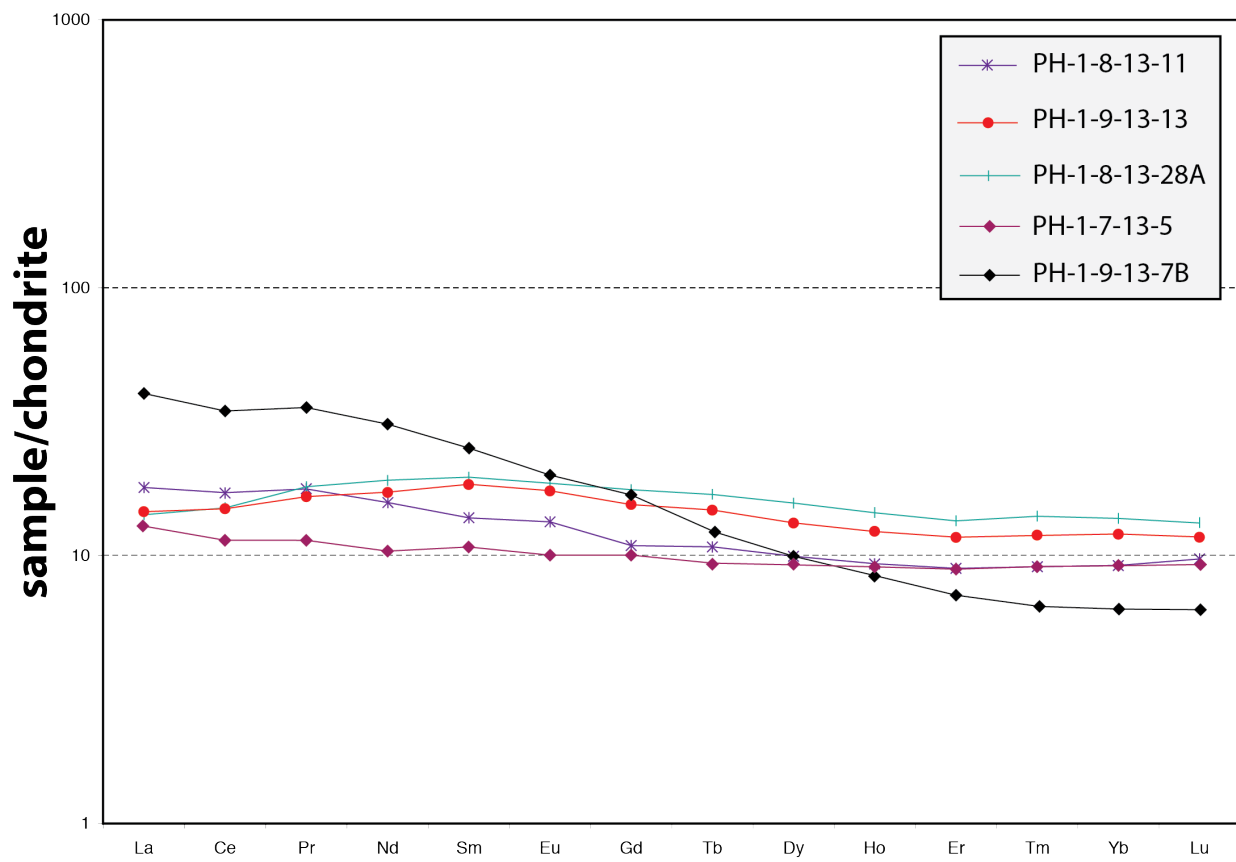


Figure A.2.8. Chondrite-normalized rare earth element spider diagram for mafic and ultramafic rocks.

Table A.2.1. U-Pb zircon geochronology data for the Western Lohit Plutonic Complex Belt

Spot ID ¹	Isotopic ratios	Ages (Ma ± 1 s.e.)										$^{207}\text{Pb}/^{206}\text{Pb}$	± 1 s.e.	U-Pb age rejected
		$^{206}\text{Pb}/^{238}\text{U}$	± 1 s.e.	$^{207}\text{Pb}/^{235}\text{U}$	± 1 s.e.	$^{207}\text{Pb}/^{206}\text{Pb}$	± 1 s.e.	^{206}Pb (%)	$^{206}\text{Pb}/^{238}\text{U}$	± 1 s.e.	$^{207}\text{Pb}/^{235}\text{U}$			
<i>PH-1-8-13-1B</i>														
1	1.737E-02	1.61 0E-03	4.571 E-02	1.090 E-01	1.908 E-02	4.430 E-02	92.97		111	10. 2	45.3 8	105	-	-
2	1.573E-02	9.16 0E-04	1.419 E-01	6.660 E-02	6.542 E-02	2.830 E-02	95.52		100.6	5.8 1	134. 8	59.3	787.9	907
3	2.136E-02	1.13 0E-03	1.739 E-01	2.830 E-02	5.905 E-02	8.940 E-03	98.54		136.2	7.1 3	162. 8	24.5	569	329
4	1.522E-02	1.04 0E-03	1.499 E-01	1.960 E-02	7.139 E-02	6.160 E-03	100		97.4	6.5 9	141. 8	17.3	968.6	176
5	1.640E-02	8.82 0E-04	1.428 E-01	1.480 E-02	6.313 E-02	4.490 E-03	100		104.9	5.6	135. 5	13.1	712.6	151
6	1.872E-02	1.20 0E-03	2.294 E-01	4.880 E-02	8.887 E-02	1.650 E-02	98.3		119.6	7.6 2	209. 7	40.3	1401	356
7	1.679E-02	7.95 0E-04	1.205 E-01	1.420 E-02	5.205 E-02	5.730 E-03	99.67		107.3	5.0 4	115. 5	12.8	287.5	251
8	1.845E-02	1.00 0E-03	1.851 E-01	1.770 E-02	7.279 E-02	6.040 E-03	100		117.8	6.3 3	172. 5	15.2	1008	168
9	1.413E-02	8.08 0E-04	8.942 E-02	5.510 E-03	4.591 E-02	1.120 E-03	99.81		90.43	5.1 3	86.9 7	5.13	-	-
10	1.455E-02	8.83 0E-04	9.585 E-02	6.760 E-03	4.776 E-02	1.700 E-03	100		93.15	5.6 1	92.9 4	6.26	87.58	84. 6
11	1.571E-02	1.17 0E-03	9.407 E-02	9.830 E-03	4.344 E-02	3.160 E-03	99.3		100.5	7.4 5	91.2 9	9.12	-	-
12	1.485E-02	9.78 0E-04	9.292 E-02	8.360 E-03	4.538 E-02	2.450 E-03	99.59		95.02	6.2 1	90.2 2	7.76	-	-
13	1.554E-02	1.33 0E-03	8.878 E-02	9.440 E-03	4.144 E-02	2.740 E-03	99.16		99.4	8.4 6	86.3 6	8.81	-	-
14	1.383E-02	8.17 0E-04	9.021 E-02	5.940 E-03	4.730 E-02	1.670 E-03	99.77		88.55	5.2	87.7	5.53	64.55	83. 8
15	1.321E-02	8.20 0E-04	8.836 E-02	5.950 E-03	4.849 E-02	9.560 E-04	99.89		84.63	5.2 2	85.9 7	5.55	123.4	46. 4
16	1.622E-02	1.11 0E-03	1.074 E-01	1.020 E-02	4.804 E-02	2.780 E-03	99.57		103.7	7.0 6	103. 6	9.35	101.1	137
17	1.588E-02	1.06 0E-03	1.026 E-01	6.950 E-03	4.687 E-02	8.990 E-04	99.86		101.6	6.7 4	99.1 9	6.4	42.59	45. 8
18	1.495E-02	9.06 0E-04	1.021 E-01	7.350 E-03	4.954 E-02	1.670 E-03	99.95		95.69	5.7 5	98.7 6	6.78	173.4	78. 8
<i>PH-1-8-13-3</i>														
1	1.522E-02	1.01 0E-03	4.431 E-02	4.910 E-02	2.112 E-02	2.280 E-02	96.2		97.37	6.4 2	44.0 2	47.8	-	-
2	1.585E-02	7.22 0E-04	9.758 E-02	8.900 E-03	4.465 E-02	3.730 E-03	99.44		101.4	4.5 8	94.5 4	8.23	-	-
3	1.742E-02	1.47 0E-03	1.558 E-02	8.240 E-02	6.485 E-03	3.400 E-02	93.7		111.4	9.3 2	15.7	82.3	-	-
4	1.590E-02	5.66 0E-04	1.065 E-01	6.390 E-03	4.856 E-02	2.240 E-03	100		101.7	3.5 9	102. 7	5.86	126.8	108

5	1.748E-02	1.310E-03	8.937E-02	4.380E-02	3.707E-02	1.760E-02	97.98		111.7	8.28	86.91	40.8	-	-	
6	1.557E-02	1.150E-03	9.994E-02	1.470E-02	4.655E-02	6.190E-03	99.3		99.6	7.27	96.72	13.6	26.33	319	
7	1.803E-02	1.270E-03	1.207E-01	9.490E-03	4.857E-02	1.690E-03	99.73		115.2	8.07	115.7	8.6	126.9	81.8	
8	1.539E-02	9.360E-04	8.710E-02	2.050E-02	4.106E-02	8.890E-03	97.97		98.43	5.94	84.8	19.2	-	-	
9	1.735E-02	1.460E-03	9.279E-02	1.920E-02	3.878E-02	7.180E-03	98.53		110.9	9.26	90.1	17.8	-	-	
10	1.674E-02	1.110E-03	8.518E-02	1.500E-02	3.690E-02	5.820E-03	98.38		107	7.04	83	14	-	-	
11	1.746E-02	5.230E-04	1.165E-01	3.960E-03	4.840E-02	5.960E-04	99.92		111.6	3.31	111.9	3.6	118.7	29	
<i>PH-I-8-13-4B</i>															
1	1.349E-02	6.190E-04	9.397E-02	5.030E-03	5.050E-02	1.250E-03	100		86.41	3.93	91.19	4.66	218.1	57.3	
2	1.509E-02	6.890E-04	1.124E-01	9.350E-03	5.399E-02	2.740E-03	100		96.58	4.38	108.1	8.53	370.7	114	
3	1.600E-02	8.360E-04	1.028E-01	7.950E-03	4.661E-02	1.950E-03	99.83		102.3	5.3	99.39	7.32	29.06	100	
<i>PH-I-8-13-7</i>															
1	1.437E-02	7.630E-04	9.099E-02	1.670E-02	4.590E-02	7.360E-03	98.85		91.97	4.85	88.42	15.6	-	-	
2	1.501E-02	6.960E-04	8.666E-02	1.590E-02	4.190E-02	7.290E-03	98.77		96.07	4.42	84.39	14.8	-	-	
3	1.514E-02	8.930E-04	6.162E-02	3.760E-02	2.950E-02	1.730E-02	97.08		96.87	5.67	60.72	36	-	-	
4	1.464E-02	6.040E-04	9.814E-02	8.530E-03	4.860E-02	3.270E-03	99.49		93.67	3.84	95.06	7.89	130.1	158	
5	1.421E-02	5.710E-04	9.056E-02	9.610E-03	4.620E-02	4.240E-03	99.29		90.94	3.63	88.03	8.94	9.814	221	
6	1.477E-02	7.960E-04	1.065E-01	1.170E-02	5.230E-02	4.390E-03	99.51		94.54	5.06	102.7	10.7	296.8	192	
7	1.461E-02	7.200E-04	8.044E-02	1.120E-02	3.990E-02	5.070E-03	98.72		93.49	4.58	78.56	10.6	-	-	
8	1.448E-02	7.520E-04	1.076E-01	1.280E-02	5.390E-02	5.280E-03	99.68		92.68	4.78	103.8	11.7	366.7	221	
9	1.444E-02	6.730E-04	9.765E-02	1.060E-02	4.900E-02	4.850E-03	99.48		92.43	4.28	94.61	9.82	150	232	
10	1.494E-02	5.970E-04	1.114E-01	6.740E-03	5.410E-02	1.980E-03	100		95.59	3.79	107.3	6.15	374.9	82.5	
<i>PH-I-8-13-8</i>															
1	2.262E-02	1.470E-03	1.503E-01	1.040E-02	4.819E-02	1.030E-03	99.84		144.2	9.27	142.2	9.16	108.5	50.6	
2	2.102E-02	2.000E-03	1.329E-01	1.980E-02	4.586E-02	5.660E-03	99.15		134.1	12.6	126.7	17.8	-	-	
3	3.327E-02	1.510E-03	6.459E-01	2.920E-02	1.408E-01	1.080E-03	99.93		211	9.41	506	18	2237	13.3	y ^c
4	1.557E-02	9.640E-04	1.011E-01	6.550E-03	4.707E-02	8.860E-04	99.83		99.6	6.12	97.75	6.04	52.81	44.9	

5	1.805E-02	1.44 0E-03	1.049 E-01	1.370 E-02	4.214 E-02	4.210 E-03	99.11		115.3	9.1	101. 3	12.6	-	-	
6	2.103E-02	1.89 0E-03	1.371 E-01	1.320 E-02	4.729 E-02	1.310 E-03	99.73		134.2	11. 9	130. 5	11.7	63.79	66. 1	
7	3.046E-02	2.05 0E-03	1.961 E-01	1.680 E-02	4.668 E-02	2.110 E-03	99.51		193.5	12. 8	181. 8	14.3	33.08	108	y ^c
8	1.657E-02	1.06 0E-03	1.204 E-01	1.200 E-02	5.273 E-02	4.090 E-03	99.6		105.9	6.6 9	115. 5	10.9	317.3	176	
9	1.706E-02	1.10 0E-03	1.145 E-01	9.660 E-03	4.868 E-02	2.670 E-03	99.73		109.1	6.9 9	110. 1	8.8	132.4	129	
10	1.968E-02	1.58 0E-03	1.471 E-01	7.300 E-02	5.421 E-02	2.540 E-02	74.13		125.6	10	139. 3	64.6	379.9	105 0	
<i>PH-1-5-13-9</i>															
1	2.360E-02	1.60 0E-03	1.938 E-01	1.680 E-02	5.957 E-02	3.560 E-03	100		150.4	10	179. 9	14.3	587.9	130	
2	2.345E-02	1.40 0E-03	1.824 E-01	1.360 E-02	5.642 E-02	2.590 E-03	100		149.4	8.8	170. 2	11.7	469	102	
3	2.689E-02	1.91 0E-03	1.923 E-01	1.890 E-02	5.188 E-02	3.160 E-03	100		171	12	178. 6	16.1	280.1	139	
4	2.636E-02	1.67 0E-03	1.867 E-01	1.440 E-02	5.137 E-02	2.200 E-03	100		167.7	10. 5	173. 8	12.3	257.6	98. 4	
5	2.328E-02	1.50 0E-03	1.794 E-01	1.450 E-02	5.588 E-02	2.670 E-03	100		148.4	9.4 3	167. 5	12.5	447.6	106	
6	2.774E-02	2.20 0E-03	2.059 E-01	1.870 E-02	5.384 E-02	2.160 E-03	100		176.4	13. 8	190. 1	15.8	364.4	90. 5	
7	2.754E-02	2.08 0E-03	1.774 E-01	1.490 E-02	4.672 E-02	2.380 E-03	100		175.2	13	165. 9	12.8	35.06	122	
8	2.287E-02	1.30 0E-03	1.595 E-01	1.100 E-02	5.057 E-02	2.040 E-03	100		145.8	8.1 7	150. 3	9.61	221.4	93. 5	

Notes:

¹Spot ID: # is the zircon spot number

²Negative values for isotopic ratios, ages, and errors are rejected

Dashes are immeasurable quantities and rejected

E-01 = x 0.1, E-02 = x 0.01, E-03 = x 0.001

Rejected U-Pb ages:

^aLow radiogenic lead

^bAnalytical error

^cInherited zircon

^dDiscordant U-Pb age

Table A.2.2. U-Pb zircon geochronology data for the Eastern Lohit Plutonic Complex Belt

Spot ID ¹	Isotopic ratios						$^{206}\text{Pb}/^{238}\text{U}$	± 1 s.e.	$^{207}\text{Pb}/^{235}\text{U}$	± 1 s.e.	$^{207}\text{Pb}^{206}\text{Pb}$	± 1 s.e.	^{206}Pb (%)	Ages (Ma ± 1 s.e.)				$^{207}\text{Pb}/^{235}\text{U}$	± 1 s.e.	$^{207}\text{Pb}/^{206}\text{Pb}$	± 1 s.e.	U-Pb age rejected
	$^{206}\text{Pb}/^{238}\text{U}$	± 1 s.e.	$^{207}\text{Pb}/^{235}\text{U}$	± 1 s.e.	$^{207}\text{Pb}^{206}\text{Pb}$	± 1 s.e.								$^{206}\text{Pb}/^{238}\text{U}$	± 1 s.e.	$^{207}\text{Pb}/^{235}\text{U}$	± 1 s.e.	$^{207}\text{Pb}/^{206}\text{Pb}$	± 1 s.e.			
<i>PH-11-10-15-15</i>																						
1	1.498E-02	9.763E-04	8.905E-02	2.430E-02	4.311E-02	1.088E-02	94.94		95.87		6.2	86.62	22.65	-	-	-	-	-	-	-	-	-
2	9.664E-03	7.350E-04	5.131E-02	2.480E-02	3.851E-02	1.778E-02	93.77		62		4.69	50.81	23.95	-	-	-	-	-	-	-	-	-
3	8.714E-03	6.964E-04	-2.112E-02	3.325E-02	-1.758E-02	-2.812E-02	85.63		55.93		4.45	-21.68	34.49	-	-	-	-	-	-	-	y ^a	-
4	1.430E-02	1.066E-03	8.525E-02	2.840E-02	4.324E-02	1.340E-02	93.9		91.54		6.78	83.07	26.57	-	-	-	-	-	-	-	-	-
5	1.237E-02	9.084E-04	8.150E-02	6.868E-03	4.781E-02	1.766E-03	99.19		79.22		5.78	79.56	6.45	89.64	87.54	-	-	-	-	-	-	-
6	1.226E-02	1.252E-03	-9.685E-02	9.195E-02	-5.728E-02	-5.764E-02	75.95		78.58		7.98	-103.4	103.4	-	-	-	-	-	-	-	y ^a	-
7	1.424E-02	1.094E-03	3.334E-02	3.609E-02	1.698E-02	1.799E-02	90.97		91.13		6.95	33.3	35.46	-	-	-	-	-	-	-	-	-
8	1.435E-02	1.155E-03	1.054E-01	2.138E-02	5.327E-02	9.352E-03	96.88		91.84		7.34	101.7	19.64	340.5	397.5	-	-	-	-	-	-	-
9	1.041E-02	1.019E-03	5.717E-02	1.761E-02	3.983E-02	1.119E-02	94.94		66.76		6.5	56.45	16.91	-	-	-	-	-	-	-	-	-
10	1.766E-02	1.596E-03	1.043E-01	3.304E-02	4.283E-02	1.236E-02	93.42		112.8		10.11	100.7	30.38	-	-	-	-	-	-	-	-	-
11	1.189E-02	1.067E-03	1.491E-02	2.980E-02	9.094E-03	1.798E-02	90.5		76.22		6.8	15.03	29.81	-	-	-	-	-	-	-	-	-
12	1.630E-02	1.426E-03	6.511E-02	2.964E-02	2.898E-02	1.252E-02	93.48		104.2		9.04	64.04	28.26	-	-	-	-	-	-	-	-	-
13	8.988E-03	5.097E-04	4.586E-02	9.490E-03	3.700E-02	7.052E-03	96.03		57.68		3.26	45.53	9.21	-	-	-	-	-	-	-	-	-
14	1.084E-02	6.963E-04	7.847E-02	1.519E-02	5.251E-02	9.062E-03	96.43		69.5		4.44	76.7	14.3	307.5	393.1	-	-	-	-	-	-	-
15	1.091E-02	6.723E-04	6.514E-02	1.252E-02	4.331E-02	7.515E-03	96.73		69.94		4.29	64.07	11.93	-	-	-	-	-	-	-	-	-
16	1.370E-02	9.267E-04	4.686E-02	2.803E-02	2.480E-02	1.432E-02	92.78		87.74		5.89	46.5	27.19	-	-	-	-	-	-	-	-	-
17	1.487E-02	1.018E-03	9.925E-02	2.530E-02	4.840E-02	1.129E-02	95.1		95.17		6.47	96.09	23.37	118.9	550	-	-	-	-	-	-	-
<i>PH-11-10-15-13^{3,4}</i>																						
1	2.07E-01	1.76E-02	2.60E+00	2.20E-01	9.09E-02	9.05E-04	100		1214		93.9	1300	62	1444	19	-	-	-	-	-	y ^d	-
2	2.84E-01	1.33E-01	3.29E+00	1.47E-01	8.40E-02	3.16E-03	100		1612		666	1479	347	1293	73.1	-	-	-	-	-	y ^b	-
3	1.79E-01	1.49E-02	2.06E+00	1.71E-01	8.33E-02	6.85E-04	100		1064		81.3	1136	56.9	1276	16	-	-	-	-	-	-	-
4	1.88E-01	1.54E-02	2.17E+00	1.77E-01	8.34E-02	4.71E-04	100		1113		83.4	1170	56.8	1278	11	-	-	-	-	-	-	-
5	1.91E-01	1.63E-02	2.20E+00	1.87E-01	8.33E-02	1.42E-04	100		1127		88.1	1180	59.5	1277	3.32	-	-	-	-	-	-	-

6	2.09E-01	1.96E-02	2.49E+00	2.37E-01	8.62E-02	1.14E-03	100		1225	104	1268	68.9	1343	25.5	
7	2.13E-01	2.01E-02	2.47E+00	2.33E-01	8.40E-02	2.99E-04	100		1244	107	1262	68.2	1293	6.93	
8	1.80E-01	1.71E-02	1.95E+00	1.86E-01	7.88E-02	2.44E-04	100		1065	93.5	1099	64	1168	6.12	y ^d
9	2.00E-01	1.78E-02	2.34E+00	2.09E-01	8.48E-02	3.68E-04	100		1177	95.7	1226	63.6	1311	8.42	
10	2.02E-01	2.16E-02	2.35E+00	2.52E-01	8.44E-02	4.49E-04	100		1185	116	1226	76.6	1301	10.3	
11	1.88E-01	2.21E-02	2.14E+00	2.54E-01	8.26E-02	6.21E-04	100		1108	120	1160	82.2	1259	14.7	
12	2.50E-01	2.62E-02	3.33E+00	3.48E-01	9.65E-02	4.09E-04	100		1439	135	1488	81.6	1558	7.94	y ^d
13	2.00E-01	2.01E-02	2.37E+00	2.39E-01	8.60E-02	5.50E-04	100		1177	108	1235	72	1337	12.4	
14	1.62E-02	1.73E-03	3.01E-01	3.27E-02	1.35E-01	2.98E-03	100		103.7	11	267	25.5	2157	38.7	y ^d

PH-11-11-15-1

1	1.062E-02	8.823E-04	4.626E-02	1.423E-02	3.158E-02	9.008E-03	95.02		68.13	5.628	45.92	13.81	-	0.01	
2	2.077E-02	3.141E-03	1.347E-01	2.307E-02	4.702E-02	3.573E-03	99.13		132.5	19.83	128.3	20.64	50.26	181.4	
3	1.328E-01	4.978E-01	7.463E-01	2.814E+00	4.075E-02	1.367E-02	96.69		804.1	2833	566.1	1636	-	0.014	y ^b
4	2.228E-02	2.106E-03	1.378E-01	2.677E-02	4.486E-02	7.181E-03	95.83		142	13.28	131.1	23.89	-	0.007	
5	1.107E-02	1.075E-03	7.545E-02	1.003E-02	4.944E-02	4.119E-03	97.08		70.96	6.856	73.86	9.465	168.8	194.6	
6	1.805E-02	1.736E-03	1.045E-01	2.045E-02	4.197E-02	6.813E-03	97.22		115.3	10.99	100.9	18.8	-	0.01	
7	2.602E-02	4.501E-03	1.596E-01	3.205E-02	4.447E-02	4.315E-03	97.85		165.6	28.28	150.3	28.07	-	0.004	
8	1.891E-02	1.755E-03	1.209E-01	1.749E-02	4.638E-02	4.882E-03	96.77		120.8	11.1	115.9	15.85	17.43	252.9	
9	1.966E-02	1.581E-03	1.618E-01	5.498E-02	5.970E-02	1.857E-02	92.23		125.5	9.99	152.3	48.05	592.6	674.5	
10	2.133E-02	1.747E-03	1.167E-01	2.802E-02	3.968E-02	8.905E-03	95.06		136	11.03	112.1	25.48	-	0.01	
11	1.977E-02	1.745E-03	1.593E-01	2.744E-02	5.843E-02	8.154E-03	94.58		126.2	11.03	150.1	24.04	545.8	305	
12	2.156E-02	2.213E-03	1.586E-01	2.042E-02	5.337E-02	3.914E-03	98.15		137.5	13.96	149.5	17.9	344.4	165.9	
13	2.241E-02	2.041E-03	1.460E-01	1.410E-02	4.725E-02	1.300E-03	99.28		142.9	12.87	138.4	12.5	62.02	65.55	
14	2.154E-02	1.990E-03	1.218E-01	2.642E-02	4.101E-02	7.653E-03	95.66		137.4	12.56	116.7	23.92	-	0.01	
15	1.457E-02	1.370E-03	9.271E-02	1.524E-02	4.616E-02	5.425E-03	97.9		93.23	8.71	90.03	14.16	5.97	283	
16	2.429E-02	2.111E-03	7.461E-02	4.749E-02	2.228E-02	1.370E-02	92.76		154.7	13.28	73.07	44.87	-	0.01	

17	2.095E-02	1.966E-03	1.103 E-01	3.1 87E -02	3.817 E-02	1.004E -02	93.1 5		133.7	12.4 1	106.2	29.15	-	0.01	
18	2.311E-02	2.241E-03	1.643 E-01	2.3 10E -02	5.156 E-02	4.849E -03	97.9 7		147.3	14.1 2	154.4	20.15	265.9	215.8	
19	2.143E-02	1.971E-03	1.545 E-01	2.3 90E -02	5.228 E-02	6.105E -03	96.7 5		136.7	12.4 4	145.8	21.02	297.5	266.5	
20	2.475E-02	2.252E-03	1.814 E-01	2.5 70E -02	5.317 E-02	5.390E -03	96.4		157.6	14.1 6	169.3	22.09	336.2	229.7	
21	2.079E-02	2.005E-03	1.872 E-01	2.6 52E -02	6.532 E-02	6.383E -03	93.2 6		132.6	12.6 6	174.3	22.69	784.5	205.3	
22	2.389E-02	2.298E-03	1.433 E-01	1.6 49E -02	4.352 E-02	2.629E -03	98.1		152.2	14.4 7	136	14.65	-	0.03	
23	2.297E-02	1.919E-03	1.531 E-01	1.4 44E -02	4.835 E-02	1.724E -03	98.7 7		146.4	12.0 9	144.7	12.72	116.6	84.06	
24	2.411E-02	2.398E-03	1.939 E-01	2.3 87E -02	5.832 E-02	3.896E -03	97.6 2		153.6	15.1	180	20.3	541.9	146	
25	1.930E-02	1.817E-03	1.276 E-01	1.2 44E -02	4.793 E-02	9.742E -04	99.4 7		123.2	11.4 9	121.9	11.2	95.97	48.11	
26	2.223E-02	2.597E-03	1.512 E-01	2.2 61E -02	4.934 E-02	4.364E -03	97.5 9		141.7	16.3 8	143	19.94	163.8	206.8	

PH-1-5-13-5

1	1.063E-01	1.660E-02	1.571 E-02	1.3 90E -03	4.906 E-02	5.720E -03	99.4		100.5	8.84	102.6	15.2	150.8	273	
2	5.816E-02	2.180E-02	1.538 E-02	1.0 80E -03	2.742 E-02	9.770E -03	97.3 4		98.42	6.87	57.4	20.9	-	0.01	
3	6.277E-02	2.280E-02	1.435 E-02	1.2 10E -03	3.174 E-02	1.090E -02	97.2 9		91.82	7.68	61.82	21.8	-	0.01	
4	3.411E-02	4.360E-02	1.615 E-02	1.3 60E -03	1.532 E-02	1.920E -02	95.5 7		103.3	8.61	34.06	42.8	-	0.02	
5	8.848E-02	1.690E-02	1.704 E-02	1.3 60E -03	3.766 E-02	6.220E -03	98.5 3		108.9	8.63	86.08	15.8	-	0.01	
6	1.112E-01	2.120E-02	1.618 E-02	1.2 30E -03	4.987 E-02	8.550E -03	99.1 2		103.4	7.83	107.1	19.4	188.9	399	
7	4.919E-02	1.160E-01	1.551 E-02	1.5 10E -03	2.301 E-02	5.380E -02	90.9 2		99.19	9.56	48.75	112	-	0.05	
8	1.102E-01	1.120E-02	1.631 E-02	1.2 60E -03	4.900 E-02	3.380E -03	100		104.3	7.99	106.1	10.3	147.8	162	
9	6.614E-02	2.810E-02	1.606 E-02	1.3 00E -03	2.987 E-02	1.200E -02	97.0 3		102.7	8.27	65.03	26.7	-	0.01	
10	8.591E-02	2.630E-02	1.604 E-02	1.4 20E -03	3.884 E-02	1.100E -02	98.3 2		102.6	8.99	83.68	24.6	-	0.01	

Notes:

¹Spot ID: # is the zircon spot number

²Negative values for isotopic ratios, ages, and errors are rejected

³Data for PH-11-10-15-13 were calculated without the ²⁰⁶Pb correction

The weighted mean age for PH-11-10-15-13 is from the single main population of Mesoproterozoic ²⁰⁷Pb/²⁰⁶Pb ages

Dashes are immeasurable quantities and rejected

E-01 = x 0.1, E-02 = x 0.01, E-03 = x 0.001

Rejected U-Pb ages:

^aLow radiogenic lead

^bAnalytical error

^cInherited zircon

^dDiscordant U-Pb age

Table A.2.3. U-Pb detrital zircon geochronologic analyses of metasedimentary rocks of the Tidding and Mayodia mélange complexes

Sample/ analysis	Isotopic ratios		$^{207}\text{Pb}/^{235}\text{U}$	± 1 s.e.	$^{207}\text{Pb}/^{206}\text{Pb}$	± 1 s.e.	Apparent ages (Ma)			$^{207}\text{Pb}/^{235}\text{U}$	± 1 s.e.	$^{207}\text{Pb}/^{206}\text{Pb}$	± 1 s.e.	Best age	
	$^{206}\text{Pb}/^{238}\text{U}$	± 1 s.e.					$^{207}\text{Pb}/^{238}\text{U}$	± 1 s.e.	(Ma)					(Ma)	\pm (Ma)
PH-1-8-13-26-002	0.1612	0.0011	1.6902	0.0244	0.0761	0.0013	0.9	963	6	1005	9	1097	18	963	6
PH-1-8-13-26-003	0.1275	0.0008	1.7804	0.0157	0.1013	0.0013	0.9	774	4	1038	6	1648	8	-	-
PH-1-8-13-26-004	0.1665	0.0012	1.6972	0.0277	0.0739	0.0013	0.87	993	6	1007	10	1039	37	993	6
PH-1-8-13-26-005	0.0213	0.0009	0.1404	0.0492	0.0478	0.00169	0.9	136	5	133	44	91	522	136	5
PH-1-8-13-26-006	0.1976	0.0022	2.1461	0.0615	0.0788	0.0024	0.9	1162	12	1164	20	1167	39	1167	39
PH-1-8-13-26-007	0.0164	0.0005	0.1038	0.0149	0.0461	0.00068	0.71	105	3	100	14	-	-	105	3
PH-1-8-13-26-008	0.1914	0.0011	2.0896	0.0186	0.0792	0.0010	0.9	1129	6	1145	6	1178	9	1178	9
PH-1-8-13-26-009	0.0842	0.0008	0.8272	0.0244	0.0713	0.00022	0.9	521	5	612	14	966	44	-	-
PH-1-8-13-26-010	0.2167	0.0016	2.5321	0.0362	0.0848	0.00014	0.9	1265	8	1281	10	1310	17	1310	17
PH-1-8-13-26-011	0.2557	0.0017	3.2185	0.0532	0.0913	0.00016	0.87	1468	9	1462	13	1453	35	1453	35
PH-1-8-13-26-012	0.3112	0.0021	4.5534	0.0479	0.1062	0.00014	0.9	1746	10	1741	9	1735	10	1735	10
PH-1-8-13-26-013	0.0835	0.0007	0.8452	0.0172	0.0734	0.00017	0.9	517	4	622	9	1026	28	-	-
PH-1-8-13-26-014	0.4683	0.0036	12.0207	0.1518	0.1862	0.00028	0.89	2476	16	2606	12	2709	25	2709	25
PH-1-8-13-26-015	0.0983	0.0006	1.0817	0.0161	0.0799	0.00013	0.8	604	4	744	8	1193	32	-	-
PH-1-8-13-26-016	0.1465	0.0008	1.4074	0.0121	0.0697	0.00009	0.9	881	5	892	5	919	9	881	5
PH-1-8-13-26-017	0.0221	0.0009	0.2344	0.0556	0.0769	0.000185	0.9	141	6	214	46	1119	444	-	-
PH-1-8-13-26-018	0.2767	0.0017	5.6426	0.0477	0.1480	0.00018	0.9	1575	9	1923	7	2322	7	-	-
PH-1-8-13-26-019	0.1703	0.0013	1.6907	0.0293	0.0720	0.00014	0.9	1014	7	1005	11	986	23	986	23
PH-1-8-13-26-020	0.0845	0.0006	0.7210	0.0120	0.0619	0.00012	0.9	523	3	551	7	670	24	523	3
PH-1-8-13-26-021	0.1981	0.0017	2.2255	0.0423	0.0815	0.00017	0.9	1165	9	1189	13	1233	24	1233	24
PH-1-8-13-26-022	0.0582	0.0005	1.2897	0.0201	0.1608	0.00028	0.9	364	3	841	9	2464	30	-	-
PH-1-8-13-26-023	0.2474	0.0023	3.1765	0.0828	0.0931	0.00026	0.88	1425	12	1451	20	1490	54	1490	54
PH-1-8-13-26-024	0.1634	0.0011	1.7042	0.0236	0.0757	0.00013	0.9	976	6	1010	9	1086	17	976	6

PH-1-8-13-26-025	0.1176	0.008	1.1871	0.0163	0.0732	0.0012	0.9		717	4	795	8	1021	17	-	-
PH-1-8-13-26-026	0.0201	0.006	0.1293	0.0317	0.0467	0.0115	0.8		128	4	123	29	35	405	128	4
PH-1-8-13-26-027	0.2056	0.0016	2.3254	0.0397	0.0821	0.0016	0.9		1205	9	1220	12	1247	21	1247	21
PH-1-8-13-26-028	0.2609	0.0033	3.4551	0.1233	0.0960	0.0036	0.88		1494	17	1517	28	1549	73	1549	73
PH-1-8-13-26-029	0.1394	0.0010	2.2108	0.0359	0.1150	0.0021	0.88		841	6	1184	11	1880	33	-	-
PH-1-8-13-26-030	0.1215	0.0010	1.1323	0.0297	0.0676	0.0019	0.86		739	5	769	14	855	58	739	5
PH-1-8-13-26-031	0.1376	0.0010	1.4155	0.0237	0.0746	0.0014	0.9		831	6	895	10	1058	22	831	6
PH-1-8-13-26-032	0.1155	0.0011	1.0412	0.0315	0.0654	0.0021	0.86		705	6	725	16	786	68	705	6
PH-1-8-13-26-033	0.1745	0.0015	1.9249	0.0391	0.0800	0.0018	0.9		1037	8	1090	14	1198	27	-	-
PH-1-8-13-26-034	0.2283	0.0019	3.0900	0.0647	0.0982	0.0022	0.87		1325	10	1430	16	1590	43	-	-
PH-1-8-13-26-035	2.7458	0.7052	339.7022	86.6136	0.8975	0.0677	0.9		8513	1214	5921	258	5085	168	-	-
PH-1-8-13-26-036	0.0235	0.0012	0.2483	0.0651	0.0767	0.0204	0.9		150	7	225	53	1112	482	-	-
PH-1-8-13-26-037	0.1759	0.0021	1.8934	0.0609	0.0781	0.0026	0.9		1045	12	1079	21	1149	45	1149	45
PH-1-8-13-26-038	0.1750	0.0020	1.9114	0.0586	0.0792	0.0026	0.9		1040	11	1085	20	1178	43	-	-
PH-1-8-13-26-039	0.0134	0.0003	0.1264	0.0113	0.0683	0.00062	0.9		86	2	121	10	877	154	-	-
PH-1-8-13-26-040	0.1811	0.0012	1.8959	0.0255	0.0759	0.0012	0.9		1073	7	1080	9	1093	16	1093	16
PH-1-8-13-26-041	0.2384	0.0023	2.9939	0.0933	0.0911	0.0030	0.87		1378	12	1406	24	1448	64	1448	64
PH-1-8-13-26-042	0.0170	0.0005	0.3131	0.0291	0.1335	0.00130	0.9		109	3	277	23	2145	122	-	-
PH-1-8-13-26-043	0.2284	0.0016	3.9209	0.0517	0.1245	0.0019	0.9		1326	8	1618	11	2022	27	-	-
PH-1-8-13-26-044	0.1494	0.0012	1.8404	0.0352	0.0894	0.0019	0.9		897	7	1060	13	1413	24	-	-
PH-1-8-13-26-045	0.0190	0.0010	0.1581	0.0823	0.0603	0.00315	0.85		121	6	149	72	615	1044	-	-
PH-1-8-13-26-046	0.1794	0.0020	1.8610	0.0752	0.0752	0.00032	0.85		1064	11	1067	27	1075	86	1075	86
PH-1-8-13-26-047	0.0080	0.0004	0.0505	0.0037	0.0461	0.00039	0.76		51	2	50	4	-	-	51	2
PH-1-8-13-26-048	0.0487	0.0003	0.3908	0.0083	0.0582	0.00013	0.86		306	2	335	6	538	50	306	2
PH-1-8-13-26-049	0.1822	0.0012	1.9091	0.0225	0.0760	0.0011	0.9		1079	6	1084	8	1095	14	1095	14
PH-1-8-13-26-050	0.0062	0.0001	0.0393	0.0054	0.0461	0.00064	0.23		39.7	0.9	39	5	-	-	39.7	0.9

PH-1-8-13-26-051	0.0909	0.008	0.7698	0.0195	0.0614	0.0017	0.9		561	5	580	11	655	39		561	5
PH-1-8-13-26-052	0.4891	0.0065	12.4611	0.3115	0.1848	0.0052	0.89		2567	28	2640	23	2696	48		2696	48
PH-1-8-13-26-053	0.3195	0.0022	4.8286	0.0546	0.1097	0.0016	0.9		1787	11	1790	10	1794	11		1794	11
PH-1-8-13-26-054	0.0965	0.0009	0.7980	0.0235	0.0600	0.0019	0.9		594	5	596	13	603	48		594	5
PH-1-8-13-26-055	0.1692	0.0021	1.8345	0.0617	0.0787	0.0028	0.9		1008	11	1058	22	1164	47	-	-	-
PH-1-8-13-26-056	0.0788	0.0011	0.6935	0.0355	0.0638	0.0034	0.9		489	7	535	21	736	85		489	7
PH-1-8-13-26-057	0.2056	0.0024	2.3520	0.0699	0.0830	0.0026	0.9		1205	13	1228	21	1269	40		1269	40
PH-1-8-13-26-058	0.2430	0.0018	3.4629	0.0561	0.1034	0.0018	0.88		1402	9	1519	13	1686	34	-	-	-
PH-1-8-13-26-059	0.0971	0.0026	1.0819	0.1023	0.0808	0.0078	0.9		598	15	745	50	1217	145	-	-	-
PH-1-8-13-26-060	0.1197	0.0009	1.3492	0.0205	0.0818	0.0015	0.9		729	5	867	9	1240	19	-	-	-
PH-1-8-13-26-061	0.1080	0.0007	1.1008	0.0136	0.0739	0.0011	0.9		661	4	754	7	1039	15	-	-	-
PH-1-8-13-26-062	0.0887	0.0006	0.8433	0.0163	0.0690	0.0014	0.86		548	4	621	9	898	43	-	-	-
PH-1-8-13-26-063	0.1458	0.0013	2.1174	0.0433	0.1054	0.0024	0.9		877	7	1154	14	1721	24	-	-	-
PH-1-8-13-26-064	0.1987	0.0018	2.2344	0.0491	0.0816	0.0019	0.9		1168	10	1192	15	1236	29		1236	29
PH-1-8-13-26-065	0.0225	0.0011	0.1726	0.0536	0.0556	0.00175	0.9		144	7	162	46	436	508	-	-	-
PH-1-8-13-26-066	0.0232	0.0006	0.3372	0.0291	0.1053	0.00094	0.9		148	4	295	22	1719	123	-	-	-
PH-1-8-13-26-067	0.2291	0.0016	2.8813	0.0531	0.0912	0.0018	0.87		1330	8	1377	14	1451	38		1451	38
PH-1-8-13-26-068	0.1272	0.0011	1.3411	0.0295	0.0765	0.0018	0.9		772	6	864	13	1108	30	-	-	-
PH-1-8-13-26-069	0.0235	0.0007	0.2653	0.0306	0.0818	0.00097	0.9		150	4	239	25	1240	183	-	-	-
PH-1-8-13-26-070	0.2609	0.0027	3.6048	0.0806	0.1002	0.0024	0.9		1495	14	1551	18	1628	26		1628	26
PH-1-8-13-26-071	0.0177	0.0007	0.1397	0.0325	0.0573	0.00135	0.9		113	5	133	29	504	410	-	-	-
PH-1-8-13-26-072	0.2351	0.0019	3.1099	0.0698	0.0959	0.0023	0.89		1361	10	1435	17	1546	46	-	-	-
PH-1-8-13-26-073	0.1673	0.0014	1.7445	0.0341	0.0757	0.0016	0.9		997	8	1025	13	1086	26		997	8
PH-1-8-13-26-074	0.1041	0.0015	0.9023	0.0447	0.0629	0.00032	0.9		638	9	653	24	705	81		638	9
PH-1-8-13-26-075	0.0208	0.0004	0.1506	0.0124	0.0525	0.00044	0.9		133	2	142	11	306	155		133	2
PH-1-8-13-26-076	0.0067	0.0001	0.0425	0.0014	0.0461	0.00016	0.64		43	0.5	42	1	-	-		43	0.5

PH-1-8-13-26-077	0.0692	0.006	0.6320	0.0160	0.0662	0.0018	0.9		432	4	497	10	813	38	-	-
PH-1-8-13-26-078	0.0214	0.004	0.2154	0.0177	0.0732	0.0062	0.9		136	2	198	15	1019	139	-	-
PH-1-8-13-26-079	0.0203	0.004	0.1291	0.0129	0.0461	0.0047	0.74		130	2	123	12	-	-	130	2
PH-1-8-13-26-080	0.1442	0.009	1.3993	0.0175	0.0704	0.0011	0.9		868	5	889	7	940	15	868	5
PH-1-8-13-26-081	0.3070	0.018	5.3738	0.0393	0.1270	0.0014	0.9		1726	9	1881	6	2057	6	-	-
PH-1-8-13-26-082	0.0870	0.009	1.0796	0.0340	0.0900	0.0030	0.9		538	6	743	17	1426	43	-	-
PH-1-8-13-26-083	0.1486	0.013	1.7831	0.0376	0.0871	0.0020	0.9		893	7	1039	14	1362	27	-	-
PH-1-8-13-26-084	0.2625	0.017	3.6198	0.0390	0.1000	0.0014	0.9		1503	9	1554	9	1625	11	1625	11
PH-1-8-13-26-085	0.2888	0.025	4.1061	0.0761	0.1031	0.0021	0.88		1636	12	1656	15	1681	39	1681	39
PH-1-8-13-26-086	0.5751	0.037	16.9145	0.1274	0.2134	0.0024	0.9		2929	15	2930	7	2931	5	2931	5
PH-1-8-13-26-087	0.0139	0.002	0.0880	0.0025	0.0461	0.0015	0.53		89	1	86	2	-	-	89	1
PH-1-8-13-26-088	0.5050	0.038	12.8917	0.1297	0.1852	0.0024	0.9		2635	16	2672	9	2700	8	2700	8
PH-1-8-13-26-089	0.2379	0.016	2.8736	0.0362	0.0876	0.0013	0.9		1376	9	1375	9	1375	14	1375	14
PH-1-8-13-26-090	0.2721	0.018	3.5956	0.0385	0.0959	0.0013	0.9		1552	9	1549	8	1545	11	1545	11
PH-1-8-13-26-091	0.2091	0.013	3.1325	0.0281	0.1087	0.0014	0.9		1224	7	1441	7	1777	8	-	-
PH-1-8-13-26-092	0.3584	0.024	7.8188	0.0834	0.1582	0.0020	0.91		1975	11	2210	10	2437	22	-	-
PH-1-8-13-26-093	0.2152	0.014	3.4220	0.0368	0.1153	0.0014	0.89		1256	7	1509	8	1885	23	-	-
PH-1-8-13-26-094	0.0213	0.002	0.1430	0.0063	0.0487	0.0022	0.9		136	1	136	6	131	82	136	1
PH-1-8-13-26-095	0.1423	0.026	1.2972	0.0753	0.0661	0.0039	0.9		858	15	844	33	811	91	858	15
PH-1-8-13-26-096	0.0133	0.007	0.0888	0.0293	0.0484	0.00162	0.9		85	5	86	27	120	472	85	5
PH-1-8-13-26-097	0.4079	0.030	9.2192	0.1081	0.1639	0.0023	0.9		2205	14	2360	11	2497	24	-	-
PH-1-8-13-26-098	0.1827	0.011	1.8919	0.0206	0.0751	0.0011	0.9		1082	6	1078	7	1071	12	1071	12
PH-1-8-13-26-099	0.0883	0.007	0.7124	0.0163	0.0585	0.0015	0.9		546	4	546	10	549	36	546	4
PH-1-8-13-26-100	0.1858	0.013	2.0897	0.0286	0.0816	0.0013	0.9		1098	7	1145	9	1236	16	-	-
	^{206}Pb / ^{238}U	± 1 s.e.	^{207}Pb / ^{235}U	± 1 s.e.	$^{207}\text{Pb}/^{206}\text{Pb}$	± 1 s.e.	Error corr.		^{206}Pb / ^{238}U	± 1 s.e.	$^{207}\text{Pb}/^{235}\text{U}$	± 1 s.e.	$^{207}\text{Pb}/^{206}\text{Pb}$	± 1 s.e.	(Ma)	\pm (Ma)

PH-1-9-13-10-001	0.2679	0.021	3.7537	0.0524	0.1017	0.0017	0.9		1530	10	1583	11	1654	15		1654	15
PH-1-9-13-10-002	0.3464	0.043	4.7062	0.1319	0.0986	0.0029	0.9		1917	21	1768	23	1597	34		-	-
PH-1-9-13-10-003	0.2587	0.021	3.3512	0.0548	0.0940	0.0017	0.9		1483	11	1493	13	1508	19		1508	19
PH-1-9-13-10-004	0.2366	0.021	2.8791	0.0575	0.0883	0.0019	0.9		1369	11	1376	15	1388	25		1388	25
PH-1-9-13-10-005	0.2476	0.023	3.1255	0.0616	0.0916	0.0020	0.9		1426	12	1439	15	1458	24		1458	24
PH-1-9-13-10-006	0.2278	0.022	2.6309	0.0616	0.0838	0.0021	0.9		1323	12	1309	17	1287	30		1287	30
PH-1-9-13-10-007	0.2041	0.0014	2.1903	0.0296	0.0778	0.0013	0.9		1197	8	1178	9	1143	16		1143	16
PH-1-9-13-10-008	0.2613	0.024	3.4814	0.0656	0.0966	0.0020	0.9		1497	12	1523	15	1560	22		1560	22
PH-1-9-13-10-009	0.1876	0.0017	2.1695	0.0480	0.0839	0.0020	0.86		1109	9	1171	15	1289	47		-	-
PH-1-9-13-10-010	0.2445	0.034	3.1448	0.1325	0.0933	0.0041	0.84		1410	18	1444	32	1494	86		1494	86
PH-1-9-13-10-011	0.3054	0.0063	7.4809	0.2940	0.1777	0.0071	0.9		1718	31	2171	35	2632	38		-	-
PH-1-9-13-10-012	0.2440	0.0038	4.2430	0.1446	0.1262	0.0045	0.9		1407	19	1682	28	2045	38		-	-
PH-1-9-13-10-013	0.2199	0.021	2.6197	0.0579	0.0864	0.0021	0.9		1282	11	1306	16	1347	28		1347	28
PH-1-9-13-10-014	0.2508	0.027	3.2137	0.0803	0.0930	0.0025	0.9		1442	14	1460	19	1487	31		1487	31
PH-1-9-13-10-015	0.2686	0.029	4.0600	0.0904	0.1097	0.0026	0.9		1534	14	1646	18	1794	25		-	-
PH-1-9-13-10-016	0.2764	0.023	3.5735	0.0581	0.0938	0.0017	0.9		1573	12	1544	13	1504	18		1504	18
PH-1-9-13-10-017	0.2589	0.030	3.5876	0.0955	0.1005	0.0028	0.9		1484	16	1547	21	1634	32		-	-
PH-1-9-13-10-018	0.2826	0.037	3.9561	0.1206	0.1016	0.0032	0.9		1604	19	1625	25	1653	37		1653	37
PH-1-9-13-10-019	0.1256	0.0018	1.3039	0.0774	0.0753	0.0046	0.84		763	10	847	34	1077	126		-	-
PH-1-9-13-10-020	0.2395	0.025	2.9425	0.0731	0.0891	0.0024	0.9		1384	13	1393	19	1407	31		1407	31
PH-1-9-13-10-021	0.2296	0.033	3.3857	0.1167	0.1070	0.0038	0.9		1333	17	1501	27	1748	42		-	-
PH-1-9-13-10-022	0.2410	0.031	3.9353	0.1087	0.1185	0.0035	0.9		1392	16	1621	22	1933	31		-	-
PH-1-9-13-10-023	0.2390	0.049	4.6518	0.2173	0.1412	0.0068	0.9		1382	25	1759	39	2242	53		-	-
PH-1-9-13-10-024	0.2931	0.049	5.5629	0.1957	0.1377	0.0050	0.9		1657	24	1910	30	2198	38		-	-
PH-1-9-13-10-025	0.2457	0.042	3.9077	0.1606	0.1154	0.0049	0.9		1416	22	1615	33	1886	49		-	-
PH-1-9-13-10-026	0.0956	0.014	0.9242	0.0618	0.0701	0.0048	0.84		589	8	665	33	931	145		-	-

PH-1-9-13-10-027	0.2217	0.0020	2.5697	0.0536	0.0841	0.0019	0.9		1291	11	1292	15	1295	26		1295	26
PH-1-9-13-10-028	0.2542	0.0025	3.5383	0.0744	0.1010	0.0023	0.9		1460	13	1536	17	1642	24		-	-
PH-1-9-13-10-029	0.2698	0.0038	4.1577	0.1306	0.1118	0.0037	0.9		1540	19	1666	26	1829	37		-	-
PH-1-9-13-10-030	0.2463	0.0023	3.1091	0.0634	0.0916	0.0020	0.9		1419	12	1435	16	1458	25		1458	25
PH-1-9-13-10-031	0.2263	0.0024	2.7161	0.0695	0.0871	0.0024	0.9		1315	13	1333	19	1362	33		1362	33
PH-1-9-13-10-032	0.2837	0.0054	3.9265	0.1868	0.1004	0.0049	0.9		1610	27	1619	38	1632	60		1632	60
PH-1-9-13-10-033	0.2394	0.0031	4.2857	0.1182	0.1299	0.0038	0.9		1384	16	1691	23	2096	31		-	-
PH-1-9-13-10-034	0.2438	0.0037	3.2915	0.1284	0.0979	0.0039	0.9		1407	19	1479	30	1585	50		-	-
PH-1-9-13-10-035	0.3739	0.0066	5.9237	0.2328	0.1149	0.0046	0.9		2048	31	1965	34	1879	45		1879	45
PH-1-9-13-10-036	0.2832	0.0031	3.8979	0.0941	0.0999	0.0026	0.9		1607	16	1613	20	1621	29		1621	29
PH-1-9-13-10-037	0.2266	0.0028	2.7729	0.0866	0.0888	0.0029	0.9		1317	15	1348	23	1399	41		1399	41
PH-1-9-13-10-038	0.2971	0.0048	4.3631	0.1637	0.1066	0.0041	0.9		1677	24	1705	31	1741	45		1741	45
PH-1-9-13-10-039	0.1569	0.0016	1.5463	0.0488	0.0715	0.0024	0.86		940	9	949	19	971	69		940	9
PH-1-9-13-10-040	0.2066	0.0020	2.3818	0.0565	0.0836	0.0021	0.9		1211	11	1237	17	1284	31		1284	31
PH-1-9-13-10-041	0.1770	0.0017	2.1359	0.0508	0.0875	0.0022	0.9		1051	9	1160	16	1372	31		-	-
PH-1-9-13-10-042	0.2335	0.0019	2.7396	0.0485	0.0851	0.0017	0.9		1353	10	1339	13	1318	22		1318	22
PH-1-9-13-10-043	0.1779	0.0022	1.8692	0.0735	0.0762	0.0031	0.86		1056	12	1070	26	1100	85		1100	85
PH-1-9-13-10-044	0.2314	0.0026	2.7411	0.0765	0.0859	0.0025	0.9		1342	13	1340	21	1336	37		1336	37
PH-1-9-13-10-045	0.2419	0.0033	2.6474	0.0990	0.0794	0.0031	0.9		1397	17	1314	28	1182	52		-	-
PH-1-9-13-10-046	0.3039	0.0037	4.6105	0.1182	0.1101	0.0030	0.9		1711	18	1751	21	1801	29		1801	29
PH-1-9-13-10-047	0.3019	0.0039	4.7223	0.1334	0.1135	0.0033	0.9		1701	19	1771	24	1856	32		1856	32
PH-1-9-13-10-048	0.2935	0.0029	4.3198	0.0859	0.1068	0.0023	0.9		1659	14	1697	16	1745	22		1745	22
PH-1-9-13-10-049	0.2160	0.0020	2.4241	0.0521	0.0814	0.0019	0.9		1261	10	1250	15	1231	28		1231	28
PH-1-9-13-10-050	0.2899	0.0024	4.1307	0.0656	0.1034	0.0019	0.9		1641	12	1660	13	1686	17		1686	17
PH-1-9-13-10-051	0.2573	0.0023	3.2824	0.0598	0.0926	0.0019	0.9		1476	12	1477	14	1479	21		1479	21
PH-1-9-13-10-052	0.2024	0.0018	2.2976	0.0500	0.0824	0.0019	0.86		1188	10	1212	15	1254	47		1254	47

PH-1-9-13-10-053	0.2287	0.0020	2.7565	0.0526	0.0875	0.0018	0.9		1328	10	1344	14	1370	23		1370	23
PH-1-9-13-10-054	0.3413	0.0044	5.9611	0.1543	0.1267	0.0034	0.9		1893	21	1970	23	2053	28		2053	28
PH-1-9-13-10-055	0.2894	0.0031	3.8620	0.0887	0.0968	0.0024	0.9		1638	15	1606	19	1564	27		1564	27
PH-1-9-13-10-056	0.2155	0.0027	2.6445	0.0883	0.0891	0.0031	0.9		1258	14	1313	25	1405	45		-	-
PH-1-9-13-10-057	0.3291	0.0029	5.0155	0.0818	0.1106	0.0020	0.9		1834	14	1822	14	1808	17		1808	17
PH-1-9-13-10-058	0.2810	0.0023	3.8411	0.0575	0.0992	0.0017	0.9		1596	11	1601	12	1609	16		1609	16
PH-1-9-13-10-059	0.2655	0.0022	3.4128	0.0542	0.0933	0.0017	0.9		1518	11	1507	12	1493	18		1493	18
PH-1-9-13-10-060	0.2113	0.0017	2.8398	0.0483	0.0975	0.0018	0.86		1236	9	1366	13	1576	36		-	-
PH-1-9-13-10-061	0.2169	0.0019	2.5718	0.0512	0.0860	0.0019	0.9		1265	10	1293	15	1339	25		1339	25
PH-1-9-13-10-062	0.2507	0.0023	3.5062	0.0657	0.1015	0.0021	0.9		1442	12	1529	15	1651	21		-	-
PH-1-9-13-10-063	0.2112	0.0017	2.4139	0.0414	0.0829	0.0016	0.9		1235	9	1247	12	1267	21		1267	21
PH-1-9-13-10-064	0.2928	0.0033	4.6163	0.1066	0.1144	0.0028	0.9		1656	16	1752	19	1870	26		-	-
PH-1-9-13-10-065	0.2394	0.0020	3.1162	0.0536	0.0944	0.0018	0.9		1384	10	1437	13	1517	20		1517	20
PH-1-9-13-10-066	0.2390	0.0019	3.0228	0.0475	0.0918	0.0017	0.9		1382	10	1413	12	1462	18		1462	18
PH-1-9-13-10-067	0.2154	0.0015	2.5374	0.0321	0.0855	0.0013	0.9		1257	8	1283	9	1326	14		1326	14
PH-1-9-13-10-068	0.2181	0.0016	2.4855	0.0367	0.0827	0.0014	0.9		1272	9	1268	11	1262	17		1262	17
PH-1-9-13-10-069	0.2155	0.0016	2.4086	0.0355	0.0811	0.0014	0.9		1258	8	1245	11	1223	17		1223	17
PH-1-9-13-10-070	0.2007	0.0015	2.2124	0.0337	0.0800	0.0014	0.9		1179	8	1185	11	1197	18		1197	18
Isotopic ratios and ages were corrected for common lead																	
Sample/analysis designation corresponds to the sampling date, traverse stop, and analysis number																	
The youngest three concordant ages are bolded, the youngest one age is interpreted to be maximum depositional age																	

Table A.2.4. U-Pb detrital zircon geochronologic analyses of Mayodia gneiss metasedimentary rocks

Sample/ analysis	Isotopic ratios								Apparent ages (Ma)								Best age	
	^{206}Pb / ^{238}U	± 1 s.e.	^{207}Pb / ^{235}U	± 1 s.e.	$^{207}\text{Pb}/^{206}\text{Pb}$	± 1 s.e.	Error corr.	^{206}Pb / ^{238}U	± 1 s.e.	^{207}Pb / ^{235}U	± 1 s.e.	$^{207}\text{Pb}/^{206}\text{Pb}$	± 1 s.e.	(Ma)	\pm (Ma)			
PH-1-3-13-8-001	0.0088	0.0001	0.0566	0.0020	0.0467	0.0017	0.9	56.4	0.5	56	2	35	60		1130	11		
PH-1-3-13-8-002	0.1924	0.0012	2.0508	0.0208	0.0773	0.0010	0.89	1134	7	1133	7	1130	11		1236	25		
PH-1-3-13-8-003	0.1948	0.0012	2.1919	0.0233	0.0816	0.0010	0.87	1147	7	1178	7	1236	25		-	-		
PH-1-3-13-8-004	0.1247	0.0007	1.3441	0.0106	0.0782	0.0008	0.9	758	4	865	5	1151	20		1493	14		
PH-1-3-13-8-005	0.2571	0.0018	3.3029	0.0419	0.0932	0.0014	0.9	1475	9	1482	10	1493	14		1108	11		
PH-1-3-13-8-006	0.1869	0.0012	1.9696	0.0206	0.0765	0.0010	0.9	1104	6	1105	7	1108	11		1117	13		
PH-1-3-13-8-007	0.1886	0.0012	1.9974	0.0226	0.0768	0.0011	0.9	1114	7	1115	8	1117	13		1213	11		
PH-1-3-13-8-008	0.2050	0.0013	2.2791	0.0241	0.0807	0.0011	0.89	1202	7	1206	7	1213	11		-	-		
PH-1-3-13-8-009	0.2557	0.0017	3.5667	0.0426	0.1012	0.0014	0.9	1468	9	1542	9	1646	26		1528	9		
PH-1-3-13-8-010	0.2650	0.0017	3.4695	0.0322	0.0950	0.0012	0.9	1515	9	1520	7	1528	9		1356	7		
PH-1-3-13-8-011	0.2118	0.0013	2.5340	0.0209	0.0868	0.0010	0.9	1239	7	1282	6	1356	7		1244	11		
PH-1-3-13-8-012	0.2123	0.0013	2.3976	0.0243	0.0820	0.0011	0.9	1241	7	1242	7	1244	11		1170	9		
PH-1-3-13-8-013	0.1948	0.0012	2.1184	0.0195	0.0789	0.0010	0.9	1147	7	1155	6	1170	9		1088	9		
PH-1-3-13-8-014	0.1810	0.0011	1.8885	0.0165	0.0757	0.0009	0.9	1072	6	1077	6	1088	9		1228	10		
PH-1-3-13-8-015	0.2089	0.0013	2.3392	0.0235	0.0813	0.0011	0.9	1223	7	1224	7	1228	10		1134	10		
PH-1-3-13-8-016	0.1926	0.0012	2.0565	0.0197	0.0775	0.0010	0.9	1135	6	1134	7	1134	10		1368	8		
PH-1-3-13-8-017	0.2397	0.0015	2.8857	0.0254	0.0874	0.0011	0.9	1385	8	1378	7	1368	8		1163	13		
PH-1-3-13-8-018	0.1999	0.0013	2.1665	0.0251	0.0787	0.0011	0.9	1175	7	1170	8	1163	13		-	-		
PH-1-3-13-8-019	0.2444	0.0015	3.3089	0.0263	0.0982	0.0011	0.9	1410	8	1483	6	1591	7		1124	11		
PH-1-3-13-8-020	0.1974	0.0013	2.0983	0.0216	0.0771	0.0010	0.9	1162	7	1148	7	1124	11		1171	11		
PH-1-3-13-8-021	0.1891	0.0013	2.0581	0.0219	0.0790	0.0011	0.9	1116	7	1135	7	1171	11		1180	7		
PH-1-3-13-8-022	0.1994	0.0012	2.1792	0.0167	0.0793	0.0009	0.89	1172	7	1174	5	1180	7		-	-		
PH-1-3-13-8-023	0.1891	0.0012	2.1451	0.0236	0.0823	0.0011	0.88	1116	7	1163	8	1252	26		1243	26		

PH-1-3-13-8-024	0.2074	0.0013	2.3416	0.0269	0.0819	0.0011	0.91		1215	7	1225	8	1243	26		1458	25
PH-1-3-13-8-025	0.2317	0.0015	2.9237	0.0323	0.0915	0.0012	0.9		1343	8	1388	8	1458	25		1170	9
PH-1-3-13-8-026	0.1868	0.0012	2.0315	0.0187	0.0789	0.0010	0.9		1104	6	1126	6	1170	9		1162	8
PH-1-3-13-8-027	0.1804	0.0011	1.9537	0.0162	0.0786	0.0009	0.9		1069	6	1100	6	1162	8		1161	9
PH-1-3-13-8-028	0.1870	0.0012	2.0255	0.0181	0.0786	0.0010	0.9		1105	6	1124	6	1161	9		1327	28
PH-1-3-13-8-029	0.2087	0.0014	2.4605	0.0305	0.0855	0.0012	0.9		1222	7	1261	9	1327	28		1148	13
PH-1-3-13-8-030	0.1891	0.0013	2.0345	0.0242	0.0781	0.0011	0.9		1116	7	1127	8	1148	13		1489	12
PH-1-3-13-8-031	0.2584	0.0018	3.3140	0.0377	0.0930	0.0013	0.9		1482	9	1484	9	1489	12		1174	7
PH-1-3-13-8-032	0.1896	0.0012	2.0668	0.0166	0.0791	0.0009	0.9		1119	6	1138	5	1174	7		1531	6
PH-1-3-13-8-033	0.2632	0.0016	3.4507	0.0260	0.0951	0.0011	0.9		1506	8	1516	6	1531	6		-	-
PH-1-3-13-8-034	0.2313	0.0014	3.0398	0.0268	0.0953	0.0010	0.9		1341	8	1418	7	1534	21		-	-
PH-1-3-13-8-035	0.2180	0.0014	2.7237	0.0245	0.0906	0.0010	0.9		1271	7	1335	7	1439	21		1165	10
PH-1-3-13-8-036	0.1899	0.0012	2.0600	0.0205	0.0787	0.0010	0.9		1121	7	1136	7	1165	10		1218	22
PH-1-3-13-8-037	0.1883	0.0012	2.0994	0.0192	0.0809	0.0009	0.82		1112	6	1149	6	1218	22		-	-
PH-1-3-13-8-038	0.0972	0.0006	1.1014	0.0100	0.0822	0.0009	0.9		598	3	754	5	1249	22		1279	7
PH-1-3-13-8-039	0.2133	0.0013	2.4519	0.0195	0.0834	0.0010	0.9		1246	7	1258	6	1279	7		1171	9
PH-1-3-13-8-040	0.1924	0.0012	2.0943	0.0198	0.0790	0.0010	0.9		1134	7	1147	6	1171	9		1272	8
PH-1-3-13-8-041	0.2154	0.0013	2.4667	0.0219	0.0831	0.0010	0.9		1257	7	1262	6	1272	8		1240	8
PH-1-3-13-8-042	0.2052	0.0013	2.3129	0.0194	0.0818	0.0010	0.9		1203	7	1216	6	1240	8		-	-
PH-1-3-13-8-043	0.2144	0.0013	2.6240	0.0192	0.0888	0.0010	0.9		1252	7	1307	5	1400	6		1164	9
PH-1-3-13-8-044	0.1926	0.0012	2.0882	0.0195	0.0787	0.0010	0.9		1135	7	1145	6	1164	9		1093	10
PH-1-3-13-8-045	0.1872	0.0012	1.9587	0.0188	0.0759	0.0010	0.9		1106	7	1101	6	1093	10		1073	8
PH-1-3-13-8-046	0.1831	0.0012	1.8973	0.0163	0.0752	0.0009	0.9		1084	6	1080	6	1073	8		1110	7
PH-1-3-13-8-047	0.1858	0.0011	1.9609	0.0148	0.0766	0.0009	0.9		1098	6	1102	5	1110	7		1342	27
PH-1-3-13-8-048	0.2174	0.0014	2.5832	0.0309	0.0862	0.0012	0.9		1268	7	1296	9	1342	27		1069	13
PH-1-3-13-8-049	0.1802	0.0012	1.8637	0.0213	0.0750	0.0011	0.89		1068	6	1068	8	1069	13		1593	21

PH-1-3-13-8-050	0.2697	0.0017	3.6563	0.0326	0.0983	0.0011	0.9		1539	9	1562	7	1593	21		1079	11
PH-1-3-13-8-051	0.1839	0.0012	1.9113	0.0201	0.0754	0.0010	0.9		1088	7	1085	7	1079	11		1238	9
PH-1-3-13-8-052	0.2067	0.0013	2.3282	0.0211	0.0817	0.0010	0.9		1211	7	1221	6	1238	9		1290	11
PH-1-3-13-8-053	0.2088	0.0014	2.4146	0.0251	0.0839	0.0011	0.9		1223	7	1247	7	1290	11		1235	19
PH-1-3-13-8-054	0.2150	0.0015	2.4176	0.0372	0.0816	0.0014	0.9		1256	8	1248	11	1235	19		-	-
PH-1-3-13-8-055	0.1955	0.0012	2.4787	0.0197	0.0920	0.0011	0.91		1151	7	1266	6	1467	7		-	-
PH-1-3-13-8-056	0.2319	0.0015	3.0478	0.0302	0.0953	0.0011	0.9		1345	8	1420	8	1534	23		-	-
PH-1-3-13-8-057	0.2289	0.0014	2.9555	0.0253	0.0937	0.0010	0.9		1329	7	1396	7	1501	20		1259	8
PH-1-3-13-8-058	0.2136	0.0013	2.4311	0.0215	0.0826	0.0010	0.9		1248	7	1252	6	1259	8		1210	11
PH-1-3-13-8-059	0.2053	0.0013	2.2787	0.0234	0.0805	0.0011	0.89		1204	7	1206	7	1210	11		1383	23
PH-1-3-13-8-060	0.2282	0.0014	2.7693	0.0275	0.0880	0.0010	0.9		1325	8	1347	7	1383	23		1251	13
PH-1-3-13-8-061	0.2123	0.0014	2.4072	0.0284	0.0822	0.0012	0.9		1241	7	1245	8	1251	13		1204	12
PH-1-3-13-8-062	0.2048	0.0013	2.2668	0.0243	0.0803	0.0011	0.89		1201	7	1202	8	1204	12		1086	34
PH-1-3-13-8-063	0.1809	0.0012	1.8871	0.0287	0.0757	0.0013	0.9		1072	7	1077	10	1086	34		1261	12
PH-1-3-13-8-064	0.2217	0.0014	2.5260	0.0282	0.0827	0.0011	0.9		1291	8	1280	8	1261	12		1123	7
PH-1-3-13-8-065	0.1885	0.0012	2.0025	0.0156	0.0771	0.0009	0.9		1113	6	1116	5	1123	7		1743	25
PH-1-3-13-8-066	0.2921	0.0020	4.2955	0.0483	0.1067	0.0014	0.9		1652	10	1692	9	1743	25		1264	8
PH-1-3-13-8-067	0.2159	0.0013	2.4633	0.0202	0.0828	0.0010	0.9		1260	7	1261	6	1264	8		1129	10
PH-1-3-13-8-068	0.1904	0.0012	2.0284	0.0201	0.0773	0.0010	0.9		1123	7	1125	7	1129	10		1636	8
PH-1-3-13-8-069	0.2855	0.0018	3.9611	0.0340	0.1006	0.0012	0.9		1619	9	1626	7	1636	8		1457	9
PH-1-3-13-8-070	0.2477	0.0016	3.1253	0.0290	0.0915	0.0011	0.9		1427	8	1439	7	1457	9		1354	11
PH-1-3-13-8-071	0.2299	0.0015	2.7479	0.0292	0.0867	0.0012	0.9		1334	8	1342	8	1354	11		1672	9
PH-1-3-13-8-072	0.2933	0.0020	4.1501	0.0422	0.1026	0.0013	0.9		1658	10	1664	8	1672	9		1149	8
PH-1-3-13-8-073	0.2000	0.0013	2.1536	0.0190	0.0781	0.0009	0.9		1175	7	1166	6	1149	8		1458	22
PH-1-3-13-8-074	0.2354	0.0015	2.9725	0.0281	0.0916	0.0010	0.9		1363	8	1401	7	1458	22		1182	9
PH-1-3-13-8-075	0.2003	0.0013	2.1922	0.0205	0.0794	0.0010	0.9		1177	7	1179	7	1182	9		1124	10

PH-1-3-13-8-076	0.1898	0.0012	2.0177	0.0195	0.0771	0.0010	0.89		1120	7	1121	7	1124	10		1116	27
PH-1-3-13-8-077	0.1888	0.0012	1.9994	0.0225	0.0768	0.0010	0.9		1115	7	1115	8	1116	27		1177	8
PH-1-3-13-8-078	0.2014	0.0013	2.1988	0.0185	0.0792	0.0009	0.9		1183	7	1181	6	1177	8		1152	9
PH-1-3-13-8-079	0.1959	0.0013	2.1130	0.0196	0.0782	0.0010	0.9		1153	7	1153	6	1152	9		1102	9
PH-1-3-13-8-080	0.1892	0.0012	1.9888	0.0187	0.0763	0.0010	0.89		1117	7	1112	6	1102	9		1115	30
PH-1-3-13-8-081	0.1919	0.0013	2.0311	0.0268	0.0768	0.0011	0.9		1131	7	1126	9	1115	30		1091	11
PH-1-3-13-8-082	0.1875	0.0013	1.9598	0.0208	0.0758	0.0010	0.9		1108	7	1102	7	1091	11		1612	7
PH-1-3-13-8-083	0.2832	0.0018	3.8784	0.0307	0.0994	0.0011	0.9		1607	9	1609	6	1612	7		1538	9
PH-1-3-13-8-084	0.2696	0.0018	3.5492	0.0339	0.0955	0.0012	0.89		1539	9	1538	8	1538	9		-	-
PH-1-3-13-8-085	0.2344	0.0014	3.0971	0.0223	0.0958	0.0009	0.9		1357	7	1432	6	1545	18		1100	7
PH-1-3-13-8-086	0.1841	0.0012	1.9331	0.0150	0.0762	0.0009	0.9		1089	6	1093	5	1100	7		1186	10
PH-1-3-13-8-087	0.1943	0.0013	2.1310	0.0210	0.0796	0.0010	0.9		1144	7	1159	7	1186	10		1447	16
PH-1-3-13-8-088	0.2645	0.0020	3.3193	0.0482	0.0910	0.0015	0.9		1513	10	1486	11	1447	16		1325	15
PH-1-3-13-8-089	0.2272	0.0016	2.6748	0.0359	0.0854	0.0013	0.9		1320	8	1322	10	1325	15		1612	9
PH-1-3-13-8-090	0.2821	0.0019	3.8642	0.0382	0.0994	0.0013	0.9		1602	10	1606	8	1612	9		1176	9
PH-1-3-13-8-091	0.1885	0.0012	2.0562	0.0187	0.0791	0.0010	0.9		1113	7	1134	6	1176	9		1374	13
PH-1-3-13-8-092	0.2332	0.0017	2.8172	0.0352	0.0876	0.0013	0.9		1351	9	1360	9	1374	13		1591	9
PH-1-3-13-8-093	0.2788	0.0019	3.7752	0.0377	0.0982	0.0013	0.88		1585	10	1587	8	1591	9		1310	33
PH-1-3-13-8-094	0.2162	0.0015	2.5263	0.0376	0.0848	0.0014	0.9		1261	8	1280	11	1310	33		1319	9
PH-1-3-13-8-095	0.2287	0.0015	2.6848	0.0254	0.0852	0.0011	0.9		1328	8	1324	7	1319	9		1167	11
PH-1-3-13-8-096	0.1940	0.0013	2.1083	0.0220	0.0788	0.0010	0.9		1143	7	1152	7	1167	11		1499	9
PH-1-3-13-8-097	0.2644	0.0018	3.4105	0.0337	0.0936	0.0012	0.9		1512	9	1507	8	1499	9		1311	8
PH-1-3-13-8-098	0.2257	0.0015	2.6383	0.0239	0.0848	0.0010	0.9		1312	8	1311	7	1311	8		1205	9
PH-1-3-13-8-099	0.2064	0.0014	2.2853	0.0216	0.0803	0.0010	0.9		1209	7	1208	7	1205	9		1219	7
PH-1-3-13-8-100	0.2074	0.0013	2.3136	0.0182	0.0809	0.0009	0.9		1215	7	1216	6	1219	7		1183	9

	^{206}Pb / ^{238}U	± 1 s.e.	^{207}Pb / ^{235}U	± 1 s.e.	$^{207}\text{Pb}/^{206}\text{Pb}$	± 1 s.e.	Error corr.	^{206}Pb / ^{238}U	± 1 s.e.	^{207}Pb / ^{235}U	± 1 s.e.	$^{207}\text{Pb}/^{206}\text{Pb}$	± 1 s.e.	(Ma)	\pm (Ma)
PH-1-3-13-9-001	0.2319	0.0015	0.0864	0.011	0.0864	0.0011	0.9	1344	8	1345	7	1348	9	1348	9
PH-1-3-13-9-002	0.1932	0.0013	0.0779	0.011	0.0779	0.0011	0.9	1139	7	1141	8	1145	14	1145	14
PH-1-3-13-9-003	0.1946	0.0013	0.0778	0.010	0.0778	0.0010	0.9	1146	7	1145	7	1142	11	1142	11
PH-1-3-13-9-004	0.1871	0.0012	0.0837	0.010	0.0837	0.0010	0.9	1106	7	1168	6	1286	9		
PH-1-3-13-9-005	0.2385	0.0016	0.0874	0.011	0.0874	0.0011	0.9	1379	8	1375	8	1370	10	1370	10
PH-1-3-13-9-006	0.2267	0.0015	0.0849	0.010	0.0849	0.0010	0.9	1317	8	1315	7	1313	8	1313	8
PH-1-3-13-9-007	0.2024	0.0013	0.0798	0.010	0.0798	0.0010	0.9	1188	7	1189	7	1192	10	1192	10
PH-1-3-13-9-008	0.1837	0.0014	0.0761	0.013	0.0761	0.0013	0.9	1087	7	1090	10	1097	17	1097	17
PH-1-3-13-9-009	0.1856	0.0012	0.0760	0.010	0.0760	0.0010	0.9	1097	7	1097	6	1096	10	1096	10
PH-1-3-13-9-010	0.2021	0.0015	0.0792	0.014	0.0792	0.0014	0.9	1186	8	1183	11	1178	20	1178	20
PH-1-3-13-9-011	0.1951	0.0013	0.0821	0.010	0.0821	0.0010	0.9	1149	7	1183	7	1247	10	1247	10
PH-1-3-13-9-012	0.1339	0.0011	0.0662	0.019	0.0662	0.0019	0.9	810	6	811	15	812	44	810	6
PH-1-3-13-9-013	0.1628	0.0010	0.0831	0.009	0.0831	0.0009	0.9	972	6	1068	5	1271	6	972	6
PH-1-3-13-9-014	0.1415	0.0009	0.0671	0.010	0.0671	0.0010	0.9	853	5	850	7	842	14	853	5
PH-1-3-13-9-015	0.1546	0.0010	0.0786	0.010	0.0786	0.0010	0.9	927	5	999	6	1162	9	927	5
PH-1-3-13-9-016	0.2065	0.0014	0.0836	0.013	0.0836	0.0013	0.9	1210	7	1236	9	1283	15	1283	15
PH-1-3-13-9-017	0.1169	0.0008	0.0730	0.010	0.0730	0.0010	0.9	713	4	790	6	1015	11	-	-
PH-1-3-13-9-018	0.1406	0.0009	0.0680	0.009	0.0680	0.0009	0.9	848	5	853	6	868	12	848	5
PH-1-3-13-9-019	0.1806	0.0012	0.0753	0.010	0.0753	0.0010	0.9	1070	6	1072	6	1076	10	1076	10
PH-1-3-13-9-020	0.1399	0.0009	0.0741	0.010	0.0741	0.0010	0.89	844	5	901	7	1044	28	844	5
PH-1-3-13-9-021	0.1832	0.0012	0.0758	0.009	0.0758	0.0009	0.9	1084	6	1086	5	1091	7	1091	7
PH-1-3-13-9-022	0.1032	0.0006	0.0761	0.009	0.0761	0.0009	0.91	633	4	745	5	1098	23	-	-
PH-1-3-13-9-023	0.2037	0.0013	0.0882	0.012	0.0882	0.0012	0.91	1195	7	1265	8	1386	26	-	-
PH-1-3-13-9-024	0.2456	0.0019	0.0907	0.015	0.0907	0.0015	0.9	1416	10	1425	11	1440	16	1440	16
PH-1-3-13-9-025	0.1501	0.0010	0.0726	0.011	0.0726	0.0011	0.9	902	6	932	8	1004	16	902	6

PH-1-3-13-9-026	0.1649	0.0012	0.0713	0.0015	0.0713	0.0015	0.9		984	7	978	12	966	28		984	7
PH-1-3-13-9-027	0.1798	0.0012	0.0754	0.0010	0.0754	0.0010	0.9		1066	6	1070	7	1079	11		1079	11
PH-1-3-13-9-028	0.1305	0.0008	0.0751	0.0008	0.0751	0.0008	0.9		791	5	868	4	1071	7		791	5
PH-1-3-13-9-029	0.1916	0.0013	0.0776	0.0012	0.0776	0.0012	0.9		1130	7	1132	9	1137	14		1137	14
PH-1-3-13-9-030	0.2020	0.0013	0.0795	0.0010	0.0795	0.0010	0.9		1186	7	1186	7	1185	10		1185	10
PH-1-3-13-9-031	0.2054	0.0013	0.0801	0.0010	0.0801	0.0010	0.9		1204	7	1202	7	1199	10		1199	10
PH-1-3-13-9-032	0.1443	0.0009	0.0678	0.0011	0.0678	0.0011	0.9		869	5	867	8	862	18		869	5
PH-1-3-13-9-033	0.2043	0.0013	0.0803	0.0010	0.0803	0.0010	0.9		1199	7	1201	7	1205	10		1205	10
PH-1-3-13-9-034	0.2405	0.0017	0.0885	0.0012	0.0885	0.0012	0.9		1389	9	1390	9	1393	12		1393	12
PH-1-3-13-9-035	0.1995	0.0013	0.0794	0.0010	0.0794	0.0010	0.9		1173	7	1176	7	1182	9		1182	9
PH-1-3-13-9-036	0.1728	0.0011	0.0746	0.0011	0.0746	0.0011	0.9		1028	6	1037	8	1059	14		1059	14
PH-1-3-13-9-037	0.1698	0.0011	0.0729	0.0011	0.0729	0.0011	0.9		1011	6	1011	8	1012	15		1012	15
PH-1-3-13-9-038	0.2322	0.0018	0.0888	0.0014	0.0888	0.0014	0.9		1346	9	1366	10	1399	15		1399	15
PH-1-3-13-9-039	0.2203	0.0015	0.0838	0.0011	0.0838	0.0011	0.9		1283	8	1284	7	1287	10		1287	10
PH-1-3-13-9-040	0.1654	0.0011	0.0714	0.0012	0.0714	0.0012	0.9		987	6	981	10	968	20		987	6
PH-1-3-13-9-041	0.1802	0.0012	0.0752	0.0011	0.0752	0.0011	0.9		1068	7	1070	8	1074	14		1074	14
PH-1-3-13-9-042	0.1942	0.0013	0.0780	0.0010	0.0780	0.0010	0.9		1144	7	1144	6	1146	9		1146	9
PH-1-3-13-9-043	0.1501	0.0010	0.0692	0.0009	0.0692	0.0009	0.9		902	5	902	6	903	11		902	5
PH-1-3-13-9-044	0.1625	0.0010	0.0715	0.0010	0.0715	0.0010	0.9		971	6	971	7	971	12		971	6
PH-1-3-13-9-045	0.1941	0.0013	0.0736	0.0012	0.0736	0.0012	0.9		1143	7	1105	9	1032	16		1032	16
PH-1-3-13-9-046	0.1853	0.0016	0.0760	0.0018	0.0760	0.0018	0.9		1096	9	1095	15	1094	30		1094	30
PH-1-3-13-9-047	0.1861	0.0014	0.0817	0.0014	0.0817	0.0014	0.9		1100	8	1147	10	1238	18	-	-	-
PH-1-3-13-9-048	0.1858	0.0017	0.0761	0.0019	0.0761	0.0019	0.9		1099	9	1098	16	1096	32		1096	32
PH-1-3-13-9-049	0.1867	0.0012	0.0760	0.0010	0.0760	0.0010	0.9		1104	7	1100	7	1094	11		1094	11
PH-1-3-13-9-050	0.1880	0.0012	0.0768	0.0009	0.0768	0.0009	0.9		1110	7	1112	6	1115	9		1115	9
PH-1-3-13-9-051	0.2160	0.0014	0.0813	0.0011	0.0813	0.0011	0.9		1261	8	1249	8	1228	11		1228	11

PH-1-3-13-9-052	0.1867	0.0012	0.0762	0.0010	0.0762	0.0010	0.9		1104	6	1102	6	1099	10		1099	10
PH-1-3-13-9-053	0.1748	0.0012	0.0734	0.0012	0.0734	0.0012	0.9		1038	7	1034	9	1026	17		1026	17
PH-1-3-13-9-054	0.1997	0.0013	0.0859	0.0010	0.0859	0.0010	0.9		1173	7	1231	5	1335	7	-	-	-
PH-1-3-13-9-055	0.1833	0.0012	0.0746	0.0009	0.0746	0.0009	0.9		1085	6	1076	6	1058	8		1058	8
PH-1-3-13-9-056	0.1589	0.0010	0.0728	0.0008	0.0728	0.0008	0.9		951	6	968	5	1007	8		951	6
PH-1-3-13-9-057	0.1856	0.0014	0.0673	0.0014	0.0673	0.0014	0.9		1097	7	1017	12	848	27	-	-	-
PH-1-3-13-9-058	0.1777	0.0012	0.0745	0.0010	0.0745	0.0010	0.9		1055	6	1054	7	1055	11		1055	11
PH-1-3-13-9-059	0.2009	0.0029	0.0808	0.0034	0.0808	0.0034	0.9		1180	16	1192	29	1215	58		1215	58
PH-1-3-13-9-060	0.1828	0.0012	0.0755	0.0011	0.0755	0.0011	0.9		1082	7	1082	8	1081	14		1081	14
PH-1-3-13-9-061	0.1827	0.0013	0.0752	0.0012	0.0752	0.0012	0.9		1082	7	1079	9	1075	17		1075	17
PH-1-3-13-9-062	0.2293	0.0015	0.0856	0.0011	0.0856	0.0011	0.9		1331	8	1330	7	1329	9		1329	9
PH-1-3-13-9-063	0.1811	0.0012	0.0752	0.0012	0.0752	0.0012	0.9		1073	7	1073	9	1075	16		1075	16
PH-1-3-13-9-064	0.2344	0.0015	0.0871	0.0010	0.0871	0.0010	0.9		1358	8	1360	6	1363	7		1363	7
PH-1-3-13-9-065	0.1663	0.0011	0.0719	0.0010	0.0719	0.0010	0.9		992	6	989	7	984	12		992	6
PH-1-3-13-9-066	0.1937	0.0014	0.0789	0.0014	0.0789	0.0014	0.9		1141	8	1151	11	1169	20		1169	20
PH-1-3-13-9-067	0.1819	0.0012	0.0752	0.0010	0.0752	0.0010	0.9		1077	7	1076	7	1074	12		1074	12
PH-1-3-13-9-068	0.1756	0.0012	0.0749	0.0011	0.0749	0.0011	0.9		1043	6	1050	8	1065	14		1065	14
PH-1-3-13-9-069	0.2341	0.0018	0.0889	0.0015	0.0889	0.0015	0.9		1356	10	1373	11	1401	16		1401	16
PH-1-3-13-9-070	0.2223	0.0016	0.0833	0.0014	0.0833	0.0014	0.9		1294	9	1287	10	1277	16		1277	16
PH-1-3-13-9-071	0.1965	0.0015	0.0785	0.0013	0.0785	0.0013	0.9		1156	8	1157	10	1159	17		1159	17
PH-1-3-13-9-072	0.1762	0.0013	0.0748	0.0015	0.0748	0.0015	0.9		1046	7	1051	12	1062	25		1062	25
PH-1-3-13-9-073	0.2134	0.0014	0.0822	0.0010	0.0822	0.0010	0.9		1247	7	1248	6	1249	9		1249	9
PH-1-3-13-9-074	0.1916	0.0013	0.0773	0.0010	0.0773	0.0010	0.9		1130	7	1129	7	1129	11		1129	11
PH-1-3-13-9-075	0.1869	0.0012	0.0772	0.0010	0.0772	0.0010	0.9		1104	7	1111	7	1125	10		1125	10
PH-1-3-13-9-076	0.1022	0.0007	0.0735	0.0009	0.0735	0.0009	0.9		628	4	722	5	1028	9	-	-	-
PH-1-3-13-9-077	0.2013	0.0013	0.0802	0.0011	0.0802	0.0011	0.9		1182	7	1189	7	1202	11		1202	11

PH-1-3-13-9-078	0.210 1	0.001 4	0.081 3	0.0 011	0.0813 0.0 011	0.9 0.9		1230 1110	7 7	1229 1110	7 8	1229 1109	11 14		1229 1109	11 14
PH-1-3-13-9-079	0.188 0	0.001 3	0.076 5	0.0 011	0.0765 0.0 011	0.9 0.9		1071 1060	6 7	1068 1061	7 8	1064 1063	11 14		1064 1063	11 14
PH-1-3-13-9-080	0.180 7	0.001 2	0.074 8	0.0 010	0.0748 0.0 010	0.9 0.9		1060 1107	7 7	1061 1119	8 9	1063 1143	14 14		1064 1143	11 14
PH-1-3-13-9-081	0.178 8	0.001 2	0.074 8	0.0 011	0.0748 0.0 011	0.9 0.9		1060 1107	7 7	1061 1119	8 9	1063 1143	14 14		1063 1143	14 14
PH-1-3-13-9-082	0.187 4	0.001 3	0.077 8	0.0 012	0.0778 0.0 012	0.9 0.9		987 1306	6 8	994 1323	8 7	1010 1354	15 9		987 1354	6 9
PH-1-3-13-9-083	0.165 4	0.001 1	0.072 8	0.0 011	0.0728 0.0 011	0.9 0.9		1070 1306	7 8	1070 1323	10 7	1071 1354	19 9		1071 1354	19 9
PH-1-3-13-9-084	0.224 5	0.001 5	0.086 7	0.0 011	0.0867 0.0 011	0.9 0.9		1070 1306	7 8	1070 1323	10 7	1071 1354	19 9		1071 1354	19 9
PH-1-3-13-9-085	0.180 6	0.001 3	0.075 1	0.0 013	0.0751 0.0 013	0.9 0.9		1070 1194	7 7	1070 1188	10 11	1071 1176	19 21		1071 1176	19 21
PH-1-3-13-9-086	0.203 5	0.001 4	0.079 2	0.0 014	0.0792 0.0 014	0.9 0.9		1070 1194	7 7	1070 1188	10 11	1071 1176	19 21		1071 1176	19 21
PH-1-3-13-9-087	0.185 8	0.001 2	0.076 4	0.0 011	0.0764 0.0 011	0.9 0.9		1098 1070	7 7	1100 1070	8 10	1105 1071	13 19		1105 1071	13 19
PH-1-3-13-9-088	0.174 1	0.001 2	0.073 6	0.0 010	0.0736 0.0 010	0.9 0.9		1035 1098	6 7	1033 1100	7 8	1031 1105	12 13		1031 1105	12 13
PH-1-3-13-9-089	0.152 6	0.001 0	0.075 5	0.0 010	0.0755 0.0 010	0.9 0.9		916 1035	6 6	966 1033	7 7	1082 1031	12 12		916 1031	6 12
PH-1-3-13-9-090	0.199 1	0.001 3	0.079 5	0.0 010	0.0795 0.0 010	0.9 0.9		1170 916	7 6	1175 966	7 7	1184 1082	9 12		1184 916	9 6
PH-1-3-13-9-091	0.124 0	0.000 9	0.063 9	0.0 021	0.0639 0.0 021	0.9 0.9		754 648	5 4	750 787	17 8	740 1205	55 18		754 -	5 -
PH-1-3-13-9-092	0.105 8	0.000 8	0.080 3	0.0 014	0.0803 0.0 014	0.9 0.9		1087 648	6 4	1082 787	7 8	1074 1205	10 18		- -	- -
PH-1-3-13-9-093	0.183 6	0.001 2	0.075 2	0.0 010	0.0752 0.0 010	0.9 0.9		1087 1087	6 6	1082 1082	7 7	1074 1074	10 10		1074 1074	10 10
PH-1-3-13-9-094	0.176 5	0.001 2	0.074 2	0.0 009	0.0742 0.0 009	0.9 0.9		1048 1048	6 6	1047 1047	6 6	1047 1047	10 10		1047 1047	10 10
PH-1-3-13-9-095	0.203 2	0.001 3	0.079 6	0.0 010	0.0796 0.0 010	0.9 0.9		1192 1048	7 6	1190 1047	6 6	1188 1047	9 10		1188 1047	9 10
PH-1-3-13-9-096	0.183 0	0.001 2	0.075 0	0.0 010	0.0750 0.0 010	0.9 0.9		1083 1192	6 7	1078 1190	7 6	1069 1188	12 9		1069 1188	12 9
PH-1-3-13-9-097	0.080 5	0.000 5	0.056 5	0.0 012	0.0565 0.0 012	0.9 0.9		499 1083	3 6	494 1078	8 7	471 1069	33 12		499 1069	3 12
PH-1-3-13-9-098	0.160 3	0.001 1	0.069 9	0.0 013	0.0699 0.0 013	0.9 0.9		958 499	6 3	948 494	10 8	925 471	24 33		958 499	6 3
PH-1-3-13-9-099	0.214 5	0.001 4	0.081 2	0.0 010	0.0812 0.0 010	0.9 0.9		1253 1253	7 7	1243 1243	7 7	1227 1227	10 10		1227 1227	10 10
PH-1-3-13-9-100	0.182 2	0.001 2	0.075 0	0.0 012	0.0750 0.0 012	0.9 0.9		1079 1079	7 7	1075 1075	10 10	1069 1069	18 18		1069 1069	18 18
	$^{206}\text{Pb}/^{238}\text{U}$	± 1 s.e.	$^{207}\text{Pb}/^{235}\text{U}$	± 1 s.e.	$^{207}\text{Pb}/^{206}\text{Pb}$	± 1 s.e.	Error corr.	$^{206}\text{Pb}/^{238}\text{U}$	± 1 s.e.	$^{207}\text{Pb}/^{235}\text{U}$	± 1 s.e.	$^{207}\text{Pb}/^{206}\text{Pb}$	± 1 s.e.	(Ma)	\pm (Ma)	
PH-1-3-13-10A-12	0.466 0	0.003 8	11.71 00	0.1 050	0.1841 0.0 019	0.96 0.96		2465 1079	17 7	2580 1075	9 10	2690 1069	17 18		2690 1069	17 18

PH-1-3-13-10A-53	0.3226	0.0021	5.1260	0.0340	0.1140	0.0011	0.98		1802	10	1840	6	1865	18		1865	18
PH-1-3-13-10A-40	0.3260	0.0021	5.1450	0.0320	0.1137	0.0011	0.99		1818	10	1843	5	1859	18		1859	18
PH-1-3-13-10A-45	0.3083	0.0022	4.6890	0.0310	0.1093	0.0011	0.98		1732	11	1765	6	1788	18		1788	18
PH-1-3-13-10A-6	0.2865	0.0016	4.3120	0.0225	0.1092	0.0011	0.96		1624	8	1695	4	1787	18		1787	18
PH-1-3-13-10A-23	0.3045	0.0015	4.5130	0.0230	0.1076	0.0011	0.99		1713	7	1733	4	1760	18		1760	18
PH-1-3-13-10A-1	0.3112	0.0018	4.6620	0.0295	0.1073	0.0011	0.99		1750	9	1760	6	1754	18		1754	18
PH-1-3-13-10A-7	0.2824	0.0022	4.1240	0.0325	0.1065	0.0011	0.97		1603	11	1658	7	1740	18		1740	18
PH-1-3-13-10A-56	0.3081	0.0018	4.5480	0.0285	0.1061	0.0011	1.00		1731	9	1739	5	1734	18		1734	18
PH-1-3-13-10A-9	0.2935	0.0023	4.2590	0.0340	0.1058	0.0011	0.98		1659	11	1685	7	1728	19		1728	19
PH-1-3-13-10A-18	0.2963	0.0019	4.2910	0.0280	0.1054	0.0011	0.99		1673	10	1691	6	1721	19		1721	19
PH-1-3-13-10A-1	0.2937	0.0016	4.2490	0.0230	0.1052	0.0011	0.99		1660	8	1683	4	1719	19		1719	19
PH-1-3-13-10A-44	0.3079	0.0018	4.5190	0.0285	0.1050	0.0011	1.00		1730	9	1734	6	1715	19		1715	19
PH-1-3-13-10A-47	0.2997	0.0026	4.4010	0.0400	0.1046	0.0011	0.99		1689	13	1711	8	1707	19		1707	19
PH-1-3-13-10A-41	0.2742	0.0016	3.9830	0.0225	0.1044	0.0010	0.96		1562	8	1630	5	1704	18		1704	18
PH-1-3-13-10A-10	0.2905	0.0019	4.1530	0.0280	0.1042	0.0011	0.99		1644	10	1664	6	1700	19		1700	19
PH-1-3-13-10A-2	0.2761	0.0021	3.8660	0.0325	0.1005	0.0010	0.98		1571	11	1606	7	1632	19		1632	19
PH-1-3-13-10A-17	0.2693	0.0019	3.6210	0.0270	0.0975	0.0010	0.99		1537	10	1554	6	1577	19		1577	19
PH-1-3-13-10A-9	0.2671	0.0013	3.5170	0.0200	0.0957	0.0010	1.00		1526	7	1531	4	1541	20		1541	20
PH-1-3-13-10A-39	0.2530	0.0018	3.3440	0.0240	0.0952	0.0010	0.98		1454	9	1491	6	1531	19		1531	19
PH-1-3-13-10A-52	0.2607	0.0018	3.4410	0.0245	0.0948	0.0010	0.99		1493	9	1515	6	1524	19		1524	19
PH-1-3-13-10A-24	0.2625	0.0016	3.3960	0.0210	0.0940	0.0009	1.00		1503	8	1503	5	1509	19		1509	19
PH-1-3-13-10A-33	0.2609	0.0018	3.3050	0.0230	0.0925	0.0010	1.01		1494	10	1482	6	1478	20		1478	20
PH-1-3-13-10A-8	0.2514	0.0016	3.1710	0.0220	0.0921	0.0009	1.00		1445	9	1451	6	1469	19		1469	19
PH-1-3-13-10A-27	0.2438	0.0013	3.0540	0.0165	0.0908	0.0009	0.99		1406	7	1421	4	1442	19		1442	19
PH-1-3-13-10A-15	0.2453	0.0022	3.0160	0.0265	0.0902	0.0009	1.00		1414	12	1411	7	1429	19		1429	19
PH-1-3-13-10A-28	0.2367	0.0014	2.8660	0.0170	0.0881	0.0009	1.00		1369	7	1373	5	1384	19		1384	19

PH-1-3-13-10A-18	0.2185	0.0013	2.6160	0.0145	0.0878	0.0009	0.98		1276	6	1305	4	1378	19		1378	19
PH-1-3-13-10A-5	0.2439	0.0017	2.9480	0.0185	0.0875	0.0009	1.01		1410	8	1394	5	1372	19		1372	19
PH-1-3-13-10A-48	0.2347	0.0019	2.8650	0.0240	0.0875	0.0009	0.99		1359	10	1372	7	1371	20		1371	20
PH-1-3-13-10A-51	0.2258	0.0019	2.7370	0.0220	0.0870	0.0009	0.98		1312	10	1338	6	1361	20		1361	20
PH-1-3-13-10A-3	0.2307	0.0020	2.7520	0.0240	0.0870	0.0009	1.00		1338	11	1342	7	1360	21		1360	21
PH-1-3-13-10A-2	0.2332	0.0013	2.7870	0.0160	0.0869	0.0009	1.00		1351	7	1352	4	1358	20		1358	20
PH-1-3-13-10A-21	0.2234	0.0012	2.6680	0.0130	0.0869	0.0009	0.99		1300	6	1319	4	1357	19		1357	19
PH-1-3-13-10A-29	0.2337	0.0017	2.7920	0.0200	0.0867	0.0009	1.00		1353	9	1353	6	1354	20		1354	20
PH-1-3-13-10A-16	0.2310	0.0014	2.7380	0.0185	0.0866	0.0009	1.00		1339	7	1338	5	1352	19		1352	19
PH-1-3-13-10A-14	0.2248	0.0024	2.6580	0.0300	0.0865	0.0009	0.99		1306	13	1315	9	1349	20		1349	20
PH-1-3-13-10A-49	0.2164	0.0015	2.5680	0.0175	0.0856	0.0009	0.98		1262	8	1291	5	1329	21		1329	21
PH-1-3-13-10A-3	0.2306	0.0012	2.6960	0.0165	0.0845	0.0008	1.01		1338	6	1327	5	1304	20		1304	20
PH-1-3-13-10A-25	0.2191	0.0015	2.5440	0.0170	0.0844	0.0008	0.99		1277	8	1286	5	1302	20		1302	20
PH-1-3-13-10A-5	0.2060	0.0019	2.3670	0.0220	0.0833	0.0008	0.98		1207	10	1232	7	1276	20		1276	20
PH-1-3-13-10A-13	0.2094	0.0011	2.3730	0.0145	0.0826	0.0008	0.99		1226	6	1234	4	1259	20		1259	20
PH-1-3-13-10A-15	0.2010	0.0010	2.2410	0.0120	0.0810	0.0008	0.99		1181	6	1194	4	1220	20		1181	12
PH-1-3-13-10A-36	0.1992	0.0014	2.1710	0.0175	0.0794	0.0008	1.00		1171	8	1171	6	1181	21		1171	12
PH-1-3-13-10A-50	0.1983	0.0017	2.1770	0.0205	0.0784	0.0008	0.99		1166	9	1173	7	1157	21		1166	12
PH-1-3-13-10A-11	0.1980	0.0013	2.2880	0.0160	0.0840	0.0008	0.96		1165	7	1208	5	1293	20		1165	12
PH-1-3-13-10A-6	0.1976	0.0012	2.1540	0.0150	0.0794	0.0008	1.00		1162	7	1166	5	1183	20		1162	12
PH-1-3-13-10A-10	0.1954	0.0014	2.1040	0.0175	0.0781	0.0008	1.00		1151	8	1150	6	1149	22		1151	12
PH-1-3-13-10A-22	0.1941	0.0013	2.0900	0.0140	0.0783	0.0008	1.00		1144	7	1145	5	1154	21		1144	11
PH-1-3-13-10A-30	0.1919	0.0015	2.1130	0.0170	0.0800	0.0008	0.98		1131	8	1152	6	1196	20		1131	11
PH-1-3-13-10A-42	0.1914	0.0011	2.1180	0.0130	0.0793	0.0008	0.98		1129	6	1154	4	1180	20		1129	11
PH-1-3-13-10A-32	0.1878	0.0015	2.0350	0.0155	0.0790	0.0008	0.98		1109	8	1127	6	1171	20		1109	11
PH-1-3-13-10A-34	0.1877	0.0012	2.0190	0.0135	0.0782	0.0008	0.99		1109	7	1122	4	1151	20		1109	11

PH-1-3-13-10A-54	0.186 4	0.001 4	1.999 0	0.0 150	0.0769	0.0 008	0.99		1101	8	1115	5	1120	20		1101	11
PH-1-3-13-10A-31	0.167 7	0.001 3	1.648 0	0.0 120	0.0712	0.0 007	1.01		999	7	988	5	962	21		999	10
PH-1-3-13-10A-4	0.164 7	0.001 0	1.624 0	0.0 110	0.0712	0.0 007	1.00		983	5	979	4	964	21		983	10
PH-1-3-13-10A-14	0.139 5	0.002 7	1.318 0	0.0 325	0.0684	0.0 008	0.99		841	15	849	15	879	24		841	15
PH-1-3-13-10A-55	0.137 7	0.001 3	1.327 0	0.0 120	0.0691	0.0 007	0.97		832	7	857	5	900	21		832	8
PH-1-3-13-10A-25	0.105 4	0.000 7	0.924 0	0.0 055	0.0629	0.0 006	0.97		646	4	664	3	704	22		646	6
	^{206}Pb $/^{238}\text{U}$	± 1 s.e.	^{207}Pb $/^{235}\text{U}$	± 1 s.e.	$^{207}\text{Pb}/^{206}\text{Pb}$	± 1 s.e.	Error corr.		^{206}Pb $/^{238}\text{U}$	± 1 s.e.	^{207}Pb $/^{235}\text{U}$	± 1 s.e.	$^{207}\text{Pb}/^{206}\text{Pb}$	± 1 s.e.	(Ma)	\pm (Ma)	
PH-1-9-13-19B-001	0.176 9	0.001 2	1.786 3	0.0 237	0.0733	0.0 012	0.9		1050	7	1040	9	1022	16		1022	16
PH-1-9-13-19B-002	0.227 4	0.001 4	2.524 7	0.0 209	0.0806	0.0 010	0.9		1321	7	1279	6	1211	8		1211	8
PH-1-9-13-19B-003	0.251 7	0.001 7	2.841 4	0.0 342	0.0819	0.0 012	0.9		1447	9	1367	9	1244	13		-	-
PH-1-9-13-19B-004	0.233 4	0.001 4	2.553 4	0.0 216	0.0794	0.0 010	0.9		1352	7	1287	6	1182	8		-	-
PH-1-9-13-19B-005	0.211 0	0.001 2	2.352 0	0.0 178	0.0809	0.0 009	0.9		1234	7	1228	5	1219	7		1219	7
PH-1-9-13-19B-006	0.253 7	0.001 7	2.916 0	0.0 339	0.0834	0.0 012	0.9		1457	9	1386	9	1279	13		-	-
PH-1-9-13-19B-007	0.239 4	0.001 5	2.659 9	0.0 265	0.0806	0.0 011	0.9		1383	8	1317	7	1213	10		-	-
PH-1-9-13-19B-008	0.249 0	0.001 6	2.698 6	0.0 289	0.0787	0.0 011	0.9		1433	8	1328	8	1163	11		-	-
PH-1-9-13-19B-009	0.249 1	0.001 7	2.959 5	0.0 363	0.0862	0.0 013	0.9		1434	9	1397	9	1344	13		1344	13
PH-1-9-13-19B-010	0.225 1	0.001 7	2.528 6	0.0 398	0.0815	0.0 015	0.9		1309	9	1280	11	1234	19		1234	19
PH-1-9-13-19B-011	0.257 3	0.002 1	2.845 6	0.0 498	0.0803	0.0 016	0.9		1476	11	1368	13	1204	22		-	-
PH-1-9-13-19B-012	0.248 1	0.001 5	2.734 8	0.0 232	0.0800	0.0 010	0.9		1429	8	1338	6	1197	8		-	-
PH-1-9-13-19B-013	0.236 4	0.001 4	2.697 7	0.0 221	0.0828	0.0 010	0.9		1368	7	1328	6	1265	8		1265	8
PH-1-9-13-19B-014	0.232 1	0.001 5	2.528 3	0.0 260	0.0790	0.0 011	0.9		1346	8	1280	7	1173	11		-	-
PH-1-9-13-19B-015	0.244 8	0.001 8	2.938 7	0.0 389	0.0871	0.0 014	0.9		1412	9	1392	10	1363	15		1363	15
PH-1-9-13-19B-016	0.229 7	0.001 4	2.542 0	0.0 197	0.0803	0.0 009	0.9		1333	7	1284	6	1204	7		1204	7
PH-1-9-13-19B-017	0.228 4	0.001 4	2.657 6	0.0 248	0.0844	0.0 011	0.9		1326	7	1317	7	1303	9		1303	9
PH-1-9-13-19B-019	0.223 6	0.001 6	2.602 8	0.0 335	0.0845	0.0 013	0.9		1301	8	1301	9	1304	14		1304	14

PH-1-9-13-19B-020	0.1997	0.0012	2.2179	0.0180	0.0805	0.0008	0.88		1174	6	1187	6	1210	20		1210	20
PH-1-9-13-19B-021	0.2617	0.0016	3.1246	0.0255	0.0866	0.0010	0.9		1499	8	1439	6	1352	7		1352	7
PH-1-9-13-19B-022	0.2349	0.0014	2.5887	0.0211	0.0800	0.0009	0.9		1360	7	1297	6	1196	8		-	-
PH-1-9-13-19B-023	0.2284	0.0016	2.6479	0.0316	0.0841	0.0012	0.9		1326	8	1314	9	1295	13		1295	13
PH-1-9-13-19B-024	0.2195	0.0014	2.4661	0.0229	0.0815	0.0010	0.9		1279	7	1262	7	1234	9		1234	9
PH-1-9-13-19B-026	0.2272	0.0014	2.6301	0.0211	0.0840	0.0010	0.9		1320	7	1309	6	1292	7		1292	7
PH-1-9-13-19B-027	0.2261	0.0014	2.6036	0.0240	0.0836	0.0011	0.9		1314	7	1302	7	1283	9		1283	9
PH-1-9-13-19B-028	0.2204	0.0013	2.5342	0.0214	0.0834	0.0010	0.9		1284	7	1282	6	1279	8		1279	8
PH-1-9-13-19B-030	0.2138	0.0014	2.3627	0.0260	0.0802	0.0011	0.9		1249	7	1231	8	1202	12		1202	12
PH-1-9-13-19B-031	0.2026	0.0013	2.1931	0.0244	0.0785	0.0011	0.9		1189	7	1179	8	1161	12		1161	12
PH-1-9-13-19B-032	0.2518	0.0016	2.8639	0.0288	0.0826	0.0011	0.9		1448	8	1372	8	1259	10		-	-
PH-1-9-13-19B-033	0.2143	0.0013	2.3456	0.0210	0.0794	0.0010	0.9		1252	7	1226	6	1183	9		1183	9
PH-1-9-13-19B-034	0.2261	0.0013	2.5623	0.0189	0.0822	0.0009	0.9		1314	7	1290	5	1251	7		1251	7
PH-1-9-13-19B-035	0.1880	0.0011	2.0020	0.0184	0.0773	0.0009	0.87		1110	6	1116	6	1128	22		1128	22
PH-1-9-13-19B-036	0.2075	0.0014	2.3094	0.0267	0.0808	0.0012	0.9		1215	7	1215	8	1216	13		1216	13
PH-1-9-13-19B-037	0.2203	0.0013	2.4499	0.0188	0.0807	0.0009	0.9		1284	7	1257	6	1214	7		1214	7
PH-1-9-13-19B-038	0.2145	0.0014	2.4205	0.0246	0.0819	0.0011	0.9		1253	7	1249	7	1243	11		1243	11
PH-1-9-13-19B-039	0.2099	0.0014	2.3413	0.0249	0.0809	0.0011	0.9		1228	7	1225	8	1220	11		1220	11
PH-1-9-13-19B-040	0.2311	0.0014	2.6362	0.0206	0.0828	0.0010	0.9		1340	7	1311	6	1264	7		1264	7
PH-1-9-13-19B-041	0.2221	0.0014	2.4428	0.0225	0.0798	0.0010	0.9		1293	7	1255	7	1193	9		1193	9
PH-1-9-13-19B-042	0.2185	0.0013	2.4924	0.0211	0.0828	0.0010	0.9		1274	7	1270	6	1264	8		1264	8
PH-1-9-13-19B-043	0.1906	0.0012	2.0392	0.0206	0.0777	0.0010	0.9		1124	6	1129	7	1138	11		1138	11
PH-1-9-13-19B-044	0.1839	0.0011	1.9074	0.0156	0.0753	0.0009	0.9		1088	6	1084	5	1075	8		1075	8
PH-1-9-13-19B-045	0.2102	0.0013	2.3390	0.0209	0.0807	0.0010	0.9		1230	7	1224	6	1215	9		1215	9
PH-1-9-13-19B-046	0.2255	0.0015	2.4916	0.0274	0.0802	0.0011	0.9		1311	8	1270	8	1201	12		1201	12
PH-1-9-13-19B-047	0.2293	0.0014	2.6481	0.0237	0.0838	0.0010	0.9		1331	7	1314	7	1288	9		1288	9

PH-1-9-13-19B-048	0.1844	0.0011	1.9373	0.0181	0.0762	0.0008	0.87		1091	6	1094	6	1100	23		1100	23
PH-1-9-13-19B-049	0.2262	0.0014	2.6020	0.0254	0.0835	0.0011	0.9		1314	7	1301	7	1280	10		1280	10
PH-1-9-13-19B-050	0.1889	0.0012	2.0790	0.0202	0.0799	0.0010	0.9		1116	6	1142	7	1193	10		1193	10
PH-1-9-13-19B-051	0.2109	0.0013	2.3624	0.0217	0.0813	0.0010	0.9		1233	7	1231	7	1228	9		1228	9
PH-1-9-13-19B-052	0.2213	0.0014	2.5059	0.0273	0.0822	0.0011	0.9		1289	8	1274	8	1249	12		1249	12
PH-1-9-13-19B-053	0.1983	0.0012	2.1770	0.0191	0.0797	0.0010	0.9		1166	6	1174	6	1188	9		1188	9
PH-1-9-13-19B-054	0.2242	0.0015	2.5013	0.0284	0.0810	0.0012	0.9		1304	8	1272	8	1221	12		1221	12
PH-1-9-13-19B-055	0.1829	0.0011	1.9566	0.0184	0.0776	0.0010	0.9		1083	6	1101	6	1137	10		1137	10
PH-1-9-13-19B-056	0.2051	0.0012	2.2691	0.0173	0.0802	0.0008	0.88		1203	6	1203	5	1203	19		1203	19
PH-1-9-13-19B-057	0.1846	0.0011	1.9744	0.0175	0.0776	0.0010	0.9		1092	6	1107	6	1137	9		1137	9
PH-1-9-13-19B-058	0.2043	0.0012	2.2236	0.0201	0.0790	0.0010	0.9		1198	7	1189	6	1172	9		1172	9
PH-1-9-13-19B-059	0.2180	0.0013	2.5487	0.0227	0.0848	0.0011	0.9		1272	7	1286	7	1311	9		1311	9
PH-1-9-13-19B-060	0.2160	0.0012	2.4873	0.0173	0.0835	0.0008	0.88		1261	6	1268	5	1281	18		1281	18
PH-1-9-13-19B-061	0.2241	0.0014	2.4614	0.0246	0.0797	0.0011	0.9		1304	7	1261	7	1189	10		1189	10
PH-1-9-13-19B-062	0.2517	0.0016	2.8640	0.0306	0.0826	0.0011	0.9		1447	8	1373	8	1259	11	-	-	-
PH-1-9-13-19B-063	0.2254	0.0014	2.6340	0.0250	0.0848	0.0011	0.9		1310	7	1310	7	1311	9		1311	9
PH-1-9-13-19B-064	0.2151	0.0013	2.4326	0.0191	0.0820	0.0010	0.9		1256	7	1252	6	1246	7		1246	7
PH-1-9-13-19B-065	0.2118	0.0013	2.3821	0.0194	0.0816	0.0010	0.9		1238	7	1237	6	1236	8		1236	8
PH-1-9-13-19B-066	0.2278	0.0015	2.6515	0.0277	0.0845	0.0011	0.9		1323	8	1315	8	1303	11		1303	11
PH-1-9-13-19B-067	0.2486	0.0018	2.8083	0.0363	0.0820	0.0013	0.9		1431	9	1358	10	1245	15	-	-	-
PH-1-9-13-19B-068	0.2152	0.0013	2.4235	0.0199	0.0817	0.0010	0.9		1256	7	1250	6	1239	8		1239	8
PH-1-9-13-19B-069	0.2234	0.0014	2.5403	0.0261	0.0825	0.0011	0.9		1300	7	1284	7	1257	11		1257	11
PH-1-9-13-19B-070	0.2210	0.0014	2.4618	0.0226	0.0808	0.0010	0.9		1287	7	1261	7	1217	9		1217	9
PH-1-9-13-19B-071	0.2583	0.0017	2.9152	0.0320	0.0819	0.0011	0.9		1481	9	1386	8	1243	12	-	-	-
PH-1-9-13-19B-072	0.2251	0.0014	2.5132	0.0262	0.0810	0.0011	0.9		1309	8	1276	8	1222	11		1222	11
PH-1-9-13-19B-073	0.2194	0.0013	2.4607	0.0203	0.0814	0.0010	0.9		1278	7	1261	6	1231	8		1231	8

PH-1-9-13-19B-074	0.2531	0.0019	2.9567	0.0434	0.0848	0.0014	0.9		1454	10	1397	11	1310	17		1310	17
PH-1-9-13-19B-075	0.2353	0.0017	2.6609	0.0355	0.0820	0.0013	0.9		1362	9	1318	10	1246	15		1246	15
PH-1-9-13-19B-076	0.2252	0.0018	2.2698	0.0403	0.0731	0.0015	0.9		1309	9	1203	13	1017	23		-	-
PH-1-9-13-19B-077	0.2202	0.0014	2.5310	0.0237	0.0834	0.0011	0.9		1283	7	1281	7	1279	9		1279	9
PH-1-9-13-19B-078	0.2065	0.0013	2.2991	0.0202	0.0808	0.0010	0.9		1210	7	1212	6	1216	9		1216	9
PH-1-9-13-19B-079	0.1981	0.0012	2.1079	0.0197	0.0772	0.0010	0.9		1165	7	1151	6	1126	10		1126	10
PH-1-9-13-19B-080	0.2292	0.0017	2.8910	0.0382	0.0915	0.0015	0.9		1330	9	1380	10	1457	14		1457	14
PH-1-9-13-19B-081	0.2087	0.0012	2.3625	0.0180	0.0821	0.0008	0.88		1222	6	1231	5	1248	19		1248	19
PH-1-9-13-19B-082	0.2206	0.0014	2.5136	0.0260	0.0827	0.0011	0.9		1285	7	1276	8	1261	11		1261	11
PH-1-9-13-19B-083	0.2430	0.0015	2.7523	0.0257	0.0822	0.0010	0.9		1402	8	1343	7	1249	9		-	-
PH-1-9-13-19B-084	0.2213	0.0014	2.5399	0.0254	0.0833	0.0011	0.9		1289	7	1284	7	1276	10		1276	10
PH-1-9-13-19B-085	0.2164	0.0014	2.3992	0.0249	0.0804	0.0011	0.9		1263	7	1242	7	1208	11		1208	11
PH-1-9-13-19B-086	0.2039	0.0013	2.2353	0.0212	0.0796	0.0010	0.9		1196	7	1192	7	1186	10		1186	10
PH-1-9-13-19B-087	0.2158	0.0013	2.4465	0.0231	0.0823	0.0011	0.9		1259	7	1256	7	1252	9		1252	9
PH-1-9-13-19B-088	0.1920	0.0011	2.0676	0.0168	0.0781	0.0008	0.88		1132	6	1138	6	1150	20		1150	20
PH-1-9-13-19B-089	0.2192	0.0015	2.5221	0.0293	0.0835	0.0012	0.9		1278	8	1278	8	1280	13		1280	13
PH-1-9-13-19B-090	0.1874	0.0011	2.0104	0.0165	0.0778	0.0008	0.88		1107	6	1119	6	1142	20		1142	20
PH-1-9-13-19B-091	0.2005	0.0012	2.3561	0.0187	0.0853	0.0010	0.9		1178	6	1229	6	1321	7		-	-
PH-1-9-13-19B-092	0.2023	0.0013	2.2068	0.0221	0.0791	0.0010	0.9		1188	7	1183	7	1175	10		1175	10
PH-1-9-13-19B-093	0.2646	0.0017	3.1365	0.0307	0.0860	0.0011	0.9		1513	9	1442	8	1338	10		-	-
PH-1-9-13-19B-094	0.2176	0.0014	2.4841	0.0266	0.0828	0.0011	0.9		1269	7	1267	8	1265	11		1265	11
PH-1-9-13-19B-095	0.2143	0.0014	2.5101	0.0288	0.0850	0.0012	0.9		1252	8	1275	8	1315	12		1315	12
PH-1-9-13-19B-096	0.2513	0.0016	2.8214	0.0266	0.0814	0.0010	0.9		1445	8	1361	7	1232	9		-	-
PH-1-9-13-19B-097	0.2156	0.0013	2.5038	0.0211	0.0842	0.0010	0.9		1259	7	1273	6	1298	8		1298	8
PH-1-9-13-19B-098	0.1705	0.0010	1.7872	0.0170	0.0760	0.0010	0.9		1015	6	1041	6	1096	10		1096	10
PH-1-9-13-19B-099	0.1699	0.0010	1.7276	0.0153	0.0738	0.0009	0.9		1012	6	1019	6	1035	9		1035	9

	PH-1-9-13-19B-100	0.1695	0.0010	1.7186	0.0161	0.0735	0.0008	0.87		1009	6	1015	6	1029	23		1029	23
		^{206}Pb / ^{238}U	± 1 s.e.	^{207}Pb / ^{235}U	± 1 s.e.	$^{207}\text{Pb}/^{206}\text{Pb}$	± 1 s.e.	Error corr.		^{206}Pb / ^{238}U	± 1 s.e.	^{207}Pb / ^{235}U	± 1 s.e.	$^{207}\text{Pb}/^{206}\text{Pb}$	± 1 s.e.	(Ma)	\pm (Ma)	
PH-1-9-13-19A-001	0.2349	0.0015	2.8236	0.0218	0.0872	0.0010			1360	8	1362	6	1364	7		1364	7	
PH-1-9-13-19A-002	0.2316	0.0015	2.7559	0.0217	0.0863	0.0010			1343	8	1344	6	1345	7		1345	7	
PH-1-9-13-19A-003	0.2313	0.0015	2.7794	0.0230	0.0871	0.0010			1341	8	1350	6	1363	7		1363	7	
PH-1-9-13-19A-004	0.2226	0.0014	2.5974	0.0213	0.0846	0.0010			1296	7	1300	6	1307	7		1307	7	
PH-1-9-13-19A-005	0.2199	0.0014	2.5410	0.0209	0.0838	0.0010			1281	7	1284	6	1288	7		1288	7	
PH-1-9-13-19A-006	0.2276	0.0015	2.6766	0.0225	0.0853	0.0010			1322	8	1322	6	1322	8		1322	8	
PH-1-9-13-19A-007	0.2261	0.0014	2.6381	0.0187	0.0846	0.0009			1314	7	1311	5	1307	6		1307	6	
PH-1-9-13-19A-008	0.2335	0.0015	2.7943	0.0217	0.0868	0.0010			1353	8	1354	6	1356	7		1356	7	
PH-1-9-13-19A-009	0.1727	0.0010	1.7895	0.0125	0.0752	0.0007			1027	6	1042	5	1073	19		1073	19	
PH-1-9-13-19A-010	0.2332	0.0015	2.7978	0.0226	0.0870	0.0010			1351	8	1355	6	1360	7		1360	7	
PH-1-9-13-19A-011	0.2382	0.0015	2.8633	0.0237	0.0872	0.0010			1377	8	1372	6	1364	7		1364	7	
PH-1-9-13-19A-012	0.2344	0.0015	2.8026	0.0277	0.0867	0.0011			1357	8	1356	7	1354	10		1354	10	
PH-1-9-13-19A-013	0.2262	0.0015	2.6737	0.0233	0.0857	0.0010			1314	8	1321	6	1332	8		1332	8	
PH-1-9-13-19A-014	0.2265	0.0014	2.6848	0.0201	0.0860	0.0010			1316	7	1324	6	1338	7		1338	7	
PH-1-9-13-19A-015	0.2293	0.0015	2.7040	0.0225	0.0855	0.0010			1331	8	1330	6	1327	7		1327	7	
PH-1-9-13-19A-016	0.2281	0.0015	2.6870	0.0215	0.0854	0.0010			1325	8	1325	6	1325	7		1325	7	
PH-1-9-13-19A-017	0.2274	0.0014	2.6784	0.0198	0.0854	0.0009			1321	7	1323	5	1325	6		1325	6	
PH-1-9-13-19A-018	0.2387	0.0015	2.8902	0.0221	0.0878	0.0010			1380	8	1379	6	1378	7		1378	7	
PH-1-9-13-19A-019	0.2208	0.0014	2.5315	0.0210	0.0832	0.0010			1286	7	1281	6	1273	8		1273	8	
PH-1-9-13-19A-020	0.2117	0.0013	2.4930	0.0165	0.0854	0.0009			1238	7	1270	5	1325	6		1325	6	
PH-1-9-13-19A-021	0.2337	0.0015	2.7912	0.0229	0.0866	0.0010			1354	8	1353	6	1352	7		1352	7	
PH-1-9-13-19A-022	0.2272	0.0015	2.6743	0.0221	0.0854	0.0010			1320	8	1321	6	1324	7		1324	7	
PH-1-9-13-19A-023	0.2172	0.0014	2.4799	0.0192	0.0828	0.0009			1267	7	1266	6	1264	7		1264	7	

PH-1-9-13-19A-024	0.2395	0.0016	2.8107	0.0265	0.0851	0.0011			1384	8	1358	7	1318	9		1318	9
PH-1-9-13-19A-025	0.2023	0.0013	2.2138	0.0229	0.0794	0.0010			1188	7	1185	7	1181	11		1181	11
PH-1-9-13-19A-026	0.2197	0.0014	2.5340	0.0186	0.0837	0.0009			1280	7	1282	5	1285	6		1285	6
PH-1-9-13-19A-027	0.2747	0.0018	3.6762	0.0295	0.0971	0.0011			1565	9	1566	6	1568	7		1568	7
PH-1-9-13-19A-028	0.2297	0.0015	2.7216	0.0214	0.0859	0.0010			1333	8	1334	6	1337	7		1337	7
PH-1-9-13-19A-029	0.2304	0.0016	2.7469	0.0269	0.0865	0.0011			1337	8	1341	7	1348	9		1348	9
PH-1-9-13-19A-030	0.2170	0.0014	2.4806	0.0215	0.0829	0.0010			1266	7	1266	6	1267	8		1267	8
PH-1-9-13-19A-031	0.2103	0.0013	2.4395	0.0174	0.0841	0.0009			1230	7	1254	5	1296	6		1296	6
PH-1-9-13-19A-032	0.2344	0.0015	2.8042	0.0226	0.0868	0.0010			1357	8	1357	6	1356	7		1356	7
PH-1-9-13-19A-033	0.2307	0.0015	2.7149	0.0214	0.0854	0.0010			1338	8	1333	6	1324	7		1324	7
PH-1-9-13-19A-034	0.2243	0.0014	2.6399	0.0202	0.0854	0.0010			1305	7	1312	6	1324	7		1324	7
PH-1-9-13-19A-035	0.2161	0.0014	2.5078	0.0198	0.0842	0.0010			1261	7	1274	6	1296	7		1296	7
PH-1-9-13-19A-036	0.2356	0.0017	2.8366	0.0313	0.0873	0.0012			1364	9	1365	8	1368	11		1368	11
PH-1-9-13-19A-037	0.2273	0.0014	2.6660	0.0203	0.0851	0.0009			1320	8	1319	6	1317	7		1317	7
PH-1-9-13-19A-038	0.2477	0.0016	3.0712	0.0266	0.0899	0.0011			1427	8	1426	7	1424	8		1424	8
PH-1-9-13-19A-039	0.2287	0.0015	2.6985	0.0227	0.0856	0.0010			1328	8	1328	6	1329	8		1329	8
PH-1-9-13-19A-040	0.2240	0.0014	2.6292	0.0209	0.0852	0.0010			1303	8	1309	6	1319	7		1319	7
PH-1-9-13-19A-041	0.2235	0.0015	2.6021	0.0229	0.0845	0.0010			1300	8	1301	6	1303	8		1303	8
PH-1-9-13-19A-042	0.2304	0.0015	2.7703	0.0253	0.0872	0.0011			1337	8	1348	7	1365	8		1365	8
PH-1-9-13-19A-043	0.2345	0.0016	2.8127	0.0252	0.0870	0.0011			1358	8	1359	7	1361	8		1361	8
PH-1-9-13-19A-044	0.2171	0.0014	2.4924	0.0192	0.0833	0.0009			1266	7	1270	6	1276	7		1276	7
PH-1-9-13-19A-045	0.2279	0.0015	2.7003	0.0231	0.0859	0.0010			1324	8	1329	6	1337	8		1337	8
PH-1-9-13-19A-046	0.2288	0.0015	2.7532	0.0243	0.0873	0.0010			1328	8	1343	7	1367	8		1367	8
PH-1-9-13-19A-047	0.2269	0.0015	2.6314	0.0217	0.0841	0.0010			1318	8	1309	6	1295	7		1295	7
PH-1-9-13-19A-048	0.2215	0.0014	2.5504	0.0210	0.0835	0.0010			1290	8	1287	6	1282	7		1282	7
PH-1-9-13-19A-049	0.2251	0.0015	2.6568	0.0211	0.0856	0.0010			1309	8	1317	6	1330	7		1330	7

PH-1-9-13-19A-050	0.2254	0.0015	2.6927	0.0228	0.0867	0.0010			1310	8	1326	6	1353	8		1353	8
PH-1-9-13-19A-051	0.2267	0.0015	2.6521	0.0207	0.0849	0.0010			1317	8	1315	6	1313	7		1313	7
PH-1-9-13-19A-052	0.2259	0.0015	2.6401	0.0215	0.0848	0.0010			1313	8	1312	6	1311	7		1311	7
PH-1-9-13-19A-053	0.2323	0.0015	2.7653	0.0226	0.0864	0.0010			1347	8	1346	6	1346	7		1346	7
PH-1-9-13-19A-054	0.2209	0.0015	2.6169	0.0235	0.0859	0.0010			1287	8	1305	7	1337	8		1337	8
PH-1-9-13-19A-055	0.2287	0.0015	2.7345	0.0211	0.0867	0.0010			1328	8	1338	6	1355	7		1355	7
PH-1-9-13-19A-056	0.2249	0.0015	2.6386	0.0223	0.0851	0.0010			1308	8	1311	6	1318	8		1318	8
PH-1-9-13-19A-057	0.2307	0.0015	2.7564	0.0228	0.0867	0.0010			1338	8	1344	6	1354	7		1354	7
PH-1-9-13-19A-058	0.2283	0.0015	2.6861	0.0221	0.0854	0.0010			1326	8	1325	6	1324	7		1324	7
PH-1-9-13-19A-059	0.2165	0.0014	2.5792	0.0223	0.0864	0.0010			1263	8	1295	6	1348	8		1348	8
PH-1-9-13-19A-060	0.2221	0.0015	2.5810	0.0244	0.0843	0.0010			1293	8	1295	7	1300	9		1300	9
PH-1-9-13-19A-061	0.2327	0.0015	2.7976	0.0234	0.0872	0.0010			1349	8	1355	6	1366	7		1366	7
PH-1-9-13-19A-062	0.1941	0.0012	2.2381	0.0156	0.0837	0.0009			1143	7	1193	5	1285	6	-	-	-
PH-1-9-13-19A-063	0.1969	0.0012	2.1763	0.0183	0.0802	0.0008			1159	7	1173	6	1201	21		1201	21
PH-1-9-13-19A-064	0.2248	0.0015	2.6029	0.0206	0.0840	0.0009			1307	8	1301	6	1293	7		1293	7
PH-1-9-13-19A-065	0.2283	0.0015	2.7257	0.0271	0.0866	0.0010			1326	8	1335	7	1351	23		1351	23
PH-1-9-13-19A-066	0.2291	0.0015	2.7154	0.0234	0.0860	0.0010			1330	8	1333	6	1338	8		1338	8
PH-1-9-13-19A-067	0.2171	0.0014	2.5023	0.0199	0.0836	0.0009			1266	7	1273	6	1284	7		1284	7
PH-1-9-13-19A-068	0.2030	0.0013	2.2307	0.0216	0.0797	0.0010			1191	7	1191	7	1190	10		1190	10
PH-1-9-13-19A-069	0.2272	0.0015	2.7065	0.0216	0.0865	0.0010			1320	8	1330	6	1348	7		1348	7
PH-1-9-13-19A-070	0.2308	0.0015	2.7477	0.0244	0.0864	0.0010			1339	8	1341	7	1346	8		1346	8
PH-1-9-13-19A-071	0.2205	0.0014	2.5591	0.0196	0.0842	0.0009			1284	8	1289	6	1297	7		1297	7
PH-1-9-13-19A-072	0.1998	0.0013	2.1878	0.0188	0.0795	0.0009			1174	7	1177	6	1183	8		1183	8
PH-1-9-13-19A-073	0.2232	0.0015	2.5714	0.0218	0.0836	0.0010			1299	8	1293	6	1283	8		1283	8
PH-1-9-13-19A-074	0.2223	0.0015	2.5721	0.0245	0.0840	0.0010			1294	8	1293	7	1292	9		1292	9
PH-1-9-13-19A-075	0.2305	0.0015	2.7436	0.0232	0.0864	0.0010			1337	8	1340	6	1346	8		1346	8

PH-1-9-13-19A-076	0.2367	0.0016	2.8685	0.0243	0.0880	0.0010			1369	8	1374	6	1381	8		1381	8
PH-1-9-13-19A-077	0.2292	0.0015	2.7143	0.0218	0.0859	0.0010			1330	8	1332	6	1337	7		1337	7
PH-1-9-13-19A-078	0.1318	0.0008	1.4440	0.0101	0.0795	0.0008			798	5	907	4	1184	6	-	-	-
PH-1-9-13-19A-079	0.2081	0.0014	2.3418	0.0205	0.0817	0.0010			1219	7	1225	6	1237	8		1237	8
PH-1-9-13-19A-080	0.2326	0.0015	2.7753	0.0218	0.0866	0.0010			1348	8	1349	6	1351	7		1351	7
PH-1-9-13-19A-081	0.1949	0.0013	2.1076	0.0177	0.0785	0.0009			1148	7	1151	6	1158	8		1158	8
PH-1-9-13-19A-082	0.2142	0.0014	2.4327	0.0177	0.0824	0.0009			1251	7	1252	5	1255	6		1255	6
PH-1-9-13-19A-083	0.2281	0.0015	2.7147	0.0217	0.0863	0.0010			1325	8	1332	6	1346	7		1346	7
PH-1-9-13-19A-084	0.2494	0.0017	3.2069	0.0266	0.0933	0.0011			1436	9	1459	6	1494	7		1494	7
PH-1-9-13-19A-085	0.2148	0.0014	2.5439	0.0191	0.0859	0.0009			1254	7	1285	5	1337	6		1337	6
PH-1-9-13-19A-086	0.2313	0.0015	2.7441	0.0239	0.0861	0.0010			1341	8	1340	6	1340	8		1340	8
PH-1-9-13-19A-087	0.2335	0.0016	2.7883	0.0236	0.0867	0.0010			1353	8	1352	6	1353	8		1353	8
PH-1-9-13-19A-088	0.2271	0.0015	2.6554	0.0235	0.0849	0.0010			1319	8	1316	7	1312	8		1312	8
PH-1-9-13-19A-089	0.2327	0.0016	2.7300	0.0247	0.0851	0.0010			1348	8	1337	7	1319	8		1319	8
PH-1-9-13-19A-090	0.2124	0.0014	2.3880	0.0223	0.0816	0.0010			1242	8	1239	7	1235	9		1235	9
PH-1-9-13-19A-091	0.2249	0.0015	2.6128	0.0248	0.0843	0.0010			1308	8	1304	7	1299	9		1299	9
PH-1-9-13-19A-092	0.2158	0.0015	2.4881	0.0249	0.0837	0.0011			1260	8	1269	7	1285	10		1285	10
PH-1-9-13-19A-093	0.2295	0.0015	2.7161	0.0229	0.0859	0.0010			1332	8	1333	6	1335	7		1335	7
PH-1-9-13-19A-094	0.2257	0.0015	2.6551	0.0226	0.0854	0.0010			1312	8	1316	6	1324	8		1324	8
PH-1-9-13-19A-095	0.2146	0.0014	2.4418	0.0215	0.0826	0.0010			1253	8	1255	6	1259	8		1259	8
PH-1-9-13-19A-096	0.2224	0.0015	2.5713	0.0268	0.0839	0.0011			1294	8	1292	8	1290	10		1290	10
PH-1-9-13-19A-097	0.2298	0.0015	2.7303	0.0207	0.0862	0.0009			1334	8	1337	6	1343	7		1343	7
PH-1-9-13-19A-098	0.2061	0.0014	2.2783	0.0241	0.0802	0.0011			1208	8	1206	7	1202	11		1202	11
PH-1-9-13-19A-099	0.2172	0.0014	2.4525	0.0230	0.0820	0.0010			1267	8	1258	7	1244	9		1244	9
PH-1-9-13-19A-100	0.2157	0.0015	2.4570	0.0220	0.0826	0.0010			1259	8	1259	6	1261	8		1261	8

Isotopic ratios and ages were corrected for common lead except sample PH-1-3-13-10A

Sample/analysis designation corresponds to the sampling date, traverse stop, and analysis number														
The youngest three concordant ages are bolded, the youngest one age is interpreted to be maximum depositional age														

Table A.2.5. U-Pb detrital zircon geochronologic analyses of Lalpani schist metasedimentary rocks

Sample/analysis	Isotopic ratios			$\frac{^{206}\text{Pb}}{^{238}\text{U}}$	± 1 s.e.	$\frac{^{207}\text{Pb}}{^{235}\text{U}}$	± 1 s.e.	$\frac{^{207}\text{Pb}}{^{206}\text{Pb}}$	± 1 s.e.	Error corr.	Apparent ages (Ma)			$\frac{^{206}\text{Pb}}{^{238}\text{U}}$	± 1 s.e.	$\frac{^{207}\text{Pb}}{^{235}\text{U}}$	± 1 s.e.	$\frac{^{207}\text{Pb}}{^{206}\text{Pb}}$	± 1 s.e.	Best age	
	(Ma)	\pm (Ma)	(Ma)								(Ma)	\pm (Ma)	(Ma)	\pm (Ma)							
PH-1-9-13-2-001	0.0992	0.006	1.1232	0.011	0.011	0.0821	0.011	0.9	0.9		610	4	765	5	1249	10	1117	22			
PH-1-9-13-2-002	0.0458	0.005	0.5923	0.021	0.021	0.0938	0.036	0.9	0.9		289	3	472	14	1503	51	-	-			
PH-1-9-13-2-003	0.1637	0.014	1.8215	0.037	0.018	0.0807	0.018	0.9	0.9		977	8	1053	13	1215	27	-	-			
PH-1-9-13-2-004	0.0739	0.005	0.6457	0.012	0.013	0.0633	0.013	0.86	0.86		460	3	506	8	720	45	977	8			
PH-1-9-13-2-005	0.1091	0.008	0.9246	0.018	0.013	0.0615	0.013	0.9	0.9		667	5	665	10	657	29	460	3			
PH-1-9-13-2-006	0.0844	0.008	0.8776	0.022	0.021	0.0754	0.021	0.9	0.9		522	5	640	12	1080	37	667	5			
PH-1-9-13-2-007	0.1364	0.010	1.3488	0.022	0.014	0.0718	0.014	0.9	0.9		824	6	867	10	979	22	-	-			
PH-1-9-13-2-008	0.0932	0.007	0.8855	0.021	0.018	0.0689	0.018	0.86	0.86		574	4	644	12	897	54	824	6			
PH-1-9-13-2-009	0.3718	0.028	9.3139	0.111	0.026	0.1817	0.026	0.87	0.87		2038	13	2369	11	2668	24	-	-			
PH-1-9-13-2-010	0.0725	0.005	2.1533	0.021	0.029	0.2155	0.029	0.9	0.9		451	3	1166	7	2947	8	-	-			
PH-1-9-13-2-011	0.1265	0.012	1.4425	0.032	0.020	0.0827	0.020	0.9	0.9		768	7	907	13	1262	30	-	-			
PH-1-9-13-2-012	0.1934	0.013	3.1234	0.033	0.015	0.1171	0.015	0.87	0.87		1140	7	1438	8	1913	23	-	-			
PH-1-9-13-2-013	0.1049	0.026	0.8870	0.113	0.079	0.0614	0.079	0.9	0.9		643	15	645	61	652	237	-	-			
PH-1-9-13-2-014	0.0419	0.005	0.2988	0.015	0.028	0.0518	0.028	0.9	0.9		264	3	265	12	276	100	643	15			
PH-1-9-13-2-015	0.1484	0.011	1.4250	0.024	0.013	0.0697	0.013	0.9	0.9		892	6	899	10	919	23	264	3			
PH-1-9-13-2-016	0.1175	0.019	1.4650	0.070	0.045	0.0905	0.045	0.9	0.9		716	11	916	29	1436	67	892	6			
PH-1-9-13-2-017	0.1300	0.020	3.6581	0.105	0.064	0.2041	0.064	0.9	0.9		788	11	1562	23	2859	27	-	-			
PH-1-9-13-2-018	0.2033	0.022	2.2834	0.062	0.024	0.0815	0.024	0.9	0.9		1193	12	1207	19	1233	37	-	-			
PH-1-9-13-2-019	0.0538	0.006	0.5134	0.027	0.038	0.0692	0.038	0.82	0.82		338	4	421	18	905	115	1233	37			
PH-1-9-13-2-020	0.3654	0.031	6.2915	0.105	0.023	0.1249	0.023	0.88	0.88		2008	15	2017	15	2027	34	-	-			
PH-1-9-13-2-021	0.1925	0.023	3.8115	0.099	0.040	0.1437	0.040	0.9	0.9		1135	12	1595	21	2272	28	2027	34			
PH-1-9-13-2-022	0.1705	0.015	3.0579	0.052	0.025	0.1302	0.025	0.9	0.9		1015	8	1422	13	2100	18	-	-			

PH-1-9-13-2-023	0.1261	0.033	1.3615	0.205	0.0783	0.0120	0.86		766	19	873	88	1154	325		-	-
PH-1-9-13-2-024	0.1371	0.012	1.2886	0.029	0.0682	0.0017	0.9		828	7	841	13	874	33		-	-
PH-1-9-13-2-025	0.1904	0.016	2.0803	0.042	0.0793	0.0018	0.9		1124	9	1142	14	1179	26		828	7
PH-1-9-13-2-026	0.1026	0.009	0.8949	0.024	0.0633	0.0018	0.9		630	5	649	13	718	42		1179	26
PH-1-9-13-2-027	0.1051	0.011	0.8791	0.030	0.0607	0.0022	0.9		644	6	641	16	628	57		630	5
PH-1-9-13-2-028	0.1044	0.013	1.6834	0.053	0.1171	0.0040	0.9		640	8	1002	20	1912	39		644	6
PH-1-9-13-2-029	0.0543	0.008	0.4877	0.027	0.0652	0.0038	0.9		341	5	403	19	781	93		-	-
PH-1-9-13-2-030	0.0908	0.009	0.8825	0.027	0.0705	0.0023	0.9		560	5	642	15	944	47		-	-
PH-1-9-13-2-031	0.1041	0.008	0.9051	0.016	0.0631	0.0013	0.9		639	5	654	9	711	27		-	-
PH-1-9-13-2-032	0.2123	0.019	3.0185	0.060	0.1031	0.0023	0.88		1241	10	1412	15	1681	42		639	5
PH-1-9-13-2-033	0.3966	0.039	6.8524	0.118	0.1254	0.0024	0.9		2153	18	2093	15	2034	17		-	-
PH-1-9-13-2-034	0.0346	0.010	0.2199	0.032	0.0461	0.0069	0.74		219	6	202	27		271		2034	17
PH-1-9-13-2-035	0.0999	0.021	0.8515	0.076	0.0618	0.0057	0.85		614	12	625	42	669	204		219	6
PH-1-9-13-2-036	0.0849	0.027	0.7728	0.124	0.0660	0.0109	0.86		525	16	581	72	807	369		614	12
PH-1-9-13-2-037	0.0667	0.008	1.6010	0.037	0.1742	0.0046	0.9		416	5	971	15	2598	24		-	-
PH-1-9-13-2-038	0.0390	0.008	0.2479	0.020	0.0461	0.0040	0.31		247	5	225	17		192		-	-
PH-1-9-13-2-039	0.0438	0.004	0.7774	0.017	0.1287	0.0033	0.9		277	3	584	10	2080	26		247	5
PH-1-9-13-2-040	0.0374	0.013	0.2466	0.067	0.0478	0.0131	0.8		237	8	224	55	89	456		-	-
PH-1-9-13-2-041	0.0917	0.028	0.7882	0.087	0.0624	0.0071	0.9		565	16	590	50	687	187		237	8
PH-1-9-13-2-042	0.0451	0.004	0.3258	0.010	0.0524	0.0017	0.9		284	2	286	8	304	54		565	16
PH-1-9-13-2-043	0.0155	0.003	0.1198	0.030	0.0563	0.0145	0.83		99	2	115	28	462	497		284	2
PH-1-9-13-2-044	0.0168	0.004	0.1592	0.014	0.0688	0.0063	0.9		107	2	150	12	893	145		-	-
PH-1-9-13-2-045	0.1584	0.015	1.6579	0.082	0.0759	0.0038	0.76		948	8	993	31	1092	104		-	-
PH-1-9-13-2-046	0.0937	0.008	0.9578	0.021	0.0742	0.0018	0.9		577	5	682	11	1046	31		948	8
PH-1-9-13-2-047	0.2864	0.026	3.9116	0.072	0.0991	0.0020	0.9		1623	13	1616	15	1608	21		-	-
PH-1-9-13-2-048	0.0938	0.018	0.8803	0.057	0.0681	0.0046	0.9		578	10	641	31	871	105		1608	21

PH-1-9-13-2-049	0.1562	0.015	1.5029	0.0386	0.0698	0.019	0.9		936	8	932	16	923	37	-	-
PH-1-9-13-2-050	0.0701	0.009	0.5501	0.0279	0.0569	0.0030	0.9		437	5	445	18	489	90	936	8
PH-1-9-13-2-051	0.2187	0.030	2.8512	0.0956	0.0946	0.0033	0.9		1275	16	1369	25	1520	43	437	5
PH-1-9-13-2-052	0.1620	0.029	2.0085	0.0976	0.0900	0.0045	0.9		968	16	1118	33	1424	65	-	-
PH-1-9-13-2-053	0.1117	0.039	0.7091	0.6747	0.0461	0.0438	0.16		683	23	544	401		1206	-	-
PH-1-9-13-2-054	0.0567	0.018	0.3600	0.0831	0.0461	0.0107	0.78		356	11	312	62		380	-	-
PH-1-9-13-2-055	0.0461	0.008	0.3296	0.0287	0.0519	0.0046	0.9		291	5	289	22	281	167	-	-
PH-1-9-13-2-056	0.0451	0.007	0.2864	0.0244	0.0461	0.0040	0.59		284	4	256	19		190	291	5
PH-1-9-13-2-057	0.1107	0.025	1.6269	0.1010	0.1066	0.0069	0.9		677	15	981	39	1743	80	284	4
PH-1-9-13-2-058	0.0316	0.010	0.2199	0.0319	0.0506	0.0075	0.9		200	6	202	27	221	264		
PH-1-9-13-2-059	0.3222	0.027	4.8018	0.0760	0.1081	0.0019	0.9		1800	13	1785	13	1768	17	200	6
PH-1-9-13-2-060	0.0355	0.015	0.2254	0.0373	0.0461	0.0078	0.36		225	9	206	31		299	1768	17
PH-1-9-13-2-061	0.2372	0.039	2.8595	0.1205	0.0875	0.0038	0.9		1372	20	1371	32	1371	56	225	9
PH-1-9-13-2-062	0.0425	0.015	0.2995	0.0575	0.0511	0.0100	0.9		268	9	266	45	247	326	1371	56
PH-1-9-13-2-063	0.0235	0.006	0.1494	0.0280	0.0461	0.0087	0.21		150	4	141	25		323	268	9
PH-1-9-13-2-064	0.0730	0.034	0.6427	0.1231	0.0639	0.0125	0.9		454	21	504	76	737	338	150	4
PH-1-9-13-2-065	0.0893	0.026	1.8751	0.2701	0.1524	0.0224	0.89		551	15	1072	95	2373	265	-	-
PH-1-9-13-2-066	0.0901	0.015	0.7373	0.0587	0.0594	0.0048	0.9		556	9	561	34	582	145	-	-
PH-1-9-13-2-067	0.0792	0.041	1.1718	0.3089	0.1073	0.0288	0.89		491	25	787	144	1754	578	556	9
PH-1-9-13-2-068	0.0761	0.014	0.7248	0.0459	0.0691	0.0045	0.9		473	8	554	27	901	100	-	-
PH-1-9-13-2-069	0.0718	0.038	2.1304	0.4231	0.2152	0.0442	0.91		447	23	1159	137	2945	364	-	-
PH-1-9-13-2-070	0.0416	0.003	0.6634	0.0139	0.1157	0.0026	0.84		263	2	517	8	1891	41	-	-
PH-1-9-13-2-071	0.0338	0.016	0.2294	0.1044	0.0493	0.0225	0.81		214	10	210	86	161	800	-	-
PH-1-9-13-2-072	0.0622	0.011	0.4785	0.0367	0.0558	0.0044	0.9		389	7	397	25	444	139	214	10
PH-1-9-13-2-073	0.2853	0.028	8.1186	0.1207	0.2065	0.0035	0.9		1618	14	2244	13	2878	12	389	7
PH-1-9-13-2-074	0.0502	0.013	0.3420	0.0619	0.0494	0.0090	0.82		316	8	299	47	167	339	-	-

PH-1-9-13-2-075	0.0337	0.006	0.2136	0.0452	0.0461	0.0098	0.15		213	3	197	38		353		316	8
PH-1-9-13-2-076	0.0676	0.020	0.6269	0.0780	0.0673	0.0085	0.9		422	12	494	49	846	215		213	3
PH-1-9-13-2-077	0.5252	0.059	13.5086	0.217	0.1866	0.0033	0.9		2721	25	2716	16	2713	14		-	-
PH-1-9-13-2-078	0.0349	0.006	0.4164	0.0291	0.0867	0.0062	0.9		221	4	353	21	1354	108		2713	14
PH-1-9-13-2-079	0.1358	0.014	2.7687	0.0558	0.1480	0.0033	0.9		821	8	1347	15	2323	21		-	-
PH-1-9-13-2-080	0.1642	0.018	1.6456	0.0721	0.0727	0.0033	0.86		980	10	988	28	1005	94		-	-
PH-1-9-13-2-081	0.0613	0.008	0.5006	0.0230	0.0592	0.0028	0.9		384	5	412	16	576	78		980	10
PH-1-9-13-2-082	0.0367	0.015	0.3679	0.0995	0.0727	0.0199	0.88		232	9	318	74	1005	581		384	5
PH-1-9-13-2-083	0.0805	0.013	0.6831	0.0418	0.0615	0.0039	0.87		499	7	529	25	657	139		-	-
PH-1-9-13-2-084	0.0866	0.013	0.8296	0.0416	0.0695	0.0036	0.9		535	8	613	23	915	78		499	7
PH-1-9-13-2-085	0.1177	0.013	1.0185	0.0388	0.0628	0.0025	0.9		717	8	713	20	701	62		-	-
PH-1-9-13-2-086	0.1393	0.026	1.4725	0.0897	0.0767	0.0048	0.9		840	15	919	37	1114	92		717	8
PH-1-9-13-2-087	0.0743	0.009	0.9495	0.0319	0.0928	0.0033	0.9		462	5	678	17	1483	46		840	15
PH-1-9-13-2-088	0.1470	0.023	1.4043	0.0731	0.0693	0.0037	0.9		884	13	891	31	908	81		-	-
PH-1-9-13-2-089	0.2247	0.024	4.5931	0.0918	0.1483	0.0033	0.9		1307	12	1748	17	2327	20		884	13
PH-1-9-13-2-090	0.1997	0.014	2.9600	0.0416	0.1075	0.0017	0.83		1173	7	1397	11	1758	29		-	-
PH-1-9-13-2-091	0.1120	0.028	2.5559	0.2659	0.1656	0.0177	0.87		684	16	1288	76	2514	187		-	-
PH-1-9-13-2-092	0.1015	0.008	0.8456	0.0176	0.0604	0.0014	0.9		623	5	622	10	619	31		-	-
PH-1-9-13-2-093	0.0365	0.004	0.3502	0.0136	0.0696	0.0028	0.9		231	3	305	10	915	61		623	5
PH-1-9-13-2-094	0.5405	0.059	14.4333	0.2291	0.1937	0.0033	0.9		2785	25	2779	15	2774	13		-	-
PH-1-9-13-2-095	0.0703	0.006	1.3341	0.0249	0.1376	0.0029	0.9		438	4	861	11	2197	20		2774	13
PH-1-9-13-2-096	0.1857	0.026	3.8309	0.1156	0.1496	0.0050	0.87		1098	14	1599	24	2342	58		-	-
PH-1-9-13-2-097	0.0704	0.009	0.9720	0.0336	0.1002	0.0037	0.9		438	5	689	17	1628	46		-	-
PH-1-9-13-2-098	0.0246	0.005	0.1717	0.0594	0.0507	0.0176	0.82		157	3	161	51	226	603		-	-
PH-1-9-13-2-100	0.0682	0.029	1.8042	0.2685	0.1919	0.0297	0.89		425	17	1047	97	2759	269		157	3

	$^{206}\text{Pb}/^{238}\text{U}$	± 1 s.e.	$^{207}\text{Pb}/^{235}\text{U}$	± 1 s.e.	$^{207}\text{Pb}/^{206}\text{Pb}$	± 1 s.e.	Error corr.		$^{206}\text{Pb}/^{238}\text{U}$	± 1 s.e.	$^{207}\text{Pb}/^{235}\text{U}$	± 1 s.e.	$^{207}\text{Pb}/^{206}\text{Pb}$	± 1 s.e.	(Ma)	\pm (Ma)
PH-1-12-13-7-001	0.0208	0.002	0.1626	0.055	0.0566	0.0020	0.91		132.8	0.9	153	5	477	79	-	-
PH-1-12-13-7-002	0.0113	0.001	0.0923	0.045	0.0594	0.0029	0.87		72.3	0.6	90	4	581	110	-	-
PH-1-12-13-7-003	0.0815	0.005	0.6605	0.095	0.0587	0.0010	0.9		505	3	515	6	557	20	505	3
PH-1-12-13-7-004	0.0775	0.006	0.6157	0.0114	0.0576	0.0012	0.9		481	3	487	7	513	28	481	3
PH-1-12-13-7-005	0.0720	0.006	0.6120	0.0145	0.0616	0.0016	0.9		448	4	485	9	661	37	448	4
PH-1-12-13-7-006	0.0823	0.008	0.6398	0.0188	0.0563	0.0017	0.9		510	5	502	12	465	49	510	5
PH-1-12-13-7-007	0.0763	0.012	0.6097	0.0385	0.0579	0.0037	0.9		474	7	483	24	526	112	474	7
PH-1-12-13-7-008	0.0283	0.002	0.2392	0.0038	0.0614	0.0011	0.91		180	1	218	3	653	38	-	-
PH-1-12-13-7-009	0.0866	0.007	0.6940	0.0143	0.0581	0.0013	0.9		535	4	535	9	534	32	535	4
PH-1-12-13-7-010	0.0516	0.004	0.3895	0.0088	0.0548	0.0013	0.88		324	2	334	6	402	54	324	2
PH-1-12-13-7-011	0.0769	0.007	0.6633	0.0183	0.0625	0.0018	0.9		477	4	517	11	693	43	477	4
PH-1-12-13-7-012	0.0094	0.001	0.1180	0.0019	0.0913	0.0017	0.9		60.1	0.4	113	2	1453	19	-	-
PH-1-12-13-7-013	0.0763	0.005	0.6170	0.0101	0.0586	0.0011	0.9		474	3	488	6	552	24	474	3
PH-1-12-13-7-014	0.0879	0.007	0.7056	0.0211	0.0583	0.0018	0.88		543	4	542	13	539	69	543	4
PH-1-12-13-7-015	0.0214	0.002	0.2324	0.0033	0.0787	0.0013	0.9		136.6	0.9	212	3	1163	17	-	-
PH-1-12-13-7-016	0.0217	0.001	0.1831	0.0018	0.0612	0.0008	0.9		138.3	0.8	171	2	646	11	-	-
PH-1-12-13-7-017	0.1303	0.008	1.7240	0.0149	0.0960	0.0010	0.89		789	4	1018	6	1548	20	-	-
PH-1-12-13-7-018	0.0920	0.008	0.9652	0.0216	0.0761	0.0019	0.9		567	5	686	11	1097	31	-	-
PH-1-12-13-7-019	0.0816	0.005	0.6442	0.0089	0.0572	0.0009	0.9		506	3	505	6	500	19	506	3
PH-1-12-13-7-020	0.0880	0.010	1.1077	0.0343	0.0912	0.0030	0.9		544	6	757	17	1451	42	-	-
PH-1-12-13-7-021	0.0280	0.002	0.2144	0.0062	0.0556	0.0017	0.88		178	1	197	5	435	68	-	-
PH-1-12-13-7-022	0.0560	0.004	0.4468	0.0057	0.0578	0.0009	0.9		351	2	375	4	523	17	351	2
PH-1-12-13-7-023	0.0854	0.008	0.7188	0.0222	0.0610	0.0020	0.9		528	5	550	13	639	50	528	5
PH-1-12-13-7-024	0.0864	0.007	0.6952	0.0176	0.0583	0.0016	0.9		534	4	536	11	542	41	534	4
PH-1-12-13-7-025	0.0876	0.007	0.7539	0.0170	0.0624	0.0015	0.9		541	4	571	10	687	34	541	4

PH-1-12-13-7-026	0.0856	0.007	0.6846	0.0215	0.0580	0.0019	0.87		529	4	530	13	530	73		529	4
PH-1-12-13-7-027	0.0574	0.005	0.5170	0.0175	0.0654	0.0023	0.9		360	3	423	12	786	75	-	-	-
PH-1-12-13-7-028	0.0809	0.007	0.6310	0.0160	0.0566	0.0015	0.9		501	4	497	10	474	41	501	4	
PH-1-12-13-7-029	0.0642	0.004	0.5151	0.0060	0.0582	0.0008	0.9		401	2	422	4	536	15	401	2	
PH-1-12-13-7-030	0.0839	0.007	0.6643	0.0168	0.0574	0.0016	0.9		519	4	517	10	508	41	519	4	
PH-1-12-13-7-031	0.0832	0.006	0.6621	0.0098	0.0577	0.0010	0.9		515	3	516	6	519	21	515	3	
PH-1-12-13-7-032	0.3003	0.021	4.3097	0.0499	0.1041	0.0015	0.9		1693	11	1695	10	1698	11	1698	11	
PH-1-12-13-7-033	0.0247	0.002	0.1854	0.0031	0.0544	0.0010	0.89		157.5	1	173	3	386	41	158	1	
PH-1-12-13-7-034	0.0394	0.003	0.3580	0.0082	0.0659	0.0016	0.89		249	2	311	6	804	51	-	-	-
PH-1-12-13-7-035	0.0318	0.002	0.2365	0.0058	0.0539	0.0014	0.9		202	1	216	5	367	59	202	1	
PH-1-12-13-7-036	0.0821	0.008	0.6839	0.0212	0.0604	0.0020	0.9		509	5	529	13	617	50	509	5	
PH-1-12-13-7-037	0.0557	0.011	0.8704	0.0349	0.1132	0.0050	0.9		350	7	636	19	1852	45	-	-	-
PH-1-12-13-7-038	0.0692	0.005	0.5638	0.0142	0.0591	0.0016	0.88		431	3	454	9	571	58	431	3	
PH-1-12-13-7-039	0.0905	0.008	0.8248	0.0210	0.0661	0.0018	0.9		558	5	611	12	810	38	558	5	
PH-1-12-13-7-040	0.0868	0.008	0.7352	0.0193	0.0614	0.0017	0.9		537	5	560	11	654	41	537	5	
PH-1-12-13-7-041	0.0645	0.004	0.5288	0.0083	0.0595	0.0011	0.9		403	3	431	6	584	22	403	3	
PH-1-12-13-7-042	0.0257	0.002	0.2014	0.0032	0.0568	0.0010	0.89		163.6	1	186	3	485	38	-	-	-
PH-1-12-13-7-043	0.0198	0.001	0.1944	0.0053	0.0714	0.0020	0.89		126.1	0.9	180	5	968	59	-	-	-
PH-1-12-13-7-044	0.0256	0.002	0.2037	0.0023	0.0577	0.0008	0.9		163	1	188	2	518	15	-	-	-
PH-1-12-13-7-045	0.0804	0.006	0.6359	0.0124	0.0573	0.0012	0.9		499	4	500	8	504	30	499	4	
PH-1-12-13-7-046	0.0296	0.002	0.2456	0.0064	0.0602	0.0016	0.9		188	1	223	5	609	59	-	-	-
PH-1-12-13-7-047	0.0847	0.008	0.7012	0.0204	0.0600	0.0019	0.9		524	5	540	12	604	47	524	5	
PH-1-12-13-7-048	0.0847	0.006	0.6841	0.0127	0.0586	0.0012	0.9		524	4	529	8	552	28	524	4	
PH-1-12-13-7-049	0.0891	0.008	0.7644	0.0214	0.0622	0.0019	0.9		550	5	577	12	681	44	550	5	
PH-1-12-13-7-050	0.0188	0.001	0.1682	0.0016	0.0649	0.0008	0.9		120.1	0.7	158	1	769	11	-	-	-
PH-1-12-13-7-051	0.0794	0.006	0.6271	0.0110	0.0573	0.0011	0.9		493	3	494	7	502	26	493	3	

PH-1-12-13-7-052	0.0793	0.005	0.6393	0.010	0.0585	0.0011	0.9		492	3	502	6	549	23		492	3
PH-1-12-13-7-053	0.0804	0.005	0.6362	0.009	0.0574	0.0010	0.9		499	3	500	6	506	22		499	3
PH-1-12-13-7-054	0.0477	0.003	0.3987	0.007	0.0607	0.0012	0.9		300	2	341	5	627	27		-	-
PH-1-12-13-7-055	0.0315	0.002	0.2613	0.002	0.0602	0.0008	0.9		200	1	236	2	611	11		-	-
PH-1-12-13-7-056	0.0810	0.006	0.6595	0.013	0.0591	0.0013	0.9		502	4	514	8	570	32		502	4
PH-1-12-13-7-057	0.0424	0.003	0.3496	0.006	0.0598	0.0012	0.9		268	2	304	5	597	26		-	-
PH-1-12-13-7-058	0.0538	0.003	0.4330	0.005	0.0584	0.0008	0.9		338	2	365	4	543	15		338	2
PH-1-12-13-7-059	0.0889	0.009	0.8511	0.026	0.0695	0.0023	0.9		549	5	625	14	912	46		-	-
PH-1-12-13-7-060	0.0840	0.010	0.6998	0.028	0.0604	0.0026	0.9		520	6	539	17	619	68		520	6
PH-1-12-13-7-061	0.0375	0.003	0.2759	0.007	0.0534	0.0015	0.89		237	2	247	6	345	64		237	2
PH-1-12-13-7-062	0.0260	0.002	0.2184	0.002	0.0611	0.0008	0.9		165.2	0.9	201	2	641	12		-	-
PH-1-12-13-7-063	0.0276	0.002	0.2290	0.002	0.0602	0.0008	0.9		176	1	209	2	609	12		-	-
PH-1-12-13-7-064	0.0315	0.002	0.2310	0.006	0.0532	0.0015	0.89		200	1	211	5	336	67		200	1
PH-1-12-13-7-065	0.0710	0.005	0.5698	0.009	0.0582	0.0011	0.9		442	3	458	6	539	24		442	3
PH-1-12-13-7-066	0.0790	0.005	0.6275	0.008	0.0576	0.0009	0.9		490	3	495	5	515	19		490	3
PH-1-12-13-7-067	0.0826	0.006	0.6720	0.014	0.0591	0.0014	0.9		511	4	522	9	569	32		511	4
PH-1-12-13-7-068	0.0437	0.003	0.4107	0.007	0.0682	0.0014	0.9		276	2	349	5	874	26		-	-
PH-1-12-13-7-069	0.0802	0.006	0.6306	0.020	0.0571	0.0019	0.88		497	4	496	12	494	74		497	4
PH-1-12-13-7-070	0.0768	0.008	0.6371	0.021	0.0602	0.0022	0.9		477	5	500	14	611	56		477	5
PH-1-12-13-7-071	0.0450	0.003	0.3631	0.005	0.0586	0.0011	0.9		284	2	315	4	552	23		-	-
PH-1-12-13-7-072	0.0272	0.002	0.2000	0.004	0.0533	0.0012	0.91		173	1	185	4	341	54		173	1
PH-1-12-13-7-073	0.0730	0.005	0.5778	0.008	0.0575	0.0010	0.9		454	3	463	5	510	19		454	3
PH-1-12-13-7-074	0.0813	0.006	0.6391	0.014	0.0570	0.0014	0.9		504	4	502	9	492	36		504	4
PH-1-12-13-7-075	0.0825	0.005	0.7259	0.007	0.0638	0.0009	0.9		511	3	554	5	736	13		511	3
PH-1-12-13-7-076	0.0774	0.005	0.6132	0.005	0.0575	0.0007	0.9		481	3	486	4	509	10		481	3
PH-1-12-13-7-077	0.0851	0.010	0.8586	0.047	0.0732	0.0041	0.91		526	6	629	26	1019	116		-	-

PH-1-12-13-7-078	0.0184	0.0001	0.1522	0.0020	0.05990	0.0010	0.9		117.8	0.7	144	2	599	18	-	-
PH-1-12-13-7-079	0.0806	0.0006	0.6484	0.0145	0.05840	0.0014	0.9		500	4	508	9	544	35	500	4
PH-1-12-13-7-080	0.0798	0.0008	0.6579	0.0218	0.05980	0.0021	0.9		495	5	513	13	596	55	495	5
PH-1-12-13-7-081	0.0371	0.0002	0.3166	0.0040	0.06200	0.0010	0.9		235	1	279	3	673	16	-	-
PH-1-12-13-7-082	0.0459	0.0003	0.3753	0.0057	0.05940	0.0010	0.9		289	2	324	4	580	21	-	-
PH-1-12-13-7-083	0.0365	0.0002	0.3017	0.0041	0.05990	0.0010	0.9		231	1	268	3	601	19	-	-
PH-1-12-13-7-084	0.0794	0.0007	0.6357	0.0169	0.05810	0.0017	0.9		492	4	500	10	535	43	492	4
PH-1-12-13-7-085	0.0813	0.0008	0.6560	0.0216	0.05860	0.0020	0.9		504	5	512	13	552	55	504	5
PH-1-12-13-7-086	0.0456	0.0003	0.3793	0.0081	0.06040	0.0014	0.9		287	2	327	6	617	50	-	-
PH-1-12-13-7-087	0.0335	0.0002	0.2803	0.0038	0.06070	0.0010	0.9		213	1	251	3	628	18	-	-
PH-1-12-13-7-088	0.0792	0.0006	0.6357	0.0137	0.05830	0.0014	0.9		491	4	500	8	541	33	491	4
PH-1-12-13-7-089	0.0298	0.0002	0.2453	0.0048	0.05960	0.0012	0.88		190	1	223	4	590	45	-	-
PH-1-12-13-7-090	0.0802	0.0008	0.6332	0.0199	0.05730	0.0019	0.9		497	4	498	12	503	52	497	4
PH-1-12-13-7-091	0.0837	0.0010	0.7134	0.0435	0.06180	0.0038	0.88		518	6	547	26	667	137	518	6
PH-1-12-13-7-092	0.0382	0.0003	0.2864	0.0080	0.05430	0.0016	0.88		242	2	256	6	385	66	242	2
PH-1-12-13-7-093	0.0216	0.0001	0.1763	0.0017	0.05930	0.0008	0.9		137.8	0.8	165	1	577	11	-	-
PH-1-12-13-7-094	0.0824	0.0008	0.6687	0.0359	0.05890	0.0032	0.9		510	5	520	22	562	122	510	5
PH-1-12-13-7-095	0.0252	0.0001	0.2125	0.0018	0.06120	0.0008	0.9		160.4	0.9	196	2	647	9	-	-
PH-1-12-13-7-096	0.0804	0.0008	0.6585	0.0226	0.05940	0.0021	0.9		499	5	514	14	583	57	499	5
PH-1-12-13-7-097	0.0850	0.0008	0.8182	0.0223	0.06990	0.0020	0.9		526	5	607	12	925	41		
PH-1-12-13-7-098	0.0845	0.0006	0.6733	0.0141	0.05790	0.0013	0.9		523	4	523	9	524	33	523	4
PH-1-12-13-7-099	0.0777	0.0005	0.6651	0.0110	0.06210	0.0012	0.9		482	3	518	7	679	23	482	3
PH-1-12-13-7-100	0.0277	0.0002	0.2291	0.0023	0.06010	0.0008	0.9		176	1	209	2	607	12	-	-
	$^{206}\text{Pb}/^{238}\text{U}$	± 1 s.e.	$^{207}\text{Pb}/^{235}\text{U}$	± 1 s.e.	$^{207}\text{Pb}/^{206}\text{Pb}$	± 1 s.e.	Error corr.		$^{206}\text{Pb}/^{238}\text{U}$	± 1 s.e.	$^{207}\text{Pb}/^{235}\text{U}$	± 1 s.e.	$^{207}\text{Pb}/^{206}\text{Pb}$	± 1 s.e.	(Ma)	\pm (Ma)
PH-1-9-13-25-001	0.0272	0.002	0.2479	0.0022	0.06600	0.0008	0.9		173.3	0.9	225	2	807	10	-	-

PH-1-9-13-25-002	0.0863	0.007	0.8674	0.0173	0.0729	0.016	0.9		534	4	634	9	1010	28	-	-
PH-1-9-13-25-003	0.0344	0.002	0.2428	0.0060	0.0512	0.0013	0.85		218	1	221	5	249	60	218	1
PH-1-9-13-25-004	0.0797	0.005	0.6368	0.0108	0.0580	0.0011	0.9		494	3	500	7	529	25	494	3
PH-1-9-13-25-005	0.0797	0.005	0.6371	0.0110	0.0580	0.0011	0.9		494	3	500	7	529	26	494	3
PH-1-9-13-25-006	0.0276	0.002	0.2549	0.0027	0.0669	0.0009	0.9		176	1	231	2	835	13	-	-
PH-1-9-13-25-007	0.0799	0.008	0.6362	0.0246	0.0577	0.0023	0.9		496	5	500	15	520	67	496	5
PH-1-9-13-25-008	0.0817	0.009	0.6518	0.0410	0.0578	0.0037	0.89		507	6	510	25	523	144	507	6
PH-1-9-13-25-009	0.0791	0.005	0.6414	0.0084	0.0588	0.0009	0.9		491	3	503	5	561	18	491	3
PH-1-9-13-25-010	0.0550	0.005	0.5887	0.0162	0.0777	0.0023	0.9		345	3	470	10	1139	40	-	-
PH-1-9-13-25-011	0.0768	0.005	0.6294	0.0145	0.0595	0.0014	0.89		477	3	496	9	584	53	477	3
PH-1-9-13-25-012	0.0808	0.005	0.6742	0.0107	0.0605	0.0011	0.9		501	3	523	6	623	23	501	3
PH-1-9-13-25-013	0.0853	0.011	0.7330	0.0316	0.0623	0.0028	0.9		528	6	558	19	686	71	528	6
PH-1-9-13-25-014	0.0077	0.001	0.0625	0.0025	0.0586	0.0024	0.89		49.7	0.4	62	2	553	93	-	-
PH-1-9-13-25-015	0.0572	0.004	0.4892	0.0109	0.0621	0.0014	0.89		358	2	404	7	676	51	-	-
PH-1-9-13-25-017	0.0803	0.006	0.7386	0.0129	0.0667	0.0013	0.9		498	3	562	8	829	25	-	-
PH-1-9-13-25-018	0.0817	0.007	0.6650	0.0180	0.0591	0.0017	0.9		506	4	518	11	569	44	506	4
PH-1-9-13-25-019	0.0810	0.006	0.6652	0.0132	0.0596	0.0013	0.9		502	4	518	8	588	30	502	4
PH-1-9-13-25-020	0.0375	0.002	0.3145	0.0065	0.0608	0.0013	0.9		238	1	278	5	631	48	-	-
PH-1-9-13-25-021	0.0316	0.002	0.2591	0.0027	0.0595	0.0008	0.9		200	1	234	2	587	13	-	-
PH-1-9-13-25-022	0.0807	0.006	0.6594	0.0147	0.0593	0.0014	0.9		500	4	514	9	578	35	500	4
PH-1-9-13-25-023	0.0825	0.005	0.6508	0.0103	0.0572	0.0011	0.9		511	3	509	6	500	23	511	3
PH-1-9-13-25-024	0.0772	0.006	0.6464	0.0141	0.0607	0.0015	0.9		480	4	506	9	630	34	480	4
PH-1-9-13-25-025	0.0376	0.002	0.3260	0.0066	0.0629	0.0013	0.9		238	1	287	5	703	46	-	-
PH-1-9-13-25-026	0.0728	0.005	0.5609	0.0099	0.0559	0.0011	0.9		453	3	452	6	447	27	453	3
PH-1-9-13-25-027	0.0791	0.006	0.6295	0.0127	0.0577	0.0013	0.9		491	3	496	8	519	31	491	3
PH-1-9-13-25-028	0.0591	0.003	0.5035	0.0047	0.0618	0.0008	0.9		370	2	414	3	668	11	-	-

PH-1-9-13-25-029	0.0278	0.002	0.1975	0.042	0.0515	0.0011	0.88		177	1	183	4	262	52		177	1
PH-1-9-13-25-030	0.0799	0.0010	0.6359	0.0294	0.0577	0.0028	0.9		496	6	500	18	520	80		496	6
PH-1-9-13-25-031	0.0795	0.0005	0.6157	0.0089	0.0562	0.0010	0.9		493	3	487	6	459	21		493	3
PH-1-9-13-25-032	0.0246	0.0001	0.2169	0.0019	0.0639	0.0008	0.9		156.7	0.9	199	2	740	9		-	-
PH-1-9-13-25-033	0.0783	0.0006	0.6144	0.0116	0.0570	0.0012	0.9		486	3	486	7	490	29		486	3
PH-1-9-13-25-034	0.0797	0.0008	0.6340	0.0211	0.0577	0.0020	0.9		495	5	499	13	518	56		495	5
PH-1-9-13-25-035	0.0749	0.0011	0.6234	0.0327	0.0604	0.0033	0.9		466	7	492	20	617	88		466	7
PH-1-9-13-25-036	0.0801	0.0008	0.6395	0.0230	0.0580	0.0022	0.9		496	5	502	14	528	61		496	5
PH-1-9-13-25-037	0.0784	0.0006	0.6327	0.0124	0.0585	0.0013	0.9		487	3	498	8	550	30		487	3
PH-1-9-13-25-038	0.0804	0.0007	0.6510	0.0197	0.0587	0.0019	0.9		499	4	509	12	557	50		499	4
PH-1-9-13-25-039	0.0753	0.0005	0.5979	0.0077	0.0576	0.0009	0.9		468	3	476	5	514	17		468	3
PH-1-9-13-25-040	0.0844	0.0015	0.7630	0.0680	0.0656	0.0060	0.89		522	9	576	39	793	198		-	-
PH-1-9-13-25-041	0.0427	0.0002	0.3497	0.0024	0.0595	0.0007	0.9		269	1	304	2	584	7		-	-
PH-1-9-13-25-042	0.0891	0.0011	0.7637	0.0329	0.0622	0.0028	0.9		550	7	576	19	681	71		550	7
PH-1-9-13-25-043	0.0919	0.0009	0.8434	0.0226	0.0666	0.0019	0.9		567	5	621	12	825	40		567	5
PH-1-9-13-25-044	0.0817	0.0007	0.6452	0.0159	0.0573	0.0015	0.9		506	4	506	10	504	40		506	4
PH-1-9-13-25-045	0.0800	0.0017	0.6340	0.0083	0.0575	0.0076	0.89		496	10	499	52	510	303		496	10
PH-1-9-13-25-046	0.0779	0.0005	0.6213	0.0086	0.0579	0.0010	0.9		483	3	491	5	526	19		483	3
PH-1-9-13-25-047	0.0806	0.0005	0.6421	0.0096	0.0578	0.0010	0.9		499	3	504	6	524	21		499	3
PH-1-9-13-25-048	0.0796	0.0006	0.6287	0.0111	0.0573	0.0011	0.9		494	3	495	7	503	27		494	3
PH-1-9-13-25-049	0.0816	0.0008	0.6976	0.0208	0.0620	0.0020	0.9		506	5	537	12	675	47		506	5
PH-1-9-13-25-050	0.0784	0.0005	0.6203	0.0077	0.0574	0.0009	0.9		487	3	490	5	506	17		487	3
PH-1-9-13-25-051	0.0812	0.0005	0.6398	0.0085	0.0572	0.0009	0.9		503	3	502	5	499	18		503	3
PH-1-9-13-25-052	0.0807	0.0005	0.6431	0.0090	0.0578	0.0010	0.9		500	3	504	6	523	19		500	3
PH-1-9-13-25-053	0.0941	0.0010	0.8446	0.0419	0.0651	0.0033	0.9		580	6	622	23	778	110		580	6
PH-1-9-13-25-054	0.0817	0.0006	0.6657	0.0127	0.0591	0.0013	0.9		506	4	518	8	571	29		506	4

PH-1-9-13-25-055	0.0763	0.006	0.6835	0.015	0.016	0.016	0.9		474	4	529	9	776	34	-	-
PH-1-9-13-25-056	0.0266	0.002	0.2422	0.006	0.019	0.019	0.9		169	1	220	6	805	63	-	-
PH-1-9-13-25-057	0.0208	0.001	0.1814	0.001	0.008	0.008	0.9		132.9	0.8	169	1	715	8	-	-
PH-1-9-13-25-058	0.0403	0.003	0.2881	0.007	0.015	0.015	0.9		255	2	257	6	279	46	255	2
PH-1-9-13-25-059	0.0803	0.007	0.6524	0.017	0.017	0.017	0.9		498	4	510	11	566	44	498	4
PH-1-9-13-25-060	0.0507	0.003	0.3949	0.010	0.015	0.015	0.88		319	2	338	7	473	61	319	2
PH-1-9-13-25-061	0.0789	0.005	0.6234	0.010	0.011	0.011	0.9		489	3	492	7	505	26	489	3
PH-1-9-13-25-062	0.0804	0.005	0.6386	0.009	0.010	0.010	0.9		498	3	501	6	517	20	498	3
PH-1-9-13-25-063	0.0836	0.006	0.6796	0.012	0.012	0.012	0.9		518	4	527	8	567	28	518	4
PH-1-9-13-25-064	0.0837	0.005	0.6908	0.009	0.010	0.010	0.9		518	3	533	6	599	18	518	3
PH-1-9-13-25-065	0.0840	0.009	0.8266	0.028	0.026	0.026	0.9		520	5	612	16	968	52	-	-
PH-1-9-13-25-066	0.0440	0.003	0.3606	0.004	0.009	0.009	0.9		277	2	313	3	587	16	-	-
PH-1-9-13-25-067	0.0532	0.003	0.4761	0.004	0.009	0.009	0.9		334	2	395	3	774	11	-	-
PH-1-9-13-25-068	0.0858	0.007	0.7045	0.017	0.016	0.016	0.9		530	4	541	10	589	38	530	4
PH-1-9-13-25-069	0.0236	0.001	0.2152	0.001	0.008	0.008	0.9		150.3	0.8	198	1	812	8	-	-
PH-1-9-13-25-070	0.0645	0.011	0.6522	0.036	0.042	0.042	0.9		403	7	510	22	1024	86	-	-
PH-1-9-13-25-071	0.0795	0.005	0.6228	0.007	0.008	0.008	0.9		493	3	492	5	485	15	493	3
PH-1-9-13-25-072	0.0818	0.006	0.6456	0.011	0.011	0.011	0.9		507	3	506	7	503	25	507	3
PH-1-9-13-25-073	0.0879	0.013	0.7612	0.040	0.034	0.034	0.9		543	8	575	23	704	87	543	8
PH-1-9-13-25-074	0.0426	0.002	0.4050	0.003	0.008	0.008	0.9		269	1	345	2	901	8	-	-
PH-1-9-13-25-075	0.0825	0.006	0.6535	0.012	0.012	0.012	0.9		511	4	511	8	511	29	511	4
PH-1-9-13-25-076	0.0511	0.003	0.4404	0.005	0.010	0.010	0.9		321	2	371	4	692	16	-	-
PH-1-9-13-25-077	0.0811	0.006	0.6398	0.014	0.014	0.014	0.9		503	4	502	9	501	37	503	4
PH-1-9-13-25-078	0.0276	0.002	0.2338	0.002	0.009	0.009	0.9		176	1	213	2	655	16	-	-
PH-1-9-13-25-079	0.0806	0.006	0.6484	0.014	0.014	0.014	0.9		500	4	507	9	544	36	500	4
PH-1-9-13-25-080	0.0834	0.008	0.6659	0.020	0.019	0.019	0.9		516	5	518	13	528	51	516	5

PH-1-9-13-25-081	0.0834	0.006	0.6760	0.0120	0.0588	0.0012	0.9		516	3	524	7	561	26		516	3
PH-1-9-13-25-082	0.0420	0.002	0.3760	0.0033	0.0649	0.0008	0.9		265	1	324	2	771	10	-	-	-
PH-1-9-13-25-083	0.0765	0.005	0.6040	0.0063	0.0573	0.0008	0.9		475	3	480	4	504	13	475	3	
PH-1-9-13-25-084	0.0809	0.005	0.7008	0.0091	0.0629	0.0010	0.9		501	3	539	5	705	17	501	3	
PH-1-9-13-25-085	0.0145	0.001	0.1244	0.0016	0.0622	0.0010	0.9		92.9	0.6	119	1	680	17	-	-	-
PH-1-9-13-25-086	0.0852	0.007	0.7082	0.00149	0.0604	0.0014	0.9		527	4	544	9	616	32	527	4	
PH-1-9-13-25-087	0.0841	0.007	0.8836	0.0193	0.0763	0.0018	0.9		520	4	643	10	1102	30	-	-	-
PH-1-9-13-25-088	0.0813	0.005	0.6612	0.0106	0.0590	0.0011	0.9		504	3	515	6	568	23	504	3	
PH-1-9-13-25-089	0.0183	0.001	0.2093	0.0020	0.0828	0.0011	0.9		117.2	0.7	193	2	1264	9	-	-	-
PH-1-9-13-25-090	0.0794	0.006	0.6302	0.0142	0.0576	0.0014	0.9		493	4	496	9	514	36	493	4	
PH-1-9-13-25-091	0.0559	0.003	0.4731	0.0038	0.0614	0.0007	0.9		351	2	393	3	653	8	-	-	-
PH-1-9-13-25-092	0.0652	0.004	0.5354	0.0055	0.0596	0.0008	0.9		407	2	435	4	589	13	407	2	
PH-1-9-13-25-093	0.0206	0.001	0.1828	0.0014	0.0645	0.0008	0.9		131.3	0.7	170	1	757	8	-	-	-
PH-1-9-13-25-094	0.0797	0.005	0.6363	0.0084	0.0579	0.0009	0.9		495	3	500	5	526	18	495	3	
PH-1-9-13-25-095	0.0809	0.007	0.6414	0.0163	0.0575	0.0016	0.9		501	4	503	10	512	41	501	4	
PH-1-9-13-25-096	0.0840	0.006	0.6913	0.0128	0.0598	0.0012	0.9		520	4	534	8	595	28	520	4	
PH-1-9-13-25-097	0.0883	0.013	0.7174	0.0357	0.0590	0.0030	0.9		545	7	549	21	566	84	545	7	
PH-1-9-13-25-098	0.0520	0.004	0.4613	0.0116	0.0643	0.0018	0.9		327	3	385	8	752	39	-	-	-
PH-1-9-13-25-099	0.0746	0.005	0.5942	0.0080	0.0578	0.0009	0.9		464	3	474	5	523	18	464	3	
PH-1-9-13-25-100	0.0839	0.006	0.6692	0.0128	0.0579	0.0012	0.9		520	4	520	8	524	29	520	4	
	$^{206}\text{Pb}/^{238}\text{U}$	± 1 s.e.	$^{207}\text{Pb}/^{235}\text{U}$	± 1 s.e.	$^{207}\text{Pb}/^{206}$ Pb	± 1 s.e.	Error corr.		$^{206}\text{Pb}/^{238}\text{U}$	± 1 s.e.	$^{207}\text{Pb}/^{235}\text{U}$	± 1 s.e.	$^{207}\text{Pb}/^{206}$ Pb	± 1 s.e.	(Ma)	\pm (Ma)	
PH-1-3-13-11B-001	0.1764	0.010	1.8083	0.0127	0.0744	0.0008	0.9		1047	5	1048	5	1051	6	1051	6	
PH-1-3-13-11B-002	0.2045	0.012	2.2645	0.0196	0.0804	0.0010	0.9		1199	6	1201	6	1206	8	1206	8	
PH-1-3-13-11B-003	0.2075	0.013	2.3109	0.0215	0.0808	0.0010	0.9		1216	7	1216	7	1216	9	1216	9	
PH-1-3-13-11B-004	0.1923	0.012	2.0550	0.0203	0.0775	0.0010	0.9		1134	6	1134	7	1135	10	1135	10	

PH-1-3-13-11B-005	0.2228	0.013	2.5822	0.020	0.0841	0.0010	0.9		1297	7	1296	6	1295	7		1295	7
PH-1-3-13-11B-006	0.2065	0.012	2.3749	0.018	0.0835	0.0010	0.9		1210	6	1235	5	1280	7		1280	7
PH-1-3-13-11B-007	0.2220	0.013	2.5813	0.018	0.0844	0.0009	0.9		1292	7	1295	5	1301	6		1301	6
PH-1-3-13-11B-008	0.2186	0.012	2.5370	0.017	0.0842	0.0009	0.9		1274	6	1283	5	1297	6		1297	6
PH-1-3-13-11B-009	0.2029	0.012	2.2392	0.017	0.0801	0.0009	0.9		1191	6	1193	5	1198	7		1198	7
PH-1-3-13-11B-010	0.2216	0.013	2.5531	0.028	0.0836	0.0011	0.9		1290	7	1287	8	1283	25		1283	25
PH-1-3-13-11B-011	0.1385	0.008	1.4205	0.009	0.0744	0.0007	0.88		836	4	898	4	1053	18		836	4
PH-1-3-13-11B-012	0.1592	0.009	1.6204	0.020	0.0738	0.0010	0.88		952	5	978	8	1037	29		952	5
PH-1-3-13-11B-013	0.1634	0.009	1.6132	0.013	0.0716	0.0007	0.88		976	5	975	5	975	21		976	5
PH-1-3-13-11B-014	0.1119	0.006	1.0597	0.007	0.0687	0.0006	0.88		684	4	734	4	890	19		684	4
PH-1-3-13-11B-015	0.1230	0.007	1.1859	0.007	0.0699	0.0006	0.89		748	4	794	3	926	17		748	4
PH-1-3-13-11B-016	0.0861	0.005	0.8257	0.006	0.0696	0.0007	0.88		532	3	611	4	916	20		-	-
PH-1-3-13-11B-017	0.2252	0.013	2.6305	0.021	0.0848	0.0010	0.9		1309	7	1309	6	1310	8		1310	8
PH-1-3-13-11B-018	0.1555	0.009	1.5091	0.012	0.0704	0.0007	0.88		932	5	934	5	940	21		932	5
PH-1-3-13-11B-019	0.0813	0.005	0.7833	0.005	0.0699	0.0006	0.88		504	3	587	3	925	19		-	-
PH-1-3-13-11B-020	0.1882	0.011	1.9938	0.016	0.0769	0.0009	0.9		1111	6	1113	6	1118	8		1118	8
PH-1-3-13-11B-021	0.1572	0.009	1.5344	0.010	0.0708	0.0008	0.9		941	5	944	4	953	6		941	5
PH-1-3-13-11B-022	0.1552	0.009	1.4994	0.010	0.0701	0.0008	0.9		930	5	930	4	931	6		930	5
PH-1-3-13-11B-023	0.2104	0.012	2.3645	0.017	0.0815	0.0009	0.9		1231	6	1232	5	1234	7		1234	7
PH-1-3-13-11B-024	0.1556	0.009	1.5006	0.009	0.0700	0.0008	0.9		932	5	931	4	927	6		932	5
PH-1-3-13-11B-025	0.1229	0.007	1.1743	0.009	0.0693	0.0007	0.88		747	4	789	4	908	21		747	4
PH-1-3-13-11B-026	0.2083	0.013	2.3246	0.020	0.0810	0.0010	0.9		1220	7	1220	6	1220	9		1220	9
PH-1-3-13-11B-027	0.2140	0.014	2.4177	0.025	0.0820	0.0011	0.9		1250	7	1248	8	1245	11		1245	11
PH-1-3-13-11B-028	0.2198	0.013	2.5272	0.020	0.0834	0.0010	0.9		1281	7	1280	6	1279	8		1279	8
PH-1-3-13-11B-029	0.2229	0.014	2.5904	0.025	0.0843	0.0011	0.9		1297	7	1298	7	1300	10		1300	10
PH-1-3-13-11B-030	0.2155	0.013	2.4541	0.019	0.0826	0.0010	0.9		1258	7	1259	6	1260	7		1260	7

PH-1-3-13-11B-031	0.2187	0.013	2.5030	0.0196	0.08300	0.0010	0.9		1275	7	1273	6	1270	7		1270	7
PH-1-3-13-11B-032	0.1867	0.011	2.0135	0.0173	0.07820	0.0008	0.88		1103	6	1120	6	1153	21		1153	21
PH-1-3-13-11B-033	0.1664	0.010	1.6689	0.0137	0.07280	0.0009	0.9		992	5	997	5	1008	8		992	5
PH-1-3-13-11B-034	0.0867	0.005	0.8164	0.0056	0.06830	0.0006	0.88		536	3	606	3	877	18		-	-
PH-1-3-13-11B-035	0.1860	0.013	1.9521	0.0293	0.07610	0.0013	0.9		1100	7	1099	10	1099	19		1099	19
PH-1-3-13-11B-036	0.1341	0.007	1.2846	0.0082	0.06950	0.0006	0.88		811	4	839	4	913	18		811	4
PH-1-3-13-11B-037	0.2082	0.012	2.3209	0.0159	0.08090	0.0009	0.9		1219	6	1219	5	1218	6		1218	6
PH-1-3-13-11B-038	0.0655	0.004	0.6186	0.0039	0.06850	0.0006	0.89		409	2	489	2	884	18		-	-
PH-1-3-13-11B-039	0.1469	0.008	1.3933	0.0104	0.06880	0.0008	0.9		884	5	886	4	893	7		884	5
PH-1-3-13-11B-040	0.2145	0.012	2.4322	0.0194	0.08230	0.0010	0.9		1253	7	1252	6	1252	8		1252	8
PH-1-3-13-11B-041	0.1921	0.011	2.0505	0.0146	0.07740	0.0009	0.9		1133	6	1132	5	1132	7		1132	7
PH-1-3-13-11B-042	0.1566	0.009	1.5030	0.0098	0.06960	0.0008	0.9		938	5	932	4	917	6		938	5
PH-1-3-13-11B-043	0.2183	0.012	2.5035	0.0182	0.08320	0.0009	0.9		1273	7	1273	5	1274	7		1274	7
PH-1-3-13-11B-044	0.1606	0.009	1.5631	0.0106	0.07060	0.0008	0.9		960	5	956	4	946	6		960	5
PH-1-3-13-11B-045	0.1513	0.008	1.4629	0.0113	0.07010	0.0007	0.88		908	5	915	5	932	20		908	5
PH-1-3-13-11B-046	0.1768	0.010	1.8263	0.0136	0.07490	0.0009	0.9		1050	5	1055	5	1067	7		1067	7
PH-1-3-13-11B-047	0.2160	0.012	2.4649	0.0155	0.08280	0.0009	0.9		1261	6	1262	5	1264	5		1264	5
PH-1-3-13-11B-048	0.1517	0.009	1.4881	0.0114	0.07120	0.0008	0.9		911	5	926	5	962	7		911	5
PH-1-3-13-11B-049	0.1783	0.010	1.8549	0.0155	0.07550	0.0009	0.9		1058	6	1065	6	1081	8		1081	8
PH-1-3-13-11B-050	0.2013	0.012	2.2050	0.0176	0.07950	0.0009	0.9		1182	6	1183	6	1184	8		1184	8
PH-1-3-13-11B-051	0.1537	0.008	1.4703	0.0093	0.06940	0.0007	0.9		922	5	918	4	910	6		922	5
PH-1-3-13-11B-052	0.1091	0.006	1.0355	0.0065	0.06880	0.0006	0.89		668	3	722	3	894	17		668	3
PH-1-3-13-11B-053	0.0849	0.005	0.7587	0.0071	0.06480	0.0007	0.86		525	3	573	4	769	23		525	3
PH-1-3-13-11B-054	0.1507	0.008	1.4378	0.0102	0.06920	0.0008	0.9		905	5	905	4	905	7		905	5
PH-1-3-13-11B-055	0.1250	0.007	1.2038	0.0085	0.06990	0.0006	0.88		759	4	802	4	924	19		759	4
PH-1-3-13-11B-056	0.1936	0.011	2.0950	0.0182	0.07850	0.0010	0.9		1141	6	1147	6	1160	9		1160	9

PH-1-3-13-11B-057	0.2060	0.011	2.2831	0.014	0.0804	0.009	0.9		1207	6	1207	4	1207	6		1207	6
PH-1-3-13-11B-058	0.2158	0.013	2.4844	0.019	0.0835	0.010	0.9		1260	7	1267	6	1281	7		1281	7
PH-1-3-13-11B-059	0.2137	0.012	2.4176	0.019	0.0821	0.010	0.9		1248	7	1248	6	1247	8		1247	8
PH-1-3-13-11B-060	0.0919	0.005	0.8550	0.006	0.0675	0.006	0.88		567	3	627	3	853	19	-	-	-
PH-1-3-13-11B-061	0.1535	0.008	1.4738	0.009	0.0697	0.007	0.9		920	5	920	4	919	6		920	5
PH-1-3-13-11B-062	0.1918	0.011	2.0532	0.015	0.0777	0.009	0.9		1131	6	1133	5	1138	7		1138	7
PH-1-3-13-11B-063	0.1495	0.008	1.4312	0.009	0.0695	0.008	0.9		898	5	902	4	912	6		898	5
PH-1-3-13-11B-064	0.1572	0.009	1.5322	0.010	0.0707	0.008	0.9		941	5	943	4	948	6		941	5
PH-1-3-13-11B-065	0.1261	0.007	1.2062	0.009	0.0694	0.008	0.9		765	4	803	4	911	8		765	4
PH-1-3-13-11B-066	0.1620	0.009	1.6172	0.012	0.0724	0.008	0.9		968	5	977	5	998	7		968	5
PH-1-3-13-11B-067	0.2163	0.012	2.4706	0.018	0.0829	0.010	0.9		1262	7	1263	6	1266	7		1266	7
PH-1-3-13-11B-068	0.0591	0.003	0.5535	0.003	0.0680	0.006	0.88		370	2	447	2	868	18			
PH-1-3-13-11B-069	0.1218	0.007	1.1639	0.011	0.0693	0.008	0.88		741	4	784	5	909	24		741	4
PH-1-3-13-11B-070	0.2065	0.012	2.3682	0.016	0.0832	0.009	0.9		1210	6	1233	5	1274	6		1274	6
PH-1-3-13-11B-071	0.1660	0.009	1.6495	0.011	0.0721	0.008	0.9		990	5	989	4	989	7		990	5
PH-1-3-13-11B-072	0.2173	0.013	2.4907	0.022	0.0832	0.010	0.9		1267	7	1269	7	1273	9		1273	9
PH-1-3-13-11B-073	0.1751	0.010	1.7862	0.013	0.0740	0.008	0.9		1040	5	1040	5	1041	7		1041	7
PH-1-3-13-11B-074	0.1162	0.006	1.1170	0.007	0.0697	0.006	0.88		708	4	762	4	921	18		708	4
PH-1-3-13-11B-075	0.0831	0.005	0.7816	0.005	0.0682	0.006	0.88		515	3	586	3	875	18	-	-	-
PH-1-3-13-11B-076	0.2189	0.012	2.5227	0.017	0.0836	0.009	0.9		1276	6	1279	5	1283	6		1283	6
PH-1-3-13-11B-077	0.1453	0.008	1.3711	0.008	0.0685	0.007	0.9		874	4	877	4	883	6		874	4
PH-1-3-13-11B-078	0.1479	0.009	1.4207	0.016	0.0697	0.009	0.87		889	5	898	7	919	28		889	5
PH-1-3-13-11B-079	0.2141	0.012	2.4422	0.018	0.0828	0.010	0.9		1250	6	1255	5	1264	7		1264	7
PH-1-3-13-11B-080	0.2282	0.013	2.6888	0.018	0.0855	0.009	0.9		1325	7	1325	5	1326	6		1326	6
PH-1-3-13-11B-081	0.2234	0.013	2.6047	0.020	0.0846	0.010	0.9		1300	7	1302	6	1306	8		1306	8
PH-1-3-13-11B-082	0.2248	0.013	2.6327	0.020	0.0850	0.010	0.9		1307	7	1310	6	1314	7		1314	7

PH-1-3-13-11B-083	0.1425	0.008	1.3605	0.0080	0.0692	0.0006	0.89		859	4	872	3	906	17		859	4
PH-1-3-13-11B-084	0.1072	0.006	0.9961	0.0075	0.0674	0.0006	0.88		656	3	702	4	850	20		656	3
PH-1-3-13-11B-085	0.1210	0.007	1.1387	0.0076	0.0683	0.0006	0.88		736	4	772	4	877	18		736	4
PH-1-3-13-11B-086	0.2161	0.013	2.4733	0.0197	0.0830	0.0010	0.9		1261	7	1264	6	1270	7		1270	7
PH-1-3-13-11B-087	0.2152	0.012	2.4462	0.0167	0.0825	0.0009	0.9		1256	6	1256	5	1257	6		1257	6
PH-1-3-13-11B-088	0.1797	0.010	1.8874	0.0136	0.0762	0.0009	0.9		1065	5	1077	5	1101	7		1101	7
PH-1-3-13-11B-089	0.1527	0.008	1.4641	0.0092	0.0696	0.0007	0.9		916	5	916	4	916	6		916	5
PH-1-3-13-11B-090	0.1960	0.011	2.1241	0.0149	0.0786	0.0009	0.9		1154	6	1157	5	1163	6		1163	6
PH-1-3-13-11B-091	0.2129	0.012	2.4143	0.0159	0.0823	0.0009	0.9		1244	6	1247	5	1252	6		1252	6
PH-1-3-13-11B-092	0.1541	0.008	1.4786	0.0096	0.0696	0.0008	0.9		924	5	922	4	917	6		924	5
PH-1-3-13-11B-093	0.0845	0.005	0.7928	0.0049	0.0681	0.0006	0.88		523	3	593	3	870	17	-	-	-
PH-1-3-13-11B-094	0.1655	0.009	1.6536	0.0112	0.0725	0.0008	0.9		987	5	991	4	1000	6		987	5
PH-1-3-13-11B-095	0.2149	0.012	2.4463	0.0147	0.0826	0.0009	0.9		1255	6	1256	4	1259	5		1259	5
PH-1-3-13-11B-096	0.1854	0.012	1.9424	0.0215	0.0760	0.0011	0.9		1096	6	1096	7	1095	12		1095	12
PH-1-3-13-11B-097	0.2000	0.012	2.1978	0.0176	0.0797	0.0009	0.9		1176	6	1180	6	1190	8		1190	8
PH-1-3-13-11B-098	0.1484	0.008	1.4114	0.0088	0.0690	0.0007	0.9		892	5	894	4	898	6		892	5
PH-1-3-13-11B-099	0.1558	0.009	1.5114	0.0101	0.0704	0.0008	0.9		933	5	935	4	939	6		933	5
PH-1-3-13-11B-100	0.1905	0.011	2.0382	0.0143	0.0776	0.0009	0.9		1124	6	1128	5	1137	6		1137	6
	$^{206}\text{Pb}/^{238}\text{U}$	± 1 s.e.	$^{207}\text{Pb}/^{235}\text{U}$	± 1 s.e.	$^{207}\text{Pb}/^{206}\text{Pb}$	± 1 s.e.	Error corr.		$^{206}\text{Pb}/^{238}\text{U}$	± 1 s.e.	$^{207}\text{Pb}/^{235}\text{U}$	± 1 s.e.	$^{207}\text{Pb}/^{206}\text{Pb}$	± 1 s.e.	(Ma)	\pm (Ma)	
PH-1-9-13-23-001	0.3226	0.021	4.8414	0.0429	0.1089	0.0013	0.9		1802	10	1792	7	1781	8		1781	8
PH-1-9-13-23-002	0.2943	0.018	4.1743	0.0323	0.1029	0.0012	0.9		1663	9	1669	6	1677	7		1677	7
PH-1-9-13-23-003	0.3041	0.019	4.4653	0.0358	0.1065	0.0012	0.9		1712	10	1725	7	1741	7		1741	7
PH-1-9-13-23-004	0.3068	0.019	4.4515	0.0322	0.1053	0.0012	0.9		1725	9	1722	6	1719	6		1719	6
PH-1-9-13-23-005	0.2958	0.019	4.1817	0.0368	0.1026	0.0012	0.9		1670	9	1670	7	1671	8		1671	8
PH-1-9-13-23-006	0.2889	0.021	4.1431	0.0481	0.1040	0.0015	0.9		1636	10	1663	10	1697	11		1697	11

PH-1-9-13-23-007	0.2727	0.017	3.6848	0.0384	0.0980	0.013	0.9		1555	9	1568	8	1587	10		1587	10
PH-1-9-13-23-008	0.3107	0.020	4.5664	0.0377	0.1066	0.012	0.9		1744	10	1743	7	1743	7		1743	7
PH-1-9-13-23-009	0.2351	0.015	2.8189	0.0266	0.0870	0.011	0.9		1361	8	1361	7	1360	9		1360	9
PH-1-9-13-23-010	0.2932	0.019	4.1493	0.0359	0.1027	0.012	0.9		1657	9	1664	7	1673	8		1673	8
PH-1-9-13-23-011	0.2596	0.017	3.2699	0.0296	0.0914	0.011	0.9		1488	9	1474	7	1455	8		1455	8
PH-1-9-13-23-012	0.2714	0.017	3.5943	0.0306	0.0961	0.011	0.9		1548	9	1548	7	1550	8		1550	8
PH-1-9-13-23-013	0.2542	0.016	3.2249	0.0334	0.0920	0.012	0.9		1460	8	1463	8	1468	10		1468	10
PH-1-9-13-23-014	0.2739	0.017	3.6517	0.0295	0.0967	0.011	0.9		1561	9	1561	6	1562	7		1562	7
PH-1-9-13-23-015	0.3009	0.020	4.3045	0.0404	0.1038	0.013	0.9		1696	10	1694	8	1693	8		1693	8
PH-1-9-13-23-016	0.2830	0.022	3.9551	0.0723	0.1014	0.020	0.89		1607	11	1625	15	1649	38		1649	38
PH-1-9-13-23-017	0.3013	0.020	4.3300	0.0410	0.1043	0.013	0.9		1698	10	1699	8	1701	9		1701	9
PH-1-9-13-23-018	0.2988	0.022	4.2724	0.0578	0.1038	0.016	0.9		1685	11	1688	11	1692	14		1692	14
PH-1-9-13-23-019	0.3119	0.020	4.5753	0.0373	0.1064	0.012	0.9		1750	10	1745	7	1739	7		1739	7
PH-1-9-13-23-020	0.3185	0.024	4.7969	0.0653	0.1093	0.017	0.9		1783	12	1784	11	1787	14		1787	14
PH-1-9-13-23-021	0.2239	0.014	2.6127	0.0212	0.0847	0.010	0.9		1302	7	1304	6	1308	7		1308	7
PH-1-9-13-23-022	0.2688	0.018	3.5531	0.0350	0.0959	0.012	0.9		1535	9	1539	8	1546	9		1546	9
PH-1-9-13-23-023	0.3050	0.020	4.4268	0.0391	0.1053	0.013	0.9		1716	10	1717	7	1720	8		1720	8
PH-1-9-13-23-024	0.2655	0.017	3.4398	0.0285	0.0940	0.011	0.9		1518	9	1514	7	1508	7		1508	7
PH-1-9-13-23-025	0.2907	0.020	4.3921	0.0462	0.1096	0.015	0.9		1645	10	1711	9	1793	10		1793	10
PH-1-9-13-23-026	0.2244	0.014	2.6231	0.0266	0.0848	0.011	0.9		1305	8	1307	7	1311	10		1311	10
PH-1-9-13-23-027	0.2887	0.022	4.0358	0.0700	0.1014	0.020	0.9		1635	11	1641	14	1650	21		1650	21
PH-1-9-13-23-028	0.2237	0.014	2.6025	0.0208	0.0844	0.010	0.9		1302	7	1301	6	1302	7		1302	7
PH-1-9-13-23-029	0.3008	0.020	4.2915	0.0389	0.1035	0.013	0.9		1695	10	1692	7	1688	8		1688	8
PH-1-9-13-23-030	0.1765	0.012	1.8116	0.0261	0.0745	0.012	0.9		1048	6	1050	9	1054	19		1054	19
PH-1-9-13-23-031	0.2174	0.015	2.4801	0.0331	0.0828	0.013	0.9		1268	8	1266	10	1264	15		1264	15
PH-1-9-13-23-032	0.3035	0.024	4.3817	0.0601	0.1047	0.017	0.9		1709	12	1709	11	1710	14		1710	14

PH-1-9-13-23-033	0.3112	0.026	4.6327	0.0702	0.1080	0.019	0.9		1747	13	1755	13	1766	16		1766	16
PH-1-9-13-23-034	0.2420	0.017	2.9465	0.0358	0.0884	0.0013	0.9		1397	9	1394	9	1390	13		1390	13
PH-1-9-13-23-035	0.2313	0.014	2.7722	0.0196	0.0869	0.0008	0.89		1341	7	1348	5	1359	18		1359	18
PH-1-9-13-23-036	0.3074	0.023	4.5110	0.0522	0.1065	0.0015	0.9		1728	11	1733	10	1740	11		1740	11
PH-1-9-13-23-037	0.2735	0.017	3.6758	0.0282	0.0975	0.0011	0.9		1558	9	1566	6	1577	7		1577	7
PH-1-9-13-23-038	0.2740	0.018	3.9032	0.0432	0.1033	0.0013	0.9		1561	9	1614	9	1684	24		1684	24
PH-1-9-13-23-039	0.2503	0.018	3.0990	0.0443	0.0898	0.0015	0.9		1440	9	1432	11	1422	17		1422	17
PH-1-9-13-23-040	0.3029	0.019	4.3508	0.0322	0.1042	0.0012	0.9		1706	9	1703	6	1700	6		1700	6
PH-1-9-13-23-041	0.2851	0.021	3.9224	0.0651	0.0998	0.0018	0.9		1617	11	1618	13	1620	35		1620	35
PH-1-9-13-23-042	0.3044	0.020	4.3705	0.0406	0.1042	0.0013	0.9		1713	10	1707	8	1700	8		1700	8
PH-1-9-13-23-043	0.3087	0.020	4.5566	0.0397	0.1071	0.0013	0.9		1734	10	1741	7	1750	7		1750	7
PH-1-9-13-23-044	0.2756	0.023	3.6742	0.0737	0.0967	0.0021	0.9		1569	12	1566	16	1562	25		1562	25
PH-1-9-13-23-045	0.3090	0.021	4.8005	0.0471	0.1127	0.0014	0.9		1736	10	1785	8	1843	9		1843	9
PH-1-9-13-23-046	0.3138	0.021	4.6626	0.0403	0.1078	0.0013	0.9		1759	10	1761	7	1763	7		1763	7
PH-1-9-13-23-047	0.3084	0.021	4.5680	0.0443	0.1075	0.0014	0.9		1733	10	1743	8	1757	9		1757	9
PH-1-9-13-23-048	0.2649	0.018	3.4486	0.0334	0.0945	0.0012	0.9		1515	9	1516	8	1517	9		1517	9
PH-1-9-13-23-049	0.3138	0.021	4.5757	0.0407	0.1058	0.0013	0.9		1759	10	1745	7	1728	8		1728	8
PH-1-9-13-23-050	0.2628	0.017	3.3946	0.0365	0.0937	0.0013	0.9		1504	9	1503	8	1503	11		1503	11
PH-1-9-13-23-051	0.2520	0.023	3.1608	0.0763	0.0910	0.0023	0.9		1449	12	1448	19	1447	32		1447	32
PH-1-9-13-23-052	0.2357	0.015	2.8450	0.0255	0.0876	0.0011	0.9		1364	8	1367	7	1373	8		1373	8
PH-1-9-13-23-053	0.3270	0.029	5.0471	0.0766	0.1120	0.0019	0.9		1824	14	1827	13	1831	15		1831	15
PH-1-9-13-23-054	0.2732	0.019	3.6220	0.0423	0.0962	0.0014	0.9		1557	10	1554	9	1551	12		1551	12
PH-1-9-13-23-055	0.3049	0.019	4.4218	0.0330	0.1052	0.0012	0.9		1716	9	1716	6	1718	6		1718	6
PH-1-9-13-23-056	0.2327	0.014	2.7749	0.0200	0.0865	0.0009	0.9		1349	8	1349	5	1350	6		1350	6
PH-1-9-13-23-057	0.2862	0.021	3.9346	0.0477	0.0998	0.0015	0.9		1622	10	1621	10	1619	12		1619	12
PH-1-9-13-23-058	0.2883	0.019	3.9850	0.0345	0.1003	0.0012	0.9		1633	9	1631	7	1629	8		1629	8

PH-1-9-13-23-059	0.2626	0.019	3.4854	0.0389	0.0963	0.013	0.9		1503	9	1524	9	1554	11		1554	11
PH-1-9-13-23-060	0.2622	0.018	3.3693	0.0351	0.0932	0.012	0.9		1501	9	1497	8	1492	10		1492	10
PH-1-9-13-23-061	0.3050	0.021	4.4036	0.0409	0.1047	0.013	0.9		1716	10	1713	8	1710	8		1710	8
PH-1-9-13-23-062	0.3035	0.021	4.4249	0.0422	0.1058	0.013	0.9		1709	10	1717	8	1728	9		1728	9
PH-1-9-13-23-063	0.2966	0.020	4.2023	0.0392	0.1028	0.013	0.9		1675	10	1674	8	1675	8		1675	8
PH-1-9-13-23-064	0.3043	0.019	4.4383	0.0333	0.1058	0.012	0.9		1712	9	1720	6	1729	6		1729	6
PH-1-9-13-23-065	0.2393	0.015	2.9114	0.0220	0.0883	0.010	0.9		1383	8	1385	6	1389	7		1389	7
PH-1-9-13-23-066	0.3038	0.022	4.6215	0.0500	0.1104	0.015	0.9		1710	11	1753	9	1805	10		1805	10
PH-1-9-13-23-067	0.2229	0.014	2.6302	0.0222	0.0856	0.009	0.88		1297	7	1309	6	1328	21		1328	21
PH-1-9-13-23-068	0.2866	0.018	3.9692	0.0328	0.1005	0.012	0.9		1625	9	1628	7	1633	7		1633	7
PH-1-9-13-23-069	0.3089	0.020	4.5610	0.0388	0.1071	0.013	0.9		1735	10	1742	7	1751	7		1751	7
PH-1-9-13-23-070	0.3030	0.020	4.4687	0.0362	0.1070	0.012	0.9		1706	10	1725	7	1749	7		1749	7
PH-1-9-13-23-071	0.2695	0.023	3.7582	0.0847	0.1011	0.024	0.9		1538	12	1584	18	1645	46		1645	46
PH-1-9-13-23-072	0.2742	0.021	3.6466	0.0667	0.0965	0.019	0.9		1562	11	1560	15	1557	23		1557	23
PH-1-9-13-23-073	0.3035	0.022	4.3771	0.0488	0.1046	0.014	0.9		1709	11	1708	9	1708	11		1708	11
PH-1-9-13-23-074	0.2924	0.020	4.1009	0.0431	0.1018	0.014	0.9		1653	10	1654	9	1656	10		1656	10
PH-1-9-13-23-075	0.2749	0.020	3.6800	0.0430	0.0971	0.014	0.9		1566	10	1567	9	1570	12		1570	12
PH-1-9-13-23-076	0.2668	0.018	3.4914	0.0342	0.0949	0.012	0.9		1525	9	1525	8	1527	9		1527	9
PH-1-9-13-23-077	0.2254	0.014	2.6462	0.0202	0.0852	0.010	0.9		1310	7	1314	6	1319	7		1319	7
PH-1-9-13-23-078	0.1965	0.013	2.1327	0.0188	0.0787	0.009	0.9		1156	7	1159	6	1166	8		1166	8
PH-1-9-13-23-079	0.3087	0.022	4.5860	0.0484	0.1078	0.014	0.9		1734	11	1747	9	1762	10		1762	10
PH-1-9-13-23-080	0.2298	0.015	2.7054	0.0257	0.0854	0.011	0.9		1333	8	1330	7	1325	9		1325	9
PH-1-9-13-23-081	0.2858	0.020	3.9251	0.0420	0.0996	0.013	0.9		1620	10	1619	9	1617	10		1617	10
PH-1-9-13-23-082	0.3025	0.024	4.3758	0.0594	0.1050	0.017	0.9		1704	12	1708	11	1713	14		1713	14
PH-1-9-13-23-083	0.3081	0.022	4.5488	0.0503	0.1071	0.015	0.9		1731	11	1740	9	1751	10		1751	10
PH-1-9-13-23-084	0.3068	0.022	4.5013	0.0485	0.1065	0.014	0.9		1725	11	1731	9	1740	10		1740	10

PH-1-9-13-23-085	0.235 6	0.0 017	2.851 9	0.0 35 0	0.0878 0.0 013	0.9 0.9		1364 1683	9 10	1369 1688	9 8	1379 1694	13 9		1379 1694	13 9
PH-1-9-13-23-086	0.298 4	0.0 020	4.270 6	0.0 40 9	0.1038 0.0 013	0.9 0.9		1737 1580	12 10	1750 1583	10 8	1766 1586	12 10		1766 1586	12 10
PH-1-9-13-23-087	0.309 2	0.0 024	4.603 3	0.0 57 0	0.1080 0.0 016	0.9 0.9		1552 1693	10 10	1549 1705	13 8	1545 1719	18 9		1545 1719	18 9
PH-1-9-13-23-088	0.277 8	0.0 019	3.751 9	0.0 38 2	0.0980 0.0 013	0.9 0.9		1603 1592	10 9	1607 1582	8 8	1613 1570	9 9		1613 1570	9 9
PH-1-9-13-23-089	0.272 1	0.0 021	3.595 8	0.0 56 7	0.0959 0.0 017	0.9 0.9		1740 1653	12 12	1747 1650	10 11	1756 1647	12 15		1756 1647	12 15
PH-1-9-13-23-090	0.300 4	0.0 020	4.359 1	0.0 42 0	0.1053 0.0 013	0.9 0.9		1158 1161	7 7	1161 1165	7 9	1165 1165	9 9		1165 1165	9 9
PH-1-9-13-23-091	0.282 4	0.0 019	3.869 3	0.0 38 2	0.0994 0.0 013	0.9 0.9		1659 1647	10 10	1659 1659	9 9	1659 1659	10 10		1659 1659	10 10
PH-1-9-13-23-092	0.280 2	0.0 019	3.751 7	0.0 35 6	0.0971 0.0 012	0.9 0.9		1592 1570	9 9	1582 1570	8 8	1570 1570	9 9		1570 1570	9 9
PH-1-9-13-23-093	0.309 9	0.0 024	4.587 2	0.0 56 3	0.1074 0.0 016	0.9 0.9		1740 1653	12 12	1747 1650	10 11	1756 1647	12 15		1756 1647	12 15
PH-1-9-13-23-094	0.292 3	0.0 023	4.077 9	0.0 57 4	0.1012 0.0 016	0.9 0.9		1628 1659	11 10	1651 1659	10 9	1682 1659	12 10		1682 1659	12 10
PH-1-9-13-23-095	0.287 3	0.0 022	4.085 8	0.0 50 0	0.1032 0.0 015	0.9 0.9		1694 1699	11 15	1695 1699	10 16	1698 1700	12 22		1698 1700	12 22
PH-1-9-13-23-096	0.196 9	0.0 013	2.136 1	0.0 20 3	0.0787 0.0 010	0.9 0.9		1158 1161	7 7	1161 1165	7 9	1165 1165	9 9		1165 1165	9 9
PH-1-9-13-23-097	0.293 6	0.0 020	4.123 8	0.0 44 8	0.1019 0.0 014	0.9 0.9		1659 1747	10 15	1659 1750	9 15	1659 1755	10 19		1659 1755	10 19
PH-1-9-13-23-098	0.300 5	0.0 022	4.309 7	0.0 50 7	0.1041 0.0 015	0.9 0.9		1694 1747	11 15	1695 1750	10 15	1698 1755	12 19		1698 1755	12 19
PH-1-9-13-23-099	0.301 5	0.0 030	4.329 1	0.0 84 9	0.1042 0.0 022	0.9 0.9		1699 1747	15 15	1699 1750	16 15	1700 1755	22 19		1700 1755	22 19
PH-1-9-13-23-100	0.311 2	0.0 030	4.605 2	0.0 82 8	0.1074 0.0 021	0.9 0.9		1747 1747	15 15	1750 1750	15 15	1755 1755	19 19		1755 1755	19 19
	$^{206}\text{Pb}/^{238}\text{U}$	± 1 s.e.	$^{207}\text{Pb}/^{235}\text{U}$	± 1 s.e.	$^{207}\text{Pb}/^{206}\text{Pb}$	± 1 s.e.	Error corr.		$^{206}\text{Pb}/^{238}\text{U}$	± 1 s.e.	$^{207}\text{Pb}/^{235}\text{U}$	± 1 s.e.	$^{207}\text{Pb}/^{206}\text{Pb}$	± 1 s.e.	(Ma)	\pm (Ma)
PH-1-12-13-5-001	0.470 5	0.0 028	10.56 33	0.0 75 1	0.1629 0.0 018	0.9 0.9		2486 2485	12 7	2485 2486	7 5	2486 2486	5 5		2486 2486	5 5
PH-1-12-13-5-002	0.311 8	0.0 019	4.583 2	0.0 36 7	0.1066 0.0 012	0.9 0.9		1750 1746	9 7	1746 1743	7 7	1743 1743	7 7		1743 1743	7 7
PH-1-12-13-5-003	0.286 0	0.0 018	5.761 3	0.0 57 2	0.1461 0.0 017	0.92 0.92		1622 1941	9 9	1941 1941	9 9	2301 2301	21 21	-	-	-
PH-1-12-13-5-004	0.476 3	0.0 027	10.73 25	0.0 64 8	0.1635 0.0 017	0.9 0.9		2511 2500	12 6	2500 2492	6 5	2492 2492	5 5		2492 2492	5 5
PH-1-12-13-5-005	0.258 4	0.0 014	5.192 5	0.0 34 8	0.1458 0.0 013	0.89 0.89		1481 1851	7 6	1851 2297	6 6	2297 2418	15 19	-	-	-
PH-1-12-13-5-006	0.295 4	0.0 018	6.372 9	0.0 58 3	0.1565 0.0 017	0.89 0.89		1668 2029	9 8	2029 2418	8 19	2418 2418	19 19	-	-	-
PH-1-12-13-5-007	0.325 2	0.0 022	5.592 1	0.0 77 5	0.1247 0.0 019	0.91 0.91		1815 1915	11 12	1915 2025	12 28	2025 2025	28 -	-	-	-
PH-1-12-13-5-008	0.369 5	0.0 021	7.684 6	0.0 50 7	0.1509 0.0 013	0.89 0.89		2027 2195	10 6	2195 2356	6 15	2356 2356	15 15	-	-	-

PH-1-12-13-5-009	0.5004	0.030	11.2103	0.0787	0.1625	0.018	0.9		2616	13	2541	7	2482	5		2482	5
PH-1-12-13-5-010	0.4988	0.031	12.5821	0.0988	0.1830	0.018	0.9		2608	13	2649	7	2680	17		2680	17
PH-1-12-13-5-011	0.3564	0.021	7.4069	0.0603	0.1507	0.015	0.91		1965	10	2162	7	2354	18	-	-	-
PH-1-12-13-5-012	0.4575	0.029	9.9207	0.0761	0.1573	0.018	0.9		2429	13	2427	7	2427	6		2427	6
PH-1-12-13-5-013	0.4644	0.027	10.0652	0.0685	0.1572	0.017	0.9		2459	12	2441	6	2426	5		2426	5
PH-1-12-13-5-014	0.4558	0.026	9.8887	0.0614	0.1574	0.017	0.9		2421	11	2424	6	2428	5		2428	5
PH-1-12-13-5-015	0.2214	0.014	2.5624	0.0258	0.0840	0.011	0.9		1289	7	1290	7	1292	10		1292	10
PH-1-12-13-5-016	0.3110	0.020	5.7881	0.0680	0.1350	0.018	0.87		1745	10	1945	10	2164	24	-	-	-
PH-1-12-13-5-017	0.4661	0.027	10.4173	0.0683	0.1621	0.017	0.9		2466	12	2473	6	2478	5		2478	5
PH-1-12-13-5-018	0.4594	0.027	10.0453	0.0687	0.1586	0.017	0.9		2437	12	2439	6	2441	5		2441	5
PH-1-12-13-5-019	0.3998	0.023	7.5160	0.0518	0.1364	0.012	0.89		2168	11	2175	6	2181	16		2181	16
PH-1-12-13-5-020	0.4635	0.032	10.4264	0.1106	0.1632	0.021	0.89		2455	14	2473	10	2489	22		2489	22
PH-1-12-13-5-021	0.1958	0.013	2.1699	0.0279	0.0804	0.013	0.9		1153	7	1171	9	1207	15		1207	15
PH-1-12-13-5-022	0.2287	0.014	2.9407	0.0256	0.0933	0.010	0.88		1328	7	1392	7	1493	20	-	-	-
PH-1-12-13-5-023	0.4569	0.027	10.0257	0.0669	0.1592	0.017	0.9		2426	12	2437	6	2447	5		2447	5
PH-1-12-13-5-024	0.3387	0.020	7.5436	0.0506	0.1616	0.018	0.9		1881	9	2178	6	2472	5	-	-	-
PH-1-12-13-5-025	0.2984	0.017	4.2584	0.0286	0.1035	0.011	0.9		1684	8	1685	6	1688	6		1688	6
PH-1-12-13-5-026	0.2453	0.018	3.0659	0.0409	0.0907	0.014	0.9		1414	9	1424	10	1440	15		1440	15
PH-1-12-13-5-027	0.4776	0.027	10.6947	0.0682	0.1624	0.017	0.9		2517	12	2497	6	2481	5		2481	5
PH-1-12-13-5-028	0.3640	0.022	7.0054	0.0540	0.1396	0.016	0.9		2001	10	2112	7	2223	6	-	-	-
PH-1-12-13-5-029	0.4632	0.027	10.3335	0.0706	0.1619	0.018	0.9		2453	12	2465	6	2475	5		2475	5
PH-1-12-13-5-030	0.4582	0.028	10.0803	0.0876	0.1596	0.017	0.92		2432	12	2442	8	2451	18		2451	18
PH-1-12-13-5-031	0.3167	0.018	6.3014	0.0449	0.1443	0.013	0.88		1774	9	2019	6	2280	16	-	-	-
PH-1-12-13-5-032	0.3219	0.020	5.5289	0.0528	0.1246	0.014	0.9		1799	10	1905	8	2023	21	-	-	-
PH-1-12-13-5-033	0.2965	0.017	6.1814	0.0398	0.1512	0.013	0.89		1674	8	2002	6	2360	15	-	-	-
PH-1-12-13-5-034	0.4389	0.027	9.0876	0.0699	0.1502	0.017	0.9		2345	12	2347	7	2348	6		2348	6

PH-1-12-13-5-035	0.2631	0.016	3.6545	0.0324	0.1008	0.0012	0.9		1506	8	1561	7	1638	8		1638	8
PH-1-12-13-5-036	0.4579	0.028	10.0397	0.0742	0.1590	0.0018	0.9		2430	12	2438	7	2445	6		2445	6
PH-1-12-13-5-037	0.2288	0.013	4.7170	0.0326	0.1495	0.0013	0.88		1328	7	1770	6	2341	16	-	-	-
PH-1-12-13-5-038	0.4007	0.028	8.0496	0.0885	0.1457	0.0019	0.89		2172	13	2237	10	2296	23		2296	23
PH-1-12-13-5-039	0.1848	0.011	2.0623	0.0206	0.0810	0.0010	0.88		1093	6	1136	7	1220	24	-	-	-
PH-1-12-13-5-040	0.2453	0.014	3.7342	0.0289	0.1104	0.0011	0.87		1414	7	1579	6	1806	18	-	-	-
PH-1-12-13-5-041	0.4335	0.030	9.0369	0.0986	0.1512	0.0020	0.89		2321	14	2342	10	2360	23		2360	23
PH-1-12-13-5-042	0.4861	0.027	10.7099	0.0649	0.1599	0.0017	0.9		2554	12	2498	6	2454	5		2454	5
PH-1-12-13-5-043	0.2358	0.014	2.8440	0.0244	0.0875	0.0011	0.9		1365	7	1367	6	1371	8		1371	8
PH-1-12-13-5-044	0.3830	0.027	8.2632	0.0924	0.1565	0.0021	0.88		2090	13	2260	10	2418	23	-	-	-
PH-1-12-13-5-045	0.4745	0.027	10.6420	0.0689	0.1627	0.0017	0.9		2503	12	2492	6	2484	5		2484	5
PH-1-12-13-5-046	0.4849	0.028	10.4795	0.0702	0.1568	0.0017	0.9		2549	12	2478	6	2421	5		2421	5
PH-1-12-13-5-047	0.4653	0.029	10.1748	0.0768	0.1587	0.0018	0.9		2463	13	2451	7	2441	6		2441	6
PH-1-12-13-5-048	0.3731	0.025	8.1947	0.0915	0.1593	0.0021	0.89		2044	12	2253	10	2448	23	-	-	-
PH-1-12-13-5-049	0.4515	0.026	9.6403	0.0619	0.1549	0.0017	0.9		2402	11	2401	6	2401	5		2401	5
PH-1-12-13-5-050	0.2775	0.017	3.7606	0.0334	0.0983	0.0012	0.9		1579	9	1584	7	1592	8		1592	8
PH-1-12-13-5-051	0.4243	0.026	8.4806	0.0624	0.1450	0.0016	0.9		2280	12	2284	7	2288	6		2288	6
PH-1-12-13-5-052	0.4534	0.028	9.9360	0.0750	0.1590	0.0018	0.9		2410	12	2429	7	2445	6		2445	6
PH-1-12-13-5-053	0.5021	0.029	12.0824	0.0764	0.1746	0.0019	0.9		2623	12	2611	6	2602	5		2602	5
PH-1-12-13-5-054	0.4383	0.029	9.1280	0.0976	0.1511	0.0019	0.91		2343	13	2351	10	2358	22		2358	22
PH-1-12-13-5-055	0.3090	0.017	6.5520	0.0438	0.1538	0.0013	0.89		1736	9	2053	6	2388	15	-	-	-
PH-1-12-13-5-056	0.4656	0.028	10.3904	0.0733	0.1619	0.0018	0.9		2464	12	2470	7	2476	5		2476	5
PH-1-12-13-5-057	0.3381	0.020	6.7418	0.0481	0.1447	0.0016	0.9		1878	10	2078	6	2284	6			
PH-1-12-13-5-058	0.2251	0.018	2.7314	0.0463	0.0880	0.0017	0.87		1309	9	1337	13	1383	37		1383	37
PH-1-12-13-5-059	0.4948	0.031	11.4274	0.0864	0.1676	0.0019	0.9		2591	13	2559	7	2533	6		2533	6
PH-1-12-13-5-060	0.1291	0.007	2.1763	0.0147	0.1223	0.0013	0.9		783	4	1173	5	1990	5	-	-	-

PH-1-12-13-5-061	0.4628	0.028	10.3424	0.0769	0.16210.018	0.9		2452	12	2466	7	2478	6		2478	6
PH-1-12-13-5-062	0.4137	0.027	8.7741	0.0734	0.15390.018	0.9		2232	12	2315	8	2389	7		2389	7
PH-1-12-13-5-063	0.4693	0.029	11.1896	0.0923	0.17290.018	0.9		2480	13	2539	8	2586	18		2586	18
PH-1-12-13-5-064	0.4690	0.029	10.3850	0.0775	0.16070.018	0.9		2479	13	2470	7	2463	6		2463	6
PH-1-12-13-5-065	0.3708	0.020	7.6550	0.0475	0.14970.012	0.89		2033	10	2191	6	2343	15	-	-	-
PH-1-12-13-5-066	0.4604	0.061	10.1495	0.2241	0.15990.037	0.9		2441	27	2448	20	2455	20		2455	20
PH-1-12-13-5-067	0.1445	0.008	1.6542	0.0111	0.08300.007	0.88		870	4	991	4	1270	17	-	-	-
PH-1-12-13-5-068	0.4727	0.028	10.6570	0.0730	0.16360.018	0.9		2495	12	2494	6	2493	5		2493	5
PH-1-12-13-5-069	0.3998	0.024	7.7916	0.0556	0.14140.016	0.9		2168	11	2207	6	2245	6		2245	6
PH-1-12-13-5-070	0.2392	0.013	3.4139	0.0222	0.10350.009	0.89		1383	7	1508	5	1688	16	-	-	-
PH-1-12-13-5-071	0.4719	0.028	10.5299	0.0746	0.16190.018	0.9		2492	12	2483	7	2476	5		2476	5
PH-1-12-13-5-072	0.4115	0.025	8.7648	0.0654	0.15450.015	0.89		2222	11	2314	7	2396	17		2396	17
PH-1-12-13-5-073	0.4586	0.027	10.1704	0.0711	0.16090.018	0.9		2433	12	2450	6	2465	5		2465	5
PH-1-12-13-5-074	0.4581	0.030	9.9579	0.0864	0.15770.019	0.9		2431	13	2431	8	2431	7		2431	7
PH-1-12-13-5-075	0.2554	0.016	5.4896	0.0445	0.15590.016	0.88		1466	8	1899	7	2412	18	-	-	-
PH-1-12-13-5-076	0.4645	0.027	10.4541	0.0667	0.16330.017	0.9		2459	12	2476	6	2490	5		2490	5
PH-1-12-13-5-077	0.4774	0.029	10.9101	0.0810	0.16580.019	0.9		2516	13	2515	7	2516	6		2516	6
PH-1-12-13-5-078	0.4730	0.028	10.2717	0.0692	0.15760.017	0.9		2497	12	2460	6	2430	5		2430	5
PH-1-12-13-5-079	0.2607	0.016	3.5751	0.0313	0.09940.011	0.88		1494	8	1544	7	1614	20		1614	20
PH-1-12-13-5-080	0.4694	0.029	10.5253	0.0791	0.16270.018	0.9		2481	13	2482	7	2484	6		2484	6
PH-1-12-13-5-081	0.4637	0.032	10.3275	0.0945	0.16160.020	0.9		2456	14	2465	8	2472	7		2472	7
PH-1-12-13-5-082	0.4735	0.028	10.6768	0.0753	0.16360.018	0.9		2499	12	2495	7	2493	5		2493	5
PH-1-12-13-5-083	0.4671	0.027	10.5621	0.0716	0.16410.018	0.9		2471	12	2485	6	2498	5		2498	5
PH-1-12-13-5-084	0.4349	0.029	9.3552	0.0966	0.15600.019	0.9		2328	13	2373	9	2413	21		2413	21
PH-1-12-13-5-085	0.4756	0.027	10.8752	0.0672	0.16590.018	0.9		2508	12	2513	6	2517	5		2517	5
PH-1-12-13-5-086	0.4910	0.034	13.1134	0.1180	0.19370.022	0.88		2575	15	2688	8	2774	19		2774	19

PH-1-12-13-5-087	0.4664	0.026	10.3773	0.0650	0.1614	0.017	0.9		2468	12	2469	6	2471	5		2471	5
PH-1-12-13-5-088	0.3583	0.021	7.4389	0.0553	0.1506	0.014	0.88		1974	10	2166	7	2352	17	-	-	-
PH-1-12-13-5-089	0.4637	0.029	10.3620	0.0801	0.1622	0.019	0.9		2456	13	2468	7	2478	6		2478	6
PH-1-12-13-5-090	0.3285	0.018	6.4082	0.0434	0.1415	0.012	0.89		1831	9	2033	6	2245	16			
PH-1-12-13-5-091	0.4495	0.026	9.5816	0.0652	0.1547	0.017	0.9		2393	12	2395	6	2398	5		2398	5
PH-1-12-13-5-092	0.3088	0.018	4.5970	0.0348	0.1080	0.010	0.88		1735	9	1749	6	1766	18		1766	18
PH-1-12-13-5-093	0.1521	0.010	1.5637	0.0216	0.0746	0.011	0.86		913	5	956	9	1057	31		913	5
PH-1-12-13-5-094	0.4331	0.026	8.9109	0.0654	0.1493	0.017	0.9		2320	12	2329	7	2338	6		2338	6
PH-1-12-13-5-095	0.4658	0.027	10.3163	0.0666	0.1607	0.017	0.9		2465	12	2464	6	2463	5		2463	5
PH-1-12-13-5-096	0.2506	0.014	3.3949	0.0248	0.0983	0.009	0.88		1441	7	1503	6	1591	18	-	-	-
PH-1-12-13-5-097	0.1933	0.014	4.4649	0.0710	0.1675	0.029	0.86		1139	8	1724	13	2533	30	-	-	-
PH-1-12-13-5-098	0.2028	0.011	2.7941	0.0195	0.0999	0.009	0.87		1191	6	1354	5	1622	17	-	-	-
PH-1-12-13-5-099	0.1372	0.008	2.7302	0.0211	0.1443	0.014	0.9		829	4	1337	6	2279	17	-	-	-
PH-1-12-13-5-100	0.4366	0.027	9.0853	0.0714	0.1509	0.015	0.89		2335	12	2347	7	2356	17		2356	17
PH-1-12-13-5-101	0.1793	0.013	1.8420	0.0298	0.0746	0.014	0.9		1063	7	1061	11	1057	21	-	-	-
PH-1-12-13-5-102	0.4703	0.027	10.4729	0.0693	0.1617	0.017	0.9		2485	12	2478	6	2473	5		2473	5
PH-1-12-13-5-103	0.4245	0.049	9.3511	0.2384	0.1598	0.045	0.85		2281	22	2373	23	2453	48		2453	48
PH-1-12-13-5-104	0.4289	0.029	8.5893	0.0769	0.1454	0.018	0.9		2301	13	2295	8	2292	7		2292	7
PH-1-12-13-5-105	0.4646	0.032	10.3117	0.0922	0.1611	0.020	0.9		2460	14	2463	8	2468	7		2468	7
PH-1-12-13-5-106	0.1864	0.011	2.3824	0.0203	0.0927	0.010	0.88		1102	6	1237	6	1482	20	-	-	-
PH-1-12-13-5-107	0.5125	0.030	11.9496	0.0791	0.1693	0.018	0.9		2667	13	2600	6	2550	5		2550	5
PH-1-12-13-5-108	0.4782	0.029	10.8303	0.0762	0.1644	0.018	0.9		2519	13	2509	7	2502	5		2502	5
PH-1-12-13-5-109	0.2200	0.015	3.5476	0.0415	0.1170	0.016	0.88		1282	8	1538	9	1911	25	-	-	-
PH-1-12-13-5-110	0.3035	0.017	4.4069	0.0301	0.1054	0.011	0.9		1709	9	1714	6	1721	6		1721	6
PH-1-12-13-5-111	0.2353	0.015	3.7671	0.0443	0.1161	0.015	0.86		1362	8	1586	9	1897	24	-	-	-
PH-1-12-13-5-112	0.2350	0.014	4.7490	0.0462	0.1465	0.017	0.91		1361	7	1776	8	2306	20	-	-	-

PH-1-12-13-5-113	0.4668	0.029	10.3800	0.0759	0.1615	0.018	0.9		2469	13	2469	7	2471	6		2471	6
PH-1-12-13-5-114	0.2684	0.015	5.7297	0.0422	0.1548	0.0015	0.9		1533	8	1936	6	2400	16	-	-	-
PH-1-12-13-5-115	0.3393	0.019	6.8394	0.0484	0.1462	0.0013	0.89		1883	9	2091	6	2302	16	-	-	-
PH-1-12-13-5-116	0.4091	0.027	8.0809	0.0846	0.1433	0.0018	0.89		2211	12	2240	9	2267	22	2267	22	
PH-1-12-13-5-117	0.3741	0.024	7.3128	0.0758	0.1418	0.0017	0.88		2049	11	2150	9	2249	22	2249	22	
PH-1-12-13-5-118	0.4029	0.024	8.4482	0.0676	0.1521	0.0015	0.91		2182	11	2280	7	2370	17	2370	17	
PH-1-12-13-5-119	0.1438	0.008	2.8175	0.0199	0.1421	0.0013	0.89		866	5	1360	5	2253	16	-	-	-
PH-1-12-13-5-120	0.4690	0.028	10.2806	0.0741	0.1591	0.0018	0.9		2479	12	2460	7	2447	5	2447	5	
PH-1-12-13-5-121	0.1945	0.011	3.6211	0.0230	0.1350	0.0011	0.89		1146	6	1554	5	2164	15	-	-	-
PH-1-12-13-5-122	0.4511	0.026	9.7379	0.0656	0.1566	0.0014	0.9		2400	11	2410	6	2419	15	2419	15	
PH-1-12-13-5-123	0.2765	0.017	3.7032	0.0334	0.0973	0.0012	0.9		1574	9	1572	7	1572	8	1572	8	
PH-1-12-13-5-124	0.3702	0.023	7.5505	0.0687	0.1479	0.0016	0.9		2030	11	2179	8	2322	19	-	-	-
PH-1-12-13-5-125	0.4618	0.027	10.2147	0.0661	0.1606	0.0017	0.9		2448	12	2454	6	2462	5	2462	5	
PH-1-12-13-5-126	0.4715	0.030	10.5634	0.0804	0.1627	0.0018	0.9		2490	13	2485	7	2483	6	2483	6	
PH-1-12-13-5-127	0.4749	0.027	10.4507	0.0623	0.1598	0.0017	0.9		2505	12	2476	6	2453	5	2453	5	
PH-1-12-13-5-128	0.1376	0.008	1.5241	0.0130	0.0804	0.0010	0.9		831	5	940	5	1208	8	-	-	-
PH-1-12-13-5-129	0.3118	0.019	4.5605	0.0353	0.1062	0.0012	0.9		1750	9	1742	6	1735	7	1735	7	
PH-1-12-13-5-130	0.4614	0.028	10.0467	0.0700	0.1581	0.0017	0.9		2446	12	2439	6	2435	5	2435	5	
PH-1-12-13-5-131	0.4074	0.026	8.1368	0.0729	0.1449	0.0016	0.9		2203	12	2246	8	2286	19	2286	19	
PH-1-12-13-5-132	0.4482	0.026	9.6388	0.0688	0.1560	0.0014	0.9		2387	12	2401	7	2413	16	2413	16	
PH-1-12-13-5-133	0.1878	0.010	2.5261	0.0173	0.0976	0.0009	0.88		1109	6	1280	5	1578	17	-	-	-
PH-1-12-13-5-134	0.4452	0.028	10.1007	0.0776	0.1647	0.0019	0.9		2374	12	2444	7	2505	6	2505	6	
PH-1-12-13-5-135	0.2211	0.012	3.3081	0.0212	0.1085	0.0009	0.88		1288	6	1483	5	1774	16	-	-	-
PH-1-12-13-5-136	0.2535	0.016	3.2321	0.0344	0.0925	0.0011	0.88		1456	8	1465	8	1477	24	1477	24	
PH-1-12-13-5-137	0.4414	0.026	9.7625	0.0643	0.1606	0.0017	0.9		2357	12	2413	6	2462	5	2462	5	
PH-1-12-13-5-138	0.5004	0.030	12.1326	0.0837	0.1760	0.0019	0.9		2615	13	2615	6	2616	5	2616	5	

PH-1-12-13-5-139	0.4658	0.028	10.3409	0.0711	0.1612	0.018	0.9		2465	12	2466	6	2468	5		2468	5
PH-1-12-13-5-140	0.3645	0.022	7.4053	0.0534	0.1474	0.014	0.88		2003	10	2162	6	2316	16	-	-	-
PH-1-12-13-5-141	0.2637	0.016	5.2157	0.0488	0.1435	0.016	0.9		1509	8	1855	8	2269	20	-	-	-
PH-1-12-13-5-142	0.1684	0.014	1.8827	0.0365	0.0812	0.017	0.9		1003	8	1075	13	1225	25	-	-	-
PH-1-12-13-5-143	0.1760	0.010	2.5226	0.0160	0.1040	0.009	0.88		1045	5	1279	5	1696	16	-	-	-
PH-1-12-13-5-144	0.2635	0.027	3.5737	0.0762	0.0985	0.023	0.9		1508	14	1544	17	1595	25	1595	25	
PH-1-12-13-5-145	0.4577	0.027	9.9867	0.0663	0.1584	0.017	0.9		2429	12	2434	6	2439	5	2439	5	
PH-1-12-13-5-146	0.4407	0.028	9.2148	0.0753	0.1518	0.018	0.9		2354	13	2360	7	2366	6	2366	6	
PH-1-12-13-5-147	0.4624	0.028	10.4289	0.0723	0.1637	0.018	0.9		2450	12	2474	6	2495	5	2495	5	
PH-1-12-13-5-148	0.1313	0.008	1.4361	0.0151	0.0793	0.010	0.84		795	4	904	6	1180	24	-	-	-
PH-1-12-13-5-149	0.4689	0.030	10.5211	0.0810	0.1629	0.019	0.9		2479	13	2482	7	2486	6	2486	6	
PH-1-12-13-5-150	0.1872	0.011	2.1251	0.0157	0.0824	0.009	0.9		1106	6	1157	5	1255	7	-	-	-
PH-1-12-13-5-151	0.4402	0.027	9.8378	0.0700	0.1622	0.018	0.9		2352	12	2420	7	2479	5	2479	5	
PH-1-12-13-5-152	0.2237	0.018	2.8550	0.0440	0.0926	0.016	0.9		1302	9	1370	12	1480	17	-	-	-
PH-1-12-13-5-153	0.4479	0.026	10.5865	0.0666	0.1716	0.018	0.9		2386	11	2488	6	2573	5	2573	5	
PH-1-12-13-5-154	0.2231	0.013	2.5648	0.0177	0.0834	0.009	0.9		1298	7	1291	5	1280	6	1280	6	
PH-1-12-13-5-155	0.2933	0.018	4.1700	0.0385	0.1031	0.011	0.88		1658	9	1668	8	1681	21	1681	21	
PH-1-12-13-5-156	0.4763	0.029	10.7611	0.0776	0.1640	0.018	0.9		2511	13	2503	7	2497	5	2497	5	
PH-1-12-13-5-157	0.0570	0.003	0.7967	0.0079	0.1014	0.012	0.88		357	2	595	4	1650	22	-	-	-
PH-1-12-13-5-158	0.1919	0.012	3.8779	0.0330	0.1466	0.015	0.91		1132	6	1609	7	2306	18	-	-	-
PH-1-12-13-5-159	0.3103	0.019	6.5541	0.0603	0.1532	0.017	0.91		1742	9	2053	8	2382	19	-	-	-
PH-1-12-13-5-160	0.4412	0.036	9.1721	0.1130	0.1509	0.022	0.9		2356	16	2355	11	2356	11	2356	11	
PH-1-12-13-5-161	0.4747	0.029	10.6995	0.0756	0.1636	0.018	0.9		2504	13	2497	7	2493	5	2493	5	
PH-1-12-13-5-162	0.1075	0.007	1.2171	0.0115	0.0822	0.011	0.9		658	4	808	5	1249	10	-	-	-
PH-1-12-13-5-163	0.4742	0.033	10.9217	0.0976	0.1671	0.020	0.9		2502	14	2516	8	2529	7	2529	7	
PH-1-12-13-5-164	0.3080	0.020	4.4915	0.0448	0.1058	0.014	0.9		1731	10	1729	8	1729	9	1729	9	

PH-1-12-13-5-165	0.0642	0.0004	0.7081	0.0086	0.0800	0.0011	0.82		401	2	544	5	1198	27	-	-
PH-1-12-13-5-166	0.4975	0.0036	11.2831	0.1111	0.1646	0.0021	0.9		2603	16	2547	9	2503	8	2503	8
PH-1-12-13-5-167	0.3794	0.0024	7.5493	0.0657	0.1443	0.0016	0.89		2073	11	2179	8	2280	19	2280	19
PH-1-12-13-5-168	0.4458	0.0031	9.4794	0.0865	0.1543	0.0019	0.9		2377	14	2386	8	2394	7	2394	7
PH-1-12-13-5-169	0.4641	0.0027	10.4136	0.0660	0.1627	0.0014	0.89		2458	12	2472	6	2484	15	2484	15
PH-1-12-13-5-170	0.1010	0.0006	1.1023	0.0114	0.0792	0.0010	0.87		620	4	754	5	1177	24	-	-
PH-1-12-13-5-171	0.1996	0.0012	4.0565	0.0284	0.1474	0.0013	0.89		1173	6	1646	6	2316	16	-	-
PH-1-12-13-5-172	0.3010	0.0017	4.3939	0.0289	0.1059	0.0011	0.9		1696	9	1711	5	1730	5	1730	5
PH-1-12-13-5-173	0.4554	0.0027	10.5720	0.0722	0.1684	0.0018	0.9		2419	12	2486	6	2542	5	2542	5
PH-1-12-13-5-174	0.2341	0.0015	3.1527	0.0357	0.0977	0.0013	0.82		1356	8	1446	9	1581	25	-	-
PH-1-12-13-5-175	0.3530	0.0022	5.8763	0.0461	0.1208	0.0014	0.9		1949	10	1958	7	1967	6	1967	6
PH-1-12-13-5-176	0.4114	0.0035	8.5748	0.1105	0.1512	0.0023	0.9		2221	16	2294	12	2360	11	2360	11
PH-1-12-13-5-177	0.4536	0.0031	10.4373	0.0923	0.1669	0.0020	0.9		2411	14	2474	8	2527	7	2527	7
PH-1-12-13-5-178	0.4830	0.0031	11.0084	0.0850	0.1653	0.0019	0.9		2540	13	2524	7	2511	6	2511	6
PH-1-12-13-5-179	0.1542	0.0009	2.0766	0.0177	0.0977	0.0010	0.88		925	5	1141	6	1580	20	-	-
PH-1-12-13-5-180	0.4714	0.0030	10.6387	0.0803	0.1637	0.0018	0.9		2489	13	2492	7	2494	6	2494	6
PH-1-12-13-5-181	0.4559	0.0032	10.0395	0.0919	0.1597	0.0020	0.9		2421	14	2438	8	2453	7	2453	7
PH-1-12-13-5-182	0.4479	0.0028	9.6889	0.0705	0.1569	0.0017	0.9		2386	12	2406	7	2422	6	2422	6
PH-1-12-13-5-183	0.3673	0.0022	8.1004	0.0550	0.1600	0.0017	0.9		2017	10	2242	6	2455	5	-	-
PH-1-12-13-5-184	0.2614	0.0016	5.6846	0.0472	0.1577	0.0016	0.91		1497	8	1929	7	2431	18	-	-
PH-1-12-13-5-185	0.1872	0.0011	2.4851	0.0180	0.0963	0.0011	0.9		1106	6	1268	5	1553	6	-	-
PH-1-12-13-5-186	0.2591	0.0016	3.5824	0.0297	0.1003	0.0010	0.88		1485	8	1546	7	1629	19	1629	19
PH-1-12-13-5-187	0.4350	0.0025	9.6785	0.0614	0.1614	0.0017	0.9		2328	11	2405	6	2470	5	2470	5
PH-1-12-13-5-188	0.1720	0.0011	3.2875	0.0285	0.1386	0.0015	0.87		1023	6	1478	7	2210	19	-	-
PH-1-12-13-5-189	0.1952	0.0012	2.4883	0.0221	0.0925	0.0010	0.88		1149	6	1269	6	1477	21	-	-
PH-1-12-13-5-190	0.1892	0.0011	2.4639	0.0183	0.0944	0.0009	0.88		1117	6	1262	5	1517	18	-	-

PH-1-12-13-5-191	0.4714	0.029	10.7648	0.0766	0.1656	0.018	0.9		2490	13	2503	7	2513	5		2513	5
PH-1-12-13-5-192	0.4888	0.030	11.2769	0.0818	0.1673	0.019	0.9		2565	13	2546	7	2531	5		2531	5
PH-1-12-13-5-193	0.4753	0.029	10.8074	0.0751	0.1649	0.018	0.9		2507	13	2507	6	2506	5		2506	5
PH-1-12-13-5-194	0.2412	0.015	4.1898	0.0396	0.1260	0.014	0.84		1393	8	1672	8	2042	20	-	-	-
PH-1-12-13-5-195	0.3513	0.023	7.4344	0.0677	0.1535	0.017	0.88		1941	11	2165	8	2385	20	-	-	-
PH-1-12-13-5-196	0.2020	0.013	2.3777	0.0261	0.0854	0.011	0.87		1186	7	1236	8	1324	25	-	-	-
PH-1-12-13-5-197	0.3055	0.018	5.5659	0.0376	0.1321	0.014	0.9		1718	9	1911	6	2126	5	-	-	-
PH-1-12-13-5-198	0.5127	0.032	12.3684	0.0880	0.1749	0.019	0.9		2668	14	2633	7	2605	5	2605	5	
PH-1-12-13-5-199	0.4559	0.030	10.5886	0.0905	0.1684	0.018	0.89		2422	13	2488	8	2542	19	2542	19	
PH-1-12-13-5-200	0.1269	0.008	1.4532	0.0131	0.0830	0.010	0.9		770	4	911	5	1269	9	-	-	-
PH-1-12-13-5-201	0.2260	0.016	4.0986	0.0423	0.1314	0.018	0.9		1314	8	1654	8	2117	9	-	-	-
	$^{206}\text{Pb}/^{238}\text{U}$	± 1 s.e.	$^{207}\text{Pb}/^{235}\text{U}$	± 1 s.e.	$^{207}\text{Pb}/^{206}\text{Pb}$	± 1 s.e.	Error corr.		$^{206}\text{Pb}/^{238}\text{U}$	± 1 s.e.	$^{207}\text{Pb}/^{235}\text{U}$	± 1 s.e.	$^{207}\text{Pb}/^{206}\text{Pb}$	± 1 s.e.	(Ma)	\pm (Ma)	
PH-1-9-13-27-001	0.4883	0.029	11.1269	0.0759	0.1649	0.018	0.9		2563	13	2534	6	2507	5	2507	5	
PH-1-9-13-27-002	0.5118	0.034	11.9689	0.1000	0.1693	0.020	0.9		2664	15	2602	8	2551	6	2551	6	
PH-1-9-13-27-003	0.2115	0.013	4.4060	0.0448	0.1511	0.018	0.89		1237	7	1713	8	2358	21	-	-	-
PH-1-9-13-27-004	0.3510	0.025	6.8045	0.0906	0.1406	0.021	0.86		1940	12	2086	12	2234	27	-	-	-
PH-1-9-13-27-005	0.3638	0.024	6.8946	0.0692	0.1375	0.016	0.86		2000	11	2098	9	2195	21	2195	21	
PH-1-9-13-27-006	0.0550	0.004	0.6313	0.0108	0.0832	0.015	0.86		345	2	497	7	1273	37	-	-	-
PH-1-9-13-27-007	0.5012	0.033	12.1650	0.0976	0.1757	0.020	0.9		2619	14	2617	8	2613	6	2613	6	
PH-1-9-13-27-008	0.4786	0.028	10.7208	0.0688	0.1622	0.017	0.9		2521	12	2499	6	2478	5	2478	5	
PH-1-9-13-27-009	0.4986	0.033	12.0239	0.0958	0.1746	0.020	0.9		2608	14	2606	7	2602	6	2602	6	
PH-1-9-13-27-010	0.3020	0.019	5.4503	0.0493	0.1309	0.014	0.87		1701	9	1893	8	2110	20	-	-	-
PH-1-9-13-27-011	0.4551	0.028	9.8369	0.0710	0.1565	0.017	0.9		2418	12	2420	7	2418	5	2418	5	
PH-1-9-13-27-012	0.5238	0.033	12.0219	0.0892	0.1662	0.018	0.9		2715	14	2606	7	2520	6	2520	6	
PH-1-9-13-27-013	0.4333	0.027	9.8962	0.0800	0.1656	0.017	0.91		2321	12	2425	7	2514	17	2514	17	

PH-1-9-13-27-014	0.5149	0.031	11.9628	0.0818	0.1682	0.018	0.9		2677	13	2601	6	2540	5		2540	5
PH-1-9-13-27-015	0.4551	0.028	9.8944	0.0725	0.1574	0.017	0.9		2418	12	2425	7	2428	6		2428	6
PH-1-9-13-27-016	0.0924	0.005	1.1720	0.0137	0.0920	0.012	0.74		570	3	788	6	1468	25		-	-
PH-1-9-13-27-017	0.2577	0.015	5.5071	0.0379	0.1547	0.017	0.9		1478	8	1902	6	2399	5		-	-
PH-1-9-13-27-018	0.1577	0.010	1.8992	0.0225	0.0874	0.012	0.85		944	5	1081	8	1368	26		-	-
PH-1-9-13-27-019	0.4625	0.028	10.6407	0.0747	0.1666	0.018	0.9		2450	12	2492	7	2524	5		2524	5
PH-1-9-13-27-020	0.4660	0.028	10.2967	0.0683	0.1600	0.017	0.9		2466	12	2462	6	2456	5		2456	5
PH-1-9-13-27-021	0.4810	0.030	10.9893	0.0814	0.1655	0.018	0.9		2531	13	2522	7	2512	6		2512	6
PH-1-9-13-27-022	0.4559	0.029	9.8395	0.0777	0.1563	0.018	0.9		2422	13	2420	7	2416	6		2416	6
PH-1-9-13-27-023	0.4593	0.033	10.0171	0.0981	0.1580	0.020	0.9		2436	15	2436	9	2434	8		2434	8
PH-1-9-13-27-024	0.4828	0.028	11.0291	0.0712	0.1655	0.017	0.9		2539	12	2526	6	2512	5		2512	5
PH-1-9-13-27-025	0.4655	0.028	10.3386	0.0723	0.1609	0.017	0.9		2464	12	2466	6	2465	5		2465	5
PH-1-9-13-27-026	0.4599	0.030	10.1460	0.0803	0.1598	0.018	0.9		2439	13	2448	7	2453	6		2453	6
PH-1-9-13-27-027	0.4778	0.029	10.8646	0.0763	0.1647	0.018	0.9		2518	13	2512	7	2504	5		2504	5
PH-1-9-13-27-028	0.1882	0.012	1.9921	0.0220	0.0767	0.011	0.9		1112	7	1113	7	1113	12		1113	12
PH-1-9-13-27-029	0.1998	0.012	4.1851	0.0348	0.1519	0.016	0.89		1174	6	1671	7	2368	18		-	-
PH-1-9-13-27-030	0.1432	0.010	1.9234	0.0293	0.0974	0.016	0.89		862	6	1089	10	1576	32		-	-
PH-1-9-13-27-031	0.4684	0.029	10.4683	0.0737	0.1619	0.018	0.9		2477	13	2477	7	2476	5		2476	5
PH-1-9-13-27-032	0.4443	0.029	9.3178	0.0754	0.1519	0.018	0.9		2370	13	2370	7	2368	6		2368	6
PH-1-9-13-27-033	0.4881	0.030	10.6784	0.0771	0.1585	0.017	0.9		2562	13	2496	7	2440	5		2440	5
PH-1-9-13-27-034	0.4732	0.030	10.7065	0.0791	0.1639	0.018	0.9		2498	13	2498	7	2497	6		2497	6
PH-1-9-13-27-035	0.4598	0.028	10.0637	0.0721	0.1586	0.017	0.9		2439	12	2441	7	2441	5		2441	5
PH-1-9-13-27-036	0.4699	0.030	10.5440	0.0812	0.1626	0.018	0.9		2483	13	2484	7	2483	6		2483	6
PH-1-9-13-27-037	0.4588	0.031	10.3483	0.0906	0.1634	0.020	0.9		2434	14	2466	8	2492	7		2492	7
PH-1-9-13-27-038	0.4628	0.029	10.2182	0.0750	0.1600	0.018	0.9		2452	13	2455	7	2456	6		2456	6
PH-1-9-13-27-039	0.4751	0.030	10.7871	0.0795	0.1645	0.018	0.9		2506	13	2505	7	2503	6		2503	6

PH-1-9-13-27-040	0.3527	0.022	7.7132	0.0556	0.1585	0.017	0.9		1948	10	2198	6	2439	5	-	-
PH-1-9-13-27-041	0.4584	0.027	9.9178	0.0650	0.1568	0.017	0.9		2432	12	2427	6	2421	5	2421	5
PH-1-9-13-27-042	0.5218	0.034	11.8755	0.0937	0.1649	0.019	0.9		2707	14	2595	7	2507	6	2507	6
PH-1-9-13-27-043	0.5137	0.038	12.7805	0.1221	0.1803	0.022	0.9		2672	16	2664	9	2656	7	2656	7
PH-1-9-13-27-044	0.4694	0.029	10.6805	0.0760	0.1649	0.018	0.9		2481	13	2496	7	2507	5	2507	5
PH-1-9-13-27-045	0.1751	0.012	2.0385	0.0240	0.0844	0.012	0.9		1040	6	1128	8	1301	13	-	-
PH-1-9-13-27-046	0.2630	0.018	4.3450	0.0604	0.1198	0.019	0.87		1505	9	1702	11	1954	28	-	-
PH-1-9-13-27-047	0.4804	0.029	11.0672	0.0778	0.1670	0.018	0.9		2529	13	2529	7	2528	5	2528	5
PH-1-9-13-27-048	0.4872	0.030	11.3987	0.0783	0.1696	0.018	0.9		2559	13	2556	6	2553	5	2553	5
PH-1-9-13-27-049	0.4121	0.027	8.7860	0.0772	0.1546	0.017	0.9		2225	12	2316	8	2398	19	2398	19
PH-1-9-13-27-050	0.4421	0.030	9.2287	0.0818	0.1513	0.018	0.9		2360	13	2361	8	2361	7	2361	7
PH-1-9-13-27-051	0.4755	0.030	10.8238	0.0825	0.1650	0.019	0.9		2508	13	2508	7	2508	6	2508	6
PH-1-9-13-27-052	0.1681	0.010	3.3042	0.0246	0.1426	0.014	0.88		1001	5	1482	6	2259	17	-	-
PH-1-9-13-27-053	0.4639	0.030	10.2456	0.0825	0.1601	0.018	0.9		2457	13	2457	7	2457	6	2457	6
PH-1-9-13-27-054	0.1630	0.012	1.8458	0.0249	0.0821	0.013	0.9		974	6	1062	9	1248	16	974	6
PH-1-9-13-27-055	0.4684	0.029	10.4298	0.0740	0.1614	0.018	0.9		2477	13	2474	7	2471	5	2471	5
PH-1-9-13-27-056	0.5177	0.037	13.0658	0.1191	0.1830	0.022	0.9		2690	16	2684	9	2680	7	2680	7
PH-1-9-13-27-057	0.4697	0.031	10.5272	0.0851	0.1625	0.019	0.9		2482	13	2482	7	2482	6	2482	6
PH-1-9-13-27-059	0.4881	0.041	11.3724	0.1349	0.1690	0.024	0.9		2562	18	2554	11	2547	10	2547	10
PH-1-9-13-27-060	0.4667	0.028	10.3360	0.0694	0.1606	0.017	0.9		2469	12	2465	6	2462	5	2462	5
PH-1-9-13-27-061	0.4195	0.027	9.0758	0.0798	0.1569	0.017	0.91		2258	12	2346	8	2423	19	2423	19
PH-1-9-13-27-062	0.2227	0.015	2.6027	0.0295	0.0848	0.012	0.9		1296	8	1301	8	1310	12	1310	12
PH-1-9-13-27-063	0.4963	0.031	10.8826	0.0788	0.1590	0.017	0.9		2598	13	2513	7	2445	5	2445	5
PH-1-9-13-27-064	0.3060	0.019	5.8836	0.0557	0.1395	0.016	0.85		1721	9	1959	8	2221	20	-	-
PH-1-9-13-27-066	0.1494	0.009	2.7877	0.0272	0.1354	0.016	0.87		897	5	1352	7	2169	21	-	-
PH-1-9-13-27-067	0.4404	0.031	9.4326	0.0895	0.1553	0.019	0.9		2353	14	2381	9	2405	8	2405	8

PH-1-9-13-27-068	0.4601	0.031	10.1438	0.0874	0.15990	0.019	0.9		2440	14	2448	8	2455	7		2455	7
PH-1-9-13-27-069	0.4289	0.028	8.6510	0.0694	0.14630	0.017	0.9		2301	12	2302	7	2303	6		2303	6
PH-1-9-13-27-070	0.3508	0.024	5.7340	0.0670	0.11860	0.016	0.87		1938	12	1937	10	1935	25		1935	25
PH-1-9-13-27-071	0.4468	0.027	9.3986	0.0670	0.15260	0.017	0.9		2381	12	2378	7	2375	5		2375	5
PH-1-9-13-27-072	0.4832	0.030	11.0645	0.0782	0.16610	0.018	0.9		2541	13	2529	7	2519	5		2519	5
PH-1-9-13-27-073	0.3120	0.023	5.4059	0.0805	0.12570	0.021	0.84		1750	11	1886	13	2038	30		-	-
PH-1-9-13-27-074	0.2355	0.014	2.8072	0.0234	0.08650	0.010	0.9		1363	8	1357	6	1349	8		1349	8
PH-1-9-13-27-075	0.1942	0.012	3.6708	0.0285	0.13710	0.013	0.9		1144	6	1565	6	2191	17		-	-
PH-1-9-13-27-076	0.1232	0.008	1.3097	0.0139	0.07710	0.009	0.87		749	4	850	6	1124	25		-	-
PH-1-9-13-27-077	0.4723	0.029	10.6210	0.0769	0.16320	0.018	0.9		2493	13	2491	7	2489	5		2489	5
PH-1-9-13-27-078	0.4619	0.032	10.1512	0.0926	0.15950	0.019	0.9		2448	14	2449	8	2450	7		2450	7
PH-1-9-13-27-079	0.2763	0.017	4.9940	0.0440	0.13110	0.014	0.87		1573	9	1818	7	2113	19		-	-
PH-1-9-13-27-080	0.2708	0.020	3.7239	0.0736	0.09980	0.021	0.83		1545	10	1577	16	1619	40		1619	40
PH-1-9-13-27-081	0.2306	0.014	4.3652	0.0363	0.13730	0.014	0.85		1338	7	1706	7	2193	18		-	-
PH-1-9-13-27-082	0.4872	0.032	11.1310	0.0916	0.16580	0.019	0.9		2558	14	2534	8	2516	6		2516	6
PH-1-9-13-27-083	0.4600	0.030	10.0375	0.0782	0.15830	0.018	0.9		2440	13	2438	7	2438	6		2438	6
PH-1-9-13-27-085	0.5024	0.040	11.5119	0.1288	0.16630	0.023	0.9		2624	17	2566	10	2520	9		2520	9
PH-1-9-13-27-086	0.3245	0.021	5.5583	0.0632	0.12420	0.016	0.83		1812	10	1910	10	2018	24		-	-
PH-1-9-13-27-087	0.5045	0.035	11.9541	0.1052	0.17200	0.021	0.9		2633	15	2601	8	2577	7		2577	7
PH-1-9-13-27-088	0.4941	0.046	11.8089	0.1587	0.17350	0.027	0.9		2588	20	2589	13	2591	11		2591	11
PH-1-9-13-27-089	0.4795	0.033	10.8723	0.0951	0.16460	0.020	0.9		2525	14	2512	8	2503	7		2503	7
PH-1-9-13-27-090	0.4408	0.033	9.3195	0.0953	0.15350	0.020	0.9		2354	15	2370	9	2385	8		2385	8
PH-1-9-13-27-091	0.4228	0.030	8.6571	0.0950	0.14850	0.019	0.89		2273	13	2303	10	2329	23		2329	23
PH-1-9-13-27-092	0.2478	0.015	5.8126	0.0437	0.17030	0.019	0.9		1427	8	1948	7	2560	6		-	-
PH-1-9-13-27-093	0.2037	0.014	2.2433	0.0249	0.07990	0.011	0.9		1195	7	1195	8	1195	12		1195	12
PH-1-9-13-27-094	0.4827	0.042	11.1950	0.1430	0.16840	0.025	0.9		2539	18	2539	12	2542	11		2542	11

PH-1-9-13-27-095	0.5094	0.040	12.5080	0.133 6	0.1783	0.024	0.9		2654	17	2643	10	2637	8	2637	8
PH-1-9-13-27-096	0.5159	0.040	11.7419	0.126 5	0.1652	0.022	0.9		2682	17	2584	10	2510	9	2510	9
PH-1-9-13-27-097	0.4661	0.034	10.3650	0.103 4	0.1614	0.021	0.9		2467	15	2468	9	2471	8	2471	8
PH-1-9-13-27-098	0.1969	0.013	2.7878	0.043 6	0.1027	0.018	0.76		1159	7	1352	12	1673	32	-	-
PH-1-9-13-27-099	0.4520	0.031	10.0680	0.100 6	0.1615	0.020	0.9		2404	14	2441	9	2472	21	2472	21
PH-1-9-13-27-100	0.4776	0.036	10.5736	0.111 4	0.1607	0.021	0.9		2517	16	2486	10	2463	9	2463	9
Isotopic ratios and ages were corrected for common lead																
Sample/analysis designation corresponds to the sampling date, traverse stop, and analysis number																
The youngest three concordant ages are bolded, the youngest one age is interpreted to be maximum depositional age																

Table A.2.6. U-Pb detrital zircon geochronologic analyses of Sewak unit metasedimentary rocks

Sample/ analysis	Isotopic ratios								Apparent ages (Ma)								Best age	
	^{206}Pb / ^{238}U	± 1 s.e.	^{207}Pb / ^{235}U	± 1 s.e.	$^{207}\text{Pb}/^{206}\text{Pb}$	± 1 s.e.	Error corr.	^{206}Pb / ^{238}U	± 1 s.e.	^{207}Pb / ^{235}U	± 1 s.e.	$^{207}\text{Pb}/^{206}\text{Pb}$	± 1 s.e.	(Ma)	\pm (Ma)			
PH-1-14-13-4-52	0.6510	0.0033	24.4200	0.1300	0.2719	0.0027	1.02	3232	13	3285	5	3317	16	3317	16			
PH-1-14-13-4-18	0.5176	0.0027	14.3200	0.0750	0.2008	0.0020	0.97	2771	5	2689	11	2833	16	2833	16			
PH-1-14-13-4-8	0.5204	0.0026	13.6300	0.0700	0.1895	0.0019	0.99	2724	5	2700	11	2737	17	2737	17			
PH-1-14-13-4-41	0.5222	0.0039	13.4700	0.1000	0.1864	0.0019	1.00	2712	7	2708	17	2710	17	2710	17			
PH-1-14-13-4-1	0.4156	0.0023	9.2600	0.0500	0.1616	0.0016	1.05	2240	11	2363	5	2472	17	2472	17			
PH-1-14-13-4-11	0.3873	0.0022	7.8950	0.0445	0.1478	0.0015	1.05	2110	10	2219	5	2321	17	2321	17			
PH-1-14-13-4-47	0.3059	0.0016	4.5780	0.0235	0.1086	0.0011	1.01	1720	8	1745	4	1775	18	1775	18			
PH-1-14-13-4-35	0.3183	0.0021	4.7470	0.0315	0.1079	0.0011	1.00	1775	6	1781	10	1763	19	1763	19			
PH-1-14-13-4-64	0.3055	0.0016	4.4540	0.0255	0.1058	0.0011	1.00	1718	8	1722	5	1728	19	1728	19			
PH-1-14-13-4-32	0.3101	0.0020	4.5010	0.0260	0.1050	0.0011	1.00	1733	5	1741	10	1715	18	1715	18			
PH-1-14-13-4-43	0.2855	0.0016	3.9520	0.0270	0.0999	0.0010	1.00	1626	6	1619	8	1623	19	1623	19			
PH-1-14-13-4-1	0.3029	0.0028	4.1310	0.0410	0.0994	0.0010	1.03	1662	8	1705	14	1613	19	1613	19			
PH-1-14-13-4-36	0.2421	0.0015	3.0460	0.0200	0.0914	0.0009	1.02	1397	8	1419	5	1456	19	1456	19			
PH-1-14-13-4-14	0.2243	0.0014	2.7330	0.0225	0.0887	0.0010	1.03	1304	7	1337	6	1397	21	1397	21			
PH-1-14-13-4-35	0.2359	0.0014	2.8800	0.0195	0.0886	0.0009	1.01	1365	7	1376	5	1396	20	1396	20			

PH-1-14-13-4-65	0.2141	0.0013	2.5520	0.0170	0.0866	0.0099	1.03		1250	7	1287	5	1351	20		1351	20
PH-1-14-13-4-17	0.2220	0.0014	2.4810	0.0200	0.0815	0.0088	1.02		1268	6	1292	8	1234	20		1234	20
PH-1-14-13-4-23	0.2021	0.0012	2.2550	0.0150	0.0814	0.0088	1.01		1187	7	1198	5	1232	20		1198	12
PH-1-14-13-4-54	0.2030	0.0014	2.2390	0.0165	0.0798	0.0088	1.00		1191	8	1193	5	1192	20		1193	12
PH-1-14-13-4-40	0.1998	0.0010	2.1880	0.0105	0.0797	0.0088	1.00		1174	5	1177	3	1189	20		1177	12
PH-1-14-13-4-4	0.1939	0.0009	2.1340	0.0115	0.0795	0.0088	1.01		1143	5	1160	4	1184	21		1160	12
PH-1-14-13-4-34	0.1971	0.0009	2.1840	0.0105	0.0800	0.0088	0.99		1176	3	1159	5	1197	20		1159	12
PH-1-14-13-4-67	0.1952	0.0011	2.1230	0.0170	0.0781	0.0099	1.01		1149	6	1156	6	1150	22		1156	12
PH-1-14-13-4-31	0.1962	0.0013	2.1630	0.0140	0.0800	0.0088	0.99		1169	5	1155	7	1198	20		1155	12
PH-1-14-13-4-7	0.1924	0.0009	2.1130	0.0090	0.0798	0.0088	1.02		1134	4	1153	3	1193	20		1153	12
PH-1-14-13-4-60	0.1950	0.0014	2.1140	0.0145	0.0792	0.0088	1.00		1148	8	1153	5	1176	21		1153	12
PH-1-14-13-4-61	0.1907	0.0011	2.0970	0.0130	0.0799	0.0088	1.02		1125	6	1149	4	1194	20		1149	11
PH-1-14-13-4-26	0.1881	0.0010	2.0800	0.0110	0.0807	0.0088	1.03		1111	5	1142	4	1215	20		1142	11
PH-1-14-13-4-18	0.1918	0.0009	2.0770	0.0105	0.0790	0.0088	1.01		1131	5	1141	3	1172	20		1141	11
PH-1-14-13-4-66	0.1916	0.0013	2.0690	0.0145	0.0784	0.0088	1.01		1130	7	1138	5	1157	20		1138	11
PH-1-14-13-4-3	0.1917	0.0012	2.0850	0.0160	0.0792	0.0088	0.99		1143	5	1130	7	1177	20		1130	11
PH-1-14-13-4-16	0.1890	0.0008	2.0380	0.0095	0.0787	0.0088	1.01		1116	4	1128	3	1163	20		1128	11
PH-1-14-13-4-47	0.1881	0.0011	1.9430	0.0135	0.0747	0.0088	1.01		1096	5	1111	6	1061	21		1111	11
PH-1-14-13-4-11	0.1835	0.0031	2.0900	0.0600	0.0817	0.0095	1.01		1139	19	1085	17	1238	27		1085	17
PH-1-14-13-4-40	0.1816	0.0011	1.9070	0.0115	0.0759	0.0088	0.99		1083	4	1076	6	1093	20		1076	11
PH-1-14-13-4-27	0.1813	0.0012	1.9670	0.0130	0.0784	0.0088	0.97		1104	5	1074	7	1158	20		1074	11
PH-1-14-13-4-68	0.1651	0.0011	1.7190	0.0130	0.0758	0.0088	1.03		985	6	1015	5	1089	22		1015	10
PH-1-14-13-4-5	0.1652	0.0011	1.6250	0.0115	0.0717	0.0097	1.01		980	4	986	6	977	21		986	10
PH-1-14-13-4-22	0.1556	0.0011	1.5030	0.0110	0.0699	0.0097	1.00		931	5	932	6	926	21		932	9
PH-1-14-13-4-56	0.1556	0.0011	1.4910	0.0160	0.0693	0.0099	0.99		935	6	928	6	908	25		928	9
PH-1-14-13-4-63	0.1465	0.0010	1.4000	0.0100	0.0695	0.0097	1.01		881	5	889	4	913	21		889	9

PH-1-14-13-4-2	0.1476	0.0010	1.4130	0.0105	0.0695	0.0007	0.99		894	4	887	6	912	21		887	9
PH-1-14-13-4-15	0.1447	0.0010	1.3270	0.0120	0.0676	0.0007	0.98		871	6	857	6	856	23		857	9
PH-1-14-13-4-34	0.1382	0.0008	1.3090	0.0085	0.0686	0.0007	1.02		835	4	849	4	887	21		849	8
PH-1-14-13-4-53	0.1393	0.0006	1.3080	0.0100	0.0680	0.0008	1.01		841	4	849	4	868	24		849	8
PH-1-14-13-4-19	0.1401	0.0009	1.3150	0.0065	0.0682	0.0007	0.99		852	3	845	5	876	22		845	8
PH-1-14-13-4-6	0.1391	0.0009	1.2850	0.0085	0.0666	0.0007	1.00		839	4	839	5	826	21		839	8
PH-1-14-13-4-50	0.1353	0.0008	1.2760	0.0090	0.0685	0.0007	1.02		818	4	835	4	884	21		835	8
PH-1-14-13-4-29	0.1355	0.0008	1.2600	0.0085	0.0671	0.0007	1.01		819	4	828	4	842	22		828	8
PH-1-14-13-4-16	0.1365	0.0007	1.2560	0.0065	0.0666	0.0007	1.00		826	3	825	4	826	21		825	8
PH-1-14-13-4-17	0.1308	0.0006	1.2160	0.0060	0.0675	0.0007	1.02		792	3	808	3	852	21		808	8
PH-1-14-13-4-25	0.1285	0.0007	1.1670	0.0070	0.0658	0.0007	0.99		786	3	779	4	800	21		779	8
PH-1-14-13-4-15	0.1260	0.0011	1.1310	0.0110	0.0656	0.0007	0.99		769	5	765	7	793	22		765	8
PH-1-14-13-4-20	0.1213	0.0008	1.0200	0.0115	0.0609	0.0008	0.97		738	4	713	6	635	27		713	7
PH-1-14-13-4-8	0.1133	0.0007	0.9810	0.0085	0.0625	0.0007	1.00		692	4	694	4	692	26		694	7
PH-1-14-13-4-49	0.1142	0.0010	0.9740	0.0080	0.0627	0.0008	0.99		697	6	690	4	697	26		690	7
PH-1-14-13-4-43	0.1034	0.0006	0.8960	0.0065	0.0627	0.0007	1.02		634	4	649	4	697	22		649	6
PH-1-14-13-4-48	0.1043	0.0008	0.8580	0.0135	0.0598	0.0008	0.98		639	5	628	8	596	31		628	8
PH-1-14-13-4-23	0.1014	0.0007	0.8450	0.0060	0.0604	0.0006	1.00		622	3	623	4	618	23		623	6
PH-1-14-13-4-4	0.0976	0.0005	0.8069	0.0044	0.0601	0.0006	1.00		601	3	601	3	606	22		601	6
PH-1-14-13-4-13	0.0950	0.0004	0.7954	0.0036	0.0607	0.0006	1.02		585	3	594	2	628	22		594	6
PH-1-14-13-4-39	0.0965	0.0005	0.8006	0.0046	0.0600	0.0006	0.99		597	3	594	3	602	22		594	6
PH-1-14-13-4-21	0.0909	0.0005	0.7630	0.0065	0.0611	0.0006	1.02		562	3	575	4	643	23		575	6
PH-1-14-13-4-69	0.0917	0.0007	0.7490	0.0060	0.0592	0.0006	1.00		566	4	567	4	576	22		567	6
PH-1-14-13-4-38	0.0908	0.0006	0.7420	0.0055	0.0593	0.0006	1.01		560	3	563	3	577	23		563	6
PH-1-14-13-4-6	0.0902	0.0006	0.7374	0.0048	0.0593	0.0006	1.01		557	3	561	3	578	22		561	6
PH-1-14-13-4-20	0.0881	0.0007	0.7080	0.0060	0.0585	0.0006	1.00		544	4	544	4	549	23		544	5

PH-1-14-13-4-42	0.0885	0.0007	0.7030	0.0070	0.0580	0.0007	0.99		547	4	540	4	528	26		540	5
PH-1-14-13-4-44	0.0856	0.0004	0.6835	0.0041	0.0582	0.0006	1.00		529	3	529	2	535	23		529	5
PH-1-14-13-4-10	0.0852	0.0004	0.6716	0.0048	0.0571	0.0006	1.01		522	3	527	3	495	23		527	5
PH-1-14-13-4-58	0.0822	0.0004	0.6620	0.0050	0.0582	0.0007	1.01		509	3	516	3	535	26		516	5
PH-1-14-13-4-13	0.0832	0.0006	0.6640	0.0070	0.0576	0.0007	1.00		517	4	515	4	515	25		515	5
PH-1-14-13-4-32	0.0825	0.0004	0.6602	0.0041	0.0583	0.0006	1.01		511	2	515	3	540	23		515	5
PH-1-14-13-4-33	0.0829	0.0005	0.6540	0.0055	0.0572	0.0007	0.99		514	3	511	3	499	26		511	5
PH-1-14-13-4-21	0.0804	0.0007	0.6550	0.0095	0.0588	0.0009	0.98		511	6	498	4	560	32		498	5
PH-1-14-13-4-28	0.0785	0.0005	0.6232	0.0048	0.0582	0.0007	1.01		487	3	492	3	539	25		492	5
PH-1-14-13-4-44	0.0707	0.0007	0.5580	0.0055	0.0573	0.0006	0.98		450	4	440	4	501	23		440	4
PH-1-14-13-4-41	0.0579	0.0004	0.4371	0.0031	0.0548	0.0006	1.02		363	2	368	2	404	23		368	4
PH-1-14-13-4-7	0.0352	0.0002	0.2456	0.0016	0.0508	0.0005	1.00		223	1	223	1	230	24		223	2
PH-1-14-13-4-37	0.0306	0.0003	0.2159	0.0024	0.0513	0.0005	1.02		195	2	198	2	256	23		198	2
PH-1-14-13-4-45	0.0158	0.0001	0.1089	0.0015	0.0499	0.0009	0.96		105	1	101	1	190	40		101	1
PH-1-14-13-4-30	0.0140	0.0001	0.0974	0.0015	0.0506	0.0007	1.05		89	1	94	1	223	34		94	1
PH-1-14-13-4-28	0.0146	0.0001	0.1005	0.0013	0.0502	0.0008	0.96		97	1	93	1	204	38		93	1
PH-1-14-13-4-38	0.0143	0.0001	0.0979	0.0015	0.0492	0.0010	0.97		95	1	92	1	157	47		92	1
PH-1-14-13-4-42	0.0141	0.0001	0.0965	0.0019	0.0489	0.0010	0.96		94	2	90	1	143	49		90	1
PH-1-14-13-4-46	0.0104	0.0001	0.0705	0.0014	0.0492	0.0010	0.96		69	1	67	1	157	47		67	1
PH-1-14-13-4-33	0.0099	0.0001	0.0679	0.0013	0.0504	0.0010	0.95		67	1	63	1	213	45		63	1
PH-1-14-13-4-37	0.0098	0.0001	0.0642	0.0005	0.0472	0.0005	1.00		63	1	63	1	59	25		63	1
PH-1-14-13-4-24	0.0098	0.0001	0.0647	0.0006	0.0484	0.0006	0.98		64	1	63	1	118	31		63	1
PH-1-14-13-4-51	0.0086	0.0000	0.0566	0.0003	0.0476	0.0005	1.01		55	1	56	1	80	25		56	1
PH-1-14-13-4-12	0.0079	0.0000	0.0525	0.0006	0.0482	0.0007	0.98		52	1	51	1	109	36		51	1
PH-1-14-13-4-26	0.0078	0.0000	0.0531	0.0005	0.0490	0.0006	0.96		53	1	50	1	147	29		50	1
PH-1-14-13-4-55	0.0077	0.0001	0.0490	0.0008	0.0462	0.0009	0.99		49	1	49	1	8	46		49	1

PH-1-14-13-4-2	0.0047	0.0000	0.0299	0.0003	0.0457	0.0006	0.98		30	1	30	1	-19	34		30	1
PH-1-14-13-4-3	0.0046	0.0000	0.0285	0.0003	0.0451	0.0006	0.97		29	1	28	1	-53	32		28	1
PH-1-14-13-4-62	0.0042	0.0000	0.0270	0.0007	0.0464	0.0013	0.99		27	1	27	1	18	69		27	1
Sample/analysis designation corresponds to the sampling date, traverse stop, and analysis number																	
The youngest three concordant ages are bolded, the youngest one age is interpreted to be maximum depositional age																	

Table A.2.7. Whole-rock geochemical data for plutonic rocks

Sample:	PH-1-8-13-8	PH-1-8-13-1B	PH-1-8-13-4B	PH-1-8-13-22	PH-1-8-13-12A	PH-11-10-15-13
Granitoid type:	diorite	monzodiorite	monzodiorite	diorite	granodiorite ¹	migmatitic orthogneiss ²
<i>Major and minor elements (wt %)</i>						
SiO ₂	58.68	52.65	52.40	61.15	-	66.16
Al ₂ O ₃	18.46	21.33	19.71	14.68	-	14.57
Fe ₂ O ₃	5.21	7.12	11.46	4.21	-	5.37
MnO	0.09	0.08	0.11	0.10	-	0.15
MgO	2.18	2.58	3.36	0.10	-	1.84
CaO	5.85	6.91	3.74	12.73	-	3.68
Na ₂ O	4.39	4.53	3.81	3.75	-	4.2
K ₂ O	1.50	2.02	3.34	0.98	-	0.25
TiO ₂	0.46	0.71	0.92	0.48	-	0.43
P ₂ O ₅	0.13	0.16	0.07	0.13	-	0.03
LOI [@]	2.02	1.54	1.76	-	-	2.19
Total [#]	98.97	99.61	100.7	99.85	-	98.87
<i>Trace elements (ppm)</i>						
Sc	10	11	23	4	3.2	18
Be	< 1	1	2	3	0.6	< 1
V	121	127	169	20	52.9	45
Cr	30	30	50	90	28.5	< 20
Co	7	13	29	9	5.1	4
Ni	< 20	< 20	30	40	12.5	< 20
Cu	30	10	50	30	17.7	80
Zn	60	70	110	50	38.8	100
Ga	20	22	22	14	10.5	18
Ge	2	1	1	1	1.1	1
As	< 5	< 5	< 5	< 5	-	< 5
Rb	34	101	113	31	3.1	3
Sr	738	814	368	444	205	197

Y	9	15	10	12	2.1	53
Zr	52	124	98	122	53.5	214
Nb	6	3	3	4	1.7	1
Mo	< 2	< 2	< 2	< 2	-	< 2
Ag	< 0.5	< 0.5	< 0.5	< 0.5	-	1
In	< 0.2	< 0.2	< 0.2	< 0.2	-	< 0.2
Sn	1	2	1	< 1	0.6	5
Sb	1.2	< 0.5	< 0.5	1	-	< 0.5
Cs	1	2.4	3.1	1.6	0.3	< 0.5
Ba	392	339	822	130	27.1	37
La	10.4	11.5	16.4	13	3.9	7.6
Ce	21.3	25.9	33.5	25.5	7.9	23.1
Pr	2.6	3.5	4.4	3	0.9	3.67
Nd	11.1	15.3	18.3	12.4	4.7	18.1
Sm	2.2	3.6	4.1	2.7	1	5.7
Eu	0.8	1.2	1.1	0.8	0.3	1.53
Gd	1.7	3.3	3.7	2.5	0.8	7.4
Tb	0.3	0.5	0.5	0.3	0.1	1.3
Dy	1.5	3.1	2.6	2.1	0.5	9.2
Ho	0.3	0.6	0.4	0.4	0.1	2
Er	0.9	1.5	1	1.2	0.3	6.2
Tm	0.2	0.2	0.1	0.2	-	0.98
Yb	1	1.6	0.7	1.2	0.3	6.7
Lu	0.2	0.2	0.1	0.2	-	1.08
Hf	1.3	3.1	2.6	3.2	1.6	6.2
Ta	0.2	0.2	0.2	0.3	0.1	0.1
W	< 1	1	< 1	-	-	< 1
Tl	0.2	0.4	0.8	0.2	-	0.3
Pb	9	9	12	14	1.4	9
Bi	< 0.4	< 0.4	< 0.4	< 0.4	-	< 0.4
Th	0.7	1.3	3.5	5.9	1	0.7
U	0.4	0.5	0.6	1.3	0.4	0.4
S	-	-	-	-	-	-
Ti*	2696	4171	5452	2860	-	2531.1
K*	12450	16766	27722	8139	-	975
P*	567	698	305	576	-	185.7
¹ Granitoid classification determined from QAP diagram						
² Sample PH-11-10-15-13 is from the Eastern Lohit Plutonic Complex						
Undiff. is undifferentiated granitoid classification						
"@" Loss on ignition (LOI) values						

#Summed major-element oxide abundances, including LOI values				
"-" Not measured or below detection limit				
*ppm calculated from oxide weight percent				
Trace element concentrations have been normalized				

Table A.2.8. Whole-rock geochemical data for mafic and ultramafic rocks

Sample:	PH 1-8-13-11	PH 1-9-13-13	PH 1-8-13-28A	PH-1-9-13-8	PH-1-9-13-7B	PH-1-7-13-5	PH-1-8-13-12B	PH-1-9-13-10	PH-1-3-13-2B
Rock type:	mafic dike	metabasalt	metabasalt	mafic schist	ultramafic rock	metabasalt	mafic dike	metabasite	mafic schist
<i>Major and minor elements (wt %)</i>									
SiO ₂	47.86	48.37	51.36	54.38	44.42	49.01	-	-	-
Al ₂ O ₃	13.51	14.60	13.07	17.68	11.06	15.36	-	-	-
Fe ₂ O ₃	10.86	12.43	12.96	11.24	9.59	7.82	-	-	-
MnO	0.17	0.20	0.20	0.15	0.19	0.11	-	-	-
MgO	7.72	6.87	6.07	8.46	7.97	10.17	-	-	-
CaO	11.21	11.12	10.41	6.01	16.50	12.63	-	-	-
Na ₂ O	3.22	3.09	1.83	0.31	2.56	2.23	-	-	-
K ₂ O	0.26	0.61	0.87	0.01	0.90	0.19	-	-	-
TiO ₂	1.26	1.58	1.68	1.42	0.61	0.73	-	-	-
P ₂ O ₅	0.12	0.13	0.13	0.15	0.13	0.07	-	-	-
LOI [@]	2.18	0.68	0.67	-	6.62	2.01	-	-	-
Total [#]	98.37	99.68	99.25	99.81	100.5	100.3	-	-	-
<i>Trace elements (ppm)</i>									
Sc	45	39	43	-	35	37	34.5	6.8	6.7
Be	< 1	< 1	1.0	-	1.0	< 1	0.5	-	-
V	338	330	342	320	241	197	330.2	36.4	39.1
Cr	320	250	200	300	410	610	311.8	3466	2040
Co	42	42	46	52	46	38	33.6	103.9	82
Ni	140	80	70	110	130	230	108.9	2178	1784
Cu	90	< 10	110	10	260	30	17.3	2.6	12.2
Zn	80	110	110	180	70	< 30	66.5	47.6	39
Ga	16	19	19	20	15	12	15.6	0.7	1
Ge	2	2	3	2	2	1	3.1	3.4	2.8
As	< 5	< 5	< 5	28	< 5	< 5	-	-	-
Rb	7	3	14	< 2	22	< 2	5.5	0.8	0.4
Sr	188	180	134	199	310	116	195.1	2	2
Y	18	24	27	28	14	17	14.3	0.2	0.3
Zr	57	88	92	107	64	46	50	2.1	0.6

Nb	8	6	5	5	2	3	3.9	0.1	0.1
Mo	< 2	< 2	< 2	< 2	< 2	< 2	-	-	-
Ag	< 0.5	0.6	0.7	< 0.5	< 0.5	< 0.5	-	-	-
In	< 0.2	< 0.2	< 0.2	< 0.2	< 0.2	< 0.2	0.1	-	-
Sn	< 1	< 1	1	3	< 1	< 1	0.7	0.3	0.3
Sb	2.5	4	3.3	0.6	< 0.5	< 0.5	-	-	-
Cs	0.8	< 0.5	< 0.5	< 0.5	1.4	< 0.5	0.7	-	0.1
Ba	27	53	59	3	81	46	27.1	7	1.8
La	5.6	4.6	4.2	10.6	12.9	4	2.9	0.3	0.1
Ce	13.9	12.1	11.8	27.2	28.8	9.2	7.3	0.7	0.2
Pr	1.98	1.9	2	3.2	4	1.3	1.1	0.1	-
Nd	9.4	10.2	11	14.4	18.7	6.1	6.7	0.4	0.1
Sm	2.7	3.5	3.9	4.1	4.8	2.1	2.1	0.1	-
Eu	1.0	1.3	1.4	1.6	1.5	0.7	0.7	-	-
Gd	2.8	4	4.5	5.1	4.4	2.6	2.7	0.1	-
Tb	0.5	0.7	0.8	0.8	0.6	0.5	0.4	-	-
Dy	3.2	4.3	5.1	4.9	3.3	3	3	0.1	-
Ho	0.7	0.9	1	1	0.6	0.6	0.5	-	-
Er	1.9	2.5	2.8	2.7	1.5	1.9	1.9	-	-
Tm	0.3	0.4	0.4	0.4	0.2	0.3	0.2	-	-
Yb	1.9	2.5	2.8	2.6	1.3	1.9	1.8	-	0.1
Lu	0.3	0.4	0.4	0.4	0.2	1.2	0.2	-	-
Hf	1.5	2.1	2.3	2.6	1.8	0.3	1.6	0.1	-
Ta	0.3	0.2	0.2	0.4	0.1	0.3	0.3	-	-
W	< 1	2	< 1	-	< 1	< 1	-	-	-
Tl	< 0.1	< 0.1	< 0.1	< 0.1	< 0.1	< 0.1	-	-	-
Pb	< 5	< 5	8	38	< 5	< 5	2.7	0.3	0.2
Bi	< 0.4	< 0.4	0.5	0.6	< 0.4	< 0.4	0.1	-	-
Th	0.6	0.5	0.6	3.1	2	0.4	0.3	0.1	0.1
U	0.2	0.2	0.2	0.4	1.7	< 0.1	0.3	-	-
S	-	-	-	-	-	-	-	-	-
Ti*	7541	9434	10051	8481	3678	4385	-	-	-
K*	2158	5063	7221	88	7470	1577	-	-	-
P*	523	567	567	650	567	305	-	-	-

"@ Loss on ignition (LOI) values
#Summed major-element oxide abundances, including LOI values
"- Not measured or below detection limit
*ppm calculated from oxide weight percent
Trace element concentrations have been normalized

Table A.2.9. Results of Kolmogorov-Smirnov statistical test applied to the cumulative probability distributions of U-Pb detrital zircon ages

—protection against random null hypothesis ($\alpha_{\text{PR}} > 0.05$) indicates that the distribution being compared is not significantly different from the null hypothesis at the 95% confidence level.

Chapter 4: Tectonic Evolution of the northern Indo-Burma Ranges: Mesozoic-Cenozoic kinematic reconstruction and constraints on the mode of deformation across the easternmost India-Asia collisional zone

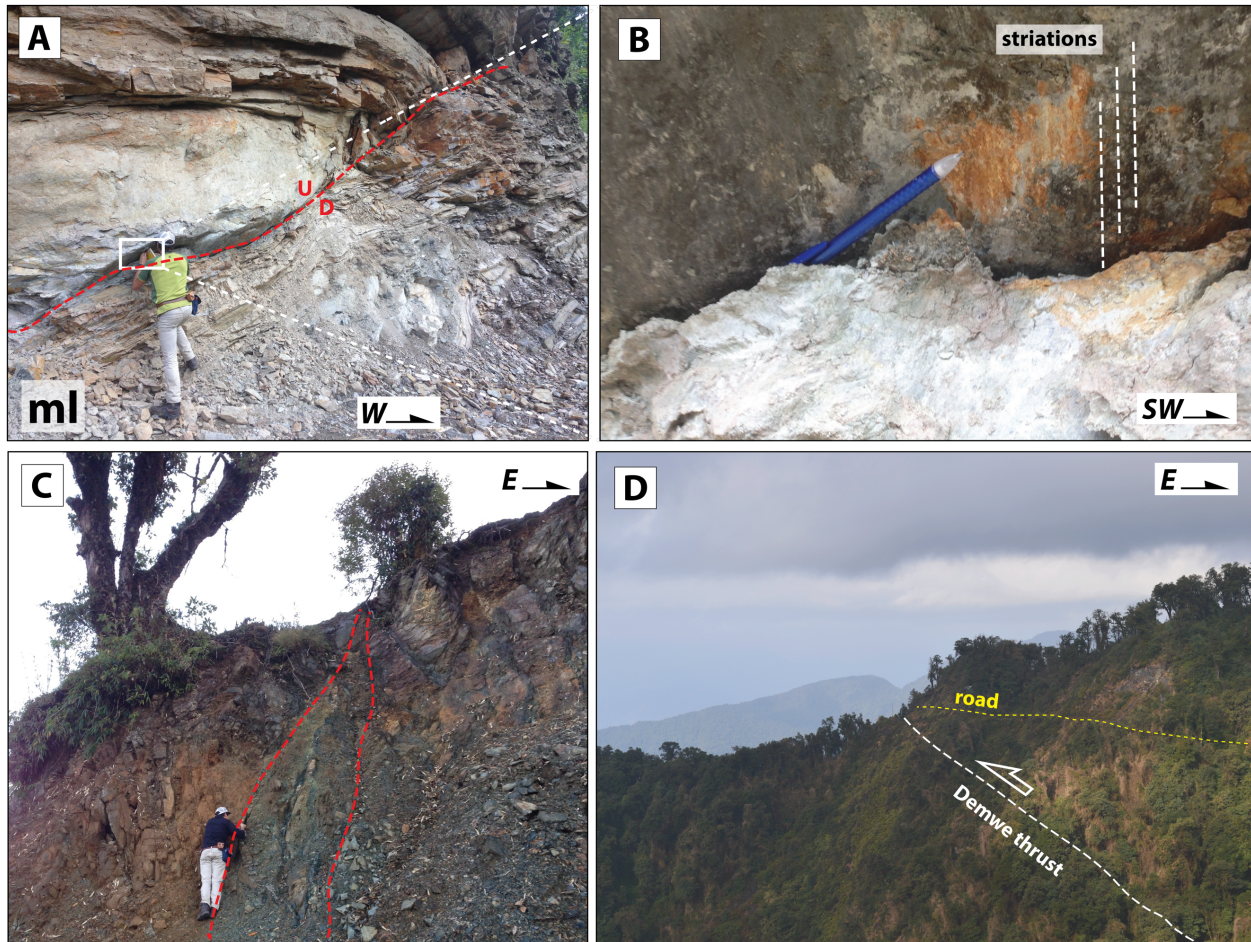


Figure A.4.1. Field photographs of (A) a brittle thrust fault within the Mayodia klippe (PH-1-7-13-4), (B) close-up view of the fault plane and striations of the previously shown thrust, (C) brittle fault gouge zone within the Mayodia klippe (PH-1-9-13-12), and (D) the Demwe thrust observed across a drainage in Dibang Valley (PH-1-3-13-11).

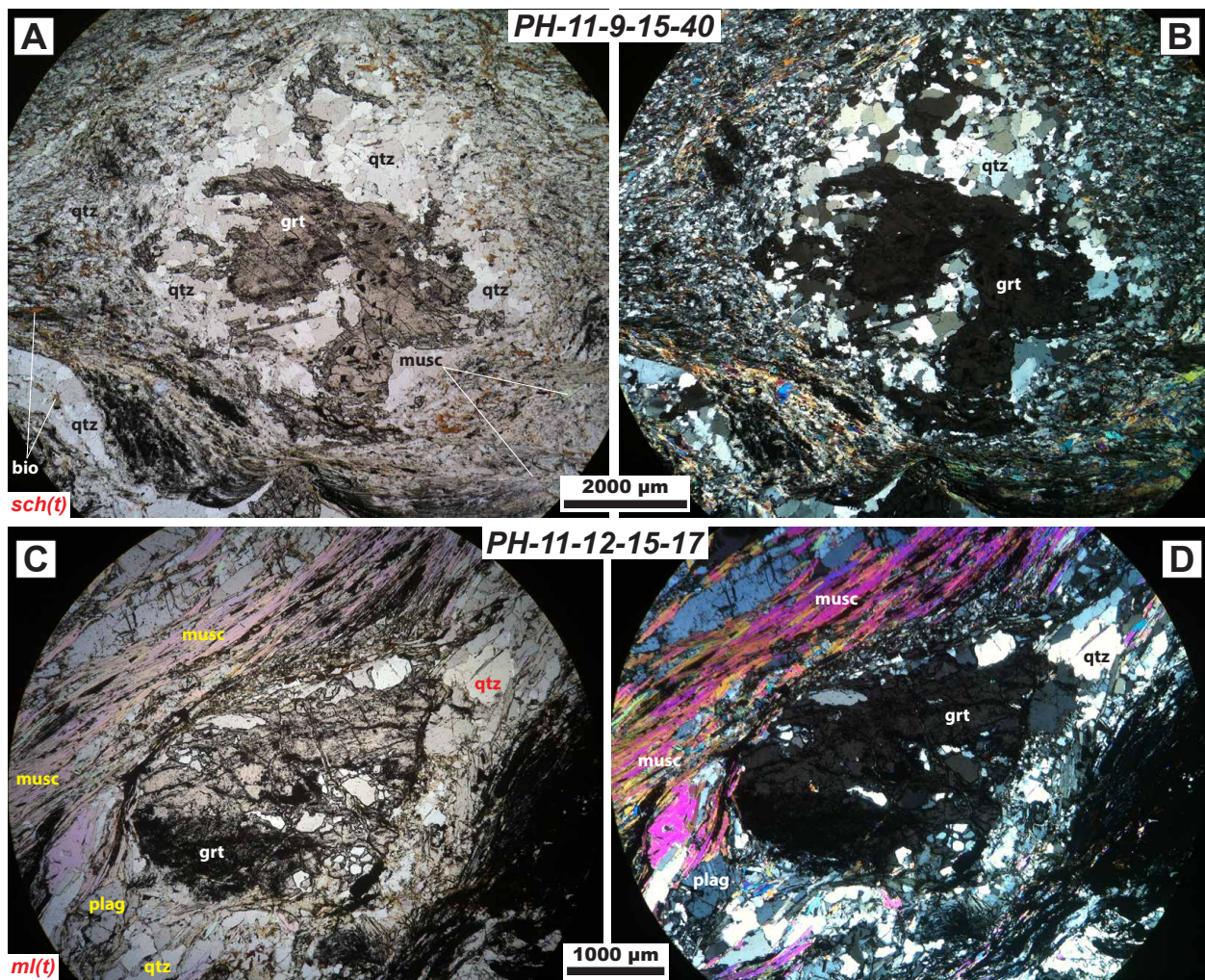


Figure A.4.2. Photomicrographs of garnet mica schist sample PH-11-9-15-40 in (A) ppl and (B) xpl and sample PH-11-12-15-17 in (C) ppl and (D) xpl. Note the quartz recrystallization along garnet grain boundaries in both samples.

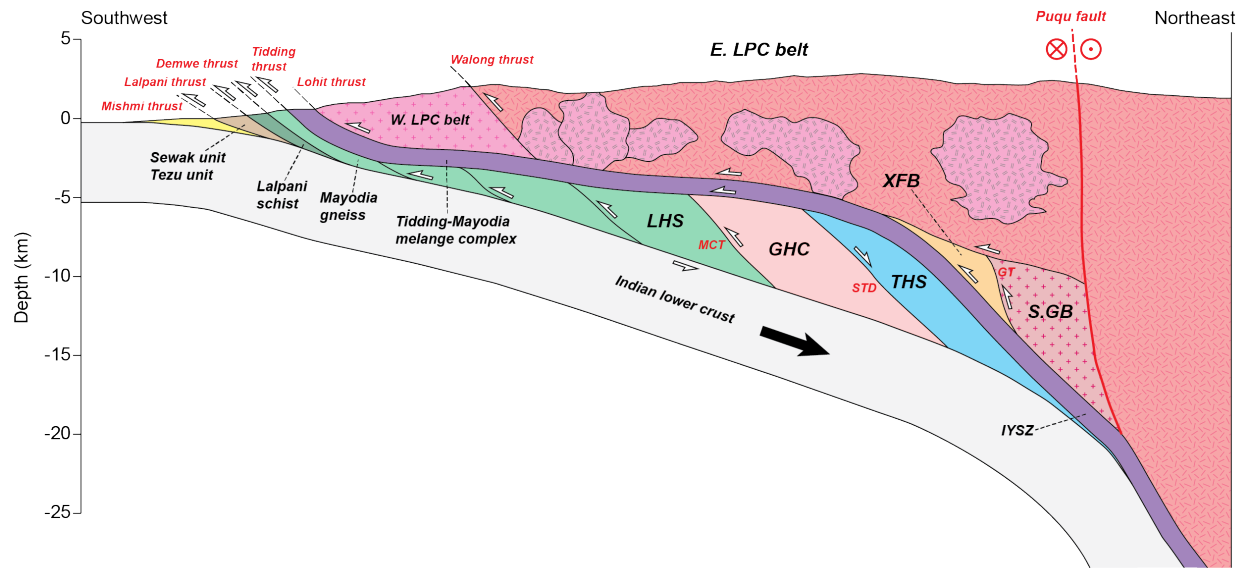


Figure A.4.3. Schematic cross section across the northern Indo-Burma Ranges showing the lithologic units of the Himalayan orogen and Lhasa terrane underthrusted beneath the overriding Lohit Plutonic Complex and Tidding-Mayodia mélange complex.

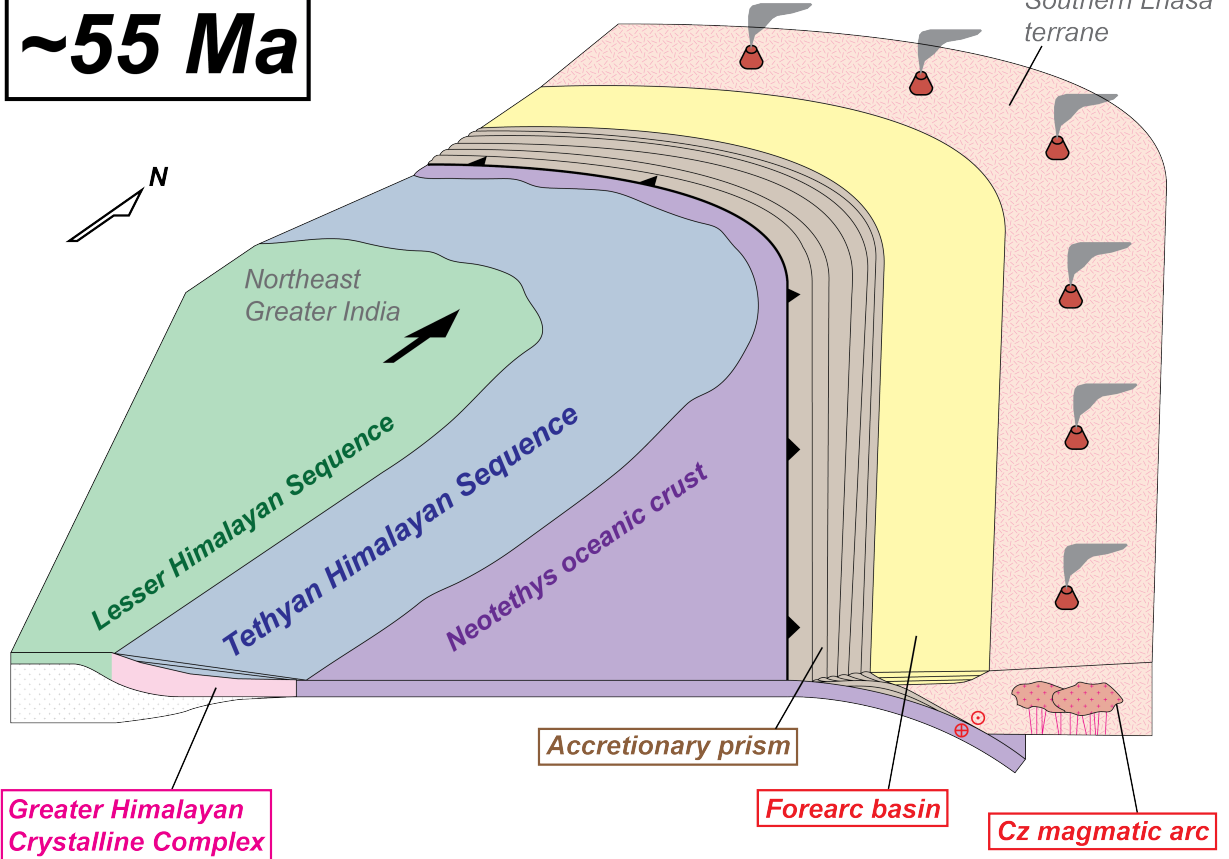


Figure A.4.4. Block diagram of the paleo-tectonic configuration of northeast Greater India and the southeast margin of Lhasa terrane at the onset of India-Asia collision.

Chapter 5: Out of sequence thrusting in the northern Indo-Burma Ranges: evidence from preliminary zircon (U-Th)/He thermochronology

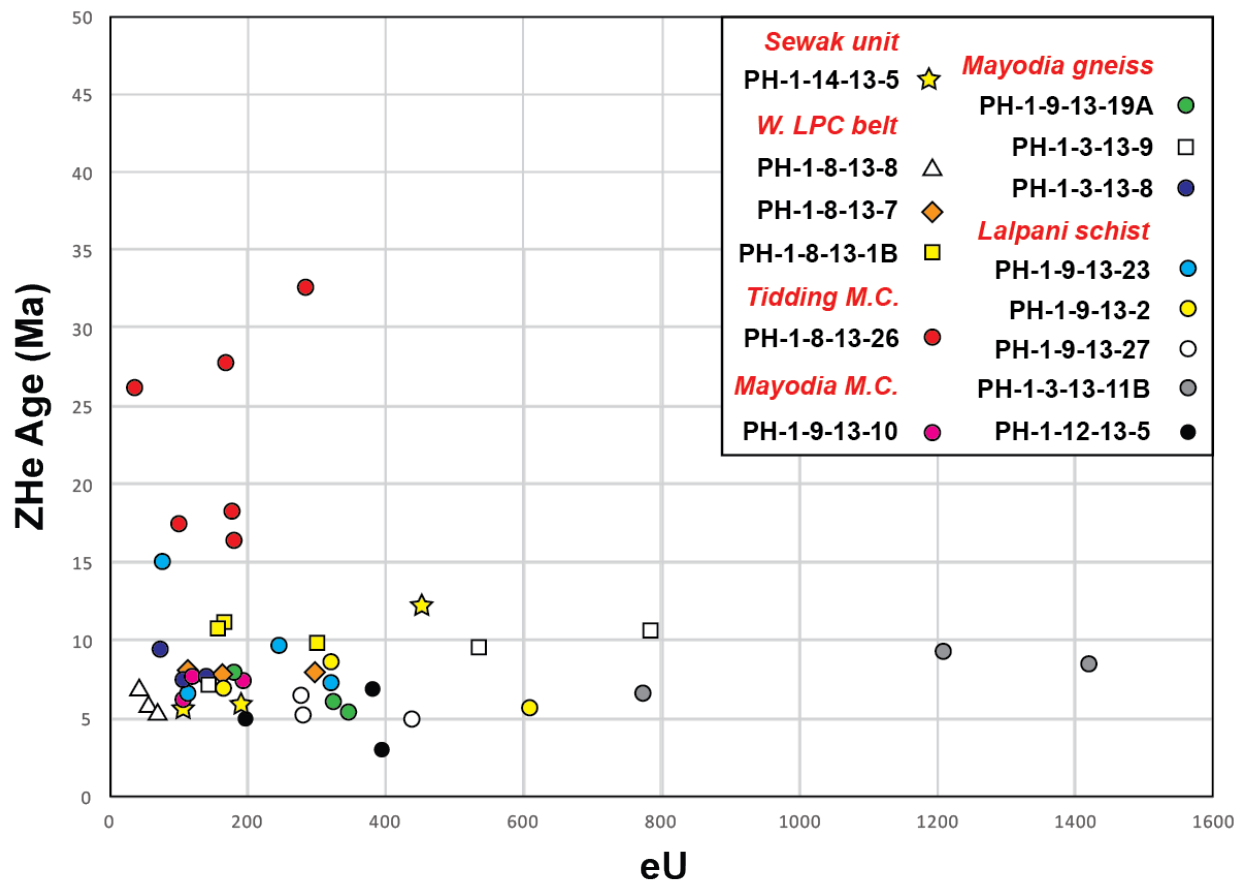


Figure A.5.1. Plot of (U-Th)/He (ZHe) age versus effective uranium (eU) for all zircon analyses.

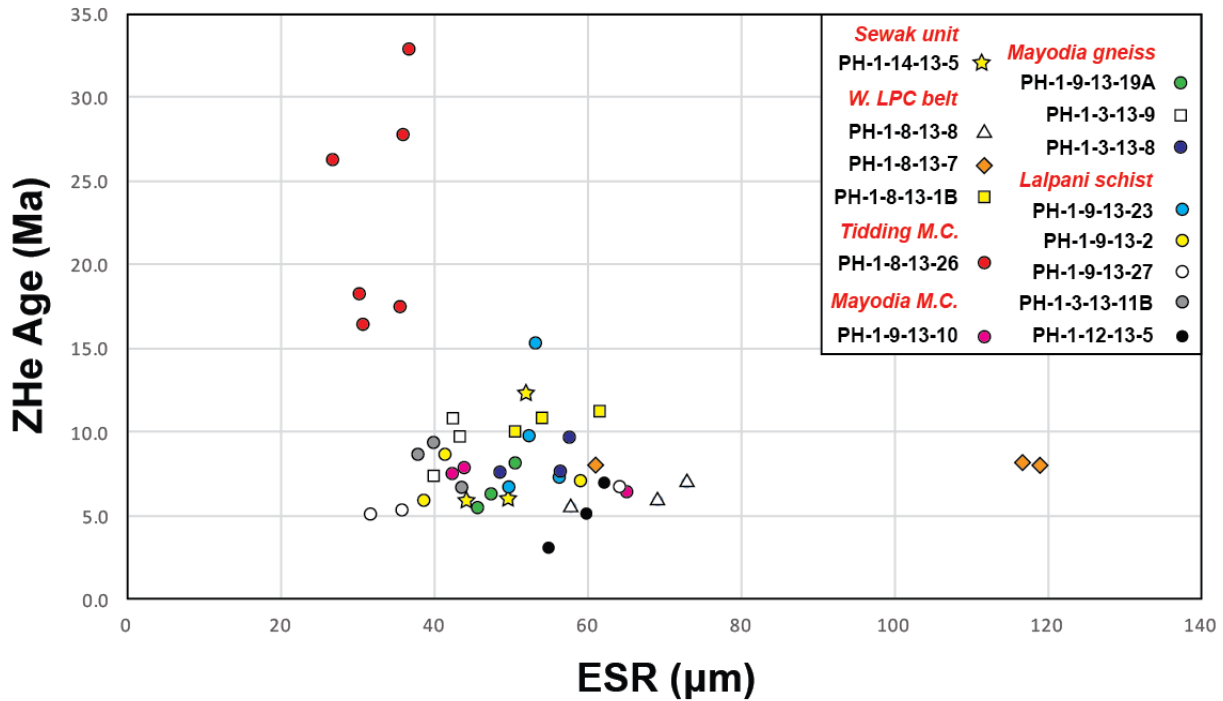


Figure A.5.2. Plot of (U-Th)/He (ZHe) age versus effective spherical radius (ESR) for all zircon analyses.

Table A.5.1. Summary of bedrock zircon (U-Th)/He ages for all aliquots from the northern Indo-Burma Ranges														
Sample	Rock type	Age (Ma)	err. (Ma)	U (ppm)	Th (ppm)	¹⁴⁷ Sm (ppm)	Ue	Th/U	He (nmol/g)	mass (ug)	Ft	ESR	Rejected ?	
<i>Western Lohit Plutonic Complex belt</i>														
PH-1-8-13-7-2	quartz monzonite	7.8	0.62	95.2	82.2	1.4	114.1	0.86	4.3	71.1 6	0.9 0	119.1 8		
PH-1-8-13-7-1	-	7.8	0.63	152.4	53.8	66.9	165.1	0.35	5.6	9.70	0.8 1	61.17		
PH-1-8-13-7-3	-	8.0	0.64	245.2	241.9	3.8	300.9	0.99	11.6	60.2 2	0.8 9	116.9 6		
PH-1-8-13-1B-3	monzodiorite	10.7	0.85	148.6	49.6	2.2	160.0	0.33	7.2	8.55	0.7 8	54.43		
PH-1-8-13-1B-2	-	11.1	0.89	151.8	71.0	1.4	168.1	0.47	8.1	13.4 4	0.8 1	61.84		
PH-1-8-13-1B-1	-	9.8	0.79	276.0	113.7	2.6	302.1	0.41	12.4	7.06	0.7 7	50.80		
PH-1-8-13-8-1	diorite	5.8	0.46	55.4	10.3	0.6	57.8	0.19	1.5	14.9 8	0.8 3	69.47		

PH-1-8-13-8-2	-	5.3	0.42	68.9	14.8	1.0	72.3	0.22	1.7	8.89	0.80	58.17	
PH-1-8-13-8-3	-	6.9	0.55	38.3	24.6	1.0	43.9	0.64	1.4	18.77	0.83	73.12	
Tidding mélange complex													
PH-1-8-13-26-1	grt mica schist	18.1	1.45	169.0	40.6	7.2	178.3	0.24	11.2	1.28	0.64	30.45	
PH-1-8-13-26-2	-	32.6	2.61	257.5	129.6	16.9	287.4	0.50	35.1	2.18	0.69	37.02	
PH-1-8-13-26-3	-	44.9	3.59	0.5	1.1	2.7	0.8	2.32	0.1	3.43	0.72	42.79	y ²
PH-1-8-13-26-4	-	17.4	1.39	92.2	46.9	5.5	103	0.51	6.6	1.74	0.68	35.82	
PH-1-8-13-26-5	-	27.6	2.21	157.5	61.4	5.5	171.7	0.39	17.6	1.74	0.64	31.06	
PH-1-8-13-26-6	-	16.3	1.31	163.6	81.5	0	182.4	0.5	10.3	1.32	0.64	31.06	
PH-1-8-13-26-7	-	26.1	2.09	35	17	0	38.9	0.49	3.3	0.81	0.59	27.02	
Mayodia mélange complex													
PH-1-9-13-10-1	grt mica schist	7.3	0.59	185.4	42.4	2.9	195.2	0.23	5.7	3.16	0.73	42.38	
PH-1-9-13-10-2	-	6.2	0.50	103.6	25.7	1.5	109.5	0.25	3.0	12.36	0.82	65.30	
PH-1-9-13-10-3	-	7.7	0.62	114.5	21.1	2.5	119.4	0.18	3.7	3.64	0.74	44.06	
Mayodia gneiss													
PH-1-9-13-19A-3	paragneiss	5.4	0.43	336.7	45.9	2.0	347.3	0.14	7.6	4.54	0.75	46.01	
PH-1-9-13-19A-1	-	8.0	0.64	174.0	36.6	3.3	182.5	0.21	6.1	5.65	0.77	50.98	
PH-1-9-13-19A-2	-	6.1	0.49	319.6	36.4	1.9	328.0	0.11	8.2	4.85	0.76	47.68	
PH-1-3-13-8-1	schist	7.5	0.60	105.3	27.4	3.6	111.6	0.26	3.4	5.18	0.76	48.92	
PH-1-3-13-8-2	-	9.5	0.76	75.4	21.0	2.1	80.3	0.28	3.3	8.94	0.80	57.83	
PH-1-3-13-8-3	-	7.5	0.60	132.4	36.7	3.4	140.9	0.28	4.5	8.13	0.79	56.76	
PH-1-3-13-9-3	paragneiss	9.6	0.77	488.4	210.9	4.9	536.9	0.43	20.4	3.75	0.73	43.57	
PH-1-3-13-9-1	-	7.2	0.57	88.4	249.6	12.8	145.9	2.82	4.0	2.87	0.70	40.15	
PH-1-3-13-9-2	-	10.6	0.85	703.5	364.7	2.6	787.4	0.52	32.9	3.49	0.73	42.60	

Lalpani schist														
PH-1-9-13-2-1	schist	8.6	0.69	275.0	207.5	2.7	322.8	0.75	10.8	3.37	0.7 2	41.69		
PH-1-9-13-2-2	-	0.0	0.00	0.2	0.1	1.4	0.2	0.46	22.1	6.44	0.7 7	51.69	y ¹	
PH-1-9-13-2-3	-	6.9	0.55	162.5	23.5	5.3	168.0	0.14	5.0	12.0 8	0.8 0	59.19		
PH-1-9-13-23-4	schist	6.6	0.53	102.2	58.7	2.9	115.7	0.57	3.1	6.31	0.7 6	49.99		
PH-1-9-13-23-5	-	7.3	0.58	300.0	107.2	25.6	324.8	0.36	10.1	8.30	0.7 9	56.57		
PH-1-9-13-23-6	-	15.0	1.20	74.6	18.9	4.1	79.0	0.25	5.0	6.76	0.7 8	53.57		
PH-1-9-13-27-1	paragneiss	-0.4	-0.03	0.2	0.2	3.7	0.3	1.02	0.0	2.49	0.6 9	37.61	y ¹	
PH-1-9-13-27-2	-	5.2	0.42	274.2	37.3	4.9	282.8	0.14	5.5	1.89	0.6 9	36.09		
PH-1-9-13-27-3	-	4.9	0.39	419.8	93.3	6.2	441.3	0.22	7.7	1.48	0.6 6	32.00		
PH-1-3-13-11B-1	paragneiss	9.3	0.74	1201. 8	47.1	3.5	1212. 6	0.04	43.7	2.61	0.7 2	40.17		
PH-1-3-13-11B-2	-	8.5	0.68	1396. 7	113.4	0.0	1422. 8	0.08	46.2	2.48	0.7 1	38.18		
PH-1-3-13-11B-3	-	6.6	0.52	762.5	55.6	2.7	775.3	0.07	20.3	3.43	0.7 4	43.82		
PH-1-12-13-5-1	paragneiss	4.9	0.39	188.4	40.7	2.1	197.8	0.22	4.2	8.66	0.8 1	60.08		
PH-1-12-13-5-2	-	6.8	0.54	380.3	19.0	1.9	384.7	0.05	11.5	9.65	0.8 1	62.31		
PH-1-12-13-5-3	-	1610. 6	128.8 5	0.4	0.7	2.4	0.6	1.74	4.0	3.82	0.7 3	44.64	y ¹	
Sewak unit														
PH-1-14-13-5-1	phyllite	5.7	0.46	95.9	51.8	2.6	107.8	0.54	2.5	3.51	0.7 4	44.38		
PH-1-14-13-5-2	-	12.1	0.97	387.2	295.3	3.2	455.2	0.76	23.1	5.84	0.7 7	52.41		
PH-1-14-13-5-3	-	5.9	0.47	175.7	83.7	4.9	195.0	0.48	4.8	5.69	0.7 7	50.01		
Rejected ZHe ages are based on ¹ analytical error or ² low uranium concentration														